Squaraine Based Dyes for Controlling the Aggregation and Charge Recombination Processes in Dye-Sensitized Solar Cells

By
Ambarish Kumar Singh
10CC15A26029

A thesis submitted to the
Academic of Scientific & Innovative Research
For the award of the degree of
DOCTOR OF PHILOSOPHY
in
Science

Under the supervision of
Dr. Jayaraj Nithyanandhan

CSIR-National Chemical Laboratory
Pune

Academy of Scientific and Innovative Research
AcSIR Headquarters, CSIR HRDC campus
Sector 19, Kamla Nehru Nagar,
Ghaziabad, U.P. - 201 002, India

January-2021

Certificate

This is to certify that the work incorporated in this Ph.D. thesis entitled, "*Squaraine Based Dyes for Controlling the Aggregation and Charge Recombination Processes in Dye-Sensitized Solar Cells*", submitted by *Ambarish Kumar Singh* to the Academy of Scientific and Innovative Research (AcSIR) in fulfilment of the requirements for the award of the Degree of *Doctor of Philosophy in Science*, embodies original research work carried-out by the student. We, further certify that this work has not been submitted to any other University or Institution in part or full for the award of any degree or diploma. Research material(s) obtained from other source(s) and used in this research work have been duly acknowledged in the thesis. Image(s), illustration(s), figure(s), table(s) etc., used in the thesis from other source(s), have also been duly cited and acknowledged.
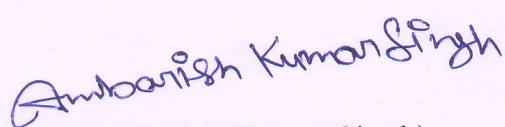
(Ambarish Kumar Singh)

Date: 05/01/2021

(Dr. Jayaraj Nithyanandhan)

Date: 05/01/2021

STATEMENTS OF ACADEMIC INTEGRITY

I, Ambarish Kumar Singh, a Ph.D. student of the Academy of Scientific and Innovative Research (AcSIR) with Registration No. 10CC15A26029 hereby undertake that, the thesis entitled "Squaraine Based Dyes for Controlling the Aggregation and Charge Recombination Processes in Dye-Sensitized Solar Cells" has been prepared by me and that the document reports original work carried out by me and is free of any plagiarism in compliance with the UGC Regulations on *"Promotion of Academic Integrity and Prevention of Plagiarism in Higher Educational Institutions (2018)"* and the CSIR Guidelines for *"Ethics in Research and in Governance (2020)"*.
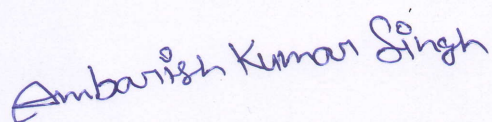
Signature of the Student
Date: 05/01/2021
Place: Pune

It is hereby certified that the work done by the student, under my supervision, is plagiarism-free in accordance with the UGC Regulations on *"Promotion of Academic Integrity and Prevention of Plagiarism in Higher Educational Institutions (2018)"* and the CSIR Guidelines for *"Ethics in Research and in Governance (2020)"*.
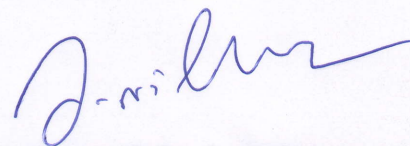
Signature of the Supervisor
Name: Dr. Jayaraj Nithyanandhan
Date : 05/01/2021
Place: Pune

Dedicated to My Family and My Gurudev

Chapter 2: Alkyl-Group-Wrapped Unsymmetrical Squaraine Dyes for Dye-Sensitized Solar Cells

Chapter 3: Position of Anchoring Group to Controls the Orientation and Self-Assembly of Unsymmetrical Squaraine Dyes on TiO₂ Surface

Chapter 4: D-A-D Based Complementary Unsymmetrical Squaraine Dyes for Co-sensitized Solar Cells

Chapter 5: Effect of Various Solvents and Electrolytes (I^-/I_3^-, Co(II/ III) and Cu(I/ II)) on the Device Performance of NIR-Light Active Squaraine Dyes

Abbreviation	Expansion
AcOH	Acetic acid
AM	Air mass
BTD	Benzo(1,2,5)thiadiazole
BuOH-1	Butanol-1
CDCA	Chenodeoxycholic acid (3α,7α-dihydroxy-5β-cholic acid)
CPDT	Cyclopentadithiophene
CIGS	Copper indium gallium diselenide
CV	Cyclic voltammetry
CH_3CN	Acetonitrile
$CDCl_3$	Chloroform-d
DFT	Density functional theory
DSCs	Dye solar cells
DSSCs	Dye-sensitized solar cells
DCM	Dichloromethane
DMSO-$d6$	Dimethyl sulfoxide-$d6$
EIS	Electrochemical impedance spectroscopy
EDOT	3,4-ethylenedioxythiophene
EtOAc	Ethyl acetate
EU-28	European Union-28 countries
FMO	Frontier molecular orbital
FTO	Fluorine-doped-tin oxide
HOMO	Highest occupied molecular orbital
HR-MS	High resolution mass spectrometry
IPCE	Incident photon-to-current conversion efficiency
IR	Infrared
I^-/I_3^-	Iodide/triiodide
ITO	Indium-doped-tin oxide
NIR	Near-Infrared
J-V	Current-Voltage
LHE	Light harvesting efficiency
LUMO	Lowest unoccupied molecular orbital
OPV	Organic photovoltaic
PCEs	Power conversion efficiencies
PV	Photovoltaic
PCC	Pyridiniumchlorochromate
PEDOT	Poly(3,4-ethylenedioxythiophene)
QDs	Quantum dots
UV-vis	Ultraviolet-visible
NMR	Nuclear magnetic resonance

REN21	Renewable Energy Policy Network for the 21st Century
SQ	Squaraine
THF	Tetrahydrofuran
TBAClO$_4$	Tetrabutylammonium perchlorate
UV-vis	Ultraviolet-visible
MeOH-d4	Methanol-d4
Eg	Energy band gap
E_{CB}	Conduction band edge
ff	Fill factor
J_{SC}	Short-circuit photocurrent
V_{OC}	Open-circuit photovoltage
R_{ct}	Charge recombination transfer/ resistance
R_s	Series resistance
R_{sh}	Shunt resistance
Cμ	Chemical capacitance
η	Solar cell efficiency
η_{inj}	Charge injection efficiency
η_{coll}	Charge collection efficiency
τ	Electron lifetime
ε	Extinction coefficient
s	Singlet
d	Doublet
t	Triplet
m	Multiplet
M$^+$	Molecular ion
mmol	Millimole
MHz	Megahertz
ppm	Parts per million
Å	Angstrom
λ	Wavelength
eV	Electron volt
ºC	Degree celsius
min	Minute(s)
h	Hour (s)
g	Gram
mg	Miligram
mL	Mililitre
kW	Kilowatt
GW	Gigawatt
TW	Terawatt

Chapter 1: Introduction

Dye sensitized solar cells (DSSCs) is a class of highly efficient low fabricating cost photovoltaic device since 1991. Light absorbing dyes are the main components of the DSSCs that harvest the light from the various regions of the solar spectrum and able to convert into the photocurrents. An ideal sensitizer needs to have an anchoring group that enhances the electronic coupling with TiO_2, high molar coefficient, panchromatic light absorption, with suitable LUMO and HOMO energy levels respect to conduction band of TiO_2 and redox level of electrolyte for an efficient charge injection and dye regeneration processes with high stability, respectively. Upon several modulations in the structures of the dyes with suitable energy levels, till now ruthenium-based dyes have reached the efficiency of 11.7%, whereas porphyrin dyes showed the device efficiency of 13%. Metal-free organic dyes have attracted considerable attention besides the ruthenium and zinc-porphyrin complexes, because of facile synthesis, low fabrication cost, flexibility of molecular design, tunable spectral properties, high molar extinction coefficient, and high-power conversion efficiency. Metal-free organic dyes have been achieved device efficiency of 13.6%. Among the metal-free organic dyes squaraine dyes are very impressive because of high extinction coefficient, and well known NIR-light sensitive with numerous applications in various areas like sensor, DSSC, organic solar cell, photodynamic-therapy, protein-labelling and fluorescent-probe due to aggregation behavior on the surface and solutions. Aggregation of dyes is a facile process on the semiconducting metal oxide surface and found as detrimental factor for the device performance of DSSC due to the self-quenching of photo-excited dyes with non-excited dyes. However, controlling the aggregation of dyes on the TiO_2 surface helps to enhance the light harvesting efficiency with improved photocurrent generation from the aggregated structures, besides reducing the charge recombination process by passivating the photoanode. The maximum efficiency achieved by unsymmetrical squaraine dye is 7.7% without co-absorbent because of the well packed aggregated structures on the TiO_2 surface.

Chapter 2: Alkyl-Group-Wrapped Unsymmetrical Squaraine Dyes for Dye-Sensitized Solar Cells

Dye-TiO$_2$ interface plays an important role in the charge injection process upon photo-exciting the sensitizers in DSSCs. Dye-dye interaction facilitated on the anatase TiO$_2$ surface due to the periodicity of dye anchoring sites (5 coordinated Ti) at the 101 facets. A strong intermolecular dye-dye interaction leads broadening the absorption spectrum because of H- and J- type aggregations. Often such aggregated structures exhibit poor charge injection capability due to deactivation of photo-excited dyes from non-excited dyes. Hence controlling the aggregation of dyes on the TiO$_2$ surface by taking the advantage of both broadening the absorption profile and efficient charge injection requires fine tuning of the dye structures with both steric and electronic factors. In this respect a series of alkyl-group-wrapped unsymmetrical squaraine dyes (SQS1-SQS6, **Figure 1**) have design, synthesized, and systematically investigated the effects of in-plane (N-centered) and out-of-plane (sp^3-C centered) alkyl groups on the V_{OC} and J_{SC}. The photophysical and electrochemical behavior of SQS1-SQS6 are almost similar in solution. Cyclic voltammetry studies of dye adsorbed on the TiO$_2$ electrode inferred that the self-hopping of charges can be modulated by the choice of both in-plane and out-of-plane alkyl groups. This particular feature helps to modulate the V_{OC} of the DSSC devices. Photovoltaic parameters such as J_{SC} and V_{OC} are modulated progressively by a judicious incorporation of branched alkyl groups which helps avoiding the charge recombination. SQS1 dye with shorter chain length at sp^3-C and N- atoms showed the cell efficiency of 4.9% with the V_{OC} 0.696 V, and J_{SC} 9.47 mA/cm^2, whereas SQS4 dye with longer chain length showed the cell efficiency of 7.1% with the V_{OC} 0.715 V and J_{SC} 13.05 mA/cm^2 respectively in the presence of CDCA. Further, importance of N-alkyl chain has been realized from SQS5 with reduced device performance of 5.24%. A correlation has been arrived for the observed V_{OC}, where alkyl group at N- atom plays importance over sp^3-C atom. Furthermore, the IPCE profile of the devices inferred that the contribution from both H- and J-type aggregates. Such observation helps to increase the DSSC device performance by effective charge injection from the self-assembled squaraine dyes, and effective passivation of the surface of TiO$_2$ which helps avoiding the charge recombination process (**Figure 2**). Systematic structure-property relationship studies in a set of similar dyes are rare, especially dyes that absorb both in the visible and NIR regions.
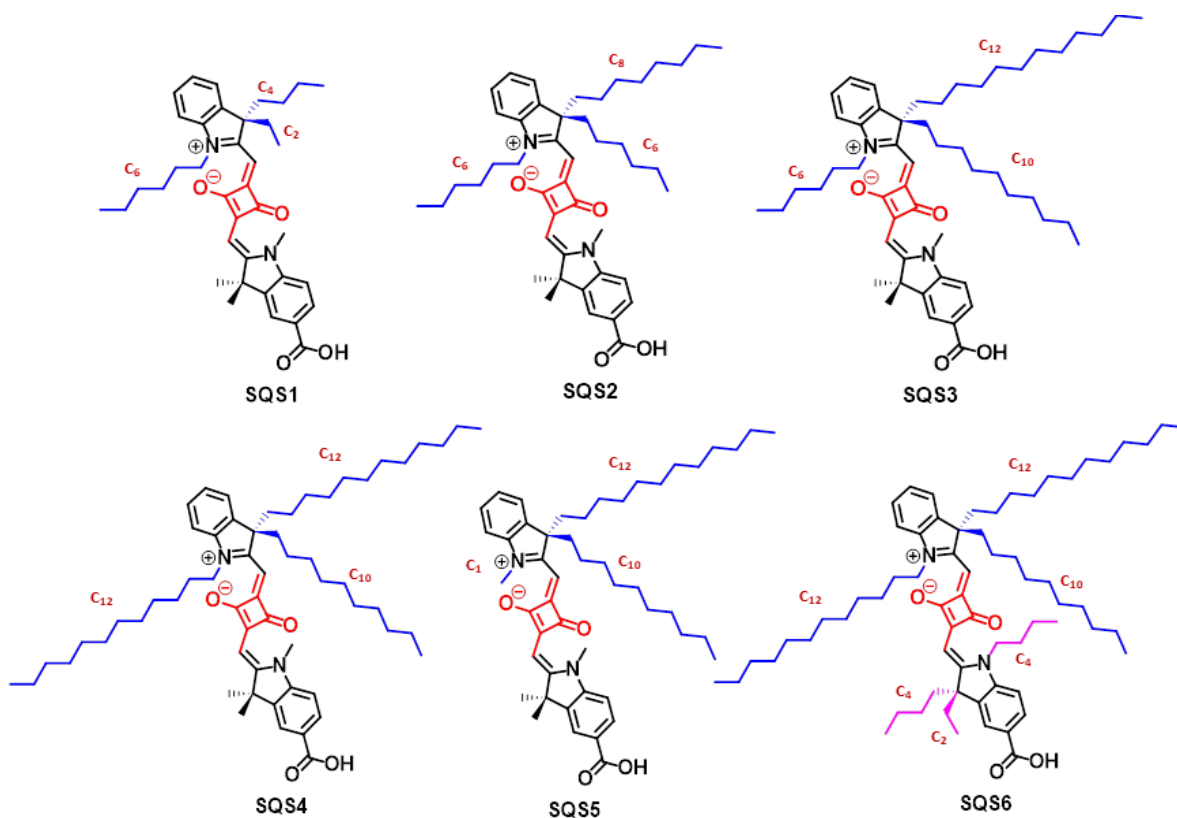
Figure 1. Structures of alkyl-group-wrapped unsymmetrical squaraine dyes.
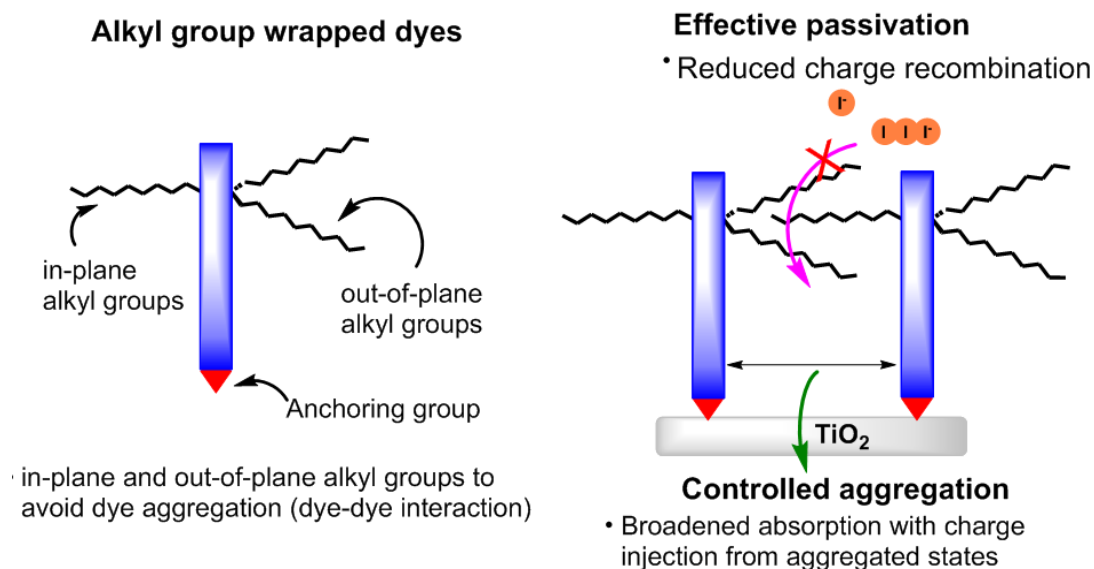
Figure 2. Controlled aggregation (broadening the spectrum) of the squaraine dyes on the TiO_2 surface, and surface passivation of TiO_2 (reduced charge recombination) by alkyl groups.

Chapter 3: Position of Anchoring Group to Controls the Orientation and Self-Assembly of Unsymmetrical Squaraine Dyes on TiO₂ Surface

Besides controlling the aggregations of dyes onto the TiO$_2$ surface and surface passivation of TiO$_2$ by introducing the alkyl groups with the donor moieties, position of anchoring group (orientation of the sensitizer onto the TiO$_2$ surface) plays an important role to determine the photovoltaic performances. In this respect a series of unsymmetrical squaraine dyes (4-SQ, 4-SQ1, 5-SQ, 6-SQ, 7-SQ, and 7-SQ1) functionalized with carboxylic acid (anchoring group) at different position with respect to N-atom (**Figure 3**) have design, synthesized, and systematically investigated the effects of the position of anchoring group on the squaraine dye to control the orientation of the dyes on the TiO$_2$ surface which modulate the self-assembly and device performance. 7-SQ, and 7-SQ1 (*ortho-*) dyes have not anchored on the TiO$_2$ surface and 5-SQ (*para-*) dye showed the highest device performance of 6.08%. It is observed that 4-SQ and 6-SQ (both are having *meta-*carboxyl groups as anchoring groups at the non-conductive site) showed varied device performance.
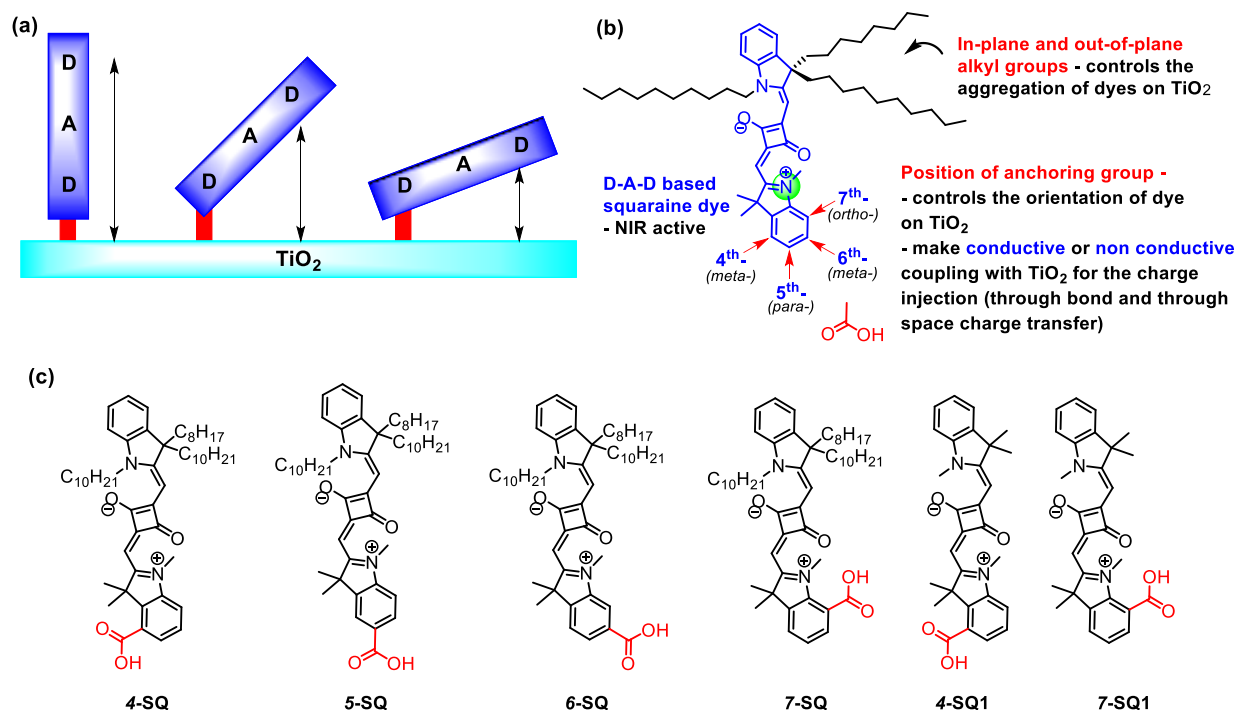
Figure 3. (a) Orientation of the D-A-D based dyes on TiO$_2$ surface, (b) structure and position of anchoring groups for the designed squaraine dyes, and (c) targeted squaraine dyes.

Fluorescence spectroscopy and computational studies revealed that the parallel orientation of 4-SQ with TiO_2 promote the formation of twisted structures for 4-SQ upon photo-excitation, whereas the self-assembly formation of 5-SQ and 6-SQ are almost similar in nature. Further, non-conductive nature of the anchoring group at 6-SQ showed the device performance of 4.14% compared to the conductive counterpart 5-SQ (6.08%) (**Figure 4**). The device performances of 4.14, 2.28, and 0.47% for the meta-carboxylic acid as anchoring group containing dye 6-SQ, 4-SQ, and 4-SQ1 showed the importance of through-space electron transfer process and self-assembled structures for the solar energy conversion. Computational studies inferred the systematic variation of the dipole moment of the dyes on the surface, which in-turn modulates the conduction band position of TiO_2.
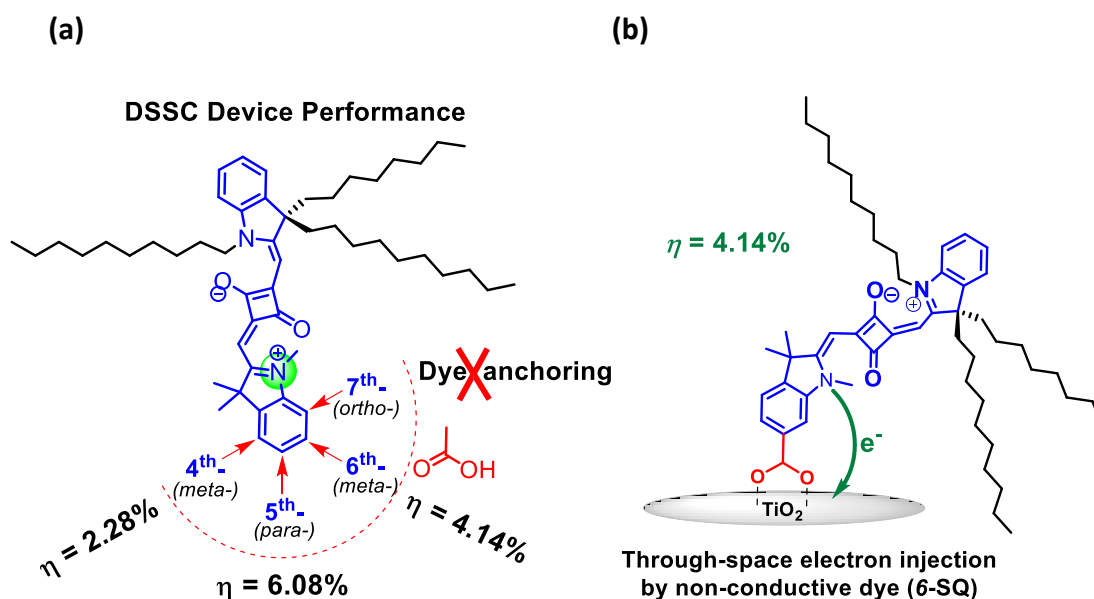
Figure 4. (a) Device performance of squaraine dyes, and **(b)** general representation of through-space electron transfer process in 6-SQ.

Chapter 4: D-A-D Based Complementary Unsymmetrical Squaraine Dyes for Co-sensitized Solar Cells

Having established the controlled self-assembly of far-red active unsymmetrical squaraine dyes, and anchoring group position for efficient photocurrent generation from the aggregated structures and photovoltage from the surface passivation of TiO_2, we have extended our design to develop visible-light active squaraine dyes. In the polymethine dyes per vinylene unit leads 100-120 nm red shift which is about 20-30 nm for the D-π-A, and D-A-π-A dyes (**Figure 5a**).

This design will help us to generalize the dye design where controlled aggregation of dyes can be used to broaden the light absorption as well as designing the visible-light active dyes for co-sensitized solar cells.
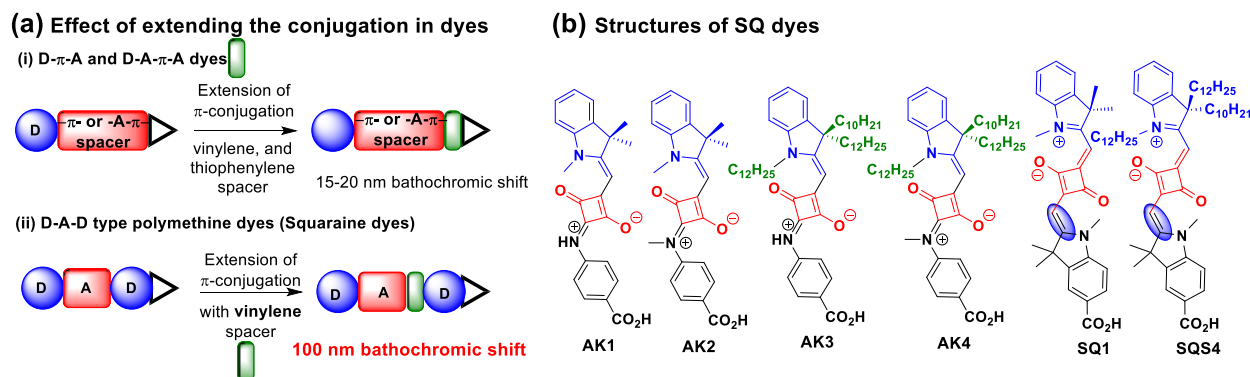
Figure 5. (a) Effect on the absorption spectrum by extension of conjugation for the sensitizers employed in DSSC, (b) structures of visible-light (targeted), and NIR active squaraine dyes.

A series of visible-light active unsymmetrical squaraine dyes (AK) with indoline and arylamine based donors were designed and synthesized. These unsymmetrical squaraine dyes showed intense absorption with high extinction coefficients ~540 nm. It is observed that by introducing alkyl groups at the indoline donor unit as well as N-methylation on arylamine donor unit boost both V_{OC} and J_{SC} of the DSSC devices. N-methylation of arylamine donor unit had profound effect on enhancing both V_{OC} and J_{SC}, whereas introducing alkyl groups at sp^3-C and N-atoms on the indoline unit had significant effect on enhancing only the V_{OC}. Visible dye with branched alkyl groups on indoline and methylation on arylamine unit gave V_{OC} 185 mV and J_{SC} 7.27 mA/cm^2 higher than the without. Device performance of 5.50% (V_{OC} 711.18 mV, J_{SC} 10.09 mA/cm^2, ff 77%) has been observed for AK2 dye in the presence of CDCA. Whereas, AK4 dye showed the device efficiency of 7.93% without CDCA with the V_{OC} of 815.8 mV, and average value is provided in **Figure 6a**. AK4 dye has achieved the maximum V_{OC} 815.8 mV which is highest obtained V_{OC} values in squaraine family. Further, visible-light active AK2 and AK4 dyes have been used to co-sensitized with NIR-light active SQ1 and SQS4 dyes that are optically complementary with each other. Co-sensitization of dyes (with different optical behavior) are the feasible and more efficient technique to gains the panchromatic light response and high photocurrents in DSSC. One of the most frequent approach used to test the DSSC device is

cocktail approach which offers easy fabrication that can control by varying the concentration of dyes, whereas sequential approach offers very high control on the density of the dye loading on the TiO$_2$ surface and that can control by varying the dipping time. AK dyes and indoline based unsymmetrical squaraine dyes SQ1 and SQS4 exhibit complementary absorption profile, cocktail approach has been used to test the device efficiency, and the maximum efficiency achieved 9.36% by the combining the dyes AK4:SQS4 (1:1), and average value is provided in **Figure 6b**.

(a)

(b)
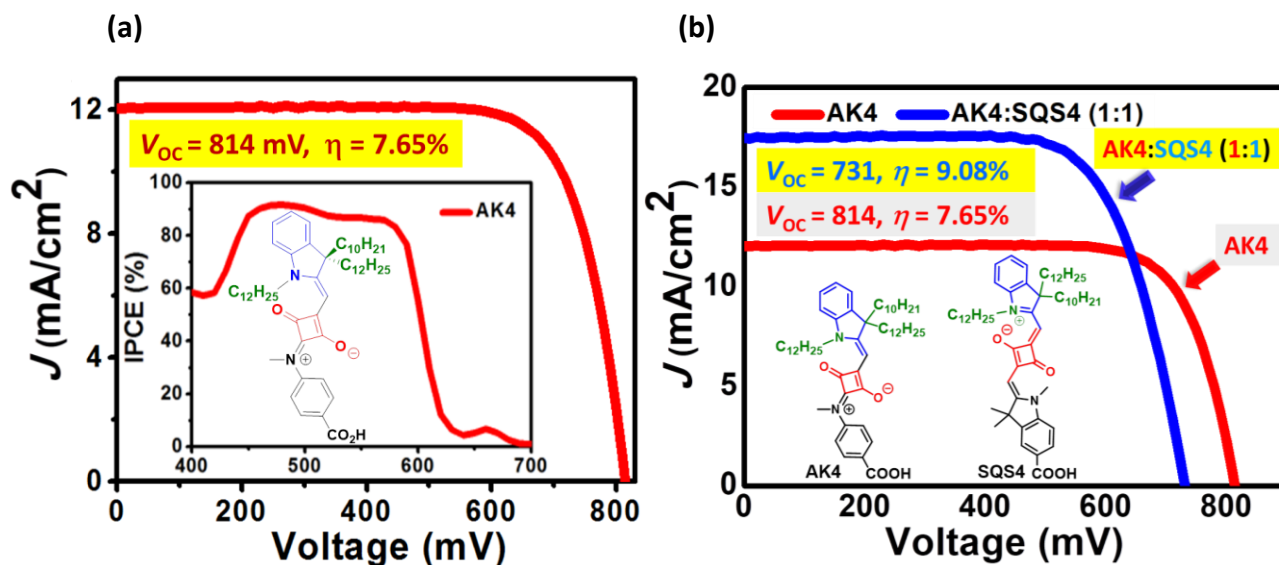
Figure 6. (a) Device performance of AK4 dye, and **(b)** combined device performance of AK4 and co-sensitization of AK4:SQS4 dyes.

Chapter 5: Effect of Various Solvents and Electrolytes (I$^-$/ I$_3^-$, Co(II/ III) and Cu(I/ II)) on the Device Performance of NIR-Light Active Squaraine Dyes

Synergistic enhancements in short-circuit current (J_{SC}), open-circuit voltage (V_{OC}), and fill factor (*ff*) of device determine the overall DSSC performance. Solvents used for the device fabrication plays an important role to achieve better device efficiencies besides the sensitizers, electrolytes, and counter electrodes. Different solvents (different dielectric constant) provides the different conditions for dyes to anchored on the TiO$_2$ surface, as the results different aggregation properties and DSSC efficiencies. In this respect NIR-light active unsymmetrical squaraine dyes SQ1, SQ5 and SQS4 that are different to each other with respect to alkyl group chain length have been used to study the aggregation behavior and its effect on the photovoltaic parameters in

CHCl$_3$ (good solvents on the basis of solubility) and CH$_3$CN (bad solvents on the basis of solubility), respectively. There is no significant change in dye aggregation on the TiO$_2$ surface and efficiencies observed when SQ1 fabricated either in the good or bad solvents, whereas the introduction of alkyl groups cause the narrowing down the IPCE curve and finally more monomeric and less dimeric response observed for SQS4 in good solvents, results efficiency of device deceased drastically. Further, addition of CDCA device fabricated in good solvents results decrease in device efficiency, whereas expected improvements in device efficiencies have been observed for all the dyes fabricated in bad solvents, respectively. SQS4 dye with good (CHCl$_3$) solvents showed more monomeric and less dimeric IPCE responses, whereas with bad (CH$_3$CN) solvents showed IPCE responses from aggregated structures in the absence of CDCA, respectively (**Figure 8a**).The maximum efficiency achieved by device fabricated in good solvents 2.71, 2.59 and 2.56% without CDCA, whereas bad solvents provided the impressive results in efficiency of 3.79, 6.67, and 7.29% with CDCA for SQ1, SQ5, and SQS4 dyes respectively.
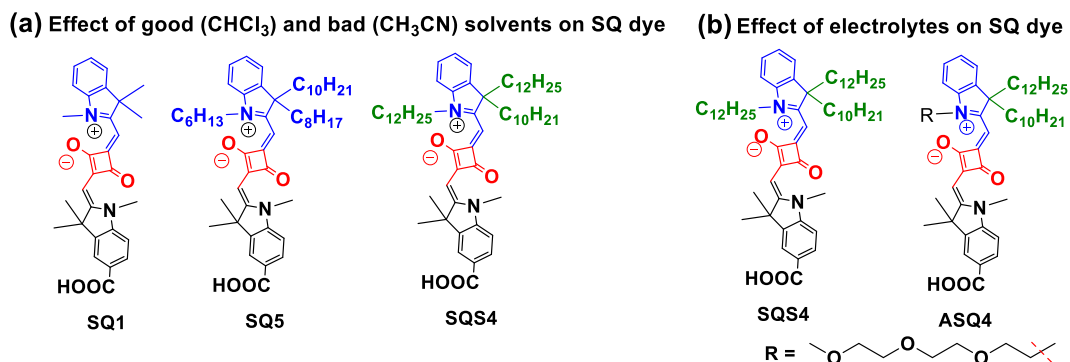
Figure 7. Structures of NIR-light active unsymmetrical squaraine dyes to study the (a) best solvent system, and (b) best electrolytes.

An electrolyte acts as a vital component for dye-regeneration process during the working time of DSSC. Photovoltaic parameters and device stability are largely influenced by the electrolytes used for the DSSC by the interfacial interactions between electrodes and electrolytes. Electrolytes, redox potential is influencing the V_{OC}, redox species transport influences J_{SC}, whereas, conductivity and interfacial resistance between electrodes and electrolyte influencing the ff values of the DSSC. Iodine, cobalt, and copper-based liquid redox-couple are well known in literature for DSSC application. Counter electrodes like platinum foil or platinum nanoparticle

paste deposited on FTO glass plate, carbon-black or nanotubes, graphite, and poly(3,4-ethylenedioxythiophene) (PEDOT) are used in DSSC. In this work NIR-light active SQS4 and ASQ4 (**Figure 7b**) dyes have been used to study the photovoltaic parameters in iodine, cobalt and copper-based electrolytes. Iodine-based electrolyte observed an efficient electrolyte to achieve high power conversion efficiency (7.18%) compare to cobalt (4.05%) and copper (1.08%) based electrolytes for SQS4 dye (where Pt-foil used as a counter electrode), whereas ASQ4 have achieved 5.52%, 3.78%, and 0.71% with iodine, cobalt, and copper-based electrolytes, respectively. The maximum efficiency achieved by SQS4 is 5.92% with cobalt (**Figure 8b**) and 2.01% with copper-based electrolytes which is highest achieved efficiency by the squaraine family, where PEDOT (regenerates Co(III) complex more efficiently than the platinum, and also good for copper-based electrolytes) used as a counter electrode. The low device efficiency of SQS4 and ASQ4 dyes with cobalt-based electrolyte compare to iodine-based electrolyte is because of the less efficient dye regeneration process and fast electron recombination between the electrons in CB of TiO_2 with oxidized redox component Co(III) complex (mass transport), results lowered the J_{SC} values. Low device efficiency of SQS4 and ASQ4 dyes with copper-based electrolytes due to poor dye regeneration process that arise from mismatching of dye HOMO and redox-potential of electrolytes.
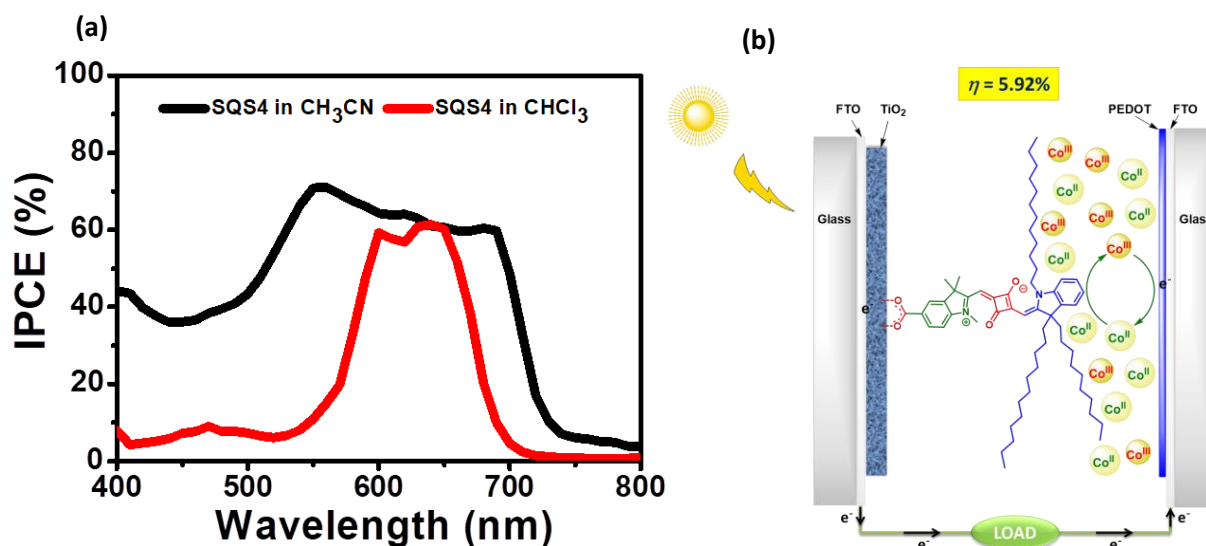
Figure 8. **(a)** Effect of good ($CHCl_3$) and bad (CH_3CN) solvents on the IPCE of SQS4 dye **(b)** device performance of SQS4 dye with cobalt-based electrolytes.

Introduction

1.1 Energy for future

Energy is the fuel of life and indispensable to keep alive the living organisms. Humans are depending on chemical energy that available from the food and energy resources for electricity generation to fulfill their daily requirements. Due to rapid improvement in the world population annually around 83 million, which results the total population will be expected to reach around 8.6 billion by the years of 2030 which will increase the energy requirements, so energy is the big task to be solved. Two types of energy resources are available to generate electricity for the humankind namely non-renewable (finite), and renewable (infinite). Non-renewable sources of energy included fossil (formed from the buried died organisms by decomposition process in the absence of oxygen) and nuclear fuels (**Figure 1**); fossil fuels like oil, coal and natural gases are more frequently used to generate the energies for the various purposes.[1] Around 73.8 % of global electricity have been produced by the non-renewable source of energy at the end of years 2018 (one year) according to the data provided by renewable energy policy network for the 21st century (REN21). The current fossil fuel resources would get consumed within two hundred years and it requires 10 million years to replenish, that means they would not be able to fulfill the future energy demand. Finite resources, consumption within very short time, production of byproduct during burning, which causes environmental damage and global warming[2], are the major drawbacks of the non-renewable sources of energy. Combustion of fossil fuels used either for electricity production or for mechanical energy production are responsible for the emission of hazardous gases (such as CO, CO_2, NO_2, NO_3, NH_3, SO_2) in air, that contaminate the environments and responsible for the acid rain, and by breathing this polluting air human develop severe diseases like lungs cancer, asthma,[3] disease of blood vessels, heart disease, skin disease, stroke,[4] diseases of digestive system, disease of nervous system,[5] vascular disease, and disease of liver. Renewable sources of energies (solar, hydropower, wind, biomass and geothermal energies) are replenished naturally time to time and will reflect our future (**Figure 1**). By keeping the drastic extension in the population growth and energy requirements in mind, only renewable resources are the vital sources to fulfill the energy demands for future without damaging our environment.

1.2 Renewable energy

Energy which is replenishes and restored naturally by renewable resources known as renewable energy. On the basis of report obtained from REN21, 18.1% of renewable energy contributed for electricity generation in 2017 whereas, electricity generation at the end of 2018 from the renewable energy resources was 26.2% (**Figure 2a**) of the total energy generation globally.[6] India situated at the 5th position in the world ranking for the generation of renewable energy (with 78 Gigawatts) from the renewable resources, whereas China on 1st, EU-28 on 2nd and the United States on 3rd positions with electricity generation of 404, 339 and 180 Gigawatts (GW) respectively at the end of year 2018 from renewable resources (**Figure 2b**). The major resources of renewable energy are classified as the hydropower, wind, solar, biomass and geothermal energies.
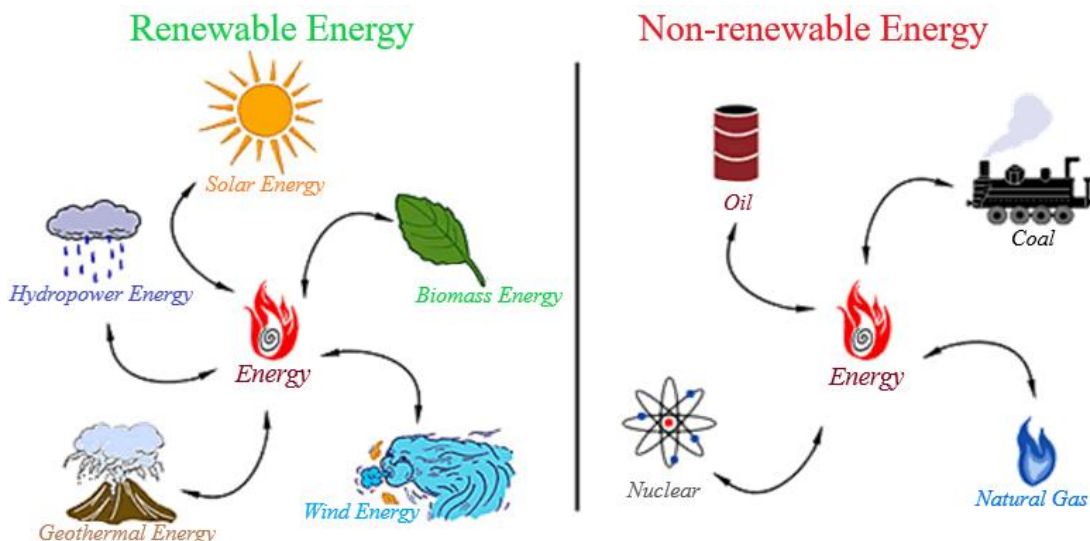
Figure 1. Renewable and non-renewable sources of energy (adapted from "https://weluvmu.wordpress.com/2011/09/11/the-politics-of-renewable-energy/").

Electricity from hydropower is the one of the powerful and leading renewable sources of energy on the basis of global electricity generation in which the electricity is generated by rotation of turbines upon water falling from the top of the dam. Electricity from hydropower without emission of hazardous gases in air, and the generation of electricity can be controlled as per

requirements. Global hydropower electricity contributed 15.8% to the total electricity generation in 2018 (**Figure 2a**). Installed capacity of electricity from hydropower at the end of 2018 with the increments of 20 GW in compare to preceding years have reached to 1132 GW globally.[6] The major disadvantages of the hydropower energy involve the construction of a dam is very expensive and maintenance costs is also high.
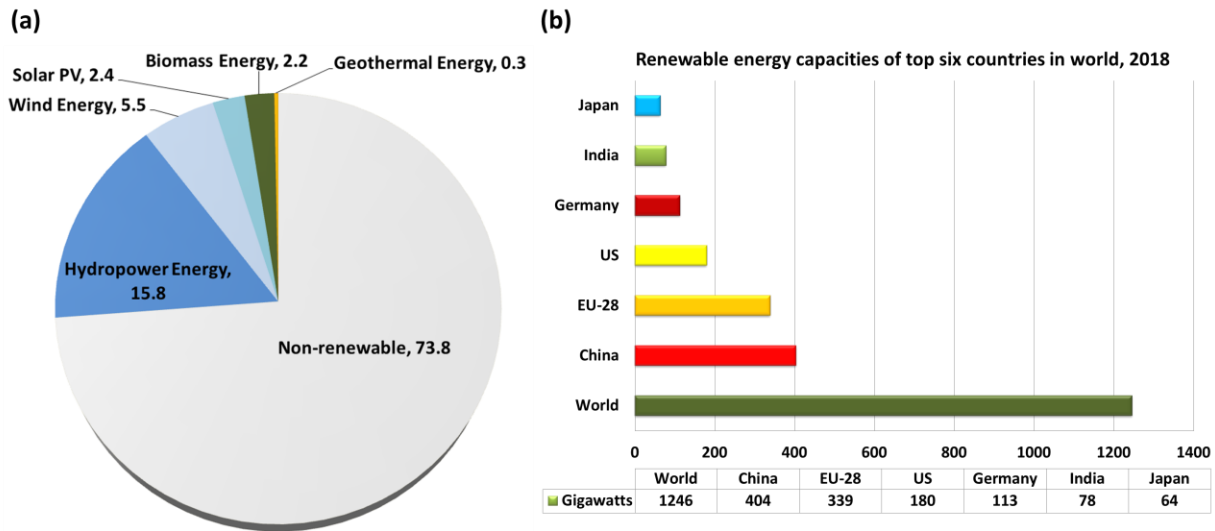
Figure 2. (a) Global electricity generation at the end of year 2018, and (b) world ranking to generate electricity from the renewable resources in 2018 (data adapted from reference no. 6).

Wind power is the second powerful and leading renewable source of energy on the basis of global electricity generation. Wind power also follows the same principle as hydropower electricity generation but only difference is that, wind required for rotation of turbines instead of water. Electricity generation from wind is also an ecofriendly process. Global electricity generated from the wind power reached to 5.5% at the end of year 2018 (**Figure 2a**). Installed capacity of wind power energy is stable with the increments of 51 GW at the end of 2018 in compare to year 2017; total electricity generation from the wind power has reached 591 GW globally.[6] The major disadvantage of the wind power energy is the availability of wind varies with time and place. The generation of electricity from the wind power is most efficient near to the coastal areas due to better continuity of wind, but is very expensive to transport the electricity from source to the cities by electric wires.

Bioenergy is the fourth renewable source of energy and available to use from the biological feedstock as electricity, and heat. Biological feedstock includes biomass (like wood, bagasse, and animal dung), biofuel (like ethanol obtained by the anaerobic decomposition of cane sugar, corn and biodiesel obtained from vegetable-oil and vegetable-fats) and biogas (like bio-methane produces from the vegetable waste). Global electricity generated from the bioenergy was 2.2% at the end of year 2018 (**Figure 2a**). Although, the use of bioenergy is responsible for the emission of CO_2 in air, but emitted CO_2 are used by higher plants during the photosynthetic process according to United Nation and European Union, due to this the bioenergy belongs to the renewable source of energy. Generation of electricity from bioenergy has reached 581 Terawatt annually on the basis of REN21. Bioenergy is very less efficient than the fossil fuels and will take more land density.

Geothermal energy is produces from the earth and the fifth renewable source of energy on the basis of global electricity generation. Global electricity generated from the geothermal and ocean energy was 0.3% at the end of year 2018 (**Figure 2a**). Due to the very high internal temperature of earth stream of water starts to come out by well and force to rotate turbines fixed inside of well, and result the electricity gets generated. The major drawbacks of geothermal energy are the expensive drilling cost and associated risk.

The most reliable and environmentally friendly source of energy with high potential to solve the demands of renewable energy for the future is solar energy (harvested by solar photovoltaics). Solar photovoltaic (PV) is the third powerful renewable source of energy on the basis of global electricity generation. Electricity generation from solar PV has no-emission of gases in air and is ecofriendly. Global electricity generated from the solar PV was 2.4% at the end of year 2018 (**Figure 2a**). Installed capacity of solar PV is stable, and the increments of 100 GW at the end of 2018 in compare to year 2017; total electricity generation from the solar PV has reached 505 GW globally.[6] Global generation of electricity from solar PV, China has 1st position and India has 5th position with 45GW and 10.8GW annual additions, respectively. The electricity generation from the hydropower is expensive, whereas wind power and geothermal energy are more efficient and cheaper than the non-renewable resources.[7]

1.3 Solar energy

Sun is the gift of universe to the solar system and only source of solar energy on the planets. Solar energy is the one of the most promising over the other renewable sources of energy. Solar energy has the various intensities of energy abundance (depends on climate, latitude, altitude and weather) around the globe with free of cost, clean and environmental-friendly. Solar energy distribution on earth and top of atmosphere is displayed in **Figure 3**. Sun continuously emits the energy with the intensity of 3.8×10^{14} terawatt (TW) without exhaustion, out of that 1.8×10^{5} TW of energy reaches to the earth.[8] Solar energy receives by earth within one hour has tendency to fulfill the energy demands of whole population for one year. So, the existing focus on research is the conversion of solar energy to the electrical energy and heat more efficiently.
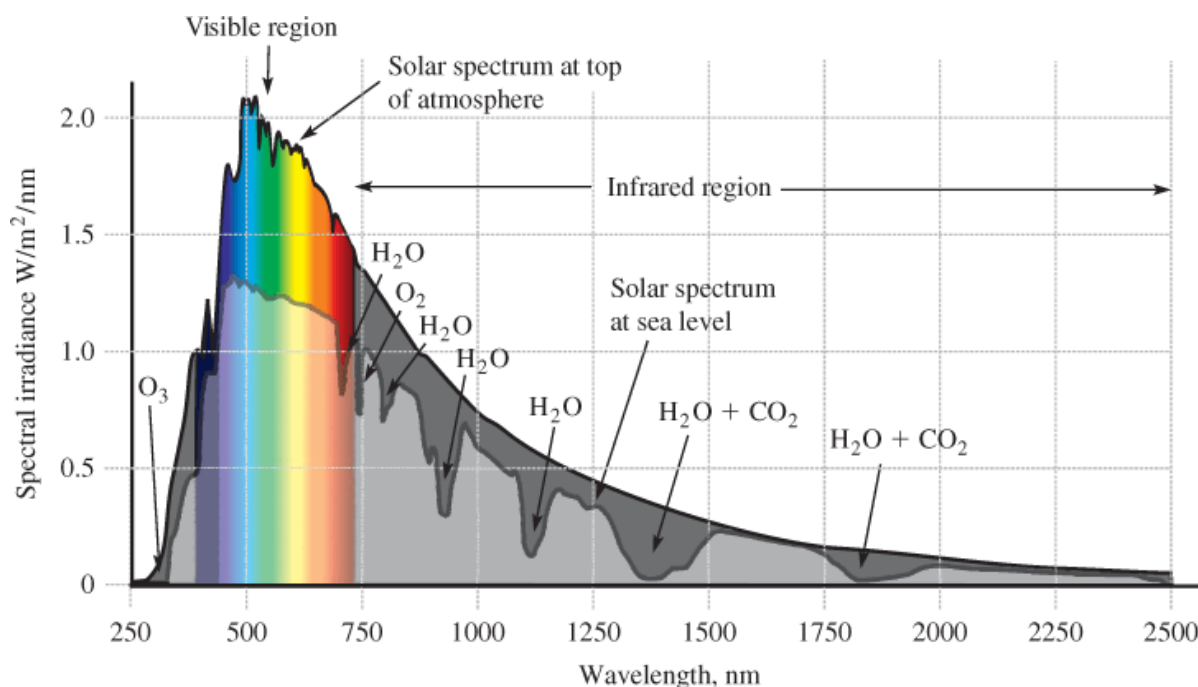
Figure 3. Solar irradiance on earth and top of the atmosphere (adapted from "https://electricala2z.com/wp-content/uploads/2018/03/Solar-Spectrum-at-the-Top-of-the-Atmosphere-and-at-Sea-Level.png").

Photovoltaics cells are very promising device to harvest the solar energy and converts into the electricity.[9] Solar energy density on earth surface observed annually in-between $1.0\text{-}2.5 \times 10^{2}$ W m^{-2} globally and enough to fulfill our needs for energy.[10]

1.4 Photovoltaics

Photovoltaics (PVs) are the semiconducting substrate or cells that generate electricity from solar energy by photovoltaic effect.[11] The term photovoltaic effect and working principle of solar cells given by Becquerel in 1839.[12] First practical report on silicon solar cell came in 1950 by Bell laboratory.[13] The best research solar cell efficiencies graph from 1976 to 2020 given by NREL is provided in **Figure 4**.
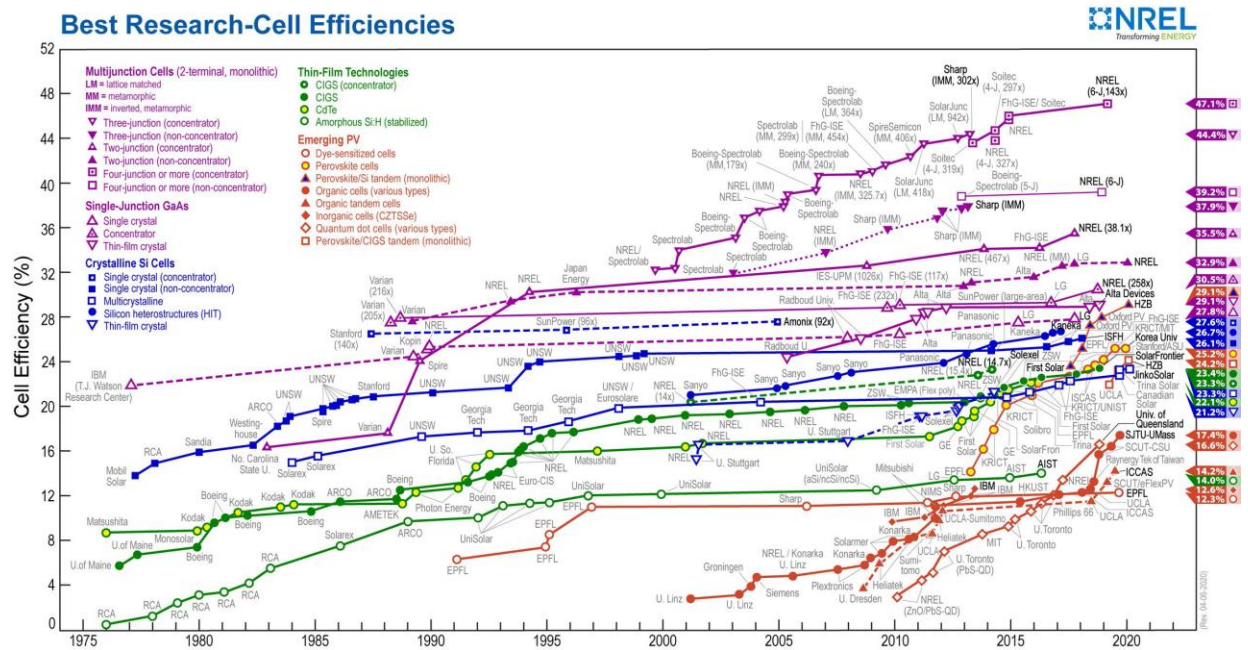
Figure 4. Best solar cell efficiencies in the world (adapted from the "NREL, best research cell efficiencies chart 2020").

Since 1976, various types of solar cells have been designed and tested by researchers, on the basis of materials specificity solar cells are categories into three generations.

1.4.1 First generation solar cells

One of the most widely used wafer-based solar technologies in the world is silicon solar cell which is belongs to the first-generation solar cell technology. Due to high conversion of photon

to electricity, abundance and lifetime, silicon semiconductors are widely used to make wafer-based solar cells. Here, silicon-wafers doped with group 3rd elements for p-type and group 5th elements for n-type semiconductor, when joined together they make a depletion zone called p-n junction. Light absorbed by p-n junction leads the generation of charge carriers namely electrons and holes that are separated from the junction and will be collected at the collector electrodes (p-type and n-type) among of electrons and holes; electrons will reach through the load to the p-type collector electrodes and recombine with holes (**Figure 5**). In the first-generation solar technology thickness of the silicon-wafer varies from 150 to 250 μm in most of the cases. On the basis of crystallinity-nature of silicon solar cells are of two types; single and multi-crystalline silicon solar cells. Efficiency wise single-crystalline silicon solar cell (24%) dominant over the multi-crystalline (19.5%) due to crystal-defects. According to the Schokley-Quessier efficiency limits on the basis of band gap of silicon (1.1 eV), the maximum efficiency achievable by a silicon solar cell will be 33.7% with air mass coefficient of 1.5.[14] Though the cost of Si-cells is still high but after several modifications the performance have reached to 47.1% with AM zero G (used in space). High fabrication cost of silicon solar cells suppressed the Scientist's attention toward the design of solar cells with low-fabrication cost. So, the second generation of solar cells came to the picture due to the thin-film solar cell to reduce the cost and substitute the first-generation solar cells.
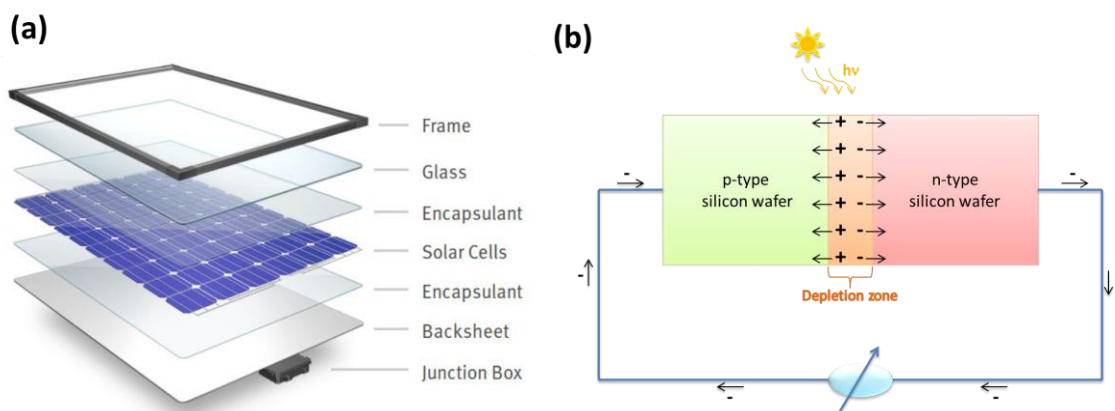
Figure 5. (a) Components of silicon solar cell (adapted from "https://ohagu.xyz/photovoltaic-panels-what-they-are-how-they-are-made"), (**b**) working principle of silicon solar cell.

1.4.2 Second generation solar cells

Second generation photovoltaic associated with the thin film solar cell technology, and designed to cost efficient. In the second generation technology thickness of the active material varies from 2 to 10 μm on polymer sheets or glass substrate, which helped in reducing the cost. This solar technology involves thin film of silicon (amorphous silicon) [15–16], non-silicon like CdTe,[17-20] GaAs,[21-23] and CIGS[24-27] with the various band gaps 1.7-1.0 eV[28] for better open circuit photo-voltage. The maximum efficiency achieved by amorphous silicon, CdTe and CIGS solar cells are 14, 22.1, and 23.4%, respectively among the thin film solar technology. However, second generation solar cell appended with the low cost but photovoltaic efficiency was low compare to wafer based crystalline silicon solar cells. Major drawbacks of the thin film technology involves abundance of indium, CdTe are highly toxic in nature and also arduous to dispose.[29] Efficiency of crystalline silicon, non-crystalline silicon and non-silicon solar cells are poor with the diffused light and also depend on the latitude. To overcome the first and second generations solar cells problems with diffused light and rotation of solar panel correspond to latitude of earth, third generation of solar cells have been developed.

1.4.3 Third generation solar cells

Third generation photovoltaic associated with emerging photovoltaic and charged by cheap semiconducting nanomaterial.[30] Photovoltaic belongs to this technology have light device weight with the tunable band-gap, HOMO-LUMO energy levels, various organic, non-organic and polymeric materials to broaden the spectrum and harvest the solar light. Now the focus of research to understand the interfacial charge transfer, charge injection, and charge collection efficiencies to enhance the solar cell efficiency. In the third generation technology thickness of nanomaterial varies from 2 to 10 μm, that mean we can make it flexible by coating it on the polymer sheets or glass substrate for low cost of the solar cells and probability to make stretchable device. The main and most prominent feature of emerging photovoltaic is the better device performance in the diffused light condition which was major drawback of first and second generation solar cells. Emerging photovoltaic further classified into four major categories.

1.4.3.1 Organic solar cells

Organic photovoltaic consist the small organic or polymeric semiconducting molecules with the behavior of n-type and p-type. In this technology polymer acts as a donor or p-type and fullerene acts as an acceptor or n-type.[31-34] Shining of light on the device leads to form a singlet excitons which is diffused on the interface of donor/ acceptor and separated as electrons/ holes. The electrons and holes are moving toward the respective electrodes and results generation of electric currents in the solar cells. Here, the donor and acceptor units have the bis-continuous networks, and behave as electron donor (hole-transporter), and electron acceptor (electron transporter). Organic solar cells have reached maximum device efficiency of 17.4%.

1.4.3.2 Quantum dot solar cells

Quantum dot (QD) photovoltaic are promising because of their low cost, better optoelectronic behavior with high rate of photon harvesting.[35-37] Variation in size of QDs offers the band gap tunability, which are capable to harvest solar energy from various ranges of solar energy spectrum. QDs of antimony and arsenic with oxidation state three are very important to cover the wide range of solar spectrum. Quantum dot acts as a sensitizer, sunshine on the device leads to excite the quantum dot and injection of one electron from conduction band of QDs to the conduction band of TiO_2 takes place. The electrolyte regenerates the hole created in the valance band of QDs and electron collected at the counter electrode regenerates the oxidized electrolytes. Quantum dot solar cells have reached maximum device efficiency of 16.6%.

1.4.3.3 Perovskite solar cells

Perovskite solar cells are highly efficient, cheaper, easier to make, and became attractive after their discovery in solar cell applications since 2013.[38-44] The active material of this solar cell is $CH_3NH_3PbI_3$ which has 3-D structure and behaves as light harvester and charge carriers. Active material band-gap can be tuned by substituting the iodide with other halides. Perovskite solar cells have reached maximum device efficiency of 25.2%, whereas perovskite/silicon tandem solar cells have achieved maximum device efficiency of 29.1%. Though, the efficiency of

perovskite solar cell is very high, but instability and chemical hazard associated with Pb based perovskites obscure their practical applications.

1.4.3.4 Dye sensitized solar cells

Among the third generation solar cells, dye sensitized solar cells (DSSCs) are the only one known solar cell which can be fabricated outside from glove-box. A widespread attention to the DSSC has been received since 1991 due to low fabrication costs and modular spectral features.[45-48] Dye cells have a lot of option to tune the band-gaps by using various dyes that can absorb in visible and NIR-regions. Recently, metal-free ZL003 have reached maximum 13.6% of DSSCs efficiency.

1.5 Dye sensitized solar cells or dye cells

DSSCs also known as dye solar cells (DSCs) or dye cells. On several modulations in the structures of dyes, till now efficiency has reached to 11.7% for ruthenium-based dyes,[49] 13% for porphyrin based dyes[50] and 13.6% for metal-free organic dyes.[51] However, dye cells have moderate device efficiency but due to lack of durability and low short circuit currents, these are not commercialized.

1.5.1 General working principle of dye cells

Working-principle of dye cells is provided in **Figure 6**. Sunshine on dye cells leads dye excitation (A) and injection of one electron from LUMO of the dye to the conduction band (CB) of TiO_2 takes place (B) (with the rate of 10^{-12} s, at the dye/TiO_2 interface), electrolyte regenerate the oxidized dye (C) (10^{-6} to 10^{-7} s, at the TiO_2/dye/electrolyte interface), injected electron will reach through the load to the counter-electrode (10^{-3} to 10^{-4} s) and electron collected at the counter electrode regenerates the oxidized electrolyte (D) (10^{-5} s, at the counter electrode/ electrolyte interface). Feasible charge injection, dye regeneration and electrolyte regeneration are necessary to complete the circuit. Though the rate of charge injection and dye regeneration are very fast still there is possibility of interfacial charge recombination (E and F), self-quenching of excited dye with non-excited dye molecule and decay of excited state dye (G) are directly

detriment the dye cells efficiency. Charge recombination at interface of dye/TiO$_2$/electrolyte happens with the rate of 10^{-2} to 10^{-4} s, and arises due to slow charge transport rate and direct contact of TiO$_2$ surface with oxidized electrolytes.[52] Self-hopping of excited dye with non-excited dye arises due to close packing of the dyes. The excited dye will stay up to 10^{-9} s, after that it will come back to ground state by losing the energy.

A Excitation of dye,

B Electron injection to the CB of TiO$_2$,

C Dye regenerate from electrolyte (I$^-$), and

D Electrolyte regenerate from collected electrons at counter electrode (Pt).

E Charge recombination with the oxidized dye (D$^+$),

F Charge recombination with the oxidized electrolyte (I$_3^-$) and

G Decay of the excited state dye (D*).
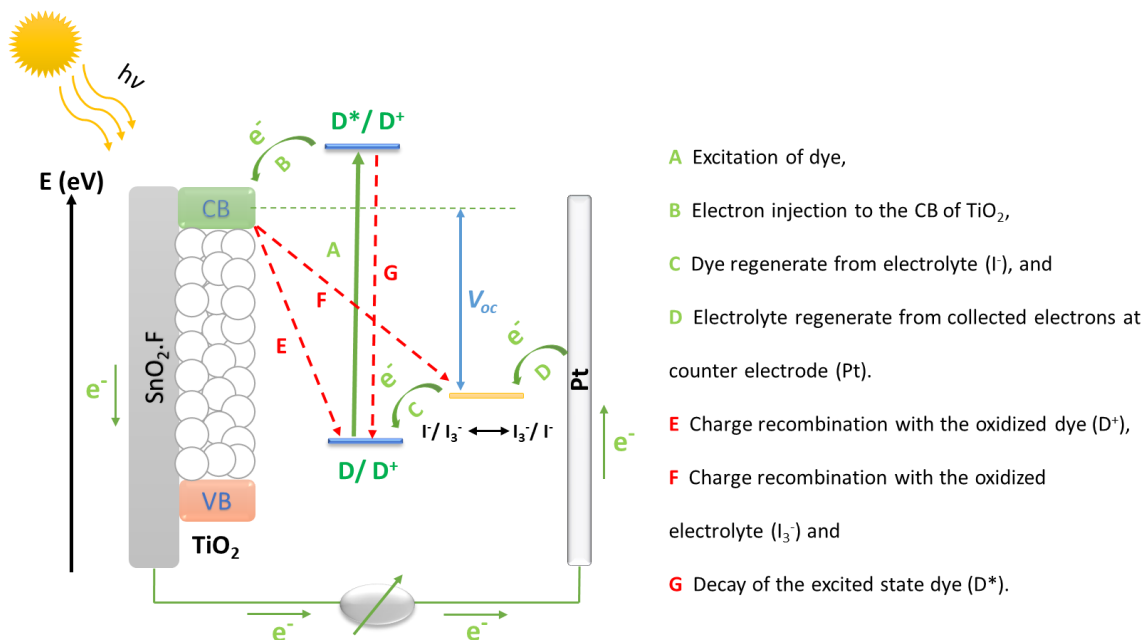
Figure 6. General working principle of dye sensitized solar cells (DSSCs).

1.5.2 Components of dye cells

There are four major components of dye cells; dye, electrolyte, photo-anode and counter electrode (**Figure 7**).
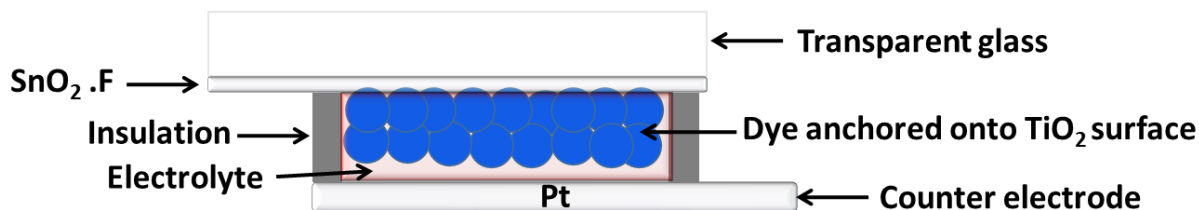
Figure 7. Components of the dye sensitized solar cells (DSSCs).

1.5.2.1 Dyes or sensitizers

Sensitizers are the main components of DSSC which harvest the light from the various regions of the solar energy spectrum and converting into the photocurrents. An ideal sensitizer needs to have an anchoring group to bind on the surface of TiO_2, high molar coefficient, panchromatic light absorption, suitable HOMO/LUMO energy levels respect to the CB of TiO_2 and redox potential of electrolyte with high stability.

1.5.2.2 Electrolyte or redox-mediator

Redox-mediator acts as a vital component for dye-regeneration process during the operation of DSSC. Electrolytes can be tuned on the basis of their redox level and HOMO/LUMO energy levels of sensitizer. Iodine, cobalt and copper-based liquid redox-mediators are well known in literature. Iodine (I^-/I_3^-) based liquid electrolytes in organic solvents[53-56] are most widely used for DSSC since 1991, because of the rapid dye regeneration behavior and offer several advantages such as molecular size of I^-/I_3^- are very small, soluble in variety of solvents, fast diffusion rate, cheap and long term-stability. The main drawbacks in use of iodine-based electrolyte are the dye regeneration needs 500 mV or more over-potential than dye HOMO level, substantial light absorption by iodine-based electrolyte from 400-500 nm if concentrations exceed more than 100 mM, and corrosive. Cobalt based redox mediator with Co(II/III) oxidation states, and tunable redox level by changing the ligands are better alternative to have good V_{OC} (up to 1V), J_{SC} and device efficiency (more than 12%).[50, 57-62] Besides the iodine and cobalt-based electrolytes copper-based electrolytes demonstrated as fast charge transfer redox mediator with the record 11% device efficiency,[63] still iodine and cobalt based redox mediator are frequently used for DSSC due to low cost. Electrolyte with smallest counter cation is preferable to achieve the high power conversion efficiency.[64] Due to high ion conductivity, and high dielectric constants of nitrile-based solvents are preferably used in DSSCs. Though, electrolytes prepared in acetonitrile are the best to achieve high device efficiency, but volatile behavior of nitrile solvents increases the possibility of leakage and evaporation risk. An ideal electrolyte required high diffusion rate, low interfacial recombination, high photo-stability and non-corrosive nature towards the metals.
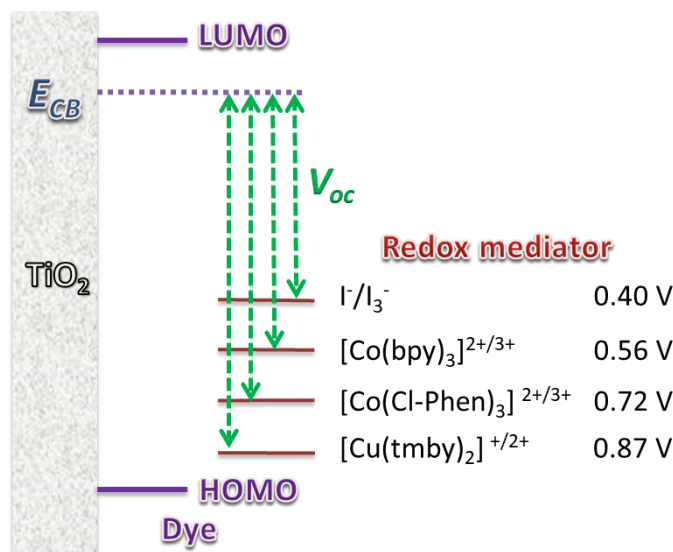
Figure 8. Redox levels of the different electrolytes respect to the conduction band of TiO_2.

1.5.2.3 Photo anode

Photo anode is the substrate where anchoring of sensitizer takes place in DSSC. The constituents required for making of photo anode involves a thin transparent conducting layer of fluorine or indium doped tin-oxide (FTO or ITO) on sterilized glass-substrate. On this glass substrate semiconducting mesoporous-TiO_2 or ZnO coated with thickness from 2-10 μm are well-explored in DSSC.[45,65] Few more metal-oxides like SnO_2 and Nb_2O_3 are tested for dye cell applications but less explored.[66-69] Among the metal-oxides TiO_2 have been well explored and promising because of non-toxic, cheap, stability towards photochemical and electrochemical, high dielectric constant, and wide band gap (~ 3.2 eV) to avoid the absorption in visible region.[70,71] Among the TiO_2 crystal structures (rutile, brookite and anatase), anatase 101 facet with particle size 20-25 nm (for iodine based electrolyte) and 30-60 nm (for cobalt and copper-based electrolytes) are commonly used as active layer, and anatase 101 facet with particle size 150-250 nm are used as reflecting layer in DSSC due to high electron conductivity.[72] Though, anatase 001 facet have only 5- coordinated Ti-atoms (more active sites for dye anchoring) which leads more dye adsorption, but have issues of long term stability.

1.5.2.4 Counter electrode

Counter electrode acts as a cathode in DSSC, where collection of electrons from load and regeneration of electrolyte by electro-catalysis happens simultaneously. Platinum foil or platinum nanoparticle paste deposited on sterilized FTO plate are frequently used as a cathode (electrocatalyst) in DSSC because of low resistance towards the electron conductivity.[73] However, natural abundance of platinum is very less and cost is high, so the significant efforts have been given towards alternatives of platinum from last few years like carbon-black or nanotubes, [74] graphite,[75-77] and poly(3,4-ethylenedioxythiophene) (PEDOT) for DSSC.[73, 78–80]

PEDOT is more efficient towards the electro-catalytic reduction reaction of Co(III) complex, and reduced charge-transfer resistance over the platinum electrode. Electro-polymerization deposition of EDOT on the FTO substrate is very feasible technique to make a thin film of PEDOT.

1.5.3 Parameters of dye cells

There are three parameters are used to characterized the DSSC efficiency and determined from the illuminated *J-V* curve.

1.5.3.1 Short-circuit current

The short-circuit current (J_{SC}) is the cell photocurrent measured at zero voltage. J_{SC} of the DSSC depends on the incident photon-to-current conversion efficiency (IPCE (λ) = LHE $(\lambda).\eta_{inj}.\eta_{coll}$). IPCE of the DSSC depends on the band gap of the dyes, density of the anchored dyes on the TiO$_2$ surface, light-harvesting, charge-injection, dye-regeneration, charge-collection efficiencies and lifetime of injected electrons on TiO$_2$ CB. Band gap of the dye can be control by the conjugation between donor and acceptor moieties. Light-harvesting properties of sensitizers can be modulated by extending the π-conjugation, ability of donor and acceptor moieties, planarity between donor and acceptor moieties that enhance the density of dyes on the surface of TiO$_2$. Co-sensitization is the one another option for broad light absorption and results better LHE and

better photocurrents generation. Charge injection efficiency depends on the energy level difference between LUMO of the dyes and conduction band of TiO_2 and can be modulated by tuning the different acceptor moieties, orientation of the dye respect to TiO_2 surface (whether electron injection occurring through-bond or space, or conducting and non-conducting bonds), aggregations of the dye can be controlled by introduction of the non-polar alkyl groups or favorable ratio of the co-adsorbent addition. Regeneration of the dyes is one of the important processes to complete the circuit and continue the device light harvesting cycle. Dye regeneration depends on the energy difference between HOMO of the dyes and redox-energy level of the respected electrolytes and modulates by using various donor moieties and also depends on the oxidized dye lifetime that controlled by the introduction of the non-polar alkyl groups or auxiliary aromatic rings. Charge collection efficiency can be controlled by introducing the non-polar alkyl groups or auxiliary aromatics wrapped with the donor moiety for better lifetime of electrons injected in the TiO_2 CB. Donor moiety wrapped with non-polar alkyl groups or auxiliary aromatic rings are also play tremendous role in the chemical thermal and photochemical stability of DSSCs.[52]

1.5.3.2 Open-circuit voltage

The open circuit photovoltage (V_{OC}) is the cell voltage measured at zero current or when the photocurrent in the cell will be zero or potential difference between redox potential of electrolytes and Fermi-level of TiO_2 CB. V_{OC} of the dye cell depends on the charge recombination processes and shift in the conduction band of TiO_2 due to interfacial dipole moments. V_{OC} of device can be enhanced by introducing the non-polar alkyl groups in the dyes by restricting the charge recombination between injected electrons in TiO_2 and oxidized dye (to enhance J_{SC}) or oxidized electrolytes (to enhance V_{OC}) also enhances the lifetime of injected electrons (additional improvement in J_{SC} and V_{OC}). Conduction band of TiO_2 shift towards negative potential, are necessary to have the better V_{OC} values which can be tuned by the direction of dipole moment of anchored dyes and density of the dyes on the TiO_2 interfaces. Positive dipole of dyes on the TiO_2 interfaces important to improve V_{OC}, and tuning the ability of donor and acceptor moieties of anchored dyes are also better to modulates the V_{OC}.[52] Density of dyes anchored on the TiO_2 surface modulate the interfacial dipole and improve the V_{OC}, more

dye density on TiO_2 surface pull the conduction band of TiO_2 towards the negative potential as the results V_{OC} can improved. Apart from that, the additions of external additive like 4-*tert*-butylpyridine into the electrolytes responsible for negative shift of TiO_2 CB. Turning of various electrolytes is another option to enhance the V_{OC} in DSSCs.[53-63] pH of dipping solution also affects the anchoring properties of dyes on the TiO_2 and responsible for high/ low V_{OC} values.[52]
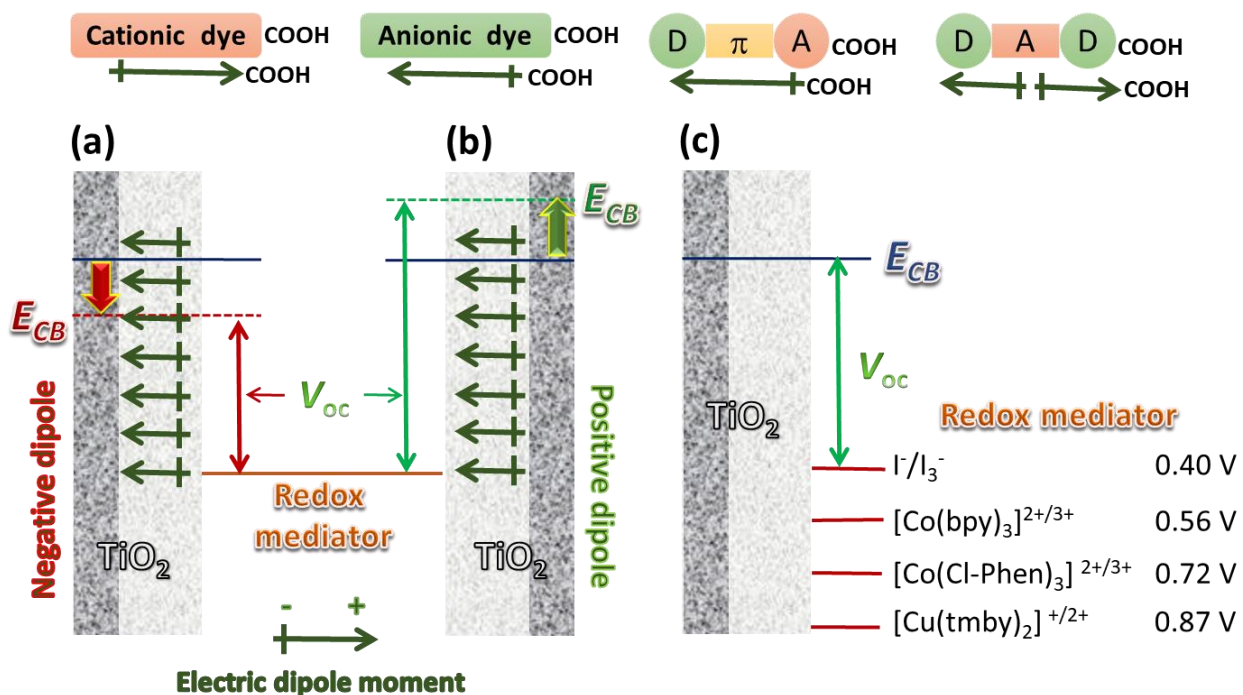
Figure 9. (a) and (b) Effect of interfacial electric dipole moment of dyes on the conduction band of TiO_2, (c) effect of various electrolytes on V_{OC} of the DSSCs.

1.5.3.3 Fill factor

The fill factor (*ff*) is the ratio between the maximum power ($P_{max} = J_{max} \times V_{max}$, **Figure 10a**) deliverable by a solar cell and the product of V_{OC} and J_{SC} (*ff* = P_{max} / $V_{OC} \times J_{SC}$).

Fill factor of the solar cell is very important parameter to know the device quality. Fill factor of solar cell depends on the series and shunt resistance. Series resistance (R_s) is the direct resistance

of current flow and arises from poor contact between the interface of metal/ semiconductor and flow of current from the absorber to the collector. High R_s value reduces the short circuit photocurrent (J_{SC}) and cell efficiency. Shunt resistance (R_{sh}) is the resistance arises during the manufacturing of solar cell. A very low R_{sh} value reduces the open circuit photovoltage (V_{OC}) and cell efficiency. From **Figure 10b**, it is clear that the R_s low and high R_{sh} values are required to get better *ff* values. An ideal solar cell needs to have zero series and infinite shunt resistance values. The series and shunt resistance can be avoided by making better interfacial contacts between metal and semiconductor, and by avoiding the defects arising during the manufacturing time, respectively.

On the basis of above parameters strategy of sensitizers, it is clear that, to have high J_{SC} values, dye-density on the TiO_2 facet and feasible energy level of dyes with respect to the conduction band of TiO_2 are necessary. Whereas, to have the better V_{OC}, suitable redox couple with respect to dyes HOMO and also dye-density on the facet of TiO_2 are necessary. The main component of DSSC is a sensitizer with suitable energy level that facilitates the favorable charge injection and sensitizer regeneration processes. So, the design of a sensitizer which can affords the better device performance with stability, durability is interesting and challenging tasks.
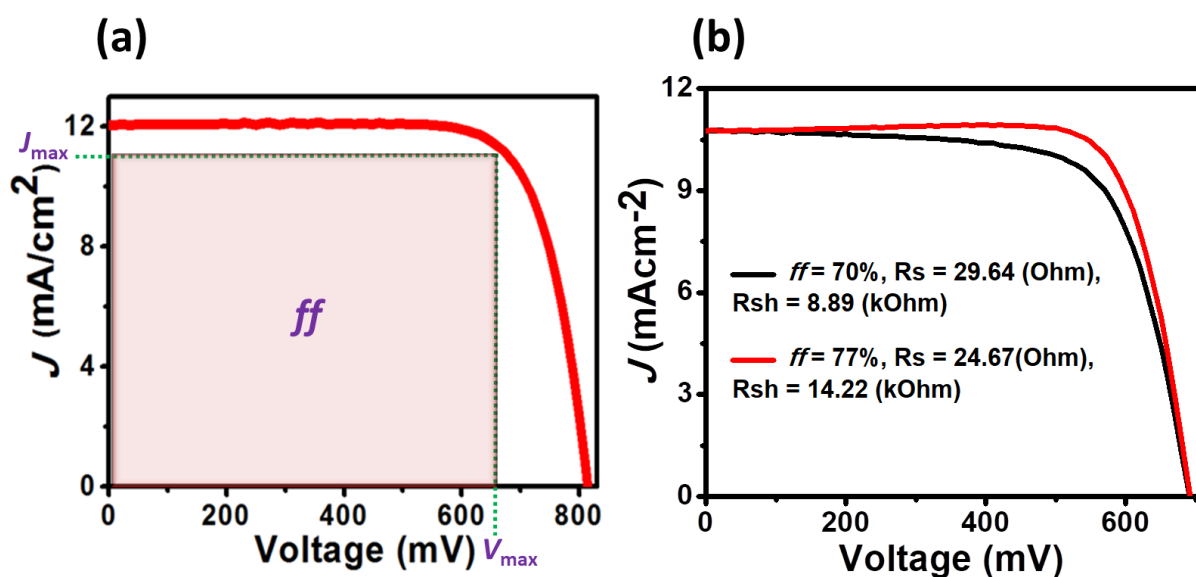
Figure 10. (a) Fill factor (b) effect of series and shunt resistance on the fill factor of DSSCs.

1.6 Dyes or sensitizers

Metallic dyes and metal-free organic dyes are two broad categories of DSSCs well-known in literature. Ruthenium,[81-83] Zinc-porphyrin[84–87] and Zinc-phthalocyanine[88,89] are belongs to the metallic dyes and are able to harvest solar light from visible as well as NIR-regions. Ruthenium dye has tendency to harvest solar light from 400 to 700 nm with the intensity of 80% as the results that achieved 11.5[90] and 11.7%[49] of device efficiency with iodine-based electrolyte. However, porphyrin has low extinction coefficient in NIR-region still by chemical engineering of donors, acceptor, and bulky groups has been reached 13%[50] Though, ruthenium-based dyes are more efficient, stable, long exciton lifetime, still not commercialized, because of ruthenium is expensive rare earth metal, low molar coefficient and hazardous nature. There are few highly efficient ruthenium-based dyes are displayed in **Figure 11** with their efficiencies. Though, lot of porphyrins have design and synthesized by different research groups for dye solar cell applications, where few dyes reached more than 10%,[61,91-94] whereas one dye have reached 13%[50] by engineering in the chemical structures of donor, acceptor with the planarity.

Metallic dyes are expensive to make, low molar coefficient, synthesis and purifications are very tricky, thus search towards the better metal-free organic dye have continued, because of cheap and easy to make, high molar coefficient, modular band-gap with flexible to tune the molecular structures, and eco-friendly. DSSC fabricated with organic dye have been achieved device efficiency 13.6%[51] by modulating the structure of dye molecule till now. Scientists are trying their best to achieve the high DSSC performance since 1991. Metal-free organic dyes constituted with a donor amine (like indoline, triarylamine analog), an acceptor (squaric acid, cyanoacrylic acid acid, benzo(1,2,5)thiadiazole) and an optional π-spacer.[95-103] There are several molecular design are explored such as donor-acceptor (D-A), donor-π-acceptor (D-π-A), donor-acceptor-π-acceptor (D-A-π-A), donor-donor-π-acceptor (D-D-π-A) and donor-acceptor-donor (D-A-D) in literature for DSSC applications.

1. N3, η = 11.03%   **2. N719, η = 11.18%**   **3. Black dye, η = 11.1%**

4. C-101, η = 11.0%   **5. C-106, η = 11.7%**   **6. CYC-B11, η = 11.5%**
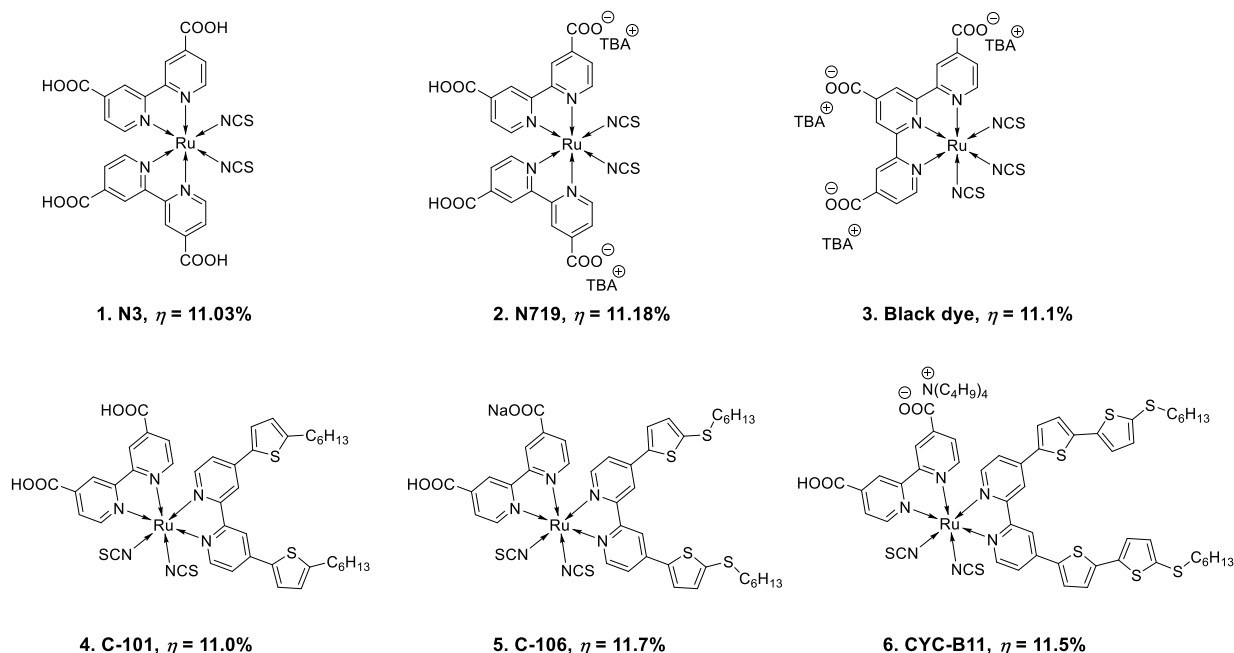
Figure 10. Structures of highly efficient ruthenium-based dyes for DSSCs.

1.6.1 Donor-acceptor dyes

Donor-acceptor (D-A) dyes are one of the most efficient dyes know in the literature, where amine wrapped with fused multi-aryl groups (to have better optical-response) works as a donor unit, benzo(1,2,5)thiadiazole (BTD) coupled with benzoic or hexylthiophenylethynylbenzoic acid works as acceptor unit and alkyl-groups introduced with donor unit to control the dye aggregation onto semiconducting TiO_2 surface. To make dyes planar for the better electronic communication between donor and acceptor units, either introduction of ethynyl group or rigidify by cyclization are preferable. Introduction of N-decylhexyl, ethynyl between D-A units and peripheral introduction of *n*-hexylphenyl groups in the dye **7** responsible for controlled dye aggregation and broad light absorption with 12.5% device efficiency.[48] Further, peripheral introduction of two *n*-octyl groups on the donor side results drop in efficiency by 0.5% for dye **8**.[104] Upon rigidifying the donor unit and peripherally introduction of *n*-hexylphenyl groups from both side (near and away from acceptor unit) leads highest cell efficiency of 13.0% by dye **9**[105] for same class of molecules, these sets of dyes were reported by Yao *et al*. Recently, Zhang *et al*

reported highly efficient metal-free D-A based organic dyes **10** with an efficiency of 13.6%[51] where triazatruxene with ethylhexyl groups on N-atom as donor and BTD as an acceptor units.

7. C275, η = 12.5%   **8. C278, η = 12.0%**   **9. C281, η = 13.0%**   **10. ZL003, η = 13.6%**
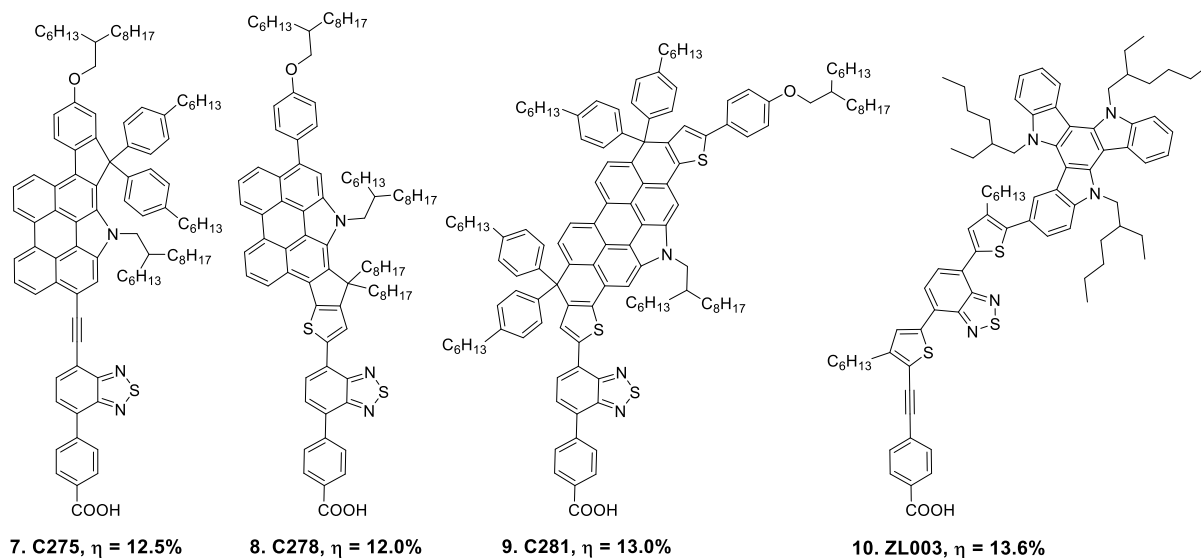
Figure 12. Structures of highly efficient D-A dyes for DSSCs.

1.6.2 Donor-π-acceptor dyes

Donor-π-acceptor (D-π-A) dyes are very promising design in DSSC and facilitate to tune the optical and electrochemical properties by tuning the different donors, acceptors and π-spacer or bridge. Donors like triarylamine analog, phenothiazine etc, acceptors like BTD with and without *n*-alkyl group, cyanoacrylic acid etc, and π-bridges like cyclopentadithiophene (CPDT), tetrathienoacene with *n*-alkyl group, thienobenzothiophene, fused anthracenethiophene with peripherally introduced *n*-hexylphenyl groups and most of the zink-porphyrins etc are commonly used for better spectral response and device efficiency in DSSC. Dye **11** with triphenyamine, tetrathienoacene with alkyl groups, and cyanoacrylic acid as donor, π-spacer, and acceptor units respectively have reached an efficiency of 10.1%,[106] whereas, dye **12** with bulky-triarylamine with alkyl groups as donor and thienobenzothiophene as π-spacer have reached 8.2% device efficiency, and CPDT as π-spacer in dye **13** have achieved 9.5% device efficiency.[107] Metal-free D-π-A based organic dyes **14** have achieved maximum efficiency of 12.6% where diarylamine, fused anthracenethiophene, and BTD used as donor, π-spacer, acceptor units respectively.[108]

11. TPA-TTAR-T-A, η = 10.1%   **12. SGT-121,** η = 8.2%   **13. Y-123,** η = 9.5%   **14. R6,** η = 12.6%

15. SM315, η = 13.0%   **16. SGT-021,** η = 12.0%   **17. GY50,** η = 12.8%   **18. XW28,** η = 10.1%
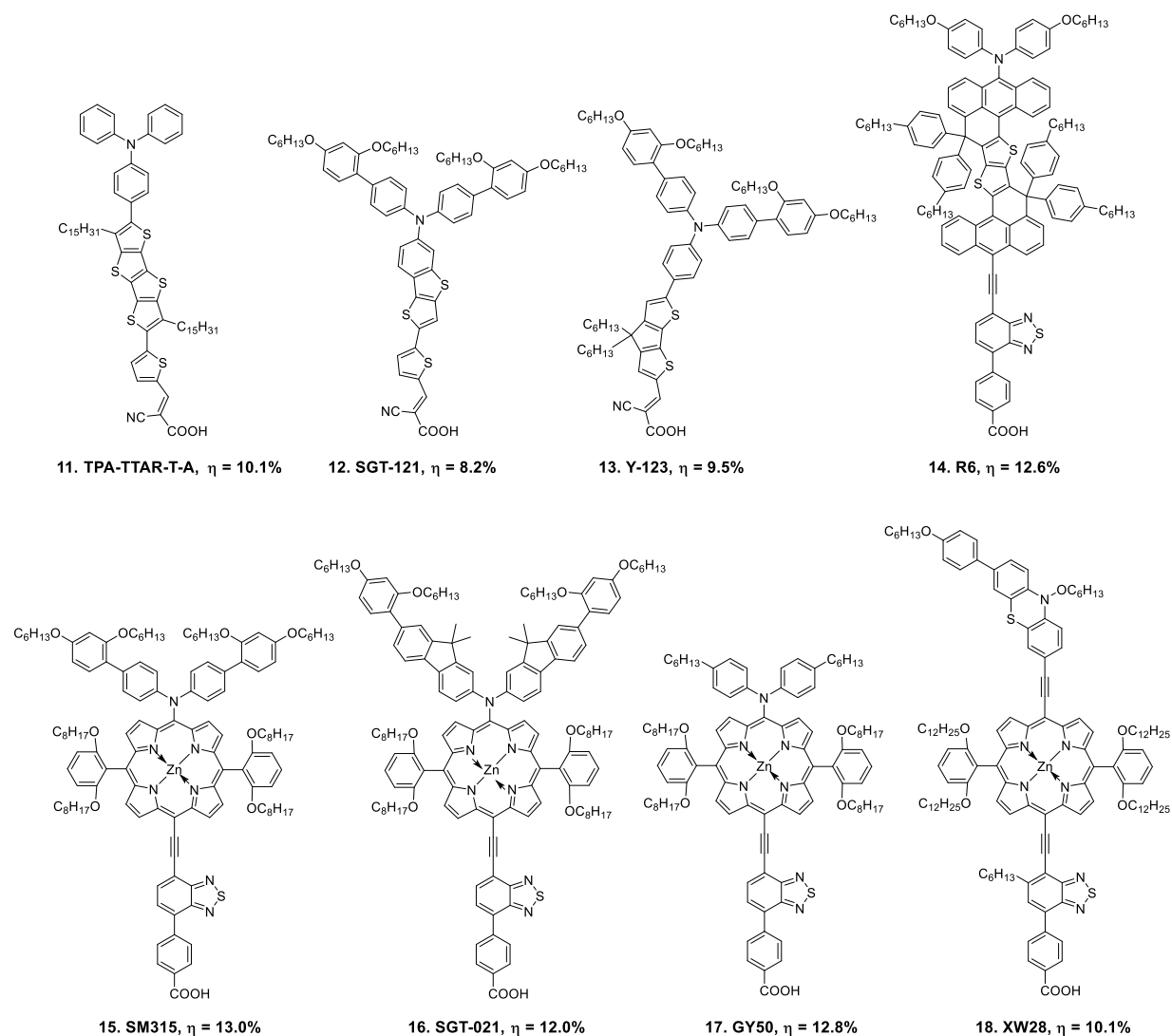
Figure 13. Structures of highly efficient D-π-A dyes for DSSCs.

Most of the highly efficient zinc-porphyrins are belongs to the D-π-A dyes. Porphyrins have Soret band with high absorbance intensity and Q-bands with low absorbance intensity in between 450-500 nm (in visible region) and 500-700 nm (in near-IR region) respectively, [109-111] and different sites are available to modulate the structures, thus are very attractive dyes for DSSCs. Spectral responses of porphyrins attracted the researchers to design and modulate the structures that can afford high dye cell efficiency. Though, several modifications done on the donor and acceptor units, orientation of dye[112,113] on TiO$_2$ surface for high device efficiency, but only few

D-π-A based porphyrin dyes have crossed 10% efficiencies, whereas dye **15** have achieved maximum device efficiency of 13.0%[50], and dye **17**[92] have achieved 12.8% device efficiency.

1.6.3 Donor-acceptor-π-acceptor dyes

In this class of dyes indoline with phenylmethyl on N-atom or triphenylamine with alkyl group as donor, cyanoacrylic acid as an acceptor, branched silolodithiophene, or branched CPDT as π-spacer and diphenylpyridopyrazine with alkyl groups or diphenylthienopyrazine or BTD as an auxiliary acceptor unit. Donor-acceptor-π-acceptor (D-A-π-A) based dyes **19**[114] and **21**[115] have achieved device efficiency of 10 and 10.1% respectively, and are the maximum values achieved by indoline based donor in literature, where cyanoacrylic acid as an acceptor, BTD as an auxiliary acceptor, only difference in π-spacer (branched silolodithiophene for dye **19** and branched CPDT for dye **21**). Substitution of BTD (auxiliary acceptor) in dye **19** with alkylated diphenylpyridopyrazine has achieved device efficiency of 9.4% for dye **20**.[114] Dye **22** with alkylated triphenylamine (donor), phenyl (π-spacer) and diphenylthienopyrazine (auxiliary acceptor) units have achieved the maximum device efficiency of 7.1%.[116] Thus, D-A-π-A based dyes indoline based donors are important to achieve high device efficiency.
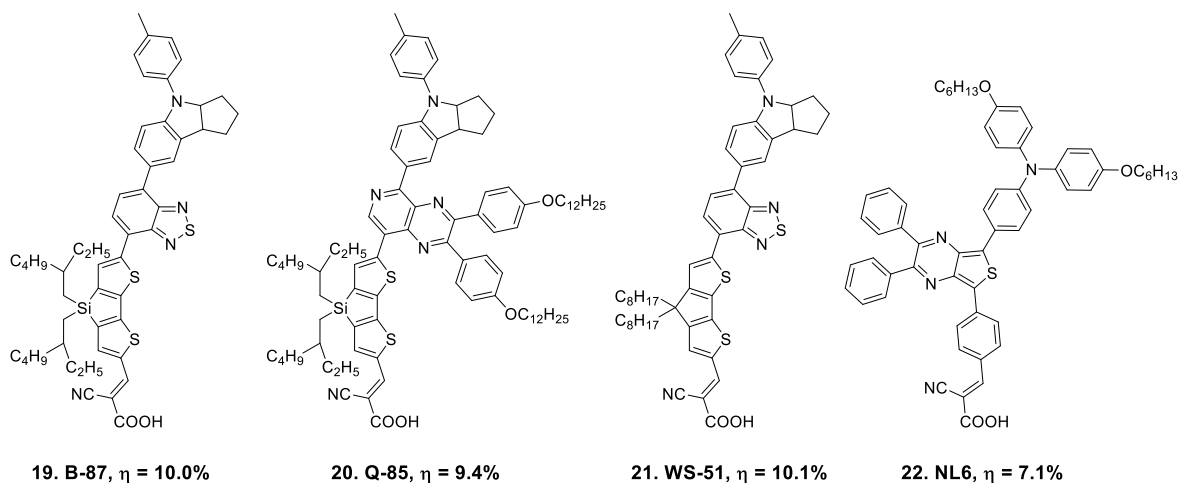
Figure 14. Structures of highly efficient D-A-π-A dyes for DSSCs.

1.6.4 Donor-donor-π-acceptor dyes

More than 15 donor-donor-π-acceptor (D-D-π-A) dyes were design and synthesized, but dyes consist with terminal donors like hexylcarbazole, hexyldithienopyrrole etc, arylamine derivatives as donor, hexyl or phenylhexyldithienopyrrole as π-spacer, cyanoacrylic acid as an acceptor and hexahexylated-dihydrodiindenofluorene as bulky group, are more efficient. Dye **24**[117] with terminal donor hexyldithienopyrrole has achieved 9.0% device efficiency, and dye **23**[118] with hexylcarbazole as terminal donor has achieved 9.5% device efficiency. Further, slight change occurs in efficiency upon introduction of the alkyl group between donor and π-spacer of dye **25**[118] with highest 9.8% efficiency for D-D-π-A dye family.
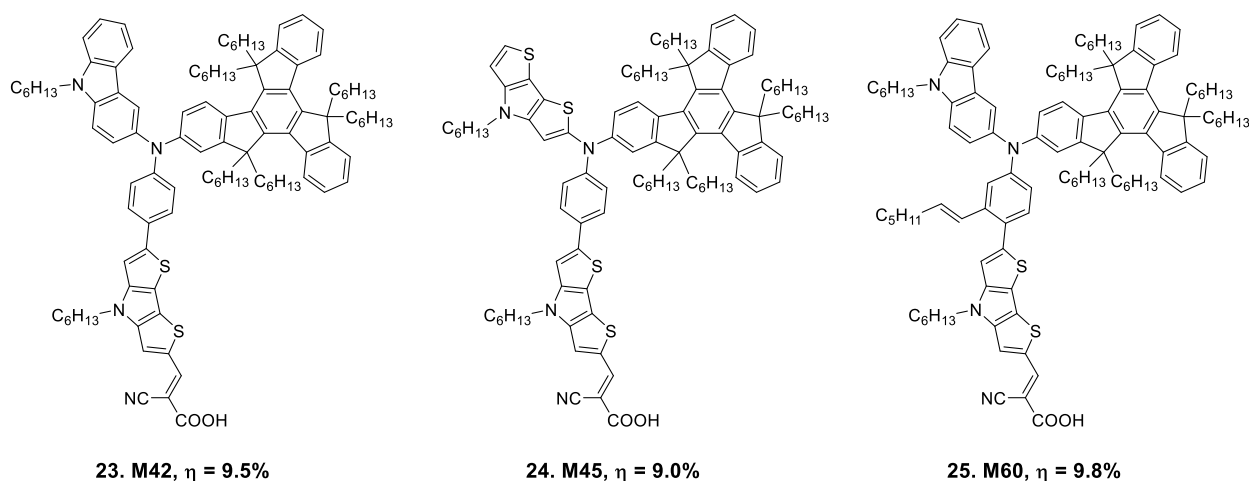
Figure 15. Structures of highly efficient D-D-π-A dyes for the DSSCs.

1.6.5 Donor-acceptor-donor dyes

Squaraine dyes have high extinction coefficient, belongs to the donor-acceptor-donor (D-A-D) dyes and well known NIR-light sensitive with numerous applications in various areas like in sensor, DSSCs, organic solar cells, photodynamic-therapy, protein-labeling and fluorescent-probe.[119-123] Squaraine dyes have achieved the maximum 7.7% of device efficiency without co-absorbent because of self-assemblies behavior in solvents and well packed structures on the TiO_2 facet.

26. η = 2.85% **27.** η = 4.5% **28.** η = 5.4% **29.** η = 0.85% **30.** η = 1.31%

SQ: CDCA (1:10) **CDCA (6 mM)**

31. η = 2.01% **32.** η = 6.53% **33.** η = 7.7% **34.** η = 4.12% **35.** η = 3.38%
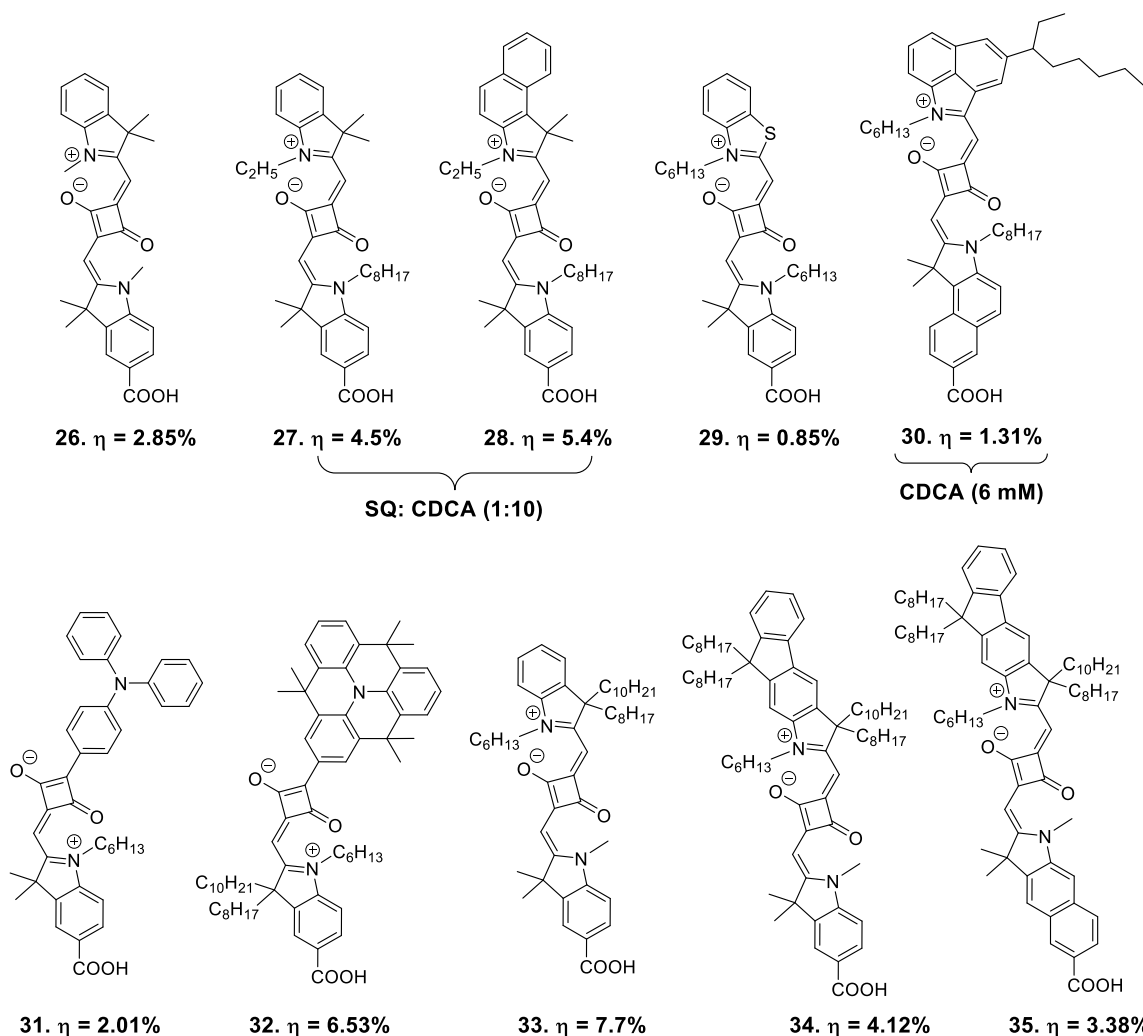
Figure 16. Structures of D-A-D based unsymmetrical squaraine dyes with their efficiency.

Kamat and coworkers have reported squaraine as a sensitizer with low IPCE response in 1993 first time.[124] After that, Zhao and co-workers have reported the symmetrical squaraine dyes that was based on indoline and aniline moieties and achieved 2.16 and 3.4% DSSC efficiencies, respectively.[125, 126] Due to low cell efficiency symmetrical squaraines are not much explored. Yum *et al*. report first indoline based unsymmetrical squaraine dye that achieved 4.5% dye cell efficiency with 10 equivalent of CDCA,[127] further Geiger *et al*. modified the one part of donor by introducing the benzo[e]indoline instead of indoline and achieved 5.4% cell efficiency with 10 equivalent of CDCA.[128] Several modifications have been done on the donor unit of D-A-D based unsymmetrical squaraine such as indoline−Sq−indoline, indoline−Sq−benzo[e]indoline, indoline−Sq−benzothiazoline, benzo[e]indoline−Sq−benzo[cd]indoline, indoline−Sq

−triphenyamine indoline−Sq−heterotriangulene, indoline−Sq−tetrahydroindenoindoline, benzo[f]indoline−Sq−tetrahydroindenoindoline etc, but it is observed that indoline−Sq−indoline (with branched alkyl-groups) based unsymmetrical squaraine dye **33**[101] have achieved 7.7% of cell efficiency, whereas indoline−Sq−heterotriangulene based dye **32**[129] have achieved 6.53% cell efficiency without co-adsorbent by controlling the aggregation of dyes on the TiO$_2$ surface helps to enhance the light harvesting efficiency of the dye with improved photocurrent generation from the self-assembled structures.

Though squaraine dyes are known for D-A-D type, but there are many architecture of squaraine based dyes have designed and synthesized for the solar cells applications, and belongs to D-A-D-A, D-A-D-π-A, D'-D-A-D, D-π-A-D, D-π-A-D-π-A, *cis*-D-A-D, *cis*-D-A-D-π-A, *spiro*-D-A-D-π-A etc. Squaraine dye based on D-A-D-A **43** achieved 5.3% cell efficiency with equal concentration of CDCA.[130] The maximum cell efficiency achieved by D-A-D-π-A squaraine dye **42a** (8.9%) and **42b** (5.0%) with 10 mM of CDCA (where, branched-silolodithiophene used as π-spacer, carboxylic acid and phosphonic acid as an anchoring group respectively),[131] whereas dithienopyrrole, dithienothiophene, thiophene and benzodithiophene based π-spacer, carboxylic acid as anchoring group have achieved cell efficiencies of 5.6, 6.0, and 6.5% for **40a**, **41a**, and **39a** dyes respectively with the 10 mM concentration of CDCA and 6.72% for **38** dye without CDCA.[131,132] Squaraine dye **38** reported by Bisht *et al*. is the highest efficient D-A-D-π-A dye without co-adsorbent.[132] The maximum cell efficiency achieved by D'-D-A-D squaraine dye **45**[133] (3.86%) with 12 mM of CDCA, where triphenylamine as a terminal donor moiety, whereas 2.61% was the highest efficiency achieved by D-π-A-D dye **46**[134] with 30 mM of CDCA. Recently, Vellimalai *et al*. have reported *cis*-D-A-D squaraine dye **50** with double-anchoring groups achieved 5.96%,[135] and *cis*-D-A-D-π-A based dye **52** achieved 4.9%[136] cell efficiencies without CDCA. Sil *et al*. have reported *spiro*-D-A-D-π-A squaraine dye **53** where two D-A-D-π-A units are connected by *spiro*-linker and achieved 2.4% of cell efficiency without CDCA, whereas same D-A-D-π-A **36** dye with 10 mM of CDCA have achieved cell efficiency 3.4%.[137] So, the results obtained from squaraine dyes tells that, the maximum efficiency achieved by dyes based on D-A-D is 7.7%, and D-A-D-π-A is 8.9%, without and with 10 mM of CDCA, respectively.
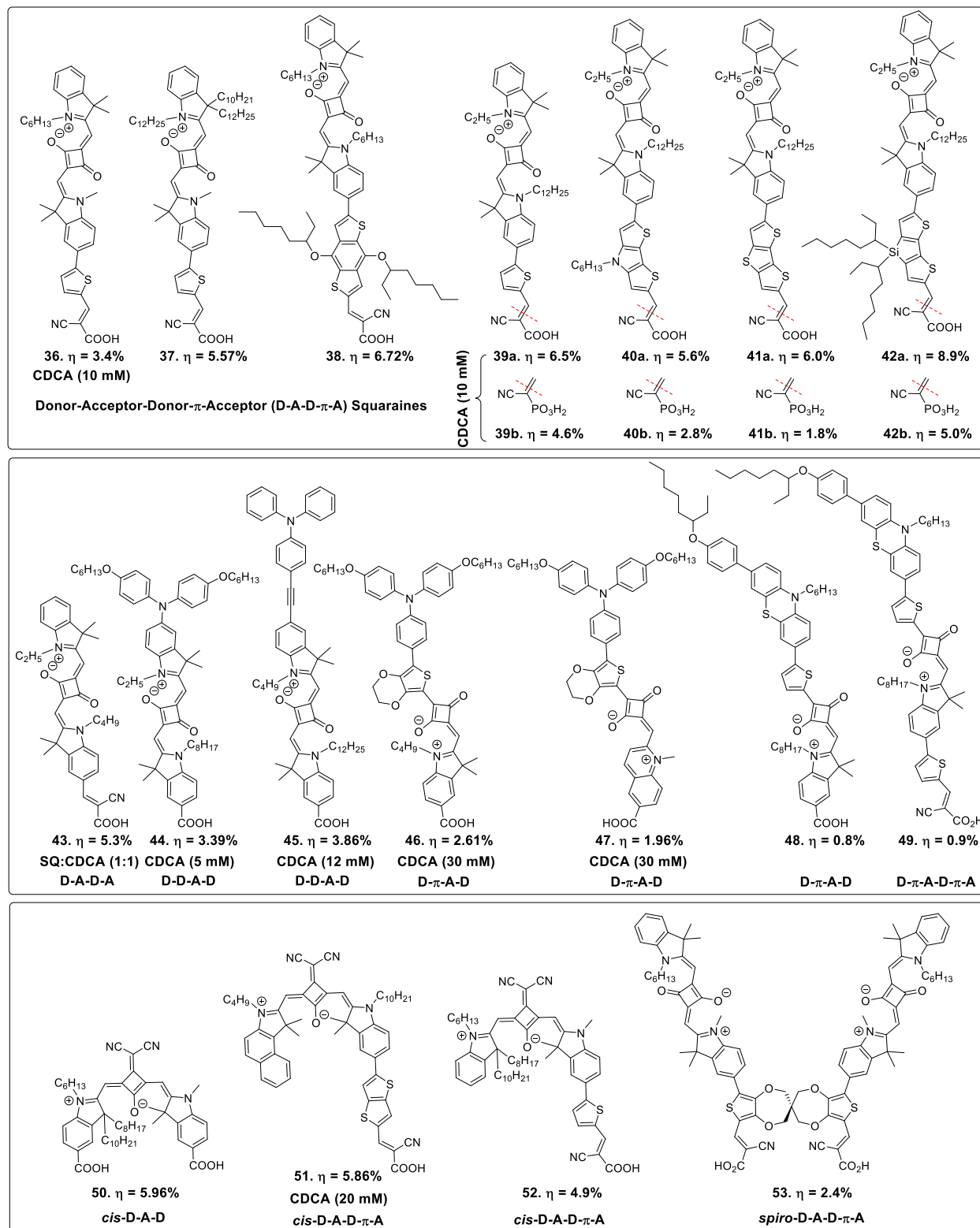
Figure 17. Structures of unsymmetrical squaraine dyes with their efficiency.

1.7 Challenges at dye-TiO₂ interfaces

Charge recombination and dye-aggregation are the two major challenges known that influence the DSSCs performance.

1.7.1 Charge recombination

One of the most challenging factors on the TiO_2/dye/electrolyte that responsible to lower the cell efficiency is the charge recombination. Injected electrons onto E_{CB} of TiO_2 metal-oxide are recombining via inner- and outer-path recombination and responsible for the lowered the J_{SC}, V_{OC}, and device efficiency. Upon electron injection onto E_{CB} of TiO_2 metal-oxide, dye gets oxidized and needs to be regenerate from electrolyte within 10^{-6} to 10^{-7} s, mostly injected electrons onto E_{CB} of TiO_2 metal-oxide are recombining with oxidized dyes and lowers the J_{SC}.[138] Charge recombination through oxidized dyes associated with the molecular design, carboxylic acid unit attached (inbuilt with alkyl chain), [139,140] and orientation of dye respect to TiO_2 metal-oxide (**Figure 18a**). Sometime injected electrons onto E_{CB} of TiO_2 metal-oxide are recombining with oxidized electrolyte and lowered the V_{OC}.[139-141] Charge recombination through oxidized electrolytes associated with the interfacial contact of TiO_2/ electrolyte.
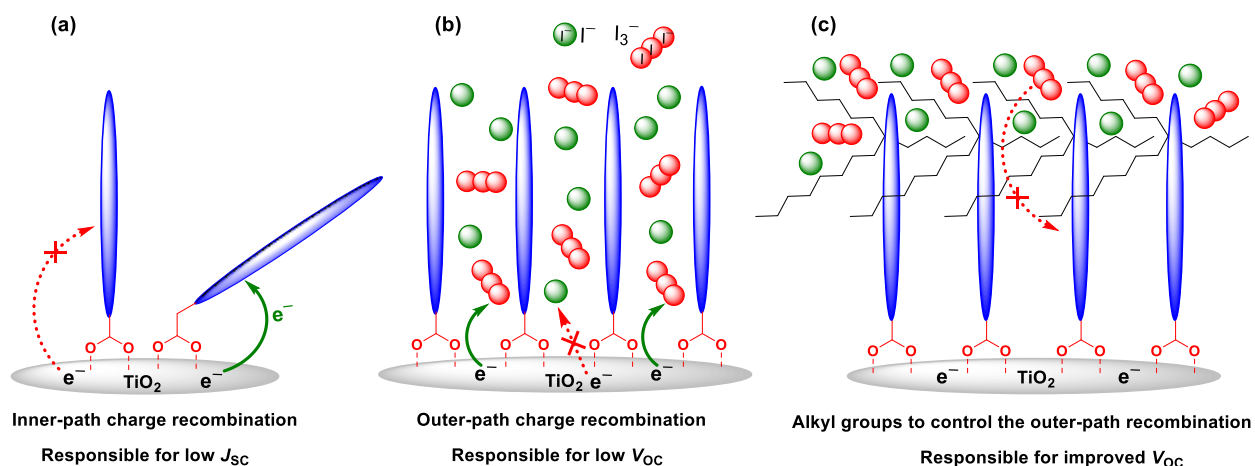
Figure 18. (a) and (b) Inner- and outer-path charge recombination respectively, and (c) controlled outer-path charge recombination by introducing the non-polar alkyl groups.

Donor moiety of dye wrapped with non-polar alkyl groups or auxiliary aromatic rings (because of polar nature of electrolyte) are important to enhance the V_{OC} by avoiding the interfacial contact between TiO$_2$/electrolyte (by surface passivation of TiO$_2$) and also enhance the lifetime of electrons.[101] Charge recombination though inner- and outer-path recombination and its presentations by introducing non-polar alkyl groups are displayed in **Figure 18**.

1.7.2 Dye-aggregation

Second most challenging factors is the interfacial interaction of dye/ TiO$_2$ that responsible to lower the cell efficiency is aggregation of dye, which is results of strong intermolecular attraction between several molecules of dye. Cyanine, merocyanine, porphyrins, perylenes and squaraine are forming the dye-aggregates due to the alignment of intrinsic molecular dipole. Two types of aggregates are well known high and low energetic aggregates corresponds to H- (stacked on top of each other with slip angle 54.7° < θ < 90°) and J-aggregate (in-line with slip angle 0° < θ < 54.7°), respectively (**Figure 19)**. Slip angle θ = 54.7° known as magic angle, where the energy of two states are same and spectroscopically none distinguishable from their monomers.[142] First example of dye aggregation found in the isocyanine (in water) by S. E. Sheppard in 1909,[143] whereas J-aggregate have been observed by Jelley in the cyanine dyes (in water).[144] Charge injection efficiency of dyes are badly affected by dye aggregation onto the TiO$_2$ metal-oxide surface. In general dye-aggregations onto the TiO$_2$ metal-oxide surface kills the cell efficiency by self-quenching of excited with non-excited dye.[145-148] Several strategy have been evolved to avoid the dye aggregation like introduction of bulky substituents,[131] linear alkyl chains and branched alkyl chains, addition of CDCA.[101] Whereas, some dye molecules with aggregated structures gave better cell efficiency, because of the broad-light absorption (improve J_{SC}) by aggregates (H-aggregates) compared to monomers,[149]An efficient charge injection have been observed from aggregated structures (H- and J-aggregates) formed on the TiO$_2$ metal-oxide surface by the chalcogenorhodamine[150] and merocyanine dye series, respectively. Though, aggregation of dyes harms the injection efficiency but it can be controlled by introducing the non-polar moiety like hydrophobic alkyl groups or non-communicable aromatics with alkyl chains into the dye backbone itself. Recently, charge injection efficiency has been tailored by controlled aggregation of dyes through introducing the in-plane, out-of-plane alkyl groups in D-

A-D based unsymmetrical squaraine dye. Donor moiety of dye wrapped with non-polar alkyl groups leads higher aggregates due to strong hydrophobic-hydrophobic attraction, that break further into smaller aggregates upon addition of CDCA and are more efficient than monomers in charge injection.[101] So, by controlling the aggregates onto TiO$_2$ metal-oxide surface we can achieve the high short circuit photocurrents (J_{SC}) (**Figure 19e**).
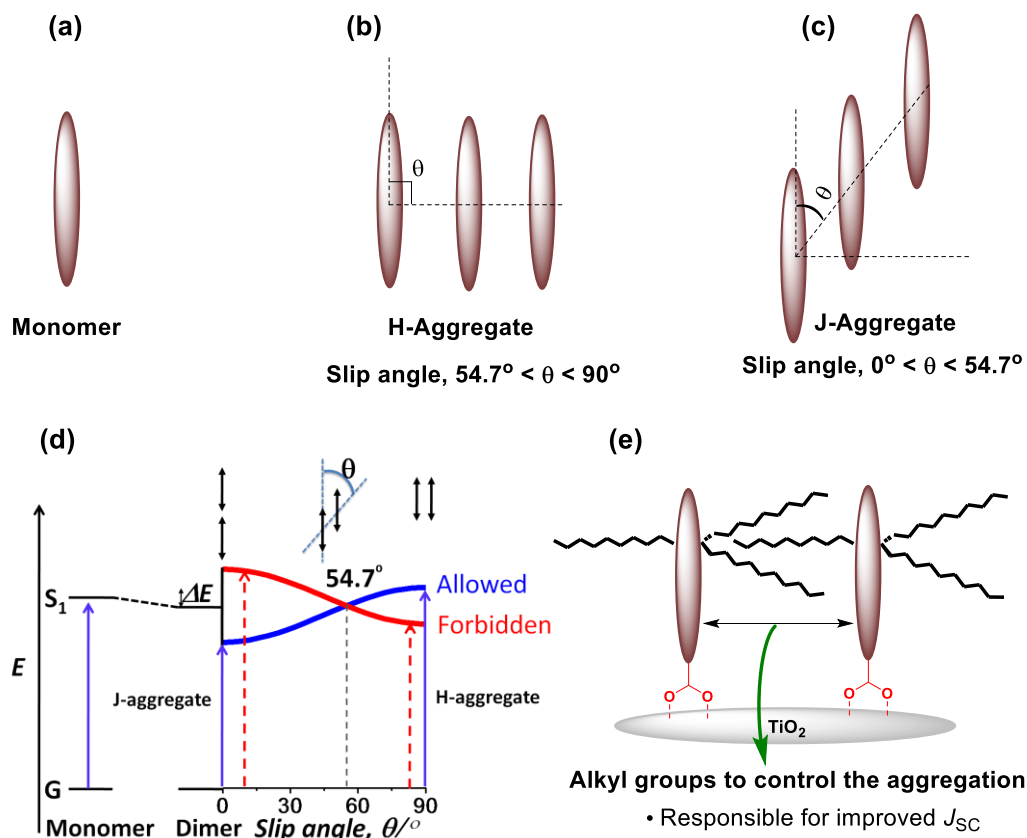
Figure 19. (a), (b) and (c) are representation monomer, H- and J-aggregates, (d) distribution of H- and J-aggregates energy level with slip angle, (e) controlled aggregation by alkyl groups to achieve high J_{SC} value.

1.8 Other factors and strategies to modulate the device efficiency

Involves orientation of dyes on TiO$_2$ surface, dipole moment of dye on the TiO$_2$ conduction band position, and panchromatic light absorption.

1.8.1 Orientation of dyes on TiO$_2$ surface

Dye orientation onto the TiO$_2$ surface playing the detrimental role on the cell efficiency if not favored the injection of electron (through-bond). [151-154] Dye orientation onto the TiO$_2$ surface have been studied firstly on the porphyrin based dyes by substituting the anchoring group on the *ortho*-position, *meta*-position, and *para*-position to know the injection of electrons from dye onto CB of TiO$_2$ happens by through-bond or space and its effects on the device performance.[152-154] Porphyrin dye with anchoring group on *para*-position has more cell efficiency than *ortho*-position, because of probability of charge recombination in *ortho*-substituted dye is much more higher (due to anchoring of dye parallel to surface) than the *para*-substituted dye (due to anchoring of dye vertical to surface) although both positions are conducting nature (**Figure 20a**).[152] Porphyrin dye with anchoring group on *meta*-position (which is non-conducting nature) injecting electron through-space results low cell efficiency than conductive *para*-position (**Figure 20b**).[151-154] Organic dye based on D-D-π-A with anchoring group at *para*-position also has maximum device efficiency than anchoring group at *ortho-* or *meta*-positions.[155] Porphyrin dyes with meso-phenyl group injection of electron takes place though-space because of porphyrin ring and meso-phenyl group are perpendicular to each other and non-electronically communicable, thus such type of dyes electron injection happens though-space with the tilted dye geometry (**Figure 20c**).[112,156,157] Such types of study have not done yet for NIR-active metal free organic dyes in particular D–A–D based squaraine dyes.
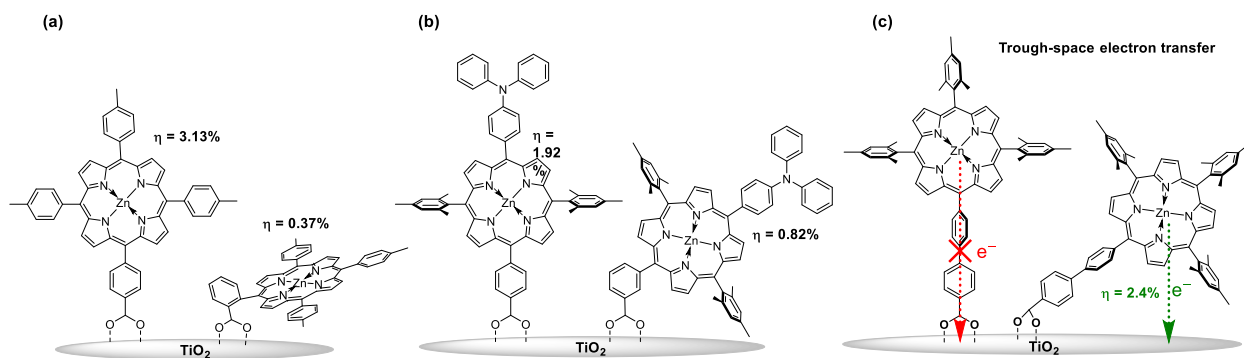
Figure 20. (a) and (b) are porphyrins with different orientation onto TiO$_2$ with their efficiency, (c) schematic representation of through space electron transfer.

1.8.2 Dipole moment of dyes and consequences on the conduction band position of TiO₂

Dipole moment of the dye plays an important role in cell efficiency by affecting the V_{OC} value directly. Changes on the value of V_{OC} due to shifts in the TiO₂ E_{CB} up or down depends on interfacial electric dipole moment of dye. There are two types of interfacial electric dipole moment known, positive dipole (for enhanced V_{OC}), and negative dipole (for reduced V_{OC}). Enhanced V_{OC} values corresponds to positive interfacial dipole moment of dyes respect to the TiO₂ surface and results of the direction of electric dipole moment towards the donor from acceptor (more electron density) unit when dyes are at the excited state.
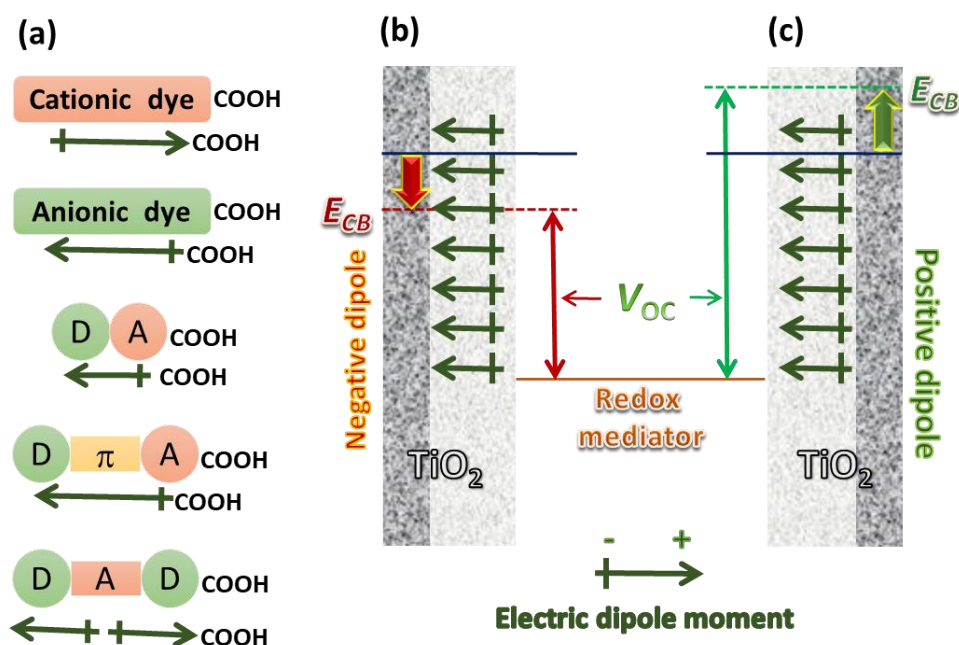
Figure 21. (a) Direction of electric dipole moment of dye on TiO₂ surface, (b) and (c) effects of negative and positive dipole on the device V_{OC}, respectively.

Diminished V_{OC} values corresponds to negative interfacial dipole moment of dyes respect to the TiO₂ surface and results of the direction of electric dipole moment towards the acceptor from donor (more electron density) unit when dyes are at the excited state. D−A,[158] D−π−A and anionic dyes having the characteristics of positive interfacial dipole thus favored high V_{OC} values, whereas cationic dyes having the characteristics of negative interfacial dipole thus favored low V_{OC} values (**Figure 21**).[159] Moderate V_{OC} values in the zwitterionic D−A−D

squaraine dyes observed because of the combination of positive and negative electric dipole moment in single dye molecule at the excited state. So, D−A−D squaraine dyes have average V_{OC} values observed commonly.

Though, dipole moment of sensitizer is playing the tremendous role to enhance the V_{OC} of device, but recently it is found that V_{OC} of device can also enhance by addition of additives to the electrolytes. Such additive attributing the conduction band of TiO_2 shift towards negative potential, and results enhanced V_{OC} values.[160,161,81] Tetra-butylammonium perchlorate (TBP) is commonly used as additive in electrolyte.

1.8.3 Panchromatic light absorption

There are two ways to obtained panchromatic (broad) light absorption in DSSC. First is dye design that contains multi-chromophore, and second is panchromatic light absorption by co-sensitization of dyes are well known in literature.

1.8.3.1 Multi-chromophoric dyes

Multi-chromophore dyes have tendency to harvest light from different regions of solar energy spectrum and converts into electricity. Jradi *et al*. have designed and synthesized a series of inbuilt squaraine and porphyrin (absorption, ~640 nm and 450-500 nm Soret, 500-700 nm Q-band) based dyes, in this design they varied the tert-Butyl and trihexylsilane group on porphyrin unit, thiophene and ethylhexylsilolodithiophene as π-spacer, varied the chain-length of alkyl groups on the indoline moieties. Broad light absorption have observed with IPCE onset ~830 nm to ~850 nm for dyes **54** to **57**, respectively (**Figure 22**).[162] Though, these dye are absorbing multiple spectral regions, due to low J_{SC} value the maximum efficiency achieved by this series of dyes was 7.6% with 10 mM concentration of CDCA which is 1.3% less than the D-A-D-π-A based squaraine dye **42a** (8.9%) with the similar cell conditions. Instead of making dyes with multi-chromophoric units, co-sensitization of dyes with complementary absorption properties are better option to harvest panchromatic light, to achieved high J_{SC} value and cell efficiencies in DSSCs.
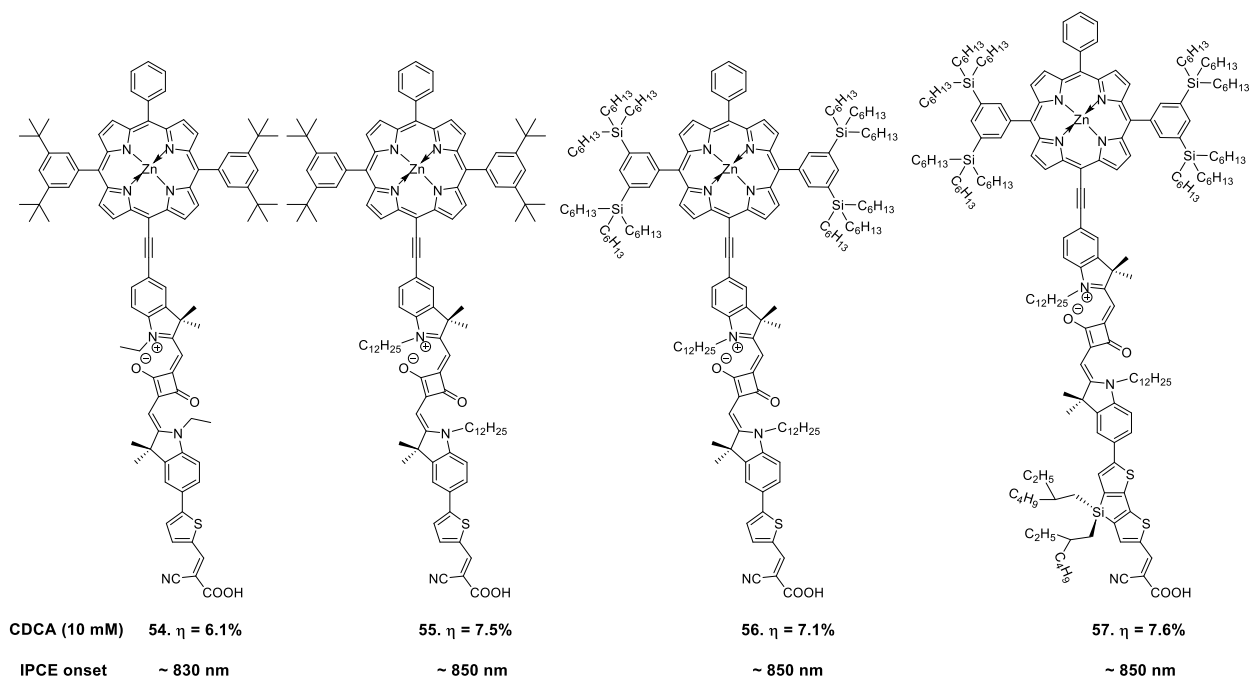
Figure 22. Structures of squaraine-porphyrin dyes with their efficiency.

1.8.3.2 Co-sensitization of dyes

Co-sensitization of dyes (with different optical behavior **Figure 23**) is the feasible and more efficient technique to gains the panchromatic light response and high photocurrents in the DSSC. Two approaches are well known for dye co-sensitization namely cocktail and sequential approaches. One of the most frequent approach for testing the device is cocktail approach which offers easy fabrication and controlled by varying the concentration of dyes, whereas sequential approach offers very high control over the density of dye loading on the TiO_2 surface and controlled by varying the cells dipping time. Structural complementary strategies are used to fill the optical absorption gap of ruthenium and porphyrin-based dyes, even device fabricated through cocktail or sequential approach (**Figure 24**).

Combination of dye **2** (N719) with organic dye **58** have reached 9.7%[163] of device efficiency due to structural complementarily, and bulky dye **3** (N749 or black dye) with small organic dye **59** have reached 11.3%[83] of device efficiency because of vacant space on TiO_2 surface between dye **3** and filled by the dye **59** (cocktail approach with iodine based electrolyte). Whereas, combination of ruthenium-based dye **2** (N719) and zinc-porphyrin dye **63** have reached 8.9%[164]

of device efficiency by following the sequential approach of co-sensitization with iodine-based electrolyte. Zinc-porphyrin dye with metal-free organic dye has reached maximum device efficiency 12.3%[61] by using cocktail co-sensitization approach with cobalt based electrolyte, Combination of two optical complementarily porphyrin dyes which are structurally monomeric **61** and dimeric **62** have reached 10.4%[165] of device efficiency due to shift in the absorption band of **62** compare to **61** (cocktail approach with iodine-based electrolyte). Further, co-sensitizers with extension in the optical absorption toward the NIR-regions have been used for panchromatic light absorption. Porphyrin, phthalocyanine and squaraine are well known NIR-active dyes. Phthalocyanine dye **60** with organic dye **64** has reached maximum 7.7%[166] of device efficiency by following the sequential approach of co-sensitization with iodine-based electrolyte. Combination of dye **2** (N719) and metal-free D-A-D based organic dye **27** (squaraine) have reached device efficiencies 5.2%, 7.5% and 7.9% by following the cocktail, ultrafast sequential and ultrafast cocktail approaches with iodine based electrolyte.[167] Whereas, 9.8%[168] device efficiency achieved by the combination of D-A-D-π-A based squaraine dye **39a** with organic dye **65** which is maximum achieved cell efficiency in literature, where cocktail approach of co-sensitization with iodine based electrolyte have been used.
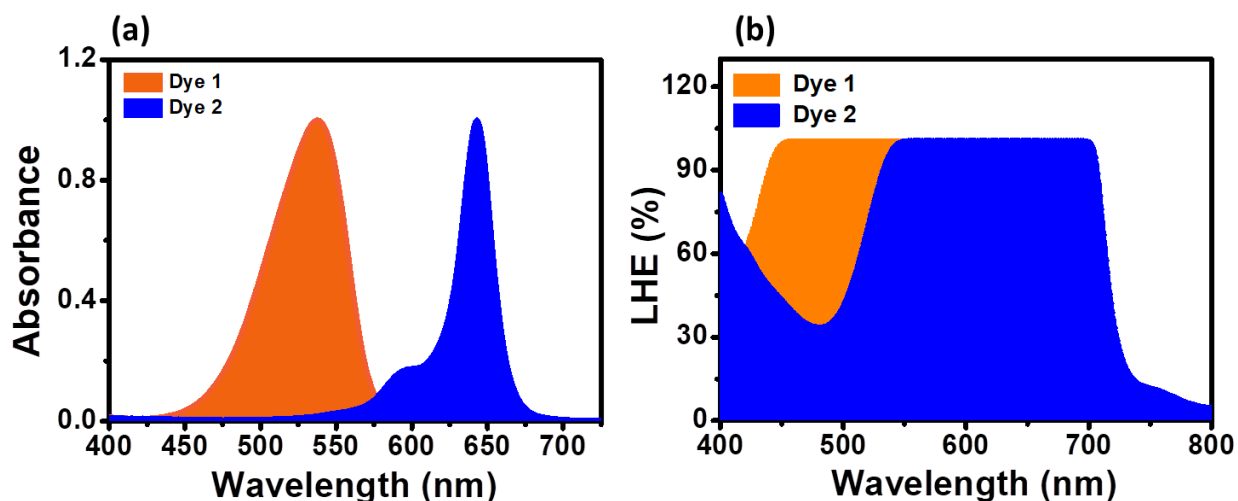
Figure 23. (a) and (b) Normalized absorbance and light harvesting efficiency (LHE) of dye 1 and 2, respectively for co-sensitization.
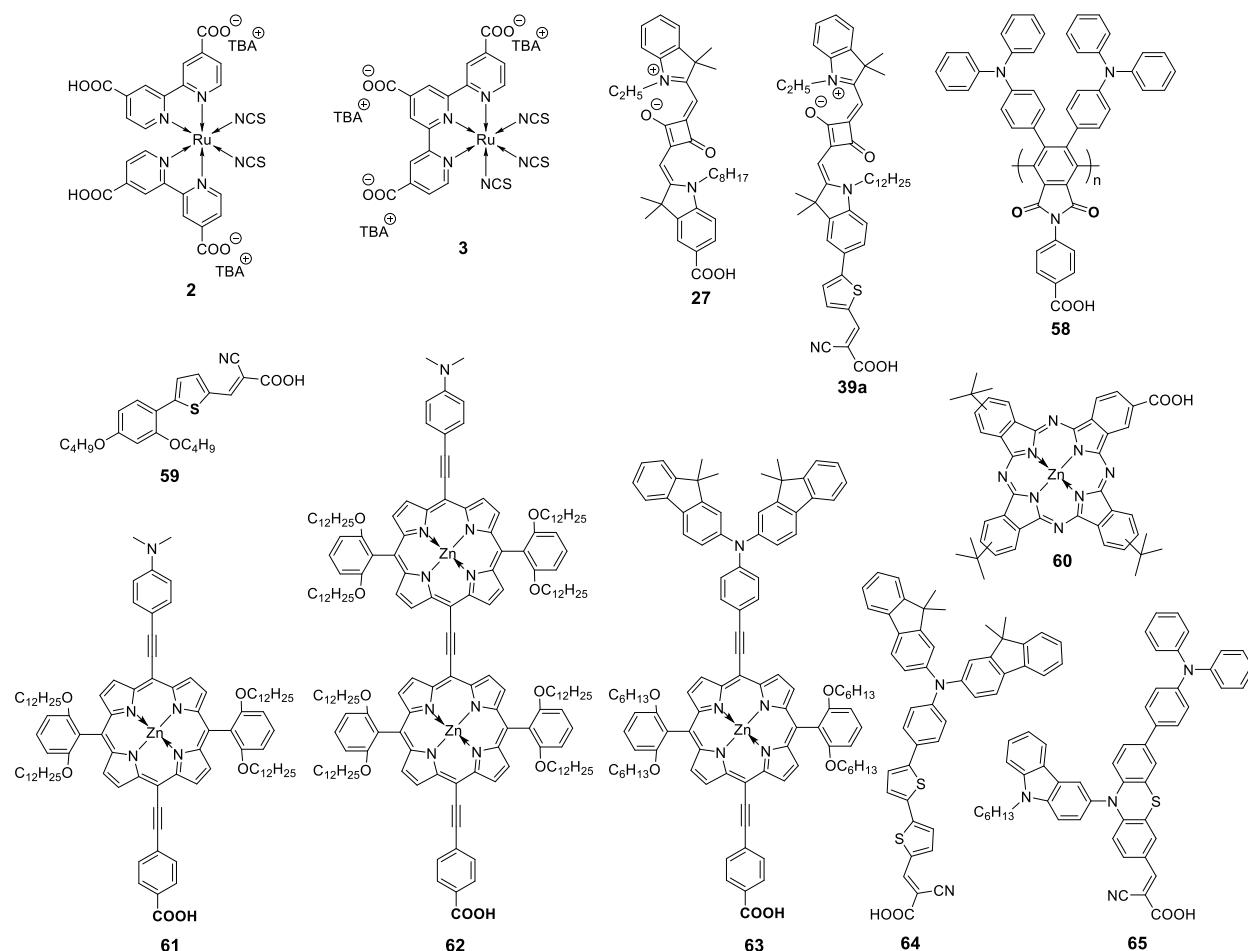
Figure 24. Structures of metallic and metal-free dyes for co-sensitized solar cells.

1.8.4 Strategy towards dye/ sensitizer design

Dye with panchromatic absorption, high extinction coefficient, suitable HOMO-LUMO levels and combination of electrolyte are required for the better cell performance in DSSCs (**Figure 25**). Different donors and π-units have their specific absorption and emission properties and offers to tune suitable energy levels. The main strategy to extend absorption from visible to NIR regions (panchromatic absorption) by the introduction of fused π-spacers to make the planar (to form J- and H-aggregates on the TiO$_2$ facet due to π−π stacking) for better electronic communication between donor and acceptor units (to enhanced J_{SC} value). More dye loading (mostly in D-A dyes) on the TiO$_2$ facet push toward the high V_{OC} and J_{SC} values. Band gap of

dyes can be controlled by introducing the conjugation between donor and acceptor units. HOMO and LUMO energy levels of the dye can be modulated by tuning the strength of donor unit, and acceptor unit. It is also observed that donor moiety of dye wrapped with non-polar alkyl groups are important to enhance the V_{OC} by surface passivation of TiO_2, enhanced J_{SC} by broadening the spectrum and enhanced the lifetime of electrons into the TiO_2 conduction band.
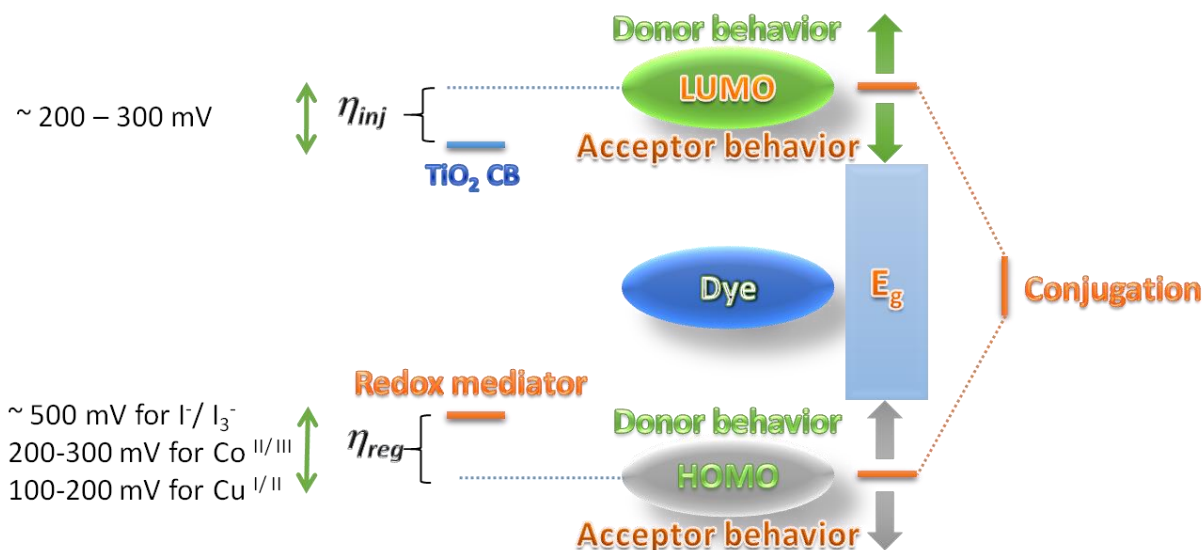
Figure 25. Strategy towards the design of highly efficient dyes for DSSCs.

1.9 Objectives of thesis

Apart from porphyrin and phthalocyanine sensitizers, squaraine dyes are found as a prominent candidate with high extinction coefficient in the far red and NIR regions. The objectives of this thesis are given as (**Figure 26**):

1. Efficient alkyl group chain length for NIR-active unsymmetrical squaraine dyes

❖ To study the aggregation of dye onto the TiO_2 surface

❖ To study the effect of alkyl group chain-length on the V_{OC}, J_{SC}, and cell efficiency

2. Position of anchoring group for better efficiency output in unsymmetrical squaraine dyes

❖ To study the effect of dye orientation on aggregation with respect to TiO_2

❖ To study the effective position of anchoring group for better V_{OC}, J_{SC}, and cell efficiency

3. Visible-light responsive unsymmetrical squaraine dyes for co-sensitized solar cells

❖ To study the aggregation and photovoltaic properties of the dyes

❖ To study the co-sensitization of complementary squaraine dyes on cell efficiency

4. Suitable solvent system and electrolytes for NIR-active unsymmetrical squaraine dyes

❖ To study the best solvent system for NIR-active squaraine dyes

❖ To study the best electrolytes for NIR-active squaraine dyes
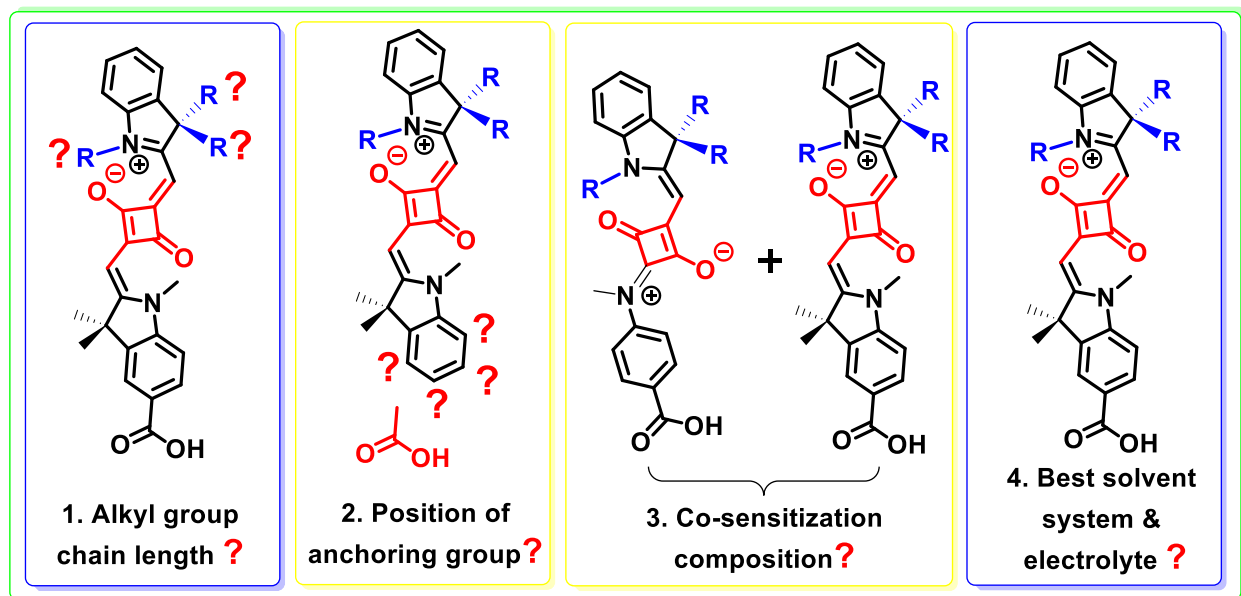
Figure 26. Objectives of thesis, where "R" are alkyl groups.

REFERENCES

1. Hubbert, M. K. Energy from Fossil Fuels. *Science* **1949**, *109*, 103–109.
2. Panwar, N. L.; Kaushik, S. C.; Kothari, S. *Renewable and Sustainable Energy Reviews* **2011**, *15*, 1513–1524.
3. Balmes, J. R.; J. M. Fine, D. *Am. Rev. Respir. Dis.* **1987**, *136*, 1117.
4. Mateen, F. J.; Brook, R. D. *JAMA*. **2011**, *305*, 1240-1241.
5. Bos, I.; De Boever, P.; Int Panis, L.; Meeusen, R. *Sports Medicine*. **2014**, *44*, 1505-1518.
6. Renewable Energy Policy Network for the 21st Century (REN21). **2019**.
7. Wackernagel, M.; Schulz, N. B.; Deumling, D.; Linares, A. C.; Jenkins, M.; Kapos, V.; Monfreda, C.; Loh, J.; Myers, N.; Norgaard, R.; et al. *PNAS* **2002**, *99*, 9266–9271.
8. Kannan, N.; Vakeesan, D. *Renew. Sustain. Energy Rev.* **2016**, *62*, 1092–1105.
9. Glaser, P. E. *Science* **1968**, *162*, 857.
10. Lewis, N. S. *Science* **2007**, *315*, 798.
11. Hagfeldt, A.; Grätzel, M. *Acc. Chem. Res.* **2000**, *33*, 269.
12. Becquerel, A. *C.R. Acad. Sci.* **1839**, *9*, 14.
13. Chapin, D. M.; Fuller, C.; Pearson, G. *J. Appl. Phys.* **1954**, *25*, 676.
14. Shockley, W.; Queisser, H. J. *J. Appl. Phys.* **1961**, *32*, 510.
15. Derkacs, D.; Lim, S. H.; Matheu, P.; Mar, W.; Yu, E. T. *Appl. Phys. Lett.* **2006**, *89*, 093103.
16. Pillai, S.; Catchpole, K. R.; Trupke, T.; Green, M. A. *Journal of Applied Physics* **2007**, *101*, 093105.
17. Nakayama, N.; Matsumoto, H.; Yamaguchi, K.; Ikegami, S.; Hioki, Y. *Jpn. J. Appl. Phys.* **1976**, *15*, 2281.
18. Aramoto, T.; Kumazawa, S.; Higuchi, H.; Arita, T.; Shibutani, S.; Nishio, T.; Nakajima, J.; Tsuji, M.; Hanafusa, A.; Hibino, T.; et al. *Jpn. J. Appl. Phys.* **1997**, *36*, 6304.
19. Gur, I.; Fromer, N. A.; Geier, M. L.; Alivisatos, A. P. *Science* **2005**, *310*, 462–465.
20. Kuribayashi, K.; Matsumoto, H.; Uda, H.; Komatsu, Y.; Nakano, A.; Ikegami, S. *Jpn. J. Appl. Phys.* **1983**, *22*, 1828.
21. Hubbard, S. M.; Cress, C. D.; Bailey, C. G.; Raffaelle, R. P.; Bailey, S. G.; Wilt, D. M. *Appl. Phys. Lett.* **2008**, *92*, 123512.
22. Krogstrup, P.; Jørgensen, H. I.; Heiss, M.; Demichel, O.; Holm, J. V.; Aagesen, M.; Nygard, J.; Fontcuberta i Morral, A. *Nature Photonics* **2013**, *7*, 306–310.
23. Yoon, J.; Jo, S.; Chun, I. S.; Jung, I.; Kim, H.-S.; Meitl, M.; Menard, E.; Li, X.; Coleman, J. J.; Paik, U.; et al. *Nature* **2010**, *465*, 329–333.
24. Liska, P.; Thampi, K. R.; Grätzel, M.; Brémaud, D.; Rudmann, D.; Upadhyaya, H. M.; Tiwari, A. N. *Appl. Phys. Lett.* **2006**, *88*, 203103.
25. Hetzer, M. J.; Strzhemechny, Y. M.; Gao, M.; Contreras, M. A.; Zunger, A.; Brillson, L. J. *Appl. Phys. Lett.* **2005**, *86*, 162105.

26. Li-Kao, Z. J.; Naghavi, N.; Erfurth, F.; Guillemoles, J. F.; Gérard, I.; Etcheberry, A.; Pelouard, J. L.; Collin, S.; Voorwinden, G.; Lincot, D. *Prog. Photovolt: Res. Appl.* **2012**, *20*, 582–587.

27. Shah, A.; Torres, P.; Tscharner, R.; Wyrsch, N.; Keppner, H. *Science* **1999**, *285*, 692–698.

28. Bube, R. H. *Phys. Rev.* **1955**, *98*, 431.

29. Fthenakis, V. *Renewable and Sustainable Energy Rev.* **2009**, *13*, 2746.

30. Beard, M. C.; Luther, J. M.; Semonin, O. E.; Nozik, A. J. *Acc. Chem. Res.* **2012**, *46*, 1252.

31. Tang, C. W. *Appl. Phys. Lett.* **1986**, *48*, 183–185.

32. Nelson, J. *Current Opinion in Solid State and Materials Science* **2002**, *6*, 87–95.

33. Pivrikas A.; Sariciftci N. S.; Juška G.; Österbacka R. *Progress in Photovoltaics: Research and Applications* **2007**, *15*, 677–696.

34. Bronstein, H.; Chen, Z.; Ashraf, R. S.; Zhang, W.; Du, J.; Durrant, J. R.; Shakya Tuladhar, P.; Song, K.; Watkins, S. E.; Geerts, Y.; et al. *J. Am. Chem. Soc.* **2011**, *133*, 3272–3275.

35. Kamat, P. V.; Tvrdy, K.; Baker, D. R.; Radich, J. G. *Chem. Rev.* **2010**, *110*, 6664–6688.

36. Albero, J.; Clifford, J. N.; Palomares, E. *Coordination Chemistry Reviews* **2014**, *263–264*, 53–64.

37. Wang, W.; Jiang, G.; Yu, J.; Wang, W.; Pan, Z.; Nakazawa, N.; Shen, Q.; Zhong, X. *ACS Appl. Mater. Interfaces* **2017**, *9*, 22549–22559.

38. Kim, H.-S.; Lee, C.-R.; Im, J.-H.; Lee, K.-B.; Moehl, T.; Marchioro, A.; Moon, S.-J.; Humphry-Baker, R.; Yum, J.-H.; Moser, J. E.; et al. *Scientific Reports* **2012**, *2*, 591.

39. Burschka, J.; Pellet, N.; Moon, S.-J.; Humphry-Baker, R.; Gao, P.; Nazeeruddin, M. K.; Grätzel, M. *Nature* **2013**, *499*, 316–319.

40. Liu, M.; Johnston, M. B.; Snaith, H. J. *Nature* **2013**, *501*, 395–398.

41. Heo, J. H.; Im, S. H.; Noh, J. H.; Mandal, T. N.; Lim, C.-S.; Chang, J. A.; Lee, Y. H.; Kim, H.; Sarkar, A.; Nazeeruddin, M. K.; et al. *Nature Photonics* **2013**, *7*, 486–491.

42. Liu, D.; Kelly, T. L. *Nature Photonics* **2014**, *8*, 133–138.

43. Jeon, N. J.; Noh, J. H.; Kim, Y. C.; Yang, W. S.; Ryu, S.; Seok, S. I. *Nature Materials* **2014**, *13*, 897–903.

44. Malinkiewicz, O.; Yella, A.; Lee, Y. H.; Espallargas, G. M.; Graetzel, M.; Nazeeruddin, M. K.; Bolink, H. J. *Nature Photonics* **2014**, *8*, 128–132.

45. O'Regan, B.; Grätzel, M. *Nature* **1991**, *353*, 737–740.

46. Grätzel, M. *Nature* **2001**, *414*, 338.

47. Thomas, S.; Deepak, T. G.; Anjusree, G. S.; Arun, T. A.; Nair, S. V.; Nair, A. S. *J. Mater. Chem. A* **2014**, *2*, 4474–4490.

48. Yao, Z.; Zhang, M.; Wu, H.; Yang, L.; Li, R.; Wang, P. *J. Am. Chem. Soc.* **2015**, *137*, 3799–3802.

49. Yu, Q.; Wang, Y.; Yi, Z.; Zu, N.; Zhang, J.; Zhang, M.; Wang, P. *ACS Nano* **2010**, *4*, 6032-6038.

50. Mathew, S.; Yella, A.; Gao, P.; Humphry-Baker, R.; Curchod, B. F. E.; Ashari-Astani, N.; Tavernelli, I.; Rothlisberger, U.; Nazeeruddin, M. K.; Grätzel, M. *Nat. Chem.* **2014**, *6*, 242–247.

51. Zhang, L.; Yang, X.; Wang, W.; Gurzadyan, G. G.; Li, J.; Li, X.; An, J.; Yu, Z.; Wang, H.; Cai, B.; Hagfeldt, A.; Sun, L. *ACS Energy Lett.* **2019**, *4*, 943–951.

52. Ji, J.-M.; Zhou, H.; Kim, H. K. *J. Mater. Chem. A,* **2018**, *6*, 14518–14545.

53. Hara, K.; Horiguchi, T.; Kinoshita, T.; Sayama, K.; Arakawa, H. *Sol. Energy Mater. Sol. Cells* **2001**, *70*, 151–161.

54. Kato, N.; Takeda, Y.; Higuchi, K.; Takeichi, A.; Sudo, E.; Tanaka, H.; Motohiro, T.; Sano, T.; Toyoda, T. *Sol. Energy Mater. Sol. Cells* **2009**, *93*, 893–897.

55. Law ChunHung; Pathirana Shehan C.; Li Xaioe; Anderson Assaf Y.; Barnes Piers R. F.; Listorti Andrea; Ghaddar Tarek H.; O'Regan Brian C. *Adv. Mater.* **2010**, *22*, 4505–4509.

56. Yu, Z.; Vlachopoulos, N.; Gorlov, M.; Kloo, L. *Dalton Trans.* **2011**, *40*, 10289.

57. Nelson, J. J.; Amick, T. J.; Elliott, C. M. *J. Phys. Chem. C* **2008**, *112*, 18255–18263.

58. Feldt, S. M.; Gibson, E. A.; Gabrielsson, E.; Sun, L.; Boschloo, G.; Hagfeldt, A. *J. Am. Chem. Soc.* **2010**, *132*, 16714–16724.

59. Wang, M.; Grätzel, C.; Zakeeruddin, S. M.; Grätzel, M. *Energy Environ. Sci.* **2012**, *5*, 9394–9405.

60. Bella, F.; Galliano, S.; Gerbaldi, C.; Viscardi, G. *Energies* **2016**, *9*, 384.

61. Yella, A.; Lee, H.-W.; Tsao, H. N.; Yi, C.; Chandiran, A. K.; Nazeeruddin, M. K.; Diau, E. W. G.; Yeh, C.-Y.; Zakeeruddin, S. M.; Grätzel, M. *Science* **2011**, *334*, 629−634.

62. Nusbaumer, H.; Zakeeruddin, S. M.; Moser, J.-E.; Grätzel, M. *Chemistry* **2003**, *9*, 3756-3763.

63. Cao, Y.; Saygili, Y.; Ummadisingu, A.; Teuscher, J.; Luo, J.; Pellet, N.; Giordano, F.; Zakeeruddin, S. M.; Moser, J.-E.; Freitag, M.; Hagfeldt, A.; Grätzel, M. *Nature Commun.* **2017**, *8*, 15390.

64. Snaith, H. J.; Schmidt-Mende, L. *Adv. Mater.* **2007**, *19*, 3187.

65. Saito, M.; Fujihara, S. *Energy Environ. Sci.,* **2008**, 1, 280–283.

66. Ramasamy, E.; Lee, J. *J. Phys Chem. C*, **2010**, 114, 22032–22037.

67. Hamann, T. W.; Jensen, R. A.; Martinson, A. B. F.; Ryswyk, H. V.; Hupp, J. T. *Energy Environ. Sci.* **2008**, *1*, 66–78.

68. Pagliaro, M.; Palmisano, G.; Ciriminna, R.; Loddo, V. *Energy Environ. Sci.* **2009**, *2*, 838–844.

69. Jose, R.; Thavasi, V.; Ramakrishna, S. *J. Am. Ceram. Soc.* **2009**, *92*, 289–301.

70. Peter, L. M. *Phys. Chem. Chem. Phys.* **2007**, *9*, 2630–2642.

71. Illa, S.; Ramireddy, B.; Manorama, S. V.; Basak, P. *J.Phys.Chem.C*, **2016,** 120, 18028-18038.

72. Park, N.-G.; Van de Lagemaat, J.; Frank, A. *J. Phys. Chem. B* **2000**, *104*, 8989.

73. Papageorgiou, N.; Maier, W. F.; Grätzel, M. *J. Electrochem. Soc.* **1997**, *144*, 876–884.

74. Murakami, T. N.; Ito, S.; Wang, Q.; Nazeeruddin, M. K.; Bessho, T.; Cesar, I.; Liska, P.; Humphry-Baker, R.; Comte, P.; Péchy, P.; Grätzel, M. *J. Electrochem. Soc.* **2006**, *153*, A2255–A2261.

75. Kay, A.; Grätzel, M. *Sol. Energy Mater. Sol. Cells* **1996**, *44*, 99–117.

76. Lindström, H.; Holmberg, A.; Magnusson, E.; Lindquist, S.-E.; Malmqvist, L.; Hagfeldt, A. *Nano Lett.* **2001**, *1*, 97–100.

77. Imoto, K.; Takahashi, K.; Yamaguchi, T.; Komura, T.; Nakamura, J.; Murata, K. *Sol. Energy Mater. Sol. Cells* **2003**, *79*, 459–469.

78. Bönnemann, H.; Khelashvili, G.; Behrens, S.; Hinsch, A.; Skupien, K.; Dinjus, E. *J Clust Sci* **2007**, *18*, 141–155.

79. Murakami, T. N.; Grätzel, M. *Inorganica Chimica Acta* **2008**, *361*, 572–580.

80. Wu, M.; Ma, T. *ChemSusChem*, **2012**, 5, 1343 – 1357.

81. Nazeeruddin, M. K.; Kay, A.; Rodicio, I.; Humphry-Baker, R.; Mueller, E.; Liska, P.; Vlachopoulos, N.; Graetzel, M. *J. Am. Chem. Soc.* **1993**, *115*, 6382–6390.

82. Nazeeruddin, M. K.; Zakeeruddin, S. M.; Humphry-Baker, R.; Jirousek, M.; Liska, P.; Vlachopoulos, N.; Shklover, V.; Fischer, C.-H.; Grätzel, M. *Inorg. Chem.* **1999**, *38*, 6298-6305.

83. Nazeeruddin, M. K.; Péchy, P.; Renouard, T.; Zakeeruddin, S. M.; Humphry-Baker, R.; Comte, P.; Liska, P.; Cevey, L.; Costa, E.; Shklover, V.; et al. *J. Am. Chem. Soc.* **2001**, *123*, 1613–1624.

84. Li, L.-L.; Diau, E. W.-G. *Chem. Soc. Rev.* **2013**, *42*, 291–304.

85. Higashino, T.; Imahori, H. *Dalton Trans.* **2014**, *44*, 448–463.

86. Urbani, M.; Grätzel, M.; Nazeeruddin, M. K.; Torres, T. *Chem. Rev.* **2014**, *114*, 12330–12396.

87. Birel, Ö.; Nadeem, S.; Duman, H. *J. Fluoresc.* **2017**, *27*, 1075–1085.

88. Ragoussi, M.-E.; Ince, M.; Torres, T. *Eur. J. Org. Chem.* **2013**, *2013*, 6475–6489.

89. Martín-Gomis, L.; Fernández-Lázaro, F.; Sastre-Santos, Á. *J. Mater. Chem. A* **2014**, *2*, 15672–15682.

90. Chen, C.-Y.; Wang, M.; Li, J.-Y.; Pootrakulchote, N.; Alibabaei, L.; Ngoc-le, C.-h.; Decoppet, J.-D.; Tsai, J.-H.; Grätzel, C.; Wu, C.-G.; Zakeeruddin, S. M.; Grätzel, M. *ACS Nano* **2009**, *3*, 3103.

91. Bessho, T.; Zakeeruddin, S. M.; Yeh, C.-Y.; Diau, E. W.-G.; Grätzel, M. *Angew. Chem., Int. Ed.* **2010**, *49*, 6646.

92. Yella, A.; Mai, C.-L.; Zakeeruddin, S. M.; Chang, S.-N.; Hsieh, C.-H.; Yeh, C.-Y.; Grätzel, M. *Angew. Chem., Int. Ed.* **2014**, *53*, 2973.

93. Tang, Y.; Wang, Y.; Li, X.; Ågren, H.; Zhu, W.-H.; Xie, Y. *ACS Appl. Mater. Interfaces* **2015**, *7*, 27976.

94. Xie, Y.; Tang, Y.; Wu, W.; Wang, Y.; Liu, J.; Li, X.; Tian, H.;Zhu, W.-H. *J. Am. Chem. Soc.* **2015**, *137*, 14055.

95. Hara, K.; Wang, Z.-S.; Sato, T.; Furube, A.; Katoh, R.; Sugihara, H.; Dan-oh, Y.; Kasada, C.; Shinpo, A.; Suga, S. *J. Phys. Chem. B* **2005**, *109*, 15476–15482.

96. Chen, R.; Yang, X.; Tian, H.; Wang, X.; Hagfeldt, A.; Sun, L. *Chem. Mater.* **2007**, *19*, 4007–4015.

97. Li, C.; Yang, X.; Chen, R.; Pan, J.; Tian, H.; Zhu, H.; Wang, X.; Hagfeldt, A.; Sun, L. *Solar Energy Materials and Solar Cells* **2007**, *91*, 1863–1871.

98. Stathatos, E.; Lianos, P.; Laschewsky, A.; Ouari, O.; Van Cleuvenbergen, P. *Chem. Mater.* **2001**, *13*, 3888–3892.

99. Teng, C.; Yang, X.; Yang, C.; Li, S.; Cheng, M.; Hagfeldt, A.; Sun, L. *J. Phys. Chem. C* **2010**, *114*, 9101–9110.

100. Meyer, T.; Ogermann, D.; Pankrath, A.; Kleinermanns, K.; Müller, T. J. J.. *J. Org. Chem.* **2012**, *77*, 3704–3715.

101. Alagumalai, A.; Kavungathodi, M. F. M.; Vellimalai, P.; Sil, M. C.; Nithyanandhan, J. *ACS Appl. Mater. Interfaces* **2016**, *8*, 35353–35367.

102. Yang, L.; Chen, S.; Zhang, J.; Wang, J.; Zhang, M.; Dong, X.; Wang, P. *J. Mater. Chem. A* **2017**, *5*, 3514–3522.

103. Venkatraman, V.; Abburu, S.; Alsberg, B. K.. *Phys. Chem. Chem. Phys.* **2015**, *17*, 27672–27682.

104. Yao, Z.; Zhang, M.; Li, R.; Yang, L.; Qiao, Y.; Wang, P. *Angew. Chem., Int. Ed.*, **2015**, *54*, 5994–5998.

105. Yao, Z. ; Wu, H.; Li, Y.; Wang, J.; Zhang, J.; Zhang, M.; Guo, Y. Wang, P. *Energy Environ. Sci.*, **2015**, *8*, 3192–3197.

106. Zhou, N.; Prabakaran, K.; Lee, B.; Chang, S. H.; Harutyunyan, B.; Guo, P.; Butler, M. R.; imalsina, A.; Bedzyk, M. J.; Ratner, M. A.; Vegiraju, S.; Yau, S.; Wu, C.-G.; Chang, R. P. H.; Facchetti, A.; Chen, M.-C.; Marks, T. J. *J. Am. Chem. Soc.*, **2015**, *137*, 4414–4423.

107. Eom, Y. K.; Choi, I. T.; Kang, S. H.; Lee, J.; Kim, J.; Ju, M. J.; Kim, H. K. *Adv. Energy Mater.*, **2015**, *5*, 1500300.

108. Ren, Y.; Sun, D.; Cao, Y.; Tsao, H. N.; Yuan, Y.; Zakeeruddin, S. M.; Wang, P.; Gratzel, M. *J. Am. Chem. Soc.*, **2018**, *7*, 2405–2408.

109. Campbell, W. M.; Burrell, A. K.; Officer, D. L.; Jolley, K. W. *Coord. Chem. Rev.* **2004**, *248*, 1363–1379.

110. Imahori, H.; Umeyama, T.; Ito, S. *Acc. Chem. Res.* **2009**, *42*, 1809–1818.

111. Martínez-Díaz, M. V.; Torre, G. de la; Torres, T. *Chem. Commun.* **2010**, *46*, 7090–7108.

112. Imahori, H.; Kang, S.; Hayashi, H.; Haruta, M.; Kurata, H.; Isoda, S.; Canton, S. E.; Infahsaeng, Y.; Kathiravan, A.; Pascher, T.; Chábera, P.; Yartsev, A. P.; Sundström, V. *J. Phys. Chem. A* **2011**, *115*, 3679–3690.

113. Si, L.; He, H. *J. Phys. Chem. A* **2014**, *118*, 3410−3418.

114. Gao, Y.; Li, X.; Hu, Y.; Fan, Y.; Yuan, J.; Robertson, N. Hua, J.; Marder, S. R. *J. Mater. Chem. A,* **2016**, *4*, 12865–12877.

115. Chai, Q.; Li, W.; Liu, J.; Geng, Z.; Tian, H.; Zhu, W.-H. *Sci. Rep.*, **2015**, *5*, 11330.

116. Liyanage, N. P.; Yella, A. Nazeeruddin, M.; Gratzel, M.; Delcamp, J. H. *ACS Appl. Mater. Interfaces*, **2016**, *8*, 5376–5384.

117. Dai, P.; Yang, L.; Liang, M.; Dong, H.; Wang, P.; Zhang, C.; Sun, Z. Xue, S. *ACS Appl. Mater. Interfaces*, **2015**, *7*, 22436–22447.

118. Dong, H.; Liang, M.; Zhang, C.; Wu, Y.; Sun, Z.; Xue, S. *J. Phys. Chem. C,* **2016**, *120*, 22822–22830.

119. Beverina, L.; Salice, P. *Eur J Org Chem* **2010**, 1207–1225.

120. Jiang J. Q.; Sun, C. L.; Shi, Z. F.; Zhang, H. L. *RSC Adv* **2014**, *4*, 32987.

121. Avirah, R. R.; Jayaram, D. T.; Adarsh, N.; Ramaiah, D. *Org Biomol Chem* **2012**, *10*, 911–920.

122. Wu D.; Chen, L.; Lee, W.; Ko, G.; Yin, J.; Yoon, J. *Coord Chem Rev* **2018**, *354*, 74–97.

123. Tatikolov, A. S. *J Photochem Photobiol C Photochem Rev* **2012**, *13*, 55–90.

124. Kamat, P. V.; Hotchandani, S.; Lind, M. de; Thomas, K. G.; Das, S.; George, M. V. *J. Chem. Soc. Faraday Trans.* **1993**, *89*, 2397–2402.

125. Zhao, W.; Jun Hou, Y.; Song Wang, X.; Wen Zhang, B.; Cao, Y.; Yang, R.; Bo Wang, W.; Rui Xiao, X. *Sol. Energy Mater. Sol. Cells* **1999**, *58*, 173–183.

126. Li, C.; Wang, W.; Wang, X.; Zhang, B.; Cao, Y. *Chem. Lett.* **2005**, *34*, 554–555.

127. Yum, J.-H.; Walter, P.; Huber, S.; Rentsch, D.; Geiger, T.; Nüesch, F.; De Angelis, F.; Grätzel, M.; Nazeeruddin, M. K. *J. Am. Chem. Soc.* **2007**, *129*, 10320–10321.

128. Geiger, T.; Kuster, S.; Yum, J.-H.; Moon, S.-J.; Nazeeruddin, M. K.; Grätzel, M.; Nüesch, F. *Adv. Funct. Mater.* **2009**, *19*, 2720–2727.

129. Karjule, N.; M. K., M. F.; Nithyanandhan, J. *J. Mater. Chem. A*, **2016**, *4*, 18910.

130. Shivashimpi, G.M.; Pandey, S. S.; Watanabe, R.; Fujikawa, N.; Ogomi, Y.; Yamaguchi, Y. *J. Photochem Photobiol A Chem* **2014**, 273, 1–7.

131. Jradi, F. M.; Kang, X.; Oneil, D.; Pajares, G.; Getmanenko, Y. A.; Szymanski, P. *Chem Mater* **2015**, *27*, 2480–2487.

132. Bisht, R.; Kavungathodi, M. F. M.; Singh, A. K.; Nithyanandhan, J. *J. Org. Chem.* **2017**, *82*, 1920.

133. Van, N. T.; Maeda, T.; Nakazumi, H.; Yagi, S. *Chem Lett* **2016**, *45*, 291–293.

134. Li, J.; Chen, C.; Lee, C.; Chen, S.; Lin, T.; Tsai, H. *Org Lett* **2010**, *12*, 10–13.

135. Punitharasu, V.; Kavungathodi, M. F. M.; Nithyanandhan, J. *ACS Appl. Mater. Interfaces,* **2018**, *10*, 16541-16551.

136. Punitharasu, V.; Kavungathodi, M. F. M.; Singh, A. K.; Nithyanandhan, J. *ACS Appl. Energy Mater*. **2019**, *2*, 8464−8472.

137. Sil, M. C.; Sudhakar, V.; Singh, A. K.; Kavungathodi, M. F. M.; Nithyanandhan, J. *ChemPlusChem* **2018**, *83*, 998–1007.

138. Haque, S. A.; Tachibana, Y.; Klug, D. R.; Durrant, J. R. *J. Phys. Chem. B* **1998**, *102*, 1745.

139. Tang, J.; Hua, J.; Wu, W.; Li, J.; Jin, Z.; Long, Y.; Tian, H. *Energy Environ. Sci.* **2010**, *3*, 1736–1745.

140. Tashiro, K.; Kobayashi, M.; Kawai, T.; Yoshino, K. *Polymer* **1997**, *38*, 2867–2879.

141. Planells, M.; Pellejà, L.; Clifford, J. N.; Pastore, M.; Angelis, F. D.; López, N.; Marder, S. R.; Palomares, E. *Energy Environ. Sci.* **2011**, *4*, 1820–1829.

142. Kasha, M.; Rawls, H. R.; Ashraf El-Bayoumi, M. *Pure Appl. Chem.,* **1965**, *11*, 371–392.

143. Sheppard, S. E.; *J. Chem. Soc. Trans.*, **1909**, *95*, 15–19.

144. Jelley, E. E. *Nature*, **1936**, *138*, 1009–1010.

145. Feng, S.; Li, Q.-S.; Sun, P.-P.; Niehaus, T. A.; Li, Z.-S. *ACS Appl. Mater. Interfaces* **2015**, *7*, 22504−22514.

146. Buhbut, S.; Clifford, J. N.; Kosa, M.; Anderson, A. Y.; Shalom, M.; Major, D. T.; Palomaresb, E.; Zaban, A. *Energy Environ. Sci.,* **2013**, *6*, 3046–3053.

147. Kusama, H; Sayama, K. *J. Phys. Chem. C* **2012**, *116*, 23906−23914.

148. Li, C.; Luo, L.; Wu, D.; Jiang, R.; Lan, J.; Wang, R.; Huang, L.; Yang, S.; You, J. *J. Mater. Chem. A,* **2016**, *4*, 11829–11834.

149. Mann, J. R.; Gannon, M. K.; Fitzgibbons, T. C.; Detty, M. R.; Watson, D. F. *J. Phys. Chem. C,***2008**, *112*, 13057–13061.

150. Kryman, M. W.; Nasca, J. N.; Watson, D. F.; Detty, M. R. *Langmuir* **2016**, *32*, 1521−1532.

151. Si, L.; He, H. *J. Phys. Chem. A* **2014**, *118*, 3410−3418.

152. Hart, A. S.; Kc, C. B.; Gobeze, H. B.; Sequeira, L. R.; D'Souza, F. *ACS Appl. Mater. Interfaces* **2013**, *5*, 5314–5323.

153. Gou, F.; Jiang, X.; Fang, R.; Jing, H.; Zhu, Z. *ACS Appl. Mater. Interfaces* 2014, *6*, 6697-6703.

154. Ambre, R. B.; Mane, S. B.; Chang, G.-F.; Hung C.-H. *ACS Appl. Mater. Interfaces* **2015**, *7*, 1879−1891.

155. Liu, S.; Jiao, Y.; Ding, Y.; Fan, X.; Song, J.; Mi, B.; Gao, Z. *Dyes and Pigments* **2020**, *180*, 108470.

156. Ye, S.; Kathiravan, A.; Hayashi, H.; Tong, Y.; Infahsaeng, Y.; Chabera, P.; Pascher, T.; Yartsev, A. P.; Isoda, S.; Imahori, H.; Sundström, V. *J. Phys. Chem. C* **2013**, *117*, 6066−6080.

157. Ide, R.; Fujimori, Y.; Tsuji, Y.; Higashino, T.; Imahori, H.; Ishikawa, H.; Imanishi, A.; Fukui, K.; Nakamura, M.; Hoshi, N. *ACS Omega* **2017**, *2*, 128−135.

158. Kim, B. G.; Chung, K.; Kim, J. *Chem. Eur. J.* **2013**, *19*, 5220.

159. Karjule, N.; M. K., M. F.; Nithyanandhan, J. *J. Phys. Chem. C* **2017**, *121,* 21836–21847.

160. Chen, Y.; Zeng, Z.; Li, C.; Wang, W.; Wang, X.; Zhang, B. *New J. Chem.* **2005**, *29*, 773−776.

161. Hagfeldt, A.; Boschloo, G.; Sun, L.; Kloo, L.; Pettersson, H. *Chem. Rev.* **2010**, *110*, 6595−6663.

162. Jradi, F. M.; O'Neil, D.; Kang, X.; Wong, J.; Szymanski, P.; Parker, T. C.; Anderson, H. L.; El-Sayed, M. A.; Marder, S. R. *Chem. Mater.* **2015**, *27*, 6305–6313.

163. Dong, L.; Zheng, Z.; Wang, Y.; Li, X.; Hua, L.; Hu, A. *J. Mater. Chem. A* **2015**, *3*, 11607−11614.

164. Chang, S.; Wang, H.; Lee, L. T. L.; Zheng, S.; Li, Q.; Wong, K. Y.; Wong, W.-K.; Zhu, X.; Wong, W.-Y.; Xiao, X.; et al. *J. Mater. Chem. C* **2014**, *2*, 3521−3526.

165. Shiu, J.-W.; Chang, Y.-C.; Chan, C.-Y.; Wu, H.-P.; Hsu, H.-Y.; Wang, C.-L.; Lin, C.-Y.; Diau, E. W.-G. *J. Mater. Chem. A* **2015**, *3*, 1417−1420.

166. Cid, J.-J.; Yum, J.-H.; Jang, S.-R.; Nazeeruddin, M. K.; Martínez-Ferrero, E.; Palomares, E.; Ko, J.; Grätzel, M.; Torres, T. *Angew. Chem., Int. Ed.* **2007**, *46*, 8358−8362.

167. Holliman, P. J.; Davies, M. L.; Connell, A.; Velasco, B. V.; Watson, T. M. *Chem. Commun*. **2010**, *46*, 7256−7258.

168. Hua, Y.; Lee, L. T. L.; Zhang, C.; Zhao, J.; Chen, T.; Wong, W.-Y.; Wong, W.-K.; Zhu, X. *J. Mater. Chem. A* **2015**, *3*, 13848−13855.

Alkyl-Group-Wrapped Unsymmetrical Squaraine Dyes for Dye-Sensitized Solar Cells
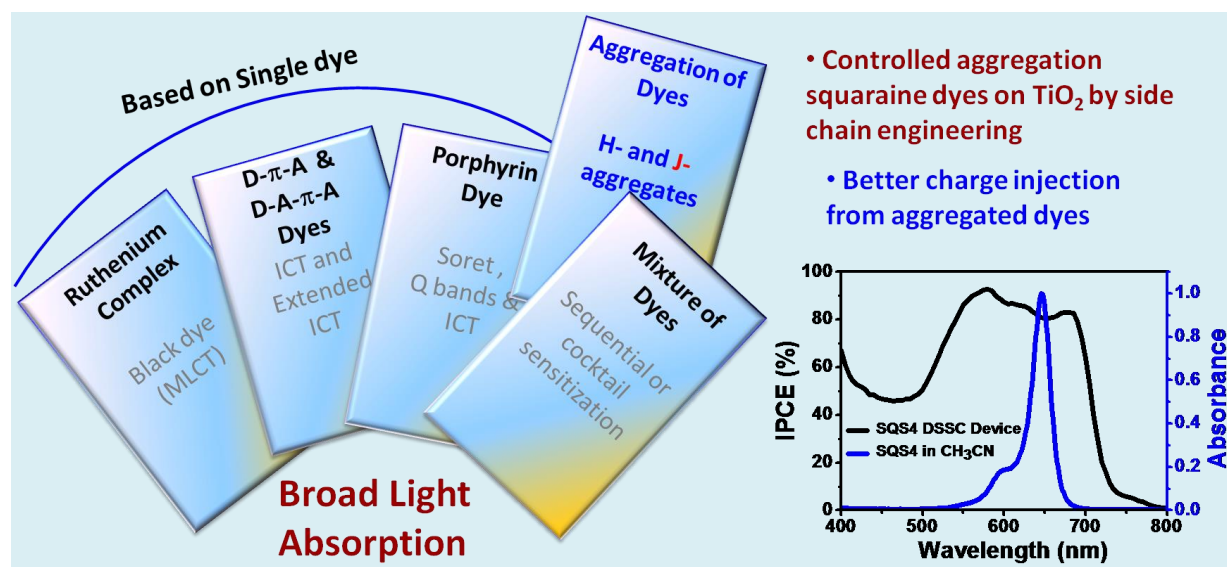
2.1 INTRODUCTION

Third generation photovoltaic technologies offer highly efficient, low fabricating cost and flexible devices for the solar energy conversion. Dye sensitized solar cell[1] belongs to third generation photovoltaic technology and light absorbing sensitizers play an important role in harvesting the solar energy. Various sensitizers have been designed based on the organometallic and metal-free organic dyes to achieve high efficiencies for DSSCs, but there are few best performing dyes are reported in literature. Judicious structural engineering of ruthenium polypyridine[2-6] dyes showed 7.0 to 12%, and zinc-porphyrin[7-19] complexes showed the varied device performance from <1 to 13%. Along with ruthenium and zinc-porphyrin complexes, organic dyes received considerable attention due to the modular molecular design of sensitizers, facile synthesis, and tunable electronic properties within the visible and near-IR-region with high device performance.[7, 20-25] Recent reports on metal-free organic dyes with cobalt (II/III) as electrolyte have shown the power conversion efficiencies (PCEs) from 10 to 10.65%[26-31] and 10.1% with I^-/I_3^- electrolyte.[32] Only few metal-free organic dyes have achieved more than 11% of power conversion efficiencies.[26-27,33-34] Porphyrines,[8,12,14] phthalocyanines[35] and polymethine (heterocyclic, cyanines and squaraines) dyes[36] are the chromophores that harvest light far-red to NIR-regions. Squaraines are well known chromophores having high molar extinction coefficient[37-39] and able to harvest light from the visible and NIR-regions. Unsymmetrical squaraines followed by structural modifications power conversion efficiencies (PCEs) have been reached from 4 to 9%,[40-46] while symmetrical squaraines have been reached 6.1%.[47] Dipole-dipole interaction between the dyes often lead to broadening the absorption profile. Variation of slip angle θ between polarization axes and the line of molecule centres lead to formation of H-aggregate ($54.7° < \theta < 90°$, blue shifted transitions) and J-aggregate ($0° < \theta < 54.7°$, red shifted transitions) assemblies (**Figure 1**), which can be naturally enhanced on the TiO_2 surface due to periodicity of 5-coordinated Ti-atoms.[48] These aggregation properties have been utilized in elegantly in organic electronics where enhanced charge transport properties of small organic molecules have been observed for well-defined self-assembled structures besides enhancing the light absorbing properties. However in case of DSSCs, aggregation of dyes on TiO_2 surface plays a detrimental role, as the aggregated structures promote the charge hopping within the monolayer of sensitizer that reduces the charge injection process to the TiO_2 and hamper the power

conversion efficiency.[49-51] While in some cases it participates to enhance the IPCE response and efficiencies by broadening the absorption spectrum.[43,52-53,] Hence controlling dye aggregations on TiO_2 to achieve synergistic effects of both spectral broadening for more light absorption and charge injection from aggregated state is a challenging task. There are reports on dyes with alkyl chains effectively controlling the charge recombination process.[54, 55]
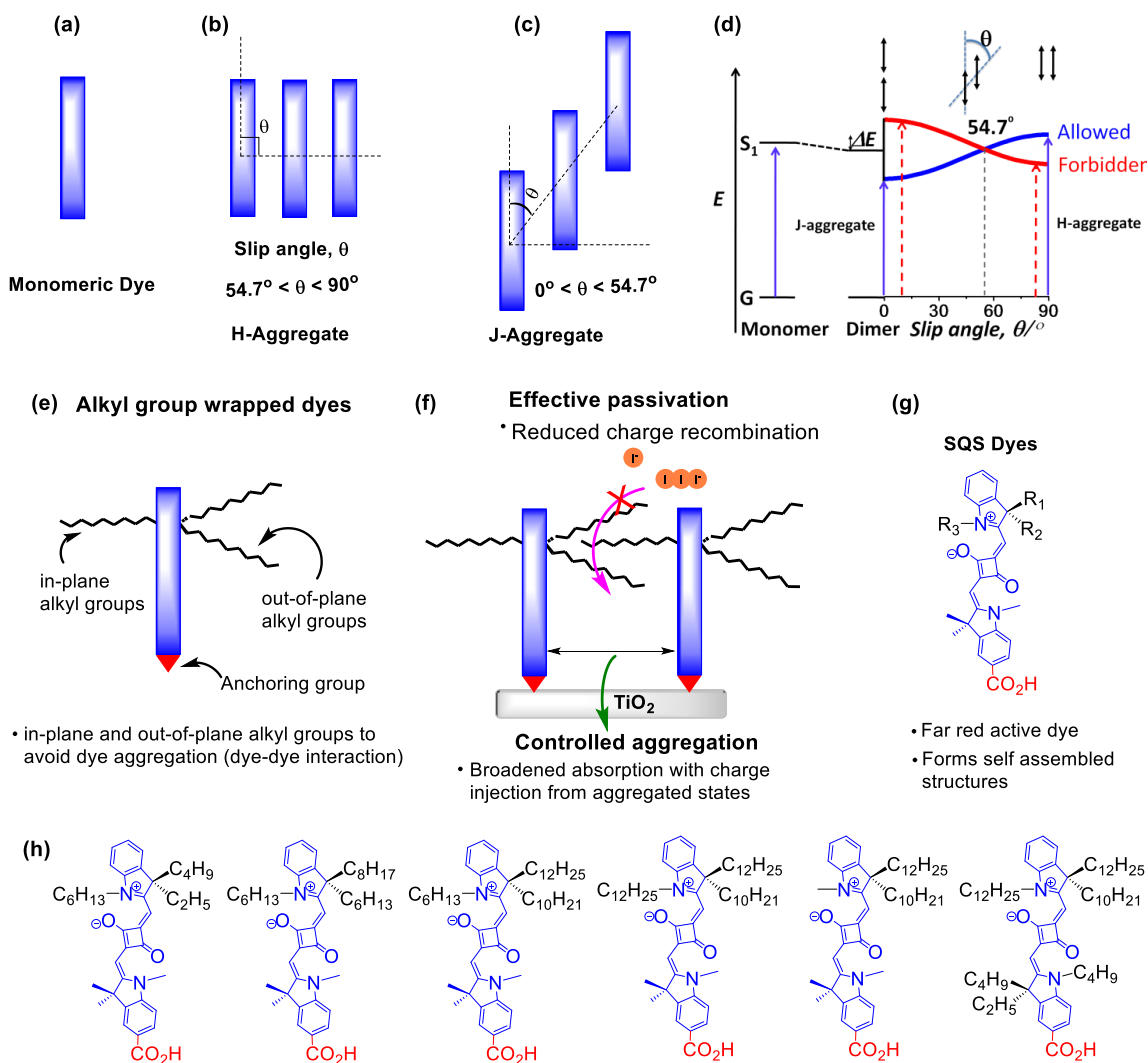
Figure 1. Schematic representation of (a) monomer dye (b) and (c) molecular arrangements of H-type and J-type aggregates, (d) energy level diagram for the allowed transitions for H-type and J-type aggregates with the slip angle (θ), (e) and (f) dyes containing branched alkyl groups and their effect on aggregation, (g) general structure of SQS dyes, and (h) structures of Y-type (SQS1−SQS4 and SQS6) and V- type (SQS5) unsymmetrical squaraine dyes.

Our previous work showed that unsymmetrical squaraine dye with alkyl groups away from the carboxylic acid provided good power conversion efficiencies and also control the organization of sensitizers on the surface of TiO_2.[43] In this respect, to understand the effect of alkyl groups on the V_{OC} and J_{SC} parameters, which originate from the effective passivation of the TiO_2 surface and broadening of the absorption spectrum by controlled aggregation (**Figure 1e,f**), we synthesized a series of unsymmetrical squaraine dyes, SQSs, with systematically varied branched alkyl groups at sp^3-C (out-of-plane) and linear alkyl groups at N-atoms (in-plane) of the indoline unit, which is away from the anchoring group (SQS1−SQS5), and in the case of SQS6, alkyl groups are present both near and away from the anchoring group (**Figure 1h**). General representation of monomer, H-aggregate, J- aggregate and SQS dye displayed in **Figure 1a-1d** and **Figure 1g**.

2.2 EXPERIMENTAL SECTION

2.2.1 General methods

The chemicals and reagents required for the SQS dyes scheme are purchased from commercial sources, and standard procedures are used for drying of solvents and were distilled before use. ^{1}H and ^{13}C NMR were recorded on Bruker NMR spectrometers AV 200 MHz, AV 400 MHz and AV-500 MHz frequency, in $CDCl_3$, MeOH-d_4 DMSO-d_6 Acetone-d_6. High-resolution mass spectrometric (HRMS) measurements were recorded on SYNAPT G2 HDM in MeOH as solvent. Absorption spectra of SQS dyes were recorded on SPECORD® 210/ PLUS, Analytikjena UV−Visible spectrophotometer at room temperature.

2.2.2 Cyclic voltammetry. Cyclic voltammetry of SQS dyes were performed on CHI660B potentiostat and done in anhydrous dichloromethane solvent at 25 ^{o}C under inert atmosphere, where platinum wire used as a working electrode, platinum foil as a counter electrode, non-aqueous Ag/Ag$^+$ (0.01M) as reference electrode, TBAClO$_4$ (0.1 M) as supporting electrolyte, Ferrocene/ Ferrocene$^+$ as the internal standard, and scan rate was 50 mV s^{-1}. Cyclic voltammetry on TiO_2 surface have done in CH_3CN, where dye adsorbed on the TiO_2 surface used as a working electrode, whereas all other electrodes and conditions are same. Thickness of electrode

was 6 μm and area was 0.22 cm^2 for all dyes, dipping solution is CH_3CN: $CHCl_3$ (90%: 10%) and dipping for 6 h.

2.2.3 Light harvesting efficiency (LHE). For the light harvesting efficiency calculation (LHE = $1\text{-}10^{-A}$), dye solution 0.1 mM in $CHCl_3$, dipping time 12 h at room temperature, where 6 μm thin film of TiO_2 coated on the transparent glass slide have used.

2.2.4 Dye-sensitized solar cells fabrication. Fluorine-doped SnO_2 glass (FTO glass; 6-8 Ω /sq; Pilkington TEC 7) was cleaned by using mucasol (2% in water), de-ionized water, and isopropanol. Freshly prepared 50 mM aqueous $TiCl_4$ solution at 70 ^{o}C for 30 min used to grow a TiO_2 layer, the substrate was washed with the de-ionized water, ethanol, and dried at 110 ^{o}C for 10 min. A paste of TiO_2 nanocrystal (< 20 nm, Ti-Nanoxide T/SP, Solaronix) was coated on FTO substrate conducting side by the doctor-blade technique and kept for 10 min in air then annealed at 125 °C in air for 20 min. The annealed films (about 6-8 μm thick) were coated with scattering layer TiO_2 paste (WER2-O, Dyesol) and annealed at 125 °C for 20 min in air, then sintered at 325 °C for 5 min, 375 °C for 5 min, 450 °C for 15 min and 500 °C for 15 min where heating rate was 5 °C per min in air. When the temperature of furnace reached at 50 °C, sintered films were immersed in freshly prepared 50 mM aqueous $TiCl_4$ solution at 70 ^{o}C for 30 min, washed with the de-ionized water, ethanol, and sintered it at 500 °C for 30 min, whenever the temperature of furnace reached at 50 °C then cells were immersed in 0.1 mM SQS dye solution MeCN: $CHCl_3$ (90: 10%) for 6 h, after washing with MeCN dry the cell at 80 ℃, here the area of TiO_2 is 0.23 cm^2. In the case of addition of co-adsorbent only the concentration of CDCA in the dye solution varied and dipping time was same (6 h). Electroplatinised platinum foil used as cathode, iodolyte (I^-/I_3^-) Z-50 (Solaronix) was used as electrolyte and 25 μm spacer, and the size of black mask is 0.23 cm^2. The device performance of SQS dyes were measured under standard simulator condition (AM 1.5 G, 100 mW/cm^2).

2.2.5 Synthesis.

The branched alcohols oxidized to branched aldehydes **2**, which was reacted with CH_3MgI at 0 ^{o}C to afford the branched alcohols **3**. Oxidation of **3** with pyridinium chlorochromate (PCC) afforded the required branched ketones **4** in moderate yield. Phenylhydrazinehydrochloride was reacted with the branched ketones (**4a-c**) to afford the indolenine derivatives (**5a-c**) in good

yield, which were further reacted with 1-iodoalkanes to afford the indolium salt (**6a-e**). The indolium salts were condensed with semi-squaric acid **12** under reflux reaction condition in Dean-Stark trap, PhMe (toluene) and *n*-BuOH (1:1) to afford the final unsymmetrical dyes **13** in moderate yields.
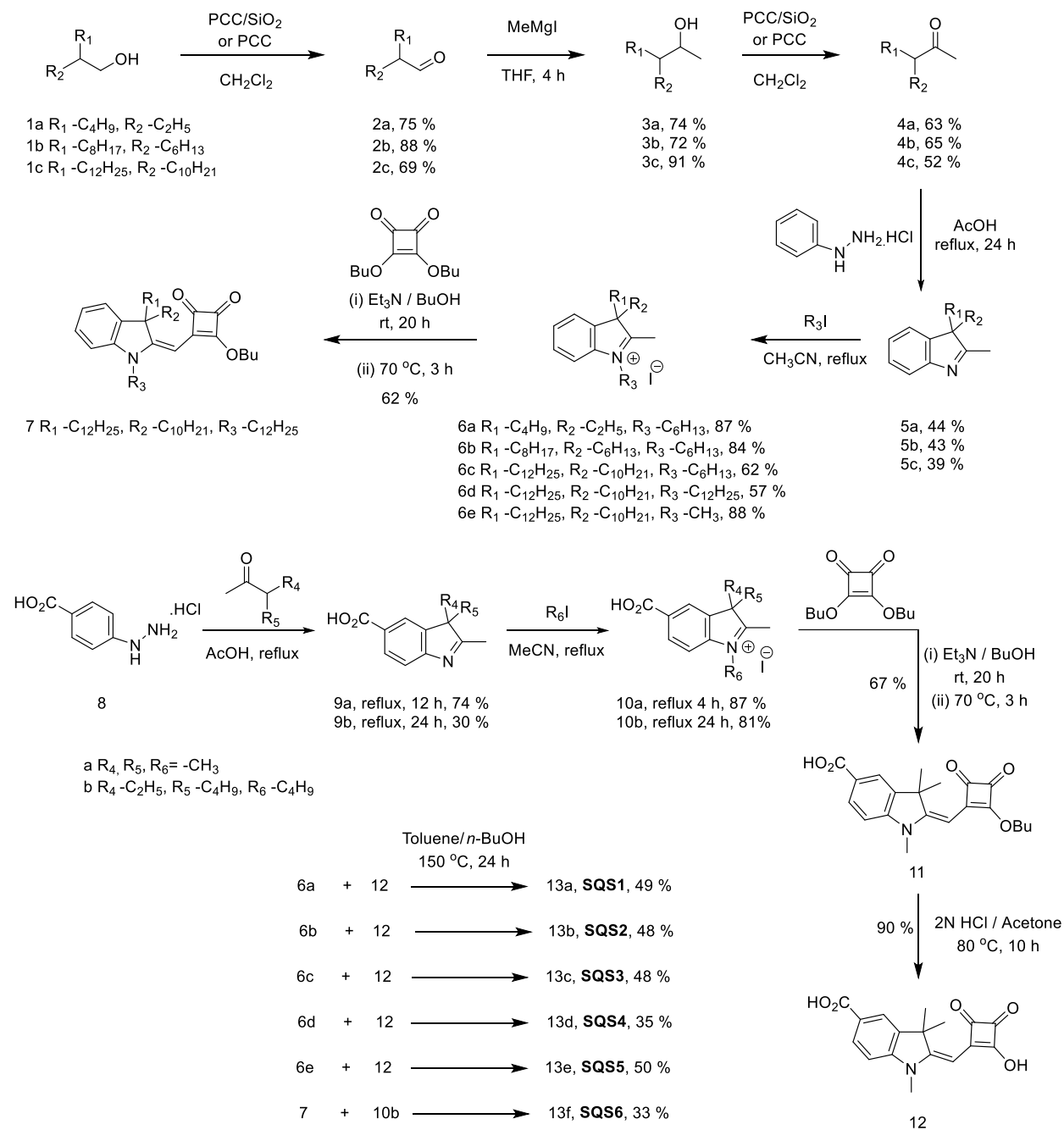
Scheme 1. Synthetic scheme for Y-type (SQS1-SQS4 and SQS6) and V- type (SQS5) unsymmetrical squaraine dyes.

Synthesis of 2-ethylhexanal (2a), 2-hexyldecanal (2b), and 2-decyltetradecanal (2c):

Procedure A: A mixture of PCC (9.93 g, 46.07 mmol) and silica gel (9.93 g, 60–200 mesh) was ground to a fine powder using a mortar and pestle. The powdered mixture added to 250 mL of round bottom flask and 120 mL of anhydrous CH_2Cl_2 was added and cooled to 0 ^{o}C. Alcohol **1a** (5 g, 38.4 mmol) added to above mixture once, stirred for 16 h at room temperature and filtered through silica gel pad and eluted with CH_2Cl_2 to provide the required aldehyde as a colorless liquid. Aldehyde used for next step without purification.[56]

Procedure B: Alcohols **1b-c** (1 equiv.) dissolved in 60 mL of anhydrous CH_2Cl_2 in a 250 mL of round bottom flask, PCC (3 equiv.) was added portion wise to the above solution, stirred for 4 h at room temperature and filtered through silica gel pad and eluted with CH_2Cl_2 to provide the required aldehyde as a colorless liquid. Aldehyde used for next step without purification.[57]

2-Ethylhexanal (2a): Procedure A, started with **1a** (5 g), Yield: 3.7 g, 75 %. ^{1}H NMR (CDCl$_3$, 200 MHz): δ 9.57 (d, *J* = 4 Hz, 1H), 2.21-2.13 (m, 1H), 1.74-1.52 (m, 4H), 1.37-1.26 (m, 4H), 0.95-86 (m, 6H).

2-Hexyldecanal (2b): Procedure B, started with **1b** (5 g), Yield: 4.4 g, 88 %. ^{1}H NMR (CDCl$_3$, 200 MHz): δ 9.55 (d, *J* = 4 Hz, 1H), 2.30-2.15 (m, 1H), 1.71-1.41 (m, 4H), 1.27 (s, 20H), 0.88 (m, 6H).

2-Decyltetradecanal (2c): Procedure B, started with **1c** (5 g), Yield: 3.44 g, 69 %. ^{1}H NMR (CDCl$_3$, 200 MHz): δ 9.55 (d, *J* = 4 Hz, 1H), 2.28-2.15 (m, 1H), 1.71-1.45 (m, 4H), 1.26 (s, 36H), 0.88 (m, 6H).

Synthesis of branched alcohol 3: Branched aldehyde **2** (1 equiv.) was taken in a 100 mL round bottom flask, charged with anhydrous THF and cooled to 0 ^{o}C. CH$_3$MgI (3M in Et$_2$O, 1.5 -1.8 equiv.) was added dropwise and stir for 4 h at room temperature. Aqueous solution of NH$_4$Cl used to quench the reaction, diluted with Ethyl acetate, washed with H$_2$O twice and Na$_2$SO$_4$ was used for drying the organic layer. Secondary alcohol used for next step without purification.

3-Ethylheptan-2-ol (3a): Started with **2a** (3 g, 23.4 mmol) and CH$_3$MgI (14 mL, 42.12 mmol) in 50 mL anhydrous THF. Yield: 2.5 g, 74 %. ^{1}H NMR (CDCl$_3$, 200 MHz): δ 3.89-3.72 (m, 1H), 2.45-2.31 (m, 1H), 1.47-1.3 (m, 8H), 1.17 (d, *J* = 4 Hz, 3H), 0.94-0.87 (m, 6H).

3-Hexylundecan-2-ol (3b): Started with **2b** (3 g, 12.48 mmol) and CH_3MgI (6.25 mL, 18.72 mmol) in 20 mL anhydrous THF. Yield: 2.31 g, 72 %. ^1H NMR ($CDCl_3$, 400 MHz): δ 3.86-3.80 (m, 1H), 2.40-2.29 (m, 1H), 1.65-1.43 (m, 4H), 1.27 (s, 20H), 1.135 (d, J = 4 Hz, 3H), 0.88 (m, 6H); ^{13}C NMR ($CDCl_3$,100 MHz): δ 69.3, 44.5, 31.6, 31.5, 30.6, 29.26, 29.0, 27.1, 22.3, 13.7.

3-Decylpentadecan-2-ol (3c): Started with **2c** (3.3 g, 9.36 mmol) and CH_3MgI (4.7 mL, 14.04 mmol) in 20 mL anhydrous THF. Yield: 3.15 g, 91 %. ^1H NMR ($CDCl_3$, 400 MHz): δ 3.92-3.88 (m, 1H), 2.36-2.29 (m, 1H), 1.66-1.54 (m, 4H), 1.26 (s, 36H), 1.13 (d, J = 4 Hz, 3H), 0.88 (m,6H); ^{13}C NMR ($CDCl_3$, 100 MHz): δ 70.8, 43.7, 32.2, 31.9, 30.2, 29.7, 29.6, 29.5, 29.3, 27.4, 27.3, 22.7, 14.1.

Synthesis of branched ketone 4: Procedure A: A mixture of PCC (4.85 g, 22.54 mmol) and silica gel (4.85 g, 60–200 mesh) was ground to a fine powder using a mortar and pestle. The powdered mixture added to 250 mL of round bottom flask and 70 mL of anhydrous CH_2Cl_2 was added and cooled to 0 ^{o}C. Alcohol **3a** (2.5 g, 17.34 mmol) added to above mixture once, stirred for 16 h at room temperature and filtered through silica gel pad and eluted with CH_2Cl_2 to provide the required ketone as a colorless liquid. Ketone used for next step without purification.

Procedure B: Alcohols **3b-c** (1 equiv.) dissolved in 60 mL of anhydrous CH_2Cl_2 in a 250 mL round bottom flask, PCC (3 equiv.) was added portion wise to the above solution, and stirred for 4 h at room temperature and filtered through silica gel pad and eluted with CH_2Cl_2.

3-Ethylheptan-2-one (4a): Procedure A, started with **3a** (2.5 g), Yield: 1.56 g, 63 %. ^1H NMR ($CDCl_3$, 200 MHz): δ 2.30 (m, 1H), 2.04 (s, 3H), 1.55-1.48 (m, 2H), 1.42-1.35 (m, 2H), 1.25-1.18 (m, 4H), 0.83-0.77 (m, 6H); ^{13}C NMR ($CDCl_3$, 125 MHz): δ 213.1, 54.7, 30.9, 29.5, 28.6, 24.5, 22.7, 13.8, 11.7; HRMS (m/z): $[M + H]^+$ calculated for $C_9H_{19}O$: 143.1430; found: 143.1430.

3-Hexylundecan-2-one (4b): Procedure B, started with **3b** (2 g, 7.8 mmol), CH_2Cl_2 (20 mL), column chromatography (SiO_2, 100-200 mesh, 8 % CH_2Cl_2 and 92 % pet. ether). Yield: 1.3 g, 64.5 %. ^1H NMR ($CDCl_3$, 500 MHz): δ 2.44-2.37 (m, 1H), 2.11 (s, 3H), 1.60-1.37 (m, 4H), 1.25 (s, 20H), 0.89-0.86 (m, 6H); ^{13}C NMR ($CDCl_3$, 125 MHz): δ 213.3, 53.36, 31.8, 31.7, 31.6, 29.7, 29.4, 29.2, 28.6, 27.5, 27.4, 22.6, 14.1, 14.0; HRMS (m/z): $[M + H]^+$ calculated for $C_{17}H_{35}O$: 255.2682; found: 255.2677.

3-Decylpentadecan-2-one (4c): Procedure B, Started with **3c** (2.9 g, 7.87 mmol), CH_2Cl_2 (30 mL), column chromatography (SiO_2, 100-200 mesh, 5 % CH_2Cl_2 and 95 % pet. ether). Yield: 1.5 g, 52 %. ^{1}H NMR ($CDCl_3$, 400 MHz): δ 2.45-2.36 (m, 1H), 2.11 (s, 3H), 1.61-1.53 (m, 2H), 1.45-1.38 (m, 2H), 1.25 (s, 36H), 0.90-0.86 (m, 6H); ^{13}C NMR ($CDCl_3$, 100 MHz): δ 213.3, 53.4, 31.9, 31.8, 29.8, 29.7, 29.5, 29.4, 28.6, 27.5, 27.3, 22.7, 14.1.

General procedure for the synthesis of 2-methyl-3, 3-dialkyl-3H-indole, 5: Phenylhydrazinehydrochloride, and 3-alkyl-2-alkanone **4** (1.2 equiv.) were dissolved in 10 mL of acetic acid in a 50 mL of round bottom flask and reflux under nitrogen atmosphere.

3-Butyl-3-ethyl-2-methyl-3H-indole (5a): Started with **4a** (1.18 g, 8.3 mmol) and phenylhydrazinehydrochloride (1 g, 6.92 mmol), reaction time: 24 h, column chromatography (SiO_2, 100-200 mesh, 12 % ethyl-acetate and 88 % pet. ether). Yield: 0.65 g, 44 %. ^{1}H NMR ($CDCl_3$, 500 MHz): δ 7.52 (d, J = 7.6 Hz, 1H), 7.32-7.28 (m, 1H), 7.20-7.19 (m, 2H), 2.21 (s, 3H), 1.96-1.85 (m, 2H), 1.81-1.70 (m, 2H), 1.16-1.11 (m, 2H), 0.73 (t, J = 7.5 Hz, 3H), 0.70-0.55 (m, 2H), 0.355 (t, J = 7.5 Hz, 3H); ^{13}C NMR ($CDCl_3$, 125 MHz): δ 186.2, 155.4, 141.9, 127.4, 124.8, 121.6, 119.5, 63.1, 36.4, 29.8, 25.8, 22.8, 16.0, 13.7, 8.1; HRMS (m/z): $[M + H]^+$ calculated for $C_{15}H_{22}N$: 216.1747; found: 216.1743.

3-Hexyl-2-methyl-3-octyl-3H-indole (5b): Started with **4b** (1 g, 3.93 mmol) and phenylhydrazinehydrochloride (0.47 g, 3.28 mmol), reaction time: 20 h, column chromatography (SiO_2, 100-200 mesh, 6 % ethyl-acetate and 94 % pet. ether). Yield: 0.45 g, 43 %. ^{1}H NMR ($CDCl_3$, 200 MHz): δ 7.52 (d, J = 7.6 Hz, 1H), 7.33-7.27 (m, 1H), 7.18 (m, 2H), 2.21 (s, 3H), 1.94-1.63 (m, 4H), 1.21-1.07 (m, 16H), 0.87-0.79 (m, 6H), 0.72-0.47 (m, 4H); ^{13}C NMR ($CDCl_3$, 100 MHz): δ 186.8, 154.9, 142.2, 127.5, 125.0, 121.7, 119.6, 62.7, 45.6, 37.0, 32.4, 31.8, 31.4, 29.8, 29.5, 29.3, 29.2, 23.6, 22.7, 22.6, 22.5, 16.0, 14.1; HRMS (m/z): $[M + H]^+$ calculated for $C_{23}H_{38}N$: 328.2999; found: 328.3001.

3-Decyl-3-dodecyl-2-methyl-3H-indole (5c): Started with **4c** (1.3 g, 3.55 mmol) and phenylhydrazinehydrochloride (0.43 g, 2.96 mmol), reaction time: 24 h, column chromatography (SiO_2, 100-200 mesh, 3 % ethyl-acetate and 97 % pet. ether). Yield: 0.5 g, 39 %. ^{1}H NMR ($CDCl_3$, 500 MHz): δ 7.51 (d, J = 7.6 Hz, 1H), 7.29 (m, 1H), 7.18 (m, 2H), 2.20 (s, 3H), 1.89-1.83 (m, 2H), 1.73-1.67 (m, 2H), 1.28-1.16 (m, 20H), 1.13-1.06 (m, 12H), 0.88-0.84 (m, 6H),

0.73-0.67 (m, 2H), 0.58-0.52 (m, 2H); ^{13}C NMR (CDCl$_3$, 125 MHz): δ 186.5, 155.3, 142.3, 127.4, 124.8, 121.6, 119.5, 62.6, 37.0, 31.9, 31.8, 29.8, 29.6, 29.6, 29.4, 29.3, 29.3, 29.2, 23.5, 22.7, 22.6, 16.1, 14.1; HRMS (*m/z*): [M + H]$^+$ calculated for C$_{31}$H$_{54}$N: 440.4251; found: 440.4241.

General procedure for the synthesis of 1-alkyl-2-methyl-3,3-dialkyl-3H-indol-1-ium iodide, (6a-c): 1-Iodohexane (2 equiv.) and 2-methyl-3,3-dialkyl-3H-indole derivative, (**5a-c**) (1 equiv.) were dissolved in 5 mL of CH$_3$CN in a 50 mL round bottom flask and refluxed under inert atmosphere, after cooling solvent were evaporate through Rota vapor. The reaction mixture washed with hexane (4 × 5 mL) to afford the required compound as a brown-red color viscous liquid.

3-Butyl-3-ethyl-1-hexyl-2-methyl-3H-indol-1-ium iodide (6a): Started with **5a** (0.3 g, 1.34 mmol) and 1-iodohexane (0.59 g, 2.79 mmol), reaction time: 40 h, Yield: 0.5 g, 87 %. ^{1}H NMR (CDCl$_3$, 500 MHz): δ 7.74 (d, *J* = 10 Hz, 1H), 7.67-7.62 (m, 2H), 7.54 (d, *J* = 10 Hz, 1H), 4.91-4.83 (m, 2H), 3.18 (s, 3H), 2.31-2.11 (m, 4H), 1.96-1.90 (m, 2H), 1.56-1.50 (m, 2H), 1.41-1.15 (m, 8H), 0.88 (m,3H), 0.78 (t, *J* = 7.5 Hz, 3H), 0.55 (t, *J* = 7.5 Hz, 3H); ^{13}CNMR (CDCl$_3$, 125 MHz): δ195.9, 142.4, 138.5, 130.1, 129.7, 123.8, 115.3, 64.2, 50.5, 36.7, 33.5, 31.2, 30.8, 30.7, 30.1, 28.6, 26.5, 26.1, 22.5, 22.3, 17.4, 14.0, 13.9, 13.5, 8.7; HRMS (*m/z*): [M]$^+$ calculated for C$_{21}$H$_{34}$N$^+$: 300.2686; found: 300.2687.

1,3-Dihexyl-2-methyl-3-octyl-3H-indol-1-ium iodide (6b): Started with **5b** (0.48 g, 1.46 mmol) and 1-iodohexane (0.62 g, 2.92 mmol), reaction time: 24 h, Yield: 0.66 g, 84 %. ^{1}H NMR (CDCl$_3$, 400 MHz): δ 7.76 (d, *J* = 8 Hz, 1H), 7.69-7.63 (m, 2H), 7.55 (d, *J* = 8 Hz, 1H), 4.83 (t, *J* = 8 Hz, 2H), 3.11 (s, 3H), 2.25-2.07 (m, 4H), 1.99-1.91 (m, 2H),1.57-1.50 (m, 2H), 1.40-1.31 (m, 4H), 1.24-1.10 (m, 16H) 0.91-0.79 (m, 11H), 0.66-0.61 (m, 2H); ^{13}CNMR (CDCl$_3$, 100 MHz): δ195.7, 142.2, 138.9, 130.3, 129.9, 123.8, 115.5, 63.9, 50.5, 37.5, 31.7, 31.3, 31.2, 29.5, 29.2, 29.1, 28.7, 26.7, 24.1, 22.6, 22.5, 17.2, 14.1, 14.0; HRMS (*m/z*): [M]$^+$ calculated for C$_{29}$H$_{50}$N$^+$: 412.3938; found: 412.3941.

3-Decyl-3-dodecyl-1-hexyl-2-methyl-3H-indol-1-ium iodide (6c): Started with **5c** (0.25 g, 0.57 mmol) and 1-iodohexane (0.24 g, 1.14 mmol), reaction time: 48 h, Yield: 0.23 g, 62 %. ^{1}H NMR (CDCl$_3$, 500 MHz): δ 7.75 (d, *J* = 10 Hz, 1H), 7.67-7.62 (m, 2H), 7.53-7.52 (m, 1H), 4.87 (t, *J* =

7.5 Hz, 2H), 3.14 (s, 3H), 2.22-2.15 (m, 2H), 2.12-2.06 (m, 2H), 1.97-1.90 (m, 2H), 1.56-1.50 (m, 2H), 1.38-1.31 (m, 4H), 1.27-1.13 (m, 32H), 0.90-0.84 (m, 9H), 0.83-0.79 (m, 2H), 0.67-0.59 (m, 2H); ^{13}CNMR (CDCl$_3$, 125 MHz): δ195.3, 141.9, 138.5, 129.8, 129.4, 123.3, 115.1, 63.4, 50.2, 37.0, 31.5, 31.0, 29.3, 29.2, 29.1, 29.0, 28.9, 28.7, 23.7, 22.3, 22.0, 16.9, 13.7, 13.6; HRMS (*m/z*): [M]$^+$ calculated for C$_{37}$H$_{66}$N$^+$: 524.5190; found: 524.5203.

3-Decyl-1,3-didodecyl-2-methyl-3H-indol-1-ium iodide (6d): Dissolved 1-iodododecane (0.4 g, 1.36 mmol) and **5c** (0.4 g, 0.91 mmol) in 5 mL of CH$_3$CN in a 50 mL round bottom flask and refluxed under inert atmosphere for 48 h, after cooling solvent were evaporate through Rota vapor. The reaction mixture washed with *n*-pentane (3× 10 mL) to afford the required compound as a brown-red color viscous liquid. Yield: 0.28 g, 57 %. ^{1}H NMR (CDCl$_3$, 400 MHz): δ 7.75 (d, *J* = 8 Hz, 1H), 7.67-7.61 (m, 2H), 7.53-7.51 (m, 1H), 4.88 (t, *J* = 8 Hz, 2H), 3.14 (s, 3H), 2.22-2.05 (m, 4H), 1.97-1.89 (m, 2H), 1.74 (b, 2H), 1.54-1.46 (m, 2H), 1.38-1.34 (m, 2H), 1.28-1.12 (m, 44H), 0.89-0.76 (m, 11H), 0.68-0.57 (m, 2H); ^{13}CNMR (CDCl$_3$, 100 MHz): δ195.7, 142.3, 138.8, 130.1, 129.7, 123.6, 115.4, 63.7, 50.5, 37.3, 31.9, 31.8, 29.6, 29.5, 29.4, 29.3, 29.2, 29.0, 28.6, 26.9, 24.0, 22.7, 22.6, 17.3, 14.1; HRMS (*m/z*): [M]$^+$ calculated for C$_{43}$H$_{78}$N$^+$: 608.6129; found: 608.6129.

3-Decyl-3-dodecyl-1,2-dimethyl-3H-indol-1-ium iodide (6e): MeI (0.29 g, 2.05 mmol) and **5c** (0.3 g, 0.68 mmol) were dissolved in 5 mL of CH$_3$CN in a 50 mL round bottom flask and refluxed under inert atmosphere for 10 h, after cooling solvent were evaporate through Rota vapor. Yield: 0.35 g, 88 %. ^{1}H NMR (CDCl$_3$, 500 MHz): δ 7.84 (d, *J* = 7.6 Hz, 1H), 7.63 (m, 2H), 7.49 (d, *J* = 7.2 Hz, 1H), 4.46 (s, 3H), 3.16 (s, 3H), 2.19-2.13 (m, 2H), 2.09-2.03 (m, 2H), 1.63-1.58 (m, 2H), 1.48-1.43 (m, 2H), 1.32-1.14 (m, 28H), 0.89-0.84 (m, 8H), 0.72-0.65 (m, 2H); ^{13}CNMR (CDCl$_3$, 125 MHz): δ196.1, 143.0, 138.5, 130.0, 129.7, 123.4, 115.4, 63.7, 45.3, 38.0, 37.0, 32.2, 31.9, 31.8, 29.7, 29.6, 29.4, 29.3, 29.2, 29.1, 29.0, 27.3, 24.1, 22.7, 22.6, 17.3, 14.1; HRMS (*m/z*): [M]$^+$ calculated for C$_{32}$H$_{56}$N$^+$: 454.4407; found: 454.4400.

3-Butoxy-4-[[3-decyl-1,3-didodecylindolin-2-ylidene]methyl]-3-cyclobutene-1,2-dione (7): 6d (0.7 g, 0.95 mmol) were dissolved in 5 mL of *n*-BuOH, NEt$_3$ (0.144 g, 1.42 mmol) added to RB flask dropwise. 3,4-dibutoxycyclobut-3-ene-1,2-dione (0.22 g, 0.95 mmol) added and stirred for 20 h at room temperature. The reaction mixture was further heated to 70 ^{o}C for 3 h, cooled and

solvent evaporate through Rota vapor. Column chromatography (SiO$_2$, 100-200 mesh, 1.5 % ethyl-acetate and 98.5 % Hexane) to furnish the required compound as yellow solid.[44] Yield: 0.45 g, 62 %. Mp: 71 ^{o}C. ^{1}H NMR (CDCl$_3$, 200 MHz): δ 7.31-7.18 (m, 2H), 7.07 (t, J = 8 Hz, 1H), 6.85 (d, J = 8 Hz, 1H), 5.51 (s, 1H), 4.87 (t, J = 8 Hz, 2H), 3.82 (t, J = 8 Hz, 2H), 2.56-2.41 (m, 2H), 1.94-1.78 (m, 4H), 1.58-1.47 (m, 2H), 1.43-0.97 (m, 55H), 0.91-0.82 (m, 11H), 0.58-0.46 (m, 2H); ^{13}C NMR (CDCl$_3$, 100 MHz): δ 192.8, 187.3, 186.8, 173.0, 166.2, 144.5, 137.2, 127.6, 122.5, 122.0, 108.0, 81.6, 73.6, 57.0, 42.9, 39.5, 32.1, 31.9, 31.8, 29.7, 29.6, 29.5, 29.5, 29.4, 29.4, 29.3, 29.3, 29.2, 27.2, 26.5, 23.9, 22.7, 22.6, 18.7, 14.1, 13.7.

2,3,3-Trimethyl-3H-indole-5-carboxylic acid (9a): 4-Hydrazinobenzoic acid hydrochloride **8** (4.0 g, 21.2 mmol.) and 3-methyl-2-butanone (3.3 g, 38.18 mmol) were dissolved in acetic acid (40mL) in a 100 mL round bottom flask and reflux for 12 h under nitrogen atmosphere, after cooling solvent were evaporate through Rota vapor. Column chromatography (100–200 mesh SiO$_2$, MeOH 2 %, CH$_2$Cl$_2$ 98 %) light brown color solid compound.[58] Yield: 3.2 g, 74 %. ^{1}H NMR (DMSO-d_6, 200 MHz): δ 8.0 (s, 1H), 7.93 (d, J = 8 Hz, 1H), 7.52 (d, J = 8 Hz, 1H), 2.26 (s, 3H), 1.28 (s, 6H).

2-Methyl-3-butyl-3-ethyl-3H-indole-5-carboxylic acid (9b): 4-Hydrazinobenzoic acid hydrochloride **8** (1.91 g, 10.13 mmol.) and **4a** (1.73 g, 12.16 mmol) were dissolved in acetic acid (20mL) in a 50 mL round bottom flask and reflux for 24 h under nitrogen atmosphere, after cooling solvent were evaporate through Rota vapor. Column chromatography (100–200 mesh SiO$_2$, MeOH 1.3 %, CH$_2$Cl$_2$ 98.7 %), colorless solid. Yield: 0.8 g, 30 %. ^{1}H NMR (CDCl$_3$, 400 MHz): δ 8.16 (d, J = 8 Hz, 1H), 7.98 (s, 1H),7.67 (d, J = 8 Hz, 1H), 2.31 (s, 3H), 2.08-1.94 (m, 2H), 1.89-1.76 (m, 2H), 1.14 (m, 2H), 0.75 (t, J = 8 Hz, 3H), 0.70-0.54 (m, 2H), 0.38 (t, J = 8 Hz, 3H); ^{13}C NMR (CDCl$_3$, 125 MHz): δ 191.3, 171.6, 159.2, 142.0, 130.9, 126.4, 123.4, 119.4, 63.6, 36.4, 29.8, 25.9, 22.8, 16.1, 13.7, 8.1; HRMS (m/z): [M + H]$^+$ calculated for C$_{16}$H$_{22}$O$_2$N: 260.1645; found: 260.1639.

5-Carboxy-1,2,3,3-tetramethyl-3H-indol-1-ium iodide (10a): 1-Iodomethane (4.19 g, 29.5 mmol) and **9a** (2 g, 9.84 mmol) were dissolved in 10 mL of CH$_3$CN in a 50 mL of round bottom flask and heated at 80 ^{o}C for 4 h under inert atmosphere, after cooling solvent were evaporate through Rota vapor. Obtained precipitate was washed with diethyl ether (4 × 20 mL) to afford the

required colorless solid compound. Compound **10a** used for next step without purification.[59] Yield: 2.95 g, 87 %. ^{1}H NMR (DMSO-d_6, 200 MHz): δ 8.38 (s, 1H), 8.2 (d, J = 8 Hz, 1H), 8.03 (d, J = 8 Hz, 1H), 4.01 (s, 3H), 2.83 (s, 3H), 1.58 (s, 6H).

5-Carboxy-1,3-dibutyl-3-ethyl-2-methyl-3H-indolium iodide (10b): 1-Iodobutane (0.82 g, 4.48 mmol) and **9b** (0.29 g, 1.12 mmol) were dissolved in 5 mL of CH_3CN in a 50 mL round bottom flask and reflux under inert atmosphere for 24 h, after cooling solvent were evaporate through Rota vapor. Obtained precipitate was washed with hexane (3 × 30 mL) to afford the required brown color solid compound. Compound **10b** used for next step without purification. Yield: 0.4 g, 81 %. ^{1}H NMR (Acetone-d_6, 200 MHz): δ 8.41-8.33 (m, 3H), 4.92 (t, J = 8 Hz, 2H), 3.30 (s, 3H), 2.65-2.35 (m, 4H), 1.63 (m, 2H), 1.30-1.14 (m, 2H), 1.03 (t, J = 8 Hz, 3H), 0.97-0.85 (m, 2H), 0.76 (t, J = 7 Hz, 3H), 0.70-0.60 (m, 2H), 0.53 (t, J = 7 Hz, 3H); ^{13}CNMR (Acetone-d_6, 125 MHz): δ199.8, 167.0, 145.9, 139.2, 131.2, 131.0, 125.0, 115.9, 64.9, 49.0, 36.2, 30.1, 25.8, 22.3, 19.8, 15.1, 13.3, 12.8 ,7.9; HRMS (*m/z*): [M]$^+$ calculated for $C_{20}H_{30}O_2N^+$: 316.2271; found: 316.2266.

3-Butoxy-4-[[5-carboxy-(1-methyl-1,3-dihydro-3,3-dimethyl-2H-indol-2-ylidene)]methyl]-3-cyclobutene-1,2-dione (11): 10a (1.5 g, 4.34 mmol) were dissolved in 10 mL of *n*-BuOH in a 100 mL of round bottom flask, NEt$_3$ (0.99 g, 9.78 mmol) added to the above solution dropwise. 3,4-dibutoxycyclobut-3-ene-1,2-dione (0.98 g, 4.34 mmol) added and stirred for 20 h at room temperature. The reaction mixture was further heated to 70 °C for 3 h, after cooling solvent were evaporate through Rota vapor. Column chromatography (SiO$_2$, 100-200 mesh, 3.5 % MeOH and 96.5 % CH_2Cl_2), light-yellow solid. Yield: 1.07 g, 67 %. Mp: 220 °C. ^{1}H NMR (DMSO-d_6, 400 MHz): δ 12.72 (s, 1H), 7.93 (s, 1H), 7.91 (d, J = 8 Hz, 1H), 7.25 (d, J = 8 Hz, 1H), 5.39 (s, 1H), 4.8 (t, J = 8 Hz, 2H), 3.41 (s, 3H), 1.83-1.76 (m, 2H), 1.57 (s, 6H), 1.47-1.4 (m, 2H), 0.94 (t, J = 6 Hz, 3H); ^{13}C NMR (DMSO-d_6, 100 MHz): δ 191.9, 188.8, 187.3, 172.2, 167.8, 167.0, 146.7, 140.1, 130.1, 124.3, 122.7, 108.4, 82.3, 73.5, 46.6, 31.3, 29.9, 26.3, 18.0, 13.4; HRMS (*m/z*): [M + H]$^+$ calculated for $C_{21}H_{24}NO_5$: 370.1649; found: 370.1651.

3-[[5-Carboxy-(1-methyl-1,3-dihydro-3,3-dimethyl-2H-indol-2-ylidene)methyl]]-4-hydroxy-cyclobutene-1,2-dione (12): Compound **11** (1.83 g, 4.96 mmol) was taken in 100 mL of round bottom flask, and dissolved with 20 mL acetone, further 6 mL of 2N-HCl was added to it and

refluxed for 10 h, after cooling solvent were evaporate through Rota vapor to afford the required compounds as a dark yellow solid. Yield: 1.4 g, 90 %. Mp: 288 °C. ^{1}H NMR (DMSO-d_6, 500 MHz): δ 7.88 (m, 2H), 7.17 (d, J = 10 Hz, 1H), 5.55 (s, 1H), 3.37 (s, 3H), 1.58 (s, 6H); ^{13}C NMR (DMSO-d_6, 125 MHz): δ 193.6, 192.9, 174.4, 167.7, 165.8, 147.7, 140.5, 130.7, 124.0, 123.2, 108.3, 83.9, 46.7, 30.2, 27.1; HRMS (m/z): [M + H]$^+$ calculated for $C_{17}H_{16}NO_5$: 314.1023; found: 314.1012.

Synthesis of unsymmetrical SQS dyes, 13a-c: Compound **6a-c** (1 equiv.), and **12** (1 equiv.) were dissolved in *n*-butanol and anhydrous PhMe (1:1, 8 mL each) in a 50 mL of round bottom flask, charged with Dean-Stark apparatus and refluxed under inert atmosphere for 24 h, after cooling solvent were evaporate through Rota vapor. The reaction mixture was subjected to column chromatography to afford the required dye as blue color solid.

5-Carboxy-2-[[3-[(1,3-dihydro-3-butyl-3-ethyl-1-hexyl-2H-indol-2-ylidene)methyl]-4-oxo-2-cyclobuten-2-olate-1-ylidene]methyl]-1,3,3-trimethyl-3H-indolium (13a): Started with **6a** (0.2 g, 0.48 mmol) and **12** (0.15 g, 0.48 mmol), reaction time: 24 h, column chromatography (SiO$_2$, 100-200 mesh, from 3.5 % MeOH and 96.5 % CH$_2$Cl$_2$). Yield: 0.14 g (golden blue color solid), 49 %. Mp: 182 °C. ^{1}H NMR (CDCl$_3$, 400 MHz): δ 8.12 (d, J = 8 Hz, 1H), 8.06 (s, 1H), 7.36-7.33 (m, 2H), 7.24 (t, J = 8 Hz, 1H), 7.06 (d, J = 8 Hz, 1H), 6.97 (d, J = 8 Hz, 1H), 6.20 (s, 1H), 5.99 (s, 1H), 4.12 (b, 2H), 3.51 (s, 3H), 3.01(b, 2H), 2.12-2.00 (m, 2H), 1.85-1.77 (m, 8H), 1.48-1.40 (m, 2H), 1.36-1.26 (m, 4H), 1.17-1.06 (m, 2H), 0.87 (t, J = 8 Hz, 3H),0.79-0.73 (m, 1H),0.68 (t, J = 8 Hz, 3H), 0.52-0.45 (m, 1H), 0.35 (t, J = 8 Hz, 3H); ^{13}C NMR (CDCl$_3$,100 MHz): δ 182.4, 176.4, 170.9, 170.4, 168.5, 147.5, 144.0, 141.8, 139.0, 131.2, 128.2, 128.0, 124.7, 124.0, 122.6, 109.8, 108.0, 88.3, 88.0, 59.9, 48.2, 44.3, 39.5, 33.2, 31.5, 30.4, 27.5, 27.3, 26.8, 26.4, 22.7, 22.5, 14.0, 13.8, 8.5; IR (KBr cm^{-1}): 2929, 2862, 1699, 1596, 1568, 1498, 1466, 1355, 1274, 1217, 1178, 1088, 1059, 938; HRMS (m/z): [M + H]$^+$ calculated for $C_{38}H_{47}N_2O_4$: 595.3530; found: 595.3529.

5-Carboxy-2-[[3-[(1,3-dihydro-1,3-dihexyl-3-octyl-2H-indol-2-ylidene)methyl]-4-oxo-2-cyclobuten-2-olate-1-ylidene]methyl]-1,3,3-trimethyl-3H-indolium (13b): Started with **6b** (0.2 g, 0.38 mmol) and **12** (0.12 g, 0.38 mmol), reaction time: 24 h, column chromatography (SiO$_2$, 100-200 mesh, from 3 % MeOH and 97 % CH$_2$Cl$_2$). Yield: 0.13 g (blue color solid), 48

%. Mp: 130 °C. ^{1}H NMR (CDCl$_3$, 400 MHz): δ 8.12 (d, J = 8 Hz, 1H), 8.05 (s, 1H), 7.38-7.32 (m, 2H), 7.23 (t, J = 8 Hz, 1H), 7.06 (d, J = 8 Hz, 1H), 6.96 (d, J = 12 Hz, 1H), 6.18 (s, 1H), 5.99 (s, 1H), 4.11 (b, 2H), 3.51 (s, 3H), 3.01(b, 2H), 2.06-1.98 (m, 2H), 1.84 (s, 6H), 1.81 (m, 2H), 1.44 (b, 2H), 1.29 (b, 4H), 1.19-1.05 (m, 16H), 0.87 (t, J = 8 Hz, 3H), 0.80-0.72 (m, 8H), 0.50-0.42 (b, 2H); ^{13}C NMR (CDCl$_3$, 100 MHz): δ 183.5, 176.2, 171.2, 170.4, 168.3, 147.5, 143.8, 141.7, 139.3, 131.1, 127.8, 124.9, 124.6, 123.9, 122.4, 109.8, 107.9, 88.3, 88.0, 59.3, 48.1, 39.9, 31.7, 31.4, 29.5, 29.2, 29.1, 29.0, 27.2, 26.8, 23.9, 22.5, 22.4, 14.0, 13.9; IR (KBr cm^{-1}): 2925, 2855, 1699, 1597, 1567, 1499, 1466, 1355, 1273, 1226, 1174, 1093, 1058, 936; HRMS (m/z): [M + H]$^+$ calculated for C$_{46}$H$_{63}$N$_2$O$_4$: 707.4782; found: 707.4769.

5-Carboxy-2-[[3-[(1,3-dihydro-3-decyl-3-dodecyl-1-hexyl-2H-indol-2-ylidene)methyl]-4-oxo-2-cyclobuten-2-olate-1-ylidene]methyl]-1,3,3-trimethyl-3H-indolium (13c): Started with **6c** (0.2 g, 0.31 mmol) and **12** (0.97 g, 0.31 mmol), reaction time: 24 h, column chromatography (SiO$_2$, 100-200 mesh, 2.8 % MeOH and 97.2 % CH$_2$Cl$_2$). Yield: 0.12 g (blue color solid), 48 %. Mp: 122 °C. ^{1}H NMR (CDCl$_3$, 500 MHz): δ 8.13 (d, J = 10 Hz, 1H), 8.07 (s, 1H), 7.35 (t, J = 7.5 Hz, 1H), 7.33 (d, J = 10 Hz, 1H), 7.23 (t, J = 7.5 Hz, 1H), 7.06 (d, J = 10 Hz, 1H), 6.97 (d, J = 10 Hz, 1H), 6.20 (s, 1H), 6.01 (s, 1H), 4.13-4.03 (b, 2H), 3.52 (s, 3H), 3.01 (b, 2H), 2.05-1.99 (m, 2H), 1.85 (s, 6H), 1.81(m, 2H), 1.43 (m, 2H), 1.30 (m, 4H), 1.23-1.05 (m, 32H), 0.88-0.81 (m, 9H), 0.78-0.71 (b, 2H), 0.50-0.42 (b, 2H); ^{13}C NMR (CDCl$_3$, 125 MHz): δ 182.2, 176.1, 171.2, 170.4, 168.4, 147.4, 143.9, 141.8, 139.4, 131.1, 127.8, 124.7, 124.1, 123.9, 122.4, 109.8, 107.9, 88.4, 88.0, 59.4, 48.1, 44.2, 39.9, 31.8, 31.5, 29.6, 29.5, 29.4, 29.3, 29.2, 27.3, 26.8, 22.6, 22.5, 18.6, 14.0, 13.9, 13.6; IR (KBr cm^{-1}): 2924, 2854, 1699, 1596, 1568, 1498, 1465, 1355, 1273, 1226, 1181, 1095, 1058, 937; HRMS (m/z): [M + H]$^+$ calculated for C$_{54}$H$_{79}$N$_2$O$_4$: 819.6034; found: 819.6057.

5-Carboxy-2-[[3-[(1,3-dihydro-3-decyl-1,3-didodecyl-2H-indol-2-ylidene)methyl]-4-oxo-2-cyclobuten-2-olate-1-ylidene]methyl]-1,3,3-trimethyl-3H-indolium (13d): Compound **6d** (0.187 g, 0.26 mmol) and **12** (0.08 g, 0.26 mmol) were dissolved in n-butanol and anhydrous PhMe (1:1, 8 mL each) in a 50 mL of round bottom flask, charged with Dean-Stark apparatus and refluxed under inert atmosphere for 24 h, after cooling solvent were evaporate through Rota vapor. The reaction mixture was subjected to column chromatography (SiO$_2$, 100-200 mesh, 2.5 % MeOH and 97.5 % CH$_2$Cl$_2$) to afford the required dye as blue color solid. Yield: 0.08 g, 35 %.

Mp: 120 °C. ^{1}H NMR (CDCl$_3$, 400 MHz): δ 8.13 (d, J = 8 Hz, 1H), 8.07 (s, 1H), 7.36 (t, J = 8 Hz, 1H), 7.33 (d, J = 8 Hz, 1H), 7.23 (t, J = 8 Hz, 1H), 7.06 (d, J = 8 Hz, 1H), 6.97 (d, J = 8 Hz, 1H), 6.21 (s, 1H), 6.02 (s, 1H), 4.12 (b, 2H), 3.52 (s, 3H), 3.02 (b, 2H), 2.07-1.99 (m, 2H), 1.85 (s, 6H), 1.82 (m, 2H), 1.42 (m, 2H), 1.31-1.05 (m, 48H), 0.89-0.80 (m, 9H), 0.77-0.72 (b, 2H), 0.51-0.44 (b, 2H); ^{13}C NMR (CDCl$_3$, 100 MHz): δ 182.0, 176.0, 171.2, 170.3, 168.4, 147.4, 143.9, 141.8, 139.4, 131.1, 127.8, 124.7, 124.3, 123.9, 122.4, 109.9, 107.9, 88.4, 88.0, 59.4, 48.1, 44.2, 39.9, 31.9, 31.8, 29.6, 29.5, 29.4, 29.3, 29.2, 27.3, 27.2, 24.0, 22.6, 14.1: IR (cm^{-1}): 2921, 2851, 1699, 1598, 1567, 1488, 1462, 1354, 1265, 1200, 1179, 1079, 1048, 933.

5-Carboxy-2-[[3-[(1,3-dihydro-3-decyl-3-dodecyl-1-methyl-2H-indol-2-ylidene)methyl]-4-oxo-2-cyclobuten-2-olate-1-ylidene]methyl]-1,3,3-trimethyl-3H-indolium (13e): Compound **6e** (0.34 g, 0.57 mmol) and **12** (0.15 g, 0.48 mmol) dissolved in *n*-butanol and anhydrous PhMe (1:1, 8 mL each) in a 50 mL round bottom flask, charged with Dean-Stark apparatus and refluxed under inert atmosphere for 24 h, after cooling solvent were evaporate through Rota vapor. The reaction mixture was subjected to column chromatography (SiO$_2$, 100-200 mesh, 2.8 % MeOH and 97.2 % CH$_2$Cl$_2$) to afford the required dye. Yield: 180 mg, 50 %. Mp: 132 °C. ^{1}H NMR (CDCl$_3$, 500 MHz): δ 8.13 (d, J = 8.8 Hz, 1H), 8.07 (s, 1H), 7.36 (t, J = 7.5 Hz, 1H), 7.32 (d, J = 7 Hz, 1H), 7.23 (t, J = 7.2 Hz, 1H), 7.08 (d, J = 7 Hz, 1H), 6.98 (d, J = 8 Hz, 1H), 6.17 (s, 1H), 6.02 (s, 1H), 3.65 (b, 3H), 3.53 (s, 3H), 3.01 (b, 1H), 2.03 (m, 2H), 1.85 (s, 6H), 1.25-1.06 (m, 33H), 0.86-0.73 (m, 8H), 0.53-0.48 (b, 2H); ^{13}CNMR (CDCl$_3$, 125 MHz): δ 182.0, 177.1, 172.0, 170.1, 168.9, 147.3, 144.4, 141.8, 139.2, 131.1, 127.9, 124.7, 124.5, 123.9, 122.4, 109.6, 108.0, 88.4, 88.1, 59.3, 48.2, 40.2, 31.8, 30.4, 29.6, 29.5, 29.4, 29.3, 29.2, 27.2, 24.0, 22.6, 14.1; IR (KBr cm^{-1}): 2922, 2852, 1699, 1592, 1566, 1497, 1477, 1357, 1272, 1218, 1156, 1093, 1058, 938; HRMS (*m/z*): [M + H]$^+$ calculated for C$_{49}$H$_{69}$N$_2$O$_4$: 749.5252; found: 749.5228.

5-Carboxy-2-[[3-[(1,3-dihydro-3-decyl-1,3-didodecyl-2H-indol-2-ylidene)methyl]-4-oxo-2-cyclobuten-2-olate-1-ylidene]methyl]-1,3-dibutyl-3-ethyl-3H-indolium (13f): Compound **10b** (0.12 g, 0.27 mmol) and **7** (0.2 g, 0.27 mmol) were dissolved in *n*-butanol and anhydrous PhMe (1:1, 8 mL each) in a 50 mL of round bottom flask, 0.5 mL of pyridine added to the above mixture and charged with Dean-Stark apparatus, refluxed under inert atmosphere for 24 h, after cooling reaction mixture was diluted with CH$_2$Cl$_2$ (50 mL) and 2N HCl (50 mL), the collective organic layer was dried over Na$_2$SO$_4$ and solvent evaporate through Rota vapor. The reaction

mixture was subjected to column chromatography (SiO$_2$, 100-200 mesh, 2.2 % MeOH and 97.8 % CH$_2$Cl$_2$) to afford the required dye as blue color solid. Yield: 0.09 g, 33 %. Mp: 138 ^{o}C. ^{1}H NMR (CDCl$_3$, 400 MHz): δ 8.13 (d, J = 8 Hz, 1H), 7.99 (s, 1H), 7.36-7.31 (m, 2H), 7.23-7.20 (m, 1H), 7.03 (d, J = 8 Hz, 1H), 6.94 (d, J = 8 Hz, 1H), 6.15 (s, 1H), 6.13 (s, 1H), 4.06-3.97 (m, 4H), 3.06-2.99 (m, 4H), 2.14-1.97 (m, 4H), 1.84-1.74 (m, 4H), 1.49-1.39 (m, 4H), 1.31-1.05(m, 50H), 0.99 (t, J = 8 Hz, 3H), 0.89-0.81 (m, 9H), 0.79-0.75 (m, 3H), 0.69 (t, J = 8 Hz, 3H), 0.58-0.44 (m, 3H), 0.39 (t, J = 8 Hz, 3H); ^{13}C NMR (CDCl$_3$, 100 MHz): δ 181.6, 176.5, 170.8, 170.6, 165.6, 149.1, 144.0, 139.3, 138.2, 131.1, 127.8, 124.4, 124.0, 123.8, 122.4, 109.6, 107.8, 88.6, 88.2, 59.2, 58.2, 44.1, 43.4, 40.0, 39.7, 33.3, 31.9, 31.8, 29.6, 29.5, 29.4, 29.3, 29.2, 29.1, 27.5, 27.2, 26.6, 24.1, 22.8, 22.7, 22.6, 20.47, 14.1, 13.9, 13.8, 8.5; IR (KBr cm^{-1}): 2923, 2853, 1699, 1591, 1570, 1493, 1463, 1375, 1266, 1251, 1179, 1159, 1098, 1076, 967, 949.

2.3 RESULTS AND DISCUSSION

2.3.1 Synthesis of SQS dyes. Synthetic scheme of SQS dyes (SQS1-SQS6) is displayed in **Scheme 1**. Un-symmetrical squaraine dyes were synthesized by condensation of semi-squaric acid and indolium salt. Branched ketones with various alkyl groups and phenyl hydrazine react and give the indolenine derivative (**5**). Branched ketones, 3-ethylhept-2-one (**4a**), 3-hexylundecan-2-one (**4b**), and 3-decylpentadecan-2-one (**4c**) were synthesized from 2-ethylhexanol, 2-hexyldecanol and 2-decyltetradecanol, respectively.

2.3.2 Photophysical properties. SQS dyes were freely soluble in CHCl$_3$, CH$_2$Cl$_2$, and EtOH and partially soluble in CH$_3$CN. The absorption and emission spectra (excited at 610 nm) of **SQS** dyes were measured in dichloromethane are showed in **Figure 2a** (**Table 1**). The UV-vis spectra of **SQS1-SQS4** (Y-type dyes) in dichloromethane solution showed λ$_{max}$ at 643 nm whereas, **SQS5** (V-type dye) and **SQS6** (Y-type dye) showed λ$_{max}$ at 642 and 650 nm, respectively corresponding to intramolecular charge transfer (π−π*) transition with the extinction coefficient of 2.9-3.5×10^5 M^{-1}cm^{-1} and emission maximum shown at 652, 652, 652, 651, 650 and 657 nm, respectively. The absorption spectra of SQS4 on the ZrO$_2$ with various dipping time are

displayed in **Figure 2b**. It is observed that the formation of H-aggregate centered at 603 nm increased progressively with the dipping time.

Light harvesting efficiency (LHE) profiles indicates that the fraction of radiation absorbed at a definite wavelength by the particular dye.[60] LHE profile of SQS1 to SQS6 dyes on TiO$_2$ is displayed in **Figure 2c** and LHE $\Delta\lambda$ at 50% given in **Table 1**. For SQS1 to SQS3 spectral broadening at 50% of LHE decreases ($\Delta\lambda$ = 183, 168, 158 nm) with increasing the chain length of sp^3-C alkyl groups, whereas in the case of SQS4, SQS5 and SQS6, the spectral broadening is $\Delta\lambda$ = 170, 176 and 139 nm respectively at 50% of LHE. Thus, aggregation of sensitizers on TiO$_2$ surface are depends on the length as well as the location of the branched alkyl groups.
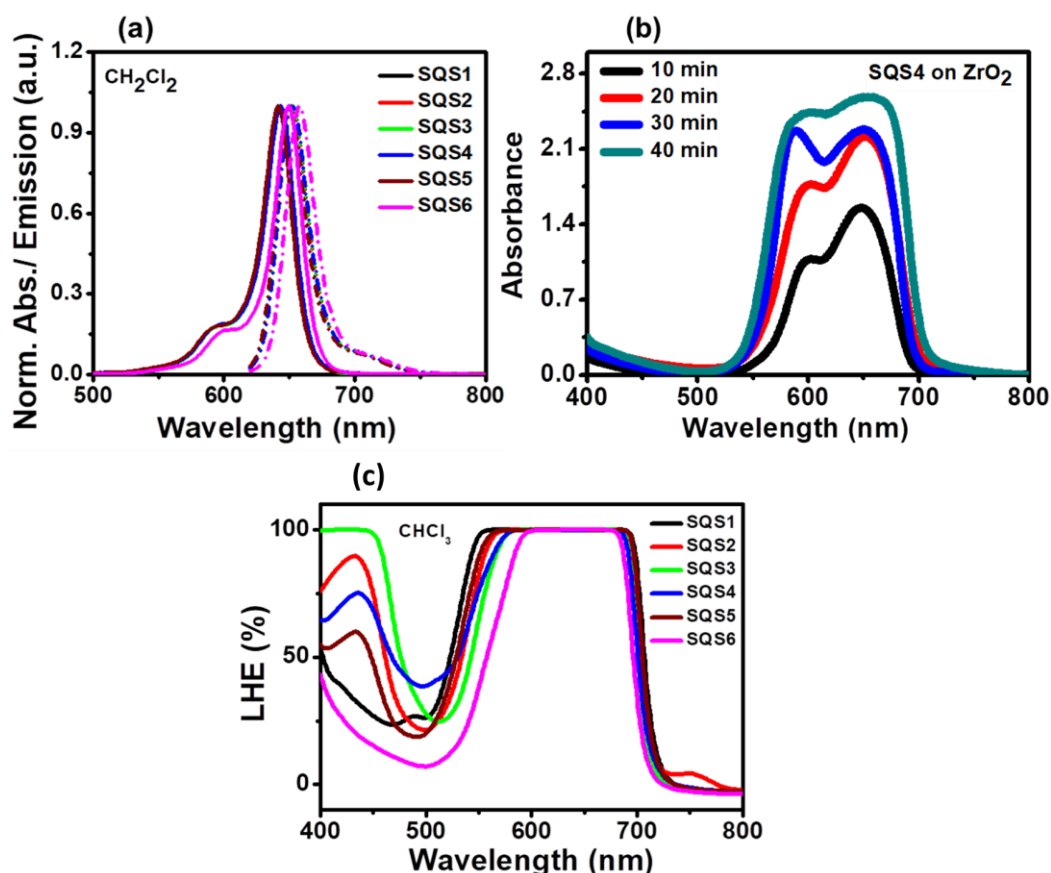
Figure 2. (a) Normalized UV-vis (solid) and fluorescence (dotted) spectra of SQS dyes in CH$_2$Cl$_2$ solution, (b) absorbance of SQS4 dye on ZrO$_2$ electrodes with various dipping time, and (c) LHE (= 1 − 10^{-A}) profiles of SQS dyes on TiO$_2$ electrodes (electrodes were dipped in CHCl$_3$ for 12 h).

2.3.3 Electrochemical properties. The electrochemical properties of SQS dyes are measured in anhydrous CH_2Cl_2; the redox potentials of SQS dyes are calculated from cyclic voltammetry and display in **Figure 3a** and **Table 1**. The first ground-state oxidation potential (E_{HOMO}) was calculated from the oxidation potential vs Ferrocene/ Ferrocene$^+$ was converting into the NHE by adding 0.70 V.[61] For an ideal sensitizer, the LUMO of the sensitizer needs to be placed above the TiO_2 conduction band for the efficient charge injection, and HOMO of the sensitizer should poised below the redox function of the electrolytes for an efficient dye regeneration process. E_{HOMO} of SQS dyes are situated between 0.79 to 0.80 V, which are lower than the liquid iodolyte electrolyte redox function and favorable for dye regeneration. The E_{LUMO} was determined by subtracting the E_g (optical band gap) from E_{HOMO}, and the E_{LUMO} of SQS dyes are situated between -1.1 to -1.2 V, which are slightly above than TiO_2 conduction band and favorable for electron injection. SQS dyes E_{HOMO} and redox potential of liquid electrolyte I^-/I_3^- difference is ~ 400 mV, whereas E_{LUMO} and TiO_2 conduction band difference is ~ 620 mV shown in **Figure 3b**.
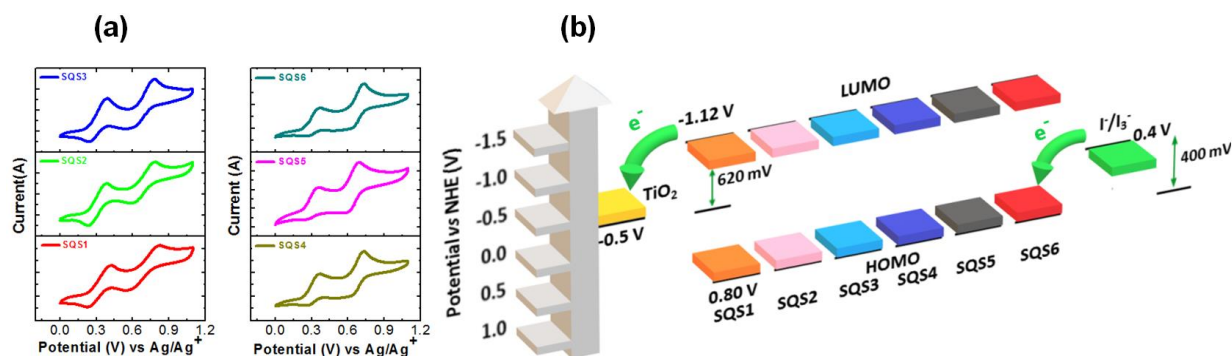
Figure 3. (a) Cyclic voltammograms of SQS dyes (CH_2Cl_2), and (b) schematic representation of energy level diagrams for SQS dyes.

2.3.4 Cyclic voltammetry on TiO_2 surface and dye desorption studies of SQS dyes. To understand the charge hopping process between the dye molecules on the TiO_2, CV studies were carried out on TiO_2 electrode. Cyclic voltammetry of SQS dyes on TiO_2 without CDCA is showed in **Figure 4a** and the peak current are provided in **Table 2**, and the results with CDCA displayed in **Figure 4c**. Graphical representation of peak current and amount of dyes adsorbed on TiO_2 surface without CDCA is provided in **Figure 4b**. Adsorption of SQS dyes in CH_3CN:

CHCl$_3$ (90%: 10%) without CDCA, path length of the cuvette was 0.1 cm^2 and 2 M HCl in EtOH was used to desorb adsorbed dyes. Area of the photoanode was 0.22 cm^2 and 6 μm thick for all dyes. UV-vis absorption spectra of desorbed SQS dyes are displayed in and **Table 2**.

Table 1. Photophysical and electrochemical characterization of SQS1 to SQS6 (Y and V-type squaraine dyes) at room temperature**.**

Dyes	$^a\lambda_{max}$ (nm)	$^b\lambda_{max}$ (nm)	ε (10^5 M^{-1} cm^{-1})	LHE Δλ at 50% (nm)	$^cE_{oxi/onset}$ (V vs Ag/Ag$^+$)	E_{HOMO} (V vs NHE)	E_{LUMO} (V vs NHE)	^dE_g (eV)	$E_{g/DFT}$ (eV)
SQS1	643	652	3.5	183	0.234	0.80	-1.11	1.91	2.18
SQS2	643	652	3.3	168	0.227	0.79	-1.12	1.91	2.18
SQS3	643	652	3.2	158	0.229	0.79	-1.11	1.91	2.20
SQS4	643	651	3.0	170	0.237	0.80	-1.10	1.91	2.18
SQS5	642	650	2.9	176	0.232	0.80	-1.11	1.92	2.18
SQS6	650	657	3.1	139	0.228	0.79	-1.10	1.90	2.16

^{a}absorption, ^{b}emission of SQS in dichloromethane, ^{c}oxidation potential, ^dE_g optical band gap (from the intersection point of absorption and fluorescence, 1240/λ).

Though the adsorbed dye on TiO$_2$ (thickness of electrode was 6 μm and area was 0.22 cm^2 for all dyes, dipping solution is CH$_3$CN: CHCl$_3$ (90%: 10%) and dipping for 6 h) is almost in the order of 1.96 - 2.29 × 10^{-7} mol/cm^2 for SQS1-SQS4, the peak current is decreased in the order of SQS1 (0.481 mA, 2.16 × 10^{-7} mol/cm^2)> SQS2 (0.245 mA, 2.29 × 10^{-7} mol/cm^2) > SQS3 (0.149 mA, 2.0 × 10^{-7} mol/cm^2) > SQS4 (0.131 mA, 1.96 × 10^{-7} mol/cm^2). Such a reduction of peak current for the similar amount of dyes on TiO$_2$ indicate the intermolecular electron hopping after initial oxidation of dye molecules across the TiO$_2$ nanoparticles.[62-64] Strong interaction between SQS1 dyes on TiO$_2$ leads facile intermolecular electron hopping and results strong current signal.

Periodical attenuation of intermolecular electron hopping is noticed by systematically changing the length of branched alkyl chains (SQS1 to SQS4, Y-type of dyes). Such controlled aggregation of dyes offers the advantage of spectral broadening due to aggregation and charge injection from aggregated state, where charge injection competes with self-quenching of photo excited dyes. In the case of SQS5 (V-type, 0.180 mA, 2.47×10^{-7} mol/cm^2), the amount of adsorbed dye is even more than SQS1, however the peak current is reduced drastically that indicates the well packed monolayer of dyes on TiO$_2$. Hence the monolayer formation with dyes SQS1, SQS4 and SQS5 on TiO$_2$ surface can be represented as in **Figure 5**.
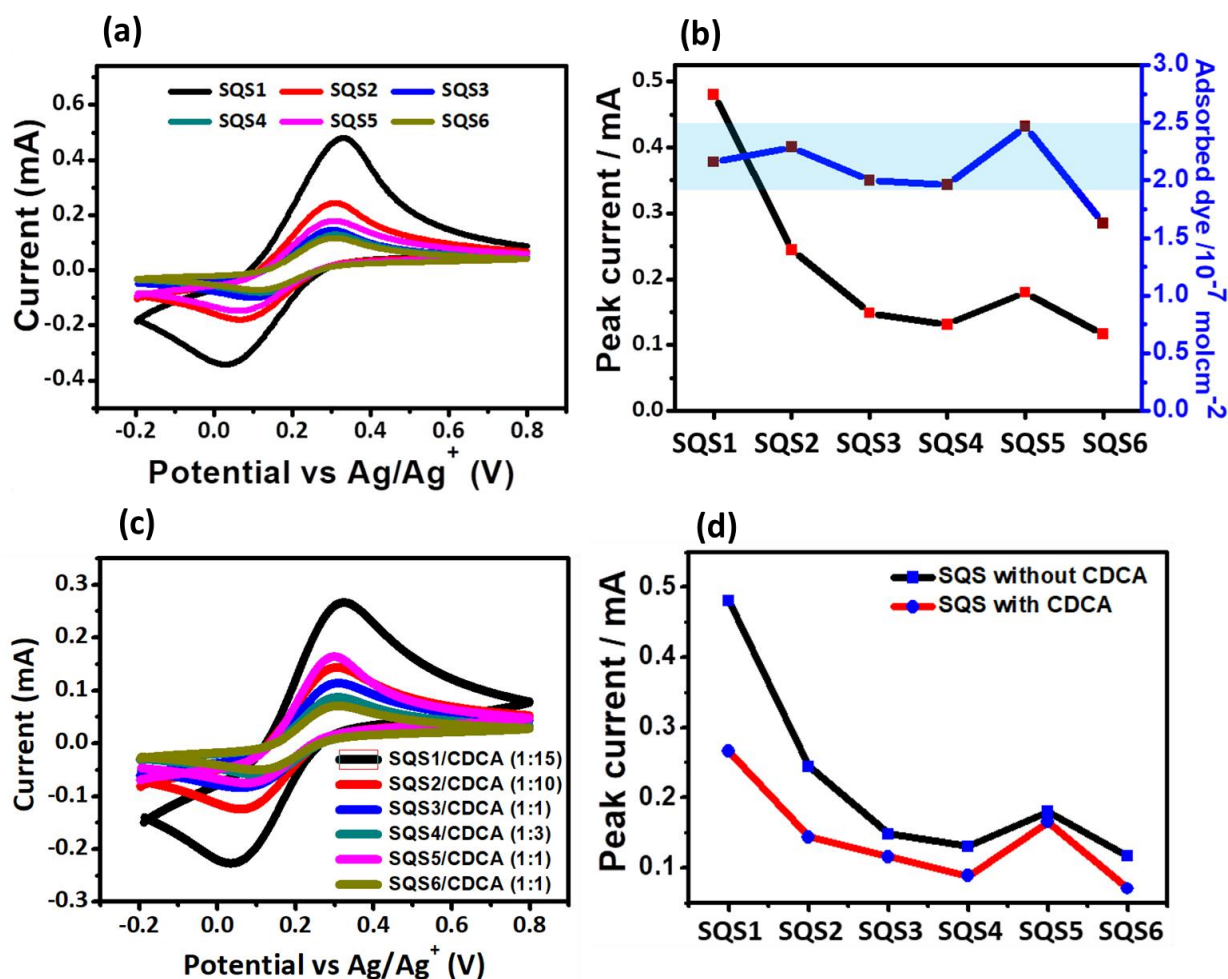
Figure 4. (a), and (C) Cyclic voltammograms of SQS dyes on TiO$_2$ (0.1M tetrabutylammonium perchlorate (C$_4$H$_9$)$_4$N(ClO$_4$) in CH$_3$CN) with and without CDCA, (b) peak current (mA, black line) and adsorbed dyes (10^{-7}mol/cm^2 blue line) on TiO$_2$ surface, (d) graphical comparisons of peak currents of SQS dyes without and with CDCA.
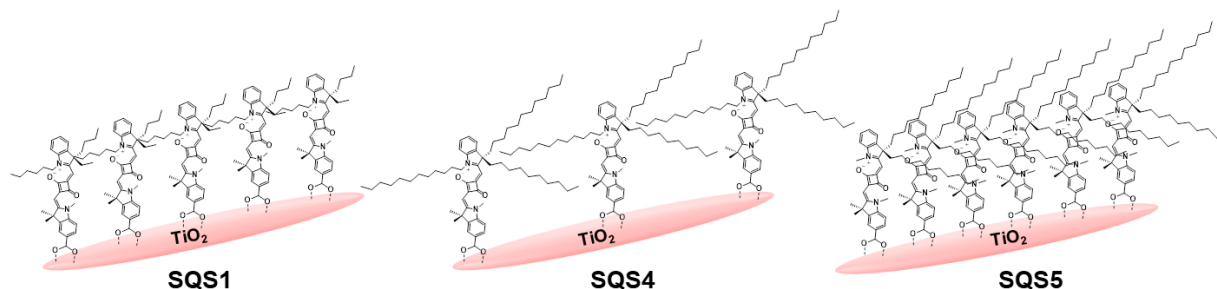
Figure 5. Simple diagrammatic representation of monolayer formation with dyes SQS1, SQS4 and SQS5 on the TiO₂ surface.

Table 2. Peak current (with and without CDCA) and desorption study of SQS1-6 at room temperature.

Dyes	Peak current (mA)	Dye amount (10^{-7}mol/cm^2)	Peak current with CDCA (mA)
SQS1	0.481	2.16	0.267 (1:15)
SQS2	0.245	2.29	0.144 (1:10)
SQS3	0.149	2.00	0.115 (1:1)
SQS4	0.131	1.96	0.089 (1:3)
SQS5	0.180	2.47	0.166 (1:1)
SQS6	0.117	1.63	0.071 (1:1)

2.3.5 Theoretical studies. To calculate the distribution of electron in SQS dyes, the structural minimization was carried out by density functional theory (DFT) at B3LYP[65-67] and 6-31G (d,p).[68] The distribution of electrons for SQS dyes (**Figure 6**, **7**), HOMO, HOMO-1, and LUMO density of electrons are mostly located on the part of squaric acid, whereas LUMO+1 density of electrons localized towards the anchoring. The HOMO-LUMO energy gap (E_g) of SQS dyes is provided in **Table 1**. The height of the dyes from anchoring group, distances between sp^3-C, sp^3-C and N-atom alkyl groups, and height of chenodeoxycholic acid (CDCA) shown in **Figure 8**, whereas dihedral angles measured from the minimized ground state geometry by DFT (**Figure 8, Table 3**).
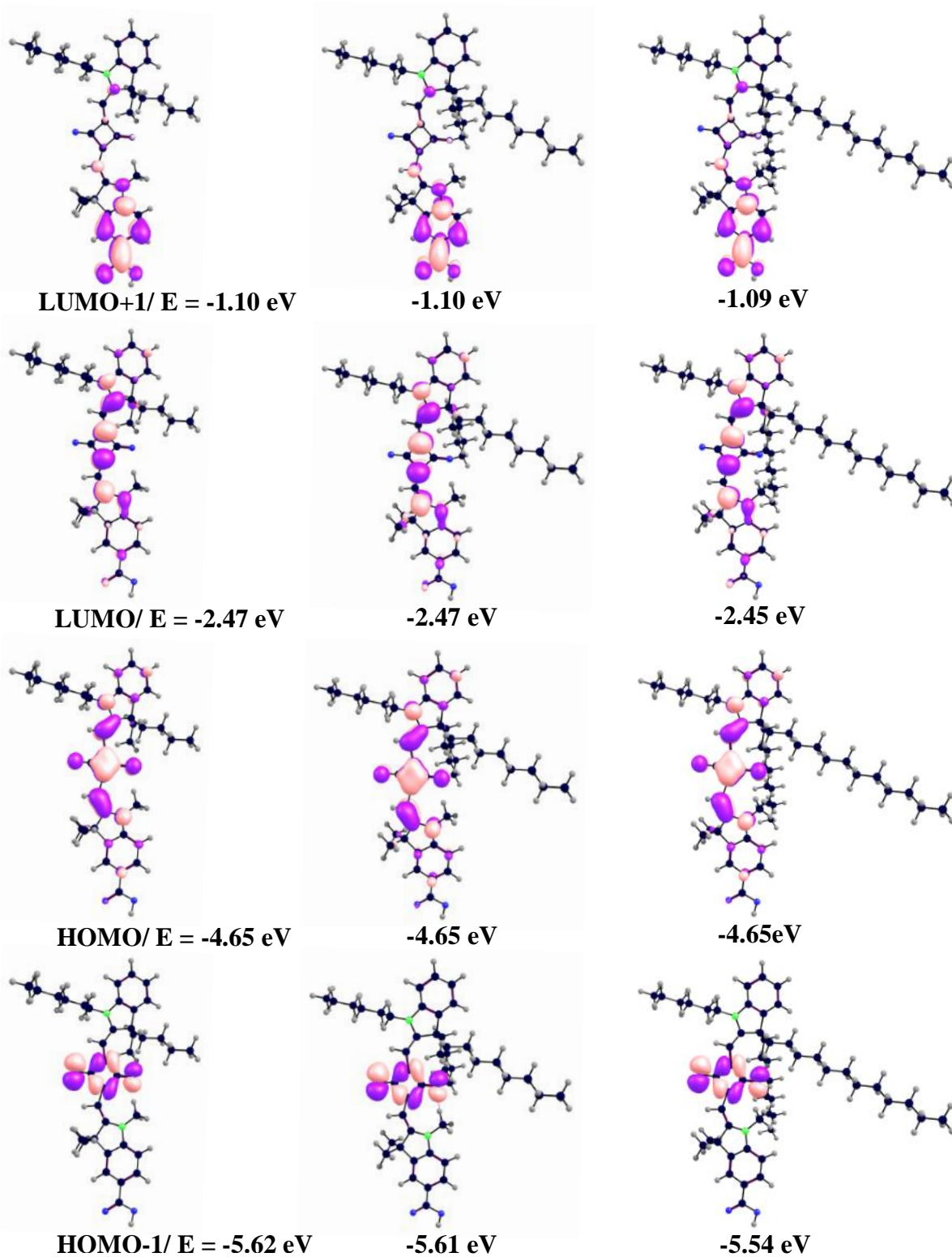
Figure 6. Isosurface plots of selected frontier orbitals (HOMO, HOMO-1, and LUMO, LUMO + 1) of SQS1 to SQS3. Fully optimized at DFT B3LYP/6-31G** level.[69] (Isovalue set to 0.036)

LUMO+1/ E = -1.10 eV   -1.13 eV   -1.07 eV

LUMO/ E = -2.46 eV   -2.51 eV   -2.47 eV

HOMO/ E = -4.64 eV   -4.69 eV   -4.63 eV

HOMO-1/ E = -5.60 eV   -5.63 eV   -5.61 eV
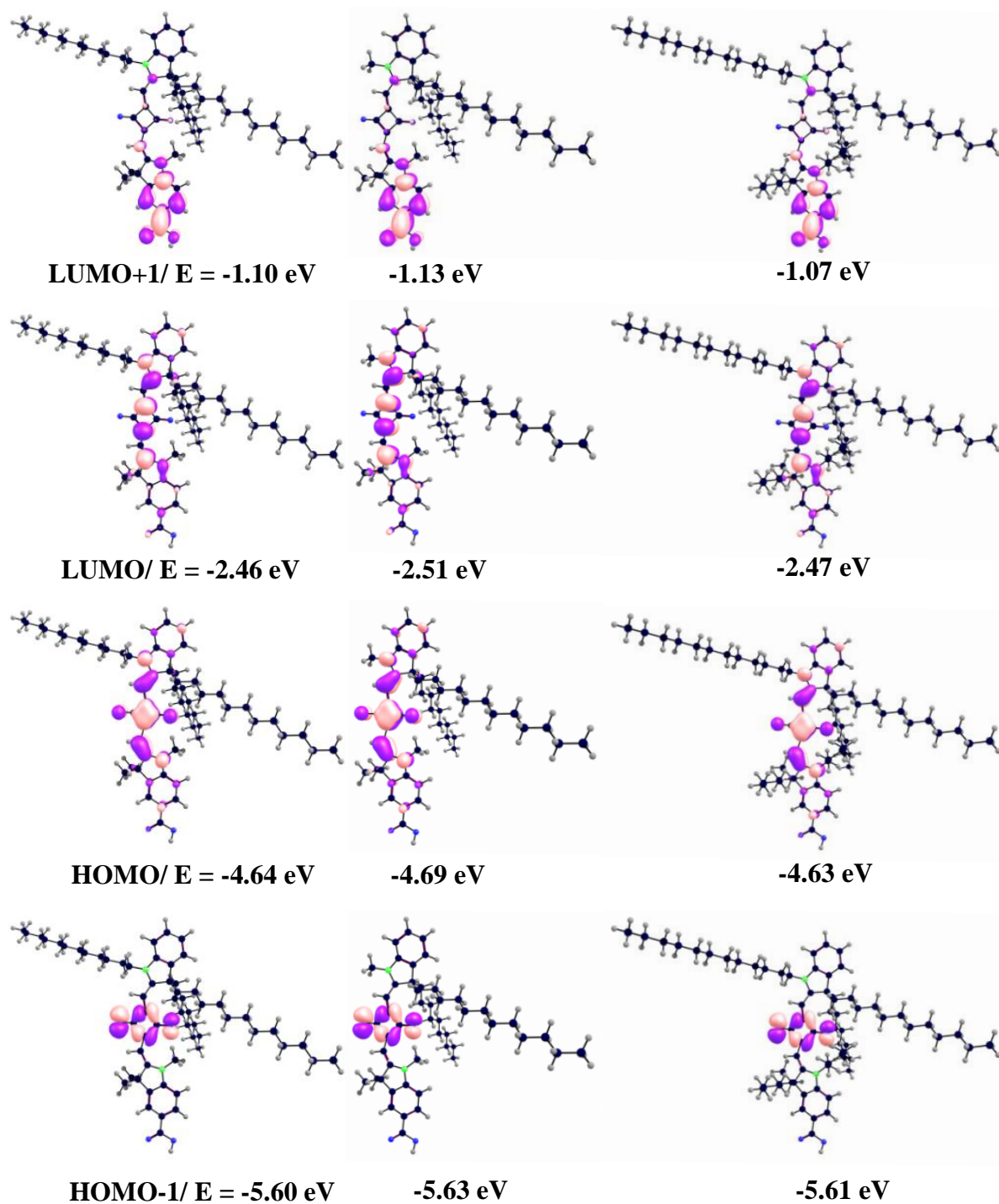
Figure 7. Isosurface plots of selected frontier orbitals (HOMO, HOMO-1, and LUMO, LUMO + 1) of SQS4 to SQS6. Fully optimized at DFT B3LYP/6-31G** level.[69] (Isovalue set to 0.036)
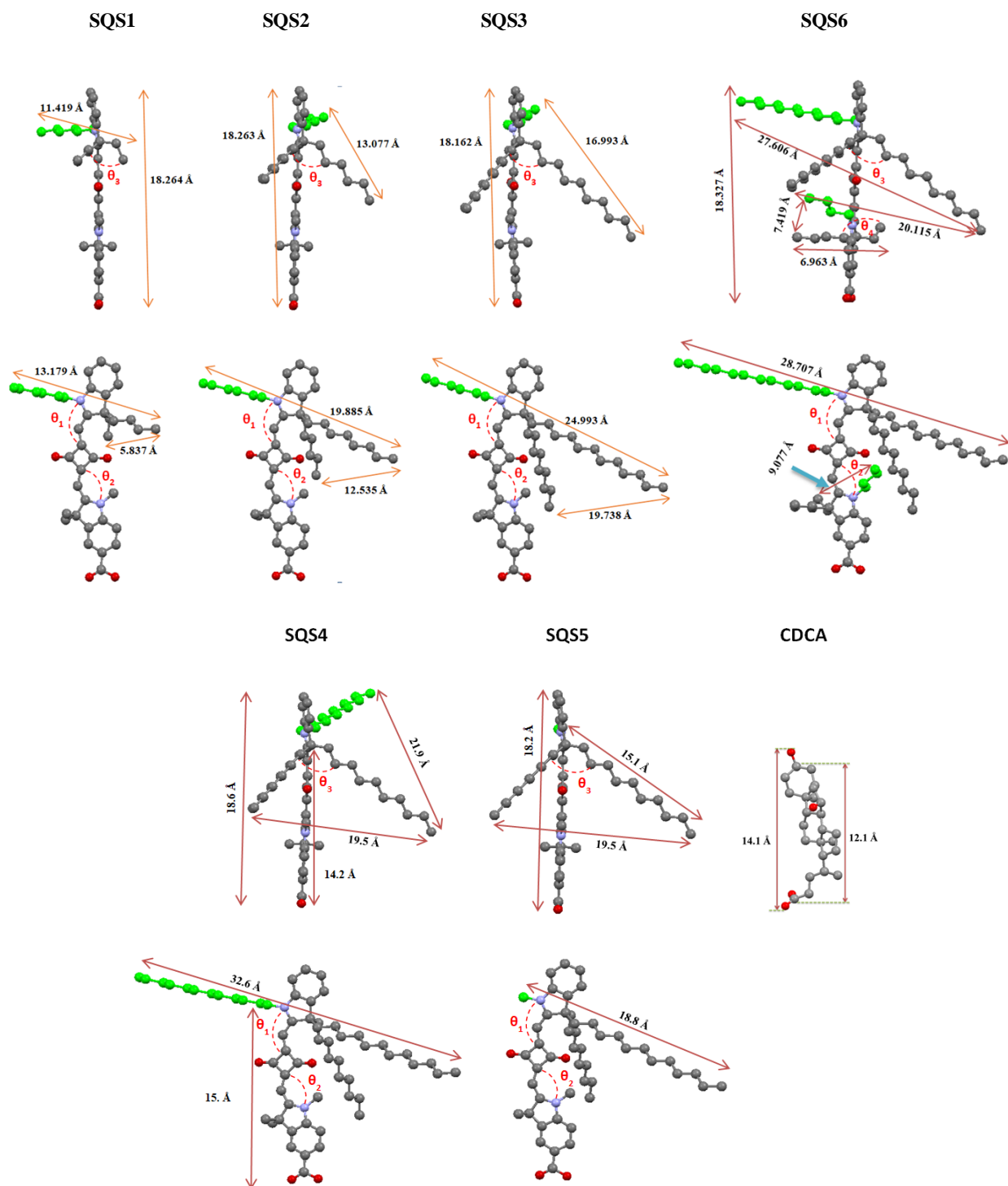
Figure 8. Dihedral angles and distance between the terminal carbon atoms of sp^3-C, and N-alkylated carbon atom of SQS dyes and chenodeoxycholic acid were determined from minimized ground state geometry (hydrogen atoms of alkyl groups and carboxylic groups are removed for clarity).

Table 3. Dihedral angles of SQS dyes.

Dyes	Dihedral Angle (Degree)			
	θ_1	θ_2	θ_3	θ_4
SQS1	-173.40	-0.72	59.32	-
SQS2	-169.40	1.09	57.91	-
SQS3	-168.91	6.78	57.78	-
SQS4	-169.35	-0.22	58.05	-
SQS5	-172.59	-0.10	58.55	-
SQS6	-174.63	8.48	59.71	58.39

2.3.6 Photovoltaic response. DSSC device fabrication with **SQS1-6** as sensitizers with iodolyte electrolyte has been carried out (area 0.23 cm^2 and mask with the aperture area of 0.23 cm^2). As the present SQS series of dyes differ with respect to the alkyl groups attached to the N- and sp^3-C atoms, the monolayer formation for the best device performance needed the optimization with optically transparent co-adsorbent chenodeoxycholic acid (CDCA). The device performance of SQS dyes were displayed in **Table 4**, and the optimized photovoltaic performance of SQS dyes with CDCA were provided in **Table 5**. *I-V* curve and IPCE response for **SQS** dyes with and without CDCA are shown in **Figure 9**, and **10**, whereas device optimization with CDCA is provided in **Figure 11**. The effect of alkyl groups on the photovoltaic parameters such as V_{OC} and J_{SC} have been discussed below.

Effect of alkyl groups on V_{OC}: The unsymmetrical squaraine dyes **SQS1-6** are wrapped with alkyl groups three dimensionally around the chromophores which may help to form well packed monolayer on the TiO$_2$ surface. Passivation of TiO$_2$ surface with alkyl groups avoids the charge recombination process between electrons in the TiO$_2$ and the oxidized electrolyte.[54-55] Such monolayer formation of SQS dyes on TiO$_2$ may impede the diffusion of oxidized electrolyte I$_3^-$ species to the TiO$_2$ surface which avoids the charge recombination process and boost the V_{OC} of the device. The V_{OC} of the devices of SQS1 (0.672 V) to SQS4 (0.717 V) to SQS6 (0.718) were increased systematically by varying the number of carbon atoms in the side chains around the dye. Further improvement of V_{OC} in the presence of CDCA for SQS1-SQS3 (0.696 V for SQS1,

0.695 V for SQS2 and 0.713 V for SQS3) indicates presence of aggregated dyes on the TiO_2 surface. The V_{OC} for the SQS5 and SQS1 are similar which suggest the importance of three dimensionally wrapped alkyl group around the dye molecule rather than alkyl groups present in only at sp^3-C center (SQS5). Further, it was observed that the extent of improvement of V_{OC} is more upon increasing the number of carbon atoms at the N-alkyl group compared to sp^3-C atom which is represented by a 3D-V_{OC} plot in **Figure 14**.

Effect of aggregated dyes on the modulation of photocurrent (J_{SC}): The IPCE responses for the devices fabricated with SQS1-6 dyes were broad (**Figure 11b**), which indicates that both monomer and aggregated structures contribute into the charge injection process. The maximum IPCE response for the DSSC devices fabricated with the SQS dyes range from 548 nm (SQS1, 58 %) to 580 nm (SQS6, 83 %) which indicates that the formation of aggregated dyes is decreased systematically from SQS1 to SQS6 (**Figure 13b, Table 7**). As the number of carbon atoms in sp^3-C and N-centers increases from SQS1 to SQS6, the maximum IPCE response from the H-aggregate is red shifted and also increased progressively, which indicates that the extent of aggregation is controlled and the charge injection from those aggregated structures can also be enhanced. Hence hydrophobic interactions between alkyl groups of SQS dyes controls the formation of aggregated structures that are efficiently inject the charges to enhance the photocurrent generation. The higher contributions in IPCE response were observed from the aggregated structures rather than the monomeric form of the sensitizer. Further in the presence of CDCA, for the dyes SQS1-3 and SQS5, the maximum IPCE is red shifted with enhanced response which suggests that the dye-dye interaction in the case of dyes SQS1-3 and SQS5 on TiO_2 is weaker, where the stability of self-assembled dye structures disturbed. Whereas, for the dyes, SQS4 and SQS6, addition of CDCA leads to only enhance the IPCE response without any spectral shift, which indicates the formation of stable monolayers of dyes with modulated dye-dye interaction which helps in both broadening the spectrum as well as contributing to the charge injection process to boost the photocurrent generation (**Figure 13b**).

Best device performance of 5.92 % (V_{OC} 0.717 V, J_{SC} 11.77 mA/cm^2, fill factor 70%) has been achieved for SQS4 without CDCA which was further improved to 7.1 % (V_{OC} 0.715 V, J_{SC} 13.05 mA/cm^2, fill factor 76%). Whereas the dye SQS1 showed the device performance of 4.9 % (V_{OC} 0.696 V, J_{SC} 9.47 mA/cm^2, fill factor 74% with 5 equiv. of CDCA), showed the importance of

optimal length of carbon chains that control the dye aggregation for enhancing the photocurrent generation. Further, qualitative evaluation of IPCE contribution from the monomer and aggregated dyes has been studied by DSSC device fabrication under different dye loading conditions. To capture the IPCE response from monomeric dyes, the TiO_2 photoanode was first saturated with non-chromophoric coadsorbent CDCA for 12 h (1.0 mM in MeCN) and further dipped in SQS4 dye solution for 2 min (0.1 mM in MeCN) (**Figure 12** and **Table 6**). The IPCE profile showed the contribution from the monomeric dyes at 650 nm. The normalized IPCE profile of DSSC device fabricated under above mentioned condition as well as the electrode dipped for 12 h in dye solutions (0.1 mM SQS4 and 0.3 mM CDCA in MeCN) is provided in **Figure 13a**. From the normalized IPCE curve of DSSC devices fabricated with SQS4 dye, it is observed that the H-type larger aggregate (570 nm), dimer (621 nm) and J-type[70, 71] (680 nm) aggregates are contributed more (to the charge injection) than the monomeric dyes.

Table 4. Photovoltaic response of SQS dyes.

Cells	CDCA (equiv.)	V_{OC} (V)	J_{SC} (mA/cm^2)	ff (%)	η (%)
SQS1	0	0.668 ± 0.004	7.64 ± 0.31	71 ± 0.63	3.62 ± 0.20
SQS1	5	0.695 ± 0.001	9.36 ± 0.11	74 ± 0.41	4.81 ± 0.09
SQS1	10	0.686 ± 0.002	8.72 ± 0.24	77 ± 0.89	4.60 ± 0.20
SQS1	15	0.684 ± 0.005	8.20 ± 0.21	78 ± 1.03	4.37 ± 0.21
SQS1	20	0.677 ± 0.003	7.58 ± 0.34	78 ± 0.07	4.00 ± 0.20
SQS2	0	0.683 ± 0.003	8.89 ± 0.19	77 ± 0.41	4.67 ± 0.15
SQS2	5	0.684 ± 0.002	9.65 ± 0.15	73 ± 0.38	4.82 ± 0.11
SQS2	10	0.694 ± 0.001	9.77 ± 0.06	76 ± 0.53	5.15 ± 0.07
SQS2	15	0.685 ± 0.003	8.80 ± 0.10	77 ± 0.15	4.64 ± 0.08
SQS2	20	0.675 ±0.004	7.54 ± 0.27	78 ± 0.63	3.96 ± 0.20

SQS3	0	0.706 ± 0.002	10.95 ± 0.06	75 ± 0.30	5.80 ± 0.07
SQS3	1	0.710 ± 0.003	12.35 ± 0.15	74 ± 0.24	6.49 ± 0.12
SQS3	2	0.712 ± 0.002	11.89 ± 0.05	75 ± 0.34	6.35 ± 0.07
SQS3	3	0.707 ± 0.001	10.86 ± 0.12	74 ± 0.57	5.68 ± 0.11
SQS3	4	0.706 ± 0.005	8.93 ± 0.03	76 ± 0.83	4.79 ± 0.10
SQS4	0	0.715 ± 0.002	11.55 ± 0.22	70 ± 0.14	5.78 ± 0.14
SQS4	1	0.718 ± 0.001	12.20 ± 0.18	72 ± 0.08	6.30 ± 0.10
SQS4	2	0.717 ± 0.001	12.49 ± 0.42	73 ± 0.17	6.54 ± 0.21
SQS4	3	0.712 ± 0.003	12.96 ± 0.09	76 ± 0.12	7.01 ± 0.09
SQS4	4	0.716 ± 0.001	11.91 ± 0.13	74 ± 0.29	6.31 ± 0.10
SQS5	0	0.671 ± 0.001	8.78 ± 0.07	77 ± 0.82	4.53 ± 0.09
SQS5	1	0.695 ± 0.003	9.80 ± 0.04	76 ± 0.30	5.17 ± 0.07
SQS5	2	0.682 ± 0.004	8.83 ± 0.39	74 ± 0.73	4.45 ± 0.27
SQS5	3	0.686 ± 0.003	7.57 ± 0.26	77 ± 0.69	3.99 ± 0.19
SQS5	4	0.664 ± 0.005	6.72 ± 0.05	77 ± 0.58	3.43 ± 0.08
SQS6	0	0.717 ± 0.001	11.95 ± 0.27	71 ± 0.06	6.08 ± 0.15
SQS6	1	0.716 ± 0.001	12.92 ± 0.33	73 ± 0.23	6.75 ± 0.21
SQS6	2	0.710 ± 0.003	12.07 ± 0.19	72 ± 0.08	6.17 ± 0.13
SQS6	3	0.697 ± 0.002	10.70 ± 0.16	72 ± 0.05	5.36 ± 0.11
SQS6	4	0.694 ± 0.003	9.10 ± 0.14	70 ± 0.37	4.42 ± 0.11

Table 5. Optimized device performance of SQS dyes with CDCA.

Cells	CDCA (equiv.)	V_{OC} (V)	J_{SC} (mA/cm^2)	ff (%)	η (%)
SQS1	0	0.668 ± 0.004	7.64 ± 0.31	71 ± 0.63	3.62 ± 0.20
SQS1	5	0.695 ± 0.001	9.36 ± 0.11	74 ± 0.41	4.81 ± 0.09
SQS2	0	0.683 ± 0.003	8.89 ± 0.19	77 ± 0.41	4.67 ± 0.15
SQS2	10	0.694 ± 0.001	9.77 ± 0.06	76 ± 0.53	5.15 ± 0.07
SQS3	0	0.706 ± 0.002	10.95 ± 0.06	75 ± 0.30	5.80 ± 0.07
SQS3	1	0.710 ± 0.003	12.35 ± 0.15	74 ± 0.24	6.49 ± 0.12
SQS4	0	0.715 ± 0.002	11.55 ± 0.22	70 ± 0.14	5.78 ± 0.14
SQS4	3	0.712 ± 0.003	12.96 ± 0.09	76 ± 0.12	7.01 ± 0.09
SQS5	0	0.671 ± 0.001	8.78 ± 0.07	77 ± 0.82	4.53 ± 0.09
SQS5	1	0.695 ± 0.003	9.80 ± 0.04	76 ± 0.30	5.17 ± 0.07
SQS6	0	0.717 ± 0.001	11.95 ± 0.27	71 ± 0.06	6.08 ± 0.15
SQS6	1	0.716 ± 0.001	12.92 ± 0.33	73 ± 0.23	6.75 ± 0.21

Thickness of TiO$_2$ 8 + 4 µm, area 0.23 cm^2, [Dye] = 0.1 mM, dipping time 6 h, Electrolyte: Iodolyte Z-50 (Solaronix).

Table 6. Photovoltaic responses of SQS4 dye (dipping time 2 min).

Cells	V_{OC} (V)	J_{SC} (mA/cm^2)	ff (%)	η (%)
SQS4	0.635 ± 0.002	2.53 ± 0.07	84 ± 1	1.35 ± 0.05

Thickness of TiO$_2$ 8 µm, area 0.23 cm^2, [Dye] = 0.1 mM, dipping time 2 min, Electrolyte: Iodolyte Z-50 (Solaronix).
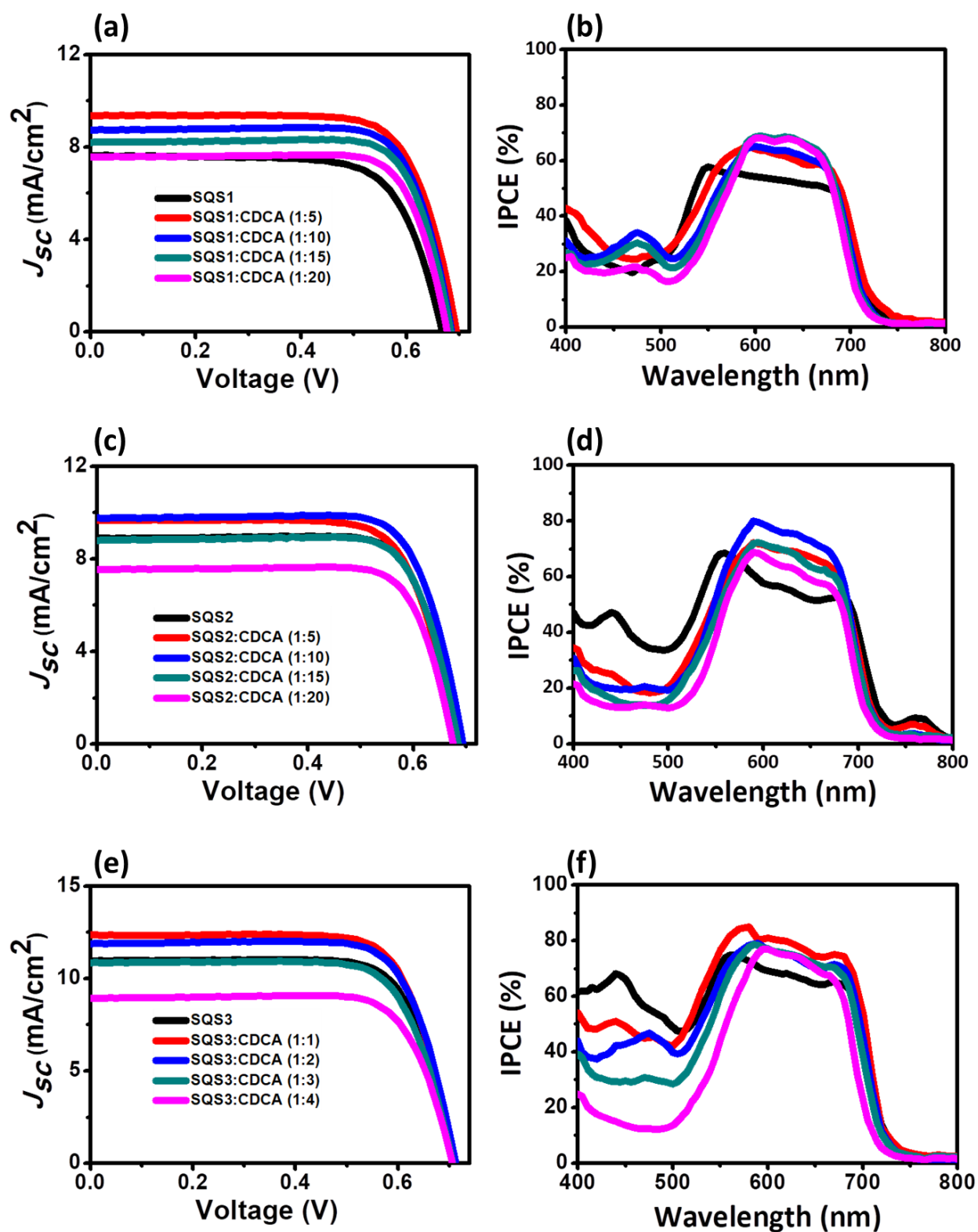
Figure 9. (a), (c), and (e) *J-V* curve of SQS1-3 dyes under AM 1.5 G illumination (1000 W/m^2), (b), (d), and (f) IPCE response of SQS1-3 dyes.
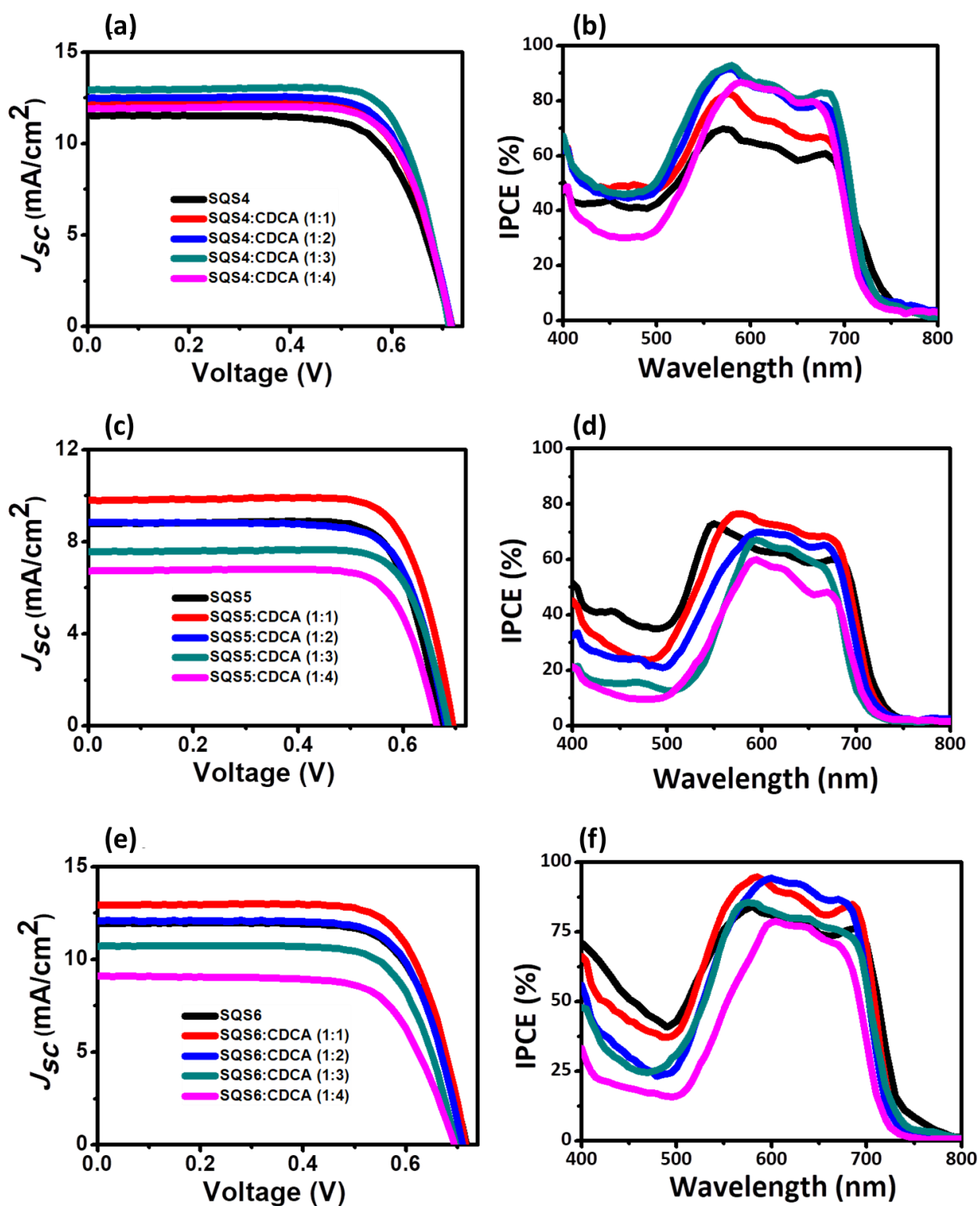
Figure 10. (a), (c), and (e) *J-V* curve of SQS4-6 dyes under AM 1.5 G illumination (1000 W/m^2), (b), (d), and (f) IPCE response of SQS4-6 dyes.
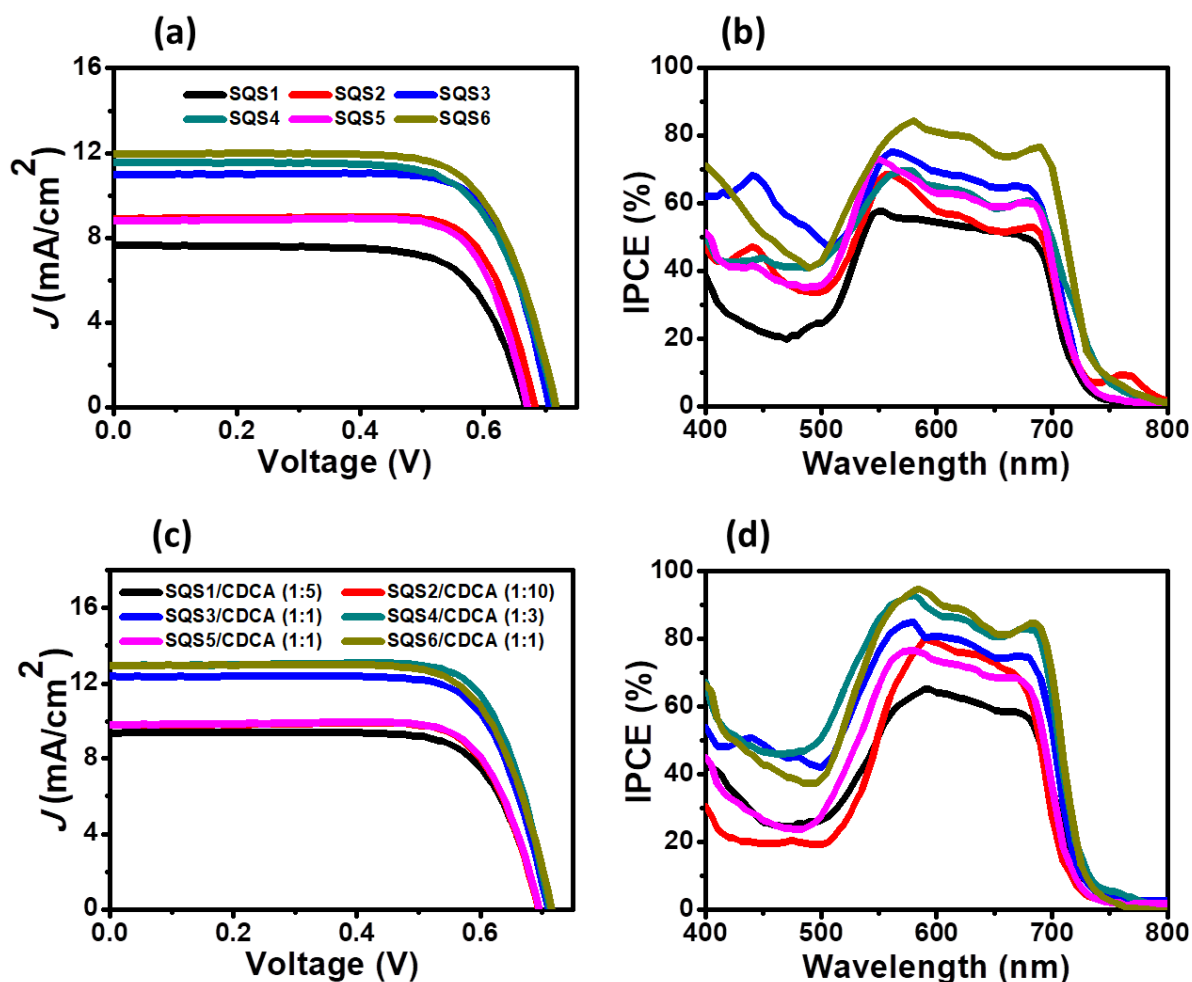
Figure 11. (a) and (c) *I-V* curve of SQS dyes with and without CDCA, respectively, (b) and (d) IPCE curve of SQS dyes with and without CDCA, respectively.

Table 7. Contribution of aggregated SQS1-SQS6 for the enhanced photovoltaic parameters.

S No	Dye	V_{OC} (V)	H-aggregate from IPCE profile (%)	Dye: CDCA	V_{OC} (V)	H-aggregate from IPCE profile (%)
1	SQS1	0.672	548 nm (58)	1:5	0.696	591 nm (65)
2	SQS2	0.686	556 nm (69)	1:10	0.695	591 nm (80)
3	SQS3	0.708	560 nm (75)	1:1	0.713	580 nm (86)
4	SQS4	0.717	570 nm (70)	1:3	0.718	570 nm (92)
5	SQS5	0.672	548 nm (73)	1:1	0.695	572 nm (77)
6	SQS6	0.718	580 nm (83)	1:1	0.717	580 nm (94)
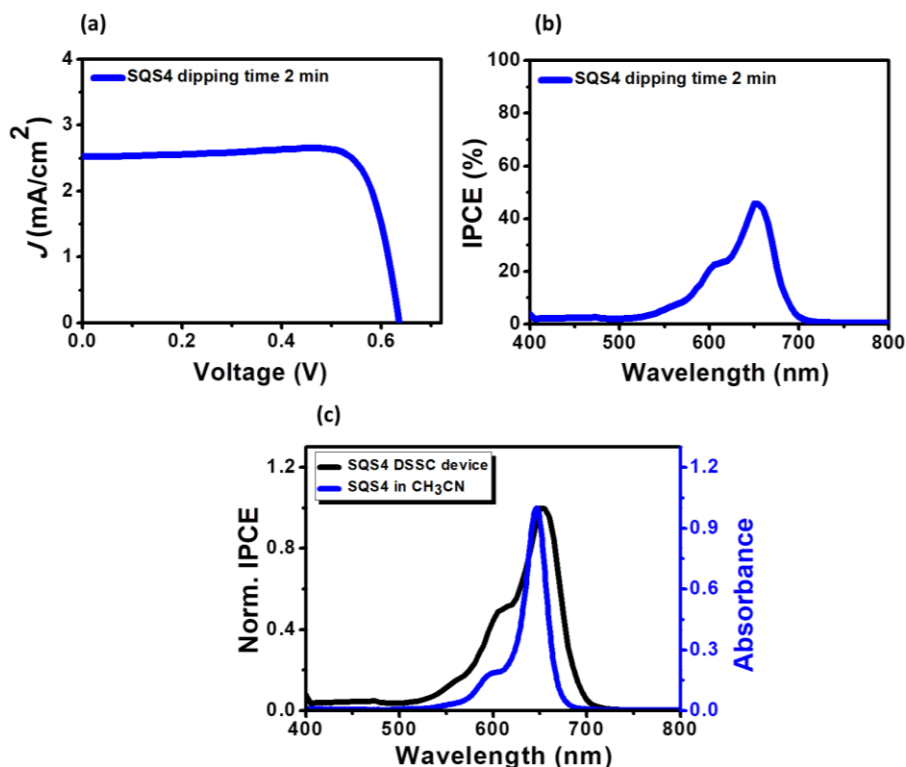
Figure 12. (a) and (b) *J-V* and IPCE curve, (c) normalized IPCE and absorbance of SQS4 dye.
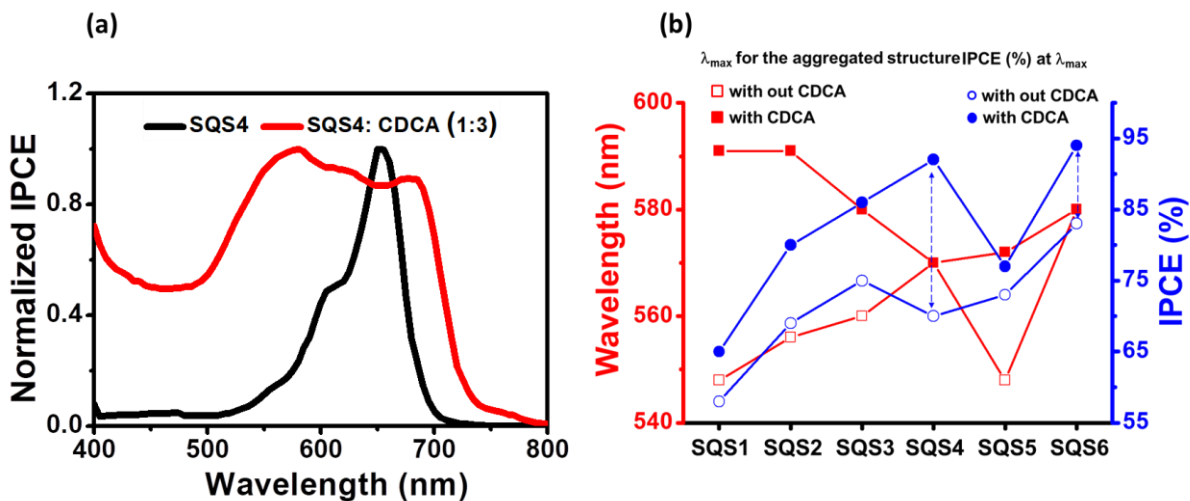
Figure 13. (a) Normalized IPCE profile of DSSC devices fabricated with the TiO$_2$ electrode dipped for 6 h in the mixture of 0.1 mM of SQS4 and 0.3 mM of CDCA in MeCN (red), the electrode was first saturated with 1.0 mM of CDCA in MeCN for 12 h and then dipped the electrode in 0.1 mM of SQS4 in MeCN for 2 min, (b) IPCE responses from the H-aggregated sensitizers of SQS1-6.
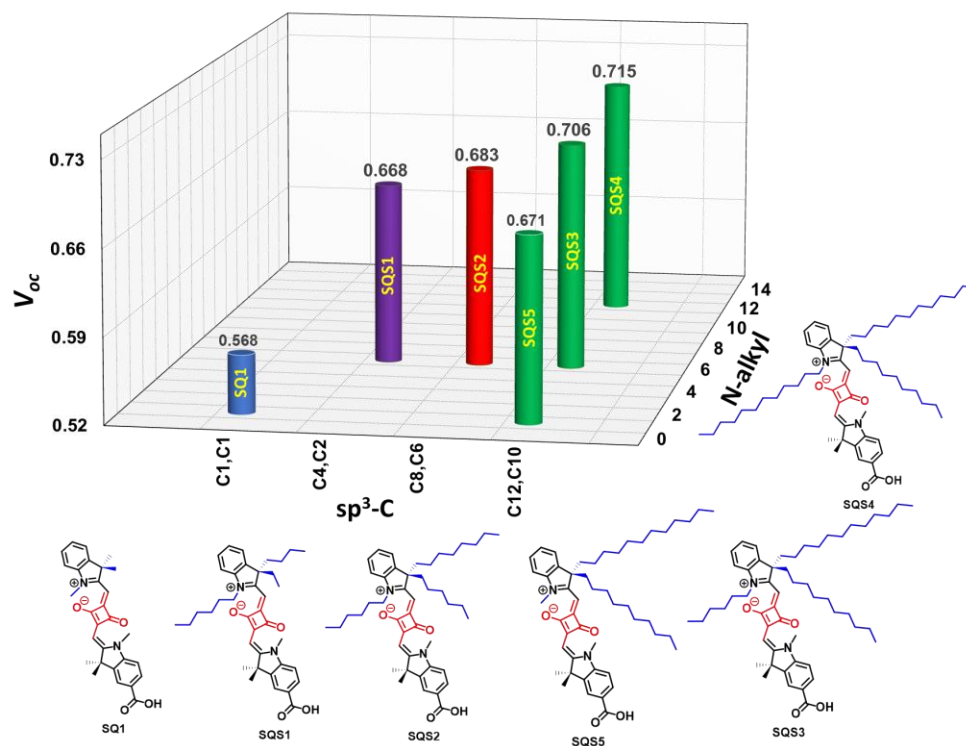
Figure 14. Three-dimensional (3D)-V_{OC} plot of SQ dyes without CDCA.

2.3.7 Electrochemical impedance spectroscopy (EIS). An EIS study was conducted to elucidate the resistance associated with the charge recombination process at the TiO_2/ electrolyte interface in DSSCs.[72, 73] EIS was carried out in the dark with the various applied bias of -0.44 to -0.68 V and scanned between 1 Hz to 1 MHz frequency range to calculate the charge transfer resistance of TiO_2/dye/electrolyte interface. Nyquist plot of the SQS dyes with and without CDCA are displayed in **Figure 15, 16** under various applied bias. There are two semicircles shows in the Nyquist diagrams of the SQS dyes, larger semicircle indicating the charge recombination resistance (R_{ct}) at the interface of TiO_2/dye/electrolyte, and smaller semicircle of SQS dyes indicating the transfer of charge at the counter electrode.[73] The radius of larger semicircle increases with increasing chain-length of alkyl groups at sp^3-C of SQS1 to SQS3 dyes, and at N-atom SQS4 without CDCA, radius of SQS6 is larger than other, whereas SQS5 is smaller than other without CDCA under an applied the bias of -0.44 V (**Figure 15**).
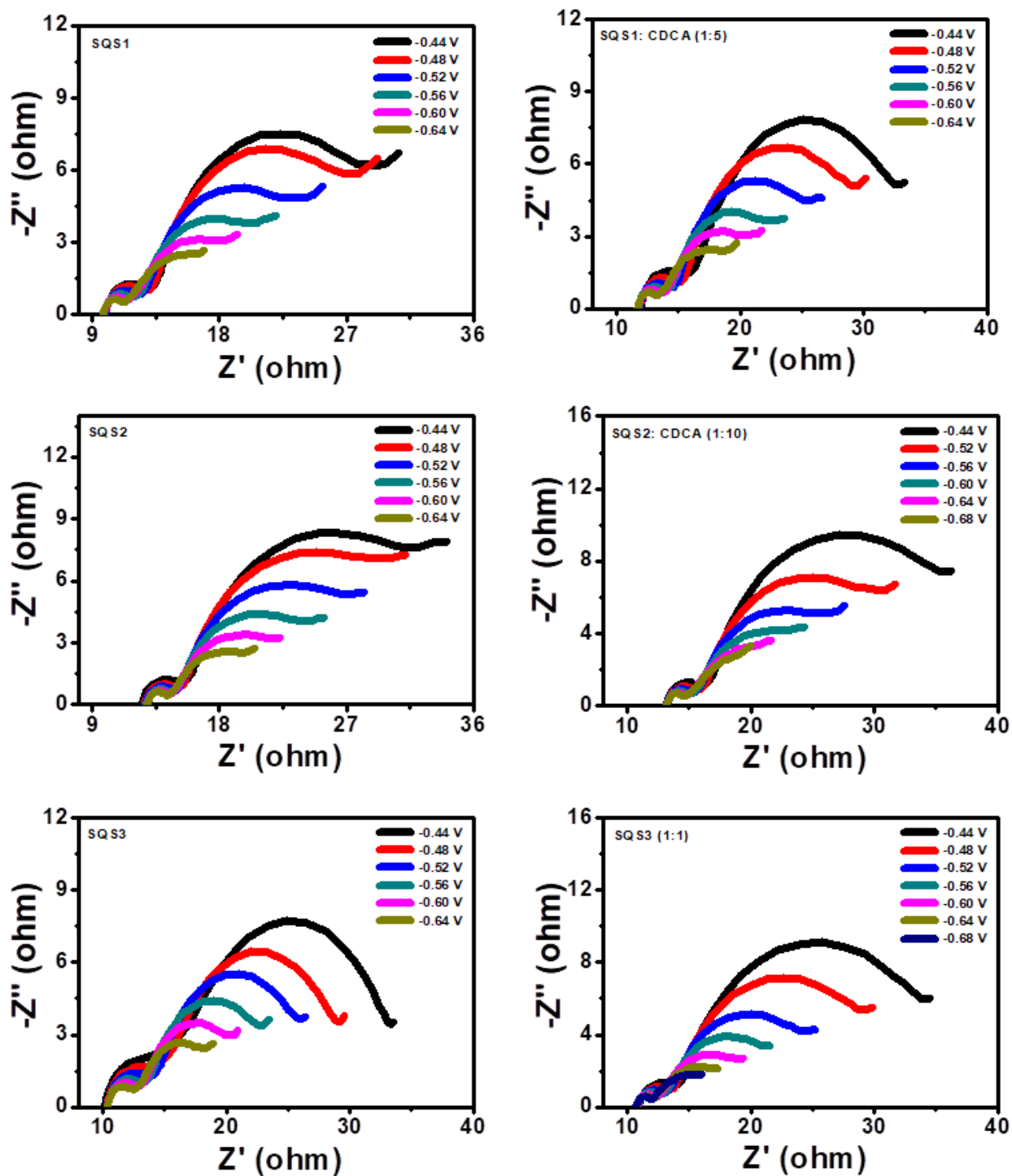
Figure 15. Nyquist plot of the SQS1-SQS3 dyes with and without CDCA under various applied bias.
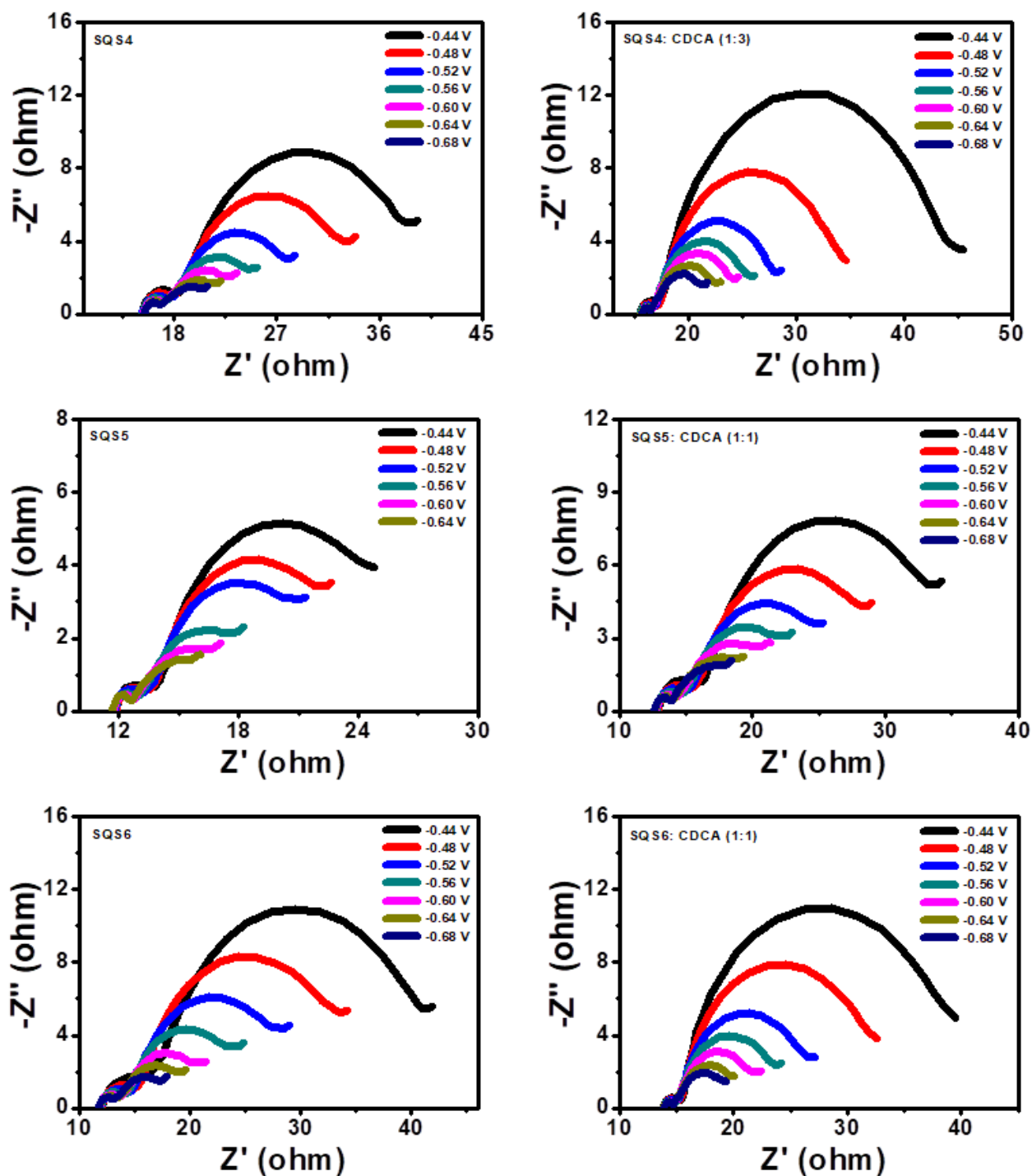
Figure 16. Nyquist plot of the SQS4-SQS6 dyes with and without CDCA under various applied bias.
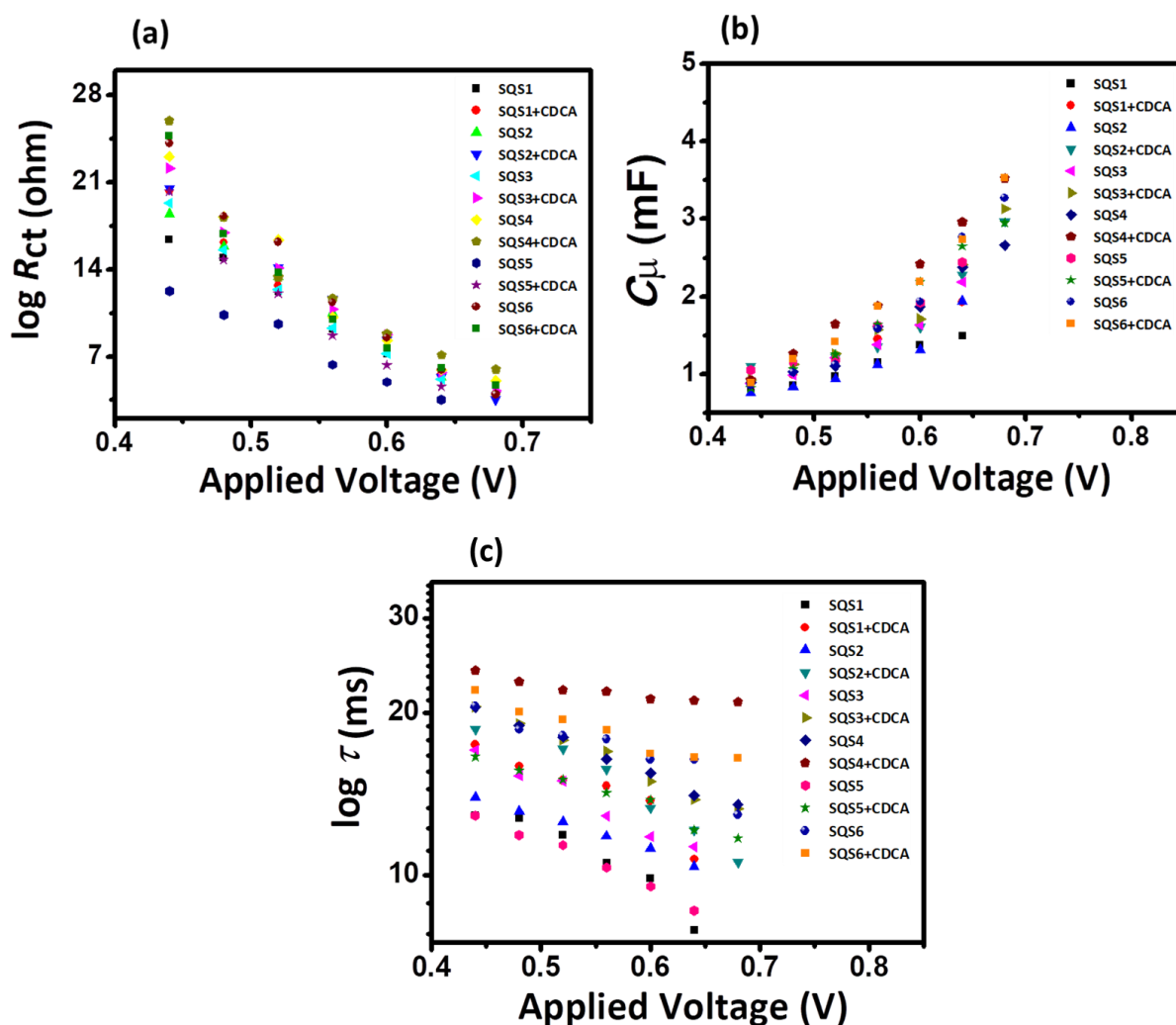
Figure 17. (a) Charge recombination resistance, (b) chemical capacitance, and (c) electron life time *vs* applied bias for the DSSC device made up of SQS dyes with and without CDCA.

The charge transfer resistance (R_{ct}) is increased for the SQS dyes in the order of SQS5 < SQS1 < SQS2 < SQS3 < SQS4 < SQS6 without CDCA (**Figure 15, 16**). Addition of CDCA increases the charge recombination resistance of SQS dyes by blocking the charge recombination sites than without CDCA are displayed in **Figure 17b**. The charge transfer resistance (R_{ct}) and the chemical capacitance ($C\mu$) were extracted by fitting the Nyquist plot by using an equivalent circuit (R1+C2/R2+C3/R3) (**Figure 19**). The chemical capacitance ($C\mu$) curve indicates the possibility of (i) shifting the conduction band position due to the dipole moment exerted by the dye on the surface for the SQS dyes, or (ii) the dye monolayer effectively passivates the TiO$_2$ surface. As the difference between the SQS dyes varies only with respect to the alkyl groups, the

change in dipole moment (μ = 1.352 to 1.567 Debye) may not be the reason for the observed results. Hence, it may be possible that SQS dyes form the well protected monolayer which helps avoiding the electron from TiO_2 reaches out to the electrolyte (**Figure 18c**). Long electron life time (τ) of SQS dyes increases for the SQS1 to SQS4 to SQS6 systematically which indicates the effective passivation of surface with controlled dye aggregation (**Figure 17c**). Maximum value of τ observed in SQS6 (without CDCA) and SQS4 (with CDCA) (**Figure 17c**), whereas minimum value of τ observed in SQS1 and SQS5 without CDCA (**Figure 17c**). Hence, alkyl group at the N-atom is important to boost the V_{OC}. EIS studies of SQS dyes, best device with CDCA displayed in **Table 8**.
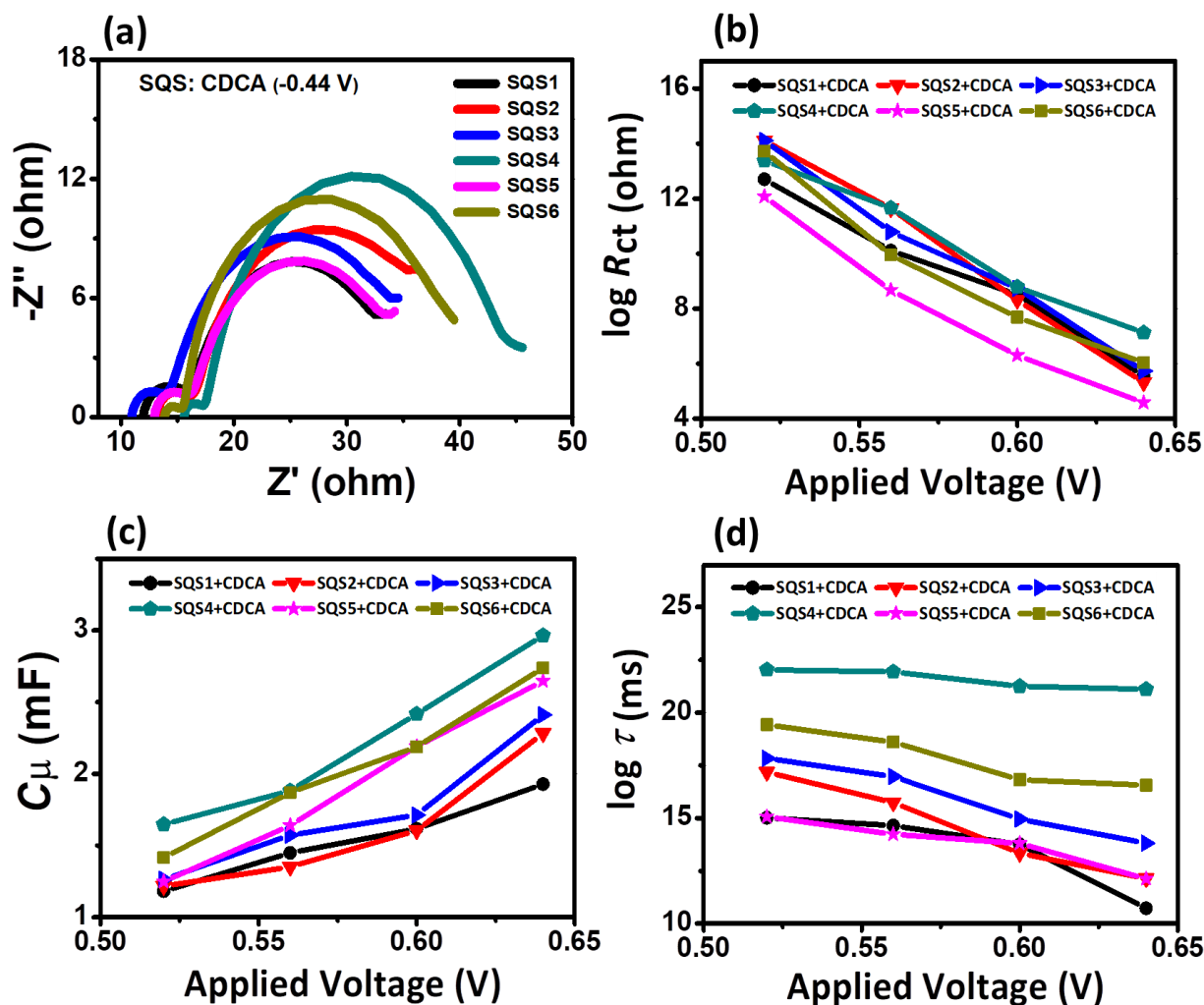
Figure 18. (a) Nyquist plot, (b) charge recombination resistance, (c) chemical capacitance, and (d) electron life time of SQS dyes *vs* applied bias with and without CDCA.
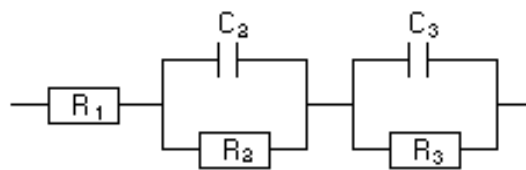
Figure 19. Equivalent circuit (R1+C2/R2+C3/R3) model, where R2/C2 represents Pt/ (I^-/ I_3^-), and R3/C3 represents TiO_2/ dye/ (I^-/ I_3^-) interfaces.

Table 8. EIS studies of SQS dyes with CDCA.

Dyes	CDCA	Applied voltage (V)	R_{ct} (ohm)	$C\mu$ (mF)	$^a\tau$ (ms)
SQS1	5	0.64	5.56	1.928	10.72
SQS2	10	0.64	5.32	2.281	12.14
SQS3	1	0.64	5.73	2.412	13.81
SQS4	3	0.64	7.12	2.965	21.11
SQS5	1	0.64	4.58	2.647	12.12
SQS6	1	0.64	6.04	2.739	16.56

$^a\tau = R_{ct} \times C\mu$

2.4 CONCLUSION

As self-assembly of organic dyes lead to aggregation of sensitizers on the TiO_2 surface, we have taken advantage of it to spread the light harvesting efficiency of the sensitizers without compromising the charge injection process. An unsymmetrical squaraine dye has been chosen with suitably functionalized branched alkyl groups to control the dye–dye interaction on the TiO_2 surface. A series of unsymmetrical squaraine dyes, SQS1-SQS6 were synthesized. Although, the photophysical and electrochemical nature of SQS1-SQS6 (in solution) are almost similar, the electrochemical properties of synthesized dyes on the TiO_2 surface indicated that self-hopping of charges can be controlled systematically by varying the chain lengths of the branching unit that is away from the TiO_2 surface. Such observation helps to increase the DSSC device performance by (i) effective charge injection from the self-assembled squaraine dyes and (ii) effectively passivates the surface of TiO_2 which helps in avoiding the charge recombination process. Shorter

chain length at sp^3-C and N- atom containing dye SQS1 showed the device performance of 4.9 % with the V_{OC} 0.696 V, and J_{SC} 9.47 mA/cm^2, whereas SQS4, dye with longer chain showed the device performance of 7.1 % with the V_{OC} and J_{SC} are 0.715 V and 13.05 mA/cm^2, respectively with CDCA. Importance of N-alkyl chain has been realized from SQS5 with reduced device performance of 5.24 %. A correlation has been arrived for the observed V_{OC} where alkyl group at N- atom plays importance over sp^3-C atom. Further, the IPCE profile of the devices inferred that the contribution from both H- and J-type aggregates. This systematic study revealed the importance of aggregation of dyes on the surface of TiO$_2$ for the enhanced the efficiency in DSSC, and further co-sensitizing with complementary sensitizer under progress.

2.5 REFERENCES

(1) O'Regan, B.; Grätzel, M. A Low-cost, High-efficiency Solar Cell Based on Dye-Sensitized Colloidal TiO$_2$ Films. *Nature*, **1991**, *353*, 737-740.

(2) Wang, P.; Zakeeruddin, S. M.; Moser, J.-E.; Nazeeruddin, M. K.; Sekiguchi, T.; Grätzel, M. A Stable Quasi-solid-state Dye-sensitized Solar Cell with an Amphiphilic Ruthenium Sensitizer and Polymer Gel Electrolyte. *Nat. Mater.* **2003**, *2*, 402-407.

(3) Wang, P.; Klein, C.; Humphry-Baker, R.; Zakeeruddin, S. M.; Grätzel, M.A High Molar Extinction Coefficient Sensitizer for Stable Dye-Sensitized Solar Cells. *J. Am. Chem. Soc.* **2005**, *127*, 808-809.

(4) Kuang, D.; Klein, C.; Ito, S.; Moser, J.-E.; Humphry-Baker, R.; Evans, N.; Duriaux, F.; Grätzel, C.; Zakeeruddin, S. M.; Grätzel, M. High-Efficiency and Stable Mesoscopic Dye-Sensitized Solar Cells Based on a High Molar Extinction Coefficient Ruthenium Sensitizer and Nonvolatile Electrolyte. *Adv. Mater.* **2007**, *19*, 1133-1137.

(5) Gao, F.; Wang, Y.; Shi, D.; Zhang, J.; Wang, M.; Jing, X.; Humphry- Baker, R.; Wang, P.; Zakeeruddin, S. M.; Grätzel, M. Enhance the Optical Absorptivity of Nanocrystalline TiO$_2$ Film with High Molar Extinction Coefficient Ruthenium Sensitizers for High Performance Dye-Sensitized Solar Cells. *J. Am. Chem. Soc*. **2008**, *130*, 10720-10728.

(6) Chen, W.-C.; Kong, F.-T.; Li, Z.-Q.; Pan, J.-H.; Liu, X.-P.; Guo, F.-L.; Zhou, Li; Huang, Y.; Yu, T.; Dai, S.-Y. Superior Light-Harvesting Heteroleptic Ruthenium (II) Complexes with Electron-Donating Antennas for High Performance Dye-Sensitized Solar Cells. *ACS Appl. Mater. Interfaces* **2016**, *8*, 19410-19417.

(7) Bessho, T.; Zakeeruddin, S. M.; Yeh, C.-Y.; Diau, E. W.-G.; Grätzel, M. Highly Efficient Mesoscopic Dye-Sensitized Solar Cells Based on Donor–Acceptor-Substituted Porphyrins. *Angew. Chem., Int. Ed*. **2010**, *49*, 6646-6649.

(8) Yella, A.; Lee, H.-W.; Tsao, H. N.; Yi, C.; Chandiran, A. K.; Nazeeruddin, M. K.; Diau, E. W.-G.; Yeh, C.-Y.; Zakeeruddin, S. M.; Grätzel, M. Porphyrin-Sensitized Solar Cells with Cobalt (II/III)–Based Redox Electrolyte Exceed 12 Percent Efficiency. *Science* **2011**, *334*, 629-634.

(9) Yella, A.; Mai, C.-L.; Zakeeruddin, S. M.; Chang, S.-N.; Hsieh, C.-H.; Yeh, C.-Y.; Grätzel, M. Molecular Engineering of Push–Pull Porphyrin Dyes for Highly Efficient Dye-Sensitized Solar Cells: The Role of Benzene Spacers. *Angew. Chem., Int. Ed*. **2014**, *53*, 2973-2977.

(10) Griffith, M. J.; Sunahara, K.; Wagner, P.; Wagner, K.; Wallace, G. G.; Officer, D. L.; Furube, A.; Katoh, R.; Mori, S.; Mozer, A. J. Porphyrins for Dye-sensitised Solar Cells: New Insights into Efficiency-determining Electron Transfer Steps. *Chem. Commun*. **2012**, *48*, 4145-4162.

(11) Li, L.-L.; Diau, E. W.-G. Porphyrin-Sensitized Solar Cells. *Chem. Soc. Rev*. **2013**, *42*, 291-304.

(12) Urbani, M.; Grätzel, M.; Nazeeruddin, M. K.; Torres, T. Meso-Substituted Porphyrins for Dye-Sensitized Solar Cells. *Chem. Rev.* **2014**, *114*, 12330-12396.

(13) Higashino, T.; Imahori, H. Porphyrins as Excellent Dyes for Dye-sensitized Solar Cells: Recent Developments and Insights. *Dalton Trans.* **2015**, *44,* 448-463.

(14) Tang, Y.; Wang, Y.; Li, X.; Ågren, H.; Zhu, W.-H.; Xie, Y. Porphyrins Containing a Triphenylamine Donor and up to Eight Alkoxy Chains for Dye-Sensitized Solar Cells: A High Efficiency of 10.9%. *ACS Appl. Mater. Interfaces* **2015**, *7*, 27976-27985.

(15) Xie, Y.; Tang, Y.; Wu, W.; Wang, Y.; Liu, J.; Li, X.; Tian, H.; Zhu, W.-H. Porphyrin Cosensitization for a Photovoltaic Efficiency of 11.5%: A Record for Non-Ruthenium Solar Cells Based on Iodine Electrolyte. *J. Am. Chem. Soc.* **2015**, *137*, 14055-14058.

(16) Zeng, K.; Lu, Y.; Tang, W.; Zhao, S.; Liu, Q.; Zhu, W.; Tian, H.; Xie, Y. Efficient Solar Cells Sensitized by a Promising New Type of Porphyrin: Dye-Aggregation Suppressed by Double Strapping. *Chem. Sci.* **2019**, *10* (7), 2186–2192.

(17) Lu, Y.; Song, H.; Li, X.; Ågren, H.; Liu, Q.; Zhang, J.; Zhang, X.; Xie, Y. Multiply Wrapped Porphyrin Dyes with a Phenothiazine Donor: A High Efficiency of 11.7% Achieved through a Synergetic Coadsorption and Cosensitization Approach. *ACS Appl. Mater. Interfaces* **2019**, *11* (5), 5046–5054.

(18) Lu,Y.; Liu, Q.; Luo, J.; Wang, B.; Feng, T.; Zhou, X.; Liu, X.; Xie, Y. Solar Cells Sensitized with Porphyrin Dyes Containing Oligo(Ethylene Glycol) Units: A High Efficiency Beyond 12 %. *ChemSusChem*, **2019**, *12*, 2802–2809.

(19) Kurumisawa, Y.; Higashino, T.; Nimura, S.; Tsuji, Y.; Iiyama, H.; Imahori, H. Renaissance of Fused Porphyrins: Substituted Methylene-Bridged Thiophene-Fused Strategy for High-Performance Dye-Sensitized Solar Cells. *J. Am. Chem. Soc.* **2019**, *141*, 9910–9919.

(20) Yang, J. B.; Guo, F. L.; Hua, J. L.; Li, X.; Wu, W. J.; Qu, Y.; Tian, H. Efficient and Stable Organic DSSC Sensitizers Bearing Quinacridone and Furan Moieties as a Planar π-spacer. *J. Mater. Chem.* **2012**, *22,* 24356-24365.

(21) Wu, Y. Z.; Marszalek, M.; Zakeeruddin, S. M.; Zhang, Q.; Tian, H.; Grätzel, M.; Zhu, W. H. High-conversion-efficiency Organic Dye-sensitized Solar Cells: Molecular Engineering on D–A– π–A Featured Organic Indoline Dyes. *Energy Environ. Sci.* **2012**, *5*, 8261-8272.

(22) Hagfeldt, A.; Boschloo, G.; Sun, L. C.; Kloo, L.; Pettersson, H. Dye-Sensitized Solar Cells. *Chem. Rev.* **2010**, *110*, 6595-6663.

(23) Jiao, Y.; Zhang, F.; Grätzel, M.; Meng, S. Structure–Property Relations in All-Organic Dye-Sensitized Solar Cells. *Adv. Funct. Mater.* **2013**, *23*, 424-429.

(24) Kozma, E.; Concina, I.; Braga, A.; Borgese, L.; Depero, L. E.; Vomiero, A.; Sberveglieri, G.; Catellani, M. Metal-free Organic Sensitizers with a Sterically Hindered Thiophene Unit for Efficient Dye-sensitized Solar Cells. *J. Mater. Chem.* **2011**, *21*, 13785-13788.

(25) Qu, S.; Wu, W.; Hua, J.; Kong, C.; Long, Y.; Tian, H. New Diketopyrrolopyrrole (DPP) Dyes for Efficient Dye-Sensitized Solar Cells. *J. Phys. Chem. C* **2010**, *114*, 1343-1349.

(26) Kakiage, K.; Aoyama, Y.; Yano, T.; Otsuka, T.; Kyomen, T.; Unno, M.; Hanaya, M. An Achievement of Over 12 Percent Efficiency in an Organic Dye-sensitized Solar Cell. *Chem. Commun.* **2014**, *50*, 6379-6381.

(27) Cao, Y.; Cai, N.; Wang, Y.; Li, R.; Yuan, Y.; Wang, P. Modulating the Assembly of Organic Dye Molecules on Titania Nanocrystals via Alkyl Chain Elongation for Efficient Mesoscopic Cobalt Solar Cells. *Phys. Chem. Chem. Phys.* **2012**, *14*, 8282-8286.

(28) Yum, J.-H.; Holcombe, T. W.; Kim, Y.; Rakstys, K.; Moehl, T.; Teuscher, J.; Delcamp, J. H.; Nazeeruddin, M. K.; Grätzel, M. Blue-Coloured Highly Efficient Dye-Sensitized Solar Cells by Implementing the Diketopyrrolopyrrole Chromophore. *Sci. Rep.* **2013**, *3*, 2446-2453.

(29) Yum, J.-H.; Baranoff, E.; Kessler, F.; Moehl, T.; Ahmad, S.; Bessho, T.; Marchioro, A.; Ghadiri, E.; Moser, J.-E.; Yi, C.; Nazeeruddin, M. K.; Grätzel, M. A Cobalt Complex Redox Shuttle for Dye-sensitized Solar Cells with High Open-circuit Potentials. *Nat. Commun.* **2012**, *3*, 627-631.

(30) Zhang, M.; Wang, Y.; Xu, M.; Ma, W.; Li, R.; Wang, P. Design of High-efficiency Organic Dyes for Titania Solar Cells Based on the Chromophoric Core of Cyclopentadithiophene-benzothiadiazole. *Energy Environ. Sci.* **2013**, *6*, 2944-2949.

(31) Yang, J.; Ganesan, P.; Teuscher, J.; Moehl, T.; Kim, Y. J.; Yi, C.; Comte, P.; Pei, K.; Holcombe, T. W.; Nazeeruddin, M. K.; Hua, J.; Zakeeruddin, S. M.; Tian, H.; Grätzel, M.Influence of the Donor Size in D−π−A Organic Dyes for Dye-Sensitized Solar Cells. *J. Am. Chem. Soc.***2014**, *136*, 5722-5730.

(32) Zhou, N.; Prabakaran, K.; Lee, B.; Chang, S.H.; Harutyunyan, B.; Guo, P.; Butler, M. R.; Timalsina, A.; Bedzyk, M. J.; Ratner, M. A.; Vegiraju, S.; Yau, S.; Wu, C.-G.; Chang, R. P. H.; Facchetti, A.; Chen, M.-C.; Marks, T. J. Metal-Free Tetrathienoacene Sensitizers for High-Performance Dye-Sensitized Solar Cells. *J. Am. Chem. Soc*. **2015**, *137*, 4414-4423.

(33) Yao, Z.; Zhang, M.; Wu, H.; Yang, L.; Li, R.; Wang, P. Donor/Acceptor Indenoperylene Dye for Highly Efficient Organic Dye-Sensitized Solar Cells. *J. Am. Chem. Soc*. **2015**, *137*, 3799-3802.

(34) Zhang, L.; Yang, X.; Wang, W.; Gurzadyan, G. G.; Li, J.; Li, X.; An, J.; Yu, Z.; Wang, H.; Cai, B.; Hagfeldt, A.; Sun, L. 13.6% Efficient Organic Dye-Sensitized Solar Cells by Minimizing Energy Losses of the Excited State. *ACS Energy Lett.* **2019**, *4* (4), 943–951.

(35) Martín-Gomis, L.; Fernández-Lázaro, F.; Sastre-Santos, Á. Advances in Phthalocyanine-Sensitized Solar Cells (PcSSCs). *J. Mater. Chem. A* **2014**, *2*, 15672-15682.

(36) Saccone, D.; Galliano, S.; Barbero, N.; Quagliotto, P.; Viscardi, G.; Barolo, C. Polymethine Dyes in Hybrid Photovoltaics: Structure–Properties Relationships. *Eur. J. Org. Chem.***2016**, *2016*, 2244-2259.

(37) Chen, G.; Sasabe, H.; Sasaki, Y.; Katagiri, H.; Wang, X.-F.; Sano, T.; Hong, Z.; Yang, Y.; Kido, J. A Series of Squaraine Dyes: Effects of Side Chain and the Number of Hydroxyl Groups on Material Properties and Photovoltaic Performance. *Chem. Mater.* **2014**, *26*, 1356-1364.

(38) Qin, C.; Wong, W.-Y.; Han, L. Squaraine Dyes for Dye-Sensitized Solar Cells: Recent Advances and Future Challenges. *Chem. Asian J*. **2013**, *8*, 1706-1719.

(39) Chen, G.; Sasabe, H.; Igarashi, T.; Hong, Z.; Kido, J. Squaraine Dyes for Organic Photovoltaic Cells. *J. Mater. Chem. A*, **2015**, *3*, 14517-14534.

(40) Shi, Y.; Hill, R. B. M.; Yum, J.-H.; Dualeh, A.; Barlow, S.; Grätzel, M.; Marder, S. R.; Nazeeruddin, M. K. A High-Efficiency Panchromatic Squaraine Sensitizer for Dye-Sensitized Solar Cells. *Angew. Chem., Int. Ed*. **2011**, *50*, 6619-6621.

(41) Delcamp, J. H.; Shi, Y.; Yum, J.-H.; Sajoto, T.; Dell'Orto, E.; Barlow, S.; Nazeeruddin, M. K.; Marder, S. R.; Grätzel, M. The Role of π Bridges in High-Efficiency DSCs Based on Unsymmetrical Squaraines. *Chem. Eur. J.***2013**, *19*, 1819-1827.

(42) Geiger, T.; Kuster, S.; Yum, J.-H.; Moon, S.-J.; Nazeeruddin, M. K.; Grätzel, M.; Nüesch, F. Molecular Design of Unsymmetrical Squaraine Dyes for High Efficiency Conversion of Low Energy Photons into Electrons Using TiO_2Nanocrystalline Films. *Adv. Funct. Mater*. **2009**, *19*, 2720-2727.

(43) Alagumalai, A.; M. K., M. F.; Vellimalai, P.; Sil, M. C.; Nithyanandhan, J. Effect of Out-of-plane Alkyl Group's Position in Dye-sensitized Solar Cell Efficiency: A Structure-Property Relationship Utilizing Indoline Based Unsymmetrical Squaraine Dyes. *ACS Appl. Mater. Interfaces* **2016**, *8*, 35353-35367.

(44) Bisht, R.; M. K., M. F.; Singh, A. K.; Nithyanandhan, J. Sensitized Solar Cells: Unsymmetrical Squaraine Dyes Incorporating Benzodithiophene π-Spacer with Alkyl Chains to Extend Conjugation, Control the Dye Assembly on TiO_2, and Retard Charge Recombination. *J. Org. Chem.* **2017**, *82*, 1920-1930.

(45) Jradi, F. M.; Kang, X.; O'Neil, D.; Pajares, G.; Getmanenko, Y. A.; Szymanski, P.; Parker, T. C.; El-Sayed, M. A.; Marder, S. R. Near-Infrared Asymmetrical Squaraine

Sensitizers for Highly Efficient Dye Sensitized Solar Cells: The Effect of π-Bridges and Anchoring Groups on Solar Cell Performance. *Chem. Mater*. **2015**, *27*, 2480-2487.

(46) Jradi, F. M.; O'Neil, D.; Kang, X.; Wong, J.; Szymanski, P.; Parker, T. C.; Anderson, H. L.; El-Sayed, M. A.; Marder, S. R. A Step Toward Efficient Panchromatic Multi-Chromophoric Sensitizers for Dye Sensitized Solar Cells. *Chem. Mater*. **2015**, *27*, 6305-6313.

(47) Park, J.; Barbero, N.; Yoon, J.; Dell'Orto, E.; Galliano, S.; Borrelli, R.; Yum,J.-H.; Censo, D. D.; Grätzel, M.; Nazeeruddin, M. K.; Barolo, C.; Viscardi, G. Panchromatic Symmetrical Squaraines: A Step Forward in the Molecular Engineering of Low Cost Blue-greenish Sensitizers for Dye-sensitized Solar Cells. *Phys. Chem. Chem. Phys.*, **2014**, *16*, 24173-24177.

(48) Kasha, M.; Rawls, H. R.; Ashraf El-Bayoumi, M. The Exciton Model in Molecular Spectroscopy. *Pure Appl. Chem*. **1965,** *11*, 371-392.

(49) Alex, S.; Santhosh, U.; Das, S. Dye Sensitization of Nanocrystalline TiO_2: Enhanced Efficiency of Unsymmetrical Versus Symmetrical Squaraine Dyes. *J. Photochem. Photobiol. A* **2005**, *172*, 63-71.

(50) Otsuka, A.; Funabiki, K.; Sugiyama, N.; Yoshida, T.; Minoura, H.; Matsui, M. Dye Sensitization of ZnO by Unsymmetrical Squaraine Dyes Suppressing Aggregation. *Chem. Lett.* **2006**, *35*, 666-667.

(51) de Miguel, G.; Ziółek, M.; Zitnan, M.; Organero, J. A.; Pandey, S. S.; Hayase, S.; Douhal, A. Photophysics of H- and J-Aggregates of Indole-Based Squaraines in Solid State. *J. Phys. Chem. C* **2012**, *116*, 9379-9389.

(52) Mulhern, K. R.; Detty, M. R.; Watson, D. F. Effects of Surface-Anchoring Mode and Aggregation State on Electron Injection from Chalcogenorhodamine Dyes to Titanium Dioxide. *J. Photochem. Photobiol. A* **2013**, *264*, 18-25.

(53) Mann, J. R.; Gannon, M. K.; Fitzgibbons, T. C.; Detty, M. R.; Watson, D. F. Optimizing the Photocurrent Efficiency of Dye-Sensitized Solar Cells through the Controlled Aggregation of Chalcogenoxanthylium Dyes on Nanocrystalline Titania Films. *J. Phys. Chem. C***2008**, *112*, 13057-13061.

(54) Hua, Y.; Chang, S.; Huang, D.; Zhou, X.; Zhu, X.; Zhao, J.; Chen, T.; Wong, W.-Y.; Wong, W.-K. Significant Improvement of Dye-Sensitized Solar Cell Performance Using Simple Phenothiazine-Based Dyes. *Chem. Mater*.**2013**, *25*, 2146-2153.

(55) Feldt, S. M.; Gibson, E. A.; Gabrielsson, E.; Sun, L. C.; Boschloo, G.; Hagfeldt, A. Design of Organic Dyes and Cobalt Polypyridine Redox Mediators for High-Efficiency Dye-Sensitized Solar Cells. *J. Am. Chem. Soc*. **2010**, *132*, 16714-16724.

(56) Gemma, S.; Gabellieri, E.; Coccone, S. S.; Martí, F.; Taglialatela-Scafati, O.; Novellino, E.; Campiani, G.; Butini. S. Synthesis of Dihydroplakortin, 6-epi- Dihydroplakortin, and Their C10-Desethyl Analogues. *J.Org. Chem*. **2010**, *75*, 2333-2340.

(57) Karjule, N.; M. K., M. F.; Nithyanandhan, J. Heterotriangulene-based Unsymmetrical Squaraine Dyes: Synergistic Effects of Donor Moiety and Out-of-plane Branched Alkyl Chains on Dye Cell Performance. *J. Mater. Chem. A*, **2016**, *4*, 18910-18921.

(58) Oushiki, D.; Kojima, H.; Terai, T.; Arita, M.; Hanaoka, K.; Urano, Y.; Nagano. T. Development and Application of a Near-Infrared Fluorescence Probe for Oxidative Stress Based on Differential Reactivity of Linked Cyanine Dyes. *J. Am. Chem. Soc.* **2010**, *132*, 2795-2801.

(59) Cusido, J.; Ragab, S. S.; Thapaliya, E. R.; Swaminathan, S.; Garcia-Amoros, J.; Roberti, M. J.; Araoz, B.; Mazza, M. M. A.; Yamazaki, S.; Scott, A. M.; Raymo, F. M.; L. Bossi. M. A Photochromic Bioconjugate with Photoactivatable Fluorescence for Superresolution Imaging. *J. Phys. Chem. C* **2016**, *120*, 12860-12870.

(60) Argazzi, R.; Bignozzi, C. A.; Heimer, T. A.; Castellano, F. N.; Meyer, G.Enhanced Spectral Sensitivity from Ruthenium(II) Polypyridyl Based Photovoltaic Devices. *J. Inorg. Chem.* **1994**, *33*, 5741-5749.

(61) Aghazada, S.; Gao, P.; Yella, A.; Marotta, G.; Moehl, T.; Teuscher, J.; Moser, J.-E.; Angelis, F. D.; Gratzel, M.; Nazeeruddin, M. K. Ligand Engineering for the Efficient Dye-Sensitized Solar Cells with Ruthenium Sensitizers and Cobalt Electrolytes. *Inorg. Chem.* **2016**, *55*, 6653-6659.

(62) Li, G.; Liang, M.; Wang, H.; Sun, Z.; Wang, L.; Wang, Z.; Xue, S. Significant Enhancement of Open-Circuit Voltage in Indoline-Based Dye-Sensitized Solar Cells via Retarding Charge Recombination. *Chem. Mater.* **2013**, *25*, 1713-1722.

(63) Cui, Y.; Wu, Y.; Lu, X.; Zhang, X.; Zhou, G.; Miapeh, F. B.; Zhu, W.; Wang, Z.-S. Incorporating Benzotriazole Moiety to Construct D-A-π-A Organic Sensitizers for Solar Cells: Significant Enhancement of Open-Circuit Photovoltage with Long Alkyl Group. *Chem. Mater.* **2011**, *23*, 4394-4401.

(64) Heimer, T. A.; D'Arcangelis, S. T.; Farzad, F.; Stipkala, J. M.; Meyer, G. J. An Acetylacetonate-Based Semiconductor-Sensitizer Linkage. *Inorg. Chem.* **1996**, *35,* 5319-5324.

(65) Becke, A. D. Density-Functional Thermochemistry. III. The Role of Exact Exchange. *J. Chem. Phys.* **1993**, *98*, 5648.

(66) Lee, C.; Yang, W.; Parr, R. G. Development of the Colle-Salvetti Correlation-Energy Formula into a Functional of the Electron Density. *Phys. Rev. B,* **1988**, *37*, 785-789.

(67) Becke, A. D. A New Mixing of Hartree-Fock and Local Density-Functional Theories. *J. Chem. Phys.* **1993**, *98*, 1372-1377.

(68) Frisch, M. J.; Pople, J. A.; Binkley, J. S. Self- Consistent Molecular Orbital Methods. 25. Supplementary Functions for Gaussian Basis Sets. *J. Chem. Phys.,* **1984**, *80*, 3265-3269.

(69) Frisch, M. J.; Trucks, G. W.; Schlegel, H. B.; Scuseria, G. E.; Robb, M. A.; Cheeseman, J. R.; Scalmani, G.; Barone, V.; Mennucci, B.; Petersson, G. A.; Nakatsuji, H.; Caricato, M.; Li, X.; Hratchian, H. P.; Izmaylov, A. F.; Bloino, J.; Zheng, G.; Sonnenberg, J. L.; Hada, M.; Ehara, M.; Toyota, K.; Fukuda, R.; Hasegawa, J.; Ishida, M.; Nakajima, T.; Honda, Y.;

Kitao, O.; Nakai, H.; Vreven, T.; Montgomery Jr., J. A.; Peralta, J. E.; Ogliaro, F.; Bearpark, M. J.; Heyd, J.; Brothers, E. N.; Kudin, K. N.; Staroverov, V. N.; Kobayashi, R.; Normand, J.; Raghavachari, K.; Rendell, A. P.; Burant, J. C.; Iyengar, S. S.; Tomasi, J.; Cossi, M.; Rega, N.; Millam, N. J.; Klene, M.; Knox, J. E.; Cross, J. B.; Bakken, V.; Adamo, C.; Jaramillo, J.; Gomperts, R.; Stratmann, R. E.; Yazyev, O.; Austin, A. J.; Cammi, R.; Pomelli, C.; Ochterski, J. W.; Martin, R. L.; Morokuma, K.; Zakrzewski, V. G.; Voth, G. A.; Salvador, P.; Dannenberg, J. J.; Dapprich, S.; Daniels, A. D.; Farkas, Ö.; Foresman, J. B.; Ortiz, J. V.; Cioslowski, J.; Fox, D. J. *Gaussian 09*; Gaussian, Inc. Wallingford, CT, USA, 2009.

(70) Chen, H.; Farahat, M. S.; Law, K. Y.; Whitten, D. G. Aggregation of Surfactant Squaraine Dyes in Aqueous Solution and Microheterogeneous Media: Correlation of Aggregation Behavior with Molecular Structure. *J. Am. Chem. Soc.* **1996**, *118* (11), 2584–2594.

(71) Maiti, N. C.; Mazumdar, S.; Periasamy, N. J- and H-Aggregates of Porphyrin - Surfactant Complexes: Time-Resolved Fluorescence and Other Spectroscopic Studies. *J. Phys. Chem. B* **1998**, *102* (9), 1528–1538.

(72) Bisquert, J.; Zaban, A.; Greenshtein, M.; Mora-Sero, I. Determination of Rate Constants for Charge Transfer and the Distribution of Semiconductor and Electrolyte Electronic Energy Levels in Dye-Sensitized Solar Cells by Open-circuit Photovoltage Decay Method. *J. Am. Chem. Soc.* **2004**, *126*, 13550-13559.

(73) Wang, Q.; Moser, J. E.; Grätzel, M. Electrochemical Impedance Spectroscopic Analysis of Dye-Sensitized Solar Cells. *J. Phys. Chem. B* **2005**, *109*, 14945-14953.

Position of Anchoring Group to Controls the Orientation and Self-Assembly of Unsymmetrical Squaraine Dyes on TiO₂ Surface
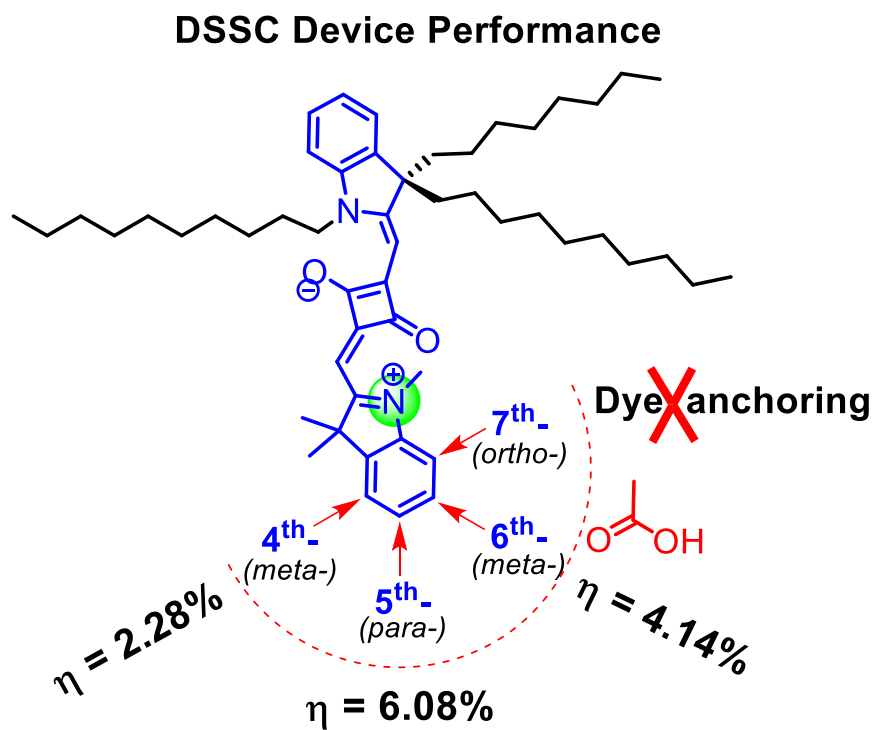
3.1 INTRODUCTION

The modulable nature of the various components associated with third-generation photovoltaic devices makes this technology very attractive.[1,2] Light absorbing dye molecules play an important role in harvesting the photons from the solar spectrum besides nano-structured metal oxide photoelectrodes,[3] electrolytes,[4] and counter electrode materials[5,6] employed in dye-sensitized solar cell (DSSC) devices. In DSSCs, the rate of charge injection from the photoexcited sensitizer to the conduction band of TiO_2 determines the overall device performance besides dye regeneration and charge recombination processes.[7] Ruthenium complexes based sensitizers exhibited the DSSC device performances of over 11%.[8] Further, metal-free organic sensitizers have attracted the wide attention due to its ease of tuning the light-harvesting properties by the synthetic design of D-π-A,[9] D-A- π-A,[10] D-D'- π-A,[11] and D-A-D[12,13] based sensitizers. High DSSC device performance has been achieved by proper molecular engineering of the sensitizers recently by considering both electronic and steric factors.[14,15] Electronic coupling between the dye-components such as donor, π-spacer, acceptor, and anchoring units are the important factors that govern light-harvesting property, photo-induced charge transfer from donor to acceptor within the sensitizer and further photoexcited dye to the semiconducting metal oxide.[16,17] Further, planarization of donor,[18,19] and π-spacer[20,21] showed modulated electronic properties with improved device performance. Moreover, the length of the π-spacer,[22,23] geometry/aggregation[24] and orientation[25-27] of the sensitizer on the TiO_2 surface also plays an important role in determining the performances of photovoltaic devices. Meso-phenyl substituted porphyrin dyes have been utilized to study the effect of orientation of the dye on the TiO_2 surface which helps to understand the through-space and through-bond electron transfer processes by the *ortho*-, *meta*-, and *para*- substituted porphyrin dyes.[26,28] Due to the orthogonal orientation of meso-phenyl group to the porphyrin ring, the electronic coupling between porphyrin core and phenyl spacer is very poor which leads to the establishment of through space charge transfer by the tilted geometry of the dye.[29-31] Seminal work by Anderson[32] and Therien[33] paved the importance of acetylenic π-spacers over phenyl π-spacers at the meso position for the electronic interaction between two porphyrin units. Several D-π-A dyes have been designed and studied with high device efficiency.[34-37] Even in meso-acetylenic π-spacer based porphyrin dyes, the position of anchoring group dictates the device performance as the

anchoring groups at non-conductive *meta-* position showed very poor photovoltaic response over sensitizer with anchoring group at the *para-* position.[27] Recently, structural design of meso-substituted porphyrins[35] such as fused porphyrin,[38] double strapping,[39] concerted companion dyes,[40] and co-sensitization[41] approaches have been used to enhance the device performance of porphyrin based sensitizers. Besides porphyrin[35] and phthalocyanine[42] based sensitizers, D-A-D type squaraine dyes possess very good absorption in the far-red region with a good extinction coefficient ($> 10^5$ $M^{-1}cm^{-1}$). This class of dyes exhibits dye-dye interaction that leads to observe H- and J-type aggregation in solution[43-45] as well as on solid-state.[46] Such self-assembled aggregated structures have been exploited in sensors,[47-50] organic photoconductive materials,[51] field-effect transistors,[52] and organic photovoltaics.[53,54] Formation of such aggregated structures on the 101 facet of anatase TiO_2 surface is facile due to the periodic arrangements of 5-coordinated Ti site, where the dye anchors and acts as a photo-anode.[24] However, the formation of such aggregated structures of sensitizers showed varied DSSC device performance due to the self-quenching of photoexcited states besides broadening the absorption profile.[24,55] Introduction of alkyl groups either in the donor or π-spacer components helps to controls the formation of aggregated structures on the TiO_2 surface for the enhanced DSSC device performance.[56-58] Thus the introduction of in-plane and out-of-plane alkyl groups in the unsymmetrical squaraine dyes boost both V_{OC} and J_{SC} by passivating the TiO_2 surface and broadened IPCE response (by controlled aggregation), respectively.[59, 60] Further, the optimal structural feature in squaraine dyes in terms of the number of carbon atoms in either sp^3-C and N-atoms of indoline units has been studied systematically. As the unsymmetrical squaraine dyes are D-A-D' structures with anchoring group at any one of the donor units, for the understanding of the charge injection process to TiO_2 either through-space or spacer is of fundamental importance. Hence to investigate the effect of the position of anchoring group which in turn to controls the orientation of the dye with respect to the TiO_2 surface, and coupling the dyes to TiO_2 either conductive *(ortho-* and *para-*carboxyl group) or non-conductive (meta-carboxyl group) charge injection, unsymmetrical squaraine dyes with carboxylic acid groups at the -4th, -5th, -6th and -7th positions of one of the indolium donor units is designed in the present work (**Figure 1**). As shown in **Figure 1**, alkyl groups at the sp^3-C and N-atoms at the indoline donor moiety far away from the anchoring group is fixed to control the aggregation of dyes and the position of anchoring group is changed in the indoline unit. Further, controlling the orientation of the dyes on the TiO_2 surface

may modulate the formation of aggregated structures which may shed the light on the importance of through space charge transfer for the device performance despite the presence of anchoring group at the non-conductive *meta-* position.
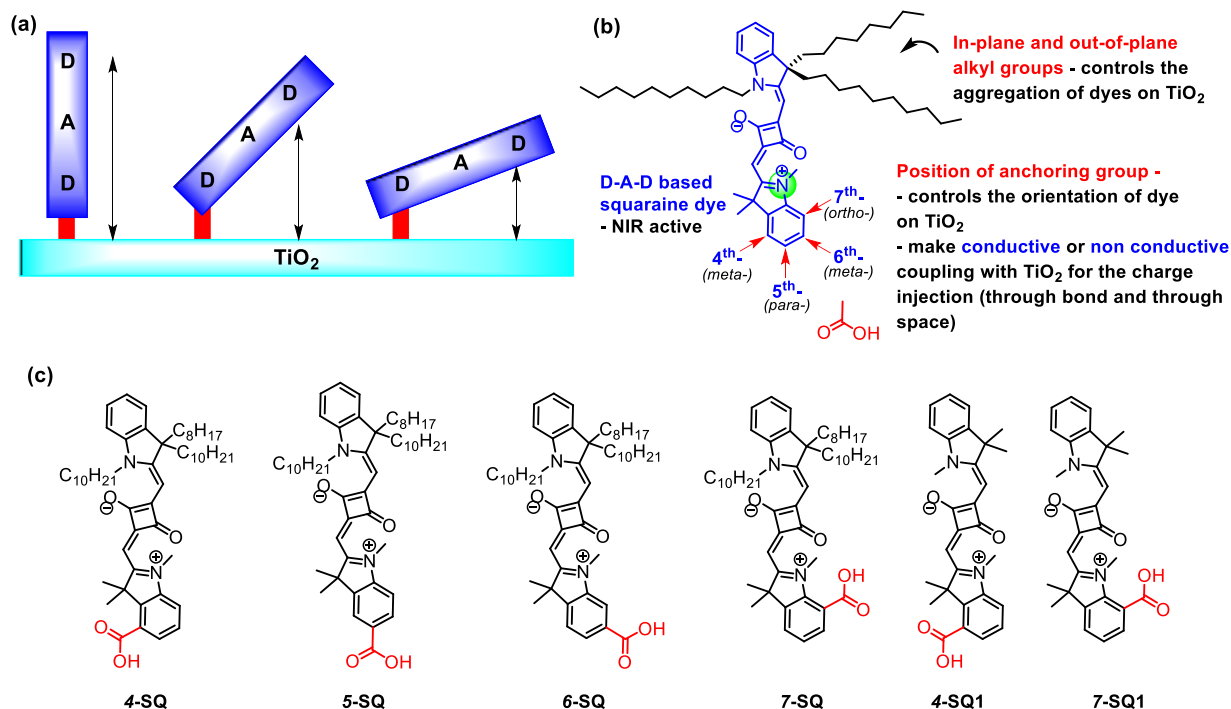
Figure 1. (a) Orientation of the D-A-D based dyes on TiO$_2$ surface, (b) structure and position of anchoring groups for the designed squaraine dyes, and (c) targeted squaraine dyes.

3.2 EXPERIMENTAL SECTION

3.2.1 General methods

Chemicals required for the synthesis of 4-SQ, 4-SQ1, 5-SQ, 6-SQ, 7-SQ, and 7-SQ1 dyes are 3-aminobenzoic acid, phenylhydrazinehydrochloride, 2-hydrazinobenzoicacid hydrochloride, 1,3,3-trimethyl-2-methyleneindoline, 3,4-dibutoxycyclobut-3-ene-1,2-dione, 1-iodomethane, 1-iododecane, Tin(II) chloride dihydrate, sodium nitrite and solvents were purchased from commercial sources. Bruker NMR spectrometers AV 200 MHz, AV 400 MHz and AV-500 MHz frequency were used to record ^{1}H and ^{13}C NMR in CDCl$_3$, DMSO-d_6. SYNAPT G2 HDM has been used to measured high-resolution mass spectrometric (HRMS) measurements in MeOH.

EZ-Melt automated melting point apparatus has been used for the melting point measurement of all solid compounds. Bruker FTIR spectrometer has been used to measure the IR-spectrum of all the squaraine dyes as such and on the surface of TiO_2. SPECORD® 210/ PLUS, Analytikjena UV−Visible spectrophotometer has been used to record both absorption spectra and light-harvesting efficiency (LHE) of SQ dyes at room temperature. For LHE, 6 μm thin film of TiO_2 or ZrO_2 coated on the transparent glass slide which is further dipped in 0.1 mM dye solution for 12 h at room temperature. Edinburgh spectrofluorometer FS5 has been used to record the emission of the SQ dyes at room temperature. BioLogic SP300 potentiostat were used to performed the cyclic voltammetric studies of 4-SQ, 5-SQ, 6-SQ, 7-SQ, and 7-SQ1 dyes in anhydrous CH_2Cl_2 solvent, whereas, for 4-SQ1 dye a mixture of 95% of CH_2Cl_2 and 5% of DMSO solvent was used at 25 °C under an inert atmosphere, where platinum wire, platinum foil and non-aqueous Ag/Ag^+ (0.01M) were used as working, counter and reference electrode respectively, $TBAClO_4$ (0.03 M) and Ferrocene/Ferrocene$^+$ has been used as a supporting electrolyte and as an internal-standard respectively, where the scan performed with 50 mV s^{-1} scan rate. PHOTO EMISSION TECH (PET, CT200AAA, USA) solar-simulator has been used for *I-V* studies of the cells and Newport QE measurement kit has been used to measured IPCE curve. For dye desorption studies of SQ dyes area of the photoanode was 0.23 cm^2 (8 μm thick), dipping time of photoanode in dye-solution (0.1mM) was 12 h at room temperature, 0.2 M NaOH in EtOH: H_2O (1:1) 9 mL was used to desorb adsorbed dyes and path length of the cuvette was 0.1 cm^2. Electrochemical impedance measurements (EIS) were performed on BioLogic SP300 potentiostat and carried out in dark with various applied potential and 3 MHz to 10 mHz frequency ranges, with 10 mV sinus amplitude.

3.2.2 Dye-sensitized solar cell fabrication. Fluorine-doped SnO_2 glass (8- 10 Ω /sq; Pilkington TEC 7) was washed with mucasol (2 % in water), de-ionized water (4 times), and isopropanol (two times) by using ultrasonic-bath to make cleaned. To grow a thin film TiO_2, FTO was treated with 40 mM aqueous $TiCl_4$ solution at 70 °C for 30 min, washed with the de-ionized water then EtOH and dried at 110 °C for 10 min. A paste of TiO_2 nanocrystal (< 20 nm, Ti-Nanoxide T/SP, Solaronix) was coated on FTO conducting side by using doctor-blade technique and kept for 15 min in air then heated at 120 °C in the air for 20 min, then coated with scattering layer TiO_2 paste (WER2-O, Dyesol) and heated at 120 °C for 10 min in air, then sintered at 325 °C for 10

min, 375 °C for 10 min, 450 °C for 10 min and 500 °C for 15 min, where the heating rate was 5 °C per min in air. After sintering, films were treated with 40 mM aqueous TiCl$_4$ solution at 70 °C for 30 min, washed with the de-ionized water then EtOH and sintered at 500 °C for 20 min. Then immersed the cells (area of TiO$_2$ is 0.23 cm^2) in 0.1 mM dye solution of 4-SQ, 5-SQ, 6-SQ, 7-SQ, and 7-SQ1 dyes (in 97.5% CH$_3$CN and 2.5% CHCl$_3$) whereas, 4-SQ (in 97.5% CH$_3$CN and 2.5% of DMSO) without and with CDCA for 12 h. Platinum foil used as a cathode, iodolyte Z-50 (Solaronix) was used as electrolyte, 25 μm spacer and area of black mask was 0.23 cm^2. The device performance of SQ dyes were measured under standard simulator condition (AM 1.5 G, 100 mW/cm^2).

3.2.3 Mott-Schottky analysis of SQ dyes. The Mott-Schottky analysis of the SQ series dyes anchored TiO$_2$ photo anodes were performed using three electrode system (dye anchored on the TiO$_2$ photo-anode as working electrode, Pt-foil as counter and non-aqueous Ag/Ag$^+$ (0.01 M) as a reference electrode) with iodolyte redox-couple (0.5M LiI and 0.05M I$_2$ in CH$_3$CN). The flat-band potential from the plot is calculated using the Mott-Schottky relation (Eq.1).[63-65]

$$(C_{CS})^{-2} = 2(E-E_{fb}-kT/e) / N_D εε_0 eA^2$$
 Equation 1

Where, C$_{CS}$= Space charge capacity, N$_D$= Charge carrier density of the sample, ε= Dielectric constant of the sample, ε$_0$= permittivity in vacuum, A= active surface area, k$_B$, T, and e are Boltzmann constant, temperature and electronic charge, respectively. The flat band potential is calculated from the intercept extrapolating a straight line from 1/C^2 versus potential plot.

3.2.4 Synthesis.

(a) Synthesis of semisquaraine

3-Decyl-2-methyl-3-octyl-3H-indole (2): Phenylhydrazinehydrochloride, **1** (0.78 g, 5.37 mmol) and 3-octyltridecan-2-one[18] (2 g, 6.44 mmol) were dissolved in 20 mL of AcOH in a round bottom flask then refluxed for 24 h. The reaction mixture was cooled to room temperature and solvents were removed under reduced pressure and purified by column chromatography (100–200 mesh SiO$_2$, EtOAc/ pet. ether). Yield: 0.75 g, 36.4 %. ^{1}H NMR (200 MHz, CDCl$_3$): δ 0.40 - 0.77 (m, 4 H) 0.77 - 0.89 (m, 6 H) 1.10 (br. s., 12 H) 1.25 (s, 6 H) 1.20 (s, 7 H) 1.58 - 1.99 (m, 4

H) 2.21 (s, 3 H) 7.07 - 7.26 (m, 2 H) 7.26 - 7.37 (m, 1 H) 7.52 (d, J=7.39 Hz, 1 H); ^{13}C NMR (101 MHz, CDCl$_3$): δ 14.03, 14.07, 15.92, 22.56, 22.62, 23.50, 29.12, 29.16, 29.23, 29.32, 29.46, 29.61, 29.78, 31.73, 31.83, 31.90, 36.96, 62.59, 119.49, 121.59, 124.92, 127.42, 142.19, 154.86, 186.78.

(a) Synthesis of semisquaraine

(b) Synthesis of indolium salts with carboxylic acid group at *4th*-, *5th*-, *6th*-, and *7th*- position

(c) Synthesis of unsymmetrical squaraine dyes
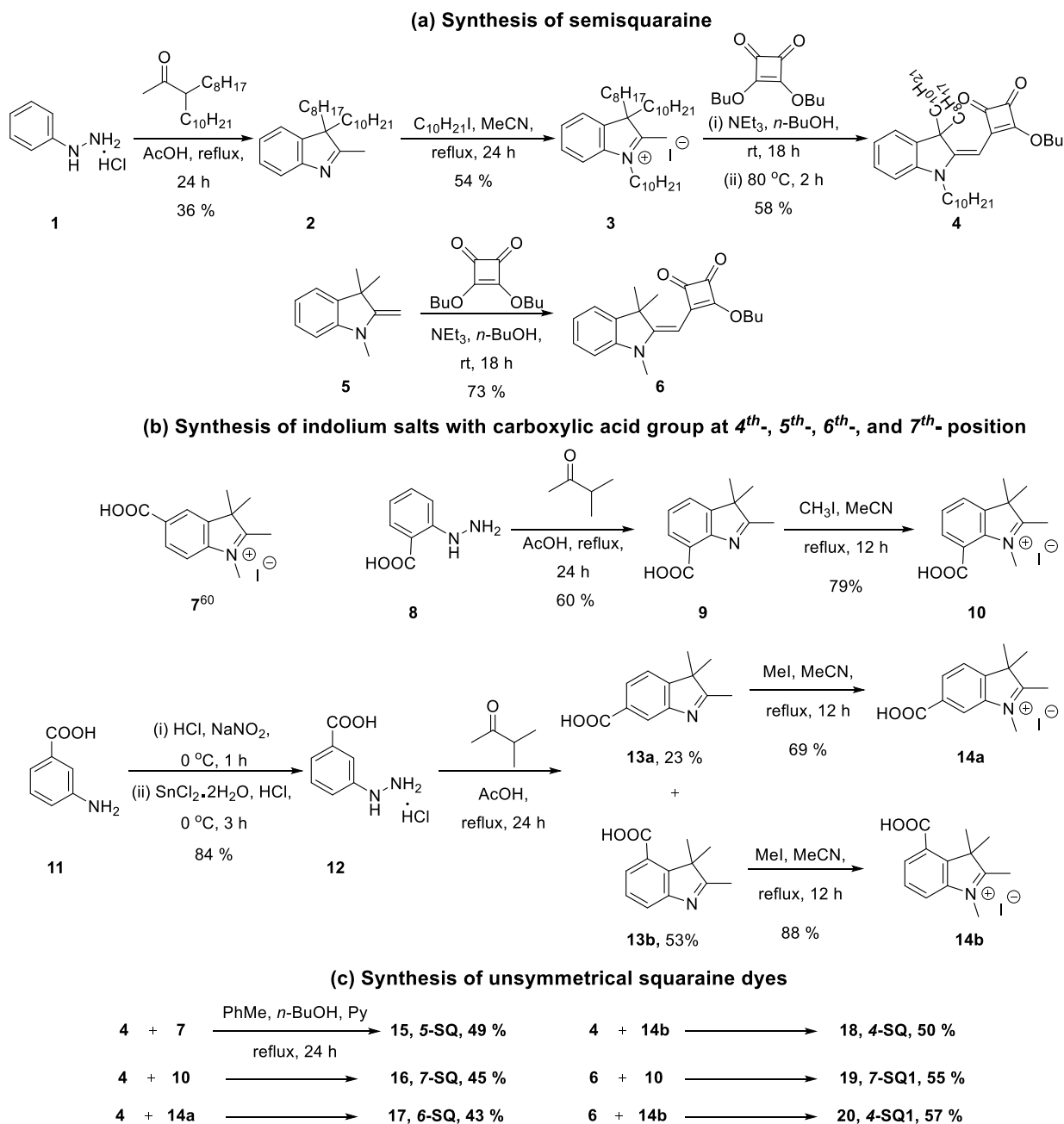
Scheme 1. Synthetic scheme of SQ dyes with anchoring group at different positions.

1,3-Didecyl-2-methyl-3-octyl-3H-indol-1-ium (3): The compound **2**[60] (0.7 g, 1.83 mmol) and 1-iododecane (0.73 g, 2.74 mmol) were dissolved in 10 mL of CH_3CN in a round bottom flask and refluxed for 24 h. The reaction mixture was cooled to room temperature and solvents were removed under reduced pressure. Reaction mixture was washed twice with *n*-pentane (20 mL) to get required indolium salt. Yield: 0.65 g, 54.5 %. ^{1}H NMR (200 MHz, CDCl$_3$): δ 0.57 - 0.72 (m, 2 H) 0.78 - 0.89 (m, 11 H) 1.06 - 1.26 (m, 36 H) 1.45 - 1.61 (m, 2 H) 1.92 (d, *J*=6.62 Hz, 2 H) 2.01 - 2.25 (m, 4 H) 3.14 (s, 3 H) 4.87 (t, *J*=7.28 Hz, 2 H) 7.48 - 7.58 (m, 1 H) 7.59 - 7.70 (m, 2 H) 7.72 - 7.79 (m, 1 H); ^{13}C NMR (101 MHz, CDCl$_3$): δ 7.35, 13.96, 14.01, 17.28, 22.46, 22.55, 23.97, 26.87, 28.45, 28.56, 28.89, 28.96, 29.15, 29.19, 29.21, 29.33, 29.39, 30.41, 31.56, 31.74, 31.79, 33.47, 37.27, 50.44, 63.67, 115.36, 123.59, 129.68, 130.03, 138.77, 142.19, 195.60; HRMS (*m/z*): [M]$^+$ calculated for $C_{37}H_{66}N$: 524.5190; found: 524.5201.

(E)-3-Butoxy-4-((1,3-didecyl-3-octylindolin-2-ylidene)methyl)cyclobut-3-ene-1,2-dione   (4): Compound **3** (0.5 g, 0.767 mmol) was dissolved in 7 mL *n*-BuOH in a round bottom flask followed by the dropwise addition of NEt$_3$ (0.116 g, 1.15 mmol). 3,4-Dibutoxycyclobut-3-ene-1,2-dione (0.17 g, 0.77 mmol) was added to the above mixture at once and the resultant mixture was stirred at room temperature for 18 h. Further, the reaction mixture was heated to 80 ^{o}C for 2 h, cooled to room temperature and solvents were removed under reduced pressure. The residue was purified by column chromatography (SiO$_2$, 100-200 mesh, 2.5 % EtOAc and 97.5 % pet. ether) to obtain the required compound as yellow solid. Yield: 0.3 g, 58 %. Mp: 76 ^{o}C. ^{1}H NMR (400 MHz, CDCl$_3$): δ 0.52 (m, 2 H) 0.76 (m, 2 H) 0.81 - 0.90 (m, 9 H) 0.99 - 1.03 (m, 3 H) 1.04 - 1.29 (m, 34 H) 1.33 - 1.44 (m, 4 H) 1.53 (m, 2 H) 1.73 (m, 2 H) 1.82 - 1.92 (m, 4 H) 2.49 (m, 2 H) 3.83 (t, *J*=7.33 Hz, 2 H) 4.87 (t, *J*=6.64 Hz, 2 H) 5.52 (s, 1 H) 6.86 (d, *J*=7.79 Hz, 1 H) 7.07 (t, *J*=7.33 Hz, 1 H) 7.20 (d, *J*=7.33 Hz, 1 H) 7.24 - 7.30 (m, 1 H); ^{13}C NMR (101 MHz, CDCl$_3$): δ 13.78, 14.14, 14.18, 18.85, 22.69, 22.73, 24.01, 26.57, 27.28, 29.17, 29.22, 29.30, 29.37, 29.46, 29.53, 29.61, 29.67, 31.85, 31.94, 32.23, 39.65, 43.07, 57.16, 73.71, 81.76, 108.15, 122.12, 122.67, 127.71, 137.36, 144.60, 166.37, 173.12, 186.95, 187.43, 192.97.

(E)-3-Butoxy-4-((1,3,3-trimethylindolin-2-ylidene)methyl)cyclobut-3-ene-1,2-dione   (6): 1,3,3-Trimethyl-2-methyleneindoline **5** (5 g, 28.86 mmol) was dissolved in 20 mL *n*-BuOH in a single neck round bottom flask followed by the dropwise addition of NEt$_3$ (4.4 g, 43.3 mmol). 3,4-Dibutoxycyclobut-3-ene-1,2-dione (6.5 g, 28.86 mmol) added to the above mixture at once

and the resultant mixture was stirred at room temperature for 18 h. Then yellow-colour residue was filtered out and washed with 50 mL of hexane and dried at high vacuum pressure pump. Yield: 6.8 g, 73 %. Mp: 132 °C. ^{1}H NMR (400 MHz, DMSO-d_6): δ 0.95 (t, J=7.56 Hz, 3 H) 1.40 - 1.49 (m, 2 H) 1.55 (s, 6 H) 1.76 - 1.85 (m, 2 H) 3.40 (s, 3 H) 4.80 (t, J=6.41 Hz, 2 H) 5.32 (s, 1 H) 7.07 (td, J=7.33, 0.92 Hz, 1 H) 7.20 (d, J=8.24 Hz, 1 H) 7.30 (td, J=7.67, 1.14 Hz, 1 H) 7.44 (dd, J=7.33, 0.92 Hz, 1 H); ^{13}C NMR (101 MHz, DMSO-d_6): δ 13.51, 18.16, 26.40, 29.83, 31.52, 47.28, 73.31, 80.79, 109.06, 121.86, 122.51, 127.80, 140.27, 142.89, 168.51, 172.40, 186.47, 187.74, 192.27; HRMS (m/z): [M + H]$^+$ calculated for $C_{20}H_{24}O_3N$: 326.1751; found: 326.1754.

(b) Synthesis of indolium salts with carboxylic acid group at 4th-, 5th-, 6th-, and 7th- position

2,3,3-Trimethyl-3H-indole-7-carboxylic acid (9): A suspension of 2-hydrazinobenzoicacid hydrochloride **8** (2.0 g, 10.63 mmol) and 3-methyl-2-butanone (1.83 g, 21.27 mmol) in 20 mL of AcOH in a round bottom flask was refluxed for 12 h. The reaction mixture was cooled and solvents were removed under reduced pressure then purified by column chromatography (100–200 mesh SiO$_2$, MeOH 1 % CH$_2$Cl$_2$ 99 %). Yield: 1.3 g, 60 %. Mp: 107 °C. ^{1}H NMR (400 MHz, CDCl$_3$): δ 1.38 (s, 6 H) 2.39 (s, 3 H) 7.36 (t, J=7.63 Hz, 1 H) 7.47 - 7.53 (m, 1 H) 8.02 - 8.08 (m, 1 H); ^{13}C NMR (101 MHz, CDCl$_3$): δ 15.73, 22.80, 54.52, 120.21, 126.04, 126.44, 129.55, 145.14, 152.14, 166.23, 191.04; HRMS (m/z): [M - H]$^+$ calculated for $C_{12}H_{12}O_2N$: 202.0863; found: 202.0864.

7-Carboxy-1,2,3,3-tetramethyl-3H-indol-1-ium iodide (10): Compound **9** (0.5 g, 2.46 mmol) and 1-iodomethane (1.048 g, 7.386 mmol) were dissolved in 5 mL of anhydrous CH$_3$CN in a round bottom flask and heated to reflux for 16 h. The reaction mixture was cooled to room temperature and solvents were removed under reduced pressure. Reaction mixture was washed twice with Et$_2$O (20 mL) to get required semisolid indolium salt. Yield: 0.67 g, 79 %. ^{1}H NMR (400 MHz, DMSO-d_6): δ 1.52 (s, 6 H) 2.76 (s, 3 H) 3.96 (s, 3 H) 7.61 - 7.63 (m, 1 H) 7.80 - 7.84 (m, 1 H) 7.88 - 7.93 (m, 1 H); ^{13}C NMR (101 MHz, DMSO-d_6): δ 14.54, 22.21, 35.14, 54.45, 115.64, 123.81, 129.35, 129.85, 142.13, 142.63, 167.66, 196.53; HRMS (m/z): [M]$^+$ calculated for $C_{13}H_{16}O_2N$: 218.1176; found: 218.1174.

3-Hydrazinobenzoicacid hydrochloride (12): A mixture of 3-aminobenzoic acid **11** (2 g, 14.58 mmol) in 30 mL of concentrated HCl in a round bottom flask was cooled to 0 ^{o}C. A solution of $NaNO_2$ (1.2 g, 17.5 mmol) in 10 mL of ice-cold water was added dropwise to the above suspension at 0 ^{o}C, and the resultant mixture was stirred for 1 h while keeping the temperature at 0 ^{o}C. In a separate 100 mL Erlenmeyer flask, $SnCl_2$. $2H_2O$ (9.87 g, 43.75 mmol) was dissolved in 15 mL of concentrated HCl, cooled to 0 ^{o}C, and added to the above ice-cold solution dropwise at 0 ^{o}C, and the resultant mixture was again stirred for 3 h while keeping the temperature at 0 ^{o}C. The residue was filtered out and washed with 100 mL of Et_2O. Compound **12** used for next step without further purification. Yield: 2.3 g, 84 %. Mp: 212 ^{o}C. ^{1}H NMR (400 MHz, DMSO-d_6): δ 7.20 (m, 1 H) 7.37 (t, *J*=7.79 Hz, 1 H) 7.44 - 7.49 (m, 1 H) 7.54 (t, *J*=2.06 Hz, 1 H); ^{13}C NMR (101 MHz, DMSO-d_6): δ 114.31, 118.28, 121.43, 129.14, 131.51, 147.02, 167.29; HRMS (*m/z*): [M + H]$^+$ calculated for $C_7H_9O_2N_2$: 153.0659; found: 153.0657.

Synthesis of compounds 13a and 13b: A suspension of 3-hydrazinobenzoicacid hydrochloride **(12)** (2 g, 10.63 mmol) and 3-methyl-2-butanone (1.373 g, 15.95 mmol) in 30 mL of AcOH in a round bottom flask was refluxed for 24 h. Solvents were removed under reduced pressure and purified by column chromatography (100–200 mesh SiO_2, CH_3OH 1.5 % and CH_2Cl_2 98.5 %) to afford the required compounds **13a** and **13b**.

2,3,3-Trimethyl-3H-indole-6-carboxylic acid (13a): Yield: 0.5 g, 23.2 %. Mp: 209 ^{o}C. ^{1}H NMR (400 MHz, CDCl$_3$): δ 1.38 (s, 6 H) 2.53 (s, 3 H) 7.40 (d, *J*=7.93 Hz, 1 H) 8.09 (d, *J*=7.93 Hz, 1 H) 8.43 (s, 1 H); ^{13}C NMR (101 MHz, CDCl$_3$): δ 14.85, 22.83, 53.93, 120.93, 121.30, 127.84, 131.06, 150.06, 152.07, 169.71, 190.42; HRMS (*m/z*): [M **-** H]$^+$ calculated for $C_{12}H_{12}O_2N$: 202.0863; found: 202.0865.

2,3,3-Trimethyl-3H-indole-4-carboxylic acid (13b): Yield: 1.15 g, 53.2 %. Mp: 270 ^{o}C. ^{1}H NMR (400 MHz, DMSO-d_6): δ 1.42 (s, 6 H) 2.23 (s, 3 H) 7.41 (t, *J*=7.79 Hz, 1 H) 7.67 (dd, *J*=7.78, 0.92 Hz, 1 H) 7.74 (dd, *J*=8.01, 1.14 Hz, 1 H); ^{13}C NMR (101 MHz, DMSO-d_6): δ 15.58, 20.37, 55.87, 124.06, 127.35, 127.75, 128.24, 146.45, 155.82, 167.98, 189.96; HRMS (*m/z*): [M **-** H]$^+$ calculated for $C_{12}H_{12}O_2N$: 202.0863; found: 202.0864.

6-Carboxy-1,2,3,3-tetramethyl-3H-indol-1-ium iodide (14a): The compound **13a** (0.3 g, 1.476 mmol) and 1-iodomethane (0.628 g, 4.43 mmol) were dissolved in 10 mL of MeCN and refluxed for 12 h. After cooling, the reaction mixture was dissolved in 2 mL of dichloromethane and added to the stirring diethyl ether portion-wise, the precipitate was collected and washed twice with the fresh portion of Et_2O (15 mL). Yield: 0.35 g, 69 %. Mp: 251 °C. ^{1}H NMR (400 MHz, DMSO-d_6): δ 1.56 (s, 6 H) 2.81 (s, 3 H) 4.04 (s, 3 H) 7.96 (d, J=7.93 Hz, 1 H) 8.19 (d, J=7.93 Hz, 1 H) 8.37 (s, 1 H); ^{13}C NMR (101 MHz, DMSO-d_6): δ 14.78, 21.96, 35.36, 54.61, 116.35, 124.02, 130.77, 132.30, 143.03, 146.41, 166.63, 197.75; HRMS (*m/z*): [M]$^+$ calculated for $C_{13}H_{16}O_2N$: 218.1176; found: 218.1177.

4-Carboxy-1,2,3,3-tetramethyl-3H-indol-1-ium iodide (14b): The compound **13b** (0.3 g, 1.476 mmol) and 1-iodomethane (0.628 g, 4.43 mmol) were dissolved in 10 mL of CH_3CN and refluxed for 12 h. After cooling, the reaction mixture was dissolved in 2 mL of dichloromethane and added to the stirring diethyl ether portion-wise, the precipitate was collected and washed twice with fresh portion of Et_2O (15 mL). Yield: 0.45 g, 88 %. Mp: 292 °C. ^{1}H NMR (400 MHz, DMSO-d_6): δ 1.69 (s, 6 H) 2.82 (s, 3 H) 4.00 (s, 3 H) 7.80 (t, J=8.01 Hz, 1 H) 8.13 (d, J=7.78 Hz, 1 H) 8.19 (d, J=8.24 Hz, 1 H); ^{13}C NMR (101 MHz, DMSO-d_6): δ 14.88, 19.58, 35.61, 56.34, 119.86, 128.87, 129.95, 131.66, 141.68, 144.25, 166.73, 197.33; HRMS (*m/z*): [M]$^+$ calculated for $C_{13}H_{16}O_2N$: 218.1176; found: 218.1177.

(c) Synthesis of unsymmetrical squaraine dyes

General synthetic procedure of 4-SQ, 4-SQ1, 5-SQ, 6-SQ, 7-SQ and 7-SQ1 dyes: Butoxy-semisquaraine (1 equiv.) and indolium salt (1 equiv.) were dissolved in anhydrous PhMe and *n*-BuOH (1:1, 10 mL of each) in a round bottom flask followed by the addition of 0.5 mL of pyridine. The contents were refluxed in Dean-Stark apparatus for 24 h under an inert atmosphere. The reaction mixture was washed with 30 mL of 2N HCl and the organic layer was separated with CH_2Cl_2 (30 mL × 2 times), dried over Na_2SO_4. The reaction mixture was purified by column chromatography (SiO_2, 100-200 mesh, MeOH and CH_2Cl_2) to afford the required dye.

5-Carboxy-2-[[3-[(1,3-dihydro-3-octyl-1,3-didecyl-2H-indol-2-ylidene)methyl]-4-oxo-2-cyclobuten-2-olate-1-ylidene]methyl]-1,3,3-trimethyl-3H-indolium (15, 5-SQ): Compound **4** (0.2 g, 0.3 mmol) and **7**^{59} (0.1 g, 0.3 mmol), column chromatography (SiO_2, 100-200 mesh, 2.5

% MeOH and 97.5 % CH_2Cl_2). Yield: 0.11 g, 49 %. Mp: 121 ^{o}C. ^{1}H NMR (400 MHz, CDCl$_3$): δ 0.46 (br. s., 2 H) 0.72 - 0.86 (m, 11 H) 1.03 - 1.25 (m, 35 H) 1.38 - 1.46 (m, 3 H) 1.83 (br. s., 8 H) 1.92 - 2.09 (m, 2 H) 3.01 (br. s., 2 H) 3.51 (br. s., 3 H) 4.08 (br. s., 2 H) 5.98 (s, 1 H) 6.17 (br. s., 1 H) 6.95 (d, J=6.87 Hz, 1 H) 7.04 (d, J=7.79 Hz, 1 H) 7.22 (t, J=7.33 Hz, 1 H) 7.28 - 7.41 (m, 2 H) 8.07 (br. s., 1 H) 8.14 (d, J=8.24 Hz, 1 H); ^{13}C NMR (101 MHz, CDCl$_3$): δ 14.17, 22.65, 22.70, 22.74, 24.10, 27.31, 27.36, 27.56, 29.15, 29.25, 29.33, 29.52, 29.59, 30.49, 31.86, 31.93, 40.06, 44.24, 48.29, 59.39, 88.02, 88.37, 107.97, 109.83, 122.52, 124.15, 124.66, 127.89, 129.55, 130.82, 131.29, 132.83, 139.52, 141.75, 144.03, 147.34, 148.63, 168.61, 170.74, 171.04, 176.61, 178.80, 180.96, 182.32; IR (cm^{-1}): 2916, 2849, 1699, 1599, 1568, 1483, 1463, 1352, 1263, 1188, 1084, 1041, 924; HRMS (m/z): [M + H]$^+$ calculated for $C_{54}H_{79}O_4N_2$: 819.6034; found: 819.6037.

7-Carboxy-2-[[3-[(1,3-dihydro-3-octyl-1,3-didecyl-2H-indol-2-ylidene)methyl]-4-oxo-2-cyclobuten-2-olate-1-ylidene]methyl]-1,3,3-trimethyl-3H-indolium (16, 7-SQ): Compound **4** (0.2 g, 0.3 mmol) and **10** (0.1 g, 0.3 mmol), column chromatography (SiO$_2$, 100-200 mesh, 2.4 % MeOH and 97.6 % CH_2Cl_2). Yield: 0.1 g, 44.8 % (semisolid). ^{1}H NMR (400 MHz, CDCl$_3$): δ 0.37 - 0.52 (m, 2 H) 0.70 - 0.88 (m, 11 H) 1.04 - 1.27 (m, 35 H) 1.38 - 1.45 (m, 3 H) 1.74 - 1.88 (m, 8 H) 1.93 - 2.07 (m, 2 H) 3.02 (br. s., 2 H) 3.50 (d, J=12.82 Hz, 3 H) 3.85 - 4.03 (m, 2 H) 5.92 (br. s., 1 H) 6.06 (br. s., 1 H) 6.95 - 6.99 (m, 1 H) 7.09 - 7.21 (m, 2 H) 7.27 - 7.40 (m, 4 H); ^{13}C NMR (101 MHz, CDCl$_3$): δ 14.09, 22.58, 22.63, 22.67, 24.05, 24.10, 27.15, 27.29, 29.10, 29.22, 29.28, 29.32, 29.47, 29.54, 29.61, 29.65, 29.70, 31.80, 31.86, 40.03, 58.76, 86.71, 87.54, 108.87, 109.36, 122.22, 122.34, 123.42, 123.79, 127.66, 127.72, 139.15, 143.14, 144.21, 148.30, 164.60, 168.89, 169.89, 173.59, 178.35; IR (cm^{-1}): 2920, 2852, 1722, 1600, 1489, 1456, 1355, 1271, 1229, 1193, 1092, 1056, 926; HRMS (m/z): [M + H]$^+$ calculated for $C_{54}H_{79}O_4N_2$: 819.6034; found: 819.6035.

6-Carboxy-2-[[3-[(1,3-dihydro-3-octyl-1,3-didecyl-2H-indol-2-ylidene)methyl]-4-oxo-2-cyclobuten-2-olate-1-ylidene]methyl]-1,3,3-trimethyl-3H-indolium (17, 6-SQ): Compound **4** (0.2 g, 0.3 mmol) and **14a** (0.1 g, 0.3 mmol), column chromatography (SiO$_2$, 100-200 mesh, 2.5 % MeOH and 97.5 % CH_2Cl_2). Yield: 0.095 g, 43 %. Mp: 167 ^{o}C. ^{1}H NMR (400 MHz, CDCl$_3$): δ 0.38 - 0.58 (m, 2 H) 0.72 - 0.91 (m, 11 H) 1.04 - 1.28 (m, 35 H) 1.36 - 1.48 (m, 3 H) 1.71 -

1.93 (m, 8 H) 1.96 - 2.13 (m, 2 H) 3.03 (br. s., 2 H) 3.58 (br. s., 3 H) 4.06 (br. s., 2 H) 6.06 (br. s., 1 H) 6.17 (br. s., 1 H) 7.02 (d, *J*=7.93 Hz, 1 H) 7.15 - 7.26 (m, 1 H) 7.29 - 7.38 (m, 2 H) 7.40 (d, *J*=6.10 Hz, 1 H) 7.74 (br. s., 1 H) 7.94 (d, *J*=7.93 Hz, 1 H); ^{13}C NMR (101 MHz, CDCl$_3$): δ 14.09, 22.57, 22.61, 22.65, 24.01, 24.05, 27.06, 27.22, 27.42, 29.09, 29.17, 29.25, 29.43, 29.45, 29.51, 29.61, 29.68, 30.49, 31.78, 31.84, 39.98, 44.01, 48.93, 59.05, 87.23, 87.98, 109.51, 110.07, 121.89, 122.39, 124.26, 125.57, 127.76, 130.87, 139.29, 143.44, 144.07, 146.95, 169.28, 169.35, 170.11, 176.43, 179.77, 182.83; IR (cm^{-1}): 2919, 2851, 1696, 1598, 1558, 1488, 1425, 1366, 1263, 1212, 1162, 1088, 1053, 933; HRMS (*m/z*): [M + H]$^+$ calculated for C$_{54}$H$_{79}$O$_4$N$_2$: 819.6034; found: 819.6034.

4-Carboxy-2-[[3-[(1,3-dihydro-3-octyl-1,3-didecyl-2H-indol-2-ylidene)methyl]-4-oxo-2-cyclobuten-2-olate-1-ylidene]methyl]-1,3,3-trimethyl-3H-indolium (18, 4-SQ): Compound **4** (0.2 g, 0.3 mmol) and **14b** (0.1 g, 0.3 mmol), column chromatography (SiO$_2$, 100-200 mesh, 2.3 % MeOH and 97.7 % CH$_2$Cl$_2$). Yield: 0.112 g, 50 %. Mp: 118 ^{o}C. ^{1}H NMR (400 MHz, CDCl$_3$): δ 0.48 (br. s., 2 H) 0.70 - 0.89 (m, 11 H) 1.06 (br. s., 12 H) 1.10 - 1.24 (m, 22 H) 1.33 (d, *J*=6.10 Hz, 2 H) 1.51 (br. s., 2 H) 1.86 (br. s., 2 H) 1.93 - 2.06 (m, 2 H) 2.18 (s, 2 H) 2.14 (s, 4 H) 3.04 (br. s., 2 H) 3.57 (br. s., 3 H) 4.32 (br. s., 2 H) 5.94 (br. s., 1 H) 6.62 (br. s., 1 H) 7.06 (d, *J*=7.32 Hz, 1 H) 7.12 - 7.26 (m, 2 H) 7.28 - 7.38 (m, 2 H) 7.41 (t, *J*=7.93 Hz, 1 H) 7.86 (d, *J*=7.32 Hz, 1 H); ^{13}C NMR (101 MHz, CDCl$_3$): δ 14.09, 22.59, 22.63, 22.65, 24.10, 24.13, 25.19, 27.21, 27.69, 29.13, 29.28, 29.30, 29.34, 29.49, 29.54, 29.61, 29.69, 31.83, 31.86, 39.96, 43.84, 46.12, 51.49, 58.97, 85.45, 88.71, 109.61, 112.43, 122.31, 124.05, 126.60, 127.59, 127.68, 128.93, 139.55, 141.74, 144.24, 144.41, 168.44, 170.24, 171.68, 174.60, 178.40, 182.63, 183.38; IR (cm^{-1}): 2918, 2849, 1687, 1586, 1555, 1486, 1450, 1359, 1260, 1192, 1160, 1087, 1046, 934; HRMS (*m/z*): [M + H]$^+$ calculated for C$_{54}$H$_{79}$O$_4$N$_2$: 819.6034; found: 819.6030.

7-Carboxy-2-[[3-[(1,3-dihydro-1,3,3-trimethyl-2H-indol-2-ylidene)methyl]-4-oxo-2-cyclobuten-2-olate-1-ylidene]methyl]-1,3,3-trimethyl-3H-indolium (19, 7-SQ1): Compound **6** (0.2 g, 0.6 mmol) and **10** (0.2 g, 0.6 mmol), column chromatography (SiO$_2$, 100-200 mesh, 2 % MeOH and 98 % CH$_2$Cl$_2$). Yield: 0.160 g, 55.6%. Mp: 265 ^{o}C. ^{1}H NMR (500 MHz, CDCl$_3$): δ 1.78 (br. s., 12 H) 3.50 (br. s., 3 H) 3.86 - 4.09 (m, 3 H) 5.92 (br. s., 1 H) 6.00 (br. s., 1 H) 7.04 -

7.21 (m, 3 H) 7.30 - 7.42 (m, 3 H) 7.50 - 7.65 (m, 1 H); ^{13}C NMR (126 MHz, CDCl$_3$): δ 26.89, 27.07, 27.43, 35.54, 47.79, 49.74, 52.54, 87.37, 88.38, 109.19, 109.73, 122.27, 122.37, 123.80, 124.53, 124.92, 127.82, 127.98, 129.29, 142.15, 142.80, 143.91, 167.52, 170.50, 170.85, 172.60, 179.29, 180.10, 182.50, 183.02; IR (cm^{-1}): 2913, 2848, 1707, 1591, 1501, 1448, 1411, 1283, 1230, 1195, 1141, 1087, 1055, 915; HRMS (*m/z*): [M + H]$^+$ calculated for C$_{29}$H$_{29}$O$_4$N$_2$: 469.2122; found: 469.2130.

4-Carboxy-2-[[3-[(1,3-dihydro-1,3,3-trimethyl-2H-indol-2-ylidene)methyl]-4-oxo-2-cyclobuten-2-olate-1-ylidene]methyl]-1,3,3-trimethyl-3H-indolium (20, 4-SQ1): Compound **6** (0.156 g, 0.58 mmol) and **14b** (0.2 g, 0.58 mmol), residue was filtered out and wash twice with CHCl$_3$ (10 mL). Yield: 0.155 g, 57 %. Mp: more than 300 ^{o}C. ^{1}H NMR (200 MHz, MeOH-d_4: CDCl$_3$ (2:4)): δ 1.76 (s, 6 H) 1.93 (s, 6 H) 3.68 (s, 3 H) 3.63 (s, 3 H) 5.85 (br. s., 1 H) 5.90 (br. s., 1 H) 7.12 (d, *J*=7.83 Hz, 1 H) 7.15 - 7.25 (m, 1 H) 7.26 - 7.39 (m, 2 H) 7.39 - 7.49 (m, 2 H) 7.78 (d, *J*=7.17 Hz, 1 H); ^{13}C NMR (101 MHz, MeOH-d_4: CDCl$_3$ (2:4)): δ 24.75, 27.04, 35.63, 51.83, 57.26, 85.96, 89.46, 110.07, 113.74, 122.52, 124.60, 126.94, 128.37, 128.53, 130.14, 142.06, 143.20, 144.48, 144.84, 168.44, 172.06, 172.42, 175.51, 177.09, 183.22, 183.78; IR (cm^{-1}): 1688, 1592, 1555, 1498, 1445, 1358, 1281, 1226, 1153, 1098, 1052, 921; HRMS (*m/z*): [M + H]$^+$ calculated for C$_{29}$H$_{29}$O$_4$N$_2$: 469.2122; found: 469.2115.

3.3 RESULTS AND DISCUSSION

3.3.1 Synthesis of Squaraine Sensitizers. Synthesis of an unsymmetrical squaraine dye requires the condensation reaction between semi-squaraine and indolium salt (**Scheme 1**). Thus alkylated semi-squaraine and indolium salt with the carboxylic acid group at 4th, -5th, -6th and -7th positions have been synthesized (**Scheme 1a** and **1b**) and condensed under the Dean-Stark distillation reaction conditions in PhMe, n-BuOH, and pyridine to afford the required unsymmetrical squaraine dyes (**Scheme 1c**, **15-20**) in moderate yield (40-60%).

3.3.2 Optical and electrochemical properties. The UV-vis spectra of 4-SQ, 4-SQ1, 5-SQ, 6-SQ, 7-SQ, and 7-SQ1 in CH_2Cl_2 are provided in **Figure 2a**. The λ_{max} and molar extinction coefficient (ε) for the synthesized dyes are provided in **Table 1**. Unsymmetrical indoline based squaraine dyes showed an intense peak between 632-643 nm in CH_2Cl_2 with the molar extinction coefficient of $2.3\text{-}3.6\times10^5$ M^{-1} cm^{-1}. The UV-vis spectra of alkylated dyes, 4-SQ, 7-SQ are 5 and 3 nm red-shifted compared to the corresponding parent dyes 4-SQ1 and 7-SQ1, respectively due to the dye-solvent interactions (**Figure 2a**). Further, the λ_{max} for the 5-SQ is red-shifted slightly compared to other derivatives, due to the conjugation of nitrogen atom of indoline unit and –CO_2H group in a *para*-type fashion. The fluorescence spectra showed the λ_{max} between 642-654 nm upon exciting at 600 nm. Further, the emission spectrum of 5-SQ is red-shifted 4-12 nm compared to other dyes (**Figure 2b**). To understand the interaction between dye and TiO_2, UV-vis spectroscopic study has been carried out by dipping the TiO_2 electrode in dye solutions (0.1 mM in MeCN). It is found that the ortho-carboxyl group containing dye 7-SQ is not anchored on the TiO_2 surface. Further, the corresponding dye with methyl groups at the sp^3-C and N-atoms, 7-SQ1 is also not anchored on the titania implies that the steric factor in the indoline unit which connected with the anchoring group plays an important role in the formation of electronic communication of dye with TiO_2 (**Figure 2d**). All the other four dyes have anchored to the TiO_2 surface. IR spectroscopy for the model squaraine dye without the carboxylic acid showed the carbonyl stretching frequency at 1592 cm^{-1} for the squaric acid unit, and ~1700 cm^{-1} for the carboxylic acid group for the 4-SQ, 4-SQ1, 5-SQ and 6-SQ dyes (**Figure 24** and **25**). However, the peak at 1700 cm^{-1} was disappeared upon anchoring to the TiO_2 surface (**Figure 26**). With 5 min of dipping of TiO_2 electrode to the 0.1 mM MeCN solutions of dyes lead to observe broad peak for the dye 4-SQ1 (500-720 nm, due to aggregation of dyes), and two peaks for the dyes 4-

SQ (643 nm and 597 nm), 5-SQ (643 nm and 602 nm) and 6-SQ (634 nm and 593 nm). The peak centred around 643-634 nm is for the monomer and 602-593 nm for the H-aggregate (**Figure 2c**). The absorption peaks for 4-SQ1 on TiO$_2$ are very broad due to the aggregation of dyes, however such broadening is narrowed down for 4-SQ, 5-SQ, and 6-SQ due to the presence of alkyl groups which controls the self-assembly of dyes. The LHE (absorptance) profile for the electrode dipped in the dye solutions 12 h showed the complete coverage from 400-700 nm with a dip in 400-500 nm regions (**Figure 9a** and **9c**).
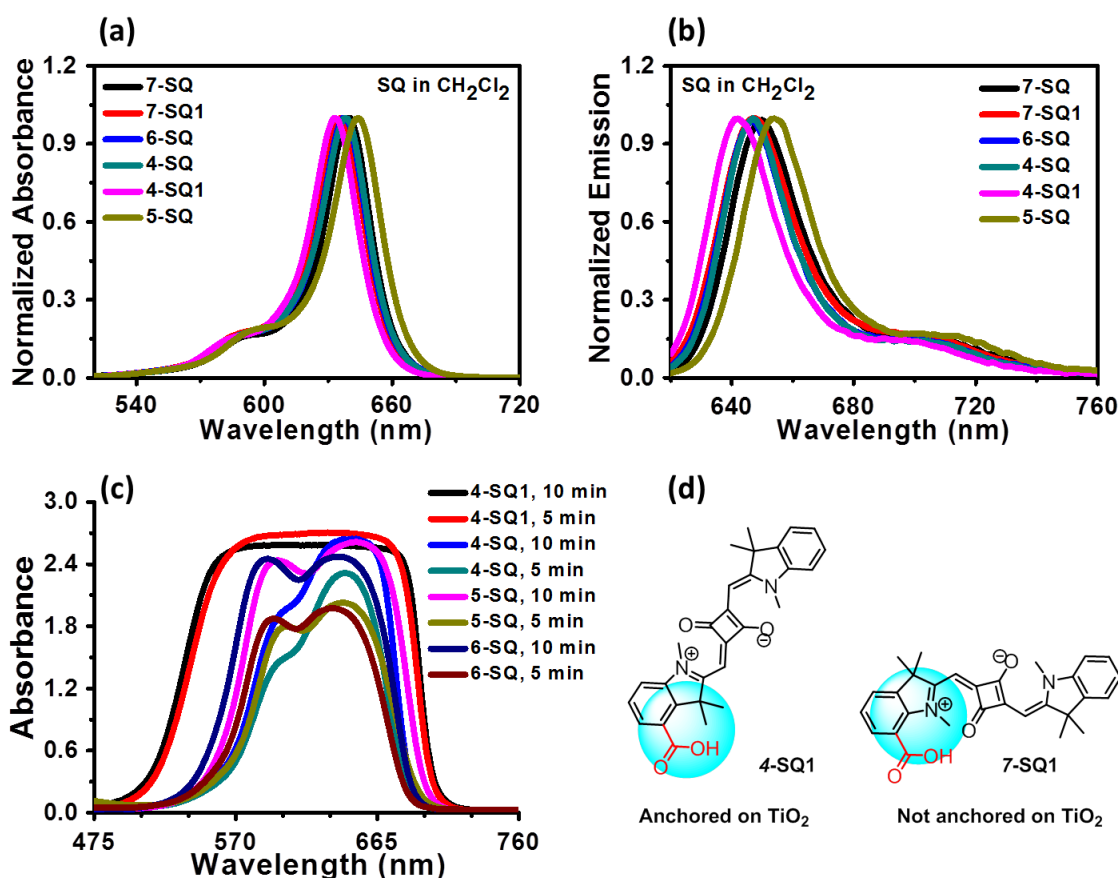
Figure 2. (a) Normalized UV-vis absorption spectra of 4-SQ, 4-SQ1, 5-SQ, 6-SQ, 7-SQ and 7-SQ1, (b) fluorescence spectra of 4-SQ, 4-SQ1, 5-SQ, 6-SQ, 7-SQ and 7-SQ1 dyes in CH$_2$Cl$_2$ solution, (c) UV-vis absorption spectra of 4-SQ, 5-SQ, 6-SQ, and 4-SQ1 on TiO$_2$ electrode (6μm thickness, [Dye] = 0.1 mM in MeCN), (d) structural differences in the anchoring sites of 4-SQ1 and 7-SQ1.

To understand the charge injection process, fluorescence experiments have been carried out in dye anchored TiO_2 and ZrO_2 electrodes. In order to have monomeric dyes on the TiO_2 surface, the electrodes are immersed in CDCA solution for 12 h (1 mM solution in MeCN) and dipped further for 2 min in dye solutions (0.1 mM in MeCN, 6 μm thickness). UV-vis studies indicated the presence of only monomeric dyes on both TiO_2 and ZrO_2 electrodes (**Figure 3a, 3c, 3e, 3g**). Further 4-SQ, 4-SQ1, 5-SQ and 6-SQ dyes showed the fluorescence (**Figure 3b, 3d, 3f, 3h**) at 659 nm, 659 nm, 673 nm and 664 nm, respectively on ZrO_2 and it was completely quenched on TiO_2. Notably, emission of spectra of 4-SQ and 4-SQ1 showed two peaks centred at 665 nm and 730 nm on ZrO_2 (**Figure 3b, 3d**). It is known in the literature that the fluorescence spectrum of squaraine dyes in solution possess α−, β−, and γ− emission peaks correspond to the emissions from the photo-excited state, photo-excited solute-solvent complex, and a twisted, relaxed excited state, respectively (**Figure 6**).[66] Red-shifted emissions for the 4-SQ and 7-SQ compared to its non-alkylated dyes, 4-SQ1 and 7-SQ1, correspond to the β-emission that is emission from the photo-excited solute-solvent complex. However, in the absence of solvent on surfaces, only α− and γ− emission peak is expected (**Figure 7**). It is possible that more spatial interaction of 4SQ and 4-SQ1 with TiO_2 may promote the formation of twisted excited state to observe the γ-emission due to the parallel arrangement of dye on the titania surface, whereas 6-SQ (a similar meta-isomer with respect to N-atom of indoline ring as 4-SQ) exhibit majorly α-emission which infers the different orientations for 4-SQ and 6-SQ on TiO_2. Though the α- and γ- emissions are quenched in the 2 min dye dipping experiments, both the emissions are not quenched even on TiO_2 for 4-SQ for the electrode dipped for 12 h (DSSC device fabrication conditions, **Figure 9b**). Hence the charge injection from 4-SQ may be less compared to 5-SQ and 6-SQ. The quenching efficiency is not calculated as the amounts of dyes are not the same for all the dyes with either 2 min or 12 h dipping time (**Table 7**, and **Figure 3**). The LHE profile on ZrO_2 is narrowed down compared to the same in TiO_2, and the complete quenching of the emission of 4-SQ1 on ZrO_2 is due to the self-quenching as the electrode was dipped for 12 h (**Figure 9d**).

Further, the cyclic voltammetry study of the dyes in CH_2Cl_2 has been carried out to evaluate the electrochemical properties (**Table 1, Figure 4a,** and **Figure A64**).
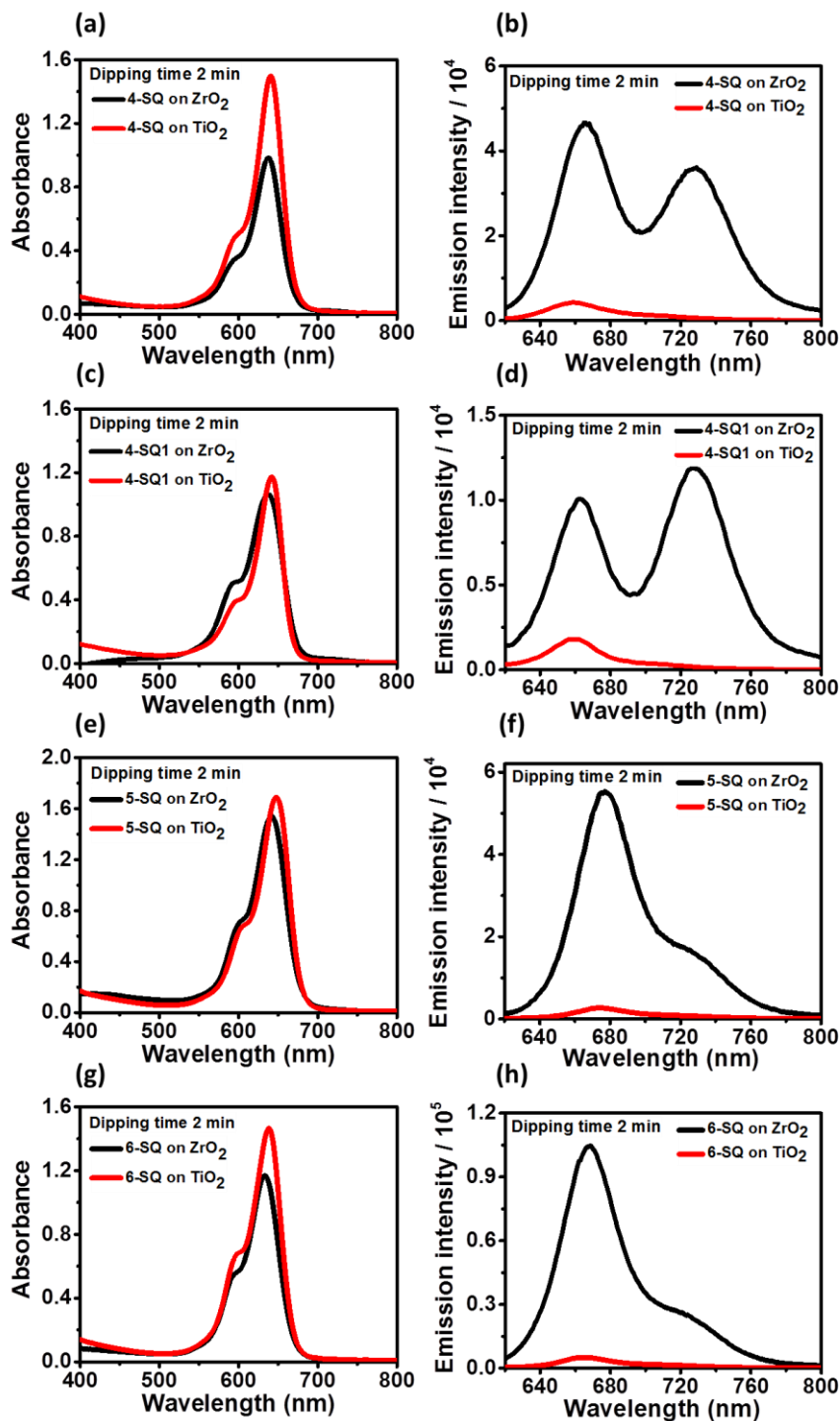
Figure 3. (a), (c), (e) and (g) absorption spectra of 4-SQ, 4-SQ1, 5-SQ, and 6-SQ dyes, (b), (d), (f) and (h) emission spectra of 4-SQ, 4-SQ1, 5-SQ and 6-SQ dyes (excited at 600 nm) on the TiO_2 and ZrO_2 respectively, where the electrodes are first dipped for 12 h in 1 mM of CDCA (in CH_3CN) solution, then 2 min in 0.1 mM dye (in CH_3CN) solution at room temperature.

The first oxidation for all the four squaraine dyes with the E_{HOMO} energy levels around 0.68 V to 0.79 V which were more positive than the redox potential of the iodide/tri-iodide (I^-/I_3^-, 0.4 V vs NHE) based electrolyte for the efficient dye regeneration, the slight difference is due to the anchoring group at different positions. The E_{LUMO} of the dyes has been calculated by using the optical bandgap of the dyes, which were around -1.12 V to -1.24 V and more negative than the conduction band position of TiO$_2$ (- 0.5 V vs NHE) to ensure the efficient charge injection.
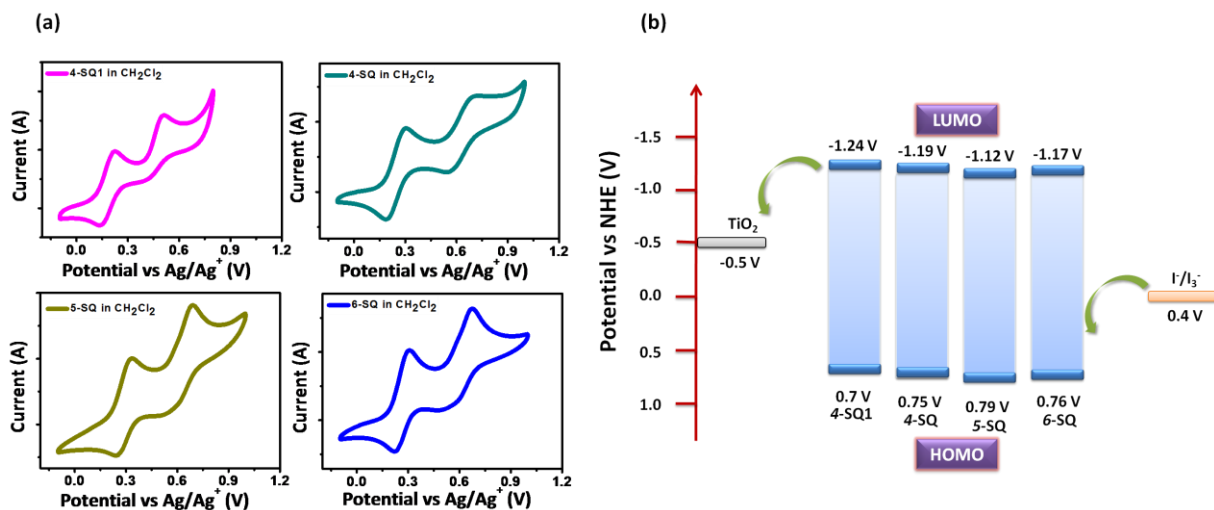
Figure 4. (a) Cyclic voltammograms of 4-SQ1, 4-SQ, 5-SQ, and 6-SQ dyes in CH$_2$Cl$_2$, (b) schematic representation of energy level diagrams of 4-SQ1, 4-SQ, 5-SQ, and 6-SQ dyes.
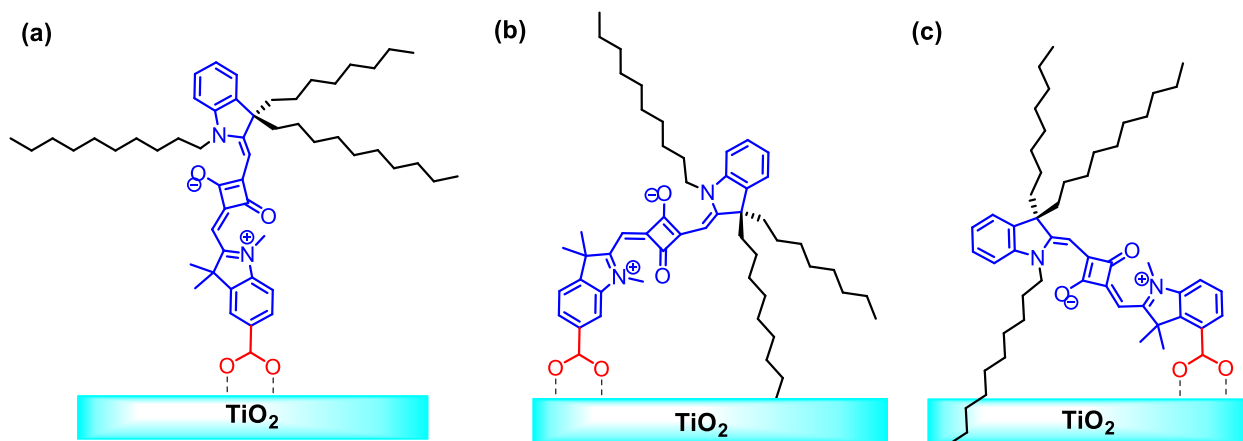
Figure 5. Representation of 4-SQ, 5-SQ and 6-SQ on TiO$_2$.
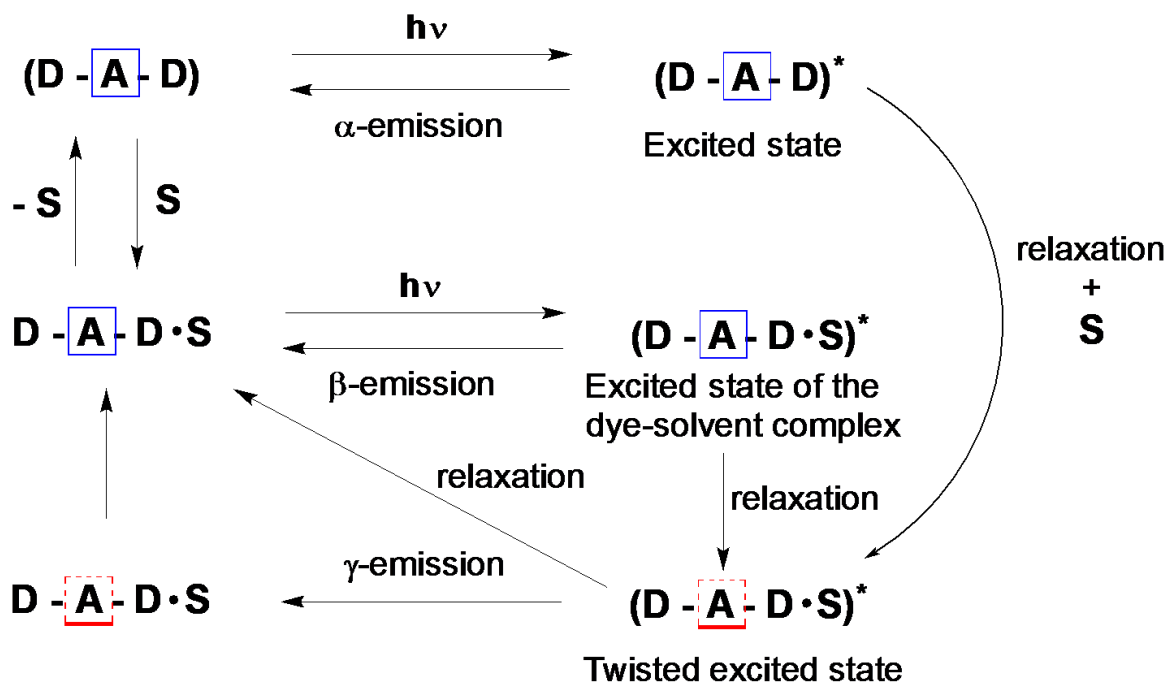
Figure 6. Emission from various states of squaraine dyes upon photoexcitation.
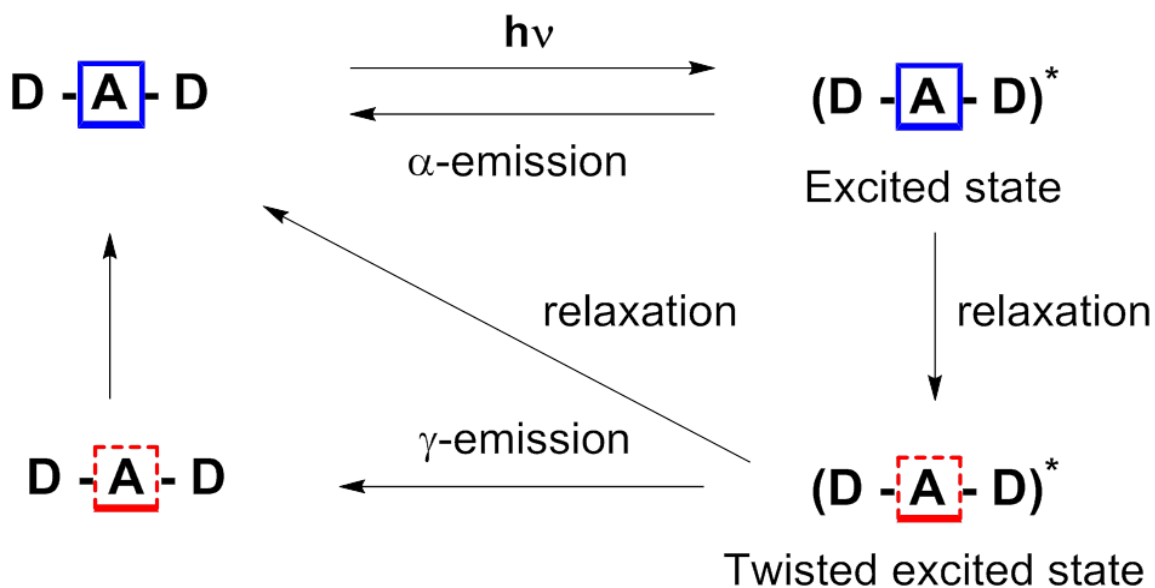
Figure 7. Photophysics of D-A-D type squaraine dyes on surfaces upon photoexcitation.

(a)

(b)

Twisted state

ZrO₂

ZrO₂

α-emission
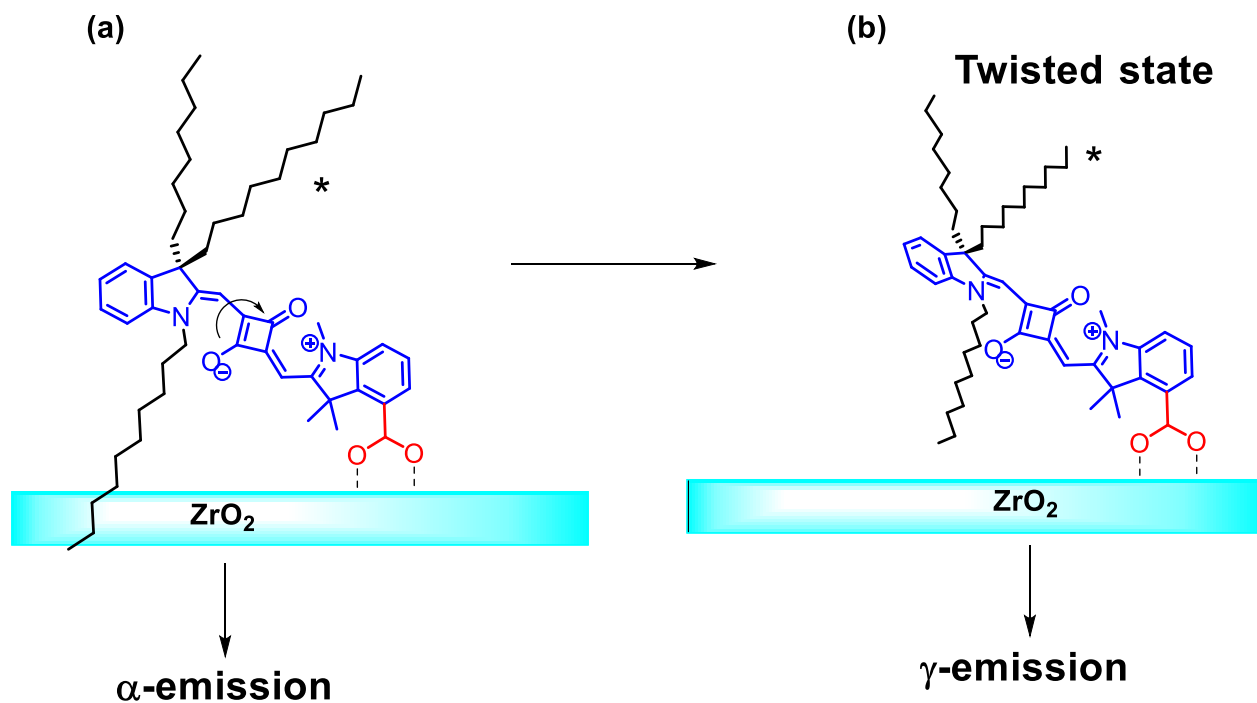
γ-emission

Figure 8. Representation for the emission of 4-SQ and 4-SQ1 on ZrO₂.

Table 1. Photophysical and electrochemical properties SQ dyes at room temperature.

Dye	$^a\lambda_{max}$ (nm)	$^b\lambda_{max}$ (nm)	$^c\lambda_{max}$ (nm) abs TiO₂	$^d\lambda_{max}$ (nm) emi TiO₂	$^f\lambda_{max}$ (nm) abs ZrO₂	$^g\lambda_{max}$ (nm) emi ZrO₂	ε $(10^5$ M^{-1} $cm^{-1})$	E_{HOMO} (V vs NHE)	E_{LUMO} (V vs NHE)	^hE_g (eV)
4-SQ1	632	642	641	659	637	662, 730	3.0	0.68	-1.25	1.94
4-SQ	637	647	641	659 (680, 750)^e	637	665, 730 (677, 742)^e	3.6	0.75	-1.18	1.93
5-SQ	643	654	647	673	641	676 (688)^e	3.1	0.79	-1.12	1.91
6-SQ	636	647	638	664	632	668 (680)^e	3.5	0.76	-1.17	1.93
7-SQ1	636	647	-	-	-	-	2.9	0.73	-1.20	1.93
7-SQ	639	650	-	-	-	-	2.3	0.72	-1.20	1.92

[a]absorption, [b]emission of 4-SQ, 4-SQ1, 5-SQ, 6-SQ, 7-SQ, and 7-SQ, dyes in CH_2Cl_2 solution, [c]absorption on TiO_2, 6 μm thickness dipped for 2 min in 0.1 mM solution of dyes in MeCN, [d]emission on TiO_2, [e]12 h dipping time, [f]absorption on ZrO_2, 6 μm thickness dipped for 2 min in 0.1 mM solution of dyes in MeCN, [g]emission on ZrO_2, [h]E_g optical bandgap.
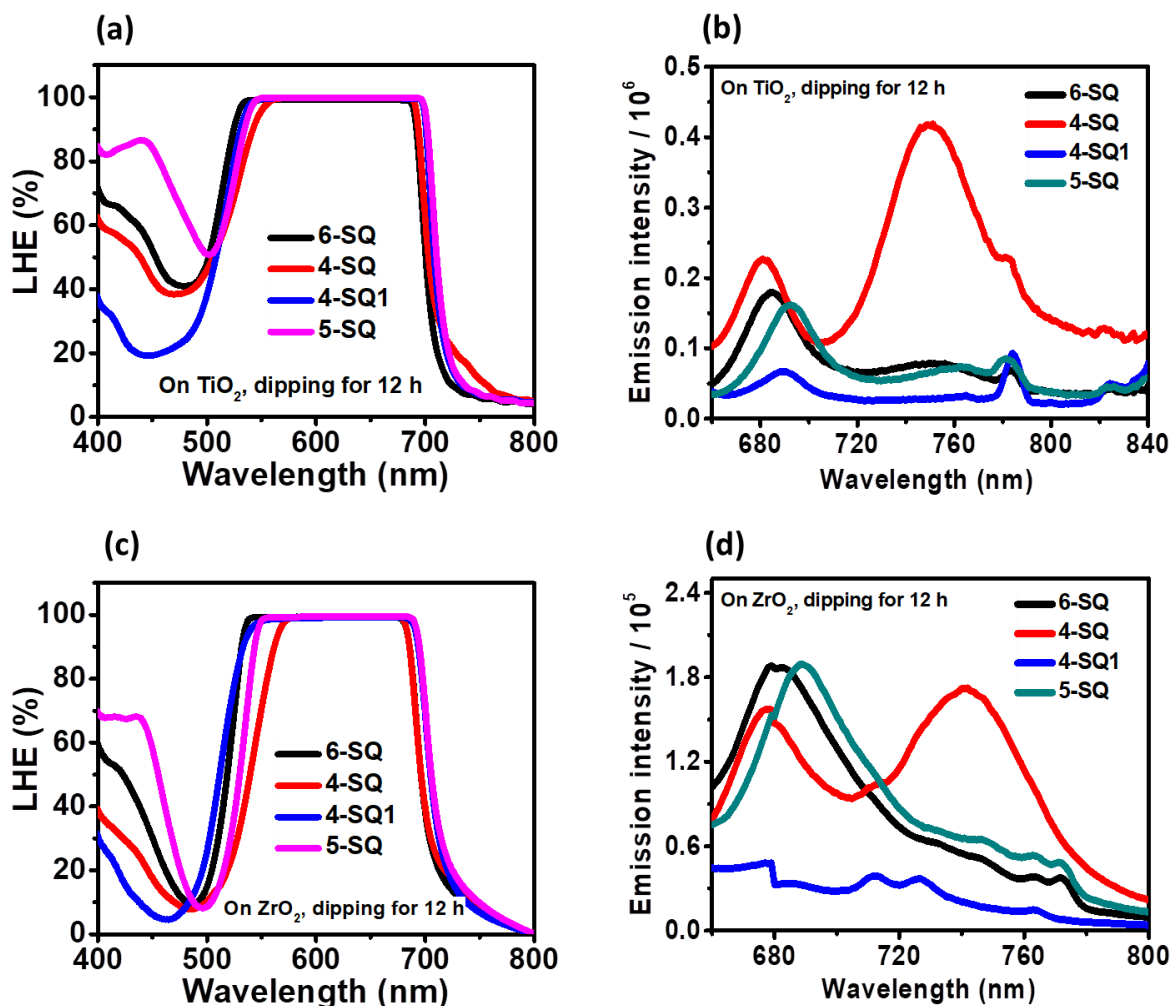
Figure 9. (a), (c) LHE ($=1–10^{-A}$), (b) and (d), emission spectra of 4-SQ1, 4-SQ, 5-SQ, and 6-SQ (0.1 mM in CH_3CN) dyes (excited at 600 nm) on the TiO_2 and ZrO_2 respectively, where the dipping time was 12 h at room temperature.

3.3.3 Theoretical studies. All the calculations on the organic dyes were carried out using the Gauusian09[61] package. A 6-311++ G basis set with B3LYP functional has been considered for the optimization of all the organic dyes without any symmetry constraints. Following the molecular property calculations, we have extended the studies to the adsorption of dyes on TiO_2 (101) surfaces with VASP[62] (Vienna Ab-initio simulation package) using a plane-wave basis and Perdew-Burke-Ernzerhof (PBE) functional. A Monkhorst-Pack scheme with $2\times2\times1$ k-point mesh has been considered with an energy cut-off set at 400 eV for all calculations. The SCF convergence threshold has been set at 10^{-5} eV with the individual forces on atoms set to be less than 0.05 eV/Å. A vacuum gap of 35 Å has been provided in the TiO_2 model to avoid interactions from the adjacent slab. The affinity of the organic dye to interact with the TiO_2 surface has been measured by adsorption energy which is calculated by the equation,

$$E_{ads} = E_{surface + dye} - E_{surface} - E_{dye}$$

Where, $E_{surface + dye}$ represents the total energy of the dye adsorbed surface, $E_{surface}$ represents the total energy of the TiO_2 surface and E_{dye} represents the total energy of the organic dye molecule.

Isosurface plots of selected frontier molecular orbitals (HOMO-1, HOMO, LUMO, LUMO+1) of SQ dyes without alkyl groups before and after adsorption on the TiO_2 surface shown in **Figure 10**, and **11**. Model squaraine dyes with methyl groups at N- and sp^3-C atoms of the indoline units with anchoring groups at various positions were taken as shown in **Figure 12**. The photovoltaic efficiency of a DSSC device largely depends on the dye-TiO_2 interface which depends on the electronic properties of the sensitizer and its orientation on the surface of the semiconductor. To understand the underlying factors, dipole moment and frontier molecular orbitals of the organic dye are analyzed along with the electronic properties of the dye anchored TiO_2 **Table 2**.

The dipole moment exerted by the dye on the TiO_2 surface plays a vital role in shifting its Fermi energy level that helps to modulate the V_{OC} of the DSSC device. The calculated resultant dipole moments for the 4-SQ, 6-SQ, and 5-SQ dyes are 2.71 D, 3.08 D and 4.56 D, respectively (**Table 3**). Further, the HOMO-LUMO energy gap and the frontier molecular orbitals composition provided in **Figure 15,** and **Table 3**. Dye 5-SQ1 has its HOMO and LUMO on the anchoring and squaraine group, dyes 6-SQ1 and 4-SQ1 have their HOMO and LUMO concentrated on the squaraine moiety.

HOMO-1	HOMO	LU MO	LUMO+1

5-SQ1

6-SQ1

4-SQ1
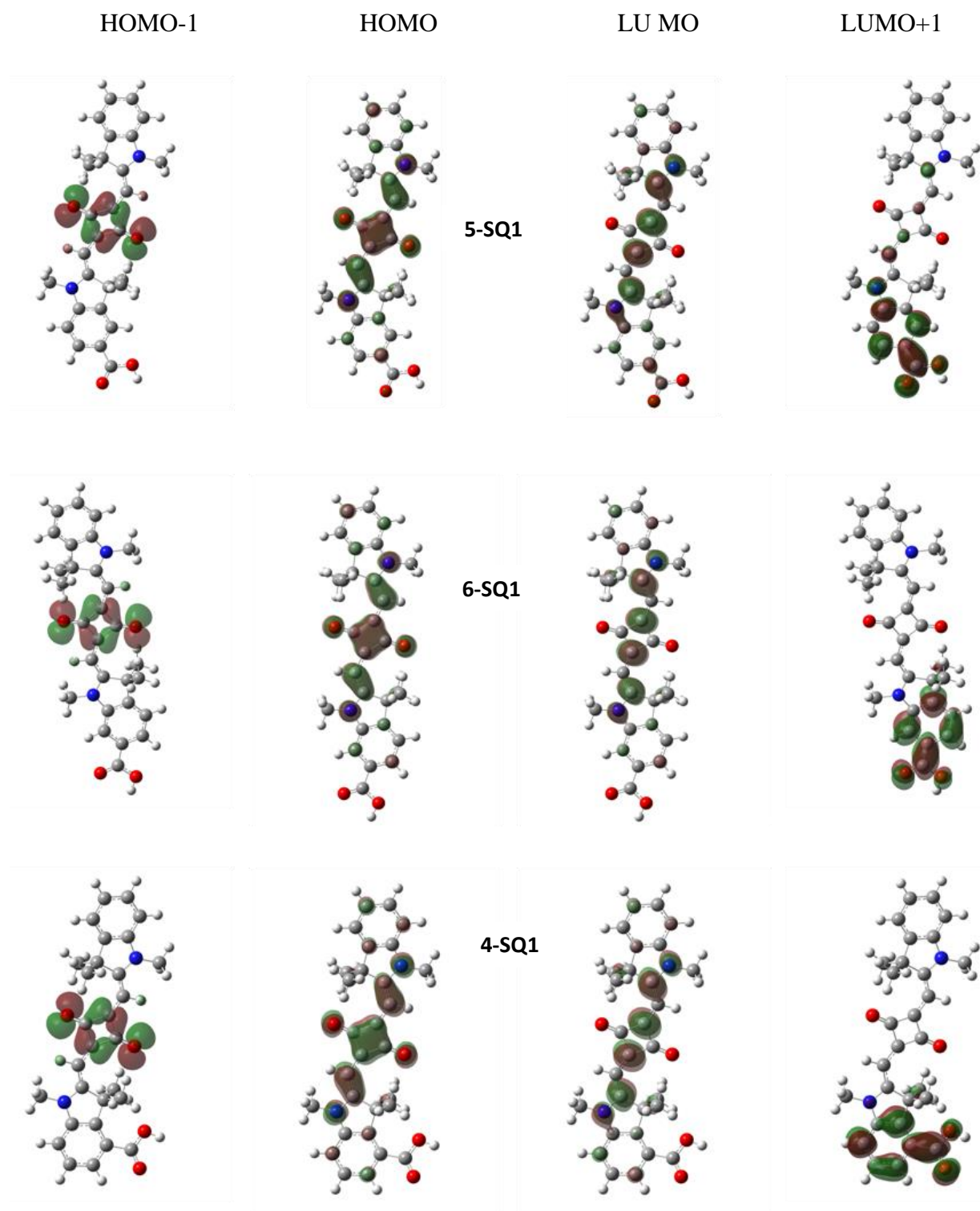
Figure 10. Isosurface plots of selected frontier molecular orbitals (HOMO-1, HOMO, LUMO, LUMO+1) of SQ dyes without alkyl groups before adsorption on the TiO_2 surface (Isosurface value at 0.03).

HOMO-1 HOMO LU MO LUMO+1
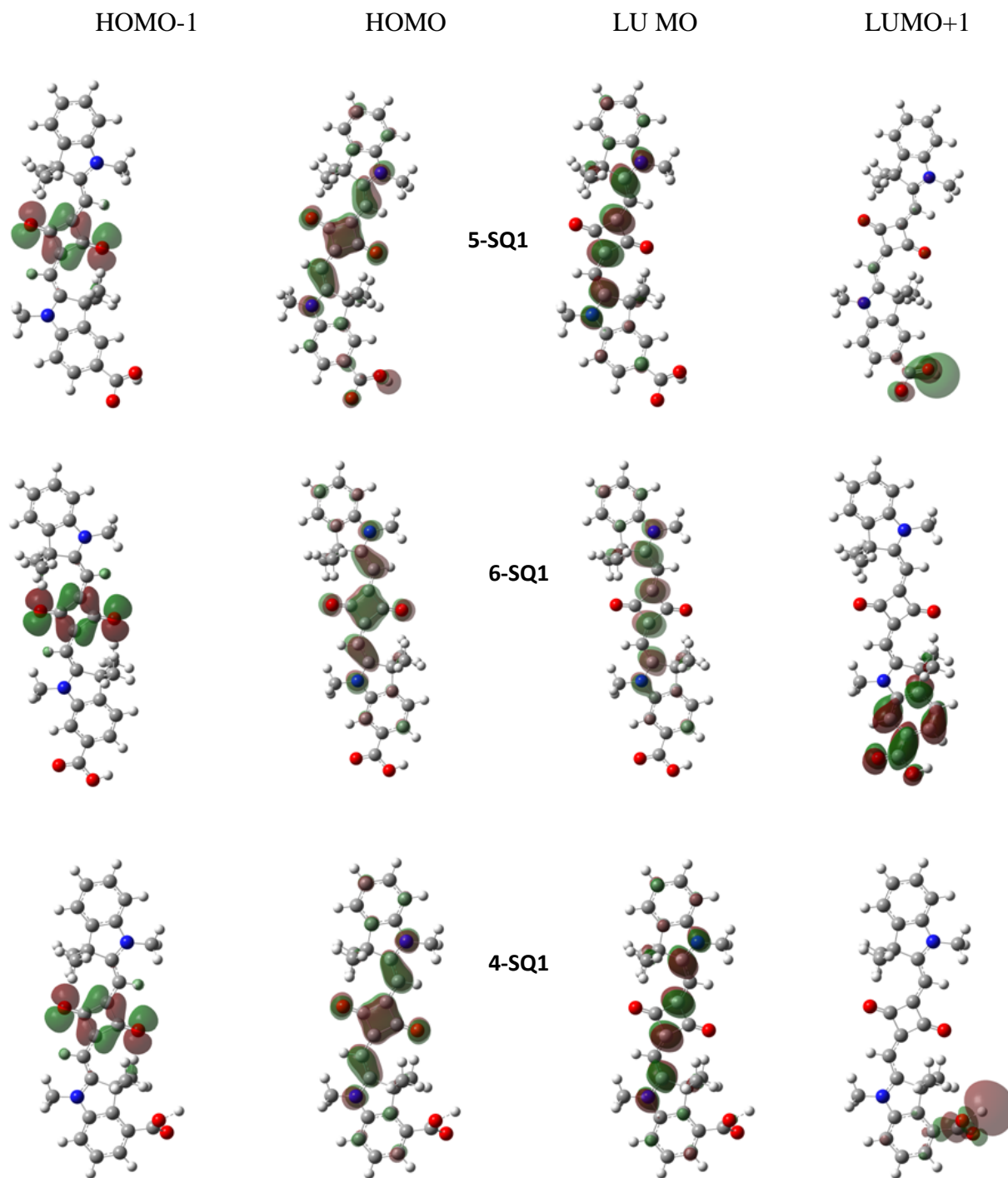
Figure 11. Isosurface plots of selected frontier molecular orbitals (HOMO-1, HOMO, LUMO, LUMO+1) of SQ dyes without alkyl groups after adsorption on the TiO$_2$ surface (Isosurface value at 0.03).

Table 2. DFT optimized band gap (HOMO-LUMO) and dipole moments of **SQ** dyes without alkyl groups before and after adsorption on the TiO_2 surface.

Dyes	Band gap (eV)		Dipole moment (Debye)	
	Before adsorption	After adsorption	Before adsorption SQ	After adsorption SQ@TiO_2
5-SQ1	2.137	0.533	$\mu_x = 4.86$, $\mu_y = 0.06$, $\mu_z = -0.29$, $\mu_{total} = 4.87$	$\mu_x = -10.24$, $\mu_y = 2.21$, $\mu_z = 1.55$, $\mu_{total} = 10.59$
6-SQ1	2.172	2.208	$\mu_x = -2.67$, $\mu_y = 1.78$, $\mu_z = -0.23$, $\mu_{total} = 3.22$	$\mu_x = -5.80$, $\mu_y = 4.00$, $\mu_z = -0.53$, $\mu_{total} = 7.06$
4-SQ1	2.173	1.733	$\mu_x = -1.92$, $\mu_y = -1.20$, $\mu_z = -0.88$, $\mu_{total} = 2.43$	$\mu_x = -2.17$, $\mu_y = -0.79$, $\mu_z = 2.05$, $\mu_{total} = 3.08$
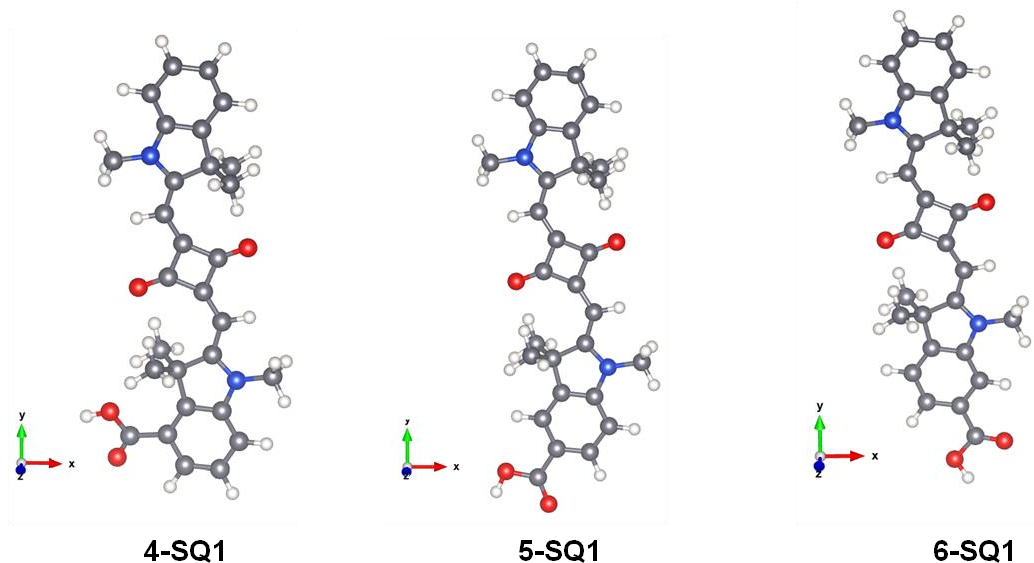
4-SQ1   **5-SQ1**   **6-SQ1**

Figure 12. Model squaraine dyes, 4-SQ1, 5-SQ1, and 6-SQ1 with anchoring group at different positions.

4-SQ1 $E_{ads} = -2.07$ eV   5-SQ1 $E_{ads} = -2.23$ eV   6-SQ1 $E_{ads} = -1.49$ eV
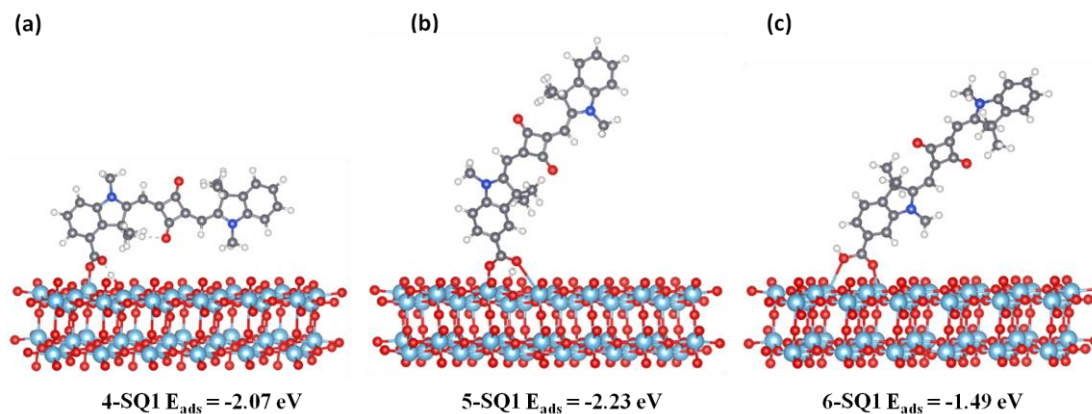
Figure 13. Relaxed orientations of dyes on the TiO_2 surface with their adsorption energies.
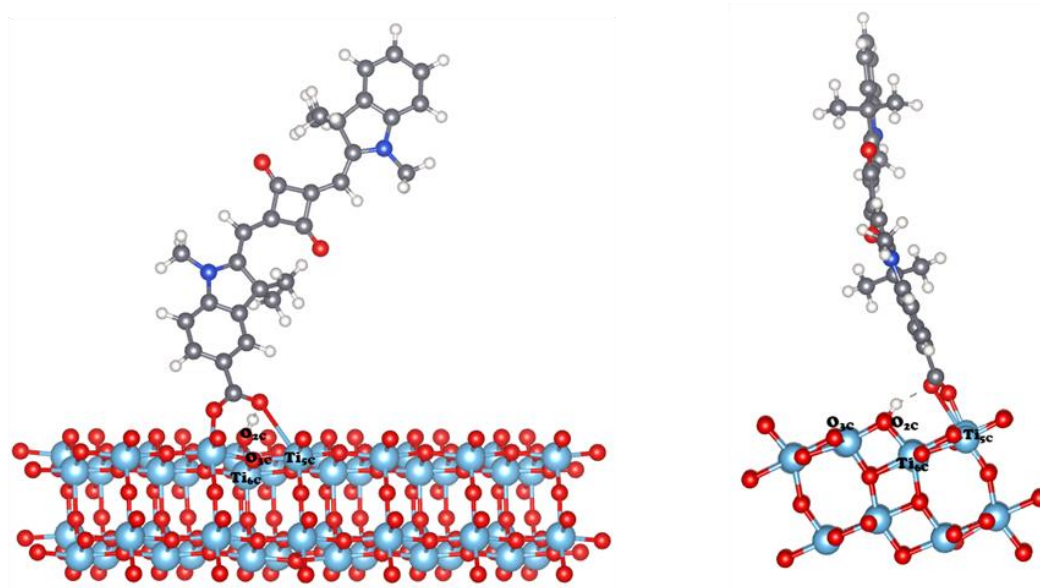
Figure 14. Side views of 5-SQ1 anchored on TiO_2 (101) binding to Ti_{5C} and O_{2C}.

The interaction of the organic dyes with TiO_2 surface is largely driven by the orientation of the anchoring group and this affects the adsorption energy (E_{ads}) and the electronic properties. The relaxed geometries of the dye adsorbed TiO_2 surface along with their adsorption energies are as shown in **Figure 13**. 5-SQ1 and 6-SQ1 dyes are seen to orient themselves in a slightly perpendicular mode by making an acute angle on theTiO$_2$ surface, whereas dye 4-SQ1 adapts a nearly parallel mode. The perpendicular mode of interaction is seen to be more favored energetically as 5-SQ1 (**Figure 14**) shows higher adsorption energy (-2.23 eV) as compared to 6-

SQ1 (-1.49 eV) and 4-SQ1 (-2.07eV). 4-SQ1 shows higher adsorption energy than 6-SQ1 owing to the H-O$_{2C}$ bond formation which is absent in 6-SQ1. The photovoltaic efficiency depends on the ability of the dye to inject electron to the semiconductor surface, this electron injection efficiency is again determined by the orientation of the dye on the surface. While a perpendicular orientation shows higher adsorption energy, it need not necessarily infer a better photovoltaic efficiency. The electronic properties of the dye adsorbed surface will give more insight into the electron injection ability of the dye.
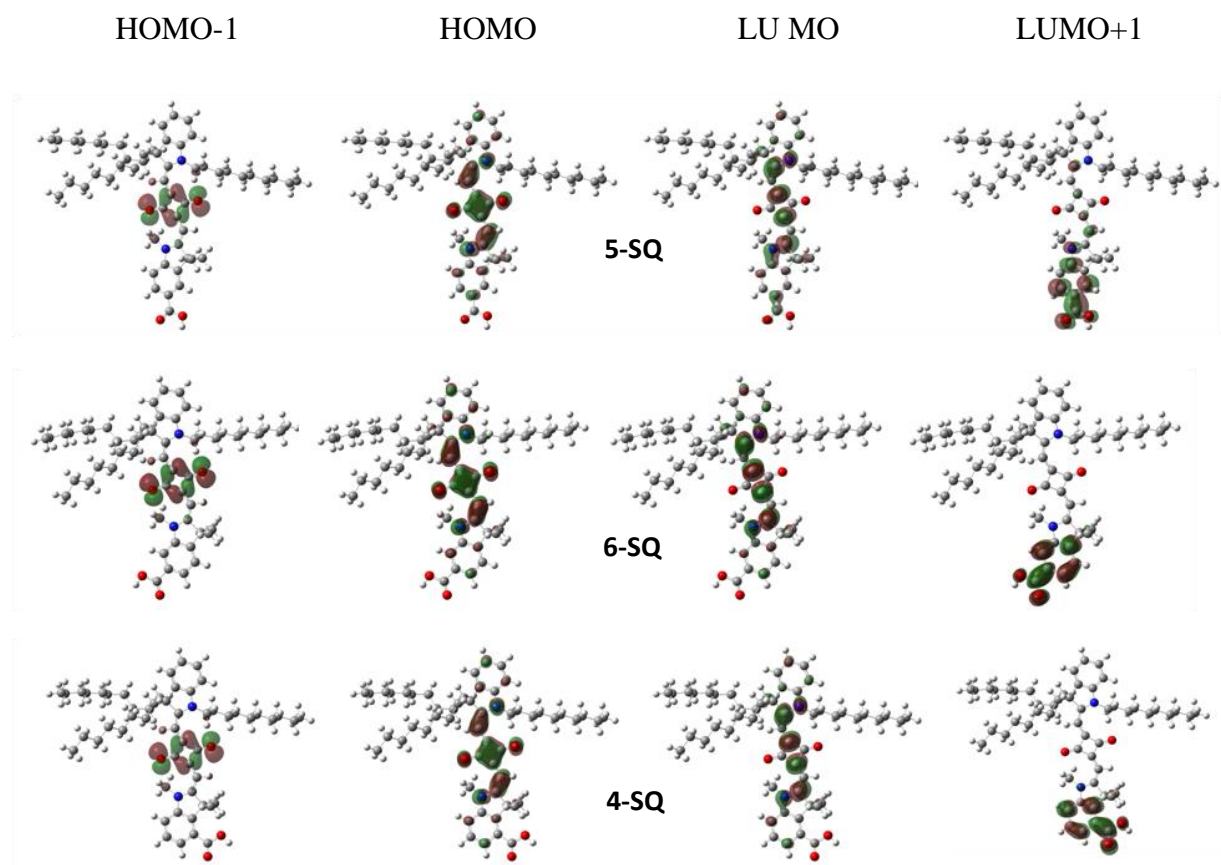
Figure 15. Isosurface plots of selected frontier molecular orbitals (HOMO-1, HOMO, LUMO, LUMO+1) of 4-SQ, 5-SQ, and 6-SQ dyes with alkyl groups (Isosurface value at 0.03).

Table 3. DFT optimized band gap and dipole moments of **SQ** dyes with alkyl groups.

Dyes	Band gap (eV)	Dipole moment (Debye)
5-SQ	2.1016	$\mu_x = -1.81$, $\mu_y = -4.18$, $\mu_z = -0.14$, $\mu_{total} = 4.56$
6-SQ	2.1413	$\mu_x = -0.75$, $\mu_y = -2.96$, $\mu_z = 0.39$, $\mu_{total} = 3.08$
4-SQ	2.1468	$\mu_x = -1.40$, $\mu_y = -1.70$, $\mu_z = 1.58$, $\mu_{total} = 2.71$
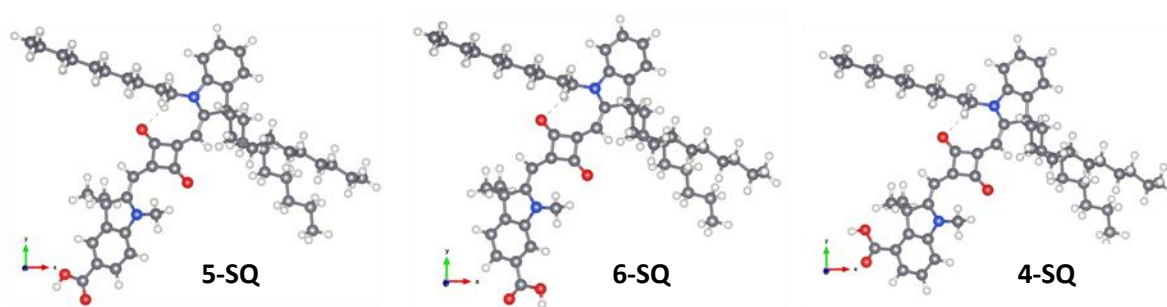
Figure 16. Fully optimized geometry of SQ dyes with alkyl groups.

The Projected Density of States (PDOS) plot along with the partial charge density plot of 5-SQ1 and 6-SQ1 dyes is shown in **Figure 17**. It can be seen from the PDOS plot that both the dyes show a bandgap of nearly 2 eV with the valence band showing contribution from the dye and the conduction region comprising of *Ti-d* orbitals. However, the partial density of charge plots brings out the contrast between these two systems very clearly. It can be seen 5-SQ1 shows electron density overlap in the anchoring region and acceptor (LUMO) of the dye while in 6-SQ1 the overlap is visible only in the anchoring region. The electron density in the anchoring region is an attribute to the higher adsorption energy observed earlier and the electron density from the squaraine region will attribute to the electron injection efficiency. The PDOS and partial charge density plots of 4-SQ1 dye which binds in a parallel mode show some interesting features. Despite a decent electron density overlap in the anchoring and squaraine region, the electron injection ability of this dye is seen to be the least from our experimental findings. This is in direct correspondence to the small bandgap as seen from the PDOS plot in **Figure 17a**. The O-p orbitals of the surface lie at a lower energy of nearly 0.6-1.0 eV causing the recombination of

electron-holes in the dye. This electron-hole recombination and low bandgap in dye 4-SQ1 leads to a lower electron injection ability and hence decreases the photovoltaic efficiency of this dye.
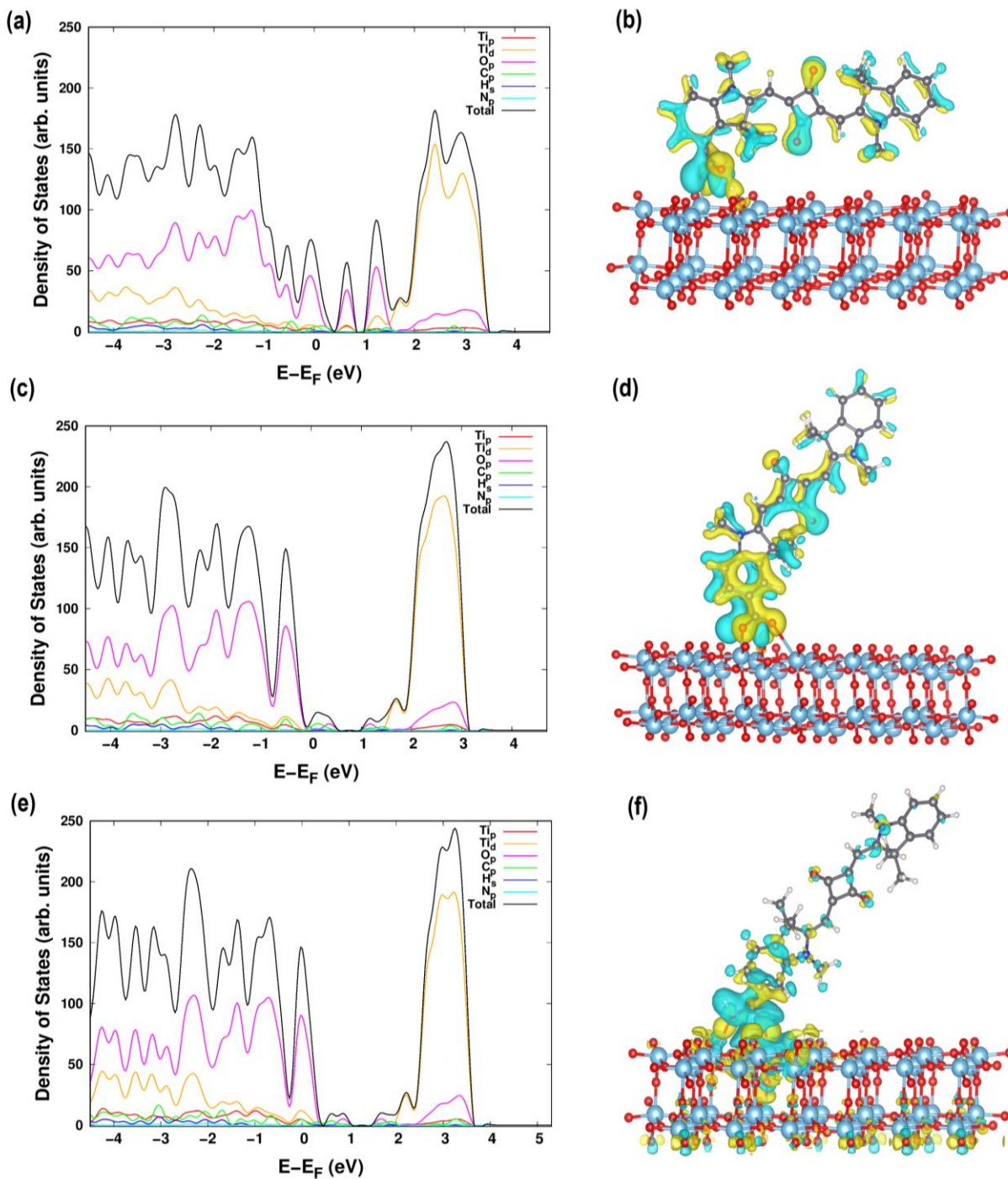
Figure 17. PDOS and partial charge density plots for 4-SQ1, 5-SQ1, and 6-SQ1 on TiO$_2$ (Isovalue set at 0.004).

The shift in the position of the conduction band of TiO_2 can be determined from the dipole moment of a sensitizer.[67, 68] The calculated dipole moment of the isolated, as well as the orientation derived from the dye@TiO_2 sensitizers without alkyl groups, has been compared (**Table 2**). The dipole moment of sensitizers under both the conditions follows the order of 5-SQ1>6-SQ1>4-SQ1, which indicates that a perpendicular orientation of dye in the case of 5-SQ1. Further, it is observed that both 4-SQ1 and 6-SQ1 have the meta-carboxyl group with respect to the N-atom of indoline unit, and differs in the dipole moment upon anchoring that indicates the different orientations on TiO_2.

3.3.4 Photovoltaic performance. To study the effect of orientation of monomeric dyes on TiO_2 surface, photovoltaic parameters have been obtained by carrying out the device fabrication with (i) dipping the TiO_2 electrode in dye solutions of 4-SQ1, 4-SQ, 5-SQ and 6-SQ for a short time, and (ii) dipping the TiO_2 electrode 1 mM solution of CDCA for 12 h prior to sensitizing it with dye solutions for 2 min. Further, to understand the importance of both orientation and aggregation of dyes on the photoanode, the TiO_2 electrodes were sensitized with dyes in MeCN. Even within 2 min of sensitizing the electrode with the dyes, the IPCE profile (**Figure 18d**) showed the interaction between the dyes as the ratio between the peaks at 650 nm, and 607 nm is significantly varied in comparison to the solution spectrum. The device efficiency of 1.55 % for the dye 5-SQ was obtained for the cell with the V_{OC} and J_{SC} of 0.625 V and 3.07 mA/cm^2, respectively (**Table 4**). The significant improvement in the V_{OC} of the devices 4-SQ1, 4-SQ indicates the importance of alkyl groups to passivate the electrode surface. The IPCE profile of the DSSC devices fabricated with loading the coadsorbent CDCA for 12 h and anchoring the dyes for 2 min in MeCN, showed only the response from the monomeric dyes (**Figure 18c**). Again, the device efficiency of 0.79 % for the dye 5-SQ was obtained for the cell with the V_{OC} and J_{SC} of 0.623 V and 1.50 mA/cm^2, respectively. In both the device fabrication conditions, the device performance for the dyes decreases in the order of 5-SQ> 4-SQ> 6-SQ. The V_{OC} obtained for the devices varied from 0.591 V (for 4-SQ1) to 0.623 V (for 5-SQ). Photoanodes loaded with the dyes 4-SQ1, 4-SQ, 5-SQ, and 6-SQ for 12 h in MeCN showed the device efficiency of 0.36%, 1.22%, 4.91%, and 3.0% respectively (**Table 5**). The V_{OC} for the 4-SQ device is 78 mV higher than that of 4-SQ1 due to the presence of branched alkyl groups. Further, DSSC devices

with 5-SQ and 6-SQ as sensitizers showed similar V_{OC}, and it may be due to the similar passivation effect offered by the monolayer of dyes on TiO_2. Further, the device performances have been significantly enhanced in the presence of 3 equivalents of CDCA, and the dye 5-SQ showed an efficiency of 6.08%. The IPCE profile showed the importance of the position of the anchoring group for the better photocurrent generation. For the 4-SQ1 dye, the monomeric dye contributed much for the photocurrent generation than the 4-SQ, 5-SQ and 6-SQ in the absence of CDCA (**Figure 19**).
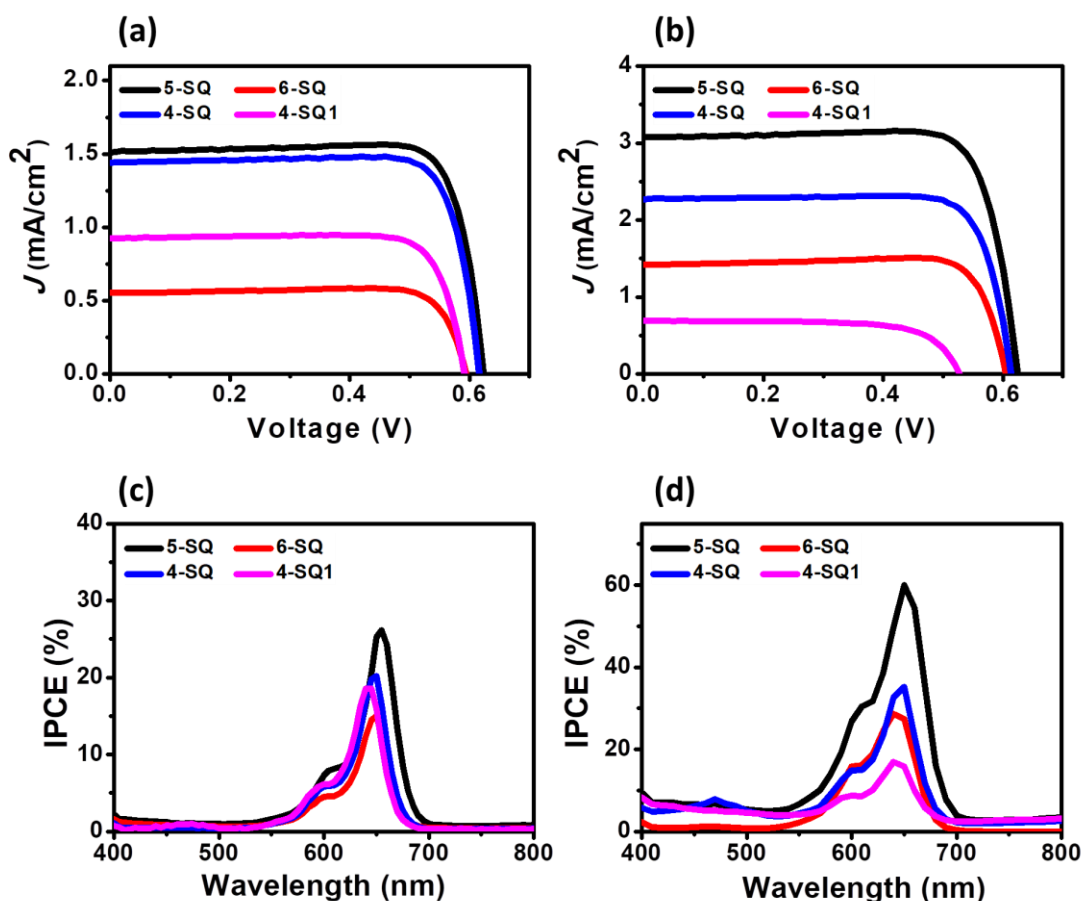
Figure 18. (a) and (c) *I-V* and IPCE curve of 4-SQ1, 4-SQ, 5-SQ, and 6-SQ dyes, where the cells are first dipped in 1 mM of CDCA (in CH_3CN) solution, then 2 min in 0.1 mM dye (in CH_3CN) solution at room temperature, (b) and (d), *I-V* and IPCE curve of 4-SQ1, 4-SQ, 5-SQ, and 6-SQ dyes, where the cells are dipped in 0.1 mM dye (in CH_3CN) solution for 2 min.
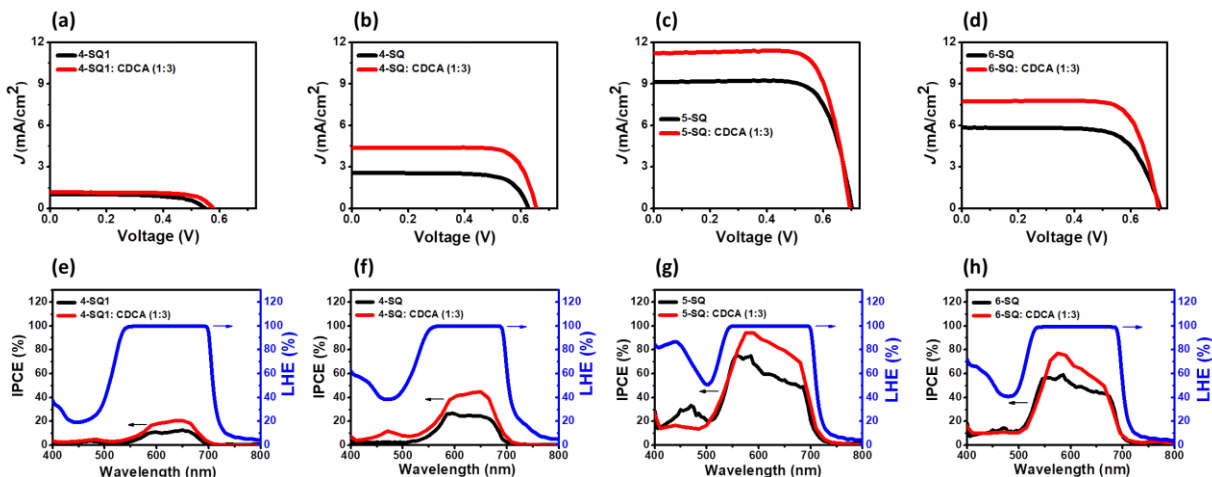
Figure 19. (a to d) *I-V* curve of 4-SQ1, 4-SQ, 5-SQ, and 6-SQ dyes in presence and absence of CDCA respectively, (e to h) IPCE curve of 4-SQ1, 4-SQ, 5-SQ, and 6-SQ dyes in presence and absence of CDCA respectively, blue line corresponds to the LHE of dye without CDCA.

Table 4. Photovoltaic response from the monomeric 4-SQ1, 4-SQ, 5-SQ, and 6-SQ dyes.

Cells	V_{OC} (V)	J_{SC} (mA/cm^2)	*ff* (%)	η (%)
[a]4-SQ1	0.591 ± 0.002	0.93 ± 0.01	82 ± 0.53	0.450 ± 0.010
[b]4-SQ1	0.528 ± 0.001	0.69 ± 0.04	71 ± 0.43	0.258 ± 0.018
[a]4-SQ	0.617 ± 0.005	1.44 ± 0.13	83 ± 0.82	0.737 ± 0.081
[b]4-SQ	0.614 ± 0.002	2.27 ± 0.09	81 ± 0.91	1.130 ± 0.060
[a]5-SQ	0.623 ± 0.002	1.50 ± 0.10	84 ± 0.34	0.785 ± 0.058
[b]5-SQ	0.625 ± 0.004	3.07 ± 0.23	81 ± 0.61	1.550 ± 0.143
[a]6-SQ	0.595 ± 0.006	0.55 ± 0.03	86 ± 0.05	0.281 ± 0.019

[b]6-SQ	0.605 ± 0.002	1.42 ± 0.12	86 ± 0.15	0.739 ± 0.066

[a]Electrodes are first dipped in 1 mM of CDCA (in CH_3CN) solution for 12 h, and then 2 min in 0.1 mM dye (in CH_3CN) solution at room temperature, [b]electrodes are dipped in 0.1 mM dye (in CH_3CN) solution at room temperature for 2 min.

Table 5. Photovoltaic response from the actual device of 4-SQ1, 4-SQ, 5-SQ, and 6-SQ dyes.

Cells	CDCA (ratio)	V_{OC} (V)	J_{SC} (mA/cm^2)	ff (%)	η (%)
4-SQ1	0	0.549 ± 0.005	1.01 ± 0.03	62 ± 1.03	0.35 ± 0.01
4-SQ1	3	0.577 ± 0.006	1.14 ± 0.05	72 ± 0.71	0.47 ± 0.03
4-SQ	0	0.627 ± 0.002	2.55 ± 0.09	73 ± 0.29	1.17 ± 0.05
4-SQ	3	0.655 ± 0.003	4.36 ± 0.07	78 ± 0.35	2.23 ± 0.05
5-SQ	0	0.701 ± 0.002	9.11 ± 0.13	75 ± 0.67	4.79 ± 0.12
5-SQ	3	0.694 ± 0.004	11.2 ± 0.15	76 ± 0.82	5.91 ± 0.17
6-SQ	0	0.704 ± 0.002	5.82 ± 0.14	71 ± 0.37	2.91 ± 0.09
6-SQ	3	0.698 ± 0.002	7.72 ± 0.04	76 ± 0.16	4.09 ± 0.05

However, the aggregated structure played a vital role in the enhanced J_{SC} for 5-SQ and 6-SQ in the presence and absence of CDCA. It is possible that both 5-SQ and 6-SQ may have similar self-assembly formation, conductive nature at the position of carboxylic acid and the TiO_2 binding site leads to the better charge injection for the 5-SQ than the 6-SQ where the dye-TiO_2 interface is non-conductive and mostly through-space charge injection lead to the observed photocurrent. The photovoltaic device by dipping the TiO_2 electrode for 12 h in dye solutions and the co-adsorbent decipher the importance of aggregation of dyes for the photocurrent generation.

3.3.5 Electrochemical impedance spectroscopy (EIS). An EIS study on the DSSC devices has been carried out to understand the charge transfer properties across the TiO$_2$-dye/electrolyte interface.[69] Nyquist plot, charge transfer resistance (R_{ct}), chemical capacitance ($C\mu$), and the electron lifetime ($\tau = R_{ct} \times C\mu$) at various applied bias are provided in **Figure 20**, **21**, and **22**. The EIS parameters by applying 0.6 V bias is provided in **Table 6**.
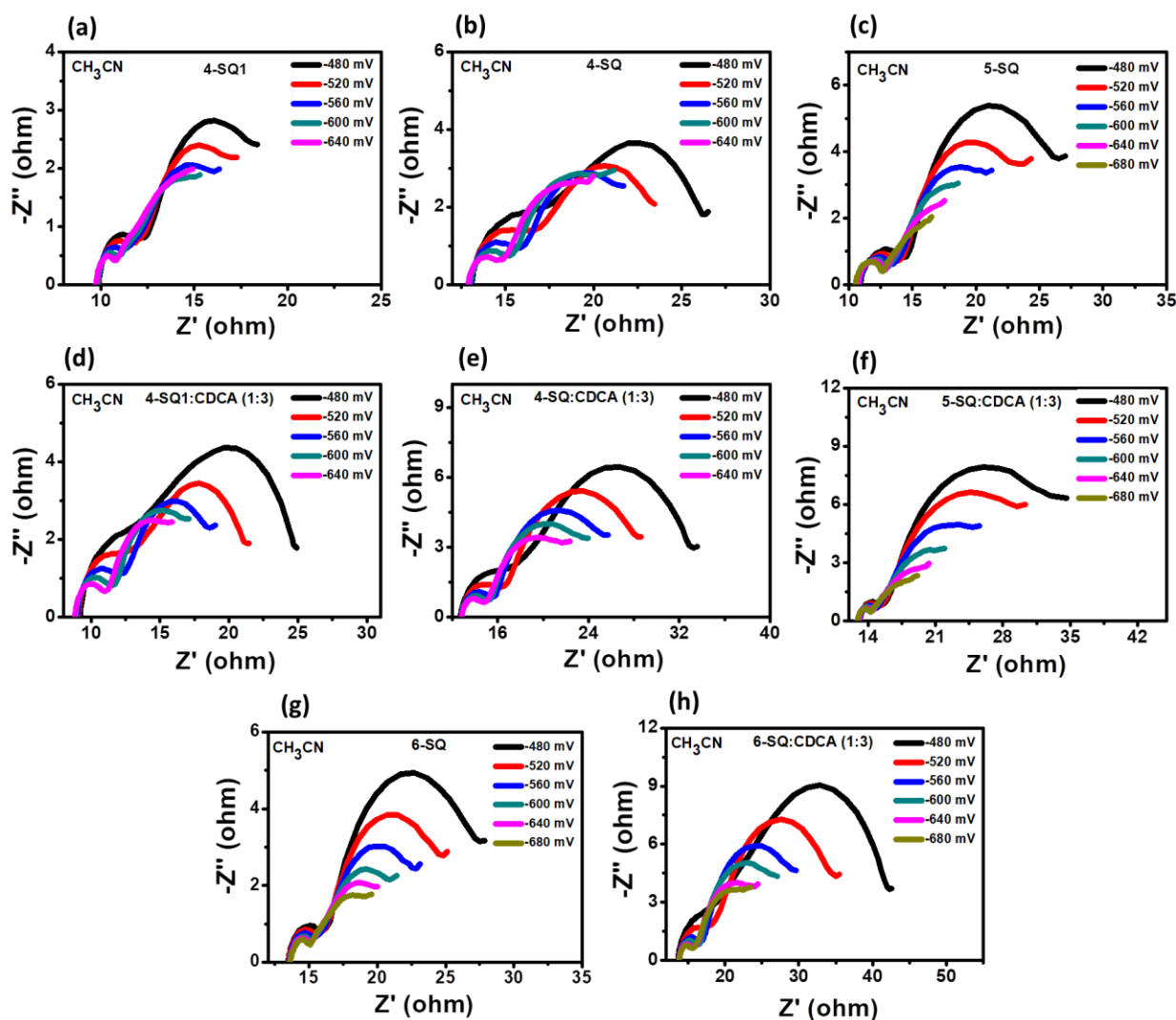
Figure 20. Nyquist plot of 4-SQ1, 4-SQ, 5-SQ, and 6-SQ dyes *vs* applied bias in the presence and absence of CDCA.
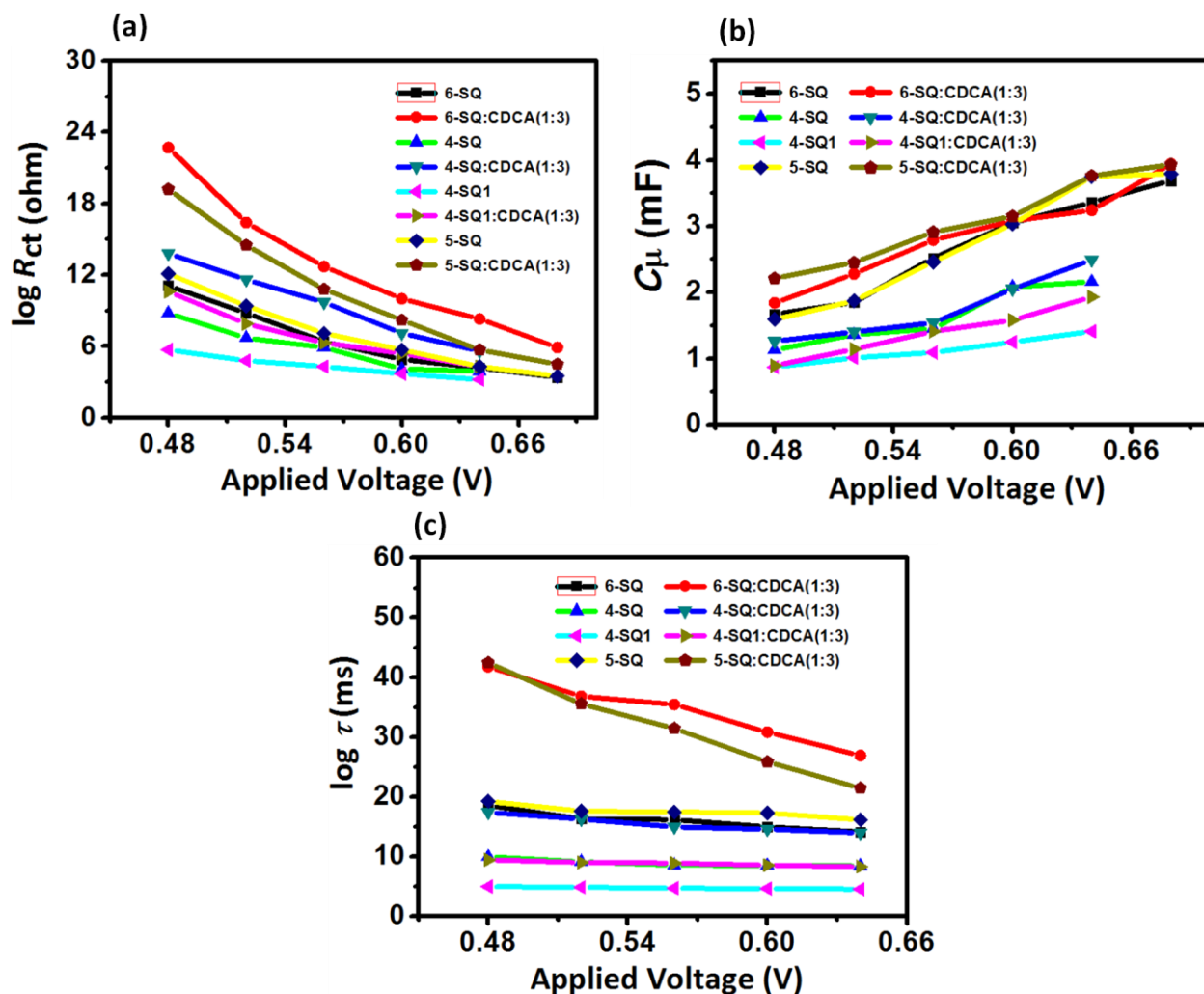
Figure 21. (a) Charge recombination resistance, (b) chemical capacitance, (c) electron life time of SQ dyes *vs* applied bias with and without CDCA.

Charge transfer resistance at the TiO$_2$-dye/electrolyte interface modulates the charge collection efficiency at the TiO$_2$ layer. In general, increment in the charge transfer resistance (R_{ct}) is reflected in the enhanced charge collection. One of the ways to improve the R_{ct} is by shielding the electrolyte components from reaching the TiO$_2$ surface which avoids the recombination of electrons in the TiO$_2$ and oxidized electrolyte component at the TiO$_2$-dye/electrolyte interface. The R_{ct} value at the applied bias of 0.6 V decreases in the order of 5-SQ (5.7 ohm)> 6-SQ (4.9 ohm)> 4-SQ (4.1 ohm) for the devices in dark. Further, the values are substantially increased in the order, 6-SQ (10 ohm)> 5-SQ (8.2 ohm)> 4-SQ (7.1 ohm) when the electrodes were coadsorbed with CDCA (3 equiv.), which indicates the well-packed monolayer of dyes as well as

dyes and CDCA have been achieved for 5-SQ and 6-SQ than 4-SQ. The fitted chemical capacitive ($C\mu$) curve under the bias potential indicates the position of the conduction band of TiO$_2$.[70-74] Similar $C\mu$ values for 5-SQ, 6-SQ, and slightly lowered value for 4-SQ indicates the similar conduction band positions for 5-SQ, 6-SQ than 4-SQ. It is known that the dipole moment of the dye normal to the TiO$_2$ surface can modulate the positions of the conduction band. As indicated by the computational studies (**Table 2**)**,** different orientation of the 4-SQ1, 5-SQ1, and 6-SQ1 dyes on the TiO$_2$ with dipole moment lead to the modulated V_{OC} besides effective passivation of the titania surface by the branched alkyl groups. Further, the electron lifetime also supported the varied V_{OC} of the 5-SQ (31.42 ms), 6-SQ (30.8 ms), and 4-SQ (14.55 ms) devices.
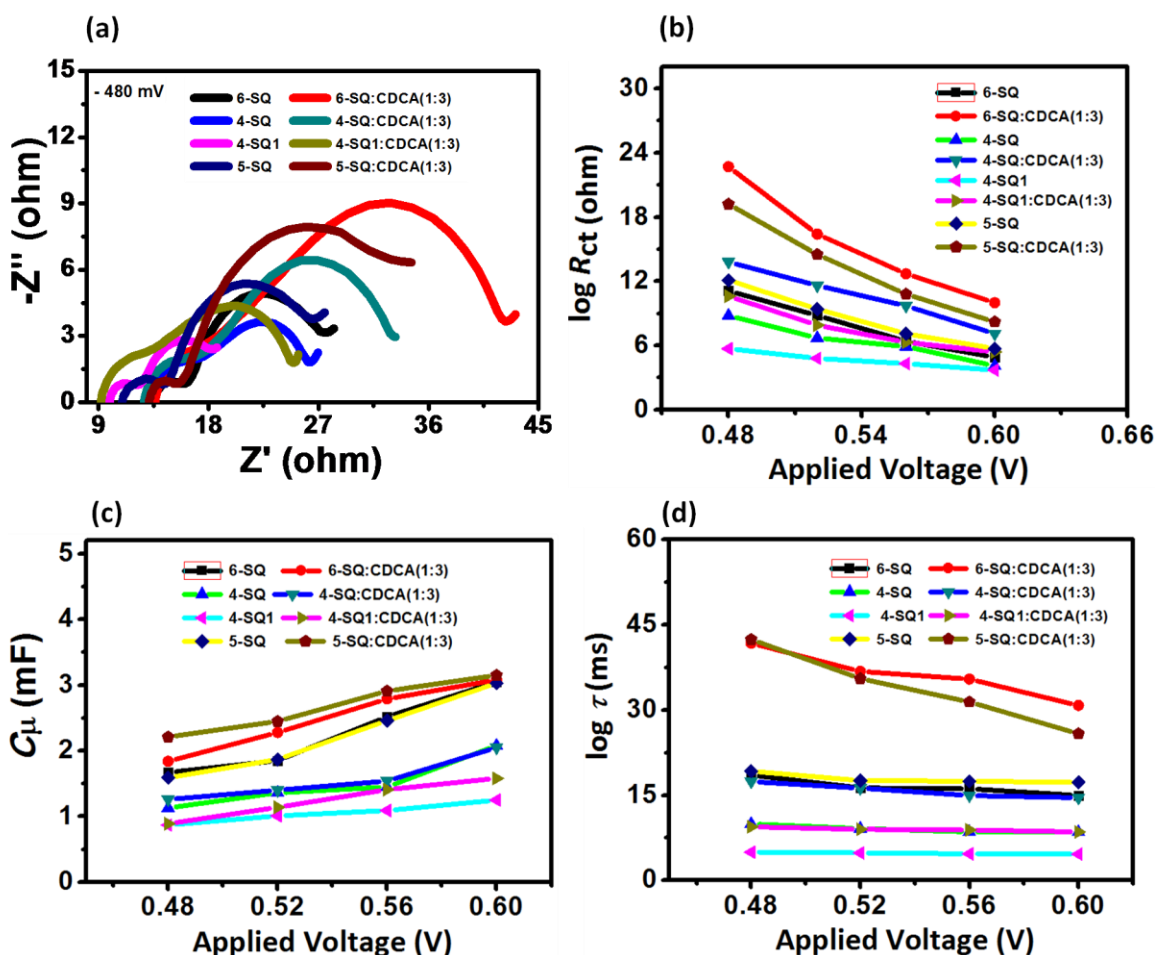
Figure 22. (a) Nyquist plot, (b) charge recombination resistance, (c) chemical capacitance, (d) electron lifetime of 4-SQ1, 4-SQ, 5-SQ, and 6-SQ dyes *vs* applied bias in the presence and absence of CDCA.

Table 6. EIS parameters of DSSC device made up of 4-SQ, 5-SQ, 6-SQ, and 4-SQ1 in dark with the applied bias of 0.6 V.

Dye	Dye: CDCA	R_{ct} (ohm)	$C\mu$ (mF)	τ (ms)
4-SQ	1:0	4.1	2.08	8.52
4-SQ	1:3	7.1	2.05	14.55
5-SQ	1:0	5.7	3.03	17.27
5-SQ	1:3	8.2	3.15	31.42
6-SQ	1:0	4.9	3.05	14.94
6-SQ	1:3	10	3.08	30.8
4-SQ1[a]	1:0	4.8	1.01	4.84
4-SQ1[a]	1:3	7.9	1.14	9.0

[a]Applied bias of 0.52 V

3.3.6 Mott-Schottky and dye-desorption studies of SQ dyes. To evaluate the conduction band position of TiO$_2$ sensitized with the 4-SQ, 5-SQ, and 6-SQ, Mott Schottky study has been carried out (**Figure 23a**).[63-65] The amount of anchored dyes on the TiO$_2$ was found to be 6.3 μmol/cm^2 for 4-SQ, 9.3 μmol/cm^2 for 5-SQ and 7.6 μmol/cm^2 for 6-SQ in the absence of CDCA by desorption method (**Table 7**), which indicates the position of anchoring unit indeed controls the extent of dye loading on the photoanode. Further, the dye retention of 74-79 % on the surface in the presence of 3 equivalents of CDCA (**Table 7**), points towards the preferential dye-dye interaction over dye-CDCA and CDCA-CDCA interactions. It is also known that the $\Delta E_{CB, TiO_2}$ also depends on the dipole moment exerted by the anchored dyes either towards or away from the TiO$_2$ surface. Mott-Schottky (**Table 7**) along with EIS ($C\mu$ vs applied bias, **Figure 22c**) studies revealed that the position of CB TiO$_2$ is modulated upon sensitizing with squaraine dyes.

Table 7. Flat band potential of TiO$_2$, upon sensitizing with squaraine dyes and amount of dye loaded on TiO$_2$ surface with and without CDCA.

Dyes	CDCA	E_{fb}	A_{max}	ε (M^{-1} cm^{-1})	Dye Loading on TiO$_2$ (mol/cm^2)
4-SQ1	0	-0.7458	0.8535	3.0×10^5	1.113×10^{-5}
4-SQ1	3	-	0.6145	3.0×10^5	8.015×10^{-6}
4-SQ	0	-0.7230	0.5751	3.6×10^5	6.251×10^{-6}
4-SQ	3	-	0.4552	3.6×10^5	4.947×10^{-6}
5-SQ	0	-0.6659	0.7398	3.1×10^5	9.338×10^{-6}
5-SQ	3	-	0.5664	3.1×10^5	7.149×10^{-6}
6-SQ	0	-0.7078	0.6803	3.5×10^5	7.605×10^{-6}
6-SQ	3	-	0.5084	3.5×10^5	5.683×10^{-6}
TiO$_2$[65]	0	-0.4200	-	-	-
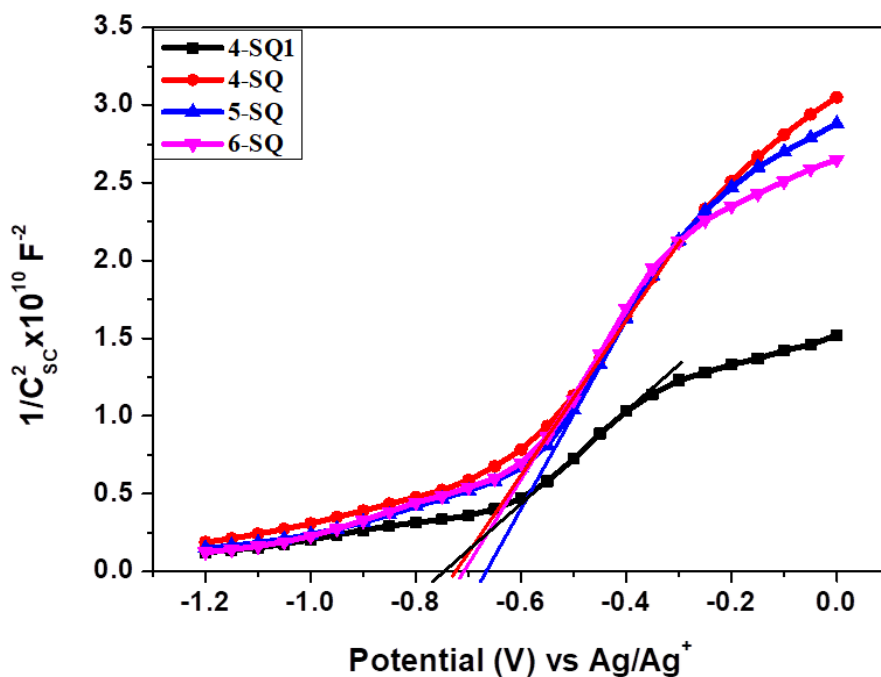
Figure 23. (a) Mott-Schottky plots of the TiO$_2$ sensitized with SQ dyes under dark condition at a frequency of 1 kHz with a voltage sweep (from -1.2 V to 0 V).

3.4 CONCLUSIONS

In the present work, a series of far-red responsive unsymmetrical squaraine dyes, 4-SQ, 5-SQ, 6-SQ, and 7-SQ have been synthesized by introducing anchoring groups at different positions to modulate the orientation of the dye on the TiO_2 surface. The position of anchoring group deciphers the importance of electronic coupling between dye and TiO_2 (both conductive and non-conductive), introducing a non-radiative decay pathway for the sensitizer upon anchoring, the orientation of dyes on the TiO_2 and self-assembly of dyes on the TiO_2. All the above-mentioned factors collectively play to optimize a better dye-sensitized photoanode for DSSC device. Our results on the D-A-D type squaraine dye indicate that the anchoring group at 7th position (7-SQ) did not anchor on TiO_2, and 4-SQ on TiO_2 formed a twisted structure upon photo-excitation. Though the aggregation pattern on TiO_2 for the 5-SQ and 6-SQ are similar, the device performance is modulated due to the conductive nature at the dye-TiO_2 interface for 5-SQ with enhanced energy conversion efficiency. The device performance of 6-SQ showed the importance of through space electron transfer for the photocurrent generation, an observation helps to design self-assembled dye structure for the DSSC device study with non-conductive anchoring group. Further, the dye-TiO_2 interface helps to modulate the flat band potential of TiO_2 due to the dipole moment exerted by the dyes on to the semiconducting metal oxide, which in turn helps to enhance the V_{OC} of the devices.

3.5 REFERENCES

(1) O'Regan, B.; Grätzel, M. A Low-Cost, High-Efficiency Solar Cell Based on Dye-Sensitized Colloidal TiO$_2$ Films. *Nature* **1991**, *353*, 737–740.

(2) Hagfeldt, A.; Boschloo, G.; Sun, L.; Kloo, L.; Pettersson, H. Dye-Sensitized Solar Cells. *Chem. Rev.* **2010**, *110*, 6595–6663.

(3) Ye, M.; Wen, X.; Wang, M.; Iocozzia, J.; Zhang, N.; Lin, C.; Lin1, Z. Recent Advances in Dye-Sensitized Solar Cells: from Photoanodes, Sensitizers and Electrolytes to Counter Electrodes. *Materials Today*, **2015**, *18*, 155-162.

(4) Wu, J.; Lan, Z.; Lin, J.; Huang, M.; Huang, Y.; Fan, L.; Luo, G. Electrolytes in Dye-Sensitized Solar Cells. *Chem. Rev.* **2015**, *115*, 2136−2173.

(5) Hao, F.; Dong, P.; Luo, Q.; Li, J.; Lou, J.; Lin, H. Recent Advances in Alternative Cathode Materials for Iodine-Free Dye-Sensitized Solar Cells. *Energy Environ. Sci.,* **2013**, *6*, 2003–2019.

(6) Wu, J.; Lan, Z.; Lin, J.; Huang, M.; Huang, Y.; Fan, L.; Luo, G.; Lin, Y.; Xie, Y.; Wei, Y. Counter Electrodes in Dye-Sensitized Solar Cells. *Chem. Soc. Rev.*, **2017**, *46*, 5975-6023.

(7) Listorti, A.; O'Regan, B.; Durrant, J. R. Electron Transfer Dynamics in Dye-Sensitized Solar Cells. *Chem. Mater.* **2011**, *23*, 3381–3399.

(8) Gao, F.; Wang, Y.; Shi, D.; Zhang, J.; Wang, M.; Jing, X.; Humphry- Baker, R.; Wang, P.; Zakeeruddin, S. M.; Grätzel, M. Enhance the Optical Absorptivity of Nanocrystalline TiO$_2$ Film with High Molar Extinction Coefficient Ruthenium Sensitizers for High Performance Dye-Sensitized Solar Cells. *J. Am. Chem. Soc*. **2008**, *130*, 10720-10728.

(9) Liang, M.; Chen, J. Arylamine Organic Dyes for Dye-Sensitized Solar Cells. *Chem. Soc. Rev.* **2013**, *42*, 3453-3488.

(10) Wu, Y.; Zhu, W. Organic Sensitizers from D–π–A to D–A– π–A: Effect of the Internal Electron-Withdrawing Units on Molecular Absorption, Energy Levels and Photovoltaic Performances. *Chem. Soc. Rev.* **2013**, *42*, 2039-2058.

(11) Park, J.-H.; Nam, D. G.; Kim, B-M.; Jin, M. Y.; Roh, D.-H.; Jung, H. S.; Ryu, D. H.; Kwon, T.-H. Planar D-D-π-A Organic Sensitizers for Thin-Film Photoanodes. *ACS Energy Lett.* **2017**, *2*, 1810-1817.

(12) Saccone, D.; Galliano, S.; Barbero, N.; Quagliotto, P.; Viscardi, G.; Barolo, C. Polymethine Dyes in Hybrid Photovoltaics: Structure-Properties Relationships. *Eur. J. Org. Chem.* **2016,** *2016*, 2244–2259.

(13) Qin, C.; Wong, W.-Y.; Han, L. Squaraine Dyes for Dye-Sensitized Solar Cells: Recent Advances and Future Challenges. *Chem. Asian J.* **2013**, *8*, 1706-1719.

(14) Yang, J.; Ganesan, P.; Teuscher, J.; Moehl, T.; Kim, Y. J.; Yi, C.; Comte, P.; Pei, K.; Holcombe, T. W.; Nazeeruddin, M. K. et al. Influence of the Donor Size in

D−π−A Organic Dyes for Dye-Sensitized Solar Cells. *J. Am. Chem. Soc.* **2014**, *136*, 5722-5730.

(15)   Yao, Z.; Zhang, M.; Wu, H.; Yang, L.; Li, R.; Wang, P. Donor/Acceptor Indenoperylene Dye for Highly Efficient Organic Dye Sensitized Solar Cells. *J. Am. Chem. Soc.* **2015**, *137*, 3799-3802.

(16)   Mishra, A.; Fischer, M. K. R.; Bauerle, P. Metal-Free Organic Dyes for Dye-Sensitized Solar Cells: From Structure: Property Relationships to Design Rules. *Angew. Chem. Int. Ed.* **2009**, *48*, 2474-2499.

(17)   Zhang, L.; Yang, X.; Wang, W.; Gurzadyan, G. G.; Li, J.; Li, X.; An, J.; Yu, Z.; Wang, H.; Cai, B. et al. 13.6% Efficient Organic Dye-Sensitized Solar Cells by Minimizing Energy Losses of the Excited State. *ACS Energy Lett. ,* **2019**, *4*, 943−951.

(18)   Karjule, N.; M. K., M. F.; Nithyanandhan, J. Heterotriangulene-based Unsymmetrical Squaraine Dyes: Synergistic Effects of Donor Moiety and Out-of-plane Branched Alkyl Chains on Dye Cell Performance. *J. Mater. Chem. A*, **2016**, *4*, 18910-18921.

(19)   Liu, Y.; Zhang, X.; Li, C.; Tian, Y.; Zhang, F.; Wang, Y.; Wu, W.; Liu, B. Energy-Level Control via Molecular Planarization and Its Effect on Interfacial Charge-Transfer Processes in Dye-Sensitized Solar Cells. *J. Phys. Chem. C* **2019**, *123*, 13531–13537.

(20)   Li, R.; Liu, J.; Cai, N.; Zhang, M.; Wang, P. Synchronously Reduced Surface States, Charge Recombination, and Light Absorption Length for High-Performance Organic Dye-Sensitized Solar Cells. *J. Phys. Chem. B* **2010**, *114*, 4461-4464.

(21)   Ren, Y.; Sun, D.; Cao, Y.; Tsao, H. N.; Yuan, Y.; Zakeeruddin, S. M.; Wang, P.; Grätzel, M. A Stable Blue Photosensitizer for Color Palette of Dye-Sensitized Solar Cells Reaching 12.6% Efficiency. *J. Am. Chem. Soc.* **2018**, *140*, 2405−2408.

(22)   Gao, P.; Tsao, H. N.; Yi, C.; Grätzel, M.; Nazeeruddin, M. K. Extended π - Bridge in Organic Dye-Sensitized Solar Cells: the Longer, the Better? *Adv. Energy Mater.* **2014**, *4*, 1301485.

(23)   Rochford, J.; Chu, D.; Hagfeldt, A.; Galoppini, E. Tetrachelate Porphyrin Chromophores for Metal Oxide Semiconductor Sensitization: Effect of the Spacer Length and Anchoring Group Position. *J. Am. Chem. Soc.* **2007**, *129*, 4655–4665.

(24)   Zhang, L.; Cole, J. M. Dye Aggregation in Dye-Sensitized Solar Cells. *J. Mater. Chem. A.***2017**, 5, 19541-19559.

(25)   Si, L.; He, H. Porphyrin Dyes on TiO_2 Surfaces with Different Orientations: A Photophysical, Photovoltaic, and Theoretical Investigation. *J. Phys. Chem. A* **2014**, *118*, 3410−3418.

(26)   Hart, A. S.; Kc, C. B.; Gobeze, H. B.; Sequeira, L. R.; D'Souza, F. Porphyrin-Sensitized Solar Cells: Effect of Carboxyl Anchor Group Orientation on the Cell Performance. *ACS Appl. Mater. Interfaces* **2013**, *5*, 5314–5323.

(27)   Gou, F.; Jiang, X.; Fang, R.; Jing, H.; Zhu, Z. Strategy to Improve Photovoltaic Performance of DSSC Sensitized by Zinc Prophyrin Using Salicylic Acid As a Tridentate Anchoring Group. *ACS Appl. Mater. Interfaces* **2014**, *6*, 6697-6703.

(28)   Ambre, R. B.; Mane, S. B.; Chang, G.-F.; Hung C.-H. Effects of Number and Position of Meta and Para Carboxyphenyl Groups of Zinc Porphyrins in Dye-Sensitized Solar Cells: Structure−Performance Relationship. *ACS Appl. Mater. Interfaces* **2015**, *7*, 1879−1891.

(29)   Imahori, H.; Kang, S.; Hayashi, H.; Haruta, M.; Kurata, H.; Isoda, S.; Canton, S. E.; Infahsaeng, Y.; Kathiravan, A.; Pascher, T. et al. Photoinduced Charge Carrier Dynamics of Zn - Porphyrin - TiO_2 Electrodes: The Key Role of Charge Recombination for Solar Cell Performance. *J. Phys. Chem. A* **2011**, *115*, 3679–3690.

(30)   Ye, S.; Kathiravan, A.; Hayashi, H.; Tong, Y.; Infahsaeng, Y.; Chabera, P.; Pascher, T.; Yartsev, A. P.; Isoda, S.; Imahori, H. et al. Role of Adsorption Structures of Zn-Porphyrin on TiO_2 in Dye-Sensitized Solar Cells Studied by Sum Frequency Generation Vibrational Spectroscopy and Ultrafast Spectroscopy. *J. Phys. Chem. C* **2013**, *117*, 6066−6080.

(31)   Ide, R.; Fujimori, Y.; Tsuji, Y.; Higashino, T.; Imahori, H.; Ishikawa, H.; Imanishi, A.; Fukui, K.; Nakamura, M.; Hoshi, N. Structural Effects on the Incident Photon-to-Current Conversion Efficiency of Zn Porphyrin Dyes on the Low-Index Planes of TiO_2. *ACS Omega* **2017**, *2*, 128−135.

(32)   Anderson, H. L. Conjugated Porphyrin Ladders. *Inorg. Chem.***1994**, *33*, 972-981.

(33)   Lin, V. S.; DiMagno, S. G.; Therien, M.J. Highly Conjugated, Acetylenyl Bridged Porphyrins: New Models for Light-harvesting Antenna Systems. *Science*, **1994**, *264*, 1105-1111.

(34)   Higashino, T.; Imahori, H. Porphyrins as Excellent Dyes for Dye-Sensitized Solar Cells: Recent Developments and Insights. *Dalton Trans.*, **2015**, *44,* 448-463.

(35)   Urbani, M.; Grätzel, M.; Nazeeruddin, M. K.; Torres, T. Meso-Substituted Porphyrins for Dye-Sensitized Solar Cells. *Chem. Rev.* **2014**, *114*, 12330−12396.

(36)   Li, L.-L.; Diau, E. W.-G. Porphyrin-Sensitized Solar Cells. *Chem. Soc. Rev*. **2013**, *42*, 291-304.

(37)   Ji, J.-M.; Zhou, H.; Kim, H. K. Rational Design Criteria for D–◻ –A Structured Organic and Porphyrin Sensitizers for Highly Efficient Dye-Sensitized Solar Cells. *J. Mater. Chem. A*, **2018**, *6*, 14518–14545.

(38)   Kurumisawa, Y.; Higashino, T.; Nimura, S.; Tsuji, Y.; Iiyama, H.; Imahori, H. Renaissance of Fused Porphyrins: Substituted Methylene-Bridged Thiophene-Fused Strategy for High-Performance Dye-Sensitized Solar Cells. *J. Am. Chem. Soc.* **2019**, *141*, 9910–9919.

(39)   Zeng, K.; Lu, Y.; Tang, W.; Zhao, S.; Liu, Q.; Zhu, W.; Tian, H.; Xie, Y. Efficient Solar Cells Sensitized by a Promising New Type of Porphyrin: Dye-Aggregation Suppressed by Double Strapping. *Chem. Sci*. **2019**, *10*, 2186-2192.

(40)   Chen, K.; Chen, Y.; Zhu, W.-H.; Tian, H.; Xie, Y. Efficient Solar Cells based on Concerted Companion Dyes Containing Two Complementary Components: An Alternative Approach for Cosensitization. *J. Am. Chem. Soc.* **2020**, *142*, 5154-5161.

(41)   Cole, J. M.; Pepe, G.; Al Bahri, O. K.; Cooper, C. B. Cosensitization in Dye-Sensitized Solar Cells. *Chem. Rev.* **2019**, *119*, 7279−7327.

(42)   Ragoussi, M.-E.; Ince , M.; Torres, T. Recent Advances in Phthalocyanine-Based Sensitizers for Dye-Sensitized Solar Cells. *Eur. J. Org. Chem.* **2013**, *2013*, 6475–6489.

(43)   McKerrow, A. J.; Buncel, E.; Kazmaier, P. M. Aggregation of Squaraine Dyes: Structure-property Relationships and Solvent Effects**.** *Can. J. Chem.* **1995**, *73*, 1605 -1615.

(44)   Alex, S.; Basheer, M. C.; Arun, K. T.; Ramaiah, D.; Das, S. Aggregation Properties of Heavy Atom Substituted Squaraine Dyes: Evidence for the Formation of J-Type Dimer Aggregates in Aprotic Solvents. *J. Phys. Chem. A* **2007**, *111*, 3226−3230.

(45)   Mor, G. K.; Kim, S.; Paulose, M.; Varghese, O. K.; Shankar, K.; Basham, J.; Grimes, C. A. Visible to Near-Infrared Light Harvesting in TiO_2 Nanotube Array−P3HT Based Heterojunction Solar Cells. *Nano Lett.* **2009**, *12*, 4250−4257.

(46)   de Miguel, G.; Ziółek, M.; Zitnan, M.; Organero, J. A.; Pandey, S. S.; Hayase, S.; Douhal, A. Photophysics of H- and J-Aggregates of Indole-Based Squaraines in Solid State. *J. Phys. Chem. C* **2012**, *116*, 9379– 9389.

(47)   Ajayaghosh, A. Chemistry of Squaraine-Derived Materials: Near-IR Dyes, Low Band Gap Systems, and Cation Sensors**.** *Acc. Chem. Res.* **2005**, *38*, 449−459.

(48)   Beverina, L.; Salice., P. Squaraine Compounds: Tailored Design and Synthesis towards a Variety of Material Science Applications. *Eur. J. Org. Chem.* **2010**, *2010*, 1207−1225.

(49)   Eldo, J.; Ajayaghosh, A. New Low Band Gap Polymers: Control of Optical and Electronic Properties in near Infrared Absorbing π-Conjugated Polysquaraines. *Chem. Mater.* **2002**, *14*, 410−418.

(50)   Sreejith, S.; Carol, P.; Chithra, P.; Ajayaghosh, A. Squaraine Dyes: A Mine of Molecular Materials, *J. Mater. Chem.* **2008**, *18*, 264-274.

(51)   Law, K. -Y. Organic Photoconductive Materials: Recent Trends and Developments. *Chem. Rev.* **1993**, *93*, 449-486.

(52)   Della Pelle, A. M.; Homnick, P. J.; Bae, Y.; Lahti, P. M.; Thayumanavan, S. Effect of Substituents on Optical Properties and Charge-Carrier Polarity of Squaraine Dyes *J. Phys. Chem. C* **2014**, *118*, 1793– 1799.

(53)   Chen, G.; Sasabe, H.; Igarashi, T.; Hong, Z.; Kido, J. Squaraine Dyes for Organic Photovoltaic Cells. *J. Mater. Chem. A*, **2015**, *3*, 14517-14534.

(54)   Chen, G.; Sasabe, H.; Lu, W.; Wang, X.-F.; Kido, J.; Hong, Z.; Yang, Y. *J*-Aggregation of a Squaraine Dye and its Application in Organic Photovoltaic Cells. *J. Mater. Chem.* C, **2013**, *1*, 6547-6552.

(55)   Mulhern, K. R.; Detty, M. R.; Watson, D. F. Aggregation-Induced Increase of the Quantum Yield of Electron Injection from Chalcogenorhodamine Dyes to TiO_2. *J. Phys. Chem. C.* **2011**, *115*, 6010-6018.

(56)   Higashino, T.; Kawamoto, K.; Sugiura, K.; Fujimori, Y.; Tsuji, Y.; Kurotobi, K.; Ito, S.; Imahori, H. Effects of Bulky Substituents of Push−Pull Porphyrins on Photovoltaic Properties of Dye-Sensitized Solar Cells. *ACS Appl. Mater. Interfaces* **2016**, *8*, 15379−15390.

(57)   Martín, L.-G.; Fernández, F.-L.; Sastre, Á.-S. Advances in Phthalocyanine-Sensitized Solar Cells (PcSSCs). *J. Mater. Chem. A,* **2014**, *2*, 15672-15682.

(58)   Bai, Y.; Zhang, J.; Zhou, D.; Wang, Y.; Zhang, M.; Wang, P. Engineering Organic Sensitizers for Iodine-Free Dye-Sensitized Solar Cells: Red-Shifted Current Response Concomitant with Attenuated Charge Recombination. *J. Am. Chem. Soc.* **2011**, *133*, 11442-11445.

(59)   Singh, A. K.; Kavungathodi, M. F. M.; Nithyanandhan, J. Alkyl-Group-Wrapped Unsymmetrical Squaraine Dyes for Dye-Sensitized Solar Cells: Branched Alkyl Chains Modulate the Aggregation of Dyes and Charge Recombination Processes. *ACS Appl. Mater. Interfaces* **2020**, *12*, 2555-2565.

(60)   Alagumalai, A.; Kavungathodi, M. F. M.; Vellimalai, P.; Sil, M. C.; Nithyanandhan, J. Effect of Out-of-Plane Alkyl Group's Position in Dye-Sensitized Solar Cell Efficiency: A Structure–Property Relationship Utilizing Indoline-Based Unsymmetrical Squaraine Dyes. *ACS Appl. Mater. Interfaces* **2016**, *8*, 35353–35367.

(61)   Frisch, M. J.; Trucks, G. W.; Schlegel, H. B.; Scuseria, G. E.; Robb, M. A.; Cheeseman, J. R.; Scalmani, G.; Barone, V.; Petersson, G. A. ; Nakatsuji, H. et al. *Gaussian 09*; Gaussian, Inc.: Wallingford, CT, 2016.

(62)   Kresse, G.; Furthmuller, J. Efficient Iterative Schemes for ab Initio Total-Energy Calculations using a Plane-Wave Basis Set. *Phys. Rev. B: Condens. Matter***, 1996**, *54*, 11169-11185.

(63)   Cheng, M.; Yang, X.; Chen, C.; Zhao, J.; Tan, Q.; Sun, L. Effect of the Acceptor on the Performance of Dye-Sensitized Solar Cells. *Phys. Chem. Chem. Phys.* **2013**, *15*, 17452−17459.

(64)   Preethi, L. K.; Antony, R. P.; Mathews, T.; Walczak, L.; Gopinath, C. S. A Study on Doped Heterojunctions in TiO_2 Nanotubes: An Efficient Photocatalyst for Solar Water Splitting. *Sci. Reports* **2017**, 7: 14314.

(65)   Gondane, V.; Bhargava, P. Tuning Flat Band Potential of TiO$_2$ using an Electrolyte Additive to Enhance Open Circuit Voltage and Minimize Current Loss in Dye Sensitized Solar Cells. *Electrochimica Acta* **2016**, *209*, 293–298.

(66)   Law, K. Y. In *Molecular and Supramolecular Photochemistry*; Ramamurthy, V., Schanze, K. S., Eds.; Marcel Dekker: New York, 1997; Vol. 1, pp 519-584.

(67)   Rühle, S.; Greenshtein, M.; Chen, S.-G.; Merson, A.; Pizem, H.; Sukenik, C. S.; Cahen, D.; Zaban, A. Molecular Adjustment of the Electronic Properties of Nanoporous Electrodes in Dye-Sensitized Solar Cells. *J. Phys. Chem. B* **2005**, *109*, 18907– 18913.

(68)   Ronca, E.; Pastore, M.; Belpassi, L.; Tarantelli, F.; De Angelis, F. Influence of the Dye Molecular Structure on the TiO$_2$ Conduction Band in Dye-Sensitized Solar Cells: Disentangling Charge Transfer and Electrostatic Effects. *Energy Environ. Sci.* **2013**, *6*, 183– 193.

(69)   Wang, Q.; Moser, J.–E.; Grätzel, M. Electrochemical Impedance Spectroscopic Analysis of Dye-Sensitized Solar Cells. *J. Phys. Chem. B* **2005**, *109*, 14945-14953.

(70)   Chai, Q.; Li, W.; Wu, Y.; Pei, K.; Liu, J.; Geng, Z.; Tian, H.; Zhu, W. Effect of a Long Alkyl Group on Cyclopentadithiophene as a Conjugated Bridge for D–A−π–A Organic Sensitizers: IPCE, Electron Diffusion Length, and Charge Recombination. *ACS Appl. Mater. Interfaces* **2014**, *6*, 14621–14630.

(71)   Fabregat-Santiago, F.; Garcia-Belmonte, G.; Mora-Seró, I.; Bisquert, J. Characterization of Nanostructured Hybrid and Organic Solar Cells by Impedance Spectroscopy. *Phys. Chem. Chem. Phys.* **2011**, *13*, 9083– 9118.

(72)   Stergiopoulos, T.; Falaras, P. Minimizing Energy Losses in Dye-Sensitized Solar Cells Using Coordination Compounds as Alternative Redox Mediators Coupled with Appropriate Organic Dyes. *Adv. Energy Mater.* **2012**, *2*, 616– 627.

(73)   Luo, J.; Xu, M.; Li, R.; Huang, K.-W.; Jiang, C.; Qi, Q.; Zeng, W.; Zhang, J.; Chi, C.; Wang, P. N-Annulated Perylene as An Efficient Electron Donor for Porphyrin-Based Dyes: Enhanced Light-Harvesting Ability and High-Efficiency Co(II/III)-Based Dye-Sensitized Solar Cells. *J. Am. Chem. Soc.* **2014**, *136*, 265– 272.

(74)   Li, L.-L.; Chang, Y.-C.; Wu, H.-P.; Diau, E. W.-G. Characterisation of Electron Transport and Charge Recombination Using Temporally Resolved and Frequency-Domain Techniques for Dye-Sensitised Solar Cells. *Int. Rev. Phys. Chem.* **2012**, *31*, 420– 467.

D-A-D Based Complementary Unsymmetrical Squaraine Dyes for Co-sensitized Solar Cells

Filling the Absorption Valley by Co-Sensitization and Aggregation

Photocurrent generation from aggregated structure

AK4 (η = 7.93%)
AK4+SQS4 (η = 9.36%)
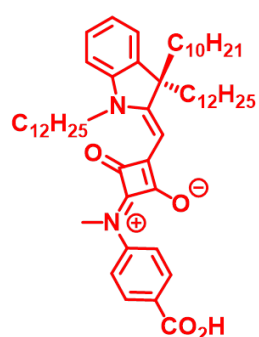
SQS4
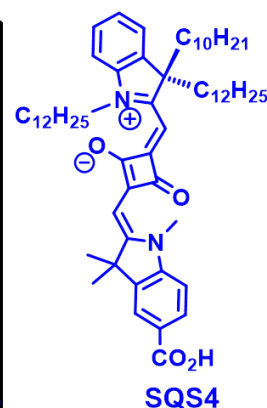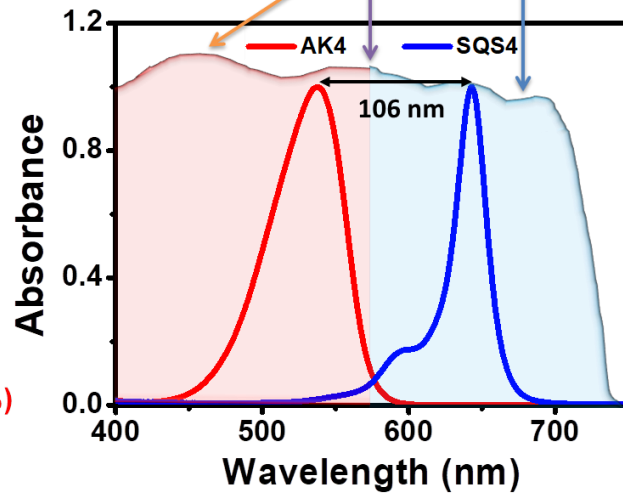
4.1 INTRODUCTION

Interfacial electron transfer kinetics associated with the photo-excited sensitizer and the semiconducting metal oxide has been the topic of frontier research for the last three decades ever since the fruition of solar energy conversion by dye-sensitized solar cells (DSSC).[1-3] Light absorbing sensitizer molecules[4] plays an important role of harvesting solar energy besides anode,[5] electrolyte[6] and cathode materials[7] in DSSC devices. Ease of tuning the HOMO and LUMO energy levels and the high extinction coefficient of organic sensitizers drew the attention of organic chemists to come up with different architectures of dyes to harvest visible, far-red and NIR regions of the solar spectrum in compared to transition mental based light absorbing complexes. Thus, D-A,[8] D-π-A,[9] D-A- π-A,[10] D-D- π-A,[11] and D-A-D[12] dye architectures have been wildly utilized to harvest the visible and NIR regions of the solar spectrum. Aggregation of dyes[13] on the semiconducting metal oxide surface,[14] and photo-injected electrons combine with the oxidized electrolyte species known as charge recombination processes are found to be detrimental factors for the DSSC device performance.[15] Hence, besides light harvesting properties of the sensitizers, design principles for controlling the aggregation of dyes on the semiconducting metal oxide surface, and diminishing the charge recombination process need to be in-built in the dye structure for the enhanced device performance.[16] Introducing alkyl groups to the dye structures and/or using optically transparent co-adsorbent helped to avoid above mentioned processes which boost the device performance.[16,17] There are several organic dyes that exceed 10-13% device performance.[18-20] Though the organic sensitizers are superior in terms of modular synthesis and having high extinction coefficient, the photocurrent generation is often rendered by either one of the visible, far-red and NIR-regions of the solar spectrum. Further there are few dyes that show panchromatic incident photon to current conversion efficiency (IPCE) response.[21,22] However the co-sensitization method that uses two or more complementary light absorbing dyes help to harvest the 400-850 nm photons of the solar spectrum.[23-25] Ruthenium complexes and porphyrin based dyes are been the choice of primary dyes, to which D-π-A,[26] D-A-π-A,[27] D-A-D[28] dyes have been utilized as a co-sensitizer for the panchromatic spectral coverage for the better photocurrent generation.

Cocktail, [29,30] sequential[28] and ultrafast methods[28,31] have been utilized for the co-sensitization process to have poised arrangements of dyes on TiO_2, preferential loading between the pair of

dyes and reducing the sensitizing the time in minutes, respectively. Further general information on the binding energy, self-assembling nature of individual dyes on TiO_2, size,[32] shape and geometry[33] of sensitizers are required to choose the method of co-sensitization to have the optimal dye arrangement for the better device performance. Further, Brønsted and Lewis acid sites on the TiO_2 surface utilized for the selective adsorption complementing dyes with pyridine and carboxylic acid anchoring groups, respectively.[34,35] Many co-sensitizers have been developed that were complement to the optical absorption gaps of near-panchromatic ruthenium- and porphyrin-based dyes. Small D-π-A based dye with N3 sensitizer provided the device performance of 11.1 and 11.3%, respectively.[24, 36-38] Ruthenium based N719 sensitizer with β- and meso substituted porphyrins showed the device performance of 4%[39] and 8.9%[40], respectively. Porphyrin dyes showed the near panchromatic photoelectron generation with dips in the IPCE profile however combination with D-π-A, and D-A-π-A showed the device performance up to 13%.[26,27,41-43] Push-pull type monomeric and dimeric porphyrin dyes with complementary light absorption property provided the device efficiencies 9.6-10.4%.[25,44] Besides, enhancing the light harvesting efficiency the co-sensitizer can reduce the aggregation of partner dye on the TiO_2 surface was studied.[45] Further, complementary light absorbing dyes with the combination of D-π-A and D-A-π-A dyes exhibited the device efficiencies of 8.7-12.8%.[46-48] Squaraine dyes have been used a NIR light absorbing component along with Ru based sensitizer[28,49], D-π-A[50,51] to provide the panchromatic photovoltaic response. NIR-light absorbing phthalocyanines dyes has been co-sensitized with JK2 to afford the device performance of 7.7%.[51,52] Tuning the band-gap of dyes with extending the conjugation is an attractive approach, as it provides the complementary dyes in the similar family of sensitizers. Pair of cyanine and D-π-A dyes with complementary absorption properties provided the device performance of 3.4%[29] and 7.3 %[53], respectively.

Recently concerted complementary dye concept has been introduced, where the dye pair has been covalently connected to have a specific control over anchoring of dyes on the surfaces.[54] It is preferable to have the complementary dyes with high extinction coefficient, and there is a mismatch in one of the dyes in most of the explored dye combinations. Squaraine, a D-A-D type dye belongs to polymethine dyes; possess a sharp absorption with high extinction coefficient in the far-red to NIR regions.[12] Besides this electronic property, these dyes self-assemble in solution

as well as in solid state to have H- and J-aggregates due to the strong dye-dye interactions.[14,55,56] Such assembled structures have been utilized in the sensor,[57,58] xerography[59] and organic solar cells.[60,61] In DSSC, such facile formation of aggregate on the TiO_2 surface plays a detrimental factor for the device performance.[14,62] We have circumvented the problem by introducing in-plane and out-of-plane alkyl groups to a series of unsymmetrical squaraine dyes and showed that controlling the aggregation of dyes synergistically boost both J_{SC} and V_{OC}.[17] Yet another property of this class dye is that the effect of extending the conjugation leads ~105 nm[63] shift in the absorption spectrum, which is merely 15-20 nm in the case of D-π-A, and D-A-π-A dye architectures (**Figure 1c**).[64,65]
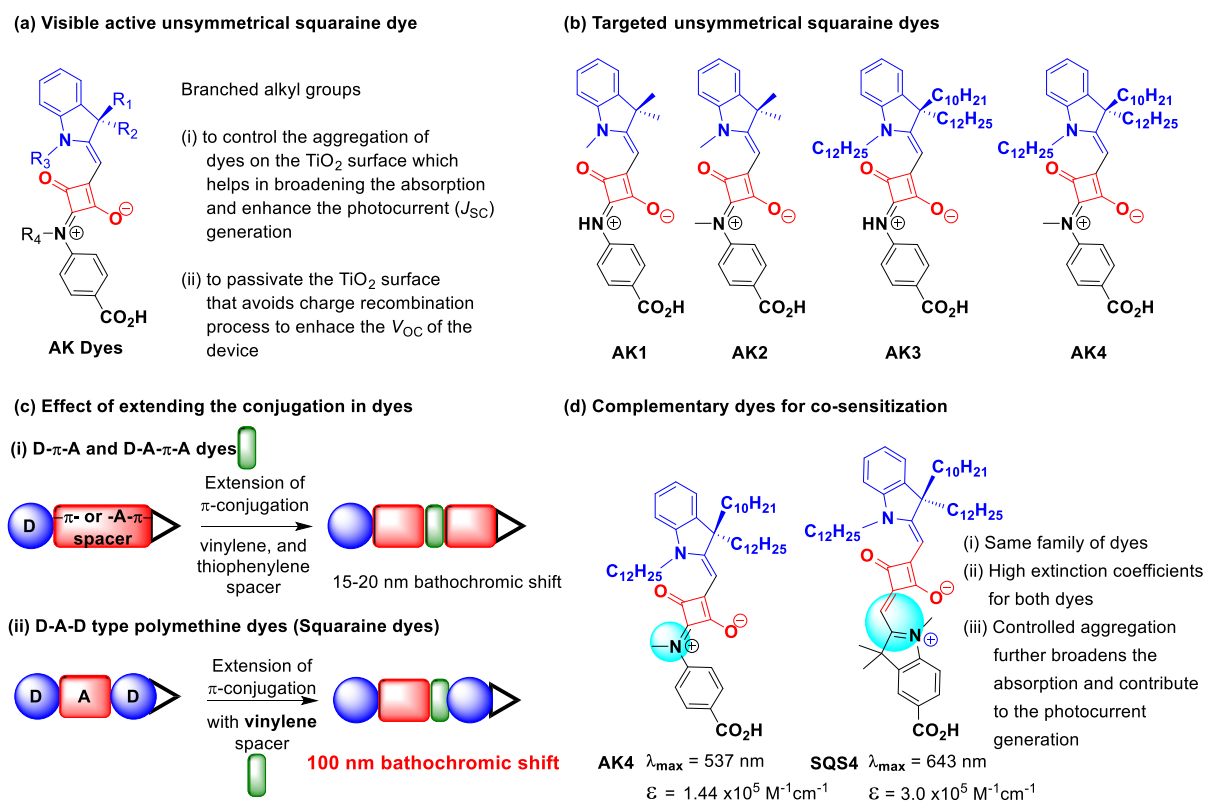
Figure 1. (a) General structure of visible active unsymmetrical squaraine dyes, (b) targeted unsymmetrical squaraine dyes with alkyl groups, (c) effect on the absorption spectrum by extension of conjugation for the sensitizers employed in DSSC, and (d) complementary squaraine dyes for co-sensitized dye-sensitized solar cells.

Hence complementary dyes for the co-sensitization purpose can be chosen from same family of D-A-D dyes with high extinction coefficients. Further, employing complementary dyes from the

same family of chromophores helps to identify the factors that can be modulated to boost the panchromatic absorption, shifting the conduction band position upon anchoring the dyes, V_{OC} and J_{SC} of the device. In the present work, a series of indoline and aniline donors based visible active unsymmetrical squaraine dyes is designed and synthesized (**Figure 1a**). Further, structural optimization for the better DSSC device performance is carried out by introducing in-plane and out-of plane alkyl groups at the N- and sp^3-C atoms of the indoline units and N-methylation at the aniline donor (**Figure 1b**). Regarding the far-red absorbing squaraine dye, we have showed the importance of aggregation of SQ1, and SQS4 dyes for broadening absorption profile which also helps to enhance the photocurrent generation. Co-sensitization of visible active AK dyes with vinylene moiety extended unsymmetrical squaraine dyes, SQ1 and SQS4, to cover the far-red region is explored to achieve the panchromatic IPCE response (**Figure 1d**).

4.2 EXPERIMENTAL SECTION

4.2.1 General methods

Chemicals and reagents required for the synthesis of AK dyes were purchased from commercial sources, and standard procedures are used for drying PhMe. ^{1}H and ^{13}C NMR were recorded on Bruker NMR spectrometers AV 400 MHz frequency, in CDCl$_3$, DMSO-d_6. High-resolution mass spectrometric (HRMS) measurements were recorded on SYNAPT G2 HDM in MeOH as a solvent. Bruker FTIR spectrometer has been used to measure the IR-spectrum of all the AK dyes. Absorption spectra of AK dyes were recorded on SPECORD$^®$ 210/ PLUS, Analytikjena UV−visible spectrophotometer at room temperature. Emissions of AK dyes were recorded on Edinburgh spectrofluorometer FS5 at room temperature. For the light-harvesting efficiency (LHE) calculation, 6 µm thin film of TiO$_2$ coated on the transparent glass slide was dipped in 0.1 mM (AK) and 0.2 mM (AK: SQ, 0.1: 0.1 mM each) dye solution for 12 h at room temperature, and absorbance spectra were recorded on SPECORD$^®$ 210/ PLUS, Analytikjena UV−visible spectrophotometer at room temperature and converted in light-harvesting efficiency (LHE = 1-10^{-A}). Differential pulse voltammetric (DPV) and cyclic voltammetric (CV) studies of AK3 and AK4 dyes were performed on BioLogic SP300 potentiostat in anhydrous CH$_2$Cl$_2$ solvent, whereas, for AK1 and AK2 dyes a mixture of 95% of CH$_2$Cl$_2$ and 5% of DMSO solvent were

used, at 25 ^{o}C under an inert atmosphere, where platinum wire as a working electrode, platinum foil as a counter electrode, non-aqueous Ag/Ag$^+$ (0.01M) as a reference electrode, TBAClO$_4$ (0.05 M) as supporting electrolyte, and Ferrocene/Ferrocene$^+$ as the internal-standard, scan rate of 100 and 50 mV s^{-1} for DPV and CV, respectively. Electrochemical impedance measurements (EIS) were performed using a BioLogic SP300 potentiostat equipped with a frequency response analyzer. EIS studies were carried out in dark with various applied potential and frequency ranges from 3 MHz to 10 mHz with sinus amplitude of 10 mV. *I-V* characteristics of the cells were measured by using PHOTO EMISSION TECH (PET, CT200AAA, USA) solar-simulator, and IPCE measurements were carried out with a Newport QE measurement kit. All the quantum mechanical calculations were conducted by using the Gaussian 09 software.[1] The optimization of the ground-state geometry was carried out at the Density Functional Theory (DFT) level, using the B3LYP hybrid functional and the 6-311G(++) atomic basis set. EZ-Melt automated melting point apparatus used for the melting point measurement of all solid compounds. AK dyes are not stable in basic as well as acidic medium; hence the condition to find out the dye loading by other method is under progress.

4.2.2 Dye-sensitized solar cell fabrication. Fluorine-doped SnO$_2$ glass (8- 10 Ω /sq; Pilkington TEC 7) was washed with mucasol (2 % in water), de-ionized water, and isopropanol by using ultrasonic-bath to make cleaned. To grow a thin film TiO$_2$, FTO was treated with 40 mM aqueous TiCl$_4$ solution at 70 ^{o}C for 30 min, washed with the de-ionized water then EtOH, and dried at 110 ^{o}C for 10 min. A paste of TiO$_2$ nanocrystal (< 20 nm, Ti-Nanoxide T/SP, Solaronix) was coated on FTO conducting side by using doctor-blade technique and kept for 15 min in the air then heated at 120 °C in the air for 20 min, then coated with scattering layer TiO$_2$ paste (WER2-O, Dyesol) and heated at 120 °C for 10 min in the air, then sintered at 325 °C for 10 min, 375 °C for 10 min, 450 °C for 10 min and 500 °C for 15 min where the heating rate was 5 °C per min in the air. After completion of sintering, films were treated with 40 mM aqueous TiCl$_4$ solution at 70 ^{o}C for 30 min, washed with the de-ionized water then with EtOH and sintered at 500 °C for 20 min. Then immersed the cells (area of TiO$_2$ is 0.23 cm^2) in 0.1 mM or 0.2 mM dye solution of AK or AK: SQ (0.1mM each) for 12 h. Electroplatinised platinum foil used as a cathode, iodolyte Z-50 (Solaronix) was used as electrolyte, 25 μm spacer, and area of

black mask was 0.23 cm^2. The device performance of AK and co-sensitized dyes were measured under standard simulator condition (AM 1.5 G, 100 mW/cm^2).

4.2.3 Synthesis.
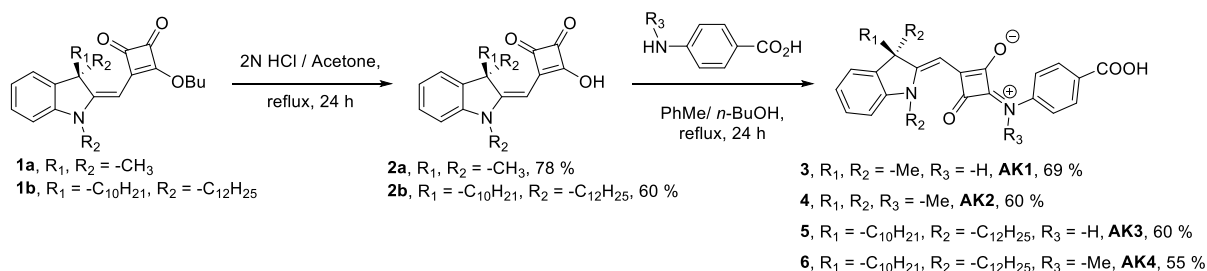
Scheme 1. Synthesis of visible active unsymmetrical squaraine dyes AK1-AK4.

Required precursors for the synthesis of AK dyes; **1a**[66], **1b**[17], **SQS4**[17] and **SQ1**[16] were synthesized by the following the procedure present in the literature, and 4-Aminobenzoic acid, 4-(Methylamino)benzoic acid are commercially available compounds.

(a) Synthesis of semisquaraine

3-hydroxy-4-((1,3,3-trimethylindolin-2-ylidene)methyl)cyclobut-3-ene-1,2-dione (2a): 3-Butoxy-4-((1,3,3-trimethylindolin-2-ylidene)methyl)cyclobut-3-ene-1,2-dione **1a** (2 g, 6.15 mmol) were dissolved in 30 mL of acetone in a single neck round bottom flask followed by the addition of 2 N aqueous HCl 6 mL, resultant mixture were refluxed for 12h. Solvents were removed under reduce pressure, washed with 30 mL of hexane and dried at high vacuum pressure pump. Yield: 1.3 g, 78.5 %. Mp: 223 ^{o}C. ^{1}H NMR (400 MHz, DMSO-d_6): δ 1.55 (s, 6 H) 3.35 (s, 3 H) 5.51 (s, 1 H) 7.02 (t, J=7.38 Hz, 1 H) 7.12 (d, J=7.75 Hz, 1 H) 7.26 (t, J=7.44 Hz, 1 H) 7.39 (d, J=7.25 Hz, 1 H); ^{13}C NMR (101 MHz, DMSO-d_6): δ 26.66, 29.68, 46.90, 81.59, 108.55, 121.82, 121.91, 127.71, 140.14, 143.18, 166.86, 173.76, 190.20, 191.80.

3-((3-decyl-1,3-didodecylindolin-2-ylidene)methyl)-4-hydroxycyclobut-3-ene-1,2-dione (2b): 3-butoxy-4-((3-decyl-1,3-didodecylindolin-2-ylidene)methyl)cyclobut-3-ene-1,2-dione **1b** (2 g, 2.63 mmol) were dissolved in 30 mL of acetone in a single neck round bottom flask followed by the addition of 4 N aqueous HCl (6 mL), resultant mixture were refluxed for 24h. Solvents were removed under reduce pressure, and reaction mixture were purified by column chromatography

(SiO$_2$, 100-200 mesh, 3-5 % MeOH and 97-95 % CH$_2$Cl$_2$) to afford the required compound as semi-solid. Yield: 1.1 g, 59.5 %. ^{1}H NMR (400 MHz, CDCl$_3$): δ 0.48 (br. s., 2 H) 0.81 - 0.87 (m, 11 H) 1.03 (br. s., 10 H) 1.13 - 1.25 (m, 38 H) 1.37 (br. s., 2 H) 1.68 - 1.78 (m, 2 H) 1.83 - 1.95 (m, 2 H) 2.70 (t, J=10.76 Hz, 2 H) 3.84 (br. s., 2 H) 5.78 (br. s., 1 H) 6.81 (d, J=7.79 Hz, 1 H) 7.03 (t, J=7.33 Hz, 1 H) 7.18 - 7.26 (m, 2 H); ^{13}C NMR (101 MHz, CDCl$_3$): δ 14.18, 22.77, 24.20, 27.42, 29.40, 29.45, 29.57, 29.73, 32.00, 40.10, 43.01, 57.15, 83.90, 107.76, 122.12, 127.41, 137.85, 145.00, 164.94, 167.42, 175.61, 178.20, 191.38.

(b) Synthesis of unsymmetrical squaraine

General synthetic procedure of AK dyes: The compound **2** (1 equiv.) and 4-Aminobenzoic acid/ 4-(Methylamino)benzoic acid (1 equiv.) were dissolved in anhydrous PhMe and n-BuOH (1:1, 10 mL of each) in a round bottom flask and refluxed in the Dean-Stark apparatus for 24 h under an inert atmosphere. The reaction mixture was purified by column chromatography (SiO$_2$, 100-200 mesh, MeOH and CH$_2$Cl$_2$) to afford the required dye.

4-((4-carboxyphenyl)iminio)-3-oxo-2-((-1,3,3-trimethylindolin-2-ylidene)methyl)cyclobut-1-en-1-olate (3, AK1): Compound **2a** (0.5 g, 1.858 mmol) and 4-Aminobenzoic acid (0.255 g, 1.858 mmol), red colour solid were filtered and dried at high vacuum pressure pump. Yield: 0.5 g, 69.3 %. Mp: more than 300 °C. ^{1}H NMR (400 MHz, DMSO-d_6): δ 1.68 (s, 6 H) 3.59 (s, 3 H) 5.77 (s, 1 H) 7.19 (m, 1 H) 7.33 - 7.45 (m, 2 H) 7.54 (d, J=7.63 Hz, 1 H) 7.83 - 8.06 (m, 4 H); ^{13}C NMR (101 MHz, DMSO-d_6): δ 26.53, 30.73, 48.83, 85.96, 110.57, 119.31, 122.23, 124.01, 125.85, 128.01, 130.72, 141.34, 142.13, 142.66, 166.88, 171.47, 175.62, 181.82; IR (cm^{-1}): 2977, 2890, 1741, 1657, 1591, 1535, 1462, 1385, 1298, 1258, 1233, 1154, 1073, 958; HRMS (m/z): [M - H]$^+$ calculated for C$_{23}$H$_{19}$O$_4$N$_2$: 387.1339; found: 387.1350.

4-((4-carboxyphenyl)(methyl)iminio)-3-oxo-2-((-1,3,3-trimethylindolin-2-ylidene)methyl)cyclobut-1-en-1-olate (4, AK2): Compound **2a** (0.2 g, 0.743 mmol) and 4-(Methylamino)benzoic acid (0.112 g, 0.743 mmol), column chromatography (SiO$_2$, 100-200 mesh, 5 % MeOH and 95 % CH$_2$Cl$_2$). Yield: 0.180 g, 60.2 %. Mp: 297 °C. ^{1}H NMR (400 MHz, DMSO- d_6): δ 1.64 (s, 6 H) 3.54 (s, 3 H) 3.94 (s, 3 H) 5.70 (s, 1 H) 7.12 - 7.19 (m, 1 H) 7.30 - 7.38 (m, 2 H) 7.51 (d, J=7.63 Hz, 1 H) 7.55 - 7.62 (m, 2 H) 7.91 - 8.02 (m, 2 H); 13C NMR (101

MHz, DMSO- d_6): δ 26.91, 29.38, 29.73, 46.97, 48.77, 81.89, 108.51, 110.71, 116.88, 121.90, 121.97, 127.88, 131.31, 140.26, 143.44, 153.58, 166.26, 167.79, 174.51, 192.40; IR (cm⁻¹): 2980, 2889, 1745, 1680, 1592,1565, 1503, 1473, 1461, 1454, 1383, 1348, 1262, 1240, 1184, 1151, 1074, 1055, 1012, 966, 954; HRMS (*m/z*): [M - H]⁺ calculated for $C_{24}H_{21}O_4N_2$: 401.1496; found: 401.1508.

4-((4-carboxyphenyl)iminio)-2-(((S)-3-decyl-1,3-didodecylindolin-2-ylidene)methyl)-3-oxocyclobut-1-en-1-olate (5, AK3): Compound **2b** (0.3 g, 0.426 mmol) and 4-Aminobenzoic acid (0.058 g, 0.426 mmol), column chromatography (SiO₂, 100-200 mesh, 2.5 % MeOH and 97.5 % CH₂Cl₂). Yield: 0.21 g, 60 %. Mp: 108 °C. ¹H NMR (400 MHz, CDCl₃): δ 0.52 (br. s., 2 H) 0.82 (m, 8 H) 0.88 (t, *J*=6.87 Hz, 3 H) 1.09-1.15(m, 30 H) 1.23 - 1.32 (m, 16 H) 1.37 (br. s., 2 H) 1.44 (m, 2 H) 1.75 - 1.89 (m, 2 H) 1.97 - 2.15 (m, 2 H) 2.96 (br. s., 2 H) 4.03 (br. s., 2 H) 6.05 (br. s., 1 H) 7.03 (d, *J*=7.63 Hz, 1 H) 7.19 - 7.25 (m, 1 H) 7.29 - 7.42 (m, 2 H) 8.11 - 8.39 (m, 4 H); ¹³C NMR (101 MHz, CDCl₃): δ 14.05, 14.08, 22.61, 22.63, 22.67, 23.89, 27.22, 29.17, 29.28, 29.30, 29.33, 29.40, 29.52, 29.57, 29.61, 31.84, 31.87, 40.02, 43.87, 58.93, 86.79, 109.44, 119.48, 122.36, 124.27, 125.64, 127.81, 132.00, 138.94, 142.74, 143.92, 170.32, 170.54, 172.67, 178.30; IR (cm⁻¹): 2955, 2921, 2852, 1765, 1665, 1639, 1595, 1532, 1480, 1466, 1415, 1357, 1300, 1273, 1247, 1182, 1154, 1104, 1084, 1021, 965, 955; HRMS (*m/z*): [M - H]⁺ calculated for $C_{54}H_{81}O_4N_2$: 821.6191; found: 821.6194.

4-((4-carboxyphenyl)(methyl)iminio)-2-(((S)-3-decyl-1,3-didodecylindolin-2-ylidene)methyl)-3-oxocyclobut-1-en-1-olate (6, AK4): Compound **2b** (0.2 g, 0.284 mmol) and 4-(Methylamino)benzoic acid (0.043 g, 0.284 mmol), column chromatography (SiO₂, 100-200 mesh, 3 % MeOH and 97 % CH₂Cl₂). Yield: 0.130 g, 54.7 %. Mp: 110 °C. ¹H NMR (400 MHz, CDCl₃): δ 0.47 (br. s., 2 H) 0.74 (br. s., 2 H) 0.86 (m, 9 H) 1.07 - 1.22 (m, 30 H) 1.25 (s, 16 H) 1.31 - 1.36 (m, 2 H) 1.38 - 1.46 (m, 2 H) 1.77 (m, 2 H) 1.90 - 2.03 (m, 2 H) 2.92 (m, 2 H) 3.94 - 4.06 (m, 5 H) 6.03 (br. s., 1 H) 7.00 (d, *J*=7.63 Hz, 1 H) 7.14 - 7.22 (m, 1 H) 7.28 - 7.36 (m, 2 H) 7.45 (d, *J*=8.39 Hz, 2 H) 8.08 (d, *J*=8.39 Hz, 2 H); ¹³C NMR (101 MHz, CDCl₃): δ 14.06, 22.59, 22.63, 23.97, 27.16, 29.24, 29.28, 29.39, 29.42, 29.47, 29.53, 29.59, 29.64, 31.83, 31.86, 38.03, 40.05, 43.74, 58.73, 86.69, 109.28, 111.03, 117.09, 121.51, 122.25, 123.96, 127.69, 131.04, 132.25, 138.78, 144.01, 144.65, 153.47, 169.12, 169.95, 171.82, 174.60, 181.64; IR (cm⁻¹): 2954,

2921, 2852, 1758, 1705, 1688, 1601, 1562, 1492, 1479, 1443, 1398, 1354, 1296, 1254, 1176, 1148, 1103, 1049, 1015, 965, 955; HRMS (*m/z*): [M - H]$^+$ calculated for $C_{55}H_{83}O_4N_2$: 835.6347; found: 835.6349.

4.3 RESULTS AND DISCUSSION

4.3.1 Synthesis of visible active unsymmetrical squaraine dyes. Synthesis of unsymmetrical squaraine dyes require semi-squaraine or semi-squaric acid intermediate with one of the donors which is then condensed with the second donor.[17] We have adopted the semi-squaric acid route for better reaction yields. The semi-squaraine derivatives **1a** and **1b** have been synthesized by following a literature known method and then treated with 2N HCl in acetone for 24 h to provide the corresponding semi-squaric acids **2a** and **2b**. Further condensing the semi-squaric acid derivatives with 4-aminobenzoic acid and 4-(methylamino)benzoic acid afforded the AK series of dyes AK1-4 (**Scheme 1**) in moderate yields.

4.3.2 Photophysical and electrochemical properties. The UV-vis spectra of AK1-AK4 dyes in CH_2Cl_2 showed intense peak between 529-541 nm with the extinction coefficients of 1.44-1.84×10^5 M^{-1}cm^{-1} (**Figure 2, Table 1**). Introducing alkyl groups at the *sp³*-C and N-atoms of indoline unit bathochromically shift the λ_{max} by 6 nm (AK1 *vs* AK3), whereas introducing N-methyl group at the arylamine donor unit shifts 6 nm hypsochromically (AK1 *vs* AK2). It is known that solvent-solute interaction is the main reason for the observation of the red shifted transitions,[17] and N-methylation around squaric acid might distort the planarity to observe the blue shifted transitions. Hence the λ_{max} observed for AK4 as a net result of hypochromic shift due to N-methyl group which distort the planarity of the molecule and bathochromic shift due to the solvent solute interaction. Further introducing N-methyl group at the arylamine donor unit broadens the UV-vis spectra of AK2 and AK4 compared to AK1 and AK3. Fluorescence emission between 546-571 nm with the Stokes's shift of 9-11 nm for the AK3, AK1 and 34-38 nm for AK4 and AK2 dyes, respectively upon exciting at 500 nm. Hence the effect of N-methylation at the arylamine donor leads to larger Stoke's shift indicates the change in dipole moment for AK2 and AK4 dyes in the excited state. To understand the aggregation of AK dyes on TiO$_2$, dipping the TiO$_2$ electrode (thickness 6μm) in AK dye solutions for a short time, 10

min, is carried out. All the AK dyes showed blue shifted peaks due to the formation of H-aggregate as wells as deprotonation of carboxylic acid upon adsorption on TiO_2 surface.[67] AK1 dye showed peaks at 523 nm, 488 nm, and 457 nm which can be assigned to monomer, dimer and aggregated dyes, respectively. In the case of AK2 dye, the peak was broad and blue shifted 38 nm on TiO_2. Further, AK3 and AK4 dyes showed 6 and 10 nm blue shifted peaks compared to the spectrum in solution with dimer peak at 506 nm for AK3. Hence introducing alkyl groups at the sp^3-C and N- atoms of indoline unit controls the aggregation of dyes on the surface (**Figure 2b**). The light harvesting property of AK1-4 dyes on TiO_2 electrode are good between 420-600 nm, introduction of alkyl groups leads to narrow down the LHE response for the AK3 and AK4 dyes due to the reduced aggregation of dyes on the TiO_2 surface (**Figure 2c**).
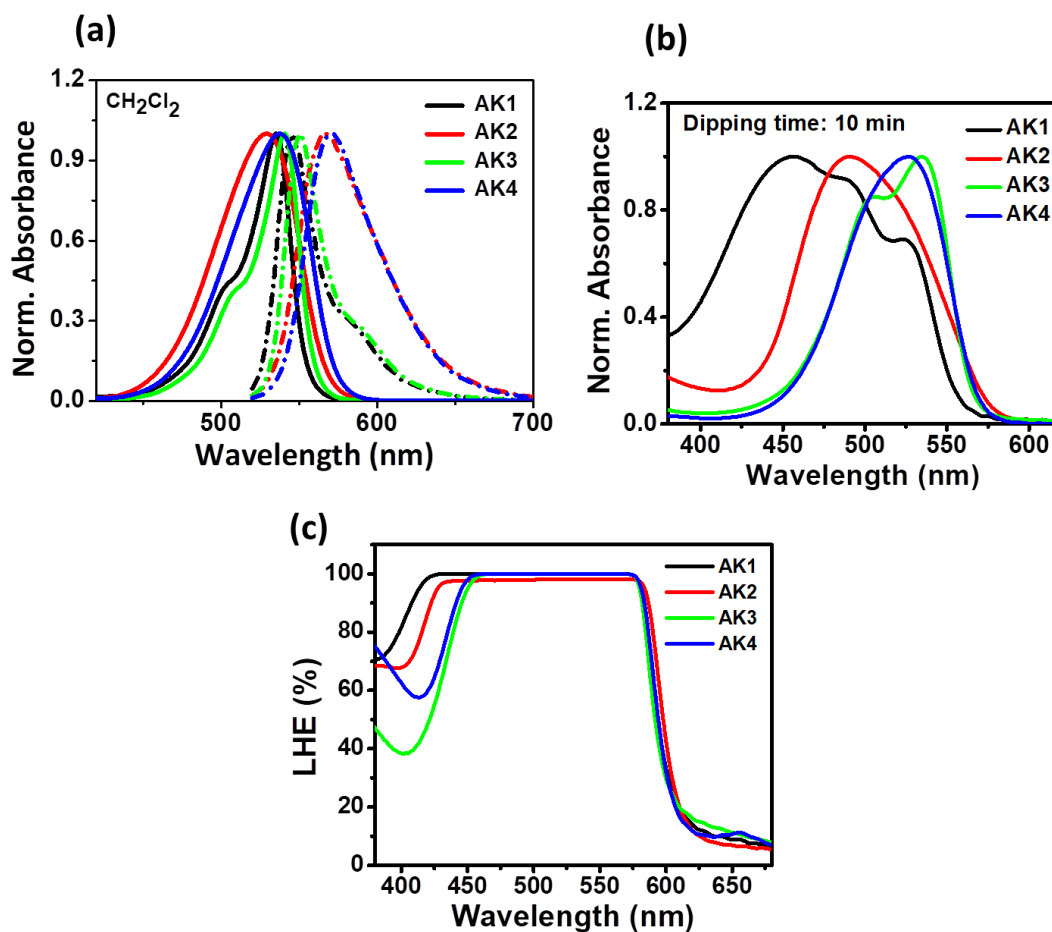
Figure 2. (a) Normalized UV-vis (solid) and fluorescence (dotted) spectra of AK dyes in CH_2Cl_2 solution, (b) UV-vis spectra of AK dyes on TiO_2 (thickness of the TiO_2 electrode 6 μm, dipping

time 10 min) and (c) LHE (=1–10^{-A}) profiles of AK dyes on TiO$_2$ electrodes (thickness 6 μm, dipping time 12 h).

To evaluate the charge injection and dye regeneration properties of the AK1-4 dyes, differential pulse voltammetry experiment was carried out (**Figure 3a**), and cyclic voltammograms with and without ferrocene/ ferrocene^{+} (**Figure 4**). Further it is better to have sufficient potentials for driving both charge injection (300 mV), and dye regeneration (500 mV) processes.[68] From the first oxidation potential of the AK1-4 dyes, the HOMO energy level is calculated. The LUMO energy level is calculated by incorporating the optical band gap which is obtained by both absorption and emission spectroscopy. The HOMO and LUMO energy levels for the dyes is found to be in the range of 0.94 – 1.12 eV (*vs* NHE) and -1.35 – -1.15 eV (*vs* NHE), respectively (**Figure 3, Table 1**). Hence all the dyes, AK1-4, are potential sensitizer for fabricating the DSSC device by using TiO$_2$ as a photoanode and I$^-$/I$_3^-$ as an electrolyte, as the availability of sufficient over potentials for charge injection (energy difference between LUMO of the dye and conduction band of TiO$_2$, more than 0.65 V), and dye regeneration processes (energy difference between HOMO of the dye and redox function of the electrolyte, more than 0.54 V).
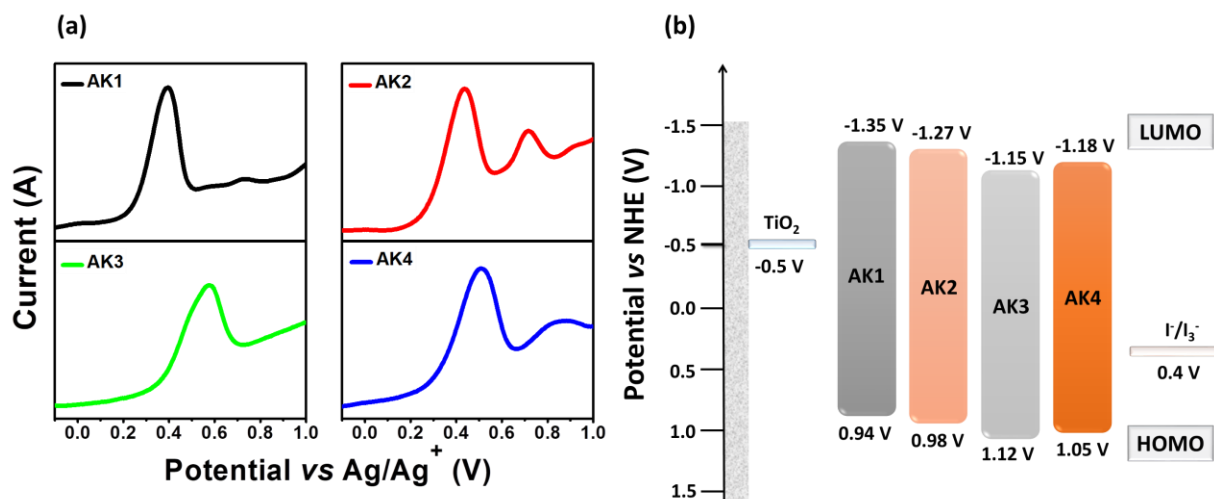
Figure 3. (a) Differential pulse voltammograms of AK1-4 dyes in CH$_2$Cl$_2$, and (b) energy level diagram of HOMO and LUMO of the AK1-4 dyes with the conduction band of TiO$_2$ and the redox function of I$^-$/I$_3^-$ electrolyte.

Table 1. Photophysical and electrochemical properties of AK1-4 dyes at room temperature.

Dyes	$^a\lambda_{max}$ (nm)	$^b\lambda_{max}$ (nm)	$^c\lambda_{max}$ (nm) on TiO$_2$	ε (M^{-1} cm^{-1})	LHE $\Delta\lambda$ at 80%(nm)	$^dE_{oxi}$ (V vs Ag/Ag$^+$)	E_{HOMO} (V vs NHE)	E_{LUMO} (V vs NHE)	^dE_g (eV)
AK1	535	546	457, 488, 523	1.80×10^5	186	0.395	0.94	-1.35	2.29
AK2	529	567	491	1.84×10^5	175	0.439	0.98	-1.27	2.25
AK3	541	550	506, 535	1.63×10^5	145	0.577	1.12	-1.15	2.27
AK4	537	571	537	1.44×10^5	151	0.507	1.05	-1.18	2.23

^{a}absorption, ^{b}emission of AK1-4 dyes in dichloromethane, ^{c}on TiO$_2$, thickness 6 µm, dipping time 10 min ^{d}oxidation potential, ^eE_g optical band gap (from the intersection point of absorption and fluorescence, 1240/λ).
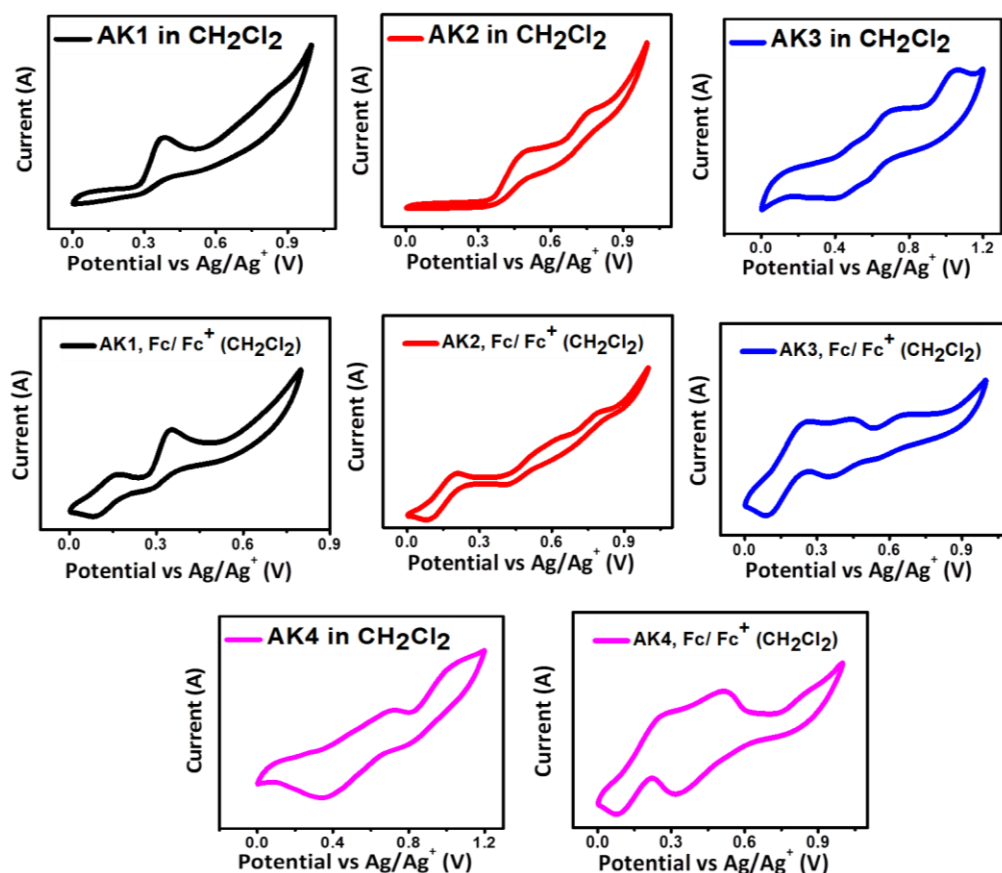
Figure 4. Cyclic voltammograms of AK dyes with and without Ferrocene/Ferrocene$^+$.

4.3.3 Theoretical studies. DFT calculation was performed at B3LYP, 6-311G (++) level[69] for the AK1 and AK2 dyes and the electronic distribution in HOMO-1, HOMO, LUMO and LUMO+1 states are provided in **Figure 5**. The electron distribution is almost uniform in the π-framework of both the dyes, and exclusively concentrated on the squaric acid unit in HOMO-1. Significant electron distribution is noted on the carboxylic acid unit in LUMO, due to the arylamine donor unit. Further the LUMO+1 possess the electronic distribution mostly on the anchoring carboxylic acid unit. The dihedral angles for the arylamine donor coupled with squaric acid unit side are 0° and 34.5° for AK1 and AK2, respectively (**Figure 6**).
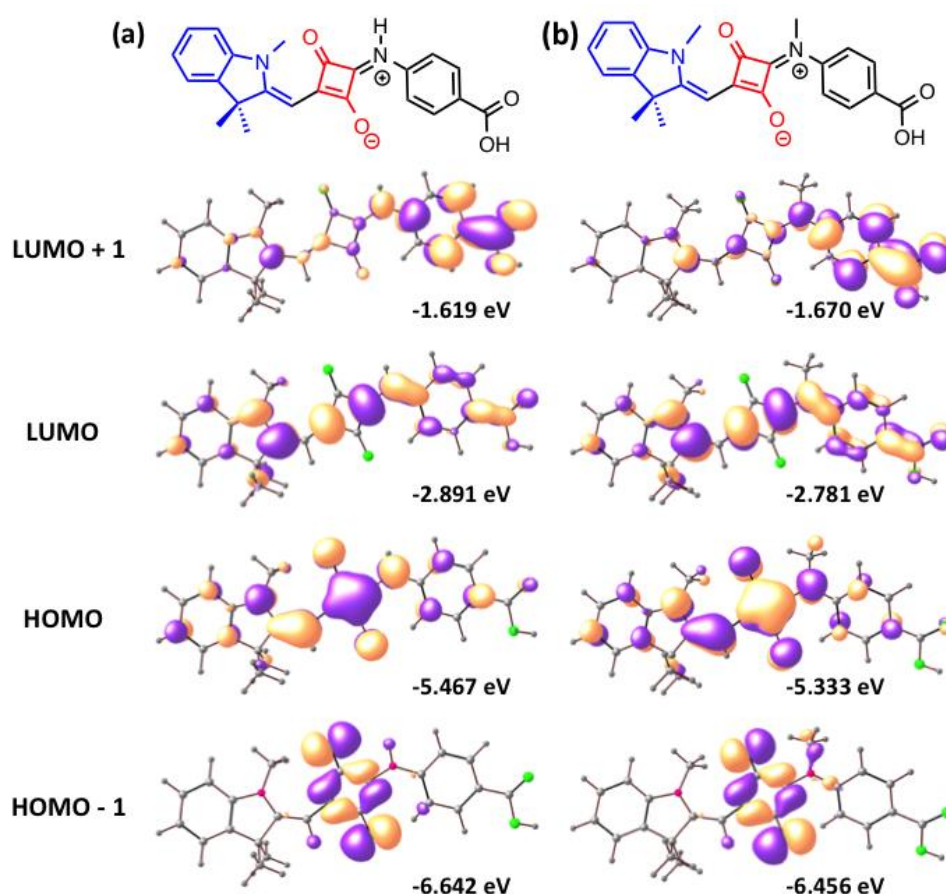
Figure 5. Frontier molecular orbital diagram for AK1 and AK2 (Isosurface value = 0.03).

The dihedral angle is the indicative of the planarity of the dyes, and AK1 is very planar and AK2 is not a planar molecule which might be the reason for the 6 nm blue shift for the dye AK2. The total calculated dipole moment for the dyes AK1 (7.662 D) and AK2 (6.235 D) are significantly varied blue to the N-methylation of arylamine donor unit (**Table 2**).
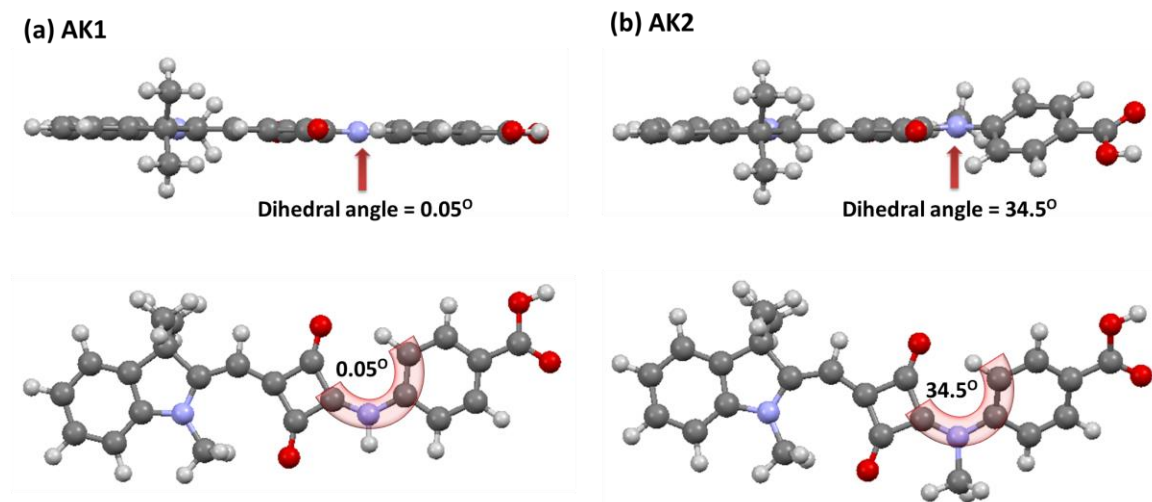
Figure 6. Optimized structure of AK1 and AK2 and the dihedral angle at the site of aniline based donor and squaric acid unit.

Table 2. DFT optimized band gap (HOMO-LUMO), dipole moments and dihedral angle of AK1 and AK2 dyes.

Dyes	Band gap (eV)	Dipole moment (Debye)	Dihedral Angle (Degree)
AK1	2.57	7.662	0.05
AK2	2.55	6.235	34.50

4.3.4 Photovoltaic performance. The result on the photovoltaic performances by fabricating the DSSC devices is provided in **Figure 7** (**Table 3**). DSSC device efficiencies of 2.52%, 4.38%, 1.73% and 7.93% were obtained for AK1, AK2, AK3 and AK4 dyes without co-adsorbing with CDCA. Further the device performances were increased to 2.49%, 5.50%, and 2.59%, respectively for AK1, AK2 and AK3 dyes in the presence of 2 equivalents of CDCA, whereas the device performance is decreased to 6.94% for AK4 in the presence of CDCA. The effect of N-methylation at the aniline donor unit and alkyl groups at the sp^3-C, N-atoms of indoline have profound effect on the V_{OC} of the devices. N-methylation at the arylamine donor unit improved the V_{OC} about 70 mV for AK2 (compared to AK1), and alkyl groups at the indoline units

improved the V_{OC} about 60 mV for AK3 (compared to AK1). However, in the case of AK4, appending alkyl groups at the indoline unit and N-methyl group at the aniline donor unit increased the V_{OC} about 185 mV, compared to AK1. It is the highest V_{OC} (815.88 mV) for the zwitterionic dye with the I^-/I_3^- electrolyte. Along with V_{OC}, J_{SC} also synergistically improved by appending the alkyl groups. The IPCE profile for all the AK dyes showed the maximum response at ~475-490 nm, and it is corresponding to the H-aggregates of the respective dyes. Further co-adsorbing the dye with CDCA (2 equivalents) has improved the IPCE response without changing the shape of the profile, which indicates that the better dye-dye interaction on the surface. It is understood from the DFT, and UV-vis studies that appending N-methyl group in AK2 make non planarity around the π-framework of squaraine unit which may help reducing he charge recombination pathways.
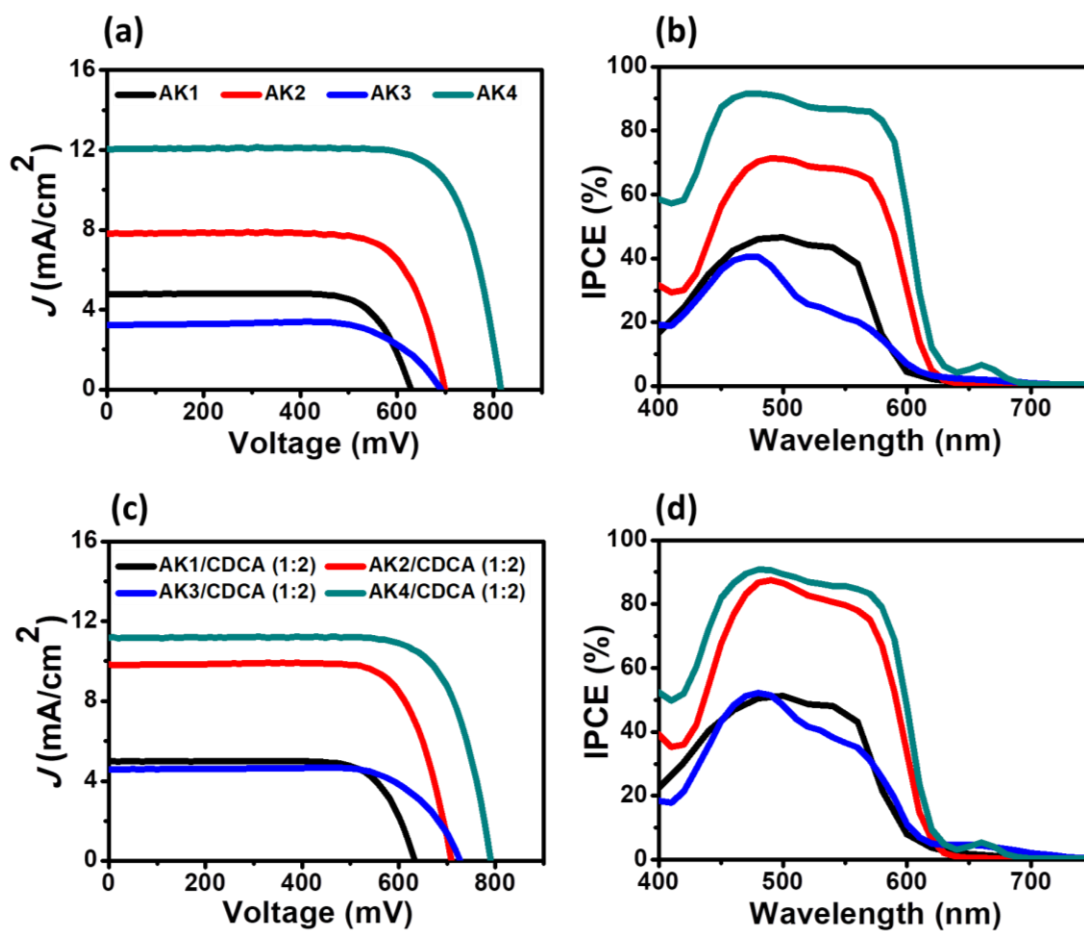
Figure 7. (a and c) *I-V* curves for AK1-AK4 dyes without and with CDCA, (b and d) IPCE curves for AK1-AK4 dyes without and with CDCA.

Table 3. Photovoltaic parameters for the DSSC devices sensitized with AK dyes in the presence and absence of CDCA (active area and black mask size was 0.23 cm^2).

Dyes	CDCA	V_{OC} (mV)	J_{SC} (mA/cm^2)	ff (%)	η (%)
AK1[a]	0	629.16 ± 1.09	4.78 ± 0.47	76 ± 0.29	2.28 ± 0.24
AK1[a]	2	633.86 ± 1.28	4.99 ± 0.17	75 ± 0.25	2.37 ± 0.12
AK2[a]	0	699.12 ± 1.22	7.80 ± 0.44	75 ± 0.87	4.09 ± 0.29
AK2[a]	2	708.92 ± 2.26	9.82 ± 0.27	76 ± 0.73	5.29 ± 0.21
AK3[b]	0	690.63 ± 1.39	3.23 ± 0.16	73 ± 0.95	1.63 ± 0.10
AK3[b]	2	727.88 ± 2.61	4.59 ± 0.31	72 ± 0.52	2.40 ± 0.19
AK4[c]	0	814.60 ± 1.28	12.05 ± 0.35	78 ± 0.37	7.65 ± 0.28
AK4[c]	2	790.91 ± 1.87	11.16 ± 0.28	76 ± 0.61	6.70 ± 0.24

[a]CH_3CN: DMSO (95: 5), [b]CH_3CN: $CHCl_3$ (85: 15), [c]CH_3CN: $CHCl_3$ (95: 5)

4.3.5 Electrochemical impedance spectroscopy (EIS). To understand the obtained V_{OC} resulted from avoided charge recombination process, systematic EIS studies in dark conditions with various applied bias is carried out (**Figure 8**).[70] From the Nyquist plot (**Figure 8**, and **10a**), the charge transfer (R_{ct}), chemical capacitance ($C\mu$), and electron lifetime (τ) were calculated (**Figure 9**, and **10**) for electrolyte/Pt electrode interface, dye-TiO$_2$/electrolyte interfaces. The R_{ct} decreases in the order AK4 (12.57 ohm) >AK2 (7.62 ohm) >AK3 (6.23 ohm) >AK1 (5.68 ohm) (**Table 4**). The high R_{ct} value for AK4 indicates that the recombination of electrons in the TiO$_2$ with the oxidized electrolyte is inhibited compared to other dyes. It is possible that the dye AK4 passivates the TiO$_2$ surface better than the other three dyes to avoid the interaction between electrolyte and TiO$_2$ surface. Further fitted capacitive curve, indicates the position of conduction band position can be modulated by anchoring of dye, which could exert the dipole moment either

towards or away from the TiO_2 surface that helps enhancing the V_{OC} of the devices. The chemical capacitance is also decreased in the order of AK4>AK2>AK3>AK1 (**Table 4**). Furthermore, the electron lifetime for AK4 dye is higher than other three dyes (**Table 4**), which could be reason for the high V_{OC} obtained for AK4 device.
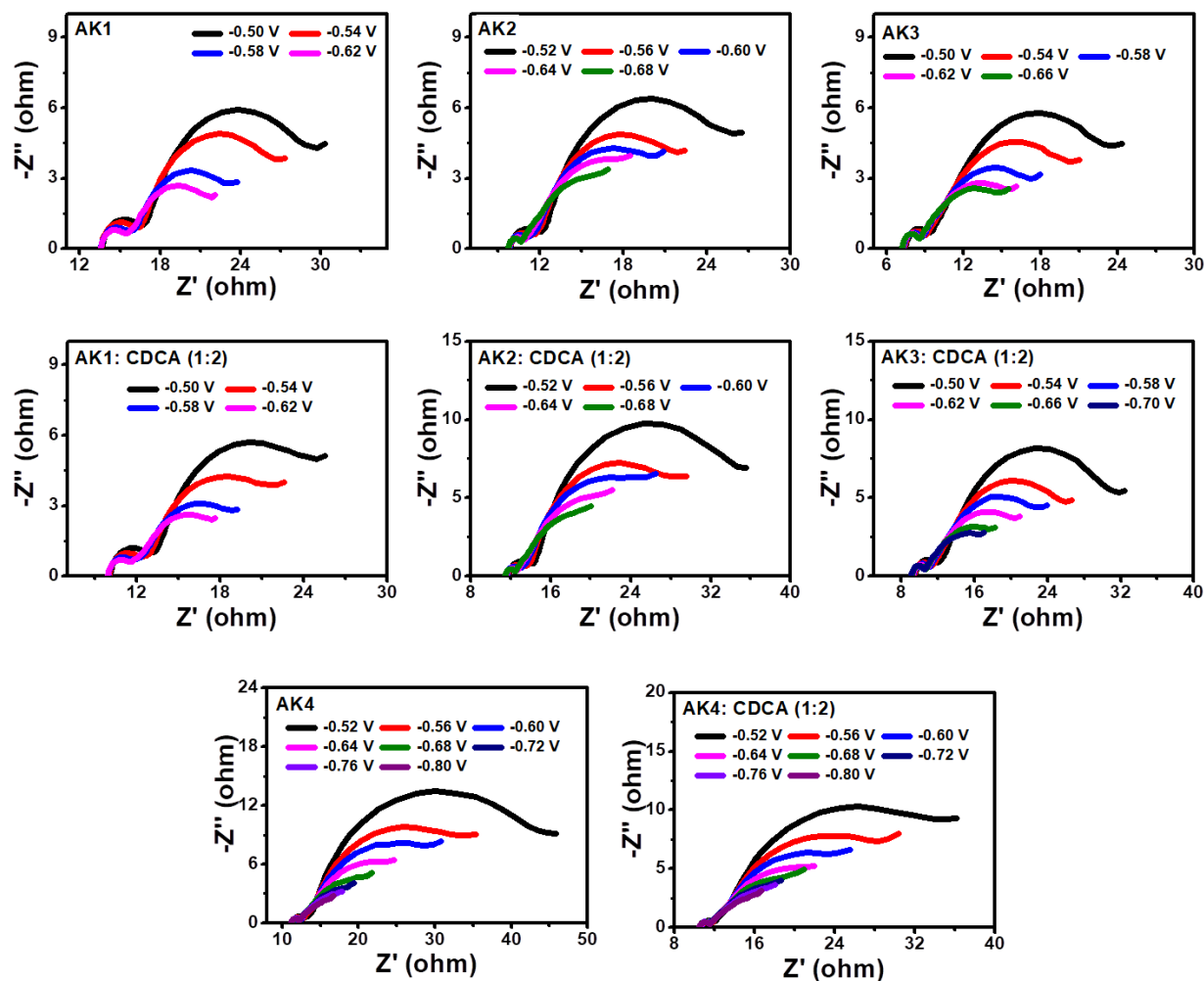
Figure 8. Nyquist plot of the AK dyes with and without CDCA under various applied bias.
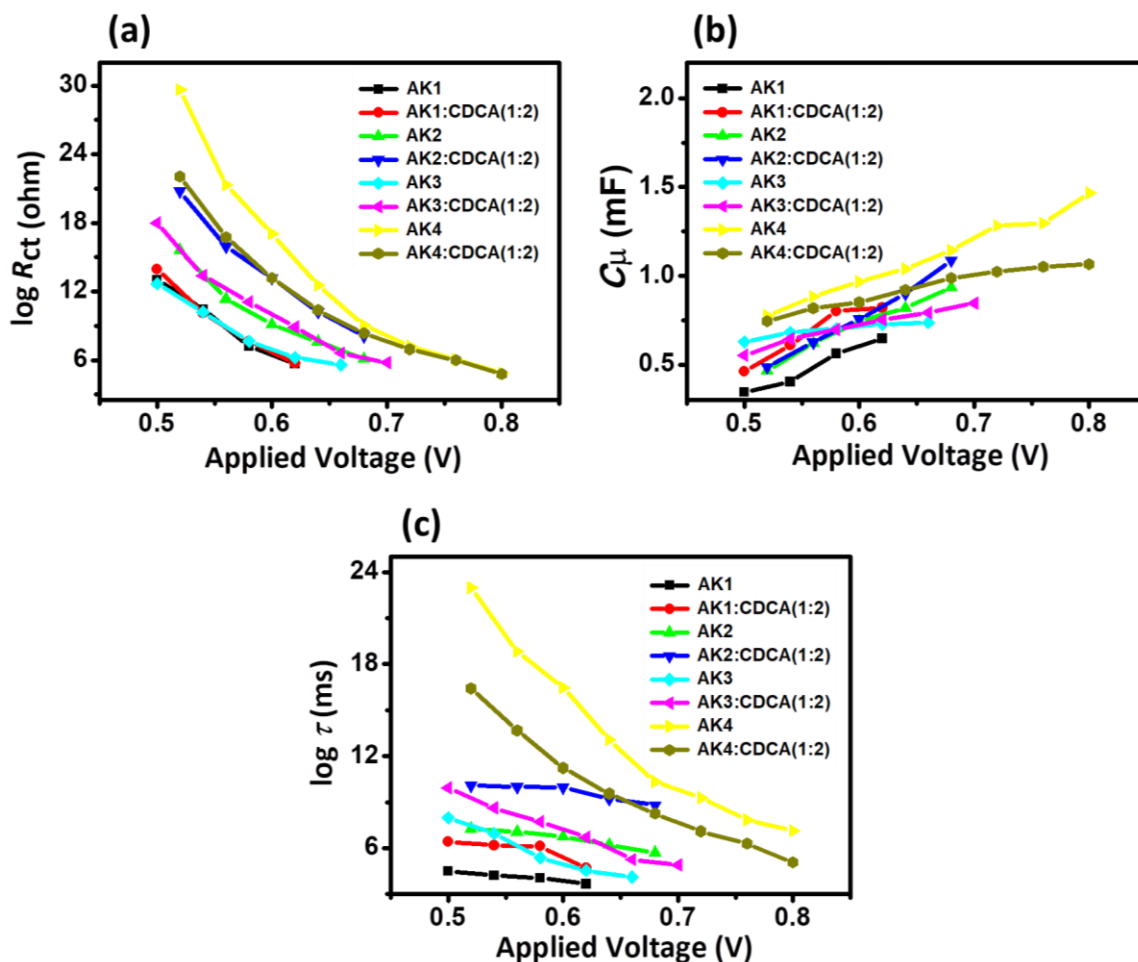
Figure 9. (a) Charge recombination resistance, (b) chemical capacitance, (c) electron life time of

AK dyes *vs* applied bias with and without CDCA.

Table 4. EIS parameters of DSSC device made up of AK1, AK2, AK3 and AK4 in dark with the applied bias of 0.62 V.

Dye	Dye: CDCA	R_{ct} (ohm)	$C\mu$ (mF)	τ (ms)
AK1	1:0	5.68	0.648	3.68
AK1	1:2	5.74	0.820	4.71
AK2[a]	1:0	7.62	0.819	6.24
AK2[a]	1:2	10.24	0.90	9.22
AK3	1:0	6.23	0.729	4.54
AK3	1:2	8.90	0.754	6.71
AK4[a]	1:0	12.57	1.04	13.07
AK4[a]	1:2	10.39	0.92	9.56

[a]Applied bias of 0.64 V
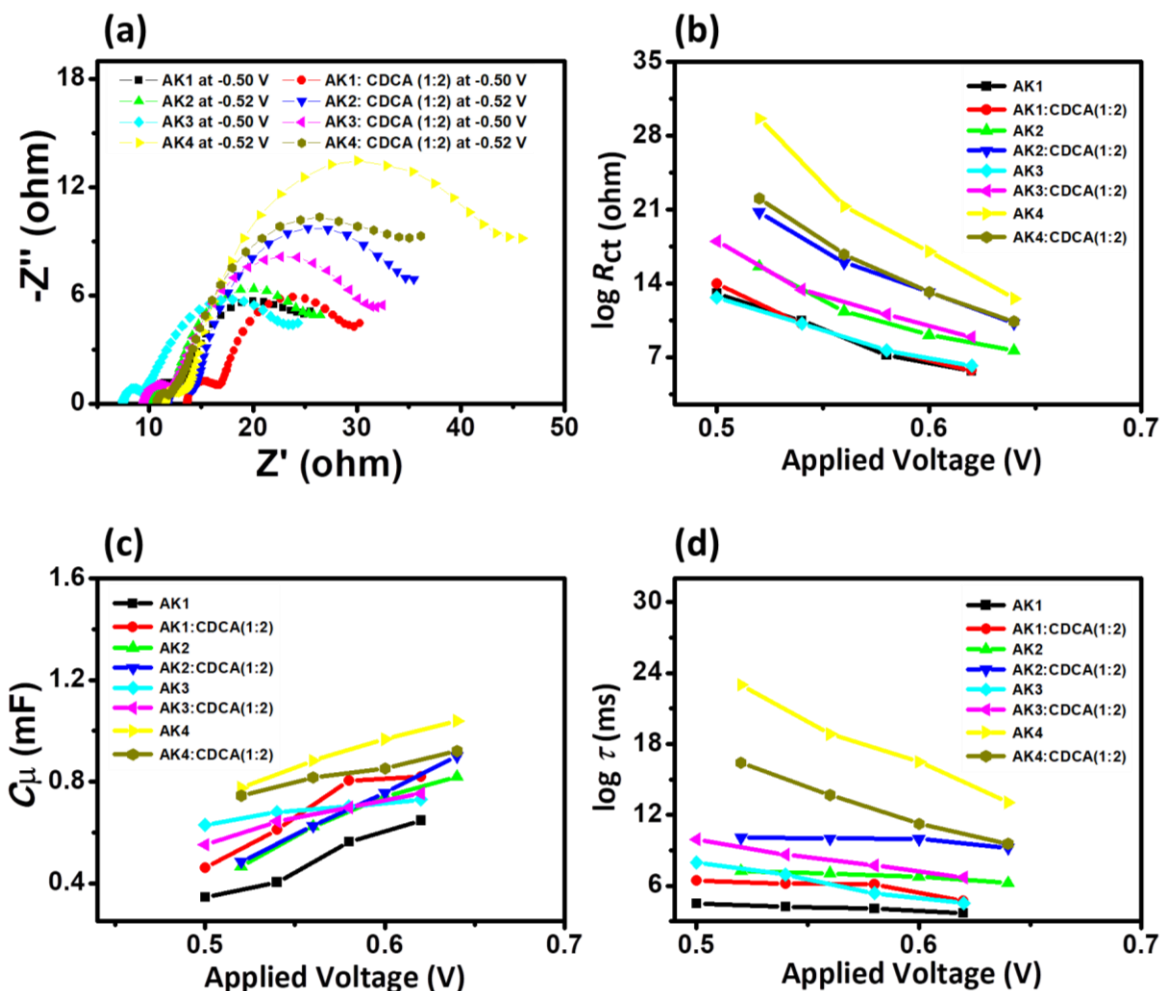
Figure 10. (a) Nyquist plot, (b) charge recombination resistance, (c) chemical capacitance and (d) lifetime of electron of AK dyes without and with CDCA.

4.3.6 Co-sensitization of complementary unsymmetrical squaraine dyes. For the efficient co-sensitized dye-sensitized solar cells, complementary light absorbing dyes with high extinction coefficients is required. AK and SQS dyes have λ_{max} in the regions of 529-541 nm and 642-650 nm, respectively (**Figure 11a, b**) with the extinction coefficients in the order of 10^5 $M^{-1}cm^{-1}$. Dyes AK2 and AK4 showed better device performance than AK1 and AK3 with the IPCE response more than 80% in the 450-610 nm regions. We have showed recently that indoline based unsymmetrical SQS4 dye showed better device performance in the region of 550-700 nm.[17] AK2, AK4 and SQS4 dyes have contributed to the photo current generation from the

aggregated state even in the presence of co-adsorbent CDCA. The model indoline based squaraine dye; SQ1 (without any alkyl groups) showed the IPCE response of 36% at 536 nm which from the aggregated dye structures on TiO_2, and in the presence of CDCA, the obtained photocurrent response is only from the monomeric structures.[16] Hence the stability of monolayer formation with the co-sensitized dyes is very important on the TiO_2 surface, and it should not happen that the formation of self-assembled structure is disturbed by the complementary dye.[28,32] Hence in order to optimize a best pair of complementary dyes for the better co-sensitized device performance, dyes SQ1, SQS4, AK2 and AK4 were chosen (**Figure 11a**).
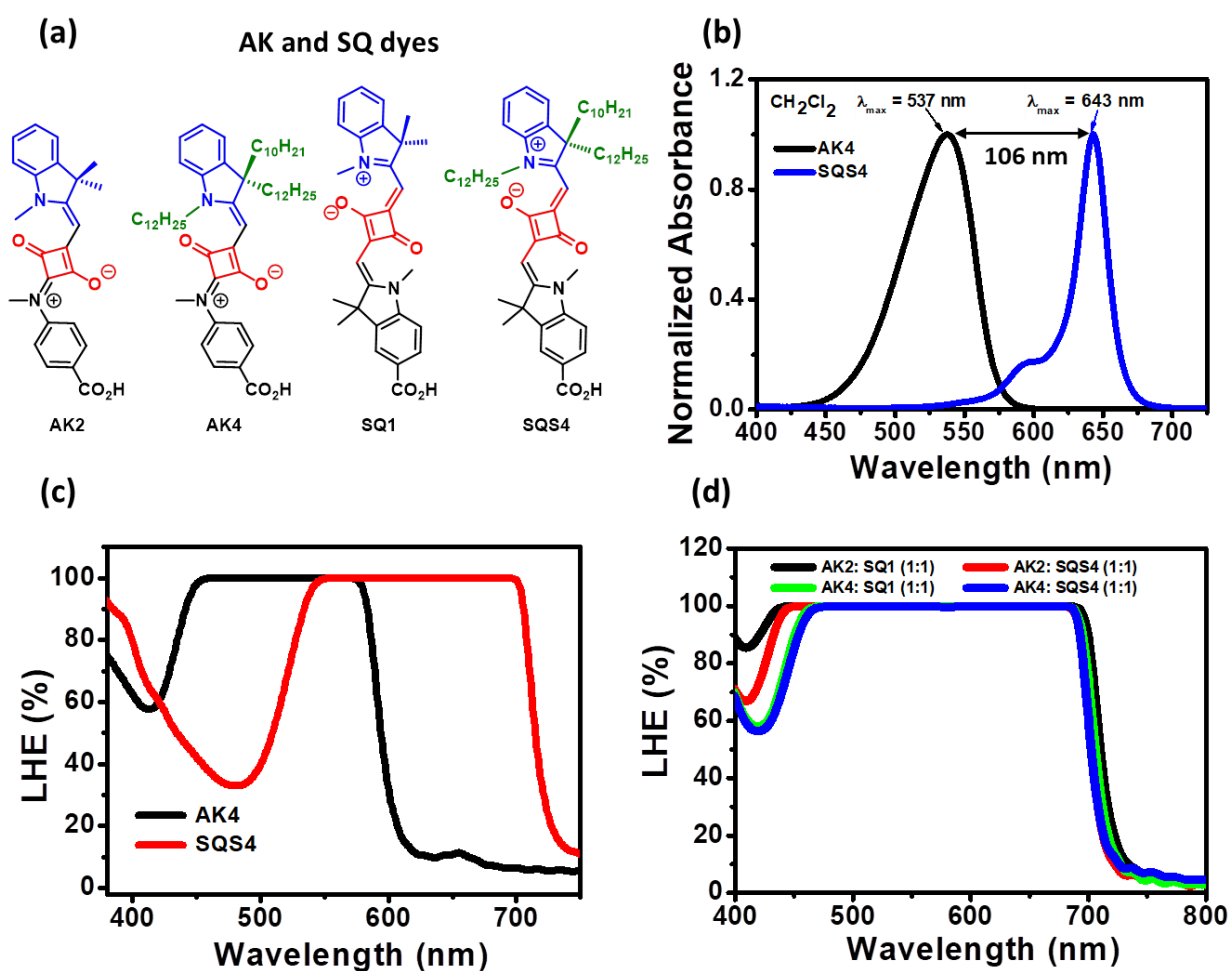
Figure 11. (a) Structures of AK2, AK4, SQ1, and SQS4, (b) normalized absorption spectra of AK4 and SQS4, (c) overlapped LHE profile of AK4 and SQS4 and (d) LHE profile of AK and SQS dyes co-sensitized TiO_2 electrode (dye dipping time 12 h).
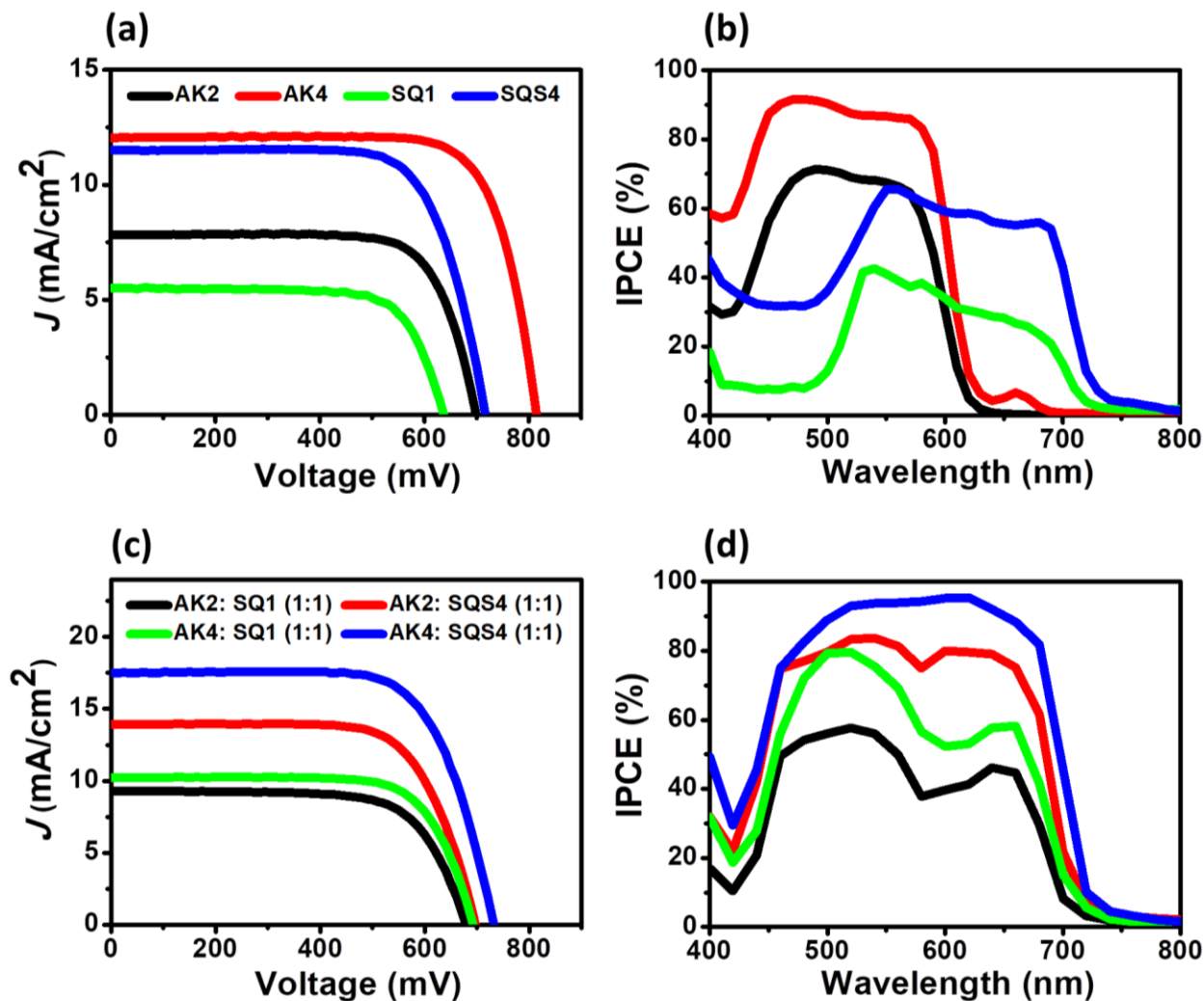
Figure 12. (a) *I-V* curve for AK2, AK4, SQ1 and SQS4 sensitized DSSC devices, (b) IPCE profile for AK2, AK4, SQ1 and SQS4 sensitized DSSC devices without CDCA, (c) *I-V* curve for co-sensitized DSSC devices of AK2+SQ1, AK2+SQS4, AK4+SQ1 and AK4+SQS4 DSSC devices and (d) IPCE profile for AK2+SQ1, AK2+SQS4, AK4+SQ1 and AK4+SQS4 co-sensitized DSSC devices.

The normalized absorption spectra of AK4 and SQS4 is provided in **Figure 11b**, and the LHE profile of the individual dye as well as combined dye showed the potential light harvesting ability from 450-700 nm (**Figure 11c, d**). The individual device performance is provided in **Figure 12a, b** (**Table 5**). Co-sensitized devices for the AK2+SQ1, AK2+SQS4, AK4+SQ1 and AK4+SQS4 dye combinations with the ratio of 1:1 are carried out without CDCA (**Figure 12c,**

d). AK2+SQS4 device performed better with 7.0% (V_{OC} 698 mV, J_{SC} 14.06 mA/cm^2) than AK2+SQ1 (4.59%, V_{OC} 679 mV, J_{SC} 9.53 mA/cm^2). Highest device performance is obtained for the AK4+SQS4 dye combination with 9.36% (V_{OC} 733 mV, J_{SC} 17.75 mA/cm^2) with the good IPCE response over a large part of the visible and far-red regions of the solar spectrum. Dye combination of AK4+SQ1 showed the device efficiency of 5.43% (V_{OC} 694 mV, J_{SC} 10.65 mA/cm^2). The high device performance of AK4+SQS4 combination may be due to the long alkyl chains present in the both of the dyes, effectively controlling the aggregation. Further addition of CDCA reduces the device performance (**Figure 13** and **Table 6**).

Table 5. Photovoltaic parameters for the co-sensitized DSSC devices (active area and black mask size was 0.23 cm^2).

Dyes	V_{OC} (mV)	J_{SC} (mA/cm^2)	ff (%)	η (%)
AK2[a]	699.12 ± 1.22	7.80 ± 0.44	75 ± 0.87	4.09 ± 0.29
AK4[b]	814.60 ± 1.28	12.05 ± 0.35	78 ± 0.37	7.65 ± 0.28
SQ1[a]	637.22 ± 1.05	5.50 ± 0.21	73 ± 0.69	2.56 ± 0.13
SQS4[b]	716.87 ± 1.12	11.52 ± 0.37	72 ± 0.61	5.94 ± 0.25
AK2: SQ1 (1:1)[c]	678.93 ± 0.36	9.27 ± 0.26	70 ± 0.91	4.41 ± 0.18
AK2: SQS4 (1:1)[c]	697.41 ± 0.65	13.89 ± 0.17	71 ± 0.39	6.88 ± 0.12
AK4: SQ1 (1:1)[c]	692.80 ± 0.76	10.22 ± 0.43	73 ± 0.55	5.17 ± 0.26
AK4: SQS4 (1:1)[c]	731.96 ± 1.32	17.46 ± 0.29	71 ± 0.93	9.08 ± 0.28

[a]CH$_3$CN: DMSO (95: 5), [b]CH$_3$CN: CHCl$_3$ (95: 5), [c]CH$_3$CN: DMSO: CHCl$_3$ (90: 5: 5)
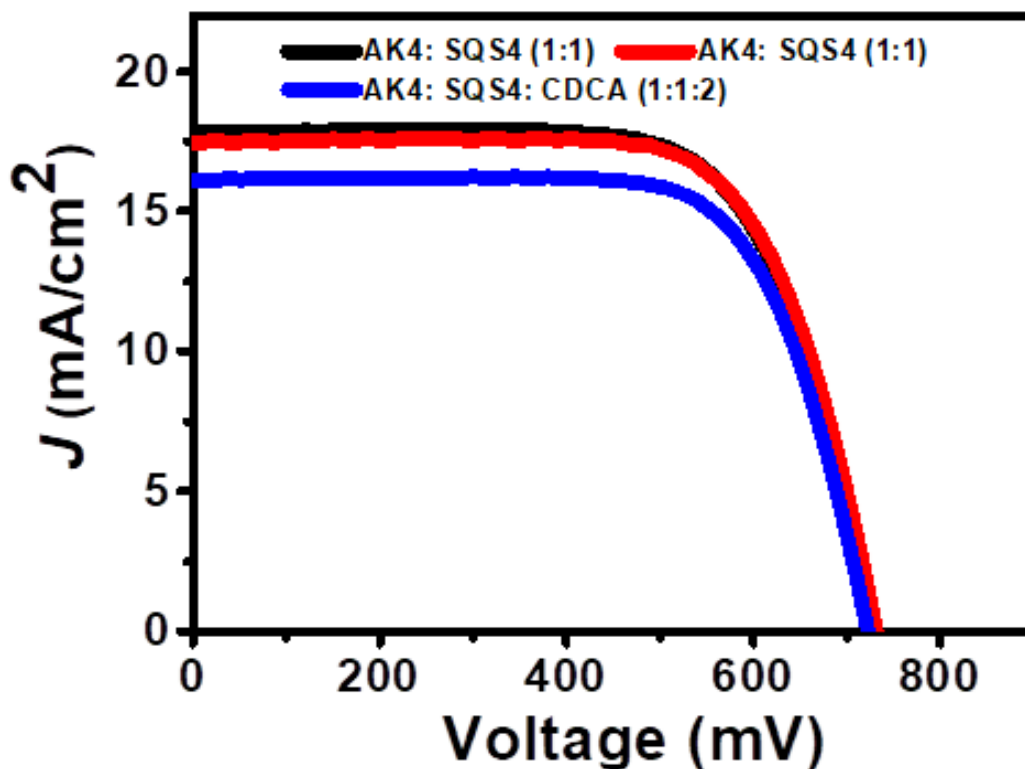
Figure 13. *J-V* curve of SQ dyes under AM 1.5 G illumination (1000 W/m^2).

Table 6. Photovoltaic performance of co-sensitized solar cells.

Dyes	CDCA ratio	V_{OC} (mV)	J_{SC} (mA/cm^2)	*ff* (%)	η (%)
AK4: SQS4 (1:1)[a]	0	731.96 ± 1.32	17.46 ± 0.29	71 ± 0.53	9.08 ± 0.23
AK4: SQS4 (1:1)[b]	0	728.26 ± 0.63	17.80 ± 0.51	70 ± 0.13	9.07 ± 0.27
AK4: SQS4 (1:1)[b]	2	722.78 ± 0.77	16.13 ± 0.81	71± 0.32	8.28 ± 0.46

[a]CH$_3$CN: DMSO: CHCl$_3$ (90: 5: 5), [b]CH$_3$CN: CHCl$_3$ (95: 5)

4.3.7 Photovoltaic response from the monomeric dyes. To understand the IPCE responses from monomeric dyes, the photoanode coated with TiO_2 (Thickness of TiO_2 8 μm, area 0.23 cm^2) was first saturated with coadsorbent CDCA for 12 h (1.0 mM in MeCN), and further dipped in dye solution for 2 min (0.1 or 0.2 mM in MeCN) (**Figure 14** and **Table 7**). Monomeric AK4 performed better with efficiency 1.17%, V_{OC} 662 mV, J_{SC} 2.21 mA/cm^2 than other dyes, whereas no much changes observed with co-sensitized solar cell efficiency from the monomeric dyes and the maximum efficiency obtained 2.58% with the AK4+SQS4 dye combinations with the ratio of 1:1.
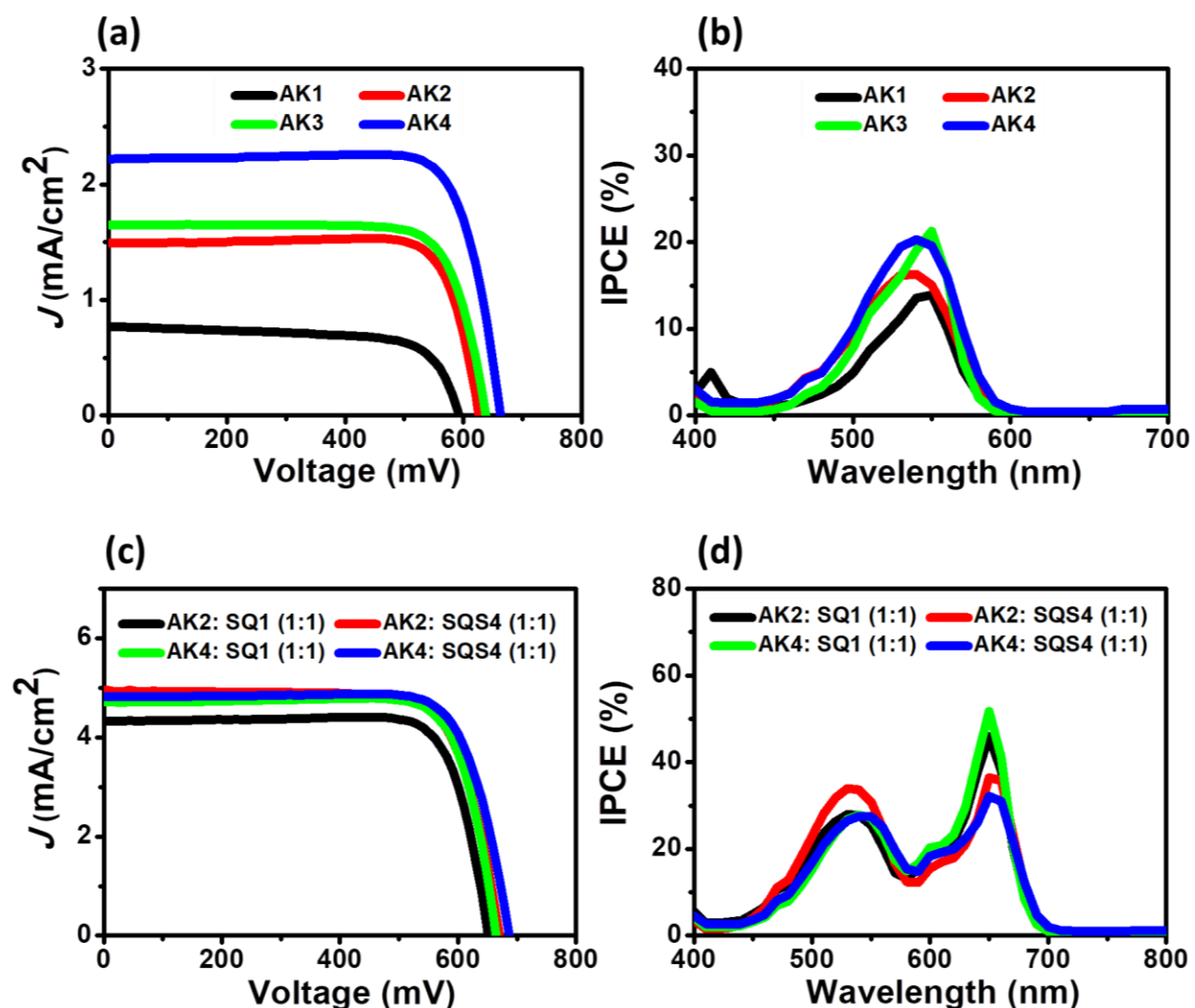
Figure 14. (**a** and **b**) *J-V* curves of SQ dyes under AM 1.5 G illumination (1000 W/m^2), (**c** and **d**) IPCE responses of SQ dyes.

Table 7. Photovoltaic performance of SQ dyes.

Dyes	V_{OC} (mV)	J_{SC} (mA/cm^2)	ff (%)	η (%)
AK1[a]	592.84	0.77	69	0.31
AK2[a]	626.20	1.49	82	0.76
AK3[b]	638.39	1.65	78	0.82
AK4[b]	662.12	2.21	80	1.17
AK2: SQ1 (1:1)[c]	650.87	4.33	80	2.25
AK2: SQS4 (1:1)[c]	670.12	4.94	76	2.51
AK4: SQ1 (1:1)[c]	664.56	4.71	80	2.50
AK4: SQS4 (1:1)[c]	687.36	4.81	78	2.58

[a]CH_3CN: DMSO (95: 5), [b]CH_3CN: $CHCl_3$ (85: 15), [c]CH_3CN: DMSO: $CHCl_3$ (90: 5: 5)

4.4 CONCLUSION

Unsymmetrical squaraine dyes with indoline and aniline based donors were designed and synthesized. These unsymmetrical squaraine dyes showed intense absorption with high extinction coefficients around 540 nm. Systematic structural optimization by means of introducing alkyl groups at the indoline donor unit as well as N-methylation of aniline donor units is required to boost both V_{OC} and J_{SC} of the DSSC devices. N-methylation of aniline donor unit had profound effect on enhancing both V_{OC} and J_{SC}, whereas introducing alkyl groups at sp^3-C and N-atoms had significant effect on enhancing only the V_{OC}. A device performance of 5.50 % (V_{OC} 711.18mV, J_{SC} 10.09 mA/cm^2, ff 77%) has been observed for AK2 device in the presence of 2 equivalent of CDCA. However, AK4 dye showed the device performance of 7.93% without adding CDCA with the V_{OC} of 815.8 mV. As AK dyes and indoline based unsymmetrical squaraine dyes (SQ1 and SQS4) exhibit complementary absorption profile, device optimization for the co-sensitized DSSC showed 9.36% for the AK4+SQS4 (1:1) dye combination. It is the first example for the co-sensitized DSSC devices that uses two different squaraine dyes which differ in extension of conjugation.

4.5 REFERENCES

(1)   O'Regan, B.; Grätzel, M. A Low-Cost, High-Efficiency Solar Cell Based on Dye-Sensitized Colloidal TiO_2 Films. *Nature* **1991**, *353*, 737–740.

(2)   Listorti, A.; O'Regan, B.; Durrant, J. R. Electron Transfer Dynamics in Dye-Sensitized Solar Cells. *Chem. Mater.* **2011**, *23*, 3381–3399.

(3) Hagfeldt, A.; Boschloo, G.; Sun, L.; Kloo, L.; Pettersson, H. Dye-Sensitized Solar Cells. *Chem. Rev.* **2010**, *110*, 6595–6663.

(4) Chen, W.-C.; Kong, F.-T.; Li, Z.-Q.; Pan, J.-H.; Liu, X.-P.; Guo, F.-L.; Zhou, Li; Huang, Y.; Yu, T.; Dai, S.-Y. Superior Light-Harvesting Heteroleptic Ruthenium (II) Complexes with Electron-Donating Antennas for High Performance Dye-Sensitized Solar Cells. *ACS Appl. Mater. Interfaces* **2016**, *8*, 19410-19417.

(5) Ye, M.; Wen, X.; Wang, M.; Iocozzia, J.; Zhang, N.; Lin, C.; Lin1, Z. Recent Advances in Dye-Sensitized Solar Cells: from Photoanodes, Sensitizers and Electrolytes to Counter Electrodes. *Materials Today*, **2015**, *18*, 155-162.

(6) Wu, J.; Lan, Z.; Lin, J.; Huang, M.; Huang, Y.; Fan, L.; Luo, G. Electrolytes in Dye-Sensitized Solar Cells. *Chem. Rev.* **2015**, *115*, 2136−2173.

(7) Wu, J.; Lan, Z.; Lin, J.; Huang, M.; Huang, Y.; Fan, L.; Luo, G.; Lin, Y.; Xie, Y.; Wei, Y. Counter Electrodes in Dye-Sensitized Solar Cells. *Chem. Soc. Rev.*, **2017**, *46*, 5975-6023.

(8) Yao, Z.; Zhang, M.; Wu, H.; Yang, L.; Li, R.; Wang, P. Donor/Acceptor Indenoperylene Dye for Highly Efficient Organic Dye-Sensitized Solar Cells. *J. Am. Chem. Soc*. **2015**, *137*, 3799-3802.

(9) Yella, A.; Mai, C.-L.; Zakeeruddin, S. M.; Chang, S.-N.; Hsieh, C.-H.; Yeh, C.-Y.; Grätzel, M. Molecular Engineering of Push–Pull Porphyrin Dyes for Highly Efficient Dye-Sensitized Solar Cells: The Role of Benzene Spacers. *Angew. Chem., Int. Ed*. **2014**, *53*, 2973-2977.

(10)   Wu, Y.; Zhu, W. Organic Sensitizers from D–π–A to D–A–π–A: Effect of the Internal Electron-Withdrawing Units on Molecular Absorption, Energy Levels and Photovoltaic Performances. *Chem. Soc. Rev.* **2013**, *42*, 2039-2058.

(11)   Park, J.-H.; Nam, D. G.; Kim, B-M.; Jin, M. Y.; Roh, D.-H.; Jung, H. S.; Ryu, D. H.; Kwon, T.-H. Planar D-D-π-A Organic Sensitizers for Thin-Film Photoanodes. *ACS Energy Lett.* **2017**, *2*, 1810-1817.

(12)   Qin, C.; Wong, W.-Y.; Han, L. Squaraine Dyes for Dye-Sensitized Solar Cells: Recent Advances and Future Challenges. *Chem. Asian J*. **2013**, *8*, 1706-1719.

(13)   Zhang, L.; Cole, J. M. Dye Aggregation in Dye-Sensitized Solar Cells. *J. Mater. Chem. A*. **2017**, 5, 19541-19559.

(14)   de Miguel, G.; Ziółek, M.; Zitnan, M.; Organero, J. A.; Pandey, S. S.; Hayase, S.; Douhal, A. Photophysics of H- and J-Aggregates of Indole-Based Squaraines in Solid State. *J. Phys. Chem. C* **2012**, *116*, 9379– 9389.

(15)   Feldt, S. M.; Gibson, E. A.; Gabrielsson, E.; Sun, L. C.; Boschloo, G.; Hagfeldt, A. Design of Organic Dyes and Cobalt Polypyridine Redox Mediators for High-Efficiency Dye-Sensitized Solar Cells. *J. Am. Chem. Soc.* **2010**, *132*, 16714-16724.

(16)   Alagumalai, A.; Kavungathodi, M. F. M.; Vellimalai, P.; Sil, M. C.; Nithyanandhan, J. Effect of Out-of-Plane Alkyl Group's Position in Dye-Sensitized Solar Cell Efficiency: A Structure–Property Relationship Utilizing Indoline-Based Unsymmetrical Squaraine Dyes. *ACS Appl. Mater. Interfaces* **2016**, *8*, 35353–35367.

(17)   Singh, A. K.; Kavungathodi, M. F. M.; Nithyanandhan, J. Alkyl-Group-Wrapped Unsymmetrical Squaraine Dyes for Dye-Sensitized Solar Cells: Branched Alkyl Chains Modulate the Aggregation of Dyes and Charge Recombination Processes. *ACS Appl. Mater. Interfaces* **2020**, *12*, 2555-2565.

(18)   Yang, J.; Ganesan, P.; Teuscher, J.; Moehl, T.; Kim, Y. J.; Yi, C.; Comte, P.; Pei, K.; Holcombe, T. W.; Nazeeruddin, M. K.; Hua, J.; Zakeeruddin, S. M.; Tian, H.; Grätzel, M.Influence of the Donor Size in D−π−A Organic Dyes for Dye-Sensitized Solar Cells. *J. Am. Chem. Soc.* **2014**, *136*, 5722-5730.

(19)   Yao, Z.; Zhang, M.; Wu, H.; Yang, L.; Li, R.; Wang, P. Donor/Acceptor Indenoperylene Dye for Highly Efficient Organic Dye-Sensitized Solar Cells. *J. Am. Chem. Soc*. **2015**, *137*, 3799-3802.

(20)   Zhang, L.; Yang, X.; Wang, W.; Gurzadyan, G. G.; Li, J.; Li, X.; An, J.; Yu, Z.; Wang, H.; Cai, B.; Hagfeldt, A.; Sun, L. 13.6% Efficient Organic Dye-Sensitized Solar Cells by Minimizing Energy Losses of the Excited State. *ACS Energy Lett.* **2019**, *4* , 943–951.

(21)   Jradi, F. M.; O'Neil, D.; Kang, X.; Wong, J.; Szymanski, P.; Parker, T. C.; Anderson, H. L.; El-Sayed, M. A.; Marder, S. R. A Step Toward Efficient Panchromatic Multi-Chromophoric Sensitizers for Dye Sensitized Solar Cells. *Chem. Mater*. **2015**, *27*, 6305-6313.

(22)   Karjule, N.; M. K., M. F.; Nithyanandhan, J. Heterotriangulene-based Unsymmetrical Squaraine Dyes: Synergistic Effects of Donor Moiety and Out-of-plane Branched Alkyl Chains on Dye Cell Performance. *J. Mater. Chem. A*, **2016**, *4*, 18910-18921.

(23)   Ogura, R. Y.; Nakane, S.; Morooka, M.; Orihashi, M.; Suzuki, Y.; Noda, K. High-Performance Dye-Sensitized Solar Cell with a Multiple Dye System. *Appl. Phys. Lett.* **2009**, *94*, 073308.

(24)   Ozawa, H.; Shimizu, R.; Arakawa, H. Significant Improvement in the Conversion Efficiency of Black-Dye-Based Dye-Sensitized Solar Cells by Cosensitization with Organic Dye. *RSC Adv*. **2012**, *2*, 3198−3200.

(25)   Shiu, J.-W.; Chang, Y.-C.; Chan, C.-Y.; Wu, H.-P.; Hsu, H.-Y.; Wang, C.-L.; Lin, C.-Y.; Diau, E. W.-G. Panchromatic Co-Sensitization of Porphyrin-Sensitized Solar Cells to Harvest Near-Infrared Light Beyond 900 nm. *J. Mater. Chem. A* **2015**, *3*, 1417−1420.

(26)   Yella, A.; Lee, H.-W.; Tsao, H. N.; Yi, C.; Chandiran, A. K.; Nazeeruddin, M. K.; Diau, E. W. G.; Yeh, C.-Y.; Zakeeruddin, S. M.; Grätzel, M. Porphyrin-Sensitized Solar Cells with Cobalt (II/III)−Based Redox Electrolyte Exceed 12% Efficiency. *Science* **2011**, *334*, 629−634.

(27)   Xie, Y.; Tang, Y.; Wu, W.; Wang, Y.; Liu, J.; Li, X.; Tian, H.; Zhu, W.-H. Porphyrin Cosensitization for a Photovoltaic Efficiency of 11.5%: A Record for Non-Ruthenium Solar Cells Based on Iodine Electrolyte. *J. Am. Chem. Soc.* **2015**, *137*, 14055−14058.

(28)   Holliman, P. J.; Davies, M. L.; Connell, A.; Velasco, B. V.; Watson, T. M. Ultra-Fast Dye Sensitisation and Co-Sensitisation for Dye Sensitized Solar Cells. *Chem. Commun*. **2010**, *46*, 7256−7258.

(29)   Guo, M.; Diao, P.; Ren, Y.-J.; Meng, F.; Tian, H.; Cai, S.-M. Photoelectrochemical Studies of Nanocrystalline TiO$_2$ Co-Sensitized by Novel Cyanine Dyes. *Sol. Energy Mater. Sol. Cells* **2005**, *88*, 23−35.

(30)   Kuang, D.; Walter, P.; Nüesch, F.; Kim, S.; Ko, J.; Comte, P.; Zakeeruddin, S. M.; Nazeeruddin, M. K.; Grätzel, M. Co-Sensitization of Organic Dyes for Efficient Ionic Liquid Electrolyte-Based Dye- Sensitized Solar Cells. *Langmuir* **2007**, *23*, 10906−10909.

(31)   Holliman, P. J.; Mohsen, M.; Connell, A.; Davies, M. L.; Al- Salihi, K.; Pitak, M. B.; Tizzard, G. J.; Coles, S. J.; Harrington, R. W.; Clegg, W.; et al. Ultra-Fast Co-Sensitization and Tri-Sensitization of Dye-Sensitized Solar Cells with N719, SQ1 and Triarylamine Dyes. *J. Mater. Chem.* **2012**, *22*, 13318−13327.

(32)   Sharma, G. D.; Singh, S. P.; Kurchania, R.; Ball, R. J. Cosensitization of Dye Sensitized Solar Cells with a Thiocyanate Free Ru Dye and a Metal Free Dye Containing Thienylfluorene Conjugation. *RSC Adv*. **2013**, *3*, 6036−6043.

(33)   Zhao, Y.; Lu, F.; Zhang, J.; Dong, Y.; Zhang, B.; Feng, Y. Stepwise Co-Sensitization of Two Metal-Based Sensitizers: Probing Their Competitive Adsorption for Improving the Photovoltaic Performance of Dye-Sensitized Solar Cells. *RSC Adv.* **2017**, *7*, 10494−10502.

(34)   Shibayama, N.; Ozawa, H.; Abe, M.; Ooyama, Y.; Arakawa, H. A New Cosensitization Method Using the Lewis Acid Sites of a TiO$_2$ Photoelectrode for Dye-Sensitized Solar Cells. *Chem. Commun*. **2014**, *50*, 6398−6401.

(35)   Jia, H.-L.; Zhang, M.-D.; Ju, Z.-M.; Zheng, H.-G.; Ju, X.-H. Picolinic Acid as an Efficient Tridentate Anchoring Group Adsorbing at Lewis Acid Sites and Bronsted Acid Sites of the TiO$_2$ Surface in Dye-Sensitized Solar Cells. *J. Mater. Chem. A* **2015**, *3*, 14809−14816.

(36)   Nazeeruddin, M. K.; Péchy, P.; Renouard, T.; Zakeeruddin, S. M.; Humphry-Baker, R.; Comte, P.; Liska, P.; Cevey, L.; Costa, E.; Shklover, V.; et al. Engineering of Efficient Panchromatic Sensitizers for Nanocrystalline TiO$_2$-Based Solar Cells. *J. Am. Chem. Soc*. **2001**, *123*, 1613−1624.

(37)   Zhang, S.; Islam, A.; Yang, X.; Qin, C.; Zhang, K.; Numata, Y.; Chen, H.; Han, L. Improvement of Spectral Response by Co-Sensitizers for High Efficiency Dye-Sensitized Solar Cells. *J. Mater. Chem. A* **2013**, *1*, 4812−4819.

(38)   Luo, J.; Wan, Z.; Jia, C.; Wang, Y.; Wu, X.; Yao, X. Co-Sensitization of Dithiafulvenyl-Phenothiazine Based Organic Dyes with N719 for Efficient Dye-Sensitized Solar Cells. *Electrochim. Acta* **2016**, *211*, 364−374.

(39)   Huang, F.; Chen, D.; Cao, L.; Caruso, R. A.; Cheng, Y.-B. Flexible Dye-Sensitized Solar Cells Containing Multiple Dyes in Discrete Layers. *Energy Environ. Sci.* **2011**, *4*, 2803−2806.

(40)   Chang, S.; Wang, H.; Lee, L. T. L.; Zheng, S.; Li, Q.; Wong, K. Y.; Wong, W.-K.; Zhu, X.; Wong, W.-Y.; Xiao, X.; et al. Panchromatic Light Harvesting by N719 with a Porphyrin Molecule for High-Performance Dye-Sensitized Solar Cells. *J. Mater. Chem. C* **2014**, *2*, 3521−3526.

(41)   Sun, X.; Wang, Y.; Li, X.; Ågren, H.; Zhu, W.; Tian, H.; Xie, Y. Cosensitizers for Simultaneous Filling up of Both Absorption Valleys of Porphyrins: a Novel Approach for Developing Efficient Panchromatic Dye-Sensitized Solar Cells. *Chem. Commun.* **2014**, *50*, 15609−15612.

(42)   Wang, C.-L.; Hu, J.-Y.; Wu, C.-H.; Kuo, H.-H.; Chang, Y.-C.; Lan, Z.-J.; Wu, H.-P.; Diau, E. W.-G.; Lin, C.-Y. Highly Efficient Porphyrin-Sensitized Solar Cells with Enhanced Light Harvesting Ability Beyond 800 nm and Efficiency Exceeding 10%. *Energy Environ. Sci.* **2014**, *7*, 1392−1396.

(43)   Kurumisawa, Y.; Higashino, T.; Nimura, S.; Tsuji, Y.; Iiyama, H.; Imahori, H. Renaissance of Fused Porphyrins: Substituted Methylene-Bridged Thiophene-Fused Strategy for High-Performance Dye-Sensitized Solar Cells. *J. Am. Chem. Soc.* **2019**, *141*, 9910–9919.

(44)   Wu, H.-P.; Ou, Z.-W.; Pan, T.-Y.; Lan, C.-M.; Huang, W.-K.; Lee, H.-W.; Reddy, N. M.; Chen, C.-T.; Chao, W.-S.; Yeh, C.-Y.; et al. Molecular Engineering of Cocktail Co-Sensitization for Efficient Panchromatic Porphyrin-Sensitized Solar Cells. *Energy Environ. Sci.* **2012**, *5*, 9843−9848.

(45)   Lee, C.-L.; Lee, W.-H.; Yang, C.-H. The Effects of Co-Sensitization in Dye-Sensitized Solar Cells. *J. Mater. Sci.* **2013**, *48*, 3448−3453.

(46)   Zhang, W.; Wu, Y.; Zhu, H.; Chai, Q.; Liu, J.; Li, H.; Song, X.; Zhu, W.-H. Rational Molecular Engineering of Indoline-Based D-A-π-A Organic Sensitizers for Long-Wavelength-Responsive Dye-Sensitized Solar Cells. *ACS Appl. Mater. Interfaces* **2015**, *7*, 26802−26810.

(47)   Hao, Y.; Saygili, Y.; Cong, J.; Eriksson, A.; Yang, W.; Zhang, J.; Polanski, E.; Nonomura, K.; Zakeeruddin, S. M.; Grätzel, M.; et al. Novel Blue Organic Dye for Dye-Sensitized Solar Cells Achieving High Efficiency in Cobalt-Based Electrolytes and by Co-Sensitization. *ACS Appl. Mater. Interfaces* **2016**, *8*, 32797−32804.

(48)   Kakiage, K.; Aoyama, Y.; Yano, T.; Oya, K.; Kyomen, T.; Hanaya, M. Fabrication of a High-Performance Dye-Sensitized Solar Cell with 12.8% Conversion Efficiency Using Organic Silyl-Anchor Dyes. *Chem. Commun*. **2015**, *51*, 6315−6317.

(49)   Rao, G. H.; Venkateswararao, A.; Giribabu, L.; Han, L.; Bedja, I.; Gupta, R. K.; Islam, A.; Singh, S. P. Near-Infrared Squaraine Co-Sensitizer for High-Efficiency Dye-Sensitized Solar Cells. *Phys. Chem. Chem. Phys*. **2016**, *18*, 14279−14285.

(50)   Qin, C.; Numata, Y.; Zhang, S.; Islam, A.; Yang, X.; Sodeyama, K.; Tateyama, Y.; Han, L. A Near-Infrared cis-Configured Squaraine Co-Sensitizer for High-Efficiency Dye-Sensitized Solar Cells. *Adv. Funct. Mater*. **2013**, *23*, 3782−3789.

(51)   Cid, J.-J.; Yum, J.-H.; Jang, S.-R.; Nazeeruddin, M. K.; Martínez-Ferrero, E.; Palomares, E.; Ko, J.; Grätzel, M.; Torres, T. Molecular Cosensitization for Efficient Panchromatic Dye-Sensitized Solar Cells. *Angew. Chem., Int. Ed*. **2007**, *46*, 8358−8362.

(52)   Kimura, M.; Nomoto, H.; Masaki, N.; Mori, S. Dye Molecules for Simple Co-Sensitization Process: Fabrication of Mixed-Dye-Sensitized Solar Cells. *Angew. Chem., Int. Ed.* **2012**, *51*, 4371−4374.

(53)   Pang, A.; Xia, L.; Luo, H.; Li, Y.; Wei, M. Highly Efficient Indoline Dyes Co-Sensitized Solar Cells Composed of Titania Nanorods. *Electrochim. Acta* **2013**, *94*, 92−97.

(54)   Chen, K.; Chen, Y.; Zhu, W.-H.; Tian, H.; Xie, Y. Efficient Solar Cells based on Concerted Companion Dyes Containing Two Complementary Components: An Alternative Approach for Cosensitization. *J. Am. Chem. Soc.* **2020**, *142*, 5154-5161.

(55)   McKerrow, A. J.; Buncel, E.; Kazmaier, P. M. Aggregation of Squaraine Dyes: Structure-property Relationships and Solvent Effects**.** *Can. J. Chem.* **1995**, *73*, 1605 - 1615.

(56)   Mor, G. K.; Kim, S.; Paulose, M.; Varghese, O. K.; Shankar, K.; Basham, J.; Grimes, C. A. Visible to Near-Infrared Light Harvesting in TiO_2 Nanotube Array−P3HT Based Heterojunction Solar Cells. *Nano Lett.* **2009**, *12*, 4250−4257.

(57)   Ajayaghosh, A. Chemistry of Squaraine-Derived Materials: Near-IR Dyes, Low Band Gap Systems, and Cation Sensors**.** *Acc. Chem. Res.* **2005**, *38*, 449−459.

(58)   Sreejith, S.; Carol, P.; Chithra, P.; Ajayaghosh, A. Squaraine Dyes: A Mine of Molecular Materials, *J. Mater. Chem.* **2008**, *18*, 264-274.

(59)   Law, K. -Y. Organic Photoconductive Materials: Recent Trends and Developments. *Chem. Rev.* **1993**, *93*, 449-486.

(60)   Chen, G.; Sasabe, H.; Igarashi, T.; Hong, Z.; Kido, J. Squaraine Dyes for Organic Photovoltaic Cells. *J. Mater. Chem. A*, **2015**, *3*, 14517-14534.

(61)   Chen, G.; Sasabe, H.; Lu, W. et al. *J*-Aggregation of a Squaraine Dye and Its Application in Organic Photovoltaic Cells. *J. Mater. Chem. C*, **2013**, *1*, 6547–6552.

(62)   Alex, S.; Santhosh, U.; Das, S. Dye Sensitization of Nanocrystalline TiO₂: Enhanced Efficiency of Unsymmetrical Versus Symmetrical Squaraine Dyes. *J. Photochem. Photobiol. A* **2005**, *172*, 63-71.

(63)   Bricks, J. L.; Kachkovskii, A. D.; Slominskii, Y. L.; Gerasov, A. O.; Popov, S. V. Molecular Design of Near Infrared Polymethine Dyes: A Review. *Dyes and Pigments*, **2015**, *121*, 238-255.

(64)   Li, H.; Wu, Y.; Geng, Z.; Liu, J.; Xu, D.; Zhu, W. Co-Sensitization of Benzoxadiazole Based D−A−π−A Featured Sensitizers: Compensating Light-Harvesting and Retarding Charge Recombination. *J. Mater. Chem. A* **2014**, *2*, 14649−14657.

(65)   Chai, Q.; Li, W.; Liu, J.; Geng, Z.; Tian, H.; Zhu, W.-H. Rational Molecular Engineering of Cyclopentadithiophene-Bridged D-A-π-A Sensitizers Combining High Photovoltaic Efficiency with Rapid Dye Adsorption. *Sci. Rep.*, **2015**, *5*, 11330.

(66)   Bisht, R.; M. K., M. F.; Singh, A. K.; Nithyanandhan, J. Sensitized Solar Cells: Unsymmetrical Squaraine Dyes Incorporating Benzodithiophene π-Spacer with Alkyl Chains to Extend Conjugation, Control the Dye Assembly on TiO₂, and Retard Charge Recombination. *J. Org. Chem.* **2017**, *82*, 1920-1930.

(67)   Marotta, G.; Lobello, M. G.; Anselmi, C.; Consiglio, G. B.; Calamante, M.; Mordini, A.; Pastore, M.; De Angelis, F. An Integrated Experimental and Theoretical Approach to the Spectroscopy of Organic-Dye-Sensitized TiO₂ Heterointerfaces: Disentangling the Effects of Aggregation, Solvation, and Surface Protonation. *ChemPhysChem* **2014**, *15*, 1116-1125.

(68)   Ji, J.-M.; Zhou, H.; Kim, H. K. Rational Design Criteria for D–π–A Structured Organic and Porphyrin Sensitizers for Highly Efficient Dye-Sensitized Solar Cells. *J. Mater. Chem. A*, **2018**, *6*, 14518–14545.

(69)   Frisch, M. J.; Trucks, G. W.; Schlegel, H. B.; Scuseria, G. E.; Robb, M. A.; Cheeseman, J. R.; Scalmani, G.; Barone, V.; Petersson, G. A. ; Nakatsuji, H. et al. *Gaussian 09*; Gaussian, Inc., Wallingford CT, **2016**.

(70)   Wang, Q.; Moser, J. E.; Grätzel, M. Electrochemical Impedance Spectroscopic Analysis of Dye-Sensitized Solar Cells. *J. Phys. Chem. B* **2005**, *109*, 14945-14953.

Effect of Various Solvents and Electrolytes (I⁻/ I$_3^-$, Co(II/ III) and Cu(I/ II)) on the Device Performance of NIR-Light Active Squaraine Dyes

Device fabricated in CH$_3$CN solvent showed aggregated IPCE response
Device fabricated in CHCl$_3$ solvent showed monomeric and dimeric IPCE response

η = 5.92%
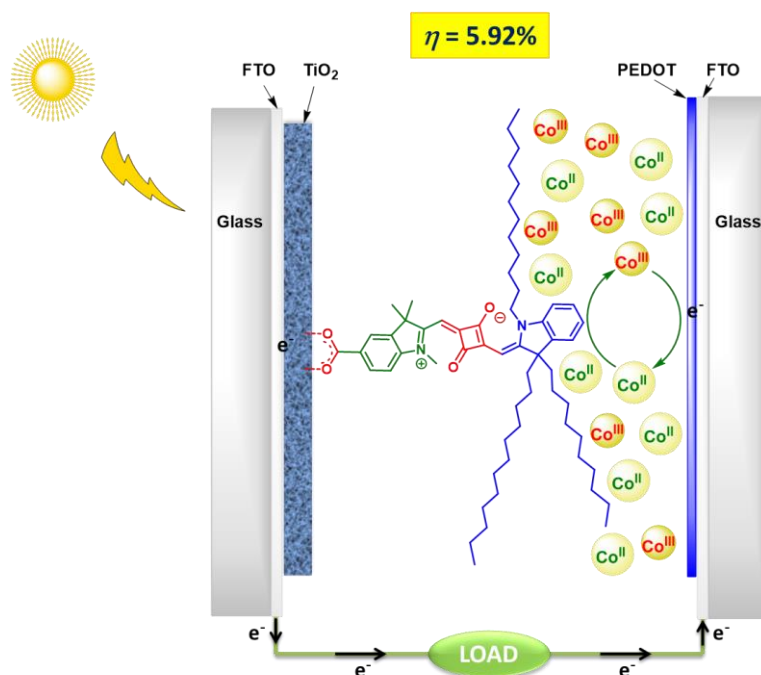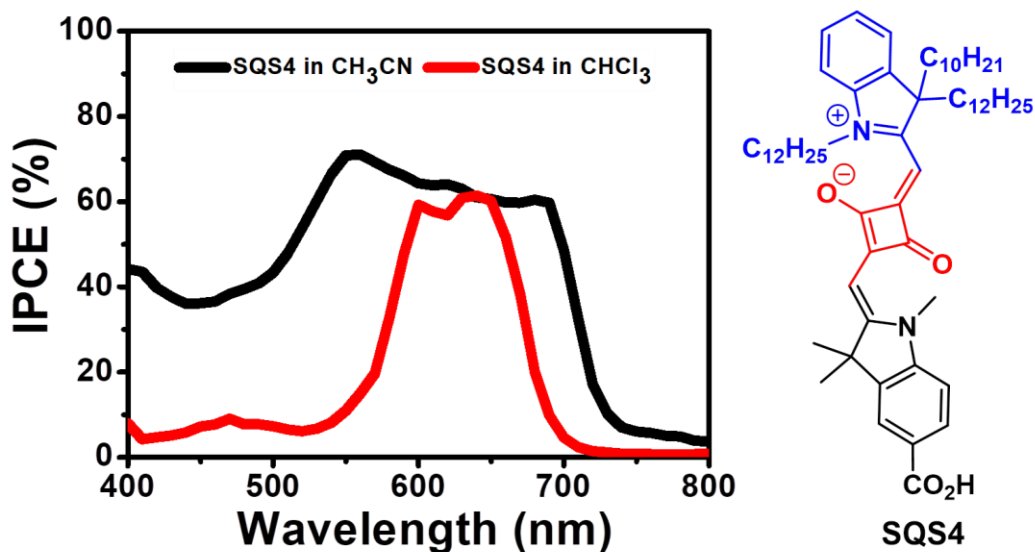
5.A Solvent Induced Aggregation of Unsymmetrical Squaraine Dyes on TiO₂ Surface and Effect on Dye-sensitized Solar Cells Performance

5.A.1 INTRODUCTION

The technology of solar energy to electrical energy conversion by photovoltaic effect has been very attractive and cheerful solar cells technology. Third generation solar cells have aroused great interest fast growing attractive and regarded as very promising photovoltaics due to low costs, and eco-friendly precursors.[1] Among the all solar cells belongs to third generation, dye-sensitized solar cells have the intense interest and potential to gain the high power conversion efficiency because of their tunable photochemical diversity by modulating the donor, acceptor, and spacer properties.[2] Scientists are devoting their great effort of research on the dye cells to solve the issues of device efficiency, stability, and costs from last two decades by developing the novel sensitizers, electrolytes, and photocathodes.[3,4] Dye is the principal components and the heart of DSSCs that leads to convert solar energy from the different regions of the solar spectrum into the electrical energy. The high power conversion efficiency gains by considering the planarity of the molecules for better electronic communications, π-spacer length, steric by introduction of the alkyl groups or auxiliary non-conjugated aromatics, controlled aggregation by introduction of the alkyl groups, and orientation of the dyes corresponds to the metal-oxide surface.[2,5-9] Though the first report on the DSSCs have been given by O'Regan and Grätzel in 1991 where ruthenium dye used as a sensitizers,[10] after several modifications the best efficiency afforded by ruthenium based dye is 12.1%.[11] Porphyrin dyes have been afforded the maximum efficiency 13% by proper structural engineering within the dye molecules.[12] Further, structural modulations in the sensitizer belongs to the metal-free organic dyes afforded the maximum efficiency 13.6%.[13] Among the metal-free organic dyes, squaraine dyes are very attractive D-A-D dye with high molar extinction coefficient in NIR region.[14] Squaraine dyes have the inherent characteristic to form aggregates in the solution as well as on the metal-oxide surface and explored well in the organic photovoltaics and sensors.[15,16]

Solvent systems used during the sensitization of dyes onto the surface of TiO₂ play a tremendous role to have better J_{SC}, V_{OC} and device efficiencies[17] besides the sensitizers,[18] electrolytes,[4] and counter electrodes.[19,20] Different solvent systems are providing the different conditions to dyes to

sensitizing onto the surface of TiO_2 due to different dielectric constant,[21] which cause the changes in the sensitizing behavior of the dyes and results different aggregation behavior and DSSC efficiencies. Ruthenium based N3 dye showed high J_{SC} and low V_{OC} values in the acetonitrile, whereas low J_{SC} and high V_{OC} values in the dimethyl sulfoxide solvent systems, due to change in the TiO_2 CB position, and interfacial electron transfer from the dye to the TiO_2.[22] Black dye showed significant changes in the device efficiencies with single solvent, and by varying the concentration of two solvents, respectively,[23] whereas Z907 dye showed difference in the device efficiencies when the dye sensitized into two or more mixed solvents.[24] Change in the adsorption conditions by changing the solvent systems either single or mixed solvent baths and adsorption time, porphyrin dyes have showed a variable changes in the J_{SC}, V_{OC} and device efficiencies.[25,26] D-A based alkylated phenothiazine dyes showed the better device efficiencies in ethanol compare to the tetrahydrofuran.[27] Drastic change in the J_{SC}, V_{OC} and device efficiencies have been observed by varying the solvent from the dichloromethane, and ethanol to N,N-dimethylformamide in the triphenylamine based D-π-A dyes.[17] BTZA-II dye showed the significant change in the J_{SC}, and device efficiencies by increasing the concentration of acetic acid in the toluene.[28] Different solvent systems provides the different electronic coupling and interaction between the dye and TiO_2, and changed the dye adsorption geometry or dye-aggregation onto the TiO_2 surface that influenced the device performance of the DSSC.[29,30]
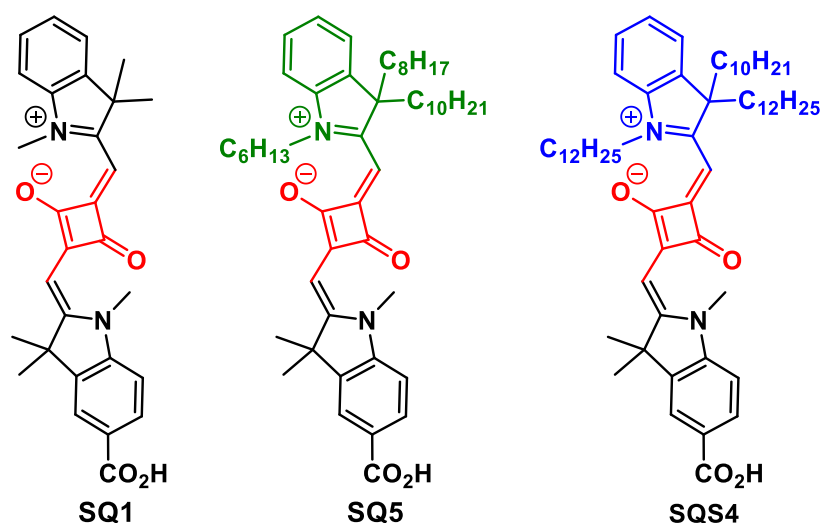
Figure 1. Structures of the unsymmetrical squaraine dyes.

NIR-light active unsymmetrical squaraine dyes SQ1,[6] SQ5[6] and SQS4[5] (which are different to each other with respect to alkyl group chain length) have been used to study the photophysical, aggregation behaviors, and effect onto the photovoltaic parameters in the chloroform (good solvents on the basis of solubility) and acetonitrile (bad solvents on the basis of solubility), respectively. Structures of the unsymmetrical squaraine dyes are displayed in **Figure 1**.

5.A.2 EXPERIMENTAL SECTION

Squaraine dyes have been synthesized by the following the procedure provided in the literature,[5,6] and required chemicals for synthesis were purchased from commercial resources.

5.A.2.1 General methods

Absorption spectra of SQ dyes were recorded on SPECORD® 210/ PLUS, Analytikjena UV−visible spectrophotometer at room temperature. For the light harvesting efficiency (LHE) calculation, (i) 6 μm thin film of TiO_2 coated on the transparent glass slide was dipped in 0.1 mM dye solution for 12 h at room temperature and absorbance spectra were recorded, (ii) 6 μm thin film of TiO_2 coated on the transparent glass slide was dipped in 0.1 mM dye solution for 12 h at room temperature then dipped in opposite solvent bath for 12 h at room temperature, and absorbance spectra were recorded and converted in light harvesting efficiency (LHE = $1-10^{-A}$). Electrochemical impedance measurements (EIS) were performed using a BioLogic SP300 potentiostat equipped with frequency response analyzer. EIS were carried out in dark with various applied potential and frequency ranges from 3 MHz to 10 mHz with sinus amplitude of 10 mV. For *I-V* characteristic of the cells were measured by using PHOTO EMISSION TECH (PET, CT200AAA, USA) solar-simulator, and IPCE measurements were carried out with a Newport QE measurement kit. For dye desorption studies of SQ dyes area of the photoanode was 0.23 cm^2 (8 μm thick), dipping time of photoanode in dye-solution (0.1mM) for 12 h at room temperature, 0.2 M NaOH in EtOH: H_2O (1:1) was used to desorb adsorbed dyes and path length of the cuvette was 0.01 cm^2. PerkinElmer FTIR spectrometer used for the measurement of IR-spectrum of all the squaraine dyes as such and on the surface of TiO_2.

5.A.2.2 Dye-sensitized solar cell fabrication. Fluorine-doped SnO_2 glass (8- 10 Ω /sq; Pilkington TEC 7) was washed with mucasol (2 % in water), de-ionized water (4 times), and isopropanol (two times) by using ultrasonic-bath to make cleaned. To grow a thin film TiO_2, FTO was treated with 40 mM aqueous $TiCl_4$ solution at 70 ^{o}C for 30 min, washed with the de-ionized water then EtOH and dried at 110 ^{o}C for 10 min. Paste of TiO_2 nanocrystal (< 20 nm, Ti-Nanoxide T/SP, Solaronix) was coated on FTO conducting side by using doctor-blade technique and kept for 15 min in air then heated at 120 °C in air for 20 min, then coated with scattering layer TiO_2 paste (WER2-O, Dyesol) and heated at 120 °C for 10 min in air, then sintered at 325 °C for 10 min, 375 °C for 10 min, 450 °C for 10 min and 500 °C for 15 min where heating rate was 5 °C per min in air. After sintering, films were treated with 40 mM aqueous $TiCl_4$ solution at 70 ^{o}C for 30 min, washed with the de-ionized water then EtOH and sintered at 500 °C for 20 min. Then immersed the cells (area of TiO_2 is 0.23 cm^2) in 0.1 mM dye solution of SQ dyes (in $CHCl_3$ or 97.5% CH_3CN and 2.5% $CHCl_3$) with and without CDCA for 12 h. Electroplatinised platinum foil used as cathode, iodolyte Z-50 (Solaronix) was used as electrolyte and 25 μm spacer and area of black mask is 0.23 cm^2. The device performance of SQ dyes were measured under standard simulator condition (AM 1.5 G, 100 mW/cm^2).

5.A.3 RESULTS AND DISCUSSION

5.A.3.1 Photophysical properties. The UV-vis and emission spectra of SQ1, SQ5, and SQS4 dyes in the bad solvents (acetonitrile) and in the good solvents (chloroform) are provided in **Figure 2** and **Table 1**. The absorption λ_{max} for SQ1 dye is appeared at 636 nm and 638 nm in MeCN and $CHCl_3$, respectively. However, the λ_{max} for the SQ5 and SQS4 dyes have been red-shifted 4-7 nm which showed that the dye-solvent complex formation in alkyl wrapped dyes in both MeCN and $CHCl_3$. There is no significant changes observed in absorption and emission of SQ5 and SQS4 dyes whether solvent was acetonitrile or chloroform. Further, absorption of SQ1, SQ5 and SQS4 dyes onto the surface of TiO_2 was carried out to understand the aggregation behavior of dyes with various concentration of CDCA in different solvent systems (thickness of the TiO_2 film 6 μm, dipping time 10 min). Normalized absorption of SQ1, SQ5 and SQS4 dyes onto the surface of TiO_2 with various concentration of CDCA in different solvent systems is provided in **Figure 3**. Two absorption peaks obtained for the SQ1 dye and corresponds to strong

H-aggregates at 570 nm and dimer at 627 nm, addition of CDCA converted H-aggregates into the dimer with decreased intensity and dimer into monomer at 638 nm in both of the solvent systems (**Figure 3a**, and **d**). SQ5 dye showed two absorption peaks corresponds to dimer at 605 nm (which is further decreased by increasing the concentration of the CDCA) and monomer at 643 nm in both of the solvent systems (**Figure 3b**, and **e**). Similarly, SQS4 dye showed two absorption peaks corresponds to dimer at 606 nm and monomer at 644 nm in both of the solvent systems and there is no significant effect CDCA concentration observed on the intensity of dimer (**Figure 3c**, and **f**).

Table 1. UV-vis and emission max of squaraine dyes in the acetonitrile and chloroform.

Dyes	SQ1		SQ5		SQS4	
Solvents	CH_3CN	$CHCl_3$	CH_3CN	$CHCl_3$	CH_3CN	$CHCl_3$
Absorbance λ_{max} (nm)	636	638	643	642	643	642
Emission λ_{max} (nm)	646	647	651	651	651	651
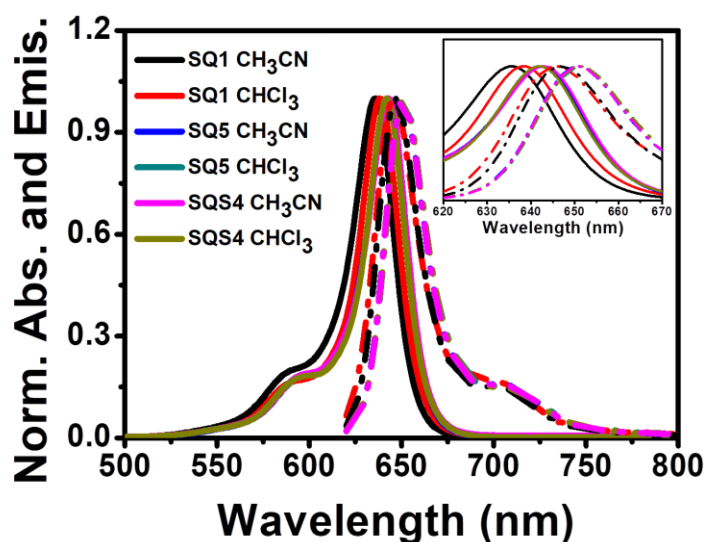
Figure 2. Normalized UV-vis (solid line), and emission (dotted line) spectra of SQ1, SQ5, and SQS4 dyes in the acetonitrile and chloroform solution.
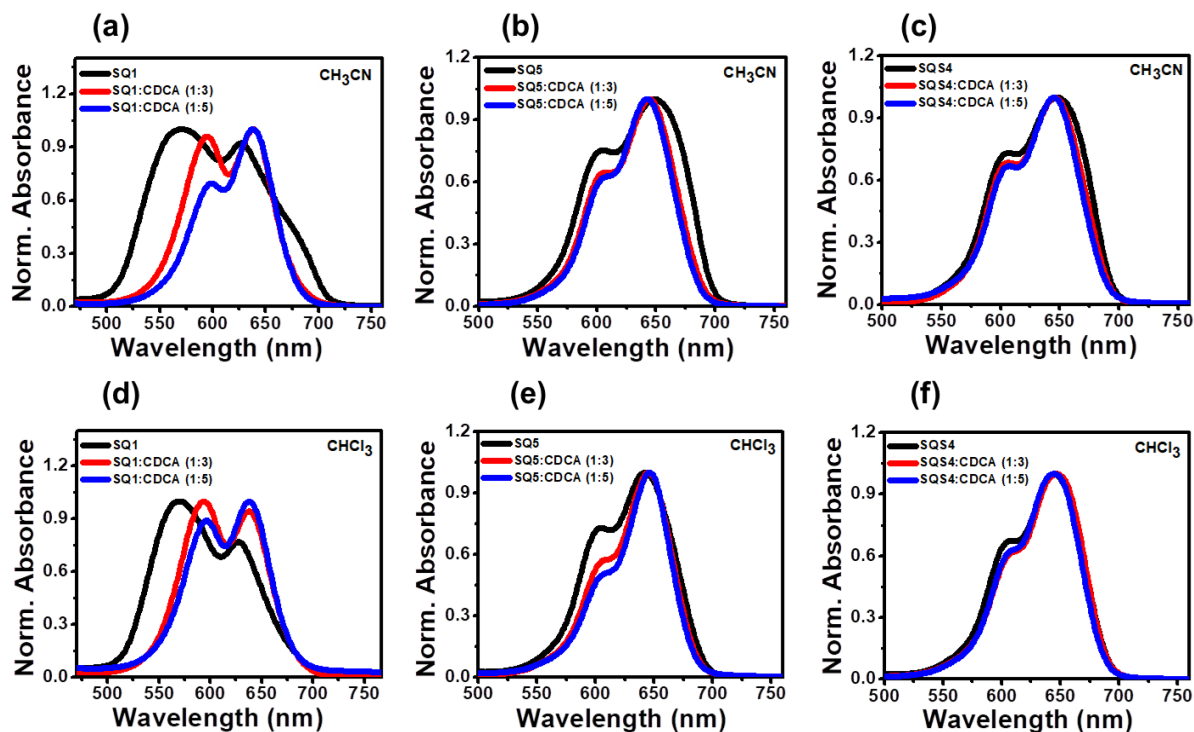
Figure 3. UV-visible spectra of squaraine dyes on TiO₂ surface (6 μm)**,** (a), (b), (c) dye solution 0.1 mM in CH₃CN, and (d), (e), (f) dye solution 0.1 mM in CHCl₃ with and without CDCA, dipping time 10 min at room temperature, respectively.

Furthermore, light harvesting efficiency (LHE) of SQ1, SQ5 and SQS4 dyes into two solvent systems and opposite solvent bath was calculated from the LHE = 1-10^{-A} (**Figure 5a, b** and **Table 2**). The order of LHE at the 60% (line width) of the squaraine dyes in bad solvent systems is 248> 201> 194 nm for the SQ1, SQ5 and SQS4 dyes respectively, that is further narrowing down to 229> 166> 155 nm for the SQ1, SQ5 and SQS4 dyes respectively in good solvent systems. Thus, the bad solvent systems favors the formation of dye aggregates onto the surface of TiO₂ for all the dyes compare to the good solvents systems (**Figure 5a,** and **Table 2**). Line width of the SQ5 and SQS4 dyes on TiO₂ are narrow, because of the hydrophobic alkyl groups present in the dyes backbone in compare to the SQ1 dye in bad as well as good solvent systems. Furthermore, LHE of squaraine dyes were calculated, where electrodes was first dipped into bad solvent dye stock solutions for 12 h at room temperature, and then immersed into opposite solvent (good solvent) bath for 12 h, and vice versa (**Figure 5b,** and **Table 2**). There is no significant change in the LHE performance of dyes observed when electrodes was first dipped

into good (chloroform) solvent dye stock solutions for 12 h, and then immersed into bad (acetonitrile) solvent bath for 12 h, whereas desorption of dyes from the surface of TiO_2 have been observed for all the dyes and line width of dyes was narrowing down, when the electrodes was first dipped into bad (acetonitrile) solvent dye stock solutions for 12 h, and then immersed into good (chloroform) solvent bath for 12 h (**Figure 4**). A proposed hypothesis of SQ1, SQ5 and SQS4 dyes desorption from the TiO_2 surface in the good solvent (chloroform) bath is provided in **Figure 6**. Procedure for the amount of squaraine dyes desorbed from the surface of TiO_2 in good solvent bath were calculated and provided in **Figure 8** and **Table 3**.
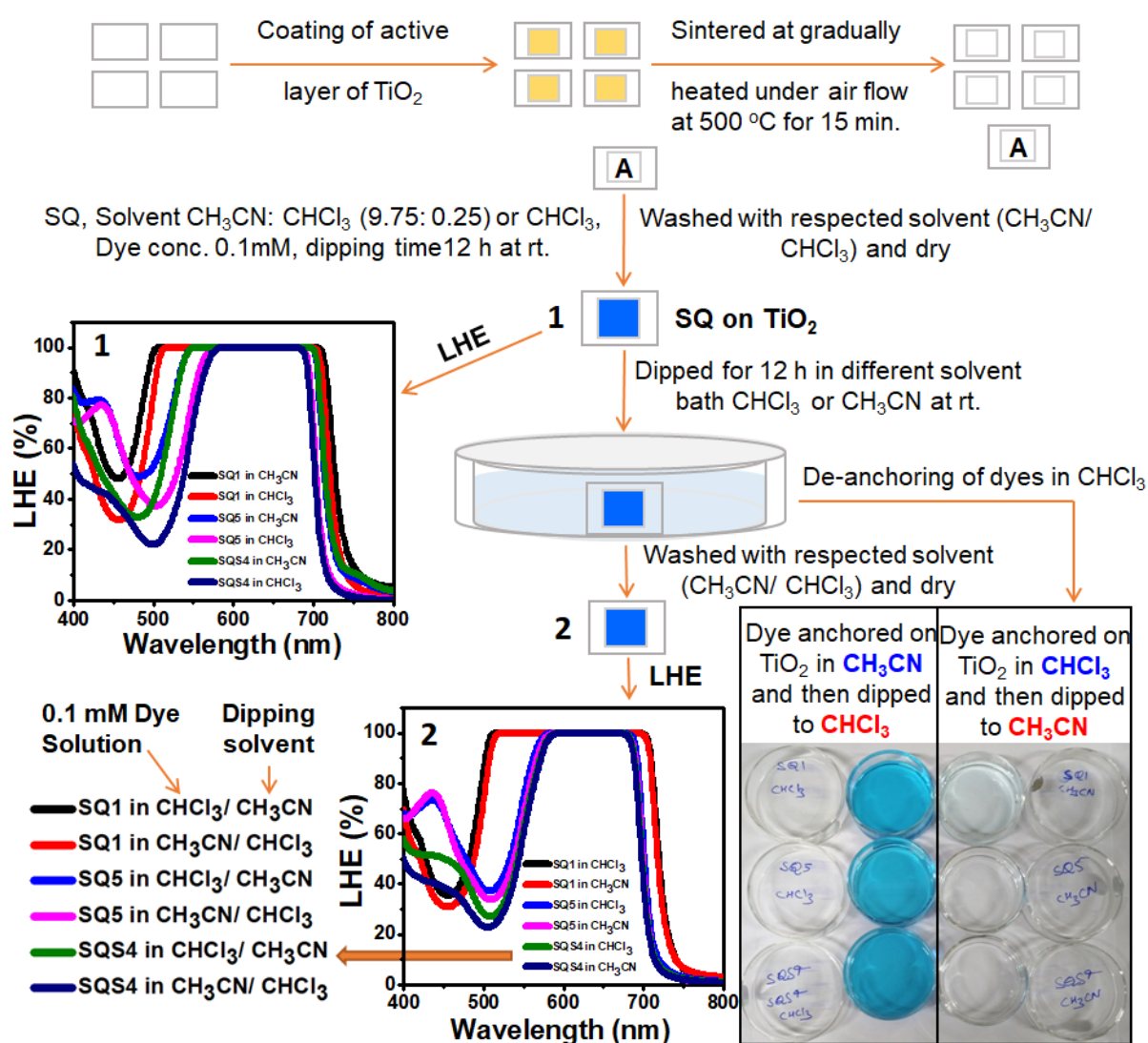
Figure 4. Procedure followed for LHE of SQ1, SQ5 and SQS4 dyes, dye solution 0.1 mM in CH_3CN and $CHCl_3$, and effect of different solvents bath.

Table 2. LHE of SQ1, SQ5 and SQS4 dyes in CH_3CN, $CHCl_3$, and opposite solvent bath.

Dyes	Dye (0.1mM) in CH_3CN line width @60% (nm)	Dye (0.1mM) in $CHCl_3$ line width @60% (nm)	CH_3CN (dye solution)/ $CHCl_3$ (solvent bath) line width @60% (nm)	$CHCl_3$ (dye solution)/ CH_3CN (solvent bath) line width @60% (nm)
SQ1	723.5-475.5 =248	718.7-489.4 =229	714.93-493.60 = 221	717.35-487.08 = 230
SQ5	710.3-509.3 =201	702.4-536.4 =166	698.00-543.95 = 154	699.61-540.22 = 159
SQS4	712.1-516.5 =194	699.4-544.2 =155	695.58-549.54 = 146	696.39-547.68 = 149
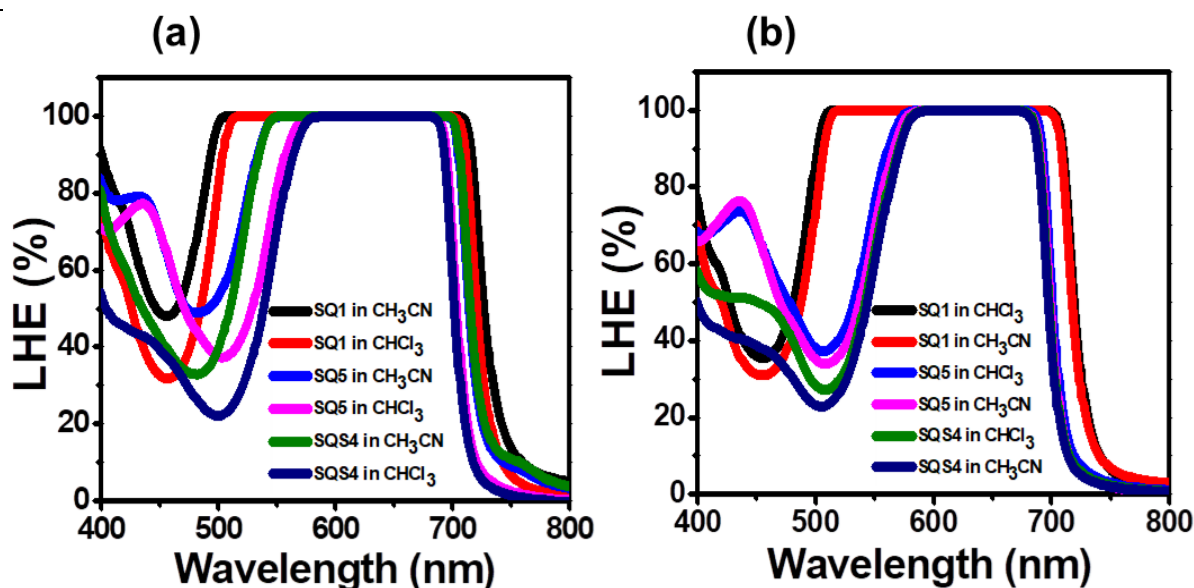
Figure 5. (a) LHE profile of squaraine dyes (dye solution 0.1 mM in CH_3CN or $CHCl_3$ dipping time 12 h at room temperature), and (b) LHE profile of squaraine dyes where electrodes was first dipped in dye solution (dye solution 0.1 mM in CH_3CN or $CHCl_3$) for 12 h at room temperature, then immediately immersed in opposite solvent bath for 12 h at room temperature.

Further, to understand the dyes desorbed in the good solvent bath was anchored onto the TiO_2 surface or only laterally interact (physisorbed) with the dyes anchored onto the TiO_2 surface, IR study of the SQ1, SQ5 and SQS4 dyes have been done as such and dyes anchored onto the TiO_2 surface into the good and bad solvent systems (**Figure 7**). The amount of SQ1 dye desorbed from the surface of the TiO_2 in the good solvent bath is 0.25×10^{-7} mol cm^{-2} more than the

amount of dyes desorbed (in 0.2 M ethanolic NaOH) from the surface of TiO_2 where dye were sensitized into good solvent systems (**Table 2**, and **6**). The carbonyl peak of carboxylic acid at 1698 cm^{-1} was disappeared for SQ1 dye (where dye anchored onto the surface of TiO_2 surface in good solvent systems), clearly tells there is no physisorbed dyes present onto the surface of TiO_2, because of amount of SQ1 dye desorbed from the surface of the TiO_2 in the good solvent bath more than that of the amount of dyes desorbed during desorption studies (in 0.2 M ethanolic NaOH) where dye sensitized into good solvent systems (**Table 2**, and **6**).
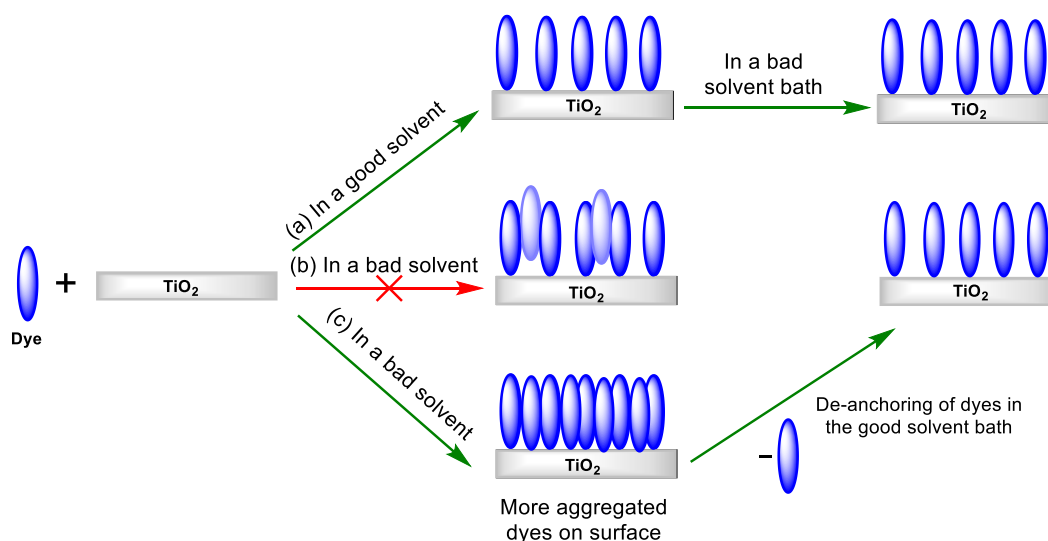
Figure 6. Proposed hypothesis for SQ1, SQ5 and SQS4 dyes desorption from the TiO_2 surface in the good solvent (chloroform) bath.
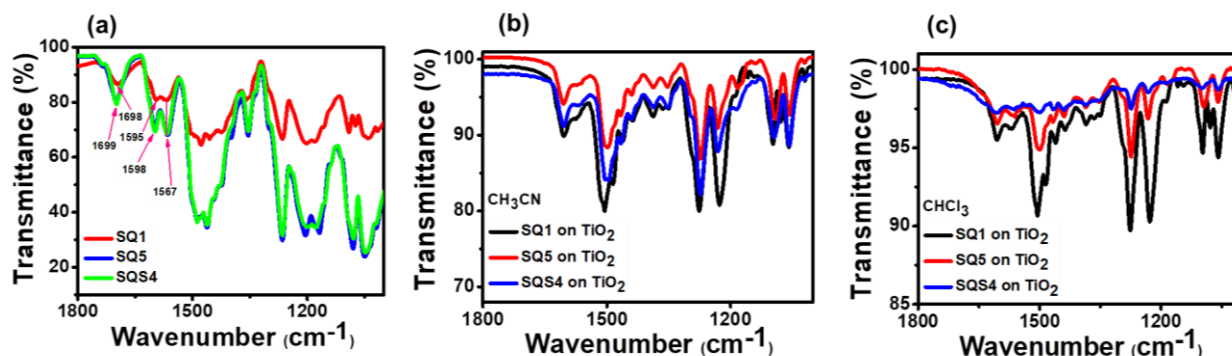
Figure 7. (a) FTIR spectrum of squaraine dyes, (b), and (c) squaraine dyes onto the TiO_2 surface, where dye stock solution 0.1 mM in CH_3CN, and $CHCl_3$, respectively and dipping time was 12 h at room temperature.

Figure 8. Procedure followed to study the dyes desorbed from the TiO$_2$ surface.

Table 3. Desorbed squaraine dyes from TiO$_2$ surface in good solvent bath (CHCl$_3$).

Cell	ε (M^{-1} cm^{-1})	Dye Loading on TiO$_2$ (mol/cm^{2}cm)
SQ1	1.4×10^5	2.30×10^{-7}
SQ5	2.1×10^5	1.46×10^{-7}
SQS4	3.4×10^5	0.96×10^{-7}

5.A.3.2 Photovoltaic performance. The photovoltaic performance of SQ1, SQ5 and SQS4 dyes have been carried out into two different solvent systems to examine the effect of solvents onto the dye aggregations and device performances. The photovoltaic studies of SQ1, SQ5 and SQS4 dyes in different solvent systems, in the absence and presence of CDCA (chenodeoxycholic acid) have been provided in the **Figure 9,** and **Table 4**. There is no significant change in aggregations of dyes onto the surface of TiO$_2$ and efficiencies observed when SQ1 dye fabricated into the good or bad solvents, whereas the introduction of hydrophobic alkyl groups cause the narrowing down the IPCE curve to dimer for SQ5 dye and finally more monomeric and less dimeric response observed for SQS4 dye in good solvents, results aggregation of dyes onto the surface of TiO$_2$ broken and efficiencies of DSSC deceases drastically. Further addition of coadsorbent (CDCA) broken the aggregation of dyes onto the surface of TiO$_2$ and only monomeric IPCE responses observed for all the three dyes when the device fabricated in good solvents system. SQ5 and SQS4 dyes are forming well packed aggregated structures in the bad solvent systems and results better IPCE performance compare to SQ1 dye in the absence of CDCA, further addition of coadsorbent (CDCA) improves the IPCE responses for all the three dyes. Length of

hydrophobic alkyl groups showed an impressive V_{OC} and J_{SC} values in the bad solvent systems due to better passivation of photoanode and controlled aggregation onto the surface of TiO_2, whereas low V_{OC} and J_{SC} values in the good solvent systems, because loading of dyes are less than the bad solvent systems for all the dyes (**Table 6**).
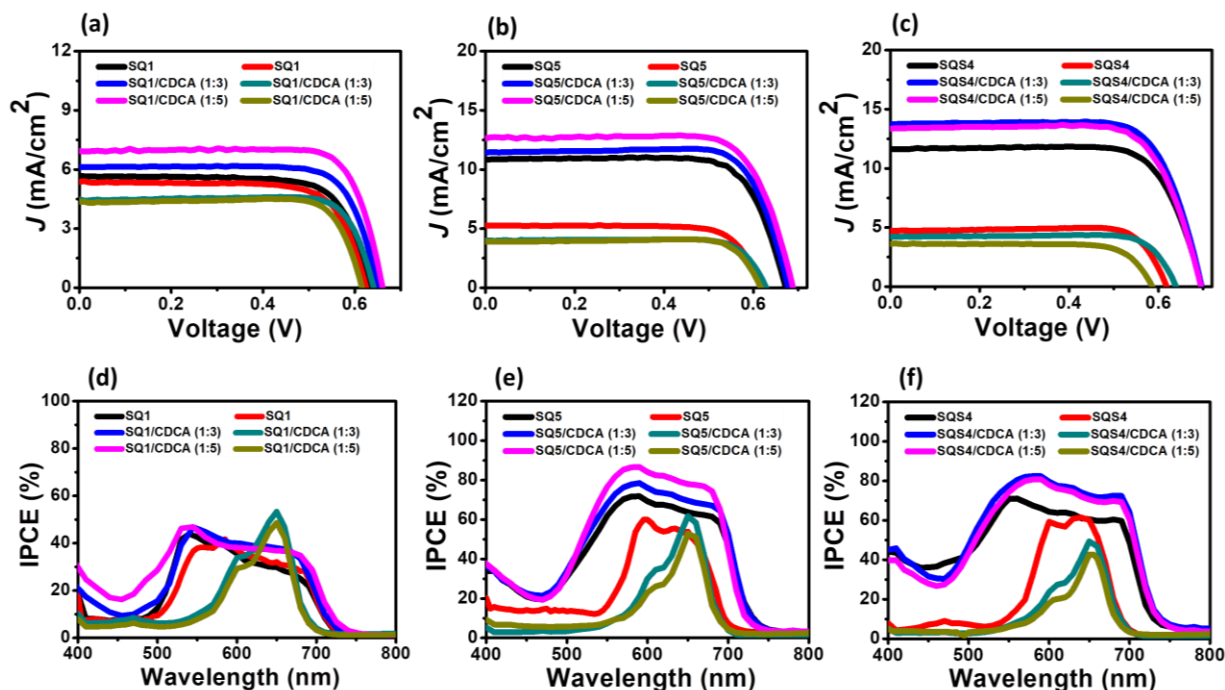
Figure 9. (a), (b), (c) *J-V* curve and (d), (e), (f) IPCE response of SQ1, SQ5 and SQS4 dyes under AM 1.5 G illumination (1000 W/m^2), respectively. Squaraine dyes in CH$_3$CN (black, blue, and magenta lines), and squaraine dyes in CHCl$_3$ (red, dark cray, and dark yellow lines), respectively.

Squaraine dyes showed the enhanced V_{OC} and J_{SC} values upon addition of CDCA in bad solvent systems, whereas decreased drastically in good solvent systems. SQ1, SQ5 and SQS4 dyes showed V_{OC} 0.642, 675, and 0.699 V, and J_{SC} 6.38, 11.1 and 11.69 mA/cm^2, which are further improved by increasing the concentration of CDCA and showed V_{OC} 0.667, 691, and 0.701 V, and J_{SC} 7.14, 12.71 and 13.82 mA/cm^2, respectively in the good solvent systems. The maximum efficiencies achieved by device fabricated in good solvent systems are 2.71, 2.59 and 2.56% without CDCA, whereas bad solvent systems gave an impressive result in efficiency of 3.79, 6.67, and 7.29% with CDCA for SQ1, SQ5, and SQS4 dyes respectively.

Table 4. Photovoltaic performance of SQ1, SQ5 and SQS4 dyes in CH_3CN and $CHCl_3$.

[a]Dyes	CDCA (mM)	V_{OC} (V)	J_{SC} (mA/cm^2)	ff (%)	η (%)
SQ1[b]	0	0.625 ± 0.005	5.37 ± 0.48	73 ± 0.71	2.43 ± 0.28
SQ1[c]	0	0.638 ± 0.004	5.66 ± 0.72	73 ± 0.38	2.61 ± 0.39
SQ1[b]	0.3	0.641 ± 0.002	4.48 ± 0.22	81 ± 0.83	2.34 ± 0.13
SQ1[c]	0.3	0.651 ± 0.004	6.12 ± 0.61	77 ± 0.59	3.07 ± 0.35
SQ1[b]	0.5	0.616 ± 0.005	4.37 ± 0.21	82 ± 0.21	2.20 ± 0.14
SQ1[c]	0.5	0.661 ± 0.007	6.94 ± 0.20	79 ± 0.44	3.62 ± 0.17
SQ5[b]	0	0.618 ± 0.002	5.25 ± 0.23	76 ± 0.18	2.45 ± 0.14
SQ5[c]	0	0.672 ± 0.003	10.81 ± 0.29	76 ± 0.33	5.43 ± 0.20
SQ5[b]	0.3	0.629 ± 0.006	4.0 ± 0.43	80 ± 0.11	2.05 ± 0.20
SQ5[c]	0.3	0.679 ± 0.001	11.43 ± 0.18	78 ± 0.62	6.13 ± 0.15
SQ5[b]	0.5	0.617 ± 0.002	3.9 ± 0.48	84 ± 0.19	2.03 ± 0.25
SQ5[c]	0.5	0.689 ± 0.002	12.62 ± 0.09	76 ± 0.43	6.56 ± 0.11
SQS4[b]	0	0.619 ± 0.013	4.72 ± 0. 12	83 ± 0.60	2.48 ± 0.08
SQS4[c]	0	0.696 ± 0.003	11.66 ± 0.03	75 ± 0.78	6.02 ± 0.11
SQS4[b]	0.3	0.640 ± 0.008	4.21 ± 0.38	82 ± 0.37	2.20 ± 0.25
SQS4[c]	0.3	0.697 ± 0.004	13.74 ± 0.08	75 ± 0.23	7.18 ± 0.11
SQS4[b]	0.5	0.586 ± 0.011	3.61 ± 0.14	76 ± 0.91	1.62 ± 0.10
SQS4[c]	0.5	0.696 ±0.001	13.36 ± 0.1	74 ± 0.28	6.93 ± 0.09

[a]thickness of TiO_2 8 + 4 μm, area 0.23 cm^2, [Dye] = 0.1 mM in [b]$CHCl_3$ or [c]CH_3CN: $CHCl_3$ (9.75: 0.25%), dipping time 12 h at rt, Electrolyte: Iodolyte Z-50 (Solaronix).
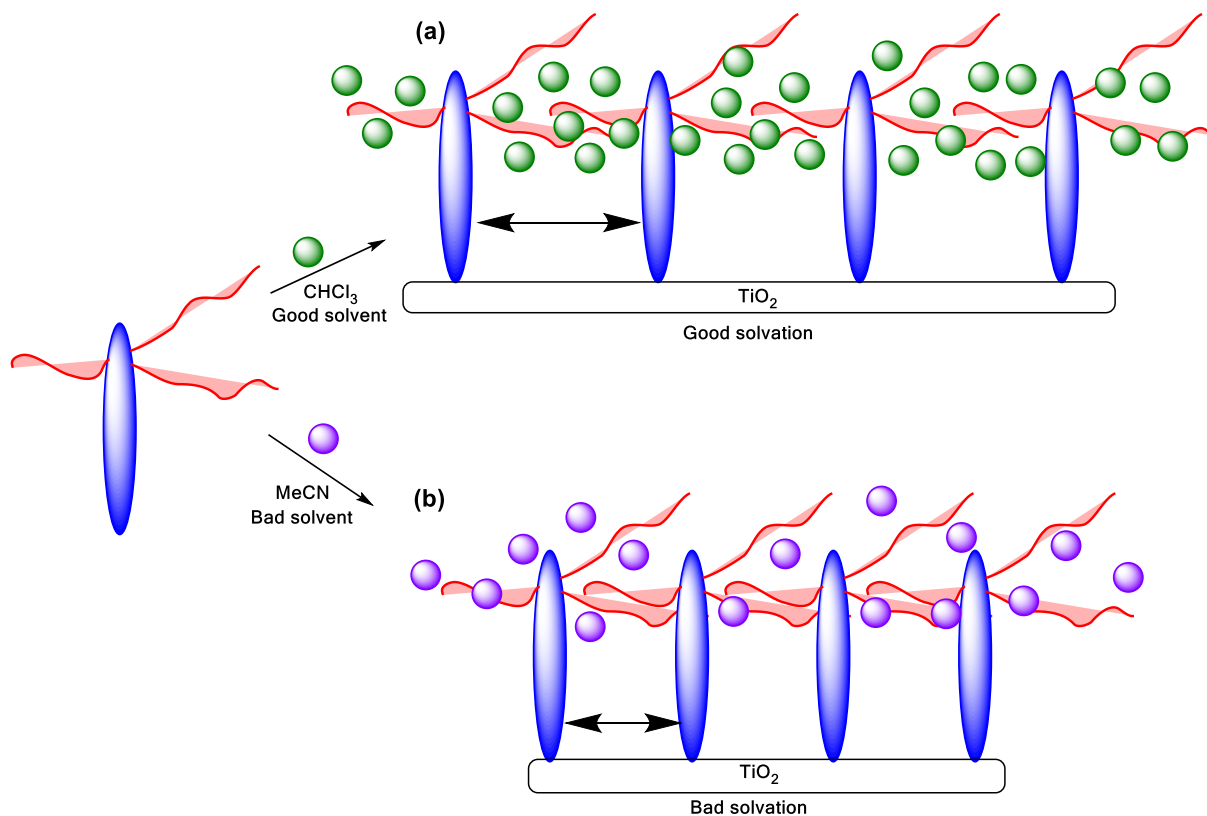
Figure 10. Effect of different solvent system on the solvation of dyes, and dye aggregation on the TiO$_2$ surface.

The efficiency difference obtained in the good and bad solvent systems is because of the change in the dye adsorption geometry due to the different interaction and the electronic coupling between the dye and TiO$_2$.[29,30] The different solvents are responsible for the different interaction between the dye molecules and alkyl groups due to change in the dielectric constant.[21] Such a low DSSC efficiency of squaraine dyes in the good solvent systems because of long hydrophobic alkyl groups are favored to formed nonpolar-nonpolar interactions between the chloroform and hydrophobic alkyl groups (good solvation) that not favorably allow to form dye aggregates onto the surface of TiO$_2$ (**Figure 10a**) and results, poor IPCE response of the dyes as well as poor device efficiencies. Whereas, the high DSSC efficiency of squaraine dyes in the bad solvent systems observed because of favorable nonpolar-nonpolar interactions between the long hydrophobic alkyl groups that partially soluble in the acetonitrile (**Figure 10b**) and favors the

formation of dye aggregates onto the surface of TiO_2 and result enhanced IPCE response of the dyes as well as high device efficiencies.

5.A.3.3 Electrochemical impedance spectroscopy (EIS).

EIS analysis for SQ1, SQ5 and SQS4 dyes in different solvent systems was carried out with various applied bias in the dark, and the frequency ranges from 1 Hz to 1 MHz to study the EIS parameters at the TiO_2/dye/electrolyte interfaces (**Figure 11**, **12** and **13**).[31] Nyquist plot of dyes SQ1, SQ5 and SQS4 in good and bad solvent systems at applied bias 0.4 V without CDCA is provided in **Figure 14a**. Charge recombination resistance (R_{ct}) values for the SQ1, SQ5, and SQS4 dyes increases by increasing the concentration CDCA with the bad solvent systems and decreases with the good solvent systems respectively. Chemical capacitance ($C\mu$) and lifetime of electron (τ) values for SQ1 dye increases by increasing the concentration CDCA with the bad solvent systems and decreases with the good solvent systems respectively, whereas in case of SQ5 and SQS4 dyes $C\mu$ and τ values increases by increasing the concentration CDCA whether solvent systems are bad or good for device fabrication. Optimized EIS parameters of squaraine dyes with and without CDCA in good and bad solvent systems are provided in **Figure 14** and **Table 5**. The order of R_{ct} values for SQ1, SQ5 and SQS4 dyes without CDCA at 0.52 V applied bias is 6.37< 7.58< 7.77 ohm which is increased by increasing the concentration CDCA 7.45< 9.60< 11.18 ohm respectively, which is corresponds to increased electron lifetime and device efficiencies in bad solvent systems, because of long electron lifetime into TiO_2 CB responsible for enhanced V_{OC} and J_{SC} values respectively.
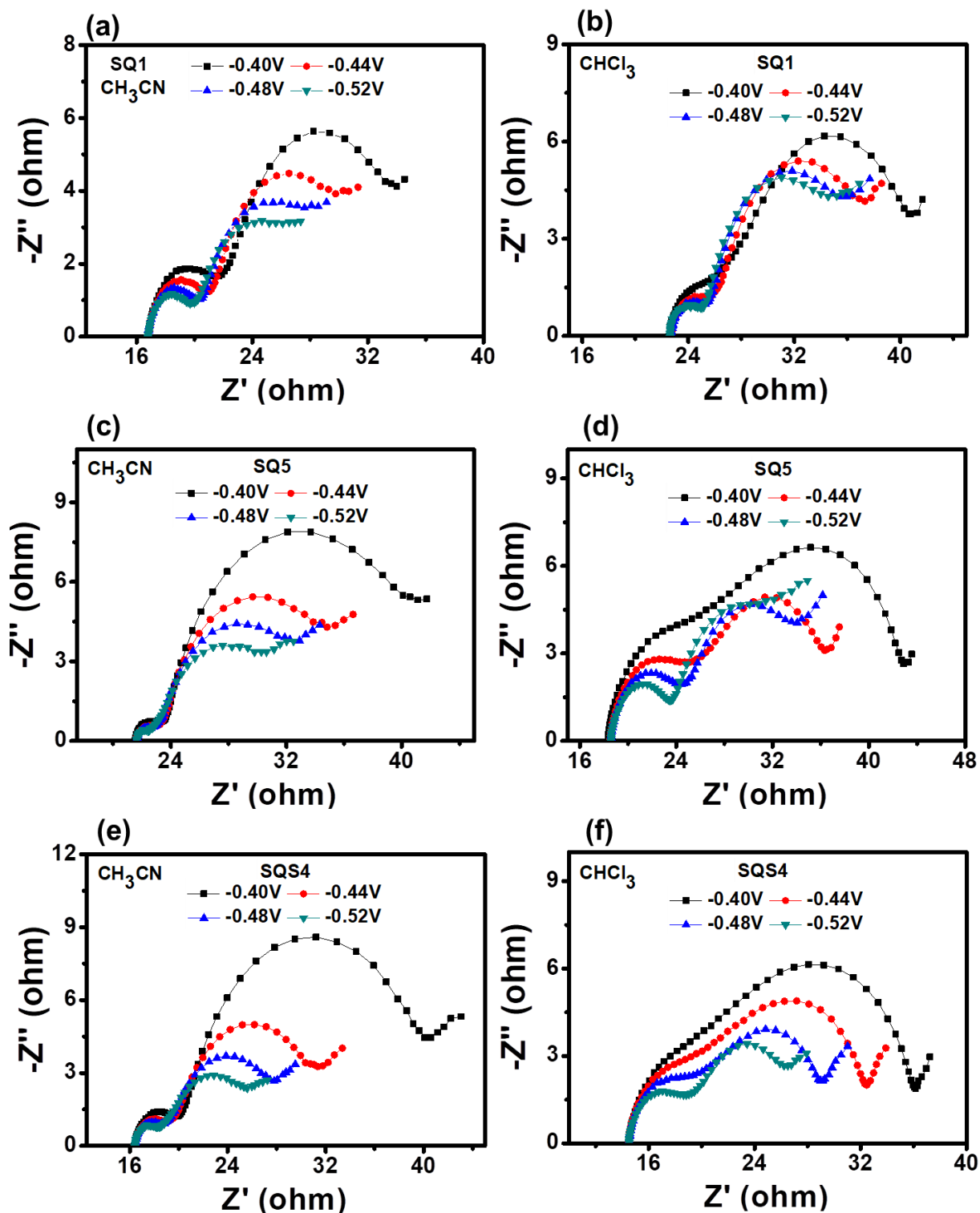
Figure 11. Nyquist plots of squaraine dyes (a), (c), (e) in CH_3CN, and (b), (d), (f) in $CHCl_3$, respectively.
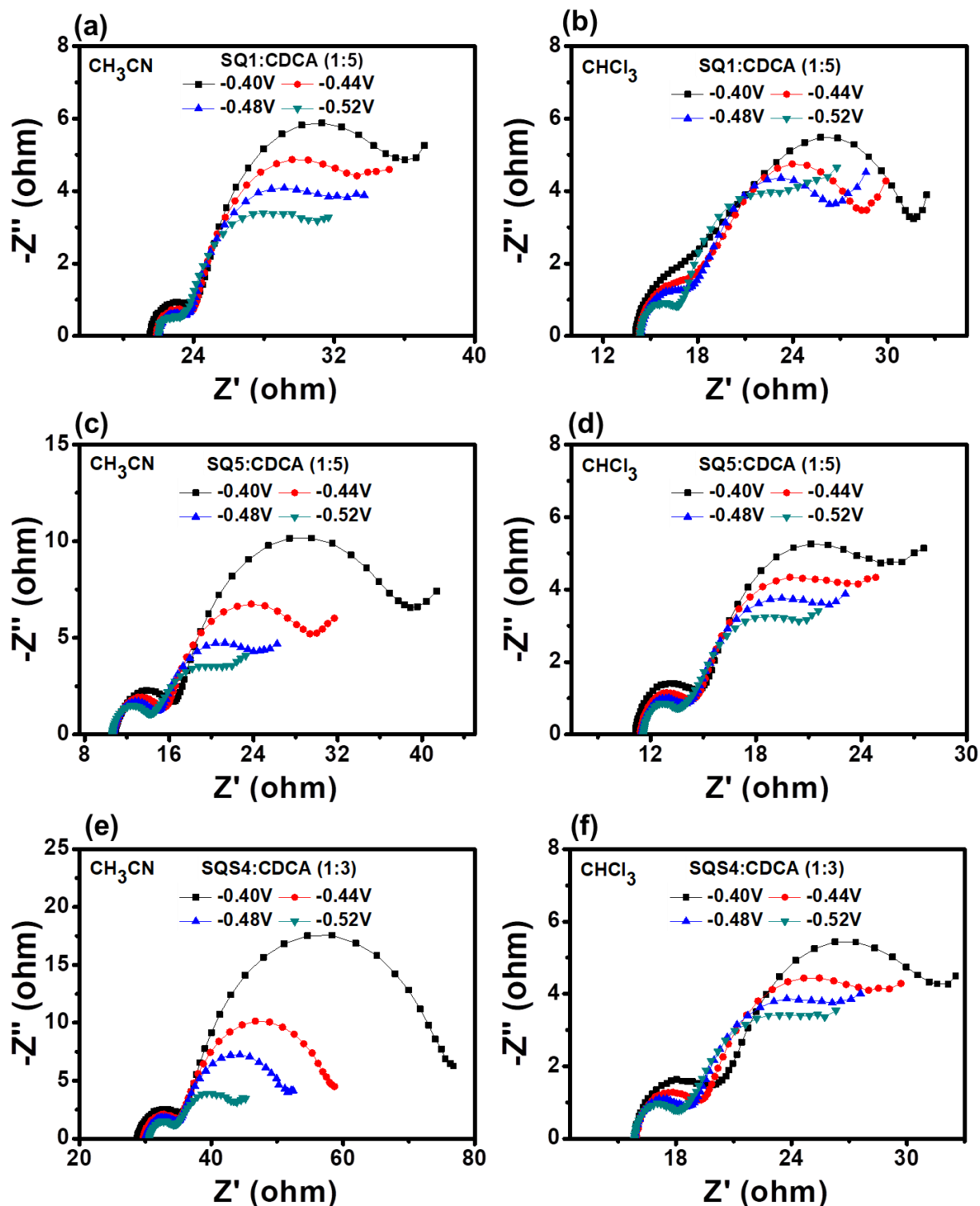
Figure 12. Nyquist plots of squaraine dyes (a), (c), (e) in CH_3CN, and (b), (d), (f) in $CHCl_3$ with CDCA, respectively.
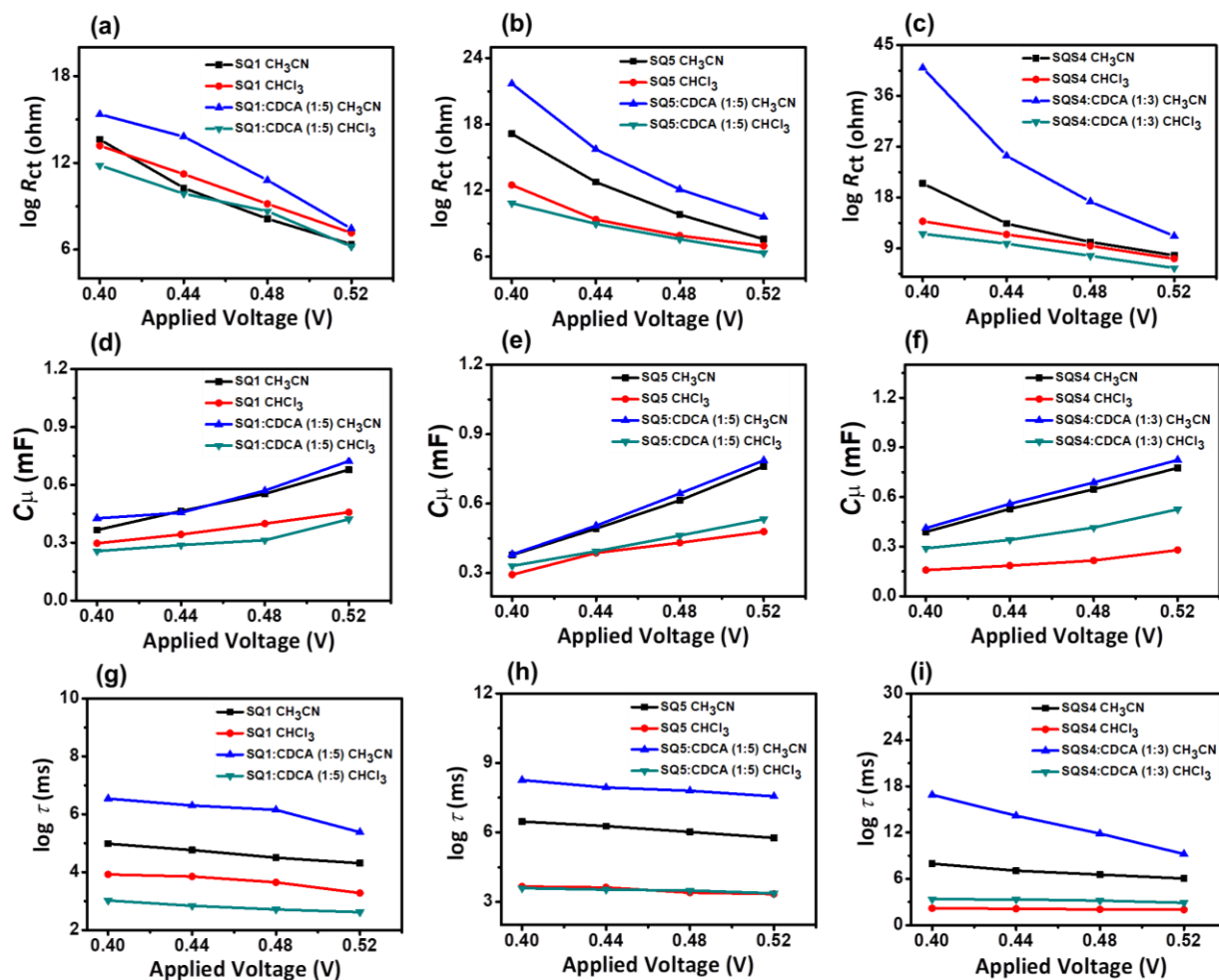
Figure 13. (a), (b), (c) charge recombination resistance, (d), (e), (f) chemical capacitance, and (g), (h), (i) life time of squaraine dyes in CH_3CN and $CHCl_3$, with and without CDCA, respectively.
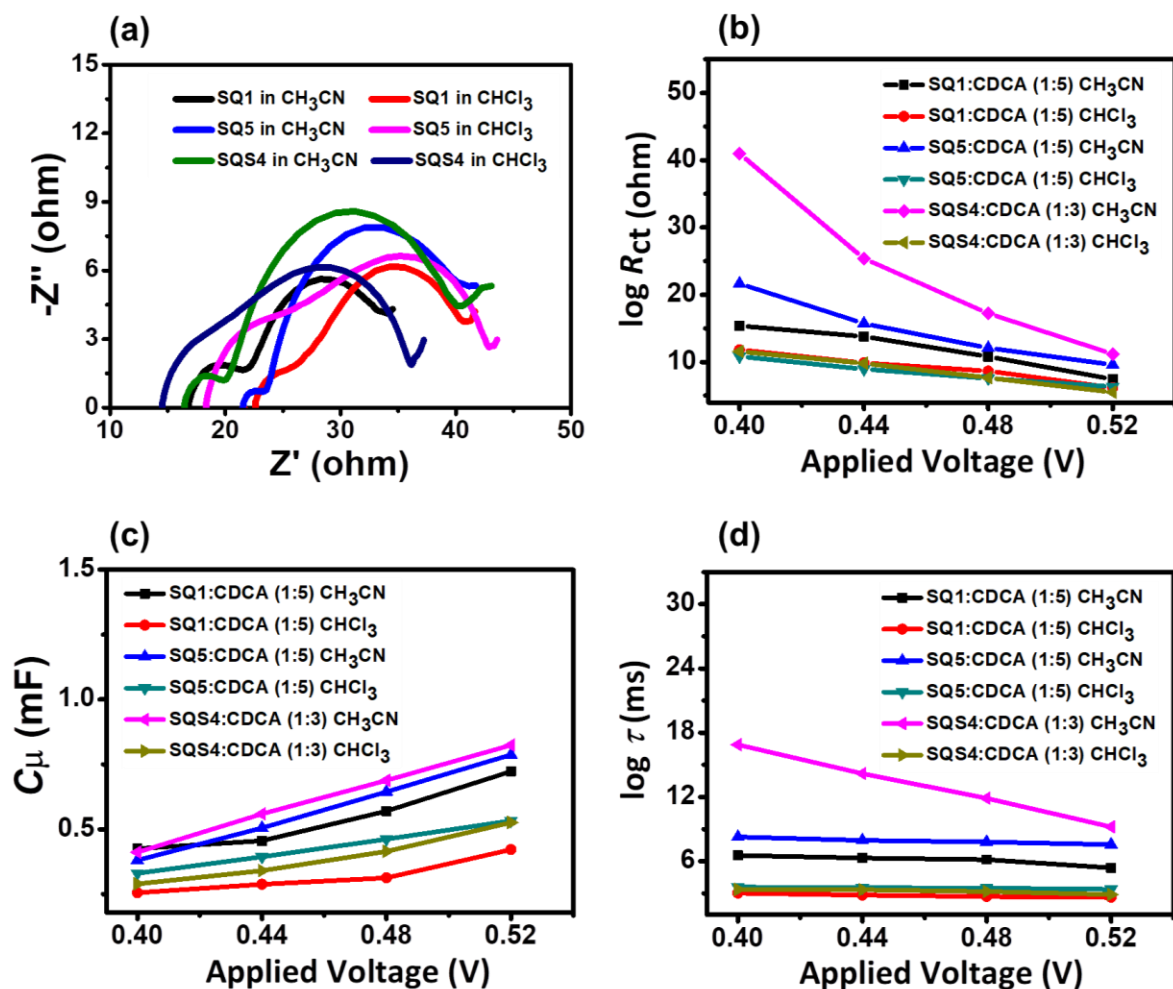
Figure 14. (a) Nyquist plot of SQ dyes in CH_3CN and $CHCl_3$ at 0.4 V applied bias without CDCA, and (b) charge recombination resistance, (c) chemical capacitance, and (d) life time of SQ dyes in CH_3CN and $CHCl_3$, optimized with CDCA, respectively.

Table 5. EIS parameter of SQ1, SQ5 and SQS4 dyes optimized with and without CDCA in CH_3CN and $CHCl_3$.

Dyes	CDCA (mM)	Applied voltage (V)	R_{ct} (ohm)	$C\mu$ (mF)	τ (ms)
SQ1	0	0.52	6.37	0.678	4.31
[a]SQ1	0	0.52	7.16	0.458	3.28
SQ1	0.5	0.52	7.45	0.723	5.38
[a]SQ1	0.5	0.52	6.22	0.422	2.62
SQ5	0	0.52	7.58	0.761	5.76
[a]SQ5	0	0.52	6.97	0.479	3.34
SQ5	0.5	0.52	9.60	0.787	7.56
[a]SQ5	0.5	0.52	6.32	0.533	3.37
SQS4	0	0.52	7.77	0.776	6.03
[a]SQS4	0	0.52	7.17	0.279	2.00
SQS4	0.3	0.52	11.18	0.824	9.21
[a]SQS4	0.3	0.52	5.52	0.526	2.90

[a]$CHCl_3$.

5.B.3.4 Dye-desorption studies of squaraine dyes. For dye desorption studies of squaraine dyes area of the photoanode was 0.23 cm^2 with the thickness of 8 μm. Photoanode was dipped into the 0.1 mM in the CH_3CN or $CHCl_3$ of dye stock solution for 12 h at room temperature, further 0.2 M NaOH in EtOH: H_2O (1:1) was used to desorb adsorbed dyes from the TiO_2 surface. Results obtained from the desorption studies of dye from TiO_2 surface is provided in the **Table 6**, where path length of the cuvette was 0.01 cm^2.

Table 6. Desorbed squaraine dyes from TiO_2 surface with and without CDCA in good and bad solvent systems.

Cell[a]	CDCA (mM)	A_{max}	ε (10^5 M^{-1} cm^{-1})	Dye Loading on TiO_2 (10^{-7} mol/cm^2)
SQ1[b]	0	0.5925	1.4	3.680
SQ1[c]	0	0.3308	1.4	2.050
SQ1[b]	0.3	0.3322	1.4	2.060
SQ1[c]	0.3	0.1223	1.4	0.759
SQ1[b]	0.5	0.2776	1.4	1.720
SQ1[c]	0.5	0.0779	1.4	0.484
SQ5[b]	0	0.5364	2.1	2.220
SQ5[c]	0	0.1849	2.1	0.765
SQ5[b]	0.3	0.2555	2.1	1.060
SQ5[c]	0.3	0.0477	2.1	0.197
SQ5[b]	0.5	0.2308	2.1	0.956
SQ5[c]	0.5	0.0449	2.1	0.186
SQS4[b]	0	0.4291	3.4	1.100
SQS4[c]	0	0.1083	3.4	0.277
SQS4[b]	0.3	0.2344	3.4	0.600
SQS4[c]	0.3	0.0347	3.4	0.0887
SQS4[b]	0.5	0.2183	3.4	0.558
SQS4[c]	0.5	0.0252	3.4	0.0645

[a]thickness of TiO_2 8 μm, area 0.23 cm^2, [Dye] = 0.1 mM in [b]CH_3CN: $CHCl_3$ (9.75: 0.25) or [c]$CHCl_3$, dipping time 12 h, at room temperature squaraine dyes was desorbed in 0.2 M NaOH solution in EtOH: H_2O (1:1), path-length of cuvette 1mm (0.01 cm^2).

5.A.4 CONCLUSION

Dye-sensitized solar cells efficiencies of the unsymmetrical squaraine dyes SQ1, SQ5, and SQS4 were carried out to find the effect of the bad solvent (acetonitrile) and good solvent (chloroform) systems on the photovoltaic properties with iodolyte (I^-/I_3^-). Device fabricated in bad solvent systems showed excellent J_{SC} and V_{OC} values compare to device fabricated in the good solvent systems for all the unsymmetrical squaraine dyes. Device fabricated for SQ1, SQ5 and SQS4 dyes in bad showed an excellent values of V_{OC} = 642, 675 and 699 mV, J_{SC} = 6.38, 11.1 and 11.69 mA/cm^2, device efficiency 3.0, 5.63 and 6.13% in the absence of CDCA, respectively, and device efficiencies was further improved to 3.79, 6.67, and 7.29% by increasing the concentration of CDCA. Device fabricated for SQ1, SQ5 and SQS4 dyes in good solvent system showed low device efficiency of 2.71, 2.59 and 2.56% without CDCA and further addition of CDCA decreases the device efficiency to 2.34, 2.28 and 1.72% respectively. Device efficiency 7.29% is the highest efficiency achieved with CDCA in bad solvent systems by the SQS4 dye, and 2.71% is the highest achieved device efficiency without CDCA in good solvent systems by the SQ1 dye respectively. From the above obtained results, bad solvent (acetonitrile) systems used for the fabrication of device were demonstrated as superior solvent systems to achieve the high device efficiencies for NIR-light active unsymmetrical squaraine dyes.

5.B Effect of Iodine Cobalt and Copper-Based Electrolytes on the Dye-Sensitized Solar Cells Performance of NIR Active Unsymmetrical Squaraine Dyes

5.B.1 INTRODUCTION

DSSC efficiencies synergistically improved by the improvement in the values of short-circuit current (J_{SC}), open-circuit voltage (V_{OC}), and fill factor (*ff*). Device J_{SC} can be enhanced by broad-light absorption,[32] co-sensitization,[33] controlled-aggregation,[5,6] lifetime of the electrons injected into the conduction band of TiO_2, whereas device V_{OC} can be enhanced by avoiding interfacial charge recombination,[2,4] positive-dipole of sensitizers corresponds to the TiO_2 surface.[34] Interfacial charge recombination is one of the major detrimental factors in DSSC, that lowered the values of J_{SC} and V_{OC} by inner and outer path recombination respectively, which can be controlled by the introducing the alkyl groups in dyes.[2,4-6] Electrolyte is the second important and indispensable component of the DSSCs, that playing vital role in the dye regeneration, and charge carrier at the time of DSSC operation.[4] Photovoltaic parameters and device stability are largely influenced by the electrolytes used for the DSSC by the interfacial interactions between electrodes and electrolytes. Electrolyte redox potential influences the V_{OC}, redox species transport influences J_{SC}, whereas, conductivity and interfacial resistance between electrodes and electrolyte influences the *ff* values of the DSSC.[4] Iodine-based electrolytes are well-explored and frequently used for DSSC due to the low cost, stable for long-time, high rate of diffusion, and fast dye regenerating behavior at the working time of the DSSC.[2,4] Iodine based electrolytes are corrosive towards the sealing components, and required at least 500 mV over potential for sensitizer regeneration. To, overcome the limitations of iodine-based electrolytes, bromine,[35] organic,[36] and pseudohalogen[37] based electrolytes have been investigated as an electrolyte for the DSSC applications. Further, cobalt based electrolytes are well explored due to its modular nature in redox potential and good alternative to substitute the iodolytes due to non-corrosive towards the sealing components, and requires ~ 250 mV over potential for the sensitizer regeneration. Recently, copper-based electrolytes were demonstrated as a rapid electron transfer species besides the electrolytes based on iodine or cobalt.[38] Further, ferrocene[39] based electrolytes have been used to studied the DSSC efficiency. Size of the counter cations in the electrolytes were demonstrated for the change in V_{OC} and J_{SC} values, larger size of counter cations leads to high V_{OC} and low J_{SC} values due to shift in the CB of TiO_2 towards the negative potential.[40] The

expensive device cost of DSSC due to very expensive platinum based cathodes, where electron-collection and reduction of electrolytes takes place simultaneously. To make the DSSC device cost effective, various types of materials, polymers are used to substitute the platinum electrode, and it is observed that the device efficiency of platinum-free cathode are more than of platinum based cathode.[4] PEDOT deposited on the FTO substrate by electropolymerization technique is the good alternative to substitute the platinum in DSSC, and good for the copper and cobalt based electrolytes, that regenerates Co(III) complex more efficiently than the platinum.[41] PEG group present in dyes may enhanced J_{SC} by capturing of Li-ion in electrolytes near to TiO$_2$ surface. SQS4, ASQ4 dyes have been used as sensitizer, and iodine,[5] cobalt,[42] copper[43,44] have been used as an electrolyte for dye-sensitized solar cell studies. The low reorganization energy for copper-based redox couple leads to the enhancement of the V_{OC} of the DSSC device.[45] The required overpotentials for the better dye-regeneration is ~ 0.5, 0.2-0.3, and 0.1-0.2 V for iodine, cobalt, and copper-based electrolytes, respectively.[2, 18] General structures, and energy level diagrams of NIR active SQ dyes and corresponding redox-potential of electrolytes is provided in **Figure 1**.
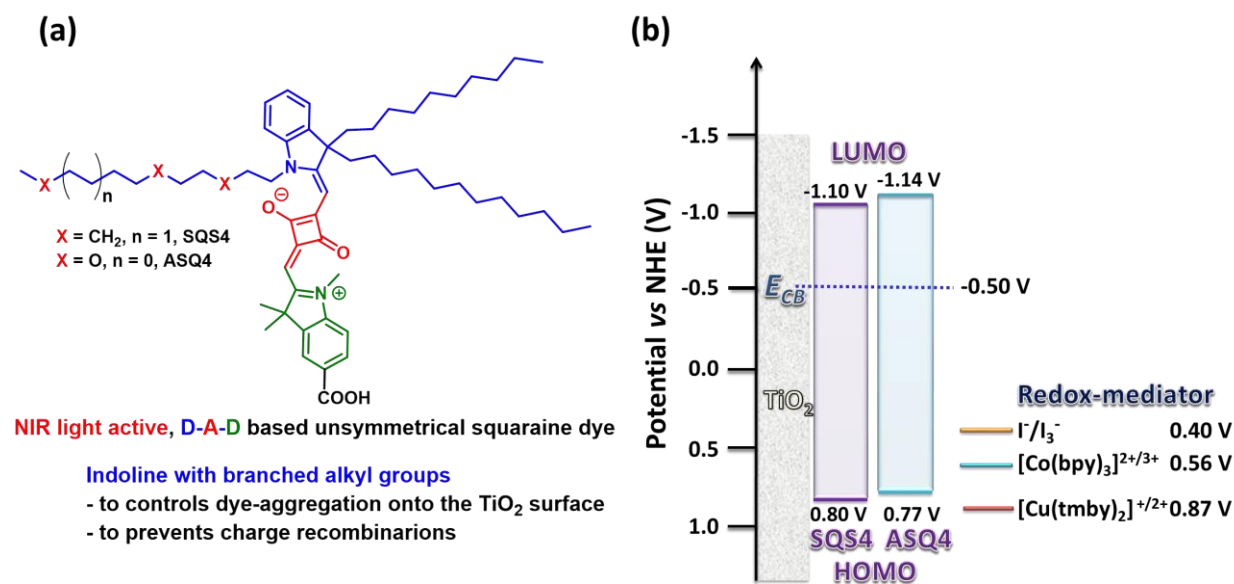
Figure 1. (a) General structure of NIR-light active SQ dyes, (b) energy level diagrams of SQ dyes, and corresponding redox-potentials of different electrolytes.

N-dodecyl group in SQS4, and N-PEG group in ASQ4 on the indoline, only the difference between these two dyes, and used for comparatively DSSC studies, due to SQS4 impressive

IPCE response in visible and NIR-regions observed by controlled aggergations.[5] Electrolytes with various redox-potential can provides the various V_{OC} and J_{CS} values. Here, acetonitrile used as solvents for the electrolyte preparation because of electrolytes prepared in the acetonitrile demonstrated as the best solvents due to solubility, stability, and low viscosity.[4]

5.B.2 EXPERIMENTAL SECTION

SQS4 dye have been synthesized by the following the literature,[5] and required chemicals for synthesis of ASQ4 dye were purchased from commercial resources. Iodine based electrolyte (Z-50) were purchased from solaronix,[5] Co(bpy)[42] and Cu(tmby)[44] based electrolytes were prepared from the procedures reported in the literature. Pt-foil and PEDOT used as a counter electrode,[46] where the thin film of PEDOT have been deposited on the clean FTO-glass by electropolymerization technique, and procedure for the DSSC fabrication is provided below.

5.B.2.1 General methods

All the required chemicals, reagents, electrolytes, solvents were purchased from commercial sources, and standard procedures are used for drying the solvents. ^1H and ^{13}C NMR were recorded on Bruker NMR spectrometers AV 400 MHz frequency, in $CDCl_3$. High-resolution mass spectrometric (HRMS) measurements were recorded on SYNAPT G2 HDM in MeOH as solvent. Absorption spectra of ASQ4 dye were recorded on SPECORD$^{®}$ 210/ PLUS, Analytikjena UV−visible spectrophotometer at room temperature. Emission ASQ4 dye was recorded on Edinburgh spectrofluorometer FS5 at room temperature. Cyclic voltammetry of ASQ4 dye were performed on BioLogic SP300 potentiostat in anhydrous dichloromethane solvent at 25 ^{o}C under inert atmosphere, where platinum wire used as a working electrode, platinum foil as a counter electrode, non-aqueous Ag/Ag^+ (0.01M) as reference electrode, $TBAClO_4$ (0.03 M) as supporting electrolyte, scan rate of 50 mV s^{-1} and Ferrocene/ Ferrocene$^+$ as the internal-standard. Electrochemical impedance measurements (EIS) were performed using a BioLogic SP300 potentiostat equipped with frequency response analyzer. EIS were carried out in dark with various applied potential and frequency ranges from 3 MHz to 10 mHz with sinus amplitude of 10 mV. Electropolymerization of PEDOT onto FTO were performed on BioLogic SP300 potentiostat at 25 ^{o}C, where cleaned FTO used as a working electrode, platinum foil as a counter electrode, non-aqueous Ag/Ag+ (0.01M) as a reference electrode. PHOTO EMISSION

TECH (PET, CT200AAA, USA) solar-simulator were used to measure the *I-V* characteristic of the dye-sensitized solar cells, whereas, Newport QE measurement kit have been used to performed the IPCE measurements. The quantum mechanical calculations were conducted using the Gaussian 09 software.[46] The optimization of the ground-state geometry was carried out at the Density Functional Theory (DFT) level, using the B3LYP hybrid functional and the 6-311G(++) atomic basis set. For dye desorption studies of SQ dyes area of the photoanode was 0.23 cm^2 (8 μm thick), dipping time of photoanode in dye-solution (0.1mM) was 12 h at room temperature, 0.2 M NaOH in EtOH: H$_2$O (1:1) 9 mL was used to desorb adsorbed dyes and path length of the cuvette was 0.1 cm^2.

5.B.2.2 DSSC fabrication, electropolymerization and electrolyte preparation.

(a) Cells fabricated for Iodolyte (I$^-$/I$_3^-$) electrolyte. FTO glass (8- 10 Ω /sq; Pilkington TEC 7) were washed with mucasol (2 % in water), de-ionized water, and isopropanol by using ultrasonic-bath to make cleaned. To grow a thin film TiO$_2$, FTO was treated with 40 mM aqueous TiCl$_4$ solution at 70 $^\circ$C for 30 min, washed with the de-ionized water and EtOH, further dried at 110 $^\circ$C for 10 min. A paste of TiO$_2$ nanocrystal (< 20 nm, Ti-Nanoxide T/SP, Solaronix) was coated on the FTO conducting side by using doctor-blade technique and kept for 15 min in the air then heated at 120 $^\circ$C in the air for 20 min, further coated with scattering layer TiO$_2$ paste (WER2-O, Dyesol) and heated at 120 $^\circ$C for 10 min in the air, then sintered at 325 $^\circ$C for 10 min, 375 $^\circ$C for 10 min, 450 $^\circ$C for 10 min and 500 $^\circ$C for 15 min, where the heating rate was 5 $^\circ$C per min in the air. After sintering, films were treated with 40 mM aqueous TiCl$_4$ solution at 70 $^\circ$C for 30 min, washed with de-ionized water then EtOH and sintered at 500 $^\circ$C for 20 min.[5]

(b) Cells fabricated for Co(II/III) and Cu(I/II) electrolytes. A paste of TiO$_2$ nanocrystal (~ 30-60 nm, Ti-Nanoxide T/SP, Solaronix) have been used as an active layer, and similar conditions has been followed as mention above. The cells were immersed (area of TiO$_2$ is 0.23 cm^2) in the 0.1 mM of SQ dyes solution for 12 h. Electroplatinised platinum foil and PEDOT coated onto FTO were used as cathode, iodolyte Z-50 (Solaronix), [Co(bpy)$_3$]$^{2+/3+}$ and [Cu(tmby)$_2$]$^{+/2+}$ were used as an electrolyte. Area of the black mask was 0.23 cm^2 and 25 μm spacer.The device performance of SQ dyes was measured under standard simulator condition (AM 1.5 G, 100 mW/cm^2).[5]

(c) Electropolymerization of PEDOT on the FTO. FTO glass (8- 10 Ω /sq; Pilkington TEC 7) were washed with mucasol (2% in water), de-ionized water, and isopropanol by using ultrasonic-bath to make cleaned. Solution for electropolymerization were prepared from a mixture of 0.01 M of 3,4-ethylenedioxythiophene (EDOT) and 0.1 M of lithium perchlorate (LiClO$_4$) in anhydrous acetonitrile by sonicating for 5 min. Electropolymerization were performed under in potentiostatic mode of chronoamperometry with 2.0 V voltage for 120 seconds, then films deposited onto FTO were washed with acetonitrile and dried.

(d) Procedure for the preparation of electrolytes. [Co(bpy)$_3$]$^{2+/3+}$ based redox couple were prepared from 0.25 M tris(2,2'-bipyridine)cobalt(II) di[bis(trifluoromethanesulfonyl)imide], 0.10 M tris(2,2'-bipyridine)cobalt(III) tris[bis(trifluoromethanesulfonyl)imide], 0.10 M Bis(trifluoromethylsulfonyl)amine lithium salt, and 0.10 M 4-*tert*-Butylpyridine in acetonitrile.[42] [Cu(tmby)$_2$]$^{+/2+}$ based redox couple were prepared from 0.20 M bis-(4,4',6,6'-tetramethyl-2,2'-bipyridine)copper(I) bis(trifluoromethanesulfonyl)imide, 0.04 M bis-(4,4',6,6'-tetramethyl-2,2'-bipyridine)copper(II) bis[bis(trifluoromethanesulfonyl)imide], 0.10 M Bis(trifluoromethylsulfonyl)amine lithium salt, and 0.60 M 4-*tert*-Butylpyridine in acetonitrile.[44]

5.B.2.3 Synthesis
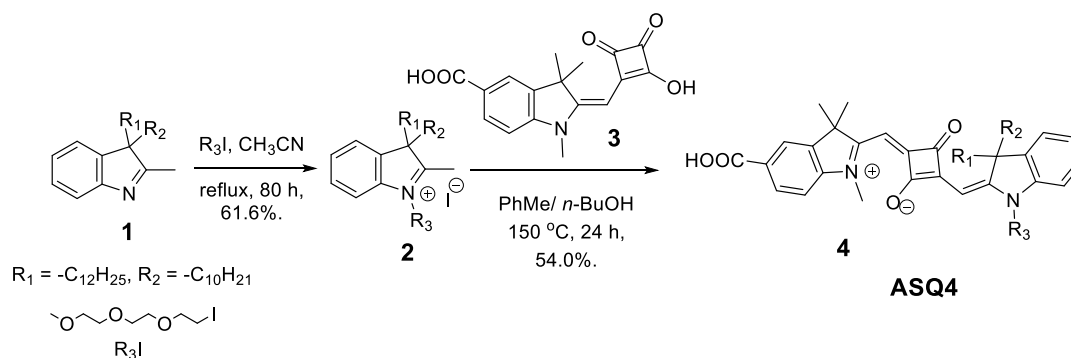
Scheme 1. Synthetic scheme of ASQ4 dye.

3-decyl-3-dodecyl-1-(2-(2-(2-methoxyethoxy)ethoxy)ethyl)-2-methyl-3H-indol-1-ium iodide (2): Compound **1** (0.250 g, 0.5685 mmol) and 1-iodo-2-(2-(2-methoxyethoxy) ethoxy) ethane (0.312 g, 1.137 mmol) were dissolved in 5 mL of CH$_3$CN and refluxed under inert atmosphere for 80 h. The reaction mixture was cooled to room temperature; solvents were removed under reduced pressure and washed with hexane (4 × 5 mL) to afford the required compound as a

brown-red viscous liquid **2**. Yield: 230 mg, 61.6%. ^{1}H NMR (CDCl$_3$, 400 MHz): δ 8.11 (d, *J* = 8 Hz, 1H), 7.67-7.59 (m, 2H), 7.49 (d, *J* = 8 Hz, 1H), 5.17 (t, *J* = 4 Hz, 2H), 4.10 (t, *J* = 4 Hz, 2H), 3.59-3.50 (m, 8H), 3.37 (s, 3H), 3.01 (s, 3H), 2.20-1.99 (m, 4H), 1.23-1.12 (m, 32H), 0.88-0.84 (m, 8H), 0.63-0.54 (m, 2H); ^{13}CNMR (CDCl$_3$, 100 MHz): δ 197.73, 142.13, 138.48, 129.94, 129.83, 123.27, 116.32, 71.88, 70.32, 70.21, 67.83, 63.96, 58.99, 50.80, 37.53, 31.89, 31.83, 29.59, 29.49, 29.44, 29.31, 29.23, 29.04, 23.73, 22.67, 22.63, 16.44, 14.12; HRMS (m/z):[M]$^+$ calcd for C$_{38}$H$_{68}$NO$_3$: 586.5194; found: 586.5196.

2-((-5-carboxy-1,3,3-trimethylindolin-2-ylidene)methyl)-4-((3-decyl-3-dodecyl-1-(2-(2-(2-methoxyethoxy)ethoxy)ethyl)-3H-indol-1-ium-2-yl)methylene)-3-oxocyclobut-1-en-1-olate (4): Compound **2** (0.180 g, 0.2521 mmol), and **3**[5] (0.079 g, 0.2521 mmol) were dissolved in anhydrous PhMe and *n*-BuOH (1:1, 10 mL of each), and reaction was refluxed in Dean-Stark apparatus for 24 h under inert atmosphere. The reaction mixture was purified by column chromatography (SiO$_2$, 100-200 mesh, 4-6% MeOH, and 96-94% CH$_2$Cl$_2$). Yield: 120 mg, 54 %. ^{1}H NMR (CDCl$_3$, 400 MHz): δ 8.14 (d, *J* = 8 Hz, 1H), 8.08 (s, 1H), 7.31 (m, 2H), 7.21 (m, 2H), 6.99 (d, *J* = 8 Hz, 1H), 6.23 (s, 1H), 6.02 (s, 1H), 4.37 (b, 2H), 3.87 (b, 2H), 3.53-3.48 (m, 11H), 3.36 (s, 3H), 3.03 (b, 2H), 2.02 (m, 2H), 1.85 (s, 6H), 1.23-1.05 (m, 32H), 0.86-0.75 (m, 8H), 0.52-0.46 (b, 2H); ^{13}C NMR (CDCl$_3$, 100 MHz): δ 181.56, 176.45, 171.21, 170.10, 168.96, 147.19, 144.53, 141.79, 138.93, 131.09, 127.67, 124.82, 124.56, 123.91, 122.07, 110.89, 108.09, 88.51, 88.04, 71.85, 71.04, 70.55, 70.46, 68.18, 59.32, 59.02, 48.29, 40.05, 31.88, 31.85, 30.49, 29.60, 29.51, 29.48, 29.30, 29.25, 27.26, 23.97, 22.65, 22.61, 14.10 ; HRMS (m/z): [M+H]$^+$ calcd for C$_{55}$H$_{81}$N$_2$O$_7$: 881.6038; found: 881.6020.

5.B.3 RESULTS AND DISCUSSION

5.A.3.1 Synthesis of Un-symmetrical amphiphilic squaraine dye. Un-symmetrical amphiphilic squaraine dyes were synthesized by condensation of semi-squaric acid and TEG-indolium. Compound **1** reacted with 1-iodo-TEG to afford the TEG-indolium salt **2**, indolium salts are further condensed with semi-sqauric acid **3** under reflux reaction condition in Dean-Stark trap in the presence of 1:1 ratio of toluene: n-BuOH to afford the final un-symmetrical amphiphilic squaraine dye **4**.

5.B.3.2 Photophysical and electrochemical properties. ASQ4 dye showed instance absorption at 644 ($\varepsilon = 3.5 \times 10^5$ M^{-1}cm^{-1}), and emission at 653 nm with the very short stock-shift (**Figure 2a**) in CH$_2$Cl$_2$. E_{HOMO} of ASQ4 dye were calculated from cyclic voltammograms first oxidation onset (**Figure 2b** and **Table 1**), and E_{LUMO} by subtracting the E_{HOMO} with optical band-gap. Slight difference in photophysical and electrochemical properties of ASQ4 and SQS4 dyes is noted. The HOMO energy levels of SQS4 and ASQ4 dyes are well matches with the redox-potential of the iodine and cobalt-based electrolytes with 0.40-0.37 V and 0.24-0.21 V positive potential and favors to efficient dye regeneration process. The CB of TiO$_2$ is 0.60-0.64 V more positive than the LUMO of SQS4 and ASQ4 dyes and favors the efficient electron injection. Though, HOMO of the dyes mismatching with redox potential of copper-based electrolyte by 70 and 100 mV negative potential and violating the process of dye regeneration for SQS4 and ASQ4 dyes respectively, but used to examine the photovoltaic responses and V_{OC} from the NIR-active squaraine dye. The CB of TiO$_2$ 0.60 V more positive than the LUMO of SQS4 and ASQ4 dyes and favored the electron injection processes.

Table 1. Photophysical and electrochemical properties of ASQ4 dye at room temperature.

Dye	$^a\lambda_{max}$ (nm)	$^b\lambda_{max}$ (nm)	ε (M^{-1} cm^{-1})	E_{HOMO} (V vs NHE)	E_{LUMO} (V vs NHE)	^cE_g (eV)	Dye Loading (10^{-7} mol/cm^2)
ASQ4	644	653	3.5×10^5	0.773	-1.14	1.91	0.310
							0.187 (CDCA)

^{a}absorption, ^{b}emission of ASQ4 dye in dichloromethane, and ^{c}optical band gap.

5.B.3.3 Theoretical studies. Theoretical studies of ASQ4 dye were performed at B3LYP, 6-311G (++) level.[47] Isosurface plots of frontier orbitals, torsional angles and distance between the terminal carbons of ASQ4 dye is provided in **Figure 3**. The distribution of electron in HOMO was uniformly and located on squaric acid and vinylene units between two donors, and in case HOMO-1 density of electron located on the squaric acid moiety, whereas density of electron in LUMO was uniformly distributed within the π-framework and slightly on carboxylic moiety, and LUMO+1 showed the density of electron located towards the anchoring group (carboxylic acid) from the adjacent donor moiety. ASQ4 dye showed 2.26 eV band gap, that 0.08 eV more than SQS4[5] dye.
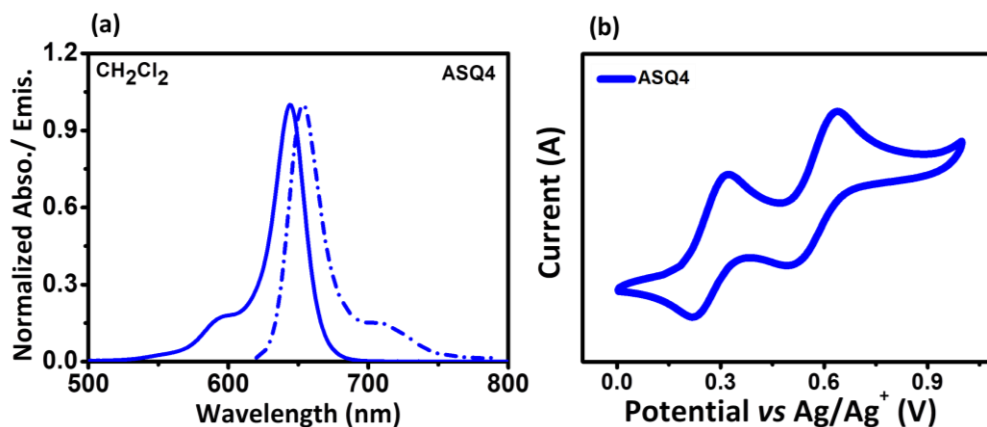
Figure 2. (a) Normalized UV-vis (solid), fluorescence (dotted) spectra, and (b) cyclic voltammograms of ASQ4 dye in CH_2Cl_2.
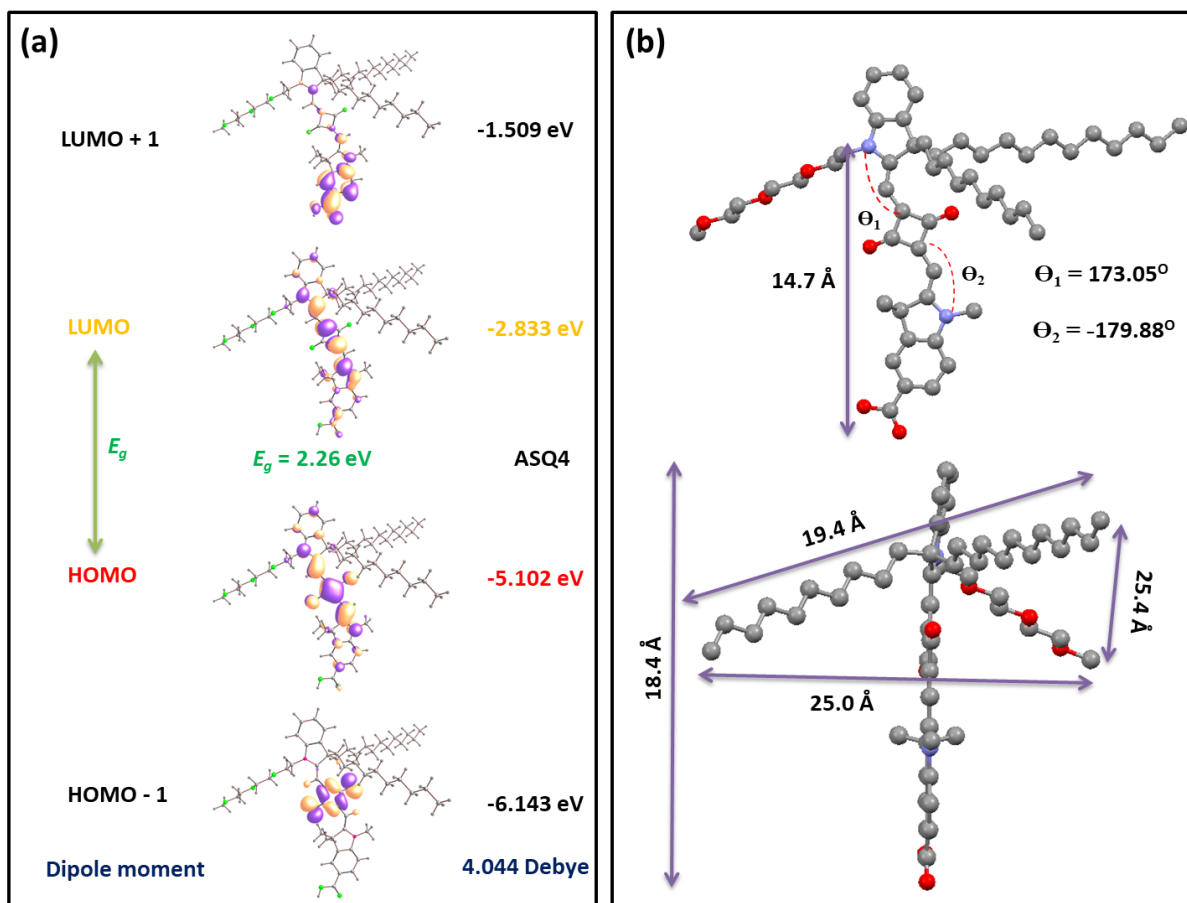
Figure 3. (a) Isosurface plots of frontier orbitals (HOMO, HOMO-1, and LUMO, LUMO + 1) of ASQ4 dye (Isovalue set to 0.03)[47], and (b) torsional angles, distance between the terminal carbon atoms of the alkyl and PEG groups of ASQ4 dye.

5.B.3.4 Photovoltaic performance. The photovoltaic studies of SQ dyes were carried out to examine the effect of the iodolyte, Co(bpy), and Cu(tmby) electrolytes on the photovoltaic parameters (**Figure 4,** and **Table 2**). Though, increment in the V_{OC} values have observed by varying the electrolytes with specific redox-potential, but the serious change in the J_{SC} values lowered the power conversion efficiency of the device. The maximum efficiency achieved for SQS4 and ASQ4 dyes with iodine-based electrolyte was 5.82 and 4.56%, that further enhanced to 7.18 and 5.78% with improvement in the J_{SC} 1.81 and 1.96 mAcm^{-2}, V_{OC} 2, and 23 mV, *ff* 4.4 and 1.15% by the addition of CDCA, respectively by using Pt-foil as a counter electrode. The maximum efficiency achieved by SQS4 and ASQ4 dyes with cobalt based electrolyte where platinum foil as a counter electrode was 4.05 and 2.5%, that further enhanced 5.92 and 3.08% with improvement in the J_{SC} 2.71 and 1.01 mAcm^{-2}, and *ff* 5.37 and 1.19%, respectively by using PEDOT as a counter electrode. Further addition of CDCA decreased the device efficiency for SQS4 dye and increased for ASQ4 dye whether the counter electrode was Pt-foil or PEDOT. Though, HOMO energy levels of the SQS4 and ASQ4 dyes was 70 mV more negative than the redox-level of the copper electrolyte, still device efficiency observed, and the maximum efficiency of 0.51 and 0.57% were achieved with Pt-foil, which is further enhanced to 1.05 and 1.25% with improved J_{SC} 0.67 and 1.24 mAcm^{-2}, *ff* 15.46 and 6.86%, respectively with PEDOT. Further, addition of CDCA increased the device efficiencies interestingly 1.08 and 0.79% with Pt-foil, whereas 2.01 and 2.69% with PEDOT, respectively for SQS4 and ASQ4 dyes. The low photovoltaic efficiencies for SQS4 and ASQ4 dyes with cobalt-based electrolyte (with Pt-foil) compare to iodine-based electrolyte, because of the fast electron recombination of the injected electrons present into CB of TiO$_2$ with oxidized redox component Co(III) complex (low mass transport),[4,45] and responsible to lowered the J_{SC} values. Whereas, low photovoltaic efficiencies for SQS4 and ASQ4 dyes with copper-based electrolytes due to poor dye regeneration process that arises from mismatching of dye HOMO and redox-potential of electrolyte. Use of PEDOT as a counter electrode leads fast regeneration of the Co(III) complex compare to Pt-foil, results improved J_{SC}, *ff*, and efficiency.[30]
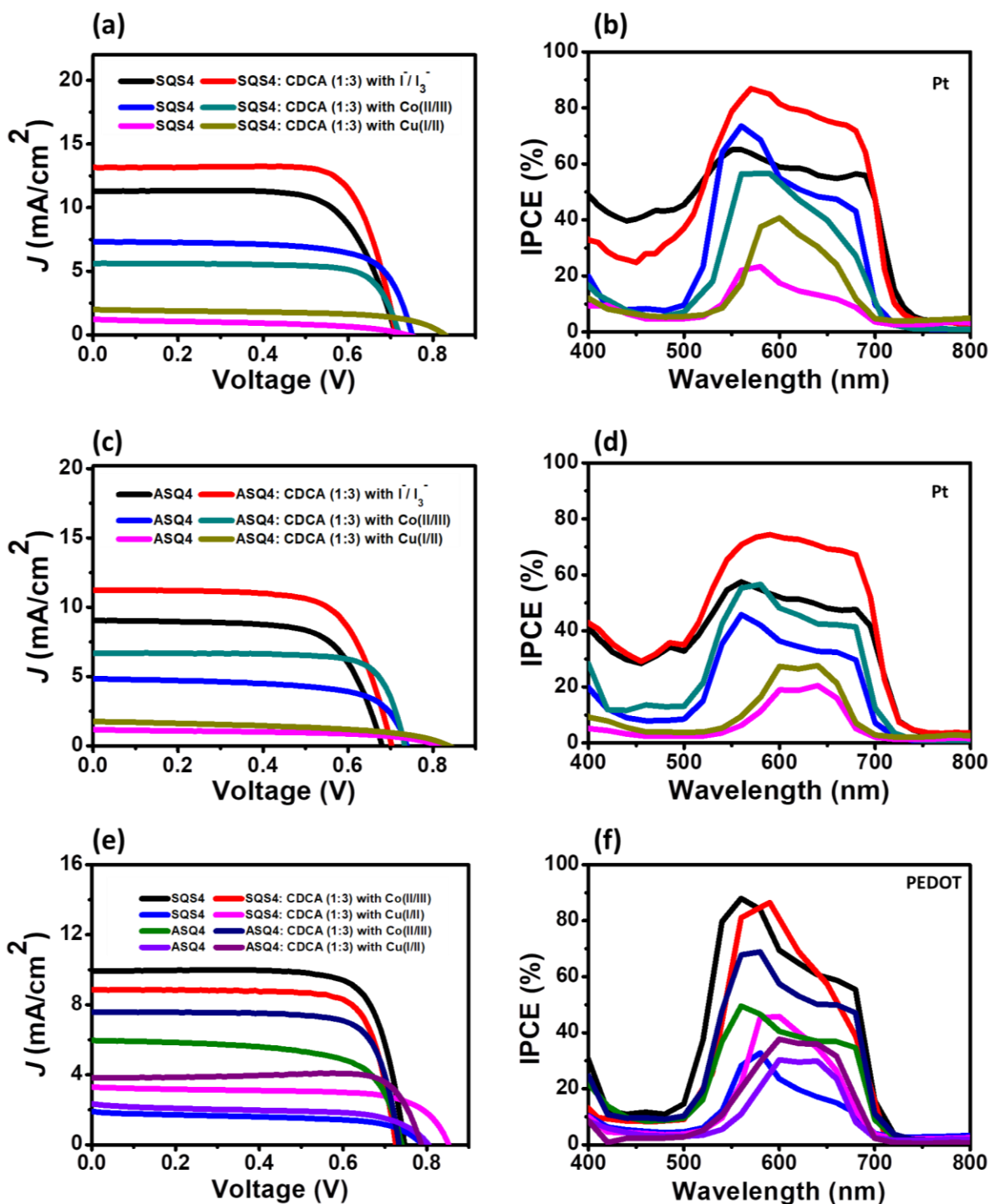
Figure 4. (a), (c) *I-V*, (b), and (d) IPCE curves of SQS4 and ASQ4 dyes with iodine, cobalt, and copper-based electrolytes respectively, where Pt-foil as a counter electrode, (e) *I-V*, and (f) IPCE curves of SQS4 and ASQ4 dyes with cobalt, and copper-based electrolytes respectively, where PEDOT coated on the FTO used as a counter electrode.

Table 2. Photovoltaic performance of squaraine dyes with iodine, cobalt, and copper-based electrolytes at room temperature.

Cell	CDCA (ratio)	V_{OC} (V)	J_{SC} (mA/cm^2)	ff (%)	η (%)
SQS4[a]	0	0.712 ± 0.001	11.28 ± 0.23	70 ± 0.95	5.63 ± 0.19
SQS4[a]	3	0.713 ± 0.002	13.17 ± 0.15	75 ± 0.39	7.04 ± 0.14
SQS4[b]	0	0.750 ± 0.003	7.30 ± 0.19	71 ± 0.88	3.89 ± 0.16
SQS4[b, d]	0	0.746 ± 0.006	9.93 ± 0.27	76 ± 1.25	5.64 ± 0.28
SQS4[b]	3	0.720 ± 0.002	5.61 ± 0.16	76 ± 0.74	3.07 ± 0.13
SQS4[b, d]	3	0.726 ± 0.005	8.85 ± 0.32	77 ± 1.23	4.95 ± 0.29
SQS4[c]	0	0.750 ± 0.001	1.25 ± 0.05	50 ± 2.32	0.47 ± 0.04
SQS4[c, d]	0	0.790 ± 0.003	1.90 ± 0.07	67 ± 0.78	1.00 ± 0.05
SQS4[c]	3	0.828 ± 0.004	2.00 ± 0.11	61 ± 0.57	1.01 ± 0.07
SQS4[c, d]	3	0.852 ± 0.002	3.31 ± 0.09	69 ± 0.10	1.95 ± 0.06
ASQ4[a]	0	0.680 ± 0.002	9.04 ± 0.52	69 ± 1.01	4.24 ± 0.32
ASQ4[a]	3	0.702 ± 0.003	11.23 ± 0.29	70 ± 1.16	5.52 ± 0.26
ASQ4[b]	0	0.740 ± 0.001	4.84 ± 0.26	66 ± 0.38	2.36 ± 0.14
ASQ4[b, d]	0	0.739 ± 0.003	5.97 ± 0.14	67 ± 0.57	2.95 ± 0.13
ASQ4[b]	3	0.733 ± 0.003	6.69 ± 0.42	77 ± 0.65	3.77 ± 0.27
ASQ4[b, d]	3	0.732 ± 0.001	7.57 ± 0.32	78 ± 1.07	4.32 ± 0.25
ASQ4[c]	0	0.814 ± 0.004	1.18 ± 0.09	54 ± 0.87	0.52 ± 0.05
ASQ4[c, d]	0	0.804 ± 0.006	2.34 ± 0.17	60 ± 1.73	1.13 ± 0.12
ASQ4[c]	3	0.838 ± 0.002	1.76 ± 0.13	48 ± 1.83	0.71 ± 0.08
ASQ4[c, d]	3	0.788 ± 0.010	3.84 ± 0.06	86 ± 0.31	2.60 ± 0.09

[a]iodine, [b]cobalt, [c]copper-based electrolytes with Pt-foil as a counter electrode, [d]PEDOT coated on the FTO used as a counter electrode.

From the IPCE curve of SQS4 dye with various redox electrolytes, the peaks from 550 nm to 590 nm (corresponds to H-aggregates) are participated more than monomers to generates the photocurrent in the DSSC efficiency, whether the counter electrode was Pt-foil or PEDOT in the presence and absence of the CDCA (**Figure 4b, 4d,** and **4f**), whereas ASQ4 dye contributed equally from aggregated and monomeric structures to generates the photocurrent with copper-based electrolytes. The IPCE curve of the SQS4 and ASQ4 dyes with iodine-based electrolyte observed good that further improved by the addition of the CDCA without disturbing the pattern of peaks. The peak intensities at 560 to 600 nm of the IPCE curve have enhanced (responsible for increased J_{SC}) when PEDOT used as a counter electrode in the presence and absence of the CDCA in case of cobalt, and copper-based electrolytes for SQS4 and ASQ4 dyes, respectively. The SQS4 dye with cobalt-based electrolyte showed good photovoltaic efficiency of 5.92% (without CDCA), and ASQ4 dye with copper-based electrolyte showed an efficiency of 2.69% (with CDCA), and are the highest photovoltaic efficiency obtained by NIR-active unsymmetrical squaraine dyes with cobalt and copper-based electrolytes first time respectively, where PEDOT used as a counter electrode.

5.B.3.5 Electrochemical impedance spectroscopy (EIS). EIS studies of SQS4 and ASQ4 dyes were carried out with different electrolytes and counter electrodes in dark experimental conditions by applying different bias (**Figure 5, 6** and **7**) near to device V_{OC}. Nyquist plot of the SQS4 and ASQ4 dyes with cobalt (at 0.75 V applied bias) and copper-based electrolyte (at 0.85 V applied bias), where Pt-foil, and PEDOT used as a counter electrode respectively (**Figure 8**).[31]
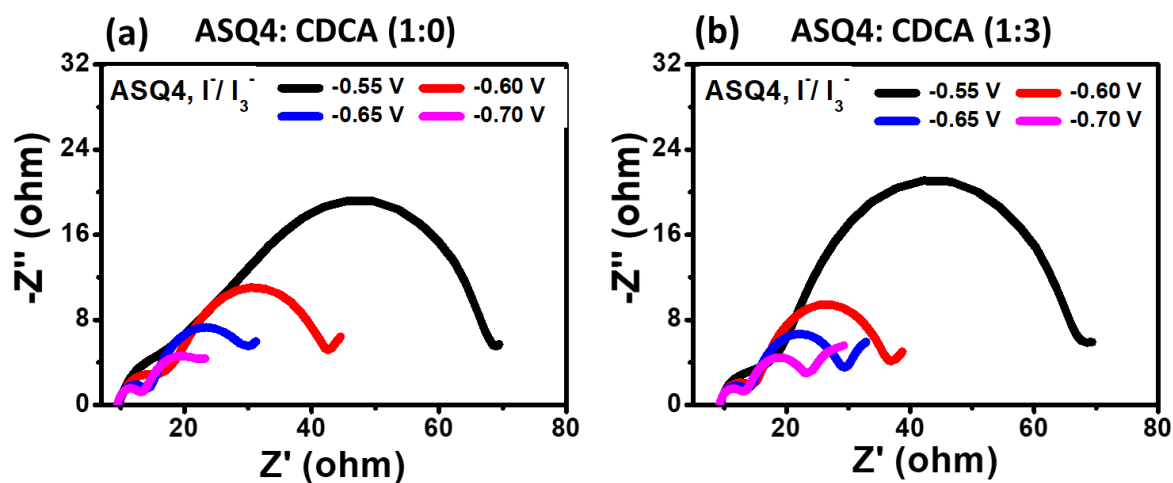
Figure 5. Nyquist plot of ASQ4 dye with and without CDCA under various applied bias.

Figure 6. Nyquist plot of ASQ4 dye with and without CDCA under various applied bias.
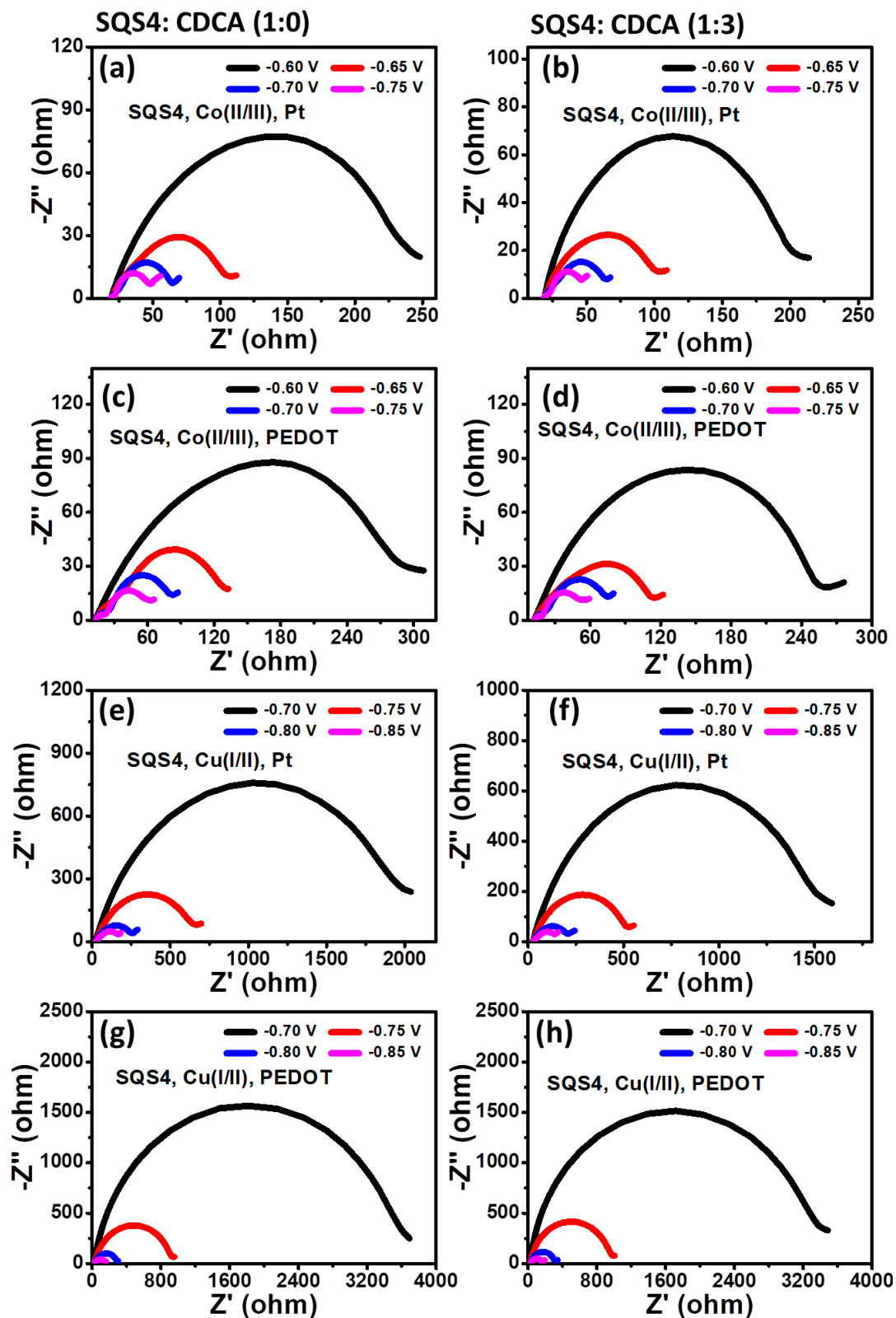
Figure 7. Nyquist plot of SQS4 dye with and without CDCA under various applied bias.

To calculate the charge recombination resistance (R_{ct}), and chemical capacitance ($C\mu$) Nyquist plot has been used, and lifetime of electron (τ) were calculated by multiplying the R_{ct} and $C\mu$ values for the SQS4 and ASQ4 dyes with various electrolytes and counter electrode conditions. EIS parameters of SQS4 and ASQ4 dyes with cobalt and copper-based electrolytes with 0.75 and 0.85 V applied bias is provided in **Table 3**, whereas ASQ4 dye with iodine-based electrolyte with 0.7 V is provided in **Table 3**. Decreased chemical capacitance ($C\mu$) values noted with PEDOT compare to Pt-foil, whether electrolyte was cobalt or copper-based. Though, R_{ct} values of SQS4 and ASQ4 dyes observed high with copper-based electrolyte, but the $C\mu$ values found very low, and results low lifetime of electron compare to the cobalt-based electrolyte. Although, the $C\mu$ value for the SQS4 dye (with PEDOT) with cobalt-based electrolyte noted lower compared to Pt-foil, but due to high R_{ct} value, lifetime of electron obtained higher than other compositions of electrolytes/ counter electrodes, and supported the increased photocurrent and device efficiency. ASQ4 dye showed maximum τ value with copper-based electrolyte and PEDOT as counter electrode.
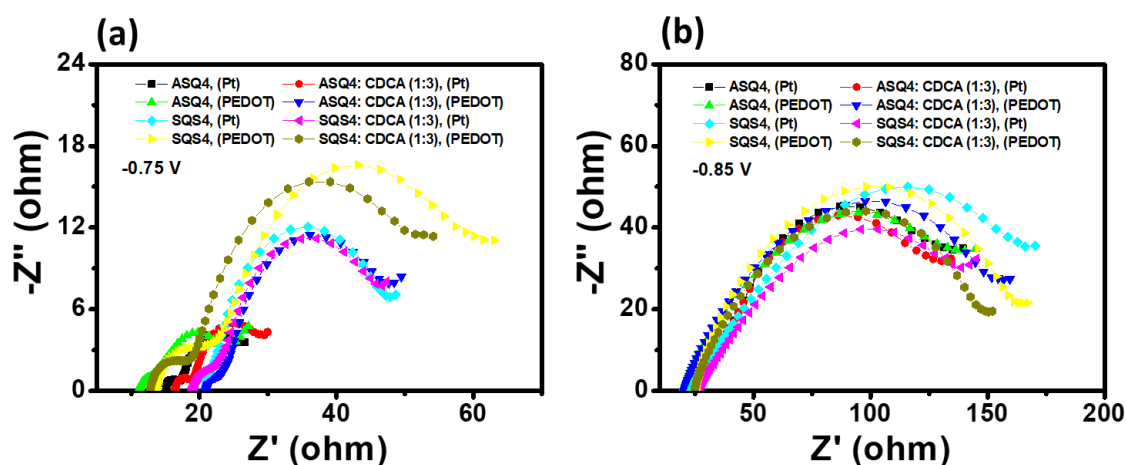
Figure 8. (a) Nyquist plot of ASQ4 and SQS4 dyes with cobalt-based electrolyte at 0.75 V applied bias, and (b) Nyquist plot of ASQ4 and SQS4 dyes with copper-based electrolytes at 0.85 V applied bias, where Pt-foil and PEDOT used as a counter electrode respectively.

Table 3. EIS parameters of SQS4 and ASQ4 dyes with cobalt and copper-based electrolytes in dark at 0.75 and 0.85 V applied bias.

Dyes	CDCA (equiv.)	Electrolyte/ Counter electrode	R_{ct} (ohm)	$C\mu$ (mF)	τ (ms)
SQS4	0	Co/ Pt	22.95	0.213	4.89
SQS4	3	Co/ Pt	23.66	0.206	4.87
SQS4	0	Co/ PEDOT	25.69	0.196	5.03
SQS4	3	Co/ PEDOT	19.63	0.134	2.63
SQS4[a]	0	Cu/ Pt	46.93	0.032	1.50
SQS4[a]	3	Cu/ Pt	44.80	0.044	1.97
SQS4[a]	0	Cu/ PEDOT	36.71	0.023	0.84
SQS4[a]	3	Cu/ PEDOT	40.39	0.028	1.13
ASQ4[b]	0	I^-/I_3^-/ Pt	13.68	0.347	4.75
ASQ4[b]	3	I^-/I_3^-/ Pt	13.83	0.486	6.72
ASQ4	0	Co/ Pt	8.57	0.384	3.29
ASQ4	3	Co/ Pt	10.36	0.348	3.60
ASQ4	0	Co/ PEDOT	11.34	0.148	1.68
ASQ4	3	Co/ PEDOT	20.42	0.231	4.72
ASQ4[a]	0	Cu/ Pt	40.15	0.065	2.61
ASQ4[a]	3	Cu/ Pt	41.33	0.067	2.77
ASQ4[a]	0	Cu/ PEDOT	41.75	0.028	1.17
ASQ4[a]	3	Cu/ PEDOT	45.78	0.061	2.79

[a]Applied bias of 0.85 V, [b]Applied bias of 0.70 V.

5.B.4 CONCLUSION

NIR-light active SQS4 and ASQ4 dyes have been used to study the photovoltaic performances in iodine, cobalt and copper-based electrolytes that possess different redox potentials, where Pt-foil/ PEDOT used as a cathode. SQS4 dye with cobalt-based electrolytes have demonstrated as a highly efficient D-A-D dyes with 5.92% (with PEDOT) photovoltaic efficiency without CDCA compare to iodine (5.82%, with Pt-foil), and copper-based electrolytes (1.05%, with PEDOT). The maximum photovoltaic efficiency achieved by SQS4 dye with iodolyte was 7.18% (with Pt-foil), and with copper-based electrolyte was 2.05% (with PEDOT) in the presence of CDCA. Photovoltaic efficiencies of 4.56, 2.5, and 0.57%, that further enhanced to 5.77, 4.04, and 0.79%, by the addition of CDCA for ASQ4 dye with iodine, cobalt, and copper-based electrolytes, where Pt-foil used as a cathode. The maximum photovoltaic efficiency achieved by ASQ4 dye with cobalt, and copper-based electrolyte was 4.57, and 2.69% (with PEDOT) respectively, in the presence of CDCA. This works tells the importance of electrolytes and counter electrodes towards the DSSC efficiency for unsymmetrical squaraine dyes for the future outlook.

5.5 REFERENCES

(1) Beard, M. C.; Luther, J. M.; Semonin, O. E.; Nozik, A. J. Third Generation Photovoltaics based on Multiple Exciton Generation in Quantum Confined Semiconductors. *Acc. Chem. Res.* **2012**, *46*, 1252-1260.
(2) Ji, J.-M.; Zhou, H.; Kim, H. K. Rational Design Criteria for D–π–A Structured Organic and Porphyrin Sensitizers for Highly Efficient Dye-Sensitized Solar Cells. *J. Mater. Chem. A*, **2018**, *6*, 14518–14545.
(3) Ye, M.; Wen, X.; Wang, M.; Iocozzia, J.; Zhang, N.; Lin, C.; Lin1, Z. Recent Advances in Dye-Sensitized Solar Cells: from Photoanodes, Sensitizers and Electrolytes to Counter Electrodes. *Materials Today*, **2015**, *18*, 155-162.
(4) Wu, J.; Lan, Z.; Lin, J.; Huang, M.; Huang, Y.; Fan, L.; Luo, G. Electrolytes in Dye-Sensitized Solar Cells. *Chem. Rev.* **2015**, *115*, 2136−2173.
(5) Singh, A. K.; Kavungathodi, M. F. M.; Nithyanandhan, J. Alkyl-Group-Wrapped Unsymmetrical Squaraine Dyes for Dye-Sensitized Solar Cells: Branched Alkyl Chains Modulate the Aggregation of Dyes and Charge Recombination Processes. *ACS Appl. Mater. Interfaces* **2020**, *12*, 2555-2565.
(6) Alagumalai, A.; Kavungathodi, M. F. M.; Vellimalai, P.; Sil, M. C.; Nithyanandhan, J. Effect of Out-of-Plane Alkyl Group's Position in Dye-Sensitized Solar Cell

Efficiency: A Structure–Property Relationship Utilizing Indoline-Based Unsymmetrical Squaraine Dyes. *ACS Appl. Mater. Interfaces* **2016**, *8*, 35353–35367.

(7) Singh, A. K.; Maibam, A.; Javaregowda, B. H.; Bisht, R.; Kudlu, A.; Krishnamurty, S.; Krishnamoorthy K.; Nithyanandhan, J. Unsymmetrical Squaraine Dyes for Dye-Sensitized Solar Cells: Position of Anchoring Group Controls the Orientation and Self-Assembly of Sensitizers on TiO_2 Surface and Modulate Its Flat Band Potential. *J. Phys. Chem. C,* **2020**, *124*, 18436–18451.

(8) Imahori, H.; Kang, S.; Hayashi, H.; Haruta, M.; Kurata, H.; Isoda, S.; Canton, S. E.; Infahsaeng, Y.; Kathiravan, A.; Pascher, T.; Chábera, P.; Yartsev, A. P.; Sundström, V. Photoinduced Charge Carrier Dynamics of Zn - Porphyrin - TiO_2 Electrodes: The Key Role of Charge Recombination for Solar Cell Performance. *J. Phys. Chem. A* **2011**, *115*, 3679–3690.

(9) Ye, S.; Kathiravan, A.; Hayashi, H.; Tong, Y.; Infahsaeng, Y.; Chabera, P.; Pascher, T.; Yartsev, A. P.; Isoda, S.; Imahori, H.; Sundström, V. Role of Adsorption Structures of Zn-Porphyrin on TiO_2 in Dye-Sensitized Solar Cells Studied by Sum Frequency Generation Vibrational Spectroscopy and Ultrafast Spectroscopy. *J. Phys. Chem. C* **2013**, *117*, 6066−6080.

(10) O'Regan, B.; Grätzel, M. A Low-Cost, High-Efficiency Solar Cell Based on Dye-Sensitized Colloidal TiO_2 Films. *Nature* **1991**, *353*, 737–740.

(11) Yu, Q.; Wang, Y.; Yi, Z.; Zu, N.; Zhang, J.; Zhang, M.; Wang, P. High-Efficiency Dye-Sensitized Solar Cells: The Influence of Lithium Ions on Exciton Dissociation, Charge Recombination, and Surface States. *ACS Nano* **2010**, *4*, 6032-6038.

(12) Mathew, S.; Yella, A.; Gao, P.; Humphry-Baker, R.; Curchod, B. F. E.; Ashari-Astani, N.; Tavernelli, I.; Rothlisberger, U.; Nazeeruddin, M. K.; Grätzel, M. Dye-Sensitized Solar Cells with 13% Efficiency Achieved through the Molecular Engineering of Porphyrin Sensitizers. *Nat. Chem.* **2014**, *6*, 242–247.

(13) Zhang, L.; Yang, X.; Wang, W.; Gurzadyan, G. G.; Li, J.; Li, X.; An, J.; Yu, Z.; Wang, H.; Cai, B. et al. 13.6% Efficient Organic Dye-Sensitized Solar Cells by Minimizing Energy Losses of the Excited State. *ACS Energy Lett.,* **2019**, *4*, 943−951.

(14) Qin, C.; Wong, W.-Y.; Han, L. Squaraine Dyes for Dye-Sensitized Solar Cells: Recent Advances and Future Challenges. *Chem. Asian J.* **2013**, *8*, 1706-1719.

(15) Chen, G.; Sasabe, H.; Igarashi, T.; Hong, Z.; Kido, J. Squaraine Dyes for Organic Photovoltaic Cells. *J. Mater. Chem. A*, **2015**, *3*, 14517-14534.

(16) Ajayaghosh, A. Chemistry of Squaraine-Derived Materials: Near-IR Dyes, Low Band Gap Systems, and Cation Sensors**.** *Acc. Chem. Res.* **2005**, *38*, 449−459.

(17) Tian, H.; Yang, X.; Chen, R.; Zhang, R.; Hagfeldt, A.; Sun, L. Effect of Different Dye Baths and Dye-Structures on the Performance of Dye-Sensitized Solar Cells Based on Triphenylamine Dyes. *J. Phys. Chem. C* **2008**, *112* (29), 11023–11033.

(18)   Hagfeldt, A.; Boschloo, G.; Sun, L. C.; Kloo, L.; Pettersson, H. Dye-Sensitized Solar Cells. *Chem. Rev.* **2010**, *110*, 6595-6663.

(19)   Hao, F.; Dong, P.; Luo, Q.; Li, J.; Lou, J.; Lin, H. Recent Advances in Alternative Cathode Materials for Iodine-Free Dye-Sensitized Solar Cells. *Energy Environ. Sci.,* **2013**, *6*, 2003–2019.

(20)   Wu, J.; Lan, Z.; Lin, J.; Huang, M.; Huang, Y.; Fan, L.; Luo, G.; Lin, Y.; Xie, Y.; Wei, Y. Counter Electrodes in Dye-Sensitized Solar Cells. *Chem. Soc. Rev.*, **2017**, *46*, 5975-6023.

(21)   Åkerlöf, G. Dielectric Constants of Some Organic Solvent-Water Mixtures at Various Temperatures. *J. Am. Chem. Soc.* **1932**, *54* (11), 4125–4139.

(22)   Pollard, J. A.; Zhang, D.; Downing, J. A.; Knorr, F. J.; McHale, J. L. Solvent Effects on Interfacial Electron Transfer from Ru(4,4′-Dicarboxylic Acid-2,2′-Bipyridine) 2(NCS) 2 to Nanoparticulate TiO_2: Spectroscopy and Solar Photoconversion. *J. Phys. Chem. A* **2005**, *109* (50), 11443–11452.

(23)   Ozawa, H.; Awa, M.; Ono, T.; Arakawa, H. Effects of Dye-Adsorption Solvent on the Performances of the Dye-Sensitized Solar Cells Based on Black Dye. *Chem. - An Asian J.* **2012**, *7* (1), 156–162.

(24)   Zhu, K.; Jang, S. R.; Frank, A. J. Effects of Water Intrusion on the Charge-Carrier Dynamics, Performance, and Stability of Dye-Sensitized Solar Cells. *Energy Environ. Sci.* **2012**, *5* (11), 9492–9495.

(25)   Imahori, H.; Hayashi, S.; Hayashi, H.; Oguro, A.; Eu, S.; Umeyama, T.; Matano, Y. Effects of Porphyrin Substituents and Adsorption Conditions on Photovoltaic Properties of Porphyrin-Sensitized TiO 2 Cells. *J. Phys. Chem. C* **2009**, *113* (42), 18406–18413.

(26)   Hayashi, H.; Higashino, T.; Kinjo, Y.; Fujimori, Y.; Kurotobi, K.; Chabera, P.; Sundström, V.; Isoda, S.; Imahori, H. Effects of Immersion Solvent on Photovoltaic and Photophysical Properties of Porphyrin-Sensitized Solar Cells. *ACS Appl. Mater. Interfaces* **2015**, *7* (33), 18689–18696.

(27)   Kafafy, H.; Wu, H.; Peng, M.; Hu, H.; Yan, K.; El-Shishtawy, R. M.; Zou, D. Steric and Solvent Effect in Dye-Sensitized Solar Cells Utilizing Phenothiazine-Based Dyes. *Int. J. Photoenergy* **2014**, *2014*.

(28)   Seintis, K.; Şahin, Ç.; Sigmundová, I.; Stathatos, E.; Hrobárik, P.; Fakis, M. Solvent-Acidity-Driven Change in Photophysics and Significant Efficiency Improvement in Dye-Sensitized Solar Cells of a Benzothiazole-Derived Organic Sensitizer. *J. Phys. Chem. C* **2018**, *122* (35), 20122–20134.

(29)   Mosconi, E.; Selloni, A.; De Angelis, F. Solvent Effects on the Adsorption Geometry and Electronic Structure of Dye-Sensitized TiO 2: A First-Principles Investigation. *J. Phys. Chem. C* **2012**, *116* (9), 5932–5940.

(30)   Marotta, G.; Lobello, M. G.; Anselmi, C.; Consiglio, G. B.; Calamante, M.; Mordini, A.; Pastore, M.; De Angelis, F. An Integrated Experimental and Theoretical

Approach to the Spectroscopy of Organic-Dye-Sensitized TiO$_2$ Heterointerfaces: Disentangling the Effects of Aggregation, Solvation, and Surface Protonation. *ChemPhysChem* **2014**, *15*, 1116−1125.

(31)   Wang, Q.; Moser, J. E.; Grätzel, M. Electrochemical Impedance Spectroscopic Analysis of Dye-Sensitized Solar Cells. *J. Phys. Chem. B* **2005**, *109*, 14945-14953.

(32)   Jradi, F. M.; O'Neil, D.; Kang, X.; Wong, J.; Szymanski, P.; Parker, T. C.; Anderson, H. L.; El-Sayed, M. A.; Marder, S. R. Near-Infrared Asymmetrical Squaraine Sensitizers for Highly Efficient Dye Sensitized Solar Cells: The Effect of π-Bridges and Anchoring Groups on Solar Cell Performance. *Chem. Mater.* **2015**, *27*, 6305–6313.

(33)   Cole, J. M.; Pepe, G.; Al Bahri, O. K.; Cooper, C. B. Cosensitization in Dye-Sensitized Solar Cells. *Chem. Rev.* **2019**, *119*, 7279−7327.

(34)   Ronca, E.; Pastore, M.; Belpassi, L.; Tarantelli, F.; De Angelis, F. Influence of the Dye Molecular Structure on the TiO$_2$ Conduction Band in Dye-Sensitized Solar Cells: Disentangling Charge Transfer and Electrostatic Effects. *Energy Environ. Sci.* **2013**, *6*, 183– 193.

(35)   Teng, C.; Yang, X.; Yuan, C.; Li, C.; Chen, R.; Tian, H.; Li, S.; Hagfeldt, A.; Sun, L. Two Novel Carbazole Dyes for Dye-Sensitized Solar Cells with Open-Circuit Voltages up to 1 V Based on Br$^-$/Br$_3^-$ Electrolytes. *Org. Lett.* **2009**, *11*, 5542-5545.

(36)   Wang, M.; Chamberland, N.; Breau, L.; Moser, J.; Humphry-Baker, R.; Marsan, B.; Zakeeruddin, S.; Gratzel, M. An Organic Redox Electrolyte to Rival Triiodide/Iodide in Dye-Sensitized Solar Cells. *Nat. Chem.* **2010**, *2*, 385-389.

(37)   Wang, P.; Zakeeruddin, S.; Moser, J.; Baker, R.; Gratzel, M. A Solvent-Free, SeCN$^-$/(SeCN)$_3^-$ Based Ionic Liquid Electrolyte for High-Efficiency Dye-Sensitized Nanocrystalline Solar Cells. *J. Am. Chem. Soc.* **2004**, *126*, 7164-7165.

(38)   Bai, Y.; Yu, Q.; Cai, N.; Wang, Y.; Zhang, M.; Wang, P. High-Efficiency Organic Dye-Sensitized Mesoscopic Solar Cells with a Copper Redox Shuttle. *Chem. Commun.* **2011**, *47*, 4376-4378.

(39)   Daeneke, T.; Kwon, T.; Holmes, A.; Duffy, N.; Bach, U.; Spiccia, L. High-Efficiency Dye-Sensitized Solar Cells with Ferrocene-based Electrolytes. *Nat. Chem.* **2011**, *3*, 211-215.

(40)   Liu, Y.; Hagfeldt, A.; Xiao, X.; Lindquist, S. Investigation of Influence of Redox Species on the Interfacial Energetics of a Dye-Sensitized Nanoporous TiO$_2$ Solar Cell. *Sol. Energy Mater. Sol. Cells* **1998**, *55*, 267-281.

(41)   Cong, J.; Kinschel, D.; Daniel, Q.; Safdari, M.; Gabrielsson, E.; Chen, H.; Svensson, P. H.; Sunce, L.; Kloo, L. Bis(1,1-bis(2-pyridyl)ethane)copper(I/II) as an Efficient Redox Couple for Liquid Dye-Sensitized Solar Cells. *J. Mater. Chem. A*, **2016**, *4*, 14550–14554.

(42)   Ren, Y.; Sun, D.; Cao, Y.; Tsao, H. N.; Yuan, Y.; Zakeeruddin, S. M.; Wang, P.; Grätzel, M. A Stable Blue Photosensitizer for Color Palette of Dye-Sensitized Solar Cells Reaching 12.6% Efficiency. *J. Am. Chem. Soc.* **2018**, *140*, 2405−2408.

(43)   Saygili, Y.; Söderberg, M.; Pellet, N.; Giordano, F.; Cao, Y.; Muñoz-García, A. B.; Zakeeruddin, S. M.; Vlachopoulos, N.; Pavone, M.; Boschloo, G.; Kavan, L.; Moser, J.-E.; Grätzel, M.; Hagfeldt, A.; Freitag, M. Copper Bipyridyl Redox Mediators for Dye-Sensitized Solar Cells with High Photovoltage. *J. Am. Chem. Soc.* **2016**, *138*, 15087−15096.

(44)   Glinka, A.; Gierszewski, M.; Gierczyk, B.; Burdziński, G.; Michaels, H.; Freitag, M.; Ziółek, M. Interface Modification and Exceptionally Fast Regeneration in Copper Mediated Solar Cells Sensitized with Indoline Dyes. *J. Phys. Chem. C,* **2020**, *124*, 2895–2906.

(45)   Pradhan, S. C.; Hagfeldt, A.; Soman, S. Resurgence of DSCs with Copper Electrolyte: A Detailed Investigation of Interfacial Charge Dynamics with Cobalt and Iodine based Electrolytes. *J. Mater. Chem. A*, **2018**, *6*, 22204–22214.

(46)   Tian, H.; Xu, Z.; Hagfeldt, A.; Kloo, L.; Sun, L. Organic Redox Couples and Organic Counter Electrode for Efficient Organic Dye-Sensitized Solar Cells. *J. Am. Chem. Soc.* **2011**, *133*, 9413-9422.

(47)   Frisch, M. J.; Trucks, G. W.; Schlegel, H. B.; Scuseria, G. E.; Robb, M. A.; Cheeseman, J. R.; Scalmani, G.; Barone, V.; Petersson, G. A. ; Nakatsuji, H. et al. *Gaussian 09*; Gaussian, Inc., Wallingford CT, **2016**.

6.1 SUMMARY

This thesis summarizes the understanding and controlling the self-assembling properties of squaraine dyes on the TiO_2 metal-oxide surfaces, and charge recombination processes in dye-sensitized solar cells (DSSCs). Increased in-plane and out-of-plane alkyl group chain length in squaraine dyes have been demonstrated for the enhanced V_{OC} and J_{SC} of device by TiO_2 surface passivation and controlled aggregation. Further, orientations of squaraine dyes on the TiO_2 surface are very sensitive towards the DSSC performance; squaraine dyes with anchoring group on the *para*-position (5th) have been demonstrated for better device efficiency than other positions. Visible-light active unsymmetrical squaraine dyes with N-methylation on arylamine unit and branched alkyl groups on indoline unit have been demonstrated for the better V_{OC} (814 mV), and device efficiency. Further, co-sensitization the visible dyes with NIR-light active squaraine dyes have achieved the maximum 9.08% co-sensitized solar cell efficiency with enhanced J_{SC}. Further, iodine-based electrolytes and acetonitrile solvent systems for device fabrication were demonstrated superior to achieve the high device efficiencies for NIR-light active unsymmetrical squaraine dyes. Furthermore, SQS4 have achieved 5.92% device efficiency which is maximum obtained efficiency by NIR-light active squaraine dyes with cobalt based electrolytes, where PEDOT used as a counter electrode.

6.2 FUTURE DIRECTIONS

This thesis works will provide the guideline to dye-design and modulation of the photovoltaic parameters by modulating the structures and conditions that used for dye-sensitized solar cell applications. In this respect, to overcome the limitations of cocktail and sequential approaches of co-sensitization a series of inbuilt optical complementary squaraine dyes for DSSC application have been design (**Figure 1**), where highly efficient NIR active dye SQS4 and visible dye AK4 are joint together with different sizes of alkyl groups to control the concentration and aggregation of the dyes on the TiO$_2$ surface.
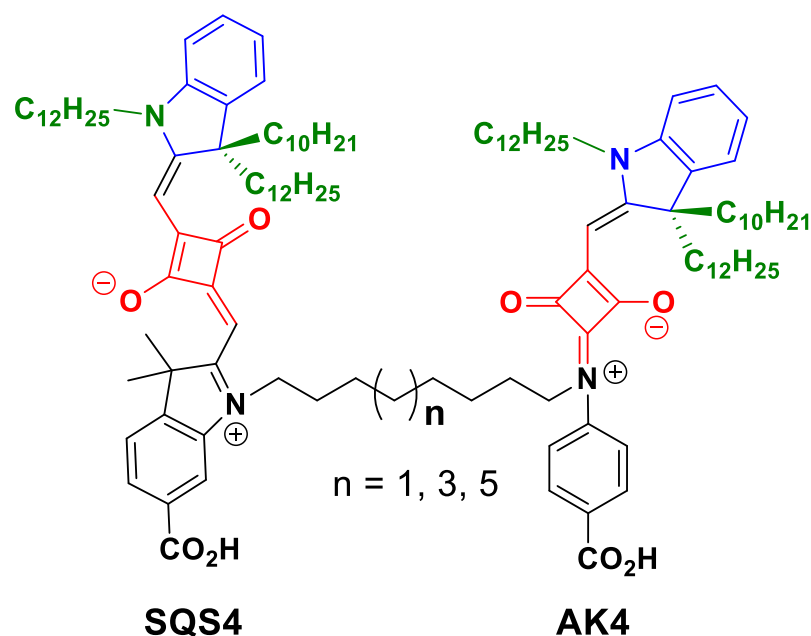
Figure 1. Inbuilt optical complementary unsymmetrical squaraine dyes for DSSCs.

Chapter 2
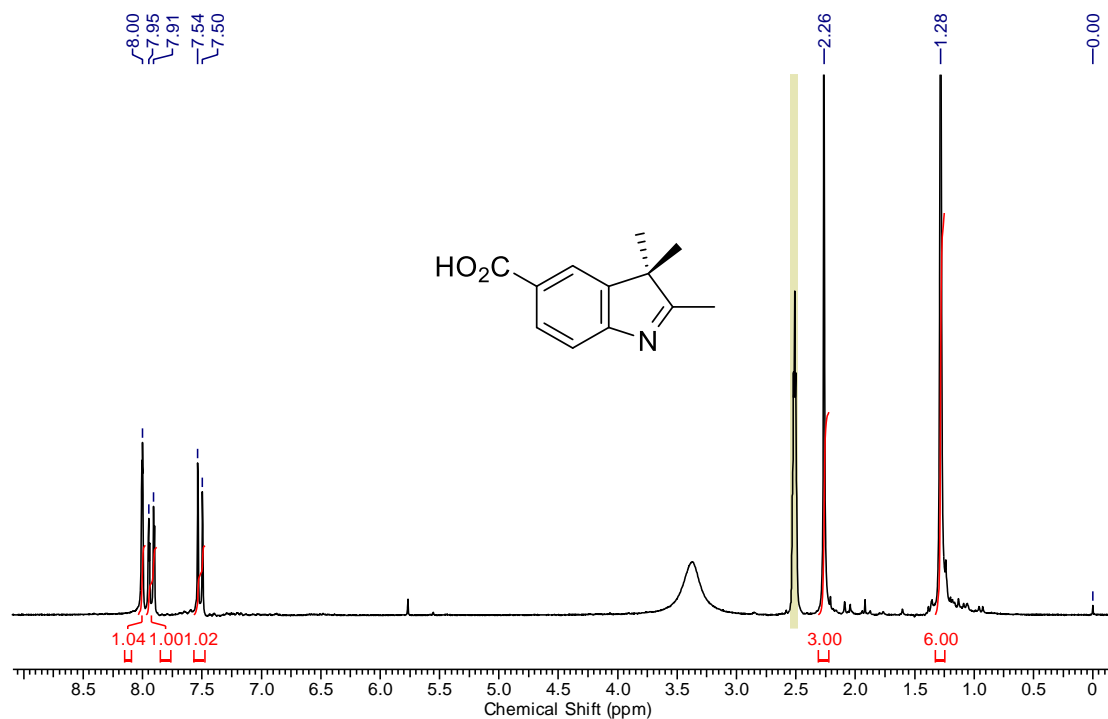
Figure A1. ^{1}H-NMR spectrum of compound **2a** in DMSO-d_6.
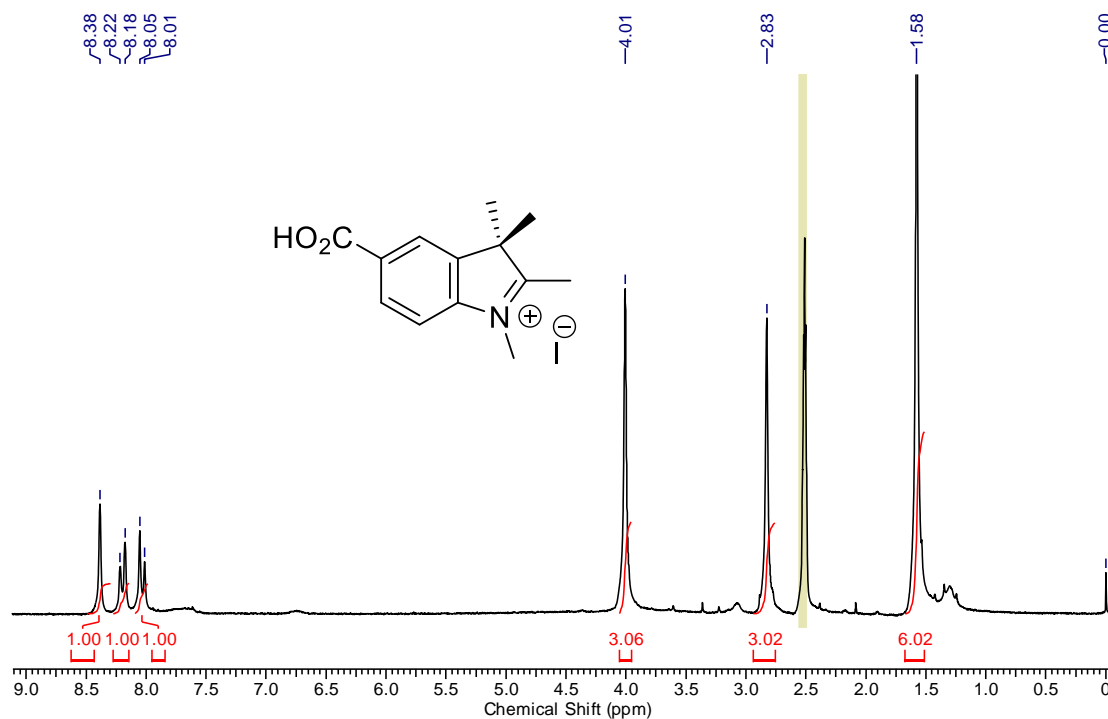
Figure A2. ^{1}H-NMR and spectrum of compound **3a** in DMSO-d_6.
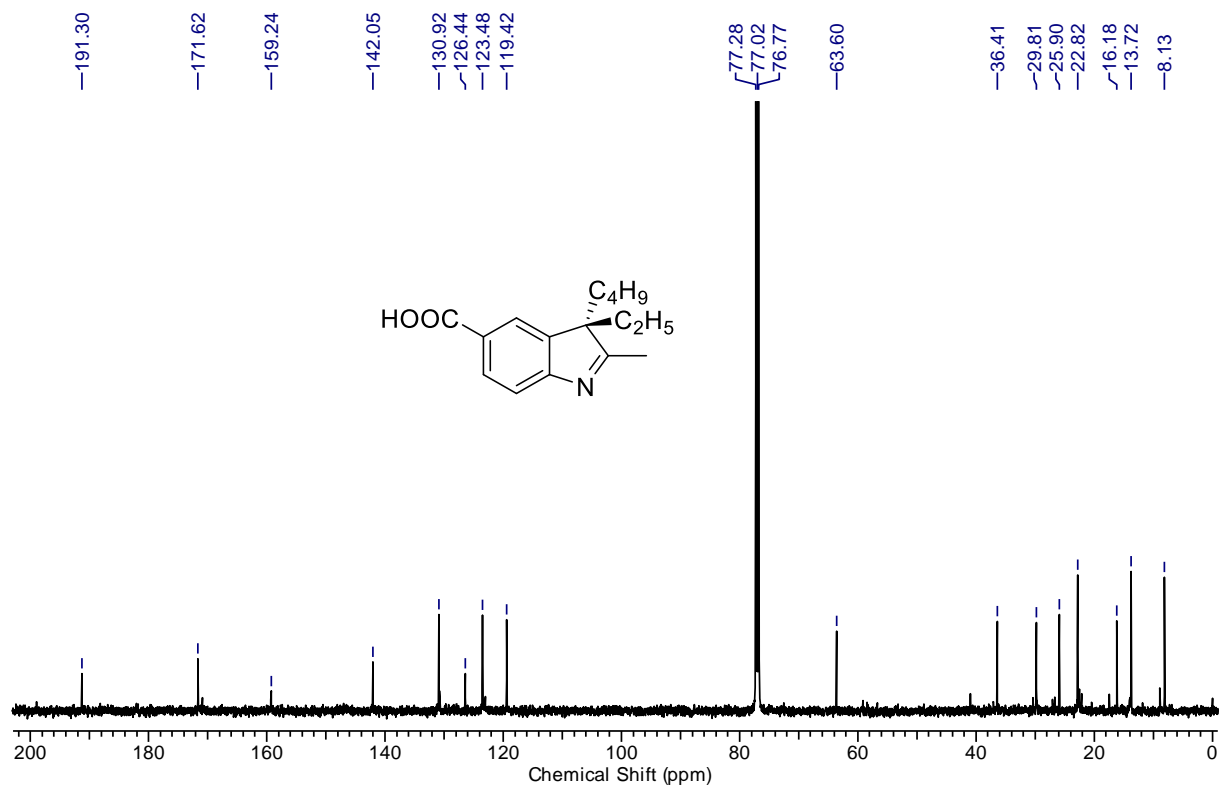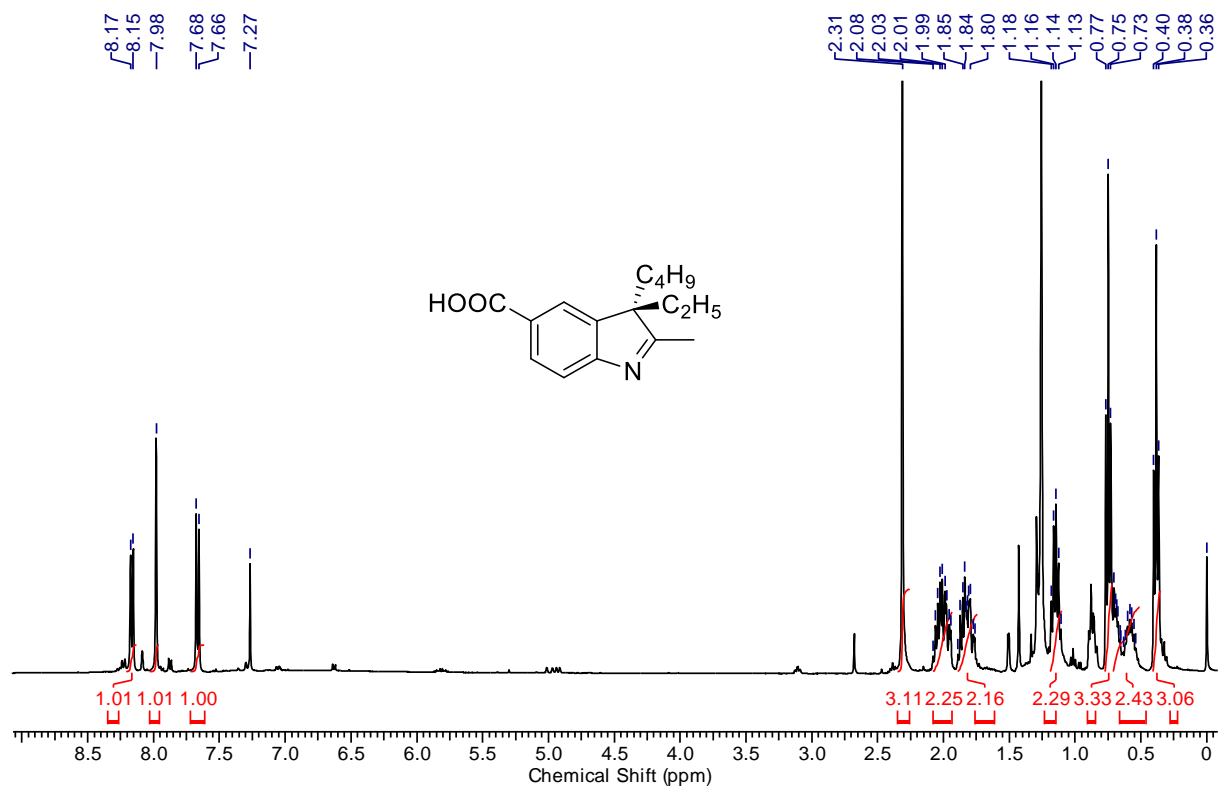
Figure A3. ^{1}H and ^{13}C NMR spectra of compound **2b** in CDCl3.
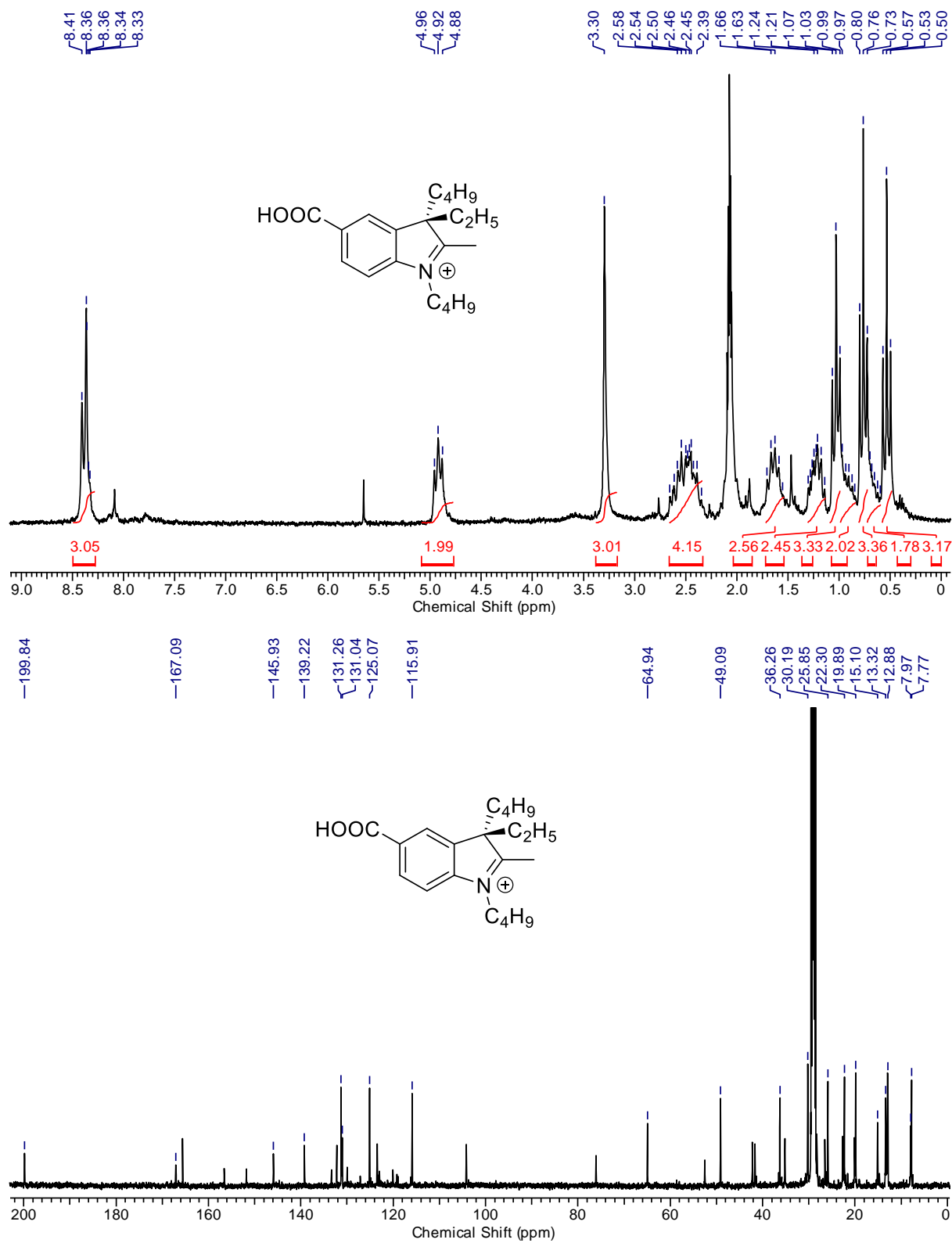
Figure A4. ^{1}H and ^{13}C NMR spectra of compound **3b** in Acetone-d_6.
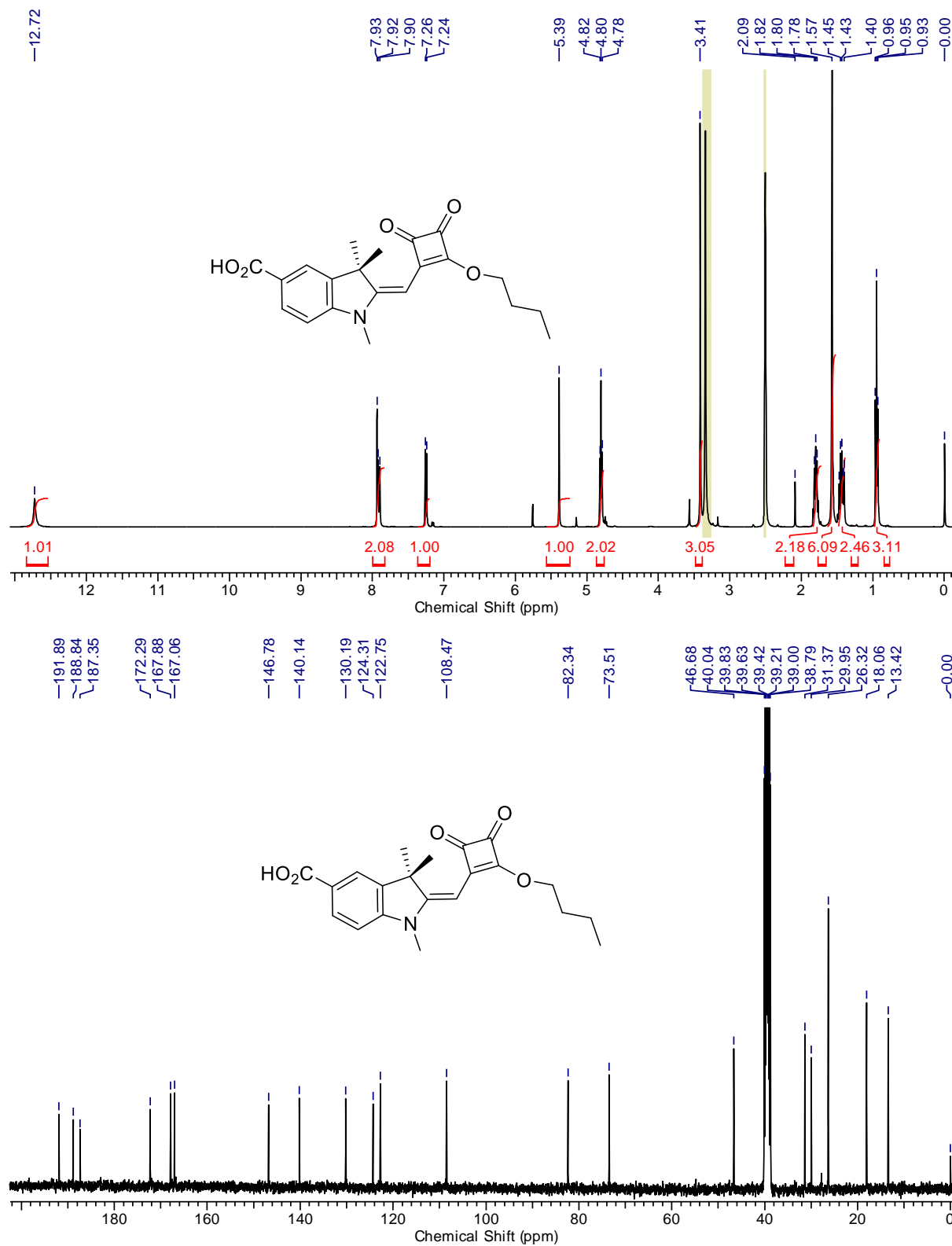
Figure A5. ^{1}H and ^{13}C NMR spectra of compound **4a** in DMSO-d_6.
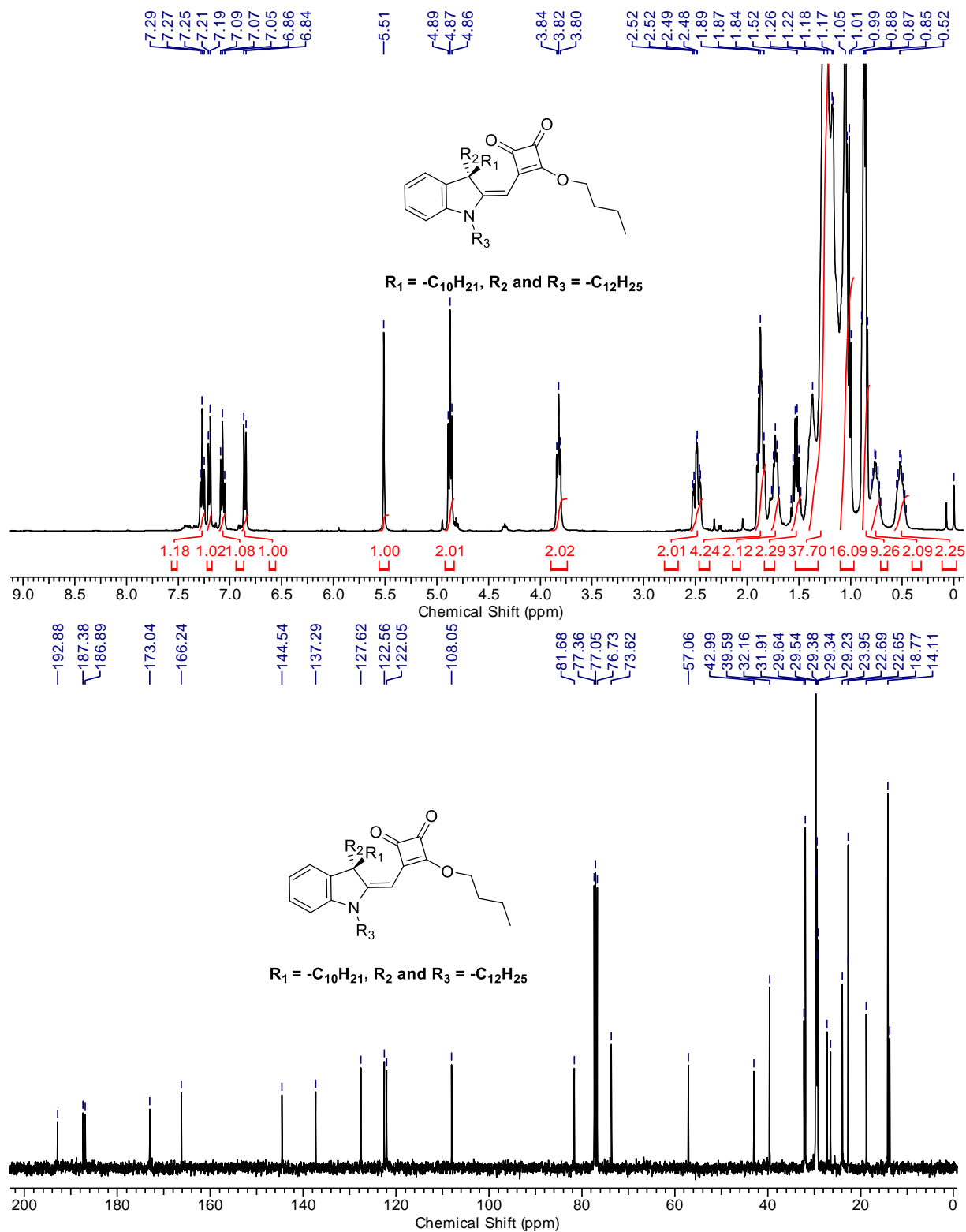
Figure A6. ^{1}H and ^{13}C NMR spectra of compound **4b** in CDCl$_3$.
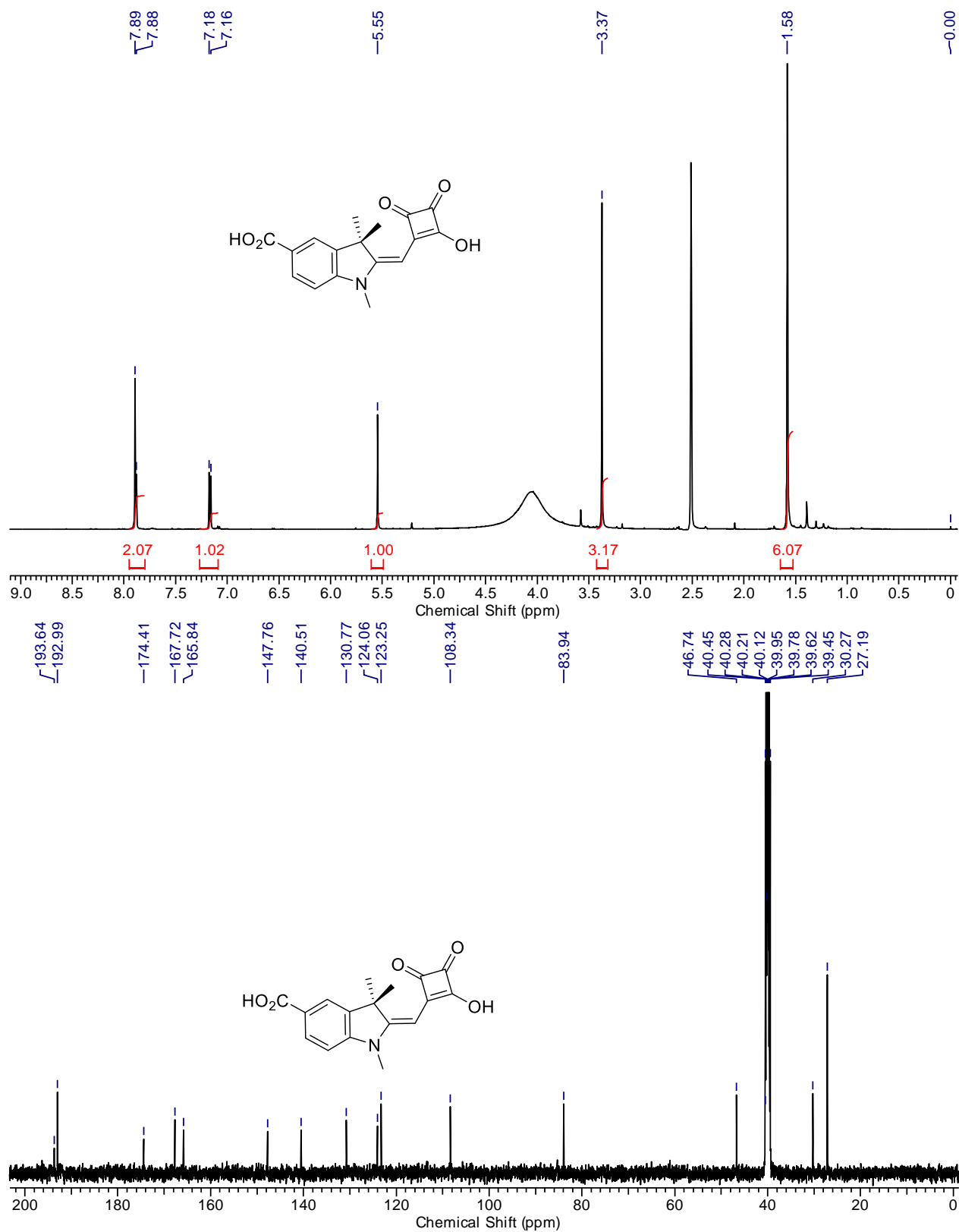
Figure A7. ^{1}H and ^{13}C NMR spectra of compound **5** in DMSO-d_6.
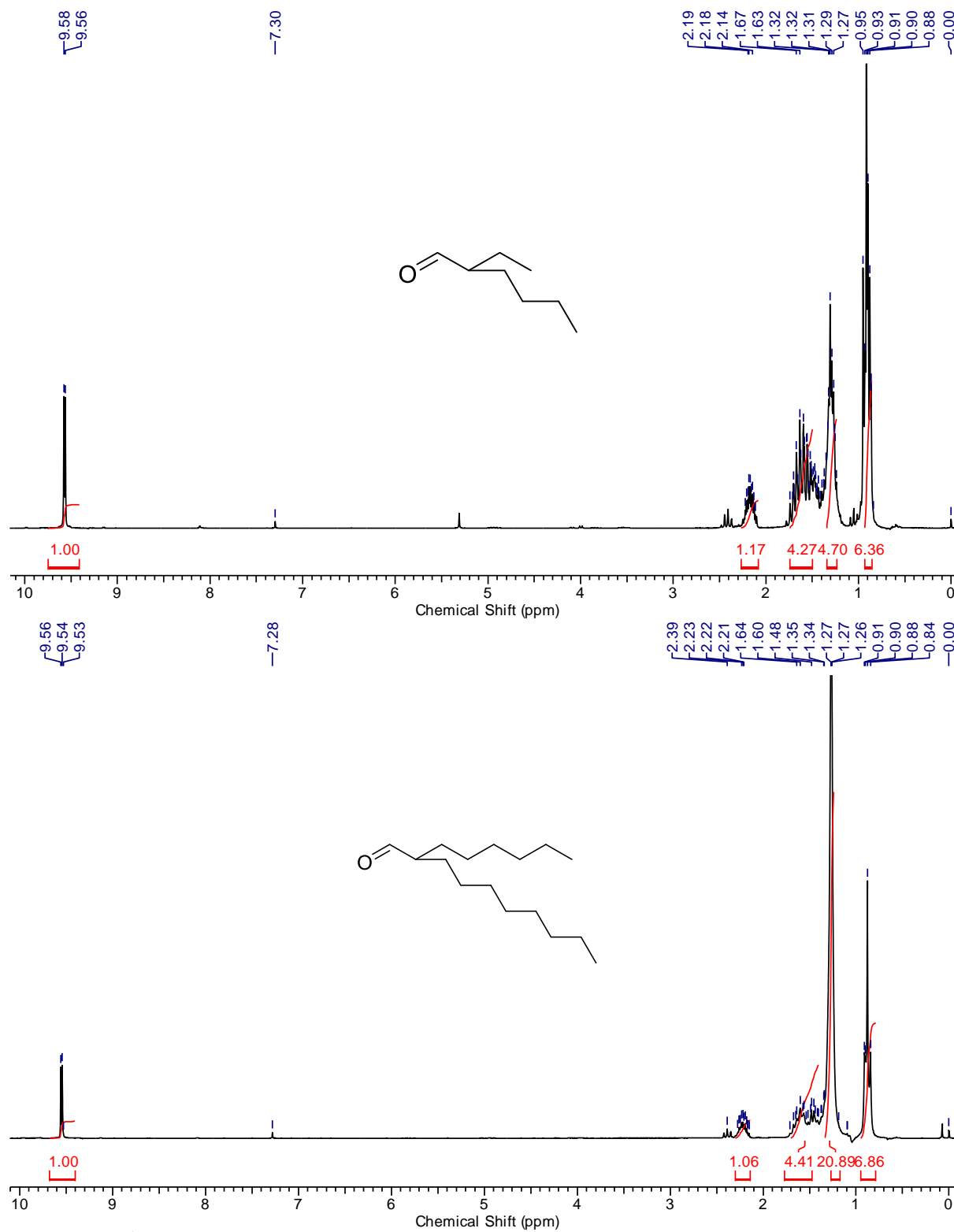
Figure A8. ^{1}H-NMR spectra of compound **7a,** and **7b** in CDCl$_3$.

9.56
9.54

7.27

2.23
2.21
2.20
1.63
1.60
1.56
1.48
1.45
1.42
1.41
1.37
1.25
0.91
0.88
0.85
0.00

1.00

1.00   4.44 36.06 6.57

10   9   8   7   6   5   4   3   2   1   0
Chemical Shift (ppm)
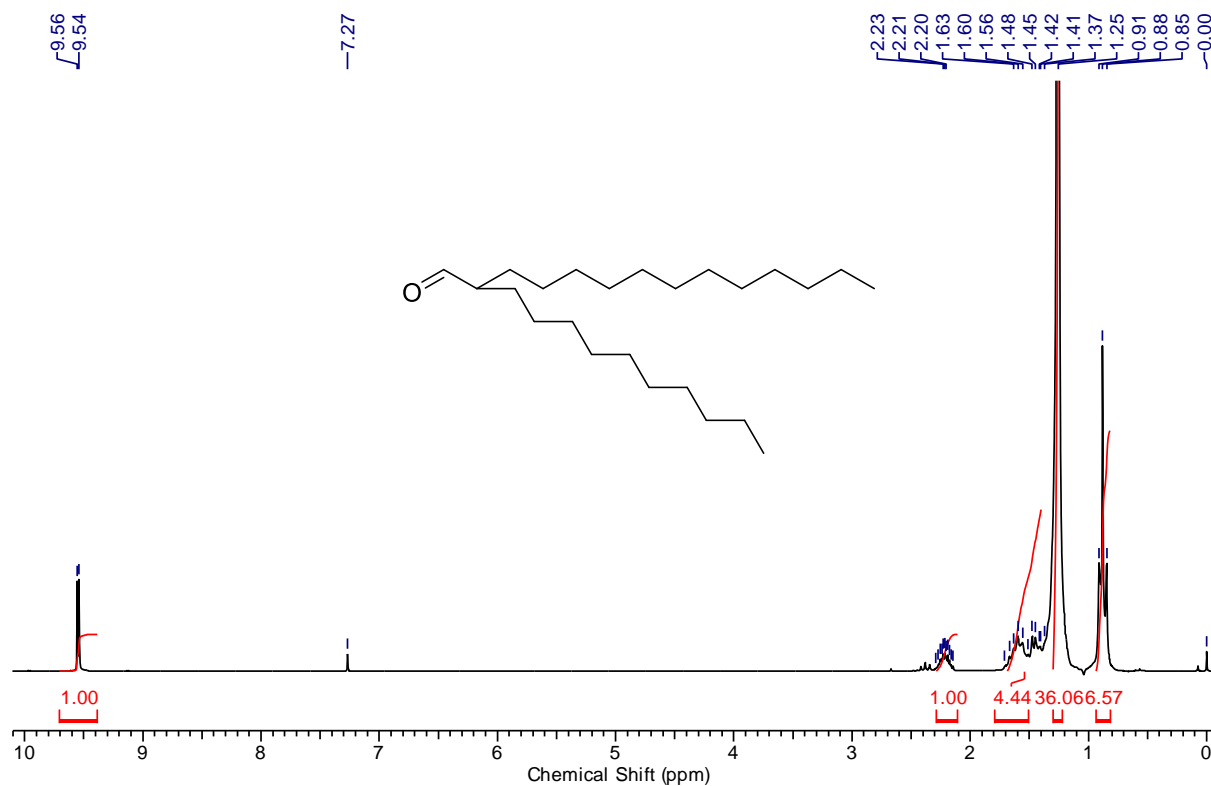
Figure A9. ^{1}H-NMR spectrum of compound **7c** in CDCl$_3$.

7.28

4.18
4.14
4.11
4.07
3.86
3.83
3.78
3.75
3.74
2.41
2.37
2.34
2.05
1.47
1.41
1.30
1.26
1.18
1.16
0.95
0.94
0.90
0.88
0.87
0.00

HO

1.09

1.17

8.84 3.00 6.14

9   8   7   6   5   4   3   2   1   0
Chemical Shift (ppm)
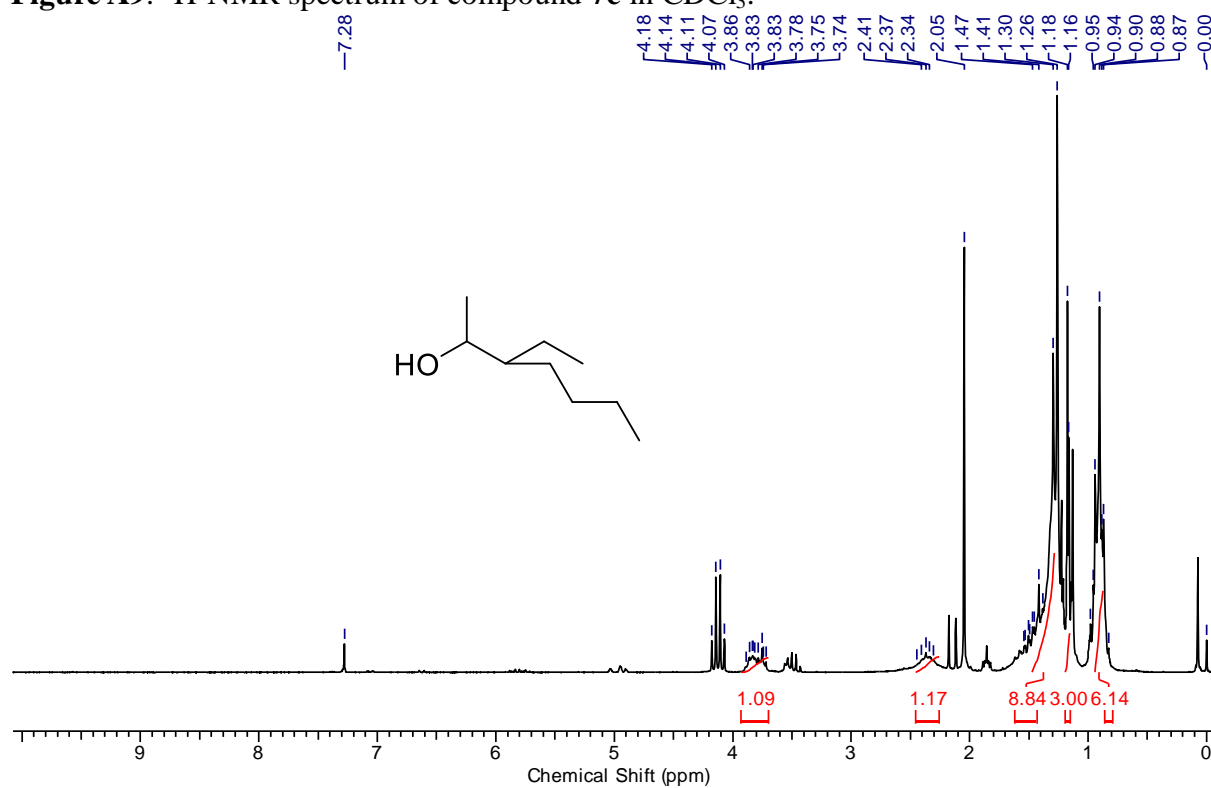
Figure A10. ^{1}H-NMR spectrum of compound **8a** in CDCl$_3$.

7.27

3.86
3.84
3.83
3.82
3.80

2.38
2.34
2.33
2.32
1.61
1.44
1.32
1.31
1.27
1.14
1.13
0.90
0.89
0.88
0.87
0.86
0.00

1.00

0.88 1.78 3.59 52.95 3.14 15.12

10 9 8 7 6 5 4 3 2 1 0
Chemical Shift (ppm)
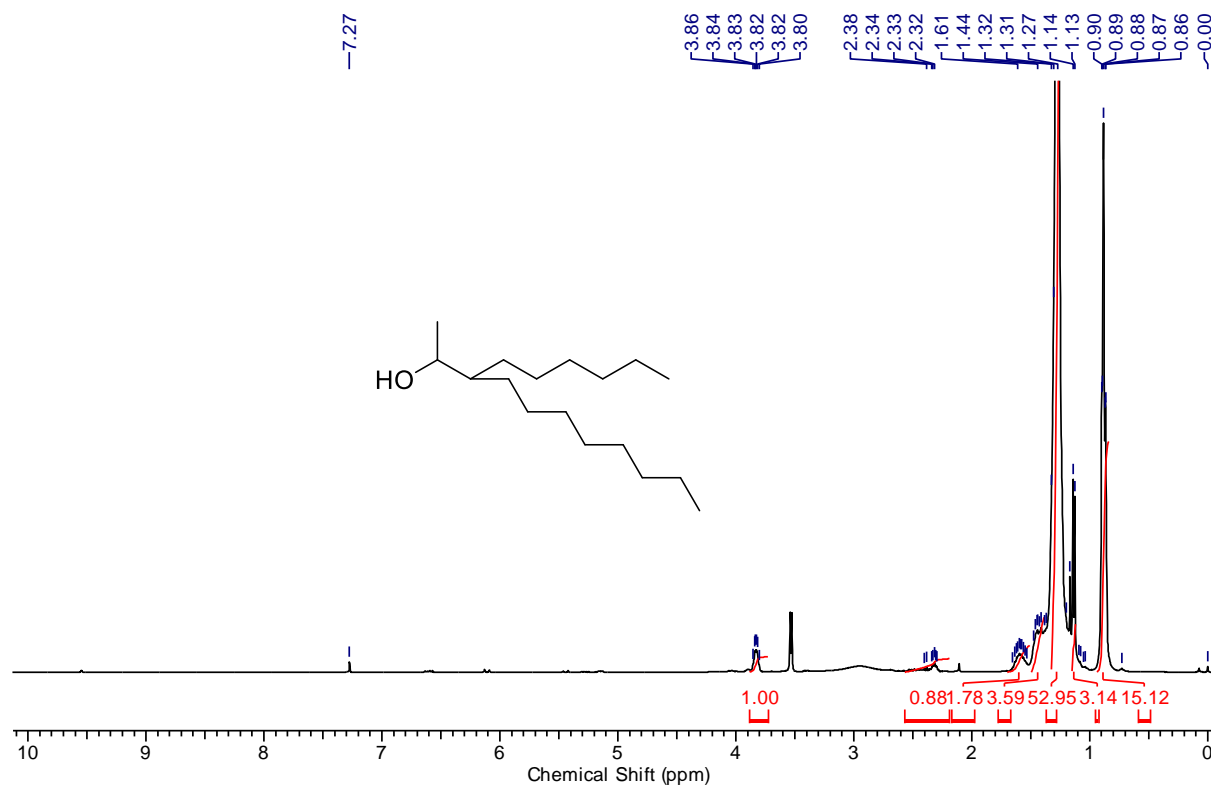
Figure A11. ^{1}H-NMR spectrum of compound **8b** in CDCl$_3$.

7.26

4.02
3.96
3.92
3.91
3.89
3.88
3.86
3.84

2.36
2.35
2.34
2.33
1.60
1.45
1.38
1.38
1.32
1.30
1.26
1.20
1.17
0.90
0.88
0.86
0.00

1.02

0.70 2.86 2.40 89.89 3.04 14.18

10 9 8 7 6 5 4 3 2 1 0
Chemical Shift (ppm)
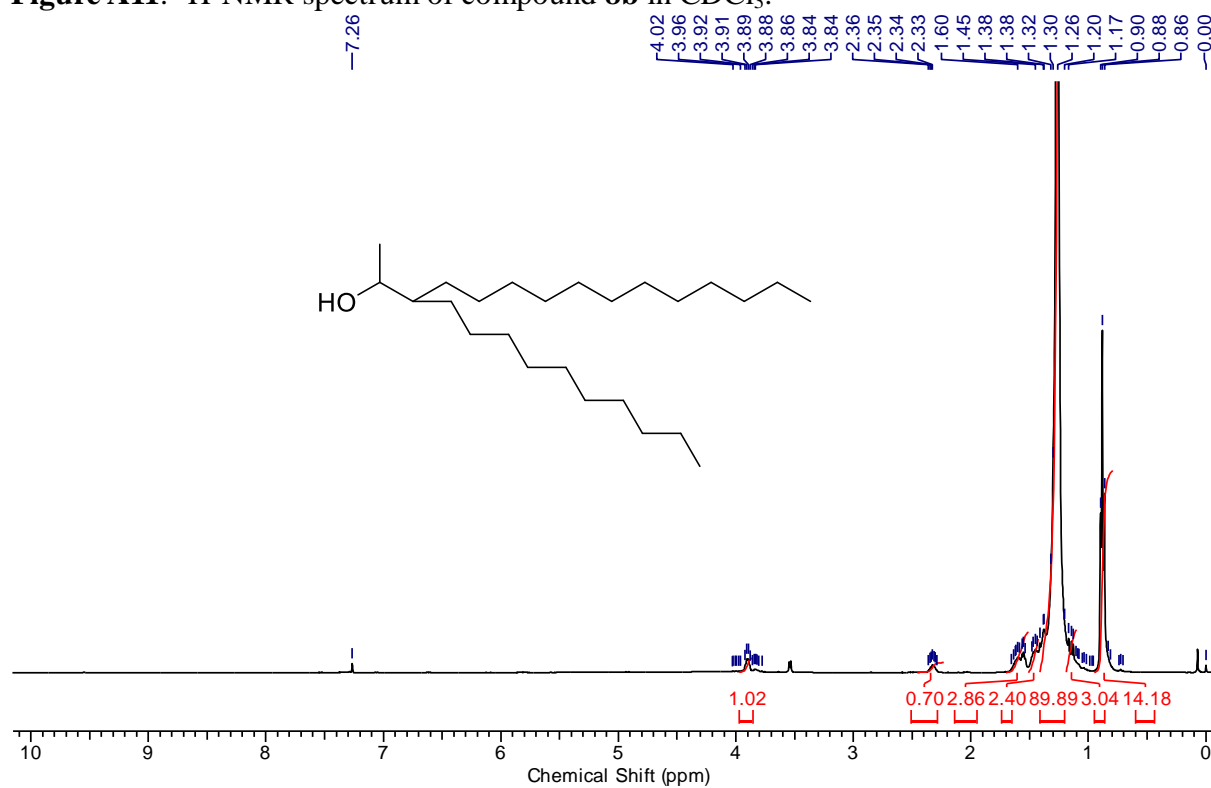
Figure A12. ^{1}H-NMR spectrum of compound **8c** in CDCl$_3$.
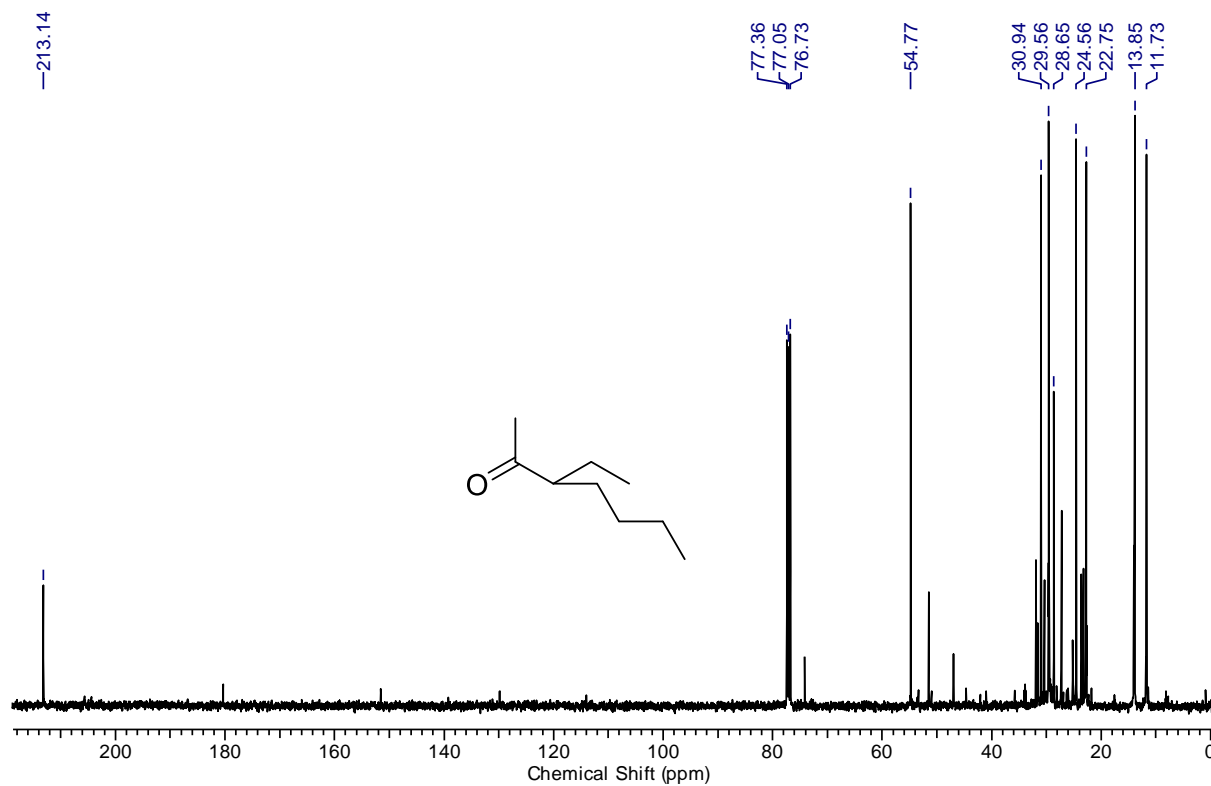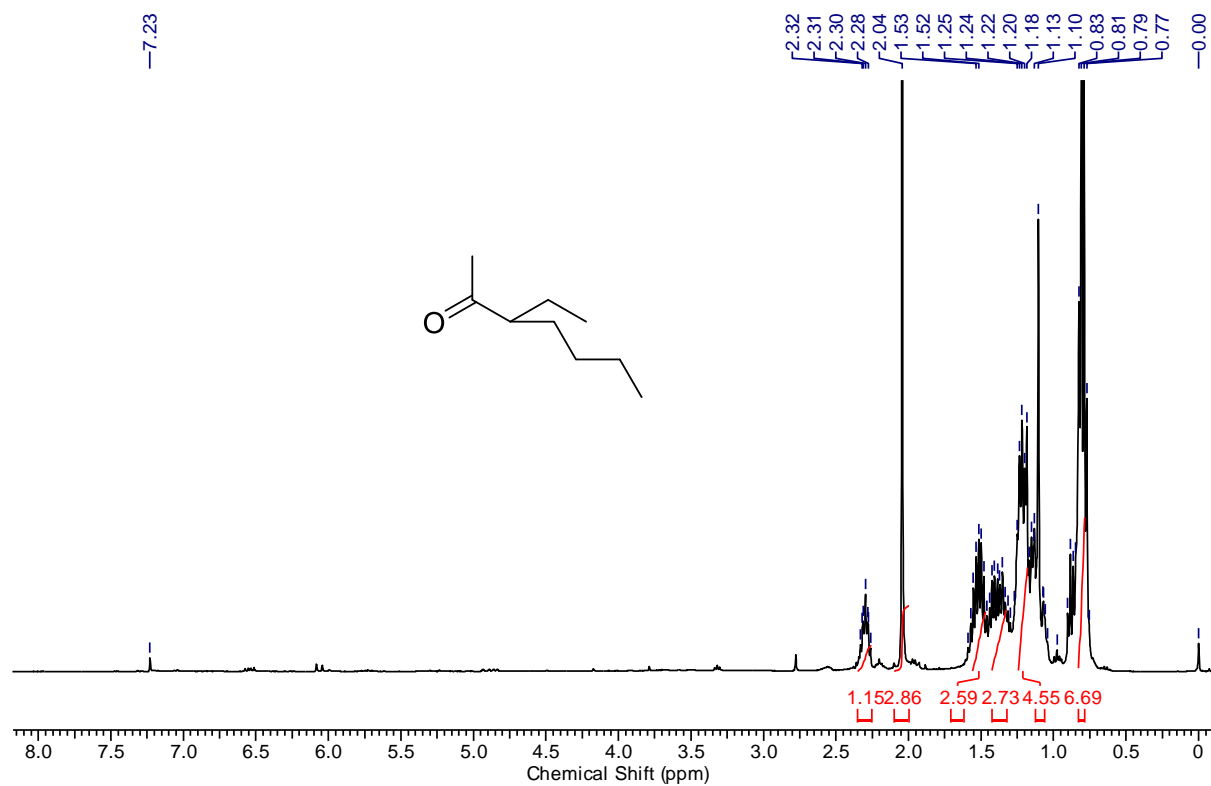
Figure A13. ^{1}H and ^{13}C-NMR spectra of compound **9a** in CDCl$_3$.
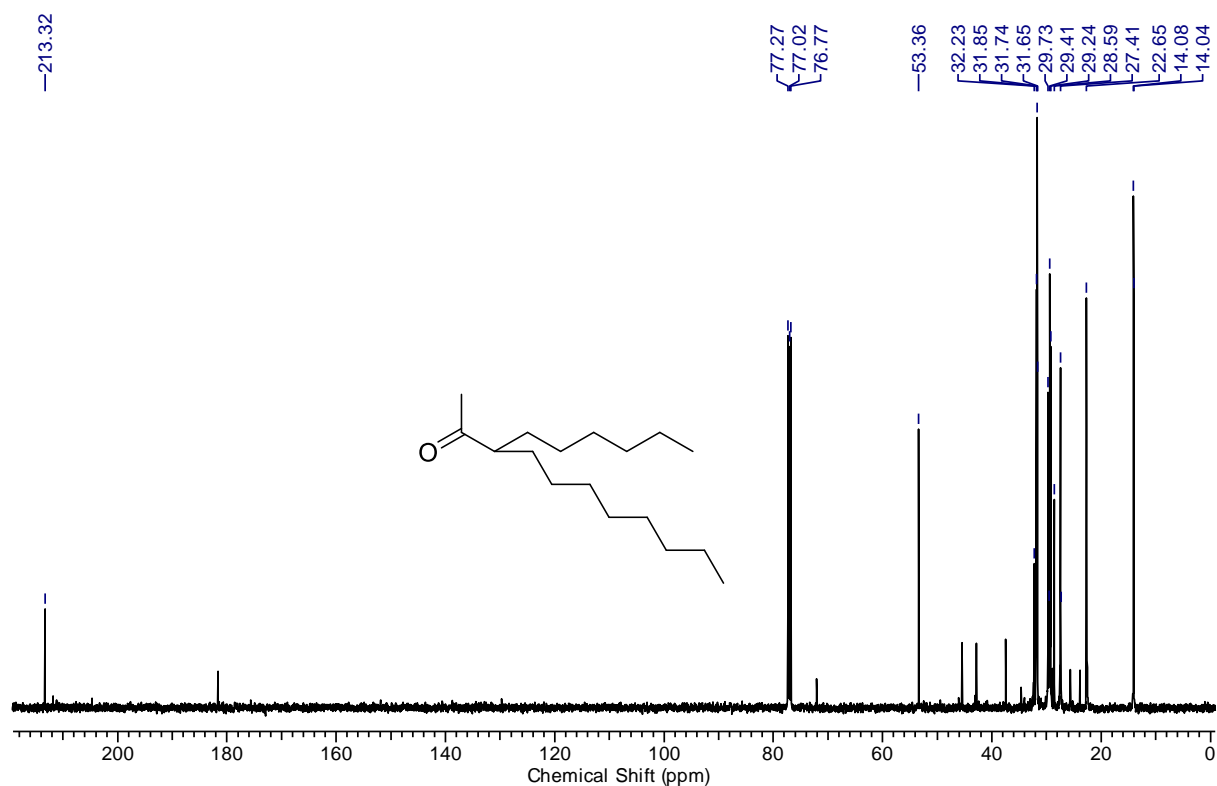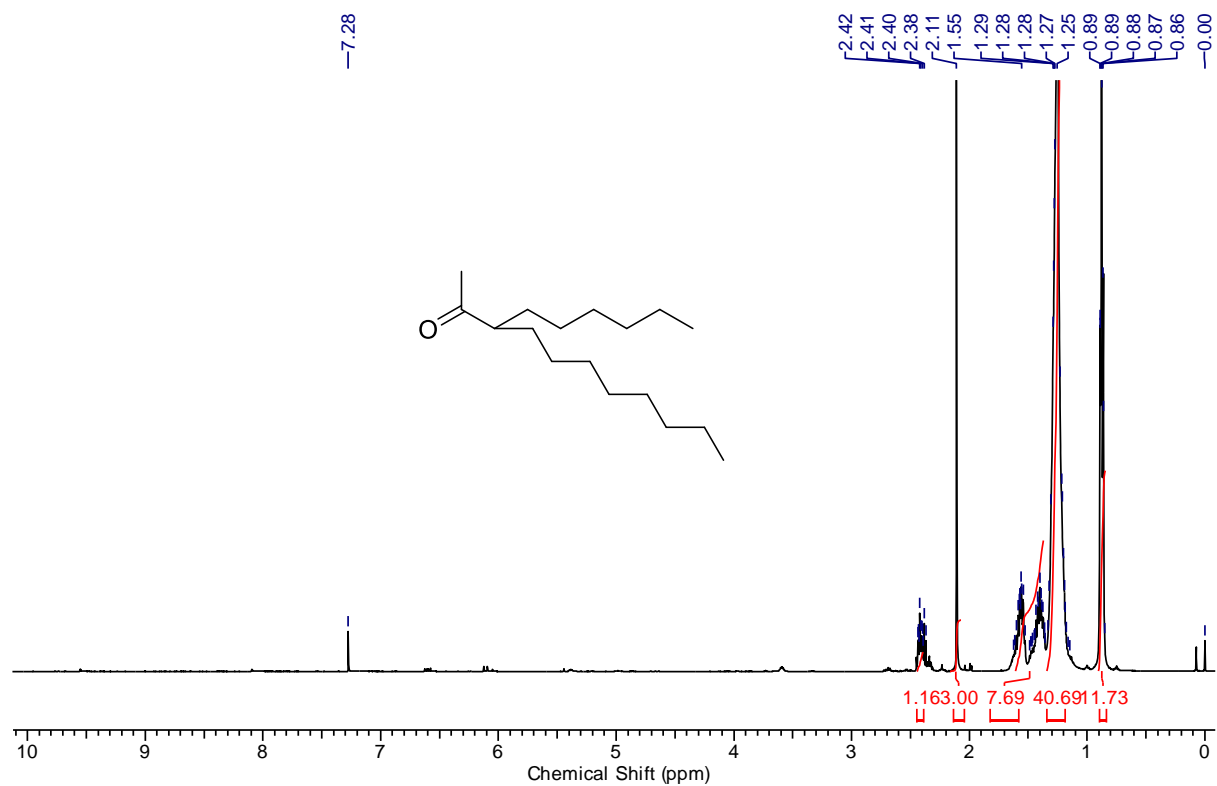
Figure A14. . ^{1}H and ^{13}C-NMR spectra of compound **9b** in CDCl$_3$.
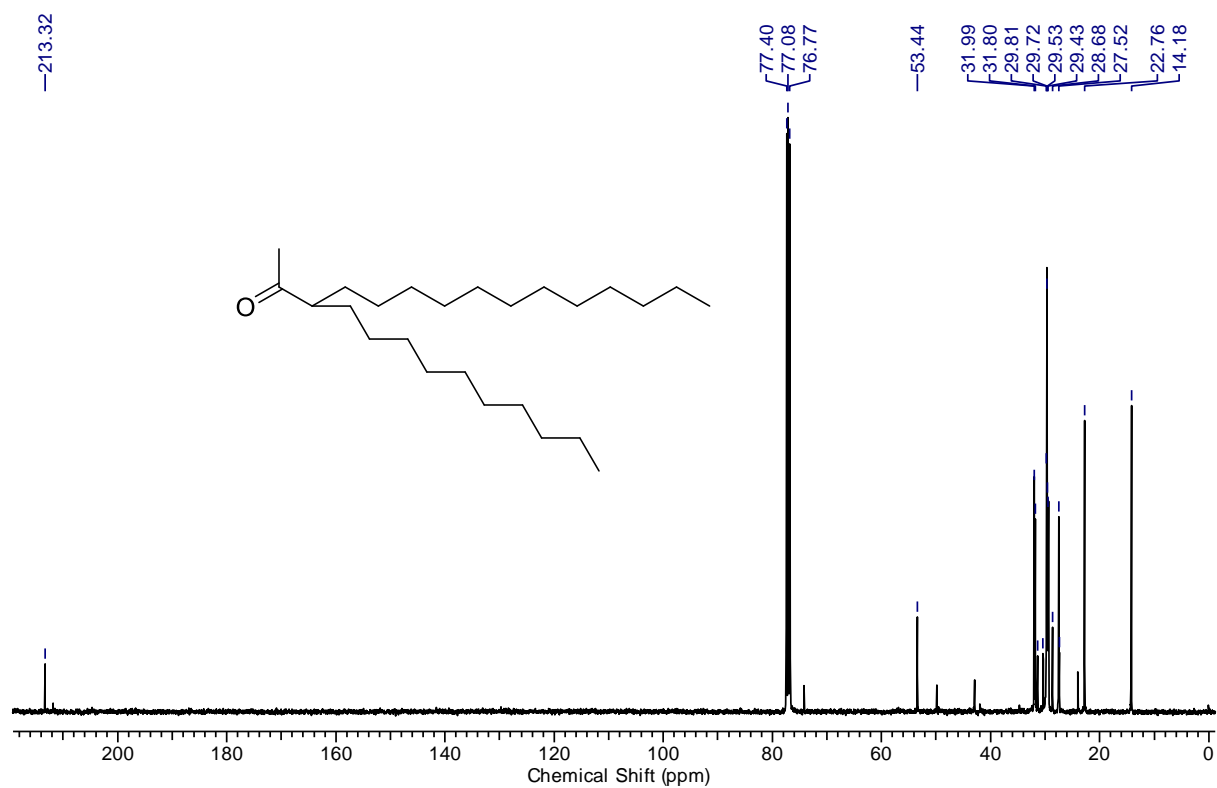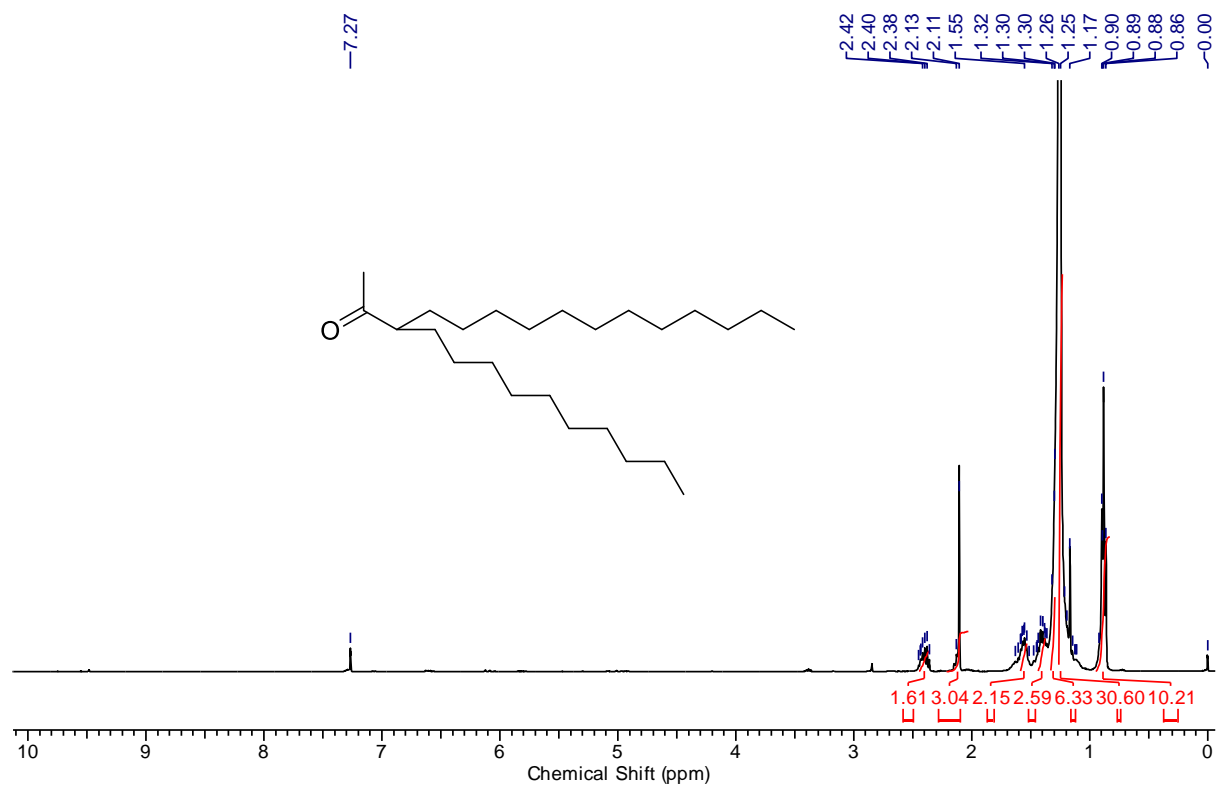
Figure A15. . ^{1}H and ^{13}C-NMR spectra of compound **9c** in CDCl₃.
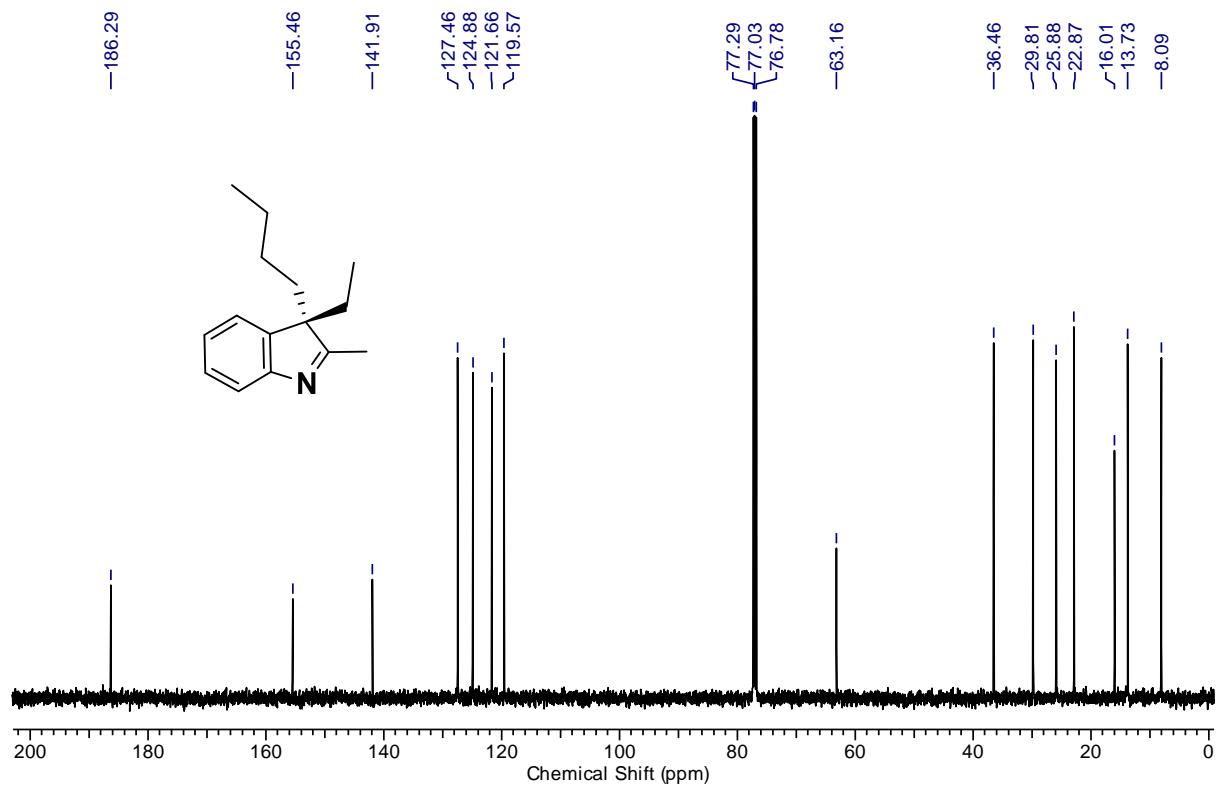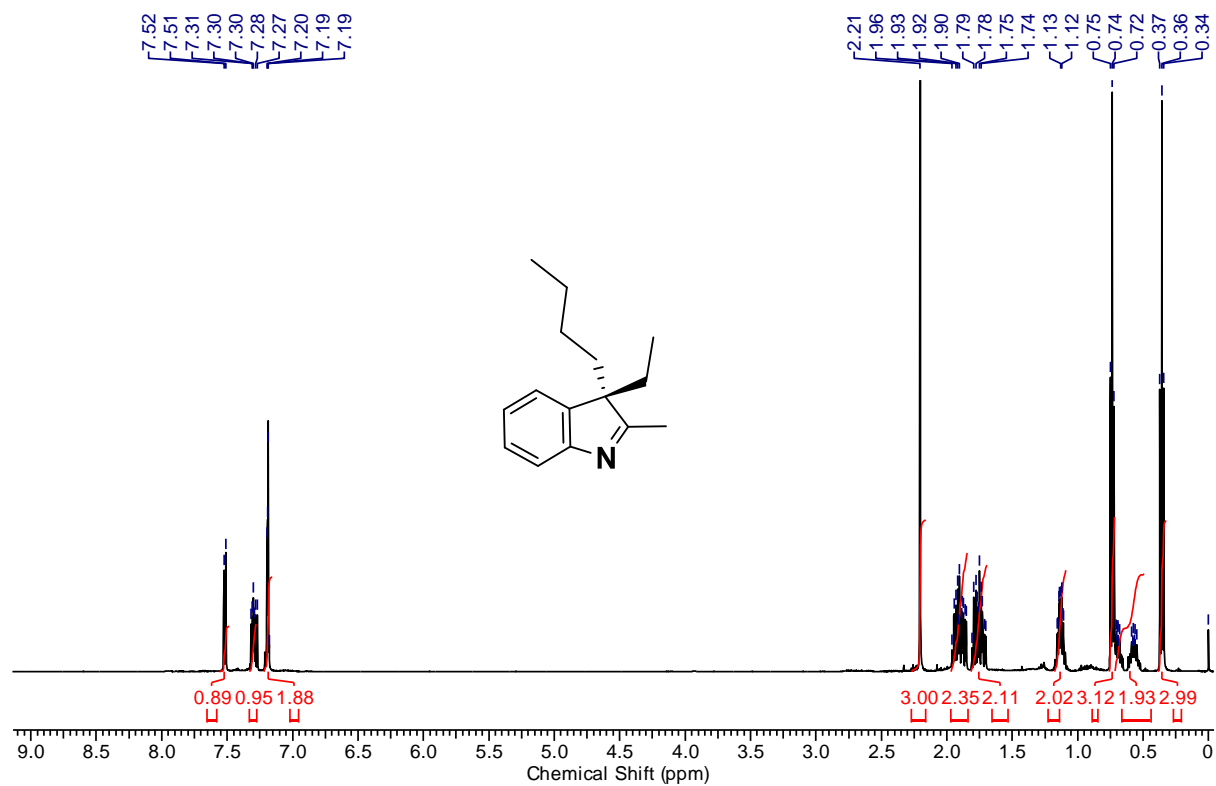
Figure A16. . ^{1}H and ^{13}C-NMR spectra of compound **10a** in CDCl$_3$.
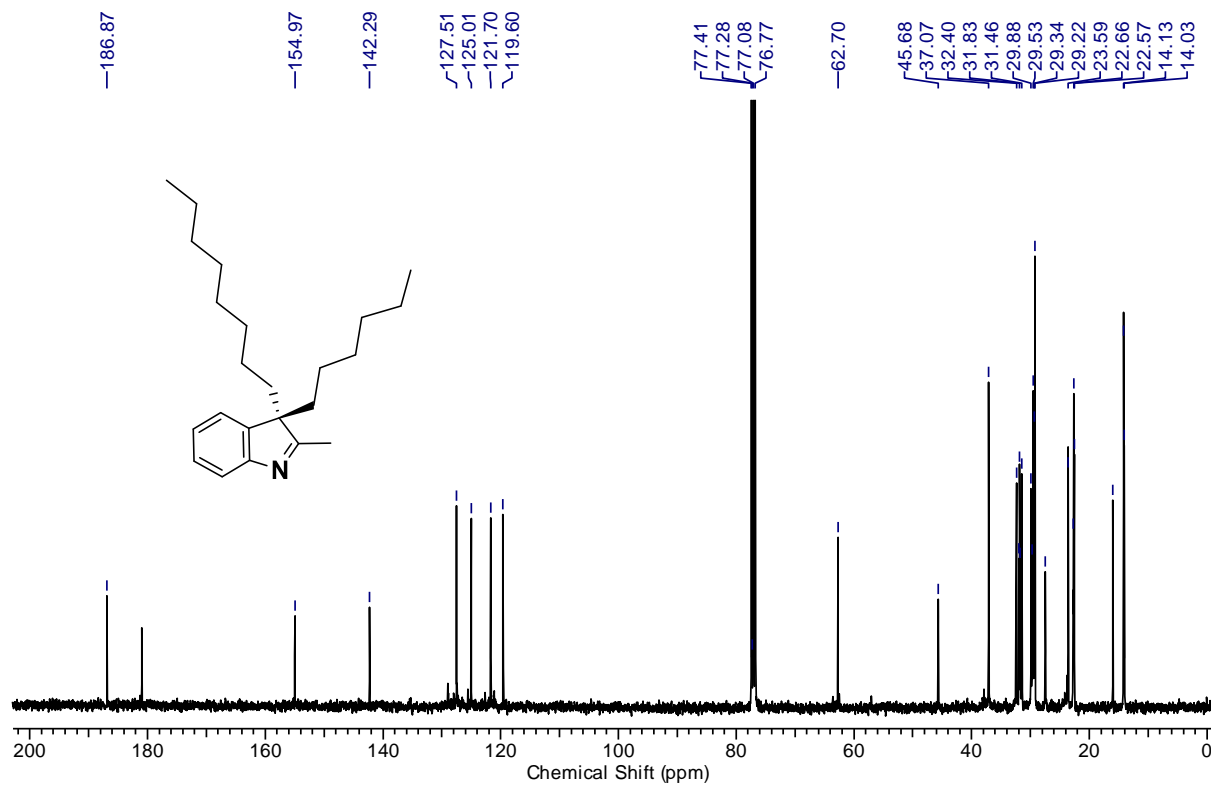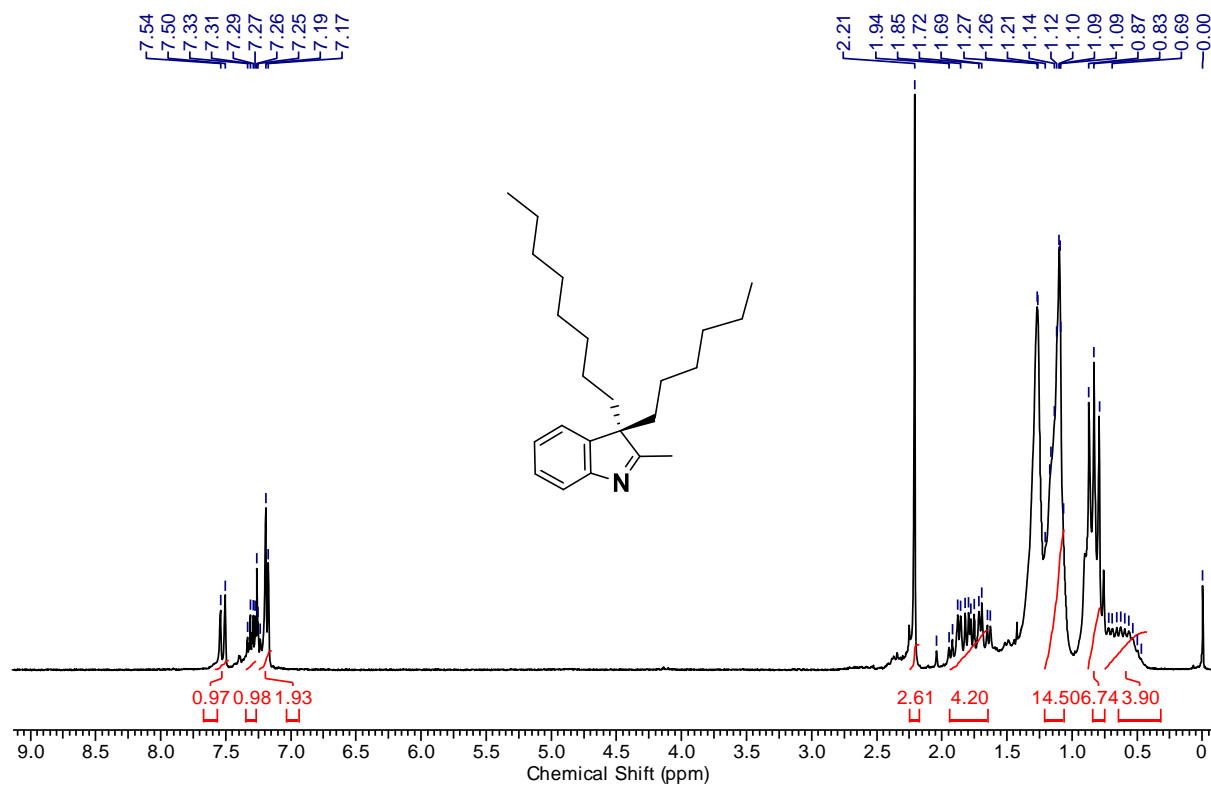
Figure A17. ^{1}H and ^{13}C-NMR spectra of compound **10b** in CDCl₃.
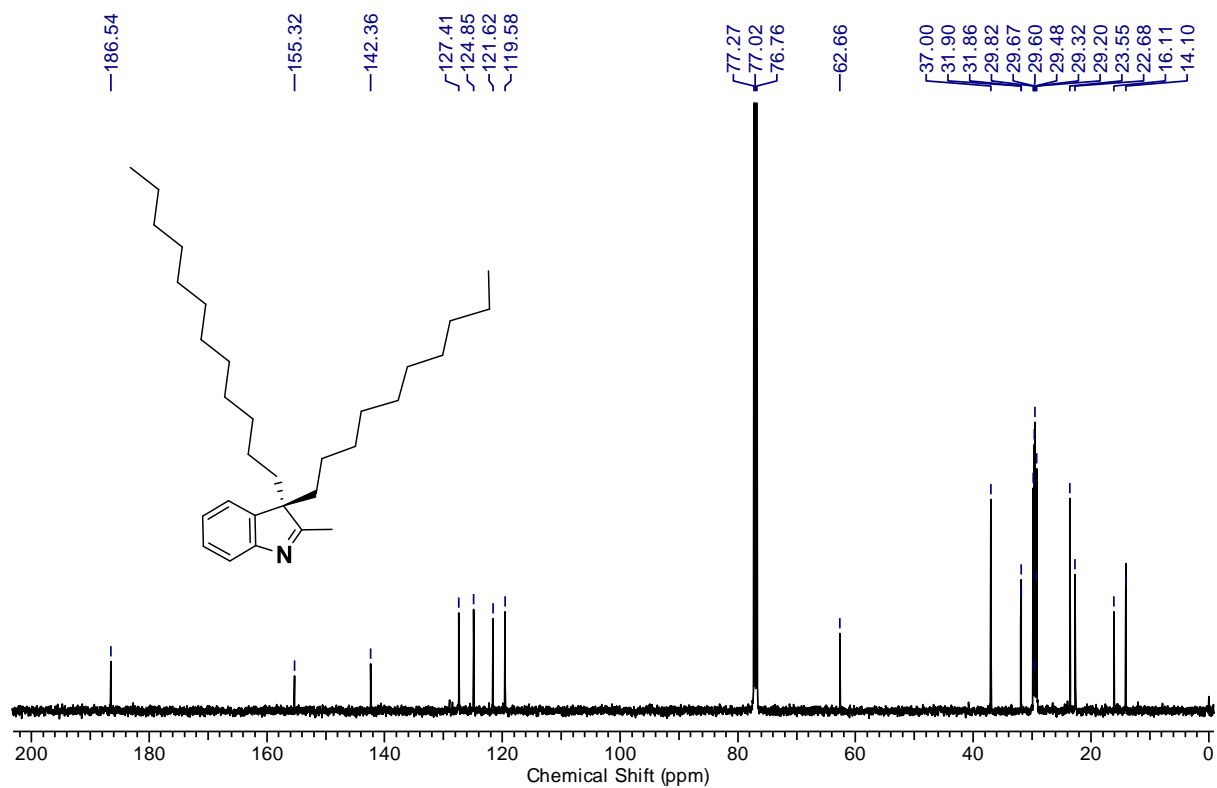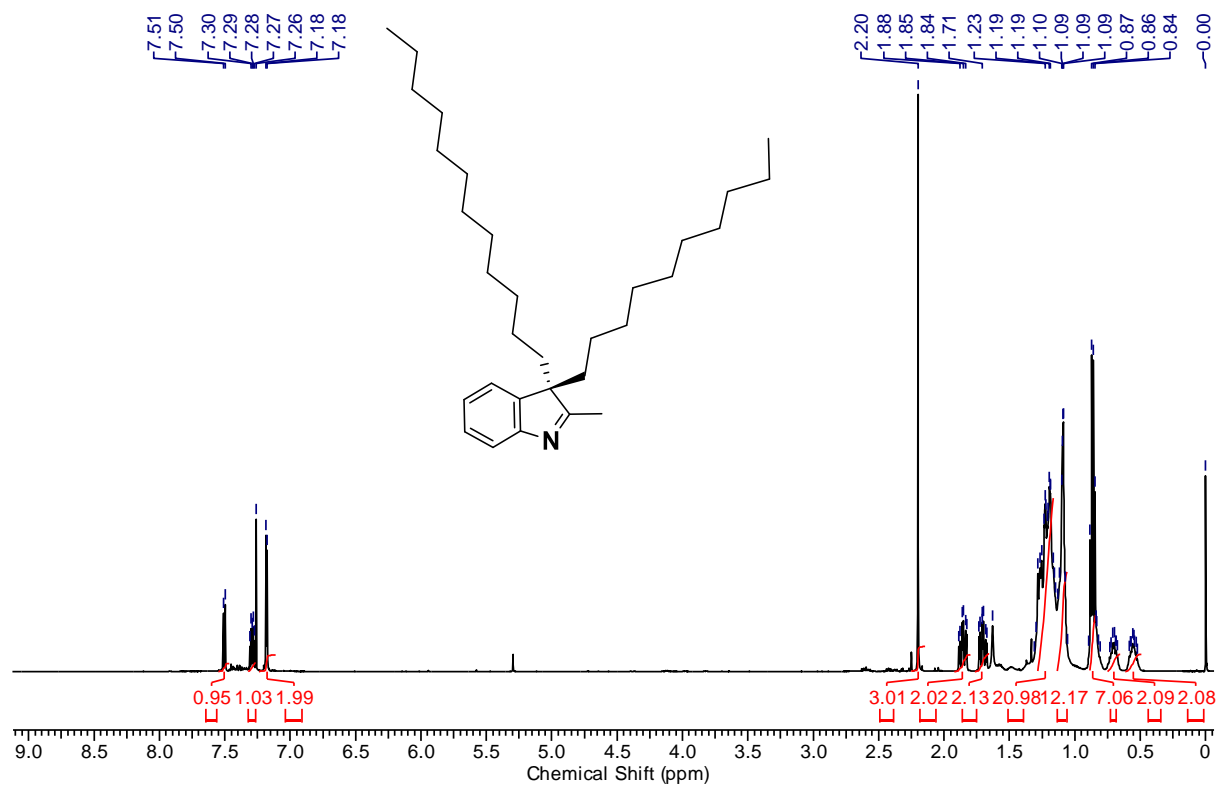
Figure A18. ^{1}H and ^{13}C-NMR spectra of compound **10c** in CDCl$_3$.
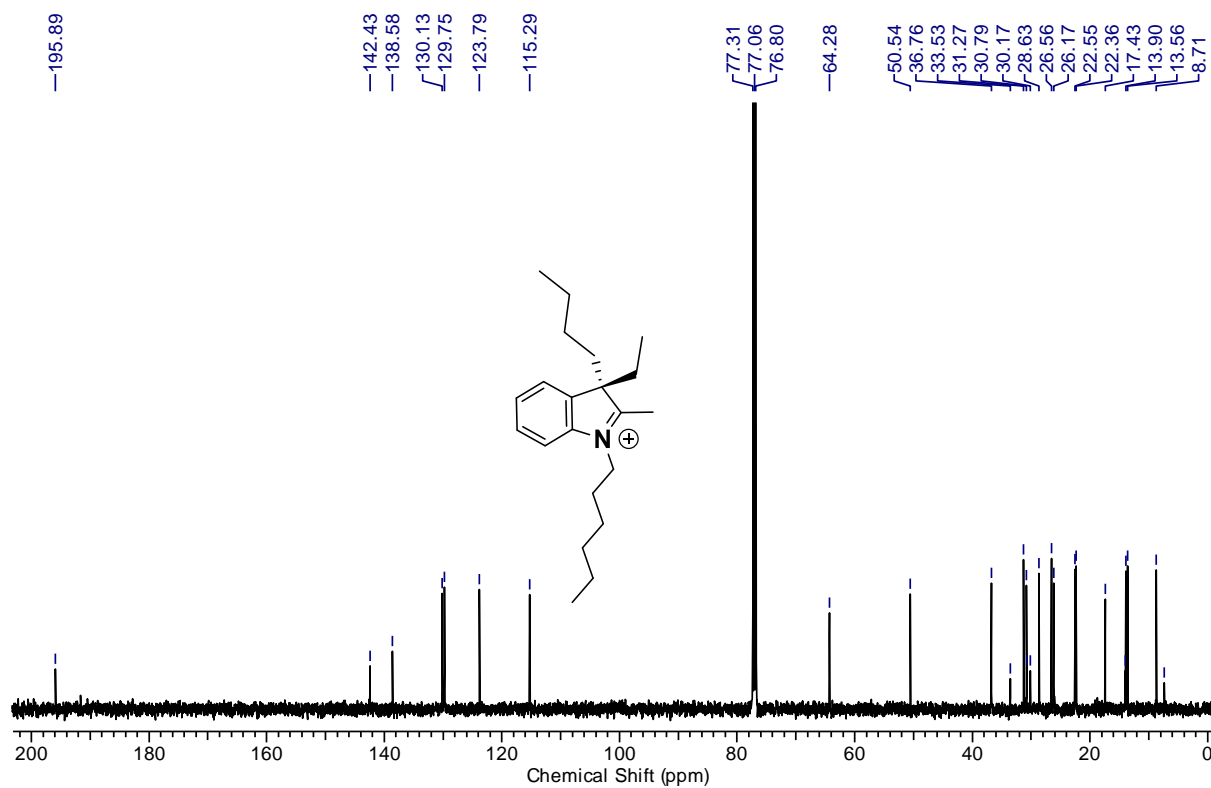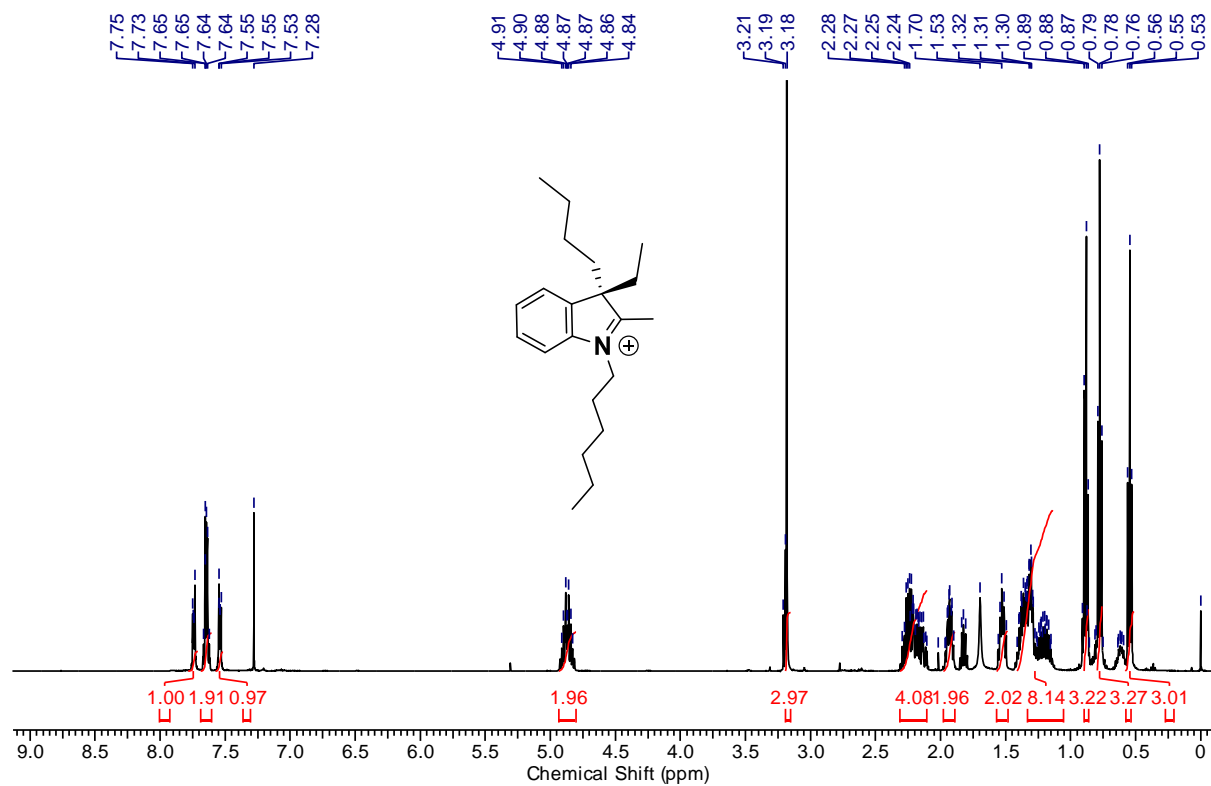
Figure A19. ^{1}H and ^{13}C-NMR spectra of compound **11a** in CDCl₃.
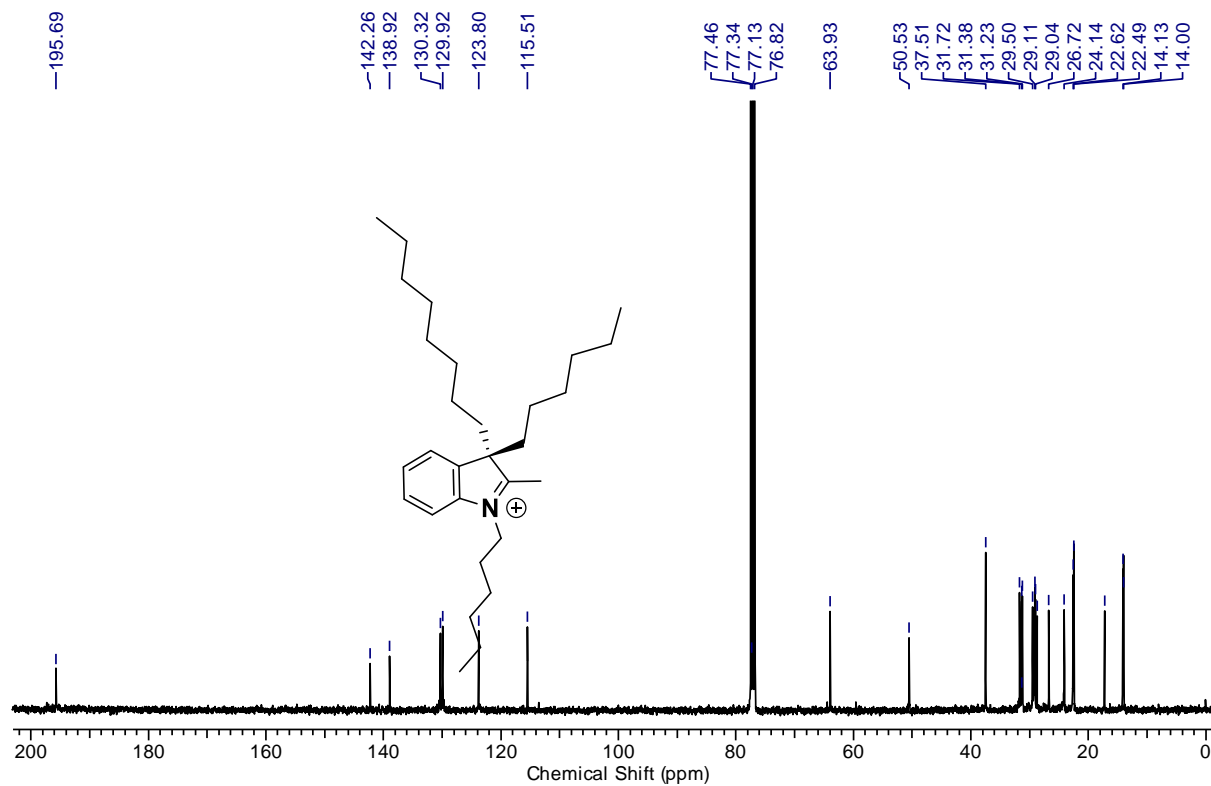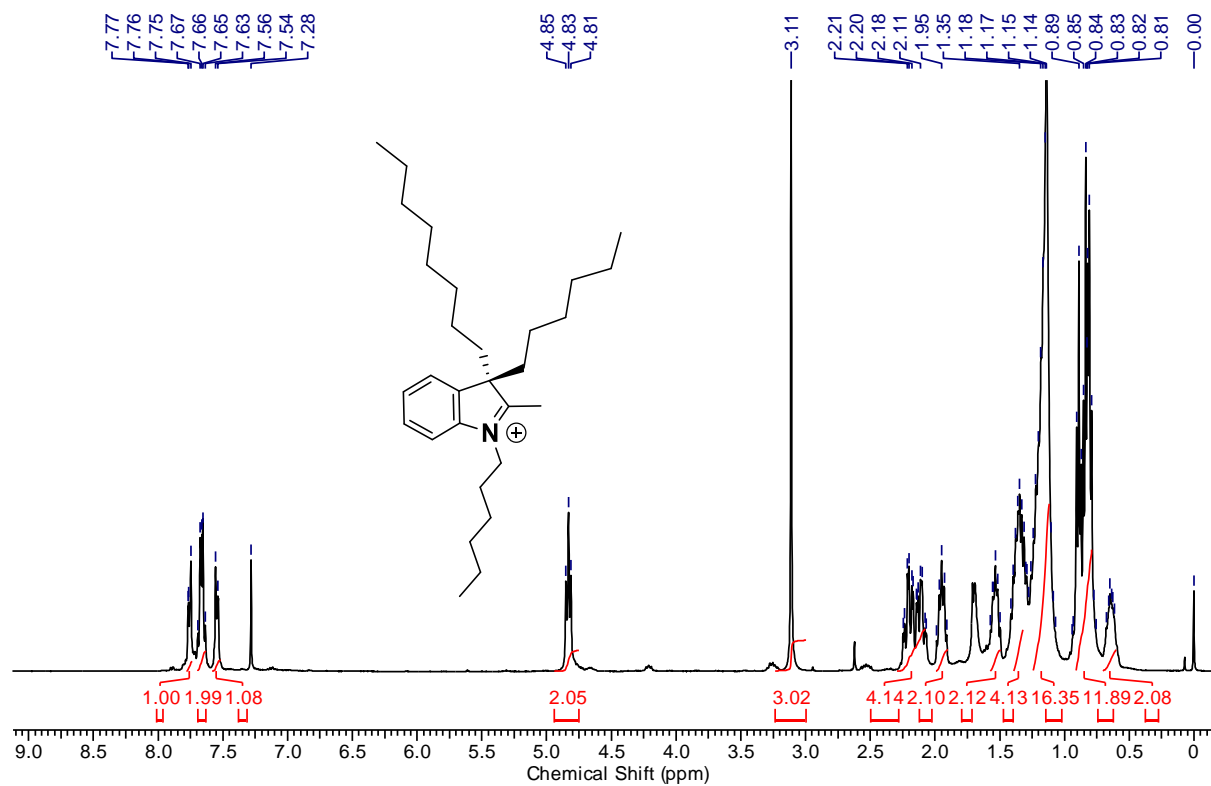
Figure A20. ^{1}H and ^{13}C-NMR spectra of compound **11b** in CDCl$_3$.
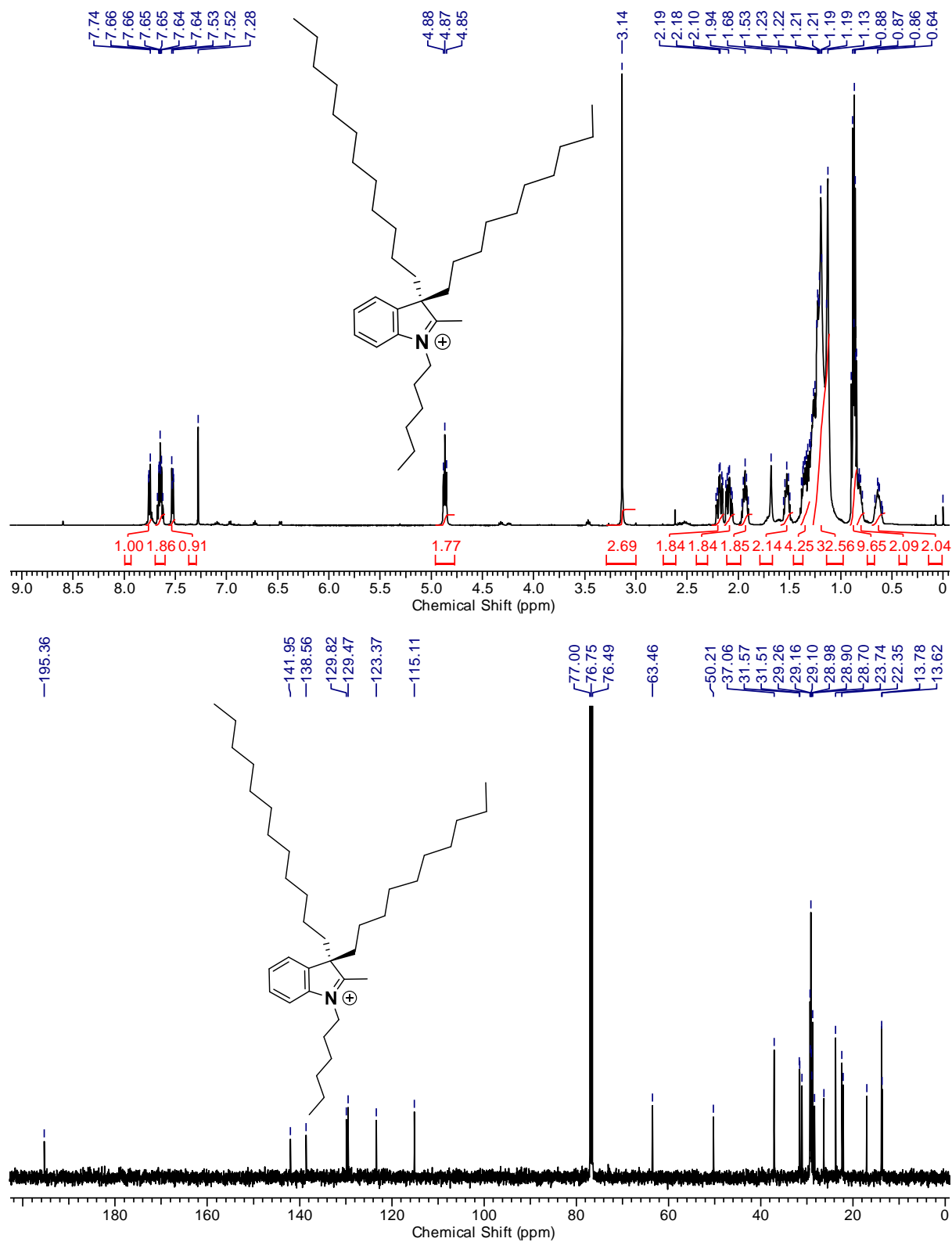
Figure A21. ^{1}H and ^{13}C-NMR spectra of compound **11c** in CDCl₃.
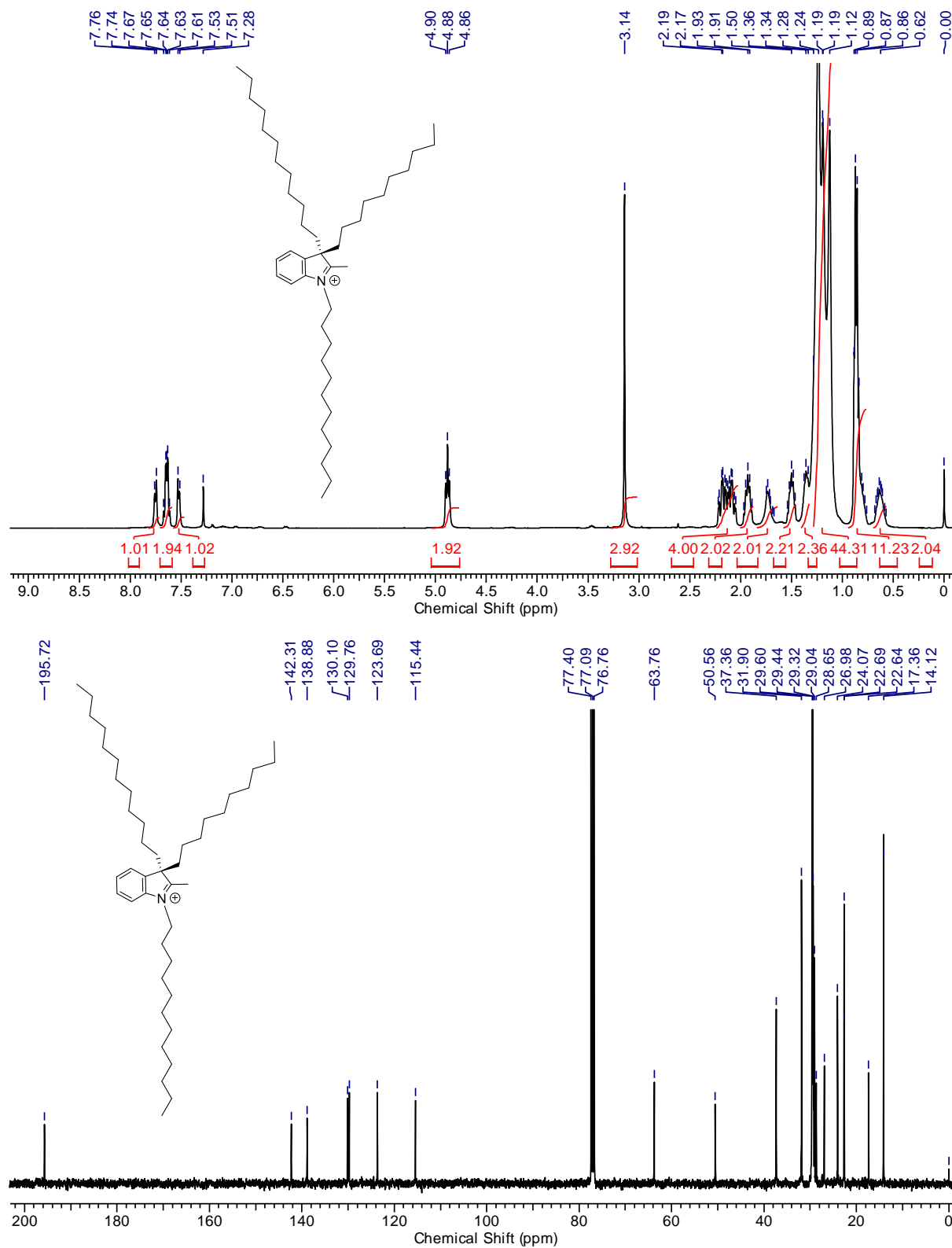
Figure A22. ^{1}H and ^{13}C-NMR spectra of compound **11d** in CDCl₃.
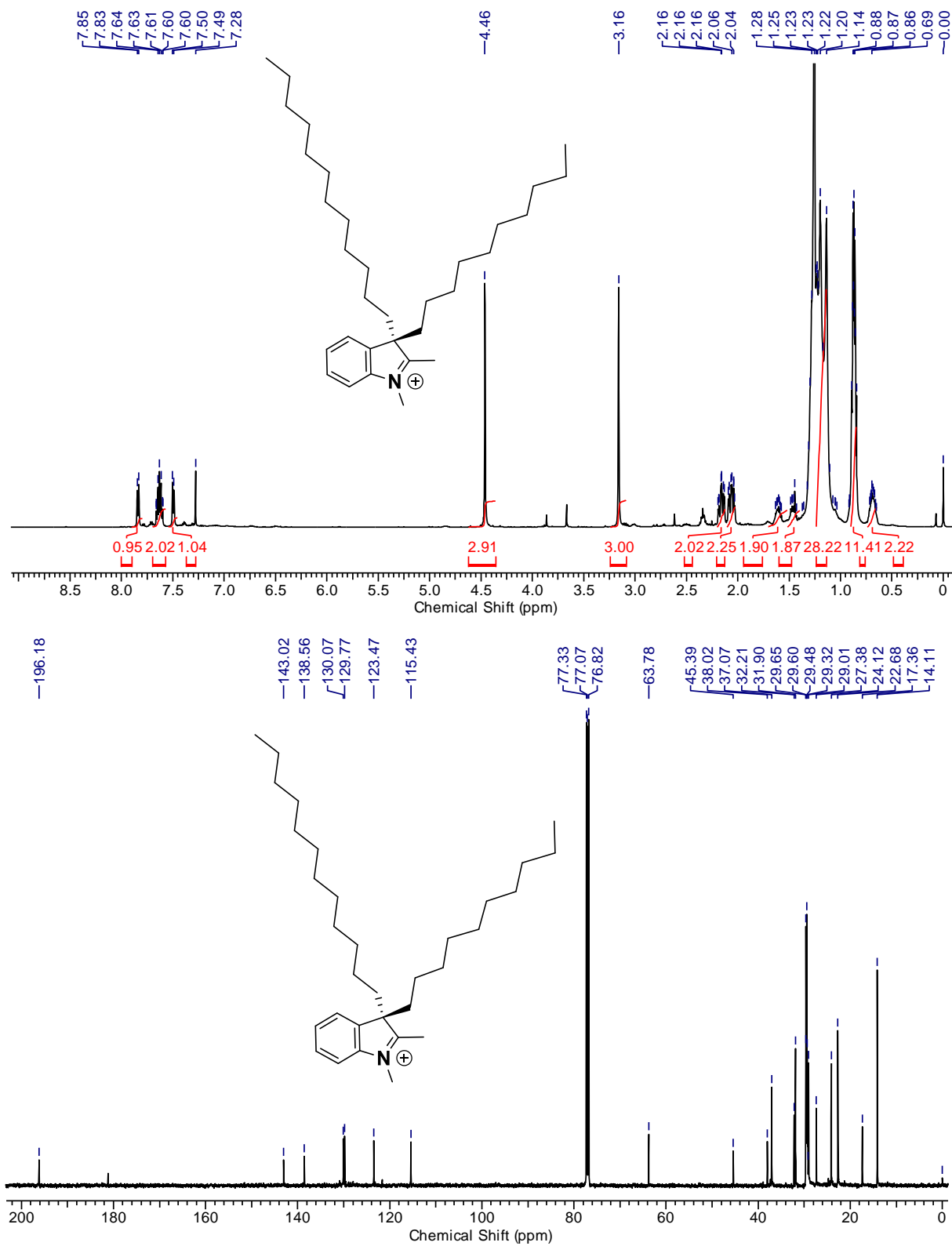
Figure A23. ^{1}H and ^{13}C-NMR spectra of compound **11e** in CDCl$_3$.
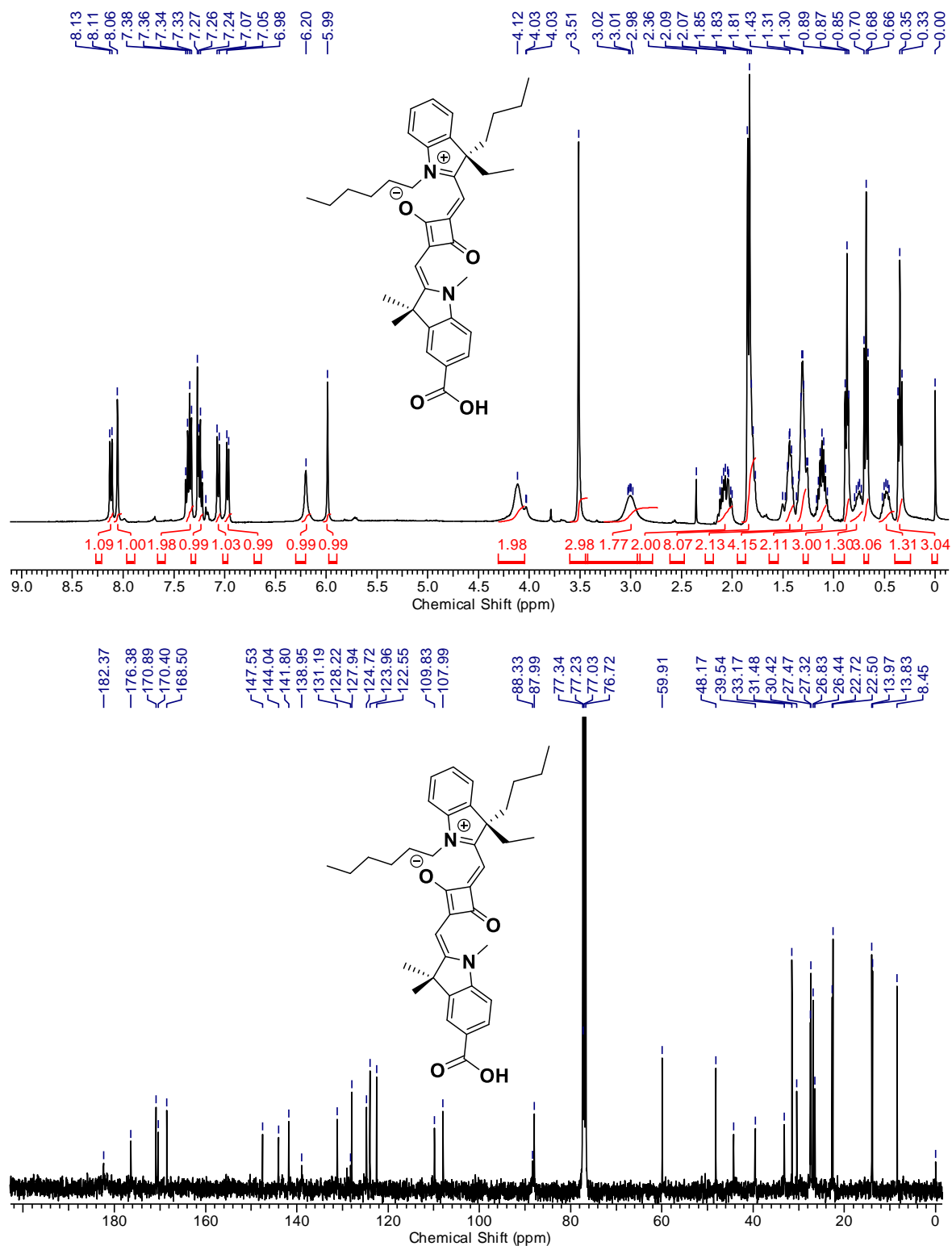
Figure A24. ^{1}H and ^{13}C NMR spectra of compound **13a (SQS1)** in CDCl$_3$.
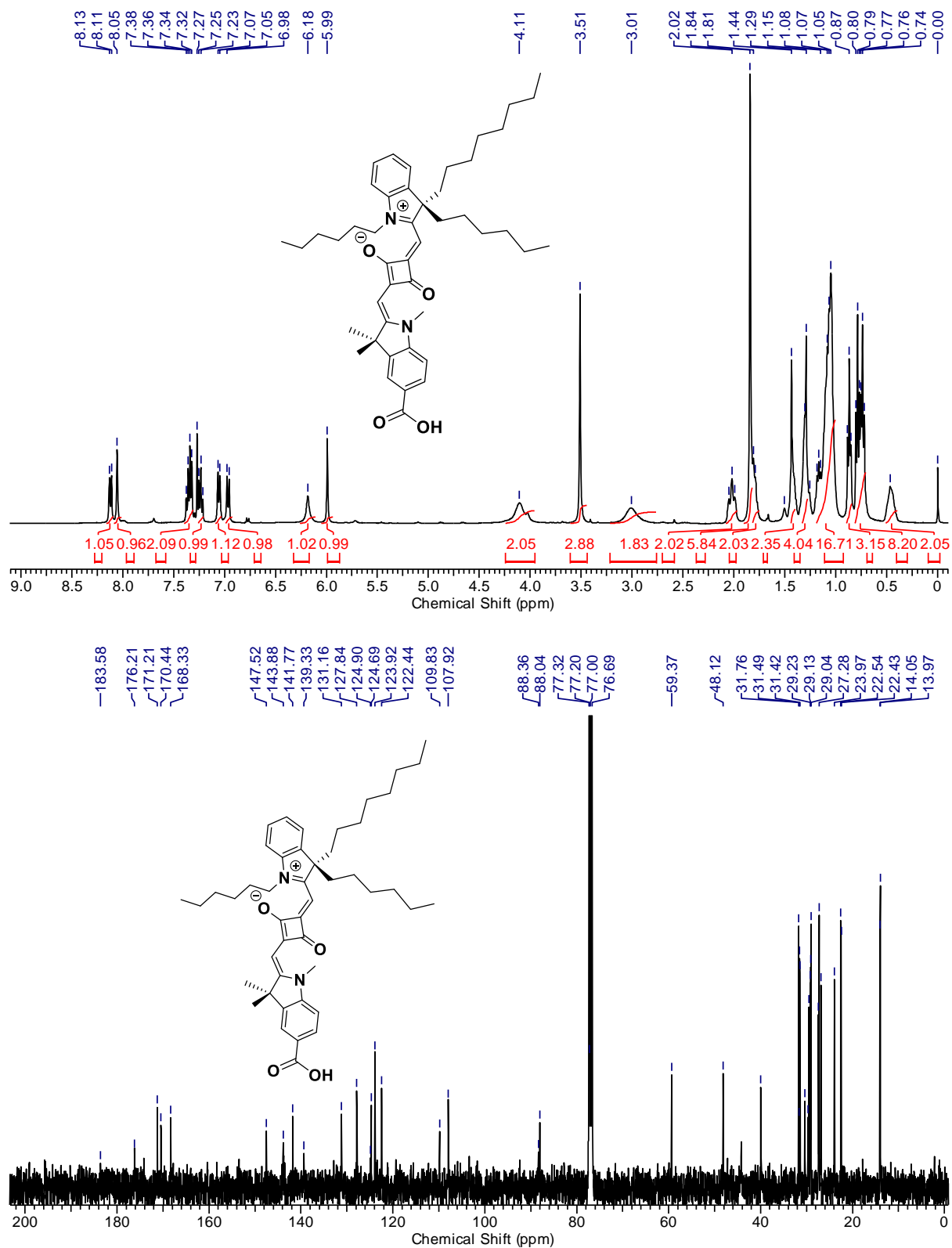
Figure A25. ^{1}H and ^{13}C NMR spectra of compound **13b (SQS2)** in CDCl$_3$.
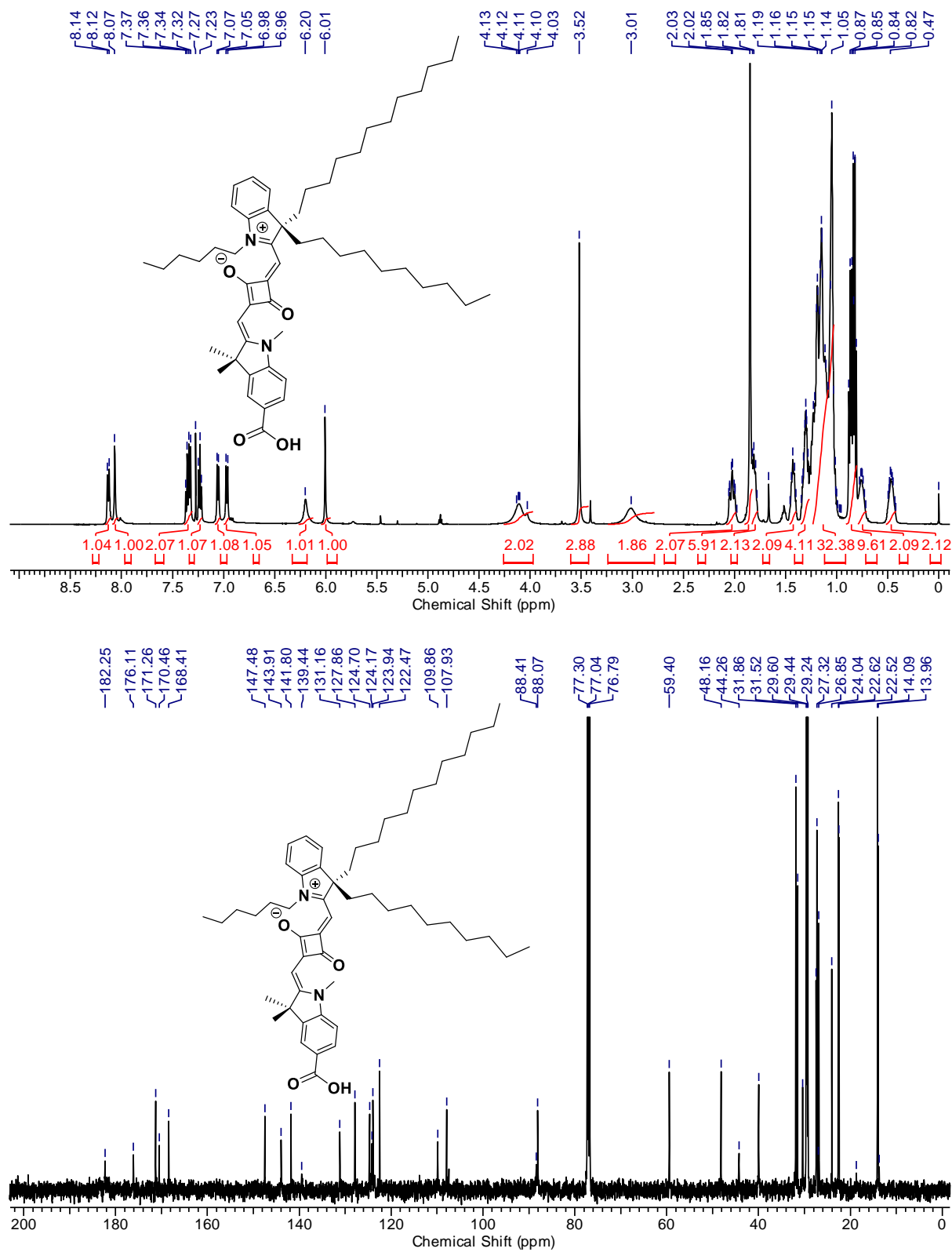
Figure A26. ^{1}H and ^{13}C NMR spectra of compound **13c (SQS3)** in CDCl$_3$.
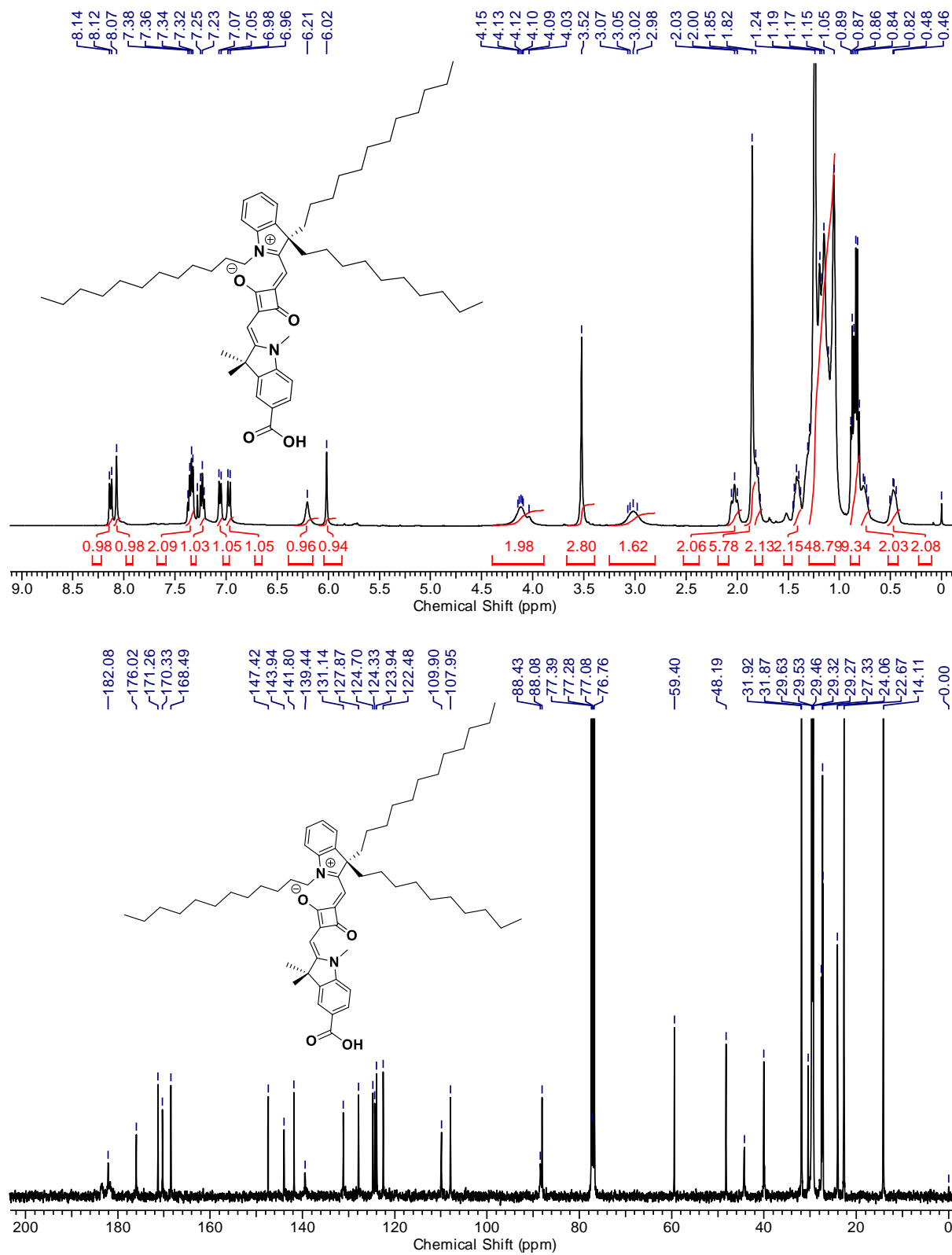
Figure A27. ^{1}H and ^{13}C NMR spectra of compound **13d (SQS4)** in CDCl$_3$.
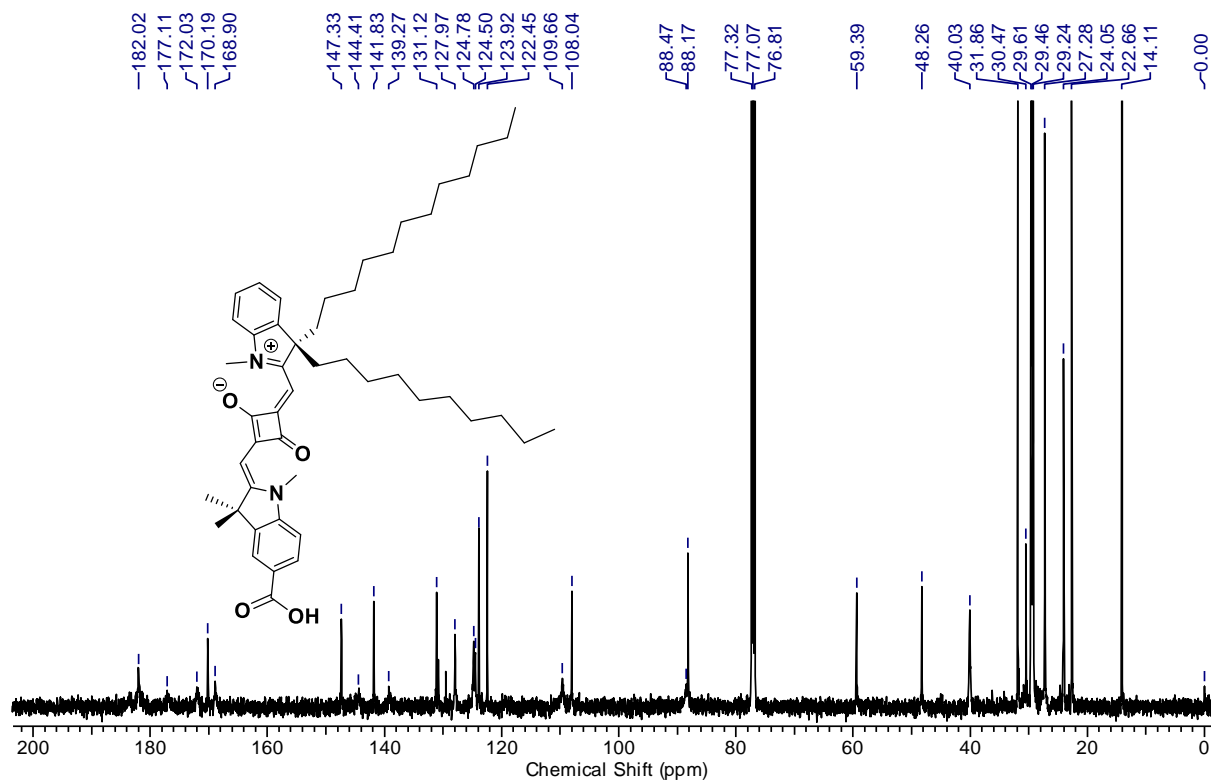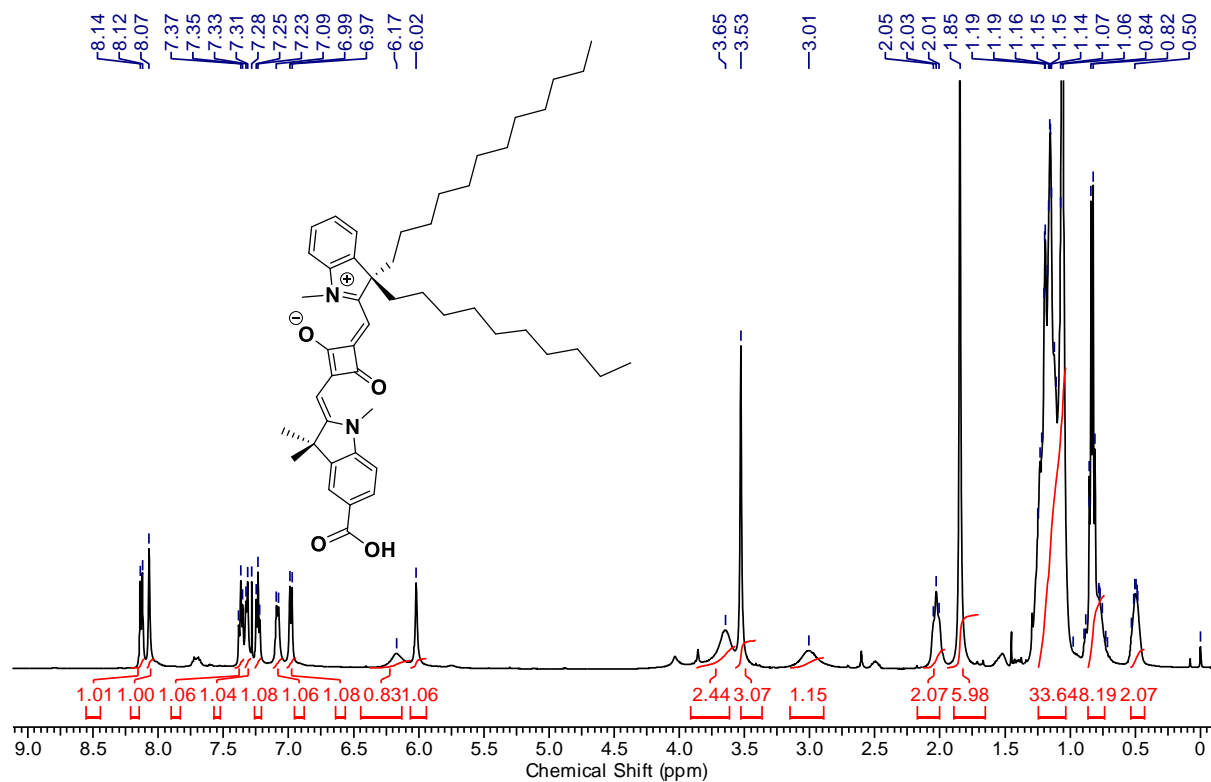
Figure A28. ^{1}H and ^{13}C NMR spectra of compound **13e (SQS5)** in CDCl$_3$.
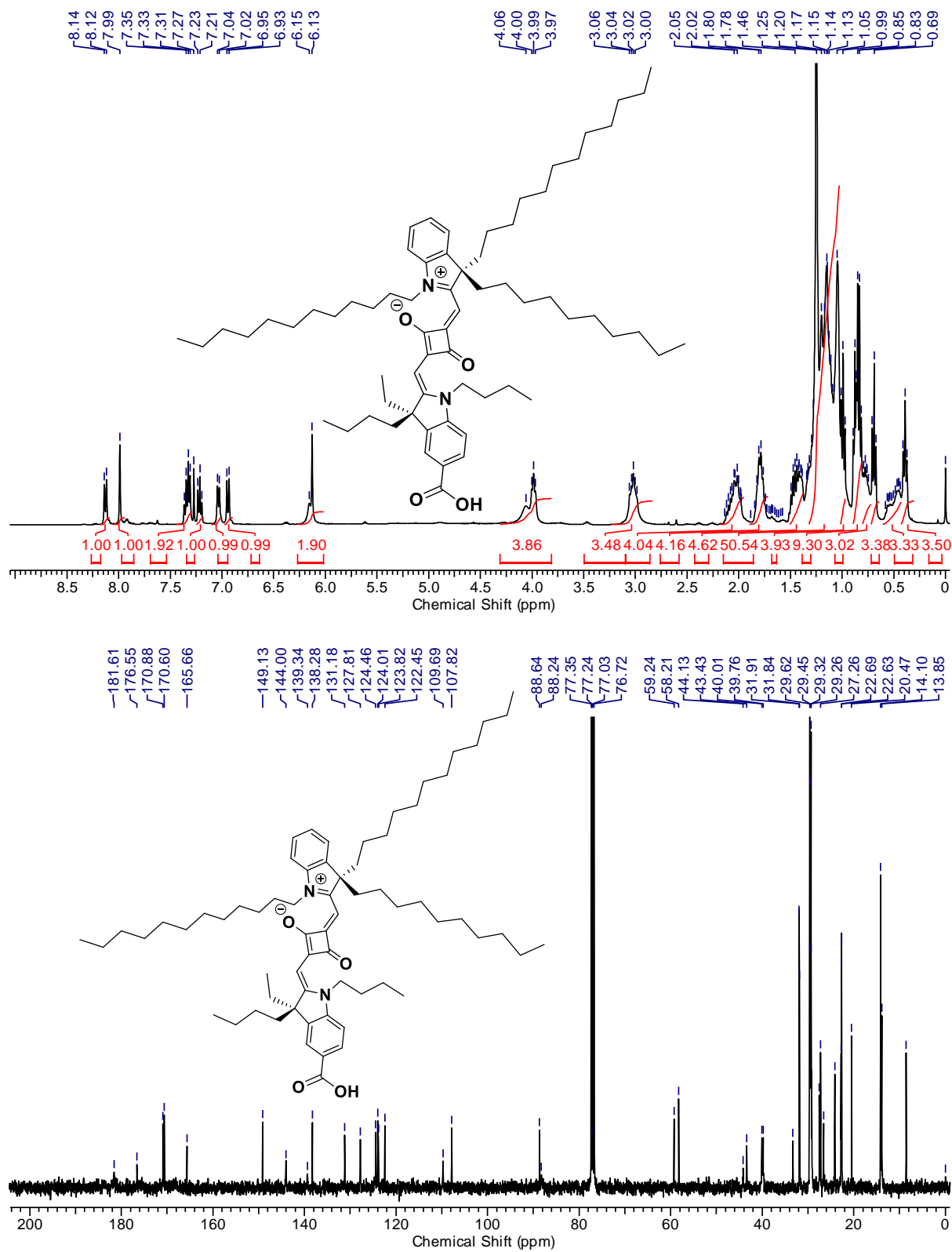
Figure A29. ^{1}H and ^{13}C NMR spectra of compound **13f (SQS6)** in CDCl$_3$.

AKS-2-110-C #119   RT: 0.53   AV: 1   NL: 4.47E9
T: FTMS + p ESI Full ms [100.00-1500.00]
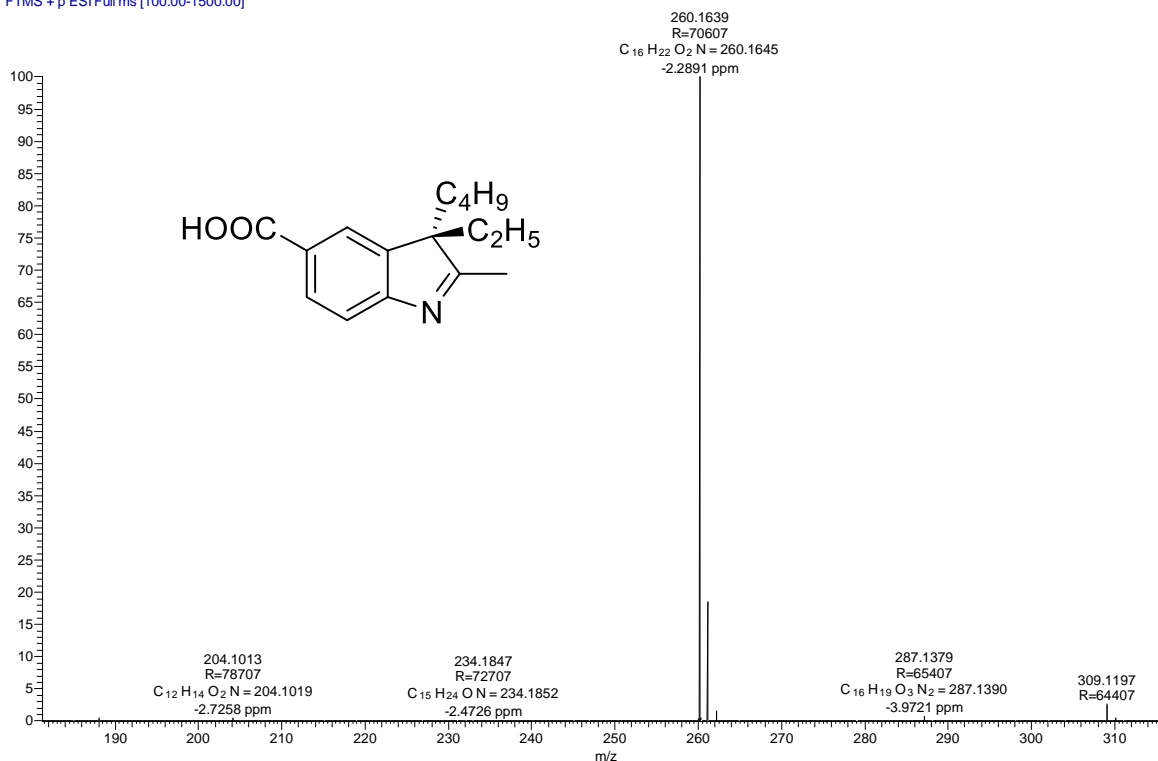
AKS-2-111-C #154   RT: 0.68   AV: 1   NL: 1.35E9
T: FTMS + p ESI Full ms [100.00-1500.00]
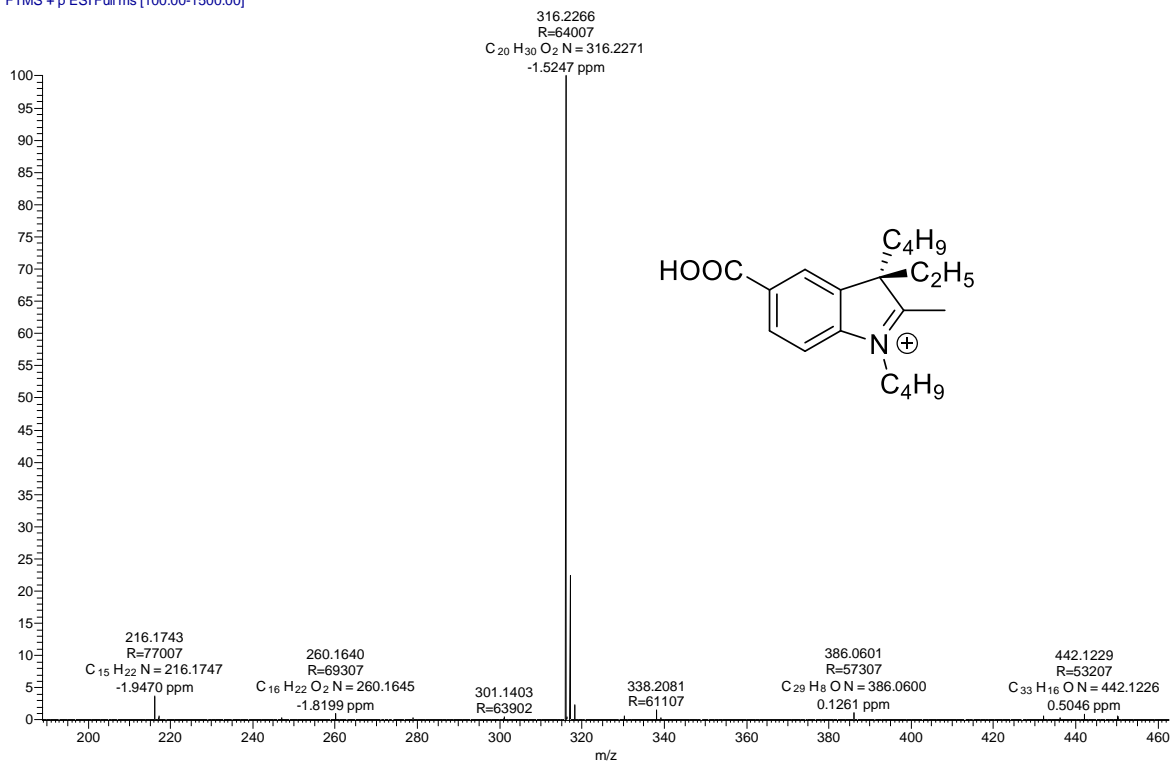
Figure A30. HRMS mass spectrometric analysis for compound **9b** and **10b**.

AKS-2-22-C #105   RT: 0.46   AV: 1   NL: 7.96E8
T: FTMS + p ESI Full ms [100.00-1500.00]
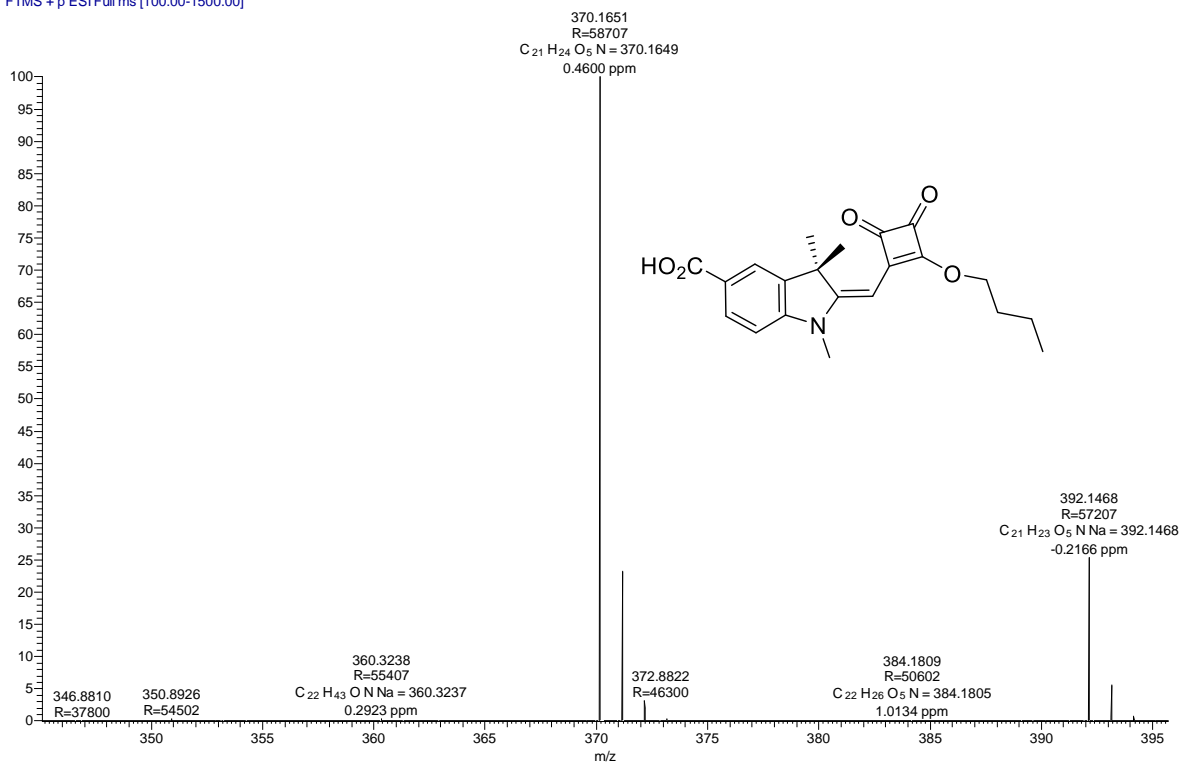
AKS-2-23-B #115   RT: 0.51   AV: 1   NL: 1.40E7
T: FTMS + p ESI Full ms [100.00-1500.00]
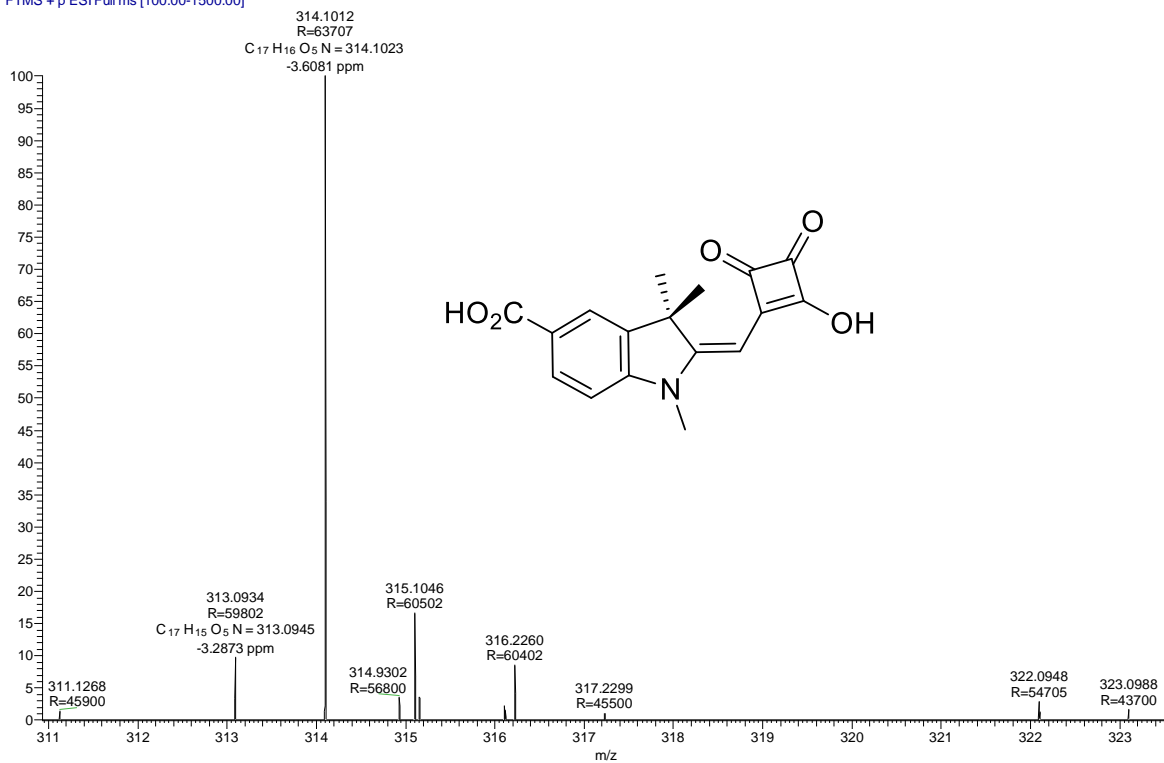
Figure A31. HRMS mass spectrometric analysis for compound **11** and **12**.

AKS-2-39-C #142 RT: 0.63 AV: 1 NL: 1.73E9
T: FTMS + p ESI Full ms [100.00-1500.00]
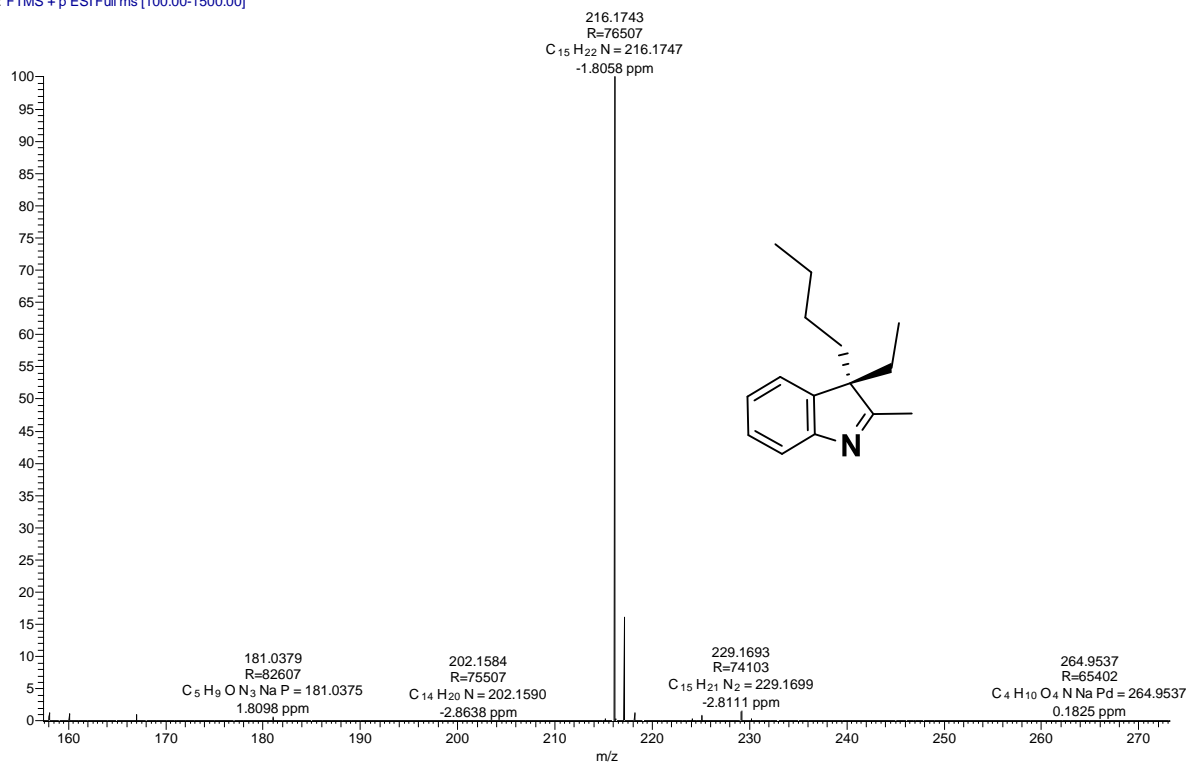
AKS-2-13-C #393 RT: 1.75 AV: 1 NL: 1.21E9
T: FTMS + p ESI Full ms [100.00-1500.00]
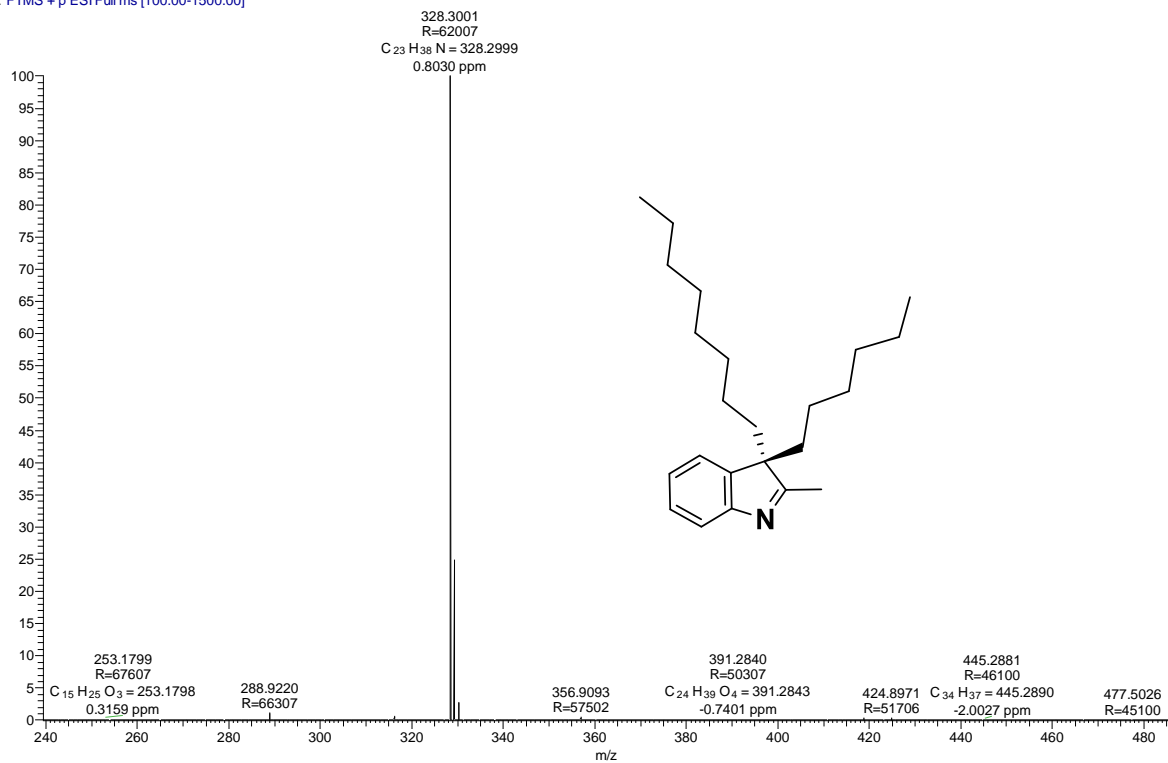
Figure A32. HRMS mass spectrometric analysis for compound **5a** and **5b**.

AKS-2-27-C_161003155144 #139 RT: 0.62 AV: 1 NL: 1.18E6
T: FTMS + p ESI Full ms [100.00-1500.00]

440.4241
R=52002
$C_{31} H_{54} N = 440.4251$
-2.2125 ppm

440.3488
R=36700

440.8988
R=45900

440.8312
R=37200

441.2959
R=46400
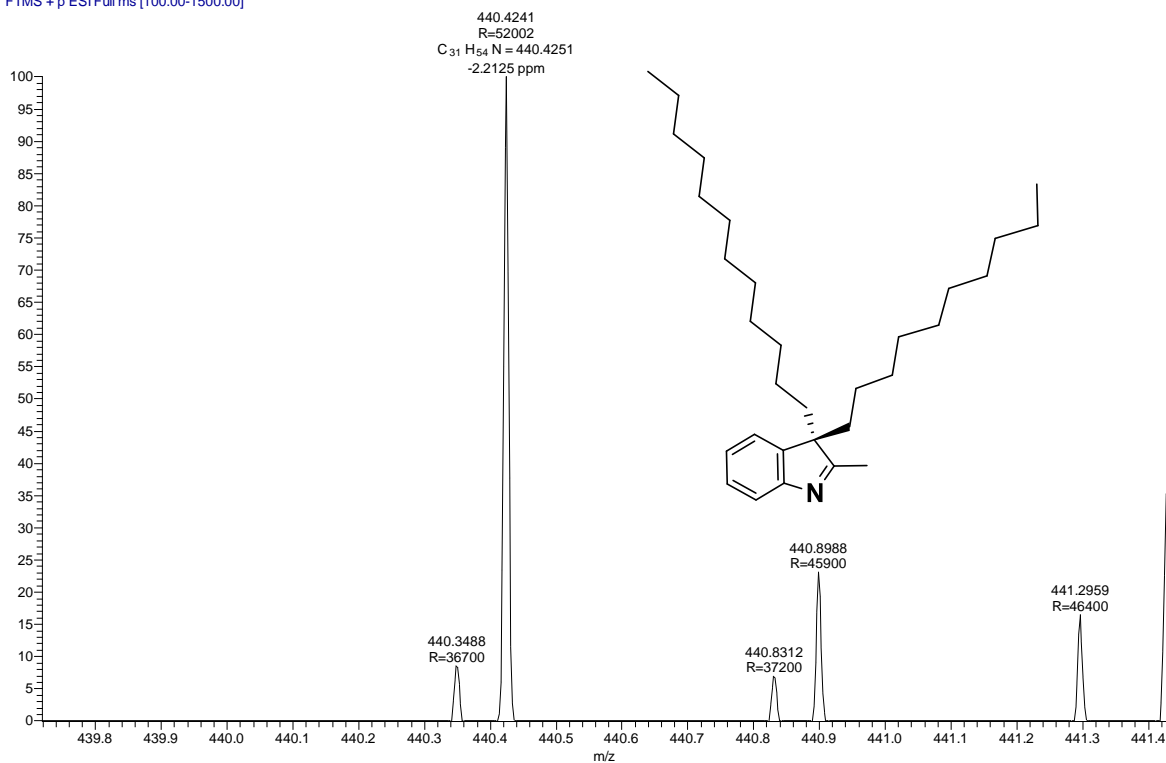
AKS-2-40-C #87 RT: 0.39 AV: 1 NL: 3.27E9
T: FTMS + p ESI Full ms [100.00-1500.00]

300.2687
R=65107
$C_{21} H_{34} N = 300.2686$
0.5368 ppm

253.1801
R=63302
$C_{16} H_{24} N Na = 253.1801$
0.1342 ppm

288.9222
R=64302

313.2636
R=63707
$C_{21} H_{33} N_2 = 313.2638$
-0.6855 ppm

341.2950
R=55002
$C_{23} H_{37} N_2 = 341.2951$
-0.5078 ppm

371.2694
R=53707
$C_{23} H_{35} O_2 N_2 = 371.2693$
0.3632 ppm
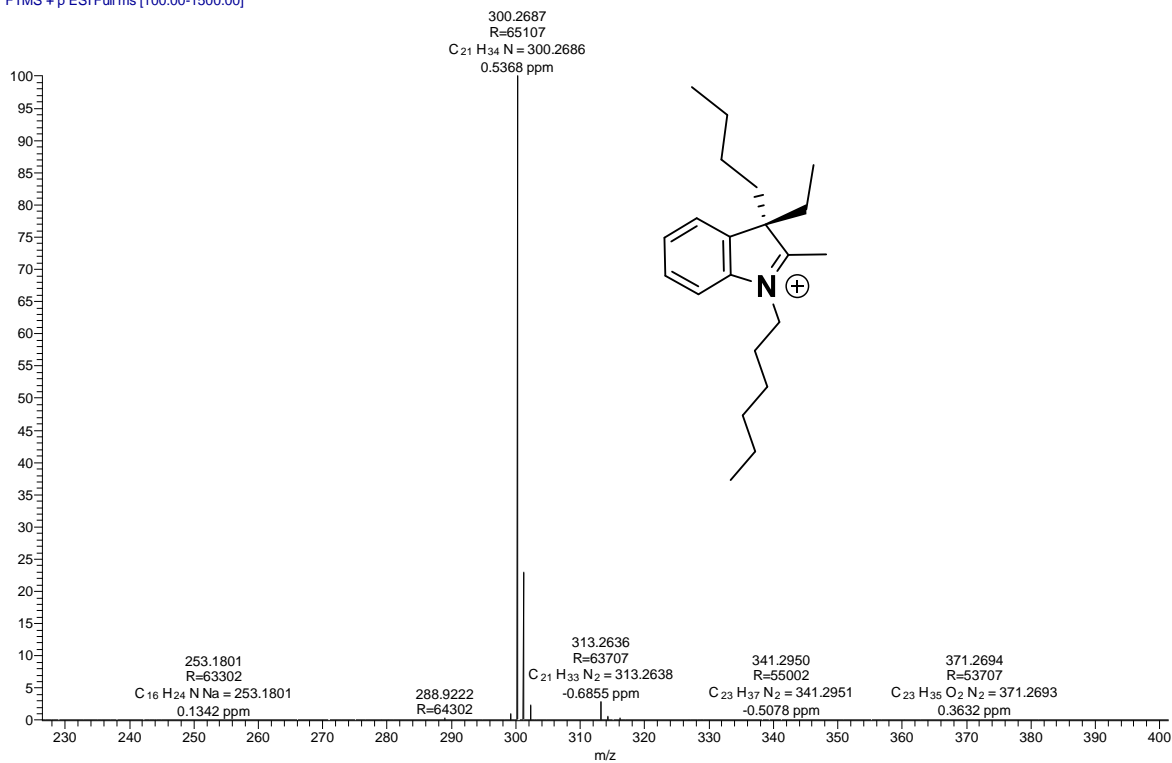
Figure A33. HRMS mass spectrometric analysis for compound **5c** and **6a**.

AKS-2-14-C #116   RT: 0.51   AV: 1   NL: 1.82E9
T: FTMS + p ESI Full ms [100.00-1500.00]

412.3941
R=55507
C$_{29}$ H$_{50}$ N = 412.3938
0.7927 ppm

338.3417
R=57402
C$_{22}$ H$_{44}$ O N = 338.3417
-0.1070 ppm

372.8837
R=36600

458.3996
R=51207
C$_{30}$ H$_{52}$ O$_2$ N = 458.3993
0.8100 ppm

486.8669
R=43400

538.2910
R=45307
C$_{33}$ H$_{41}$ O$_4$ N Na = 538.2928
-3.2776 ppm

m/z
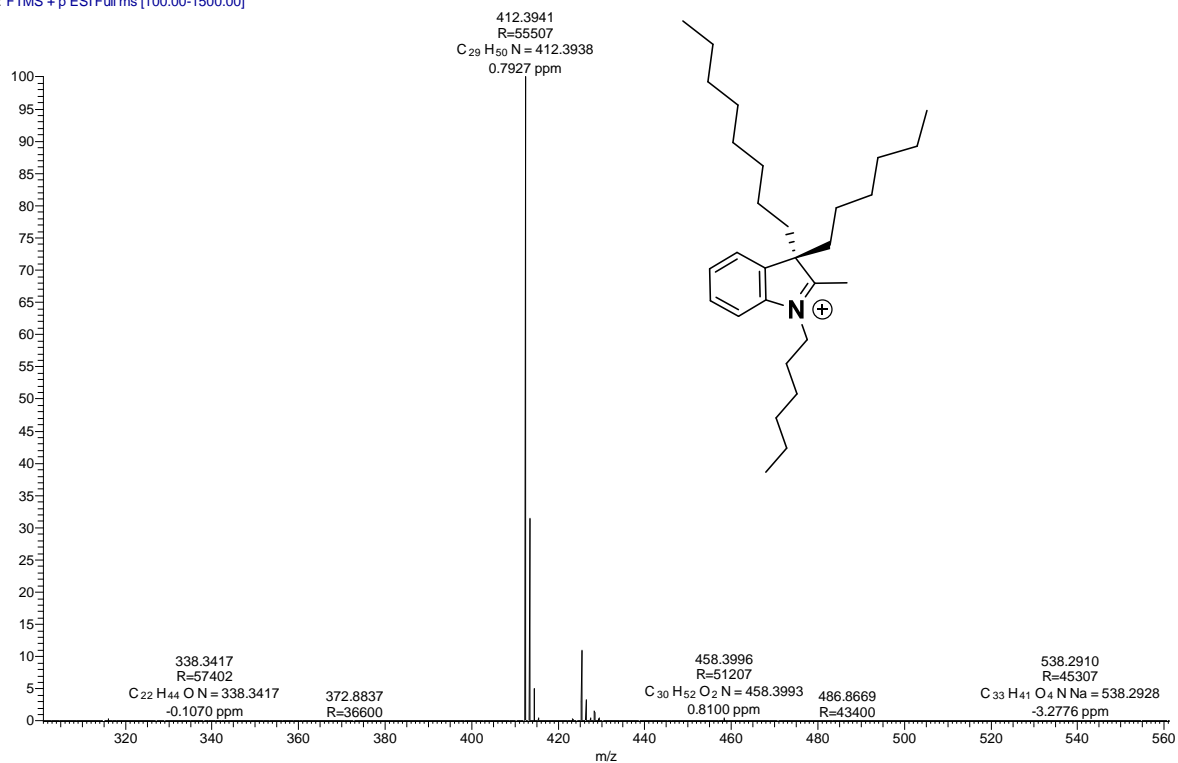
AKS-2-29-C #327   RT: 1.45   AV: 1   NL: 8.56E8
T: FTMS + p ESI Full ms [100.00-1500.00]

524.5203
R=49307
C$_{37}$ H$_{66}$ N = 524.5190
2.5683 ppm

486.8683
R=45602

492.8855
R=43702

498.9027
R=46500

510.5044
R=43600
C$_{36}$ H$_{64}$ N = 510.5033
2.0303 ppm

537.5154
R=46607
C$_{37}$ H$_{65}$ N$_2$ = 537.5142
2.2610 ppm

548.8409
R=46000

554.8558
R=44402

560.8740
R=41602

m/z
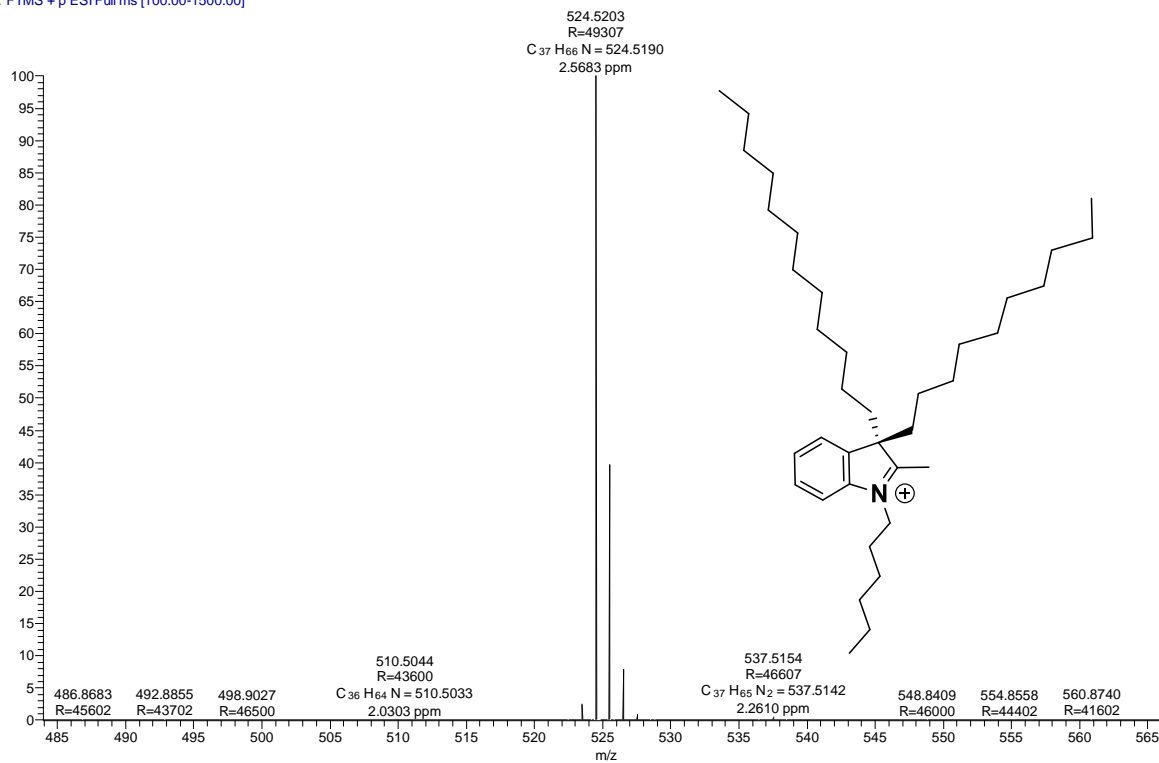
Figure A34. HRMS mass spectrometric analysis for compound **6b** and **6c**.

ASK-II-33-C #85 RT: 0.38 AV: 1 NL: 2.43E8
T: FTMS + p ESI Full ms [100.00-1500.00]

608.6129
R=45807
C$_{43}$H$_{78}$N = 608.6129
0.0610 ppm

492.3812
R=50707

508.3552
R=49307

536.8501
R=40504

554.3523
R=44806

568.8220
R=42300

621.6080
R=44007

636.6442
R=44507

650.6425
R=43702

661.5370
R=39706

684.6436
R=41200

700.6499
R=40807

m/z
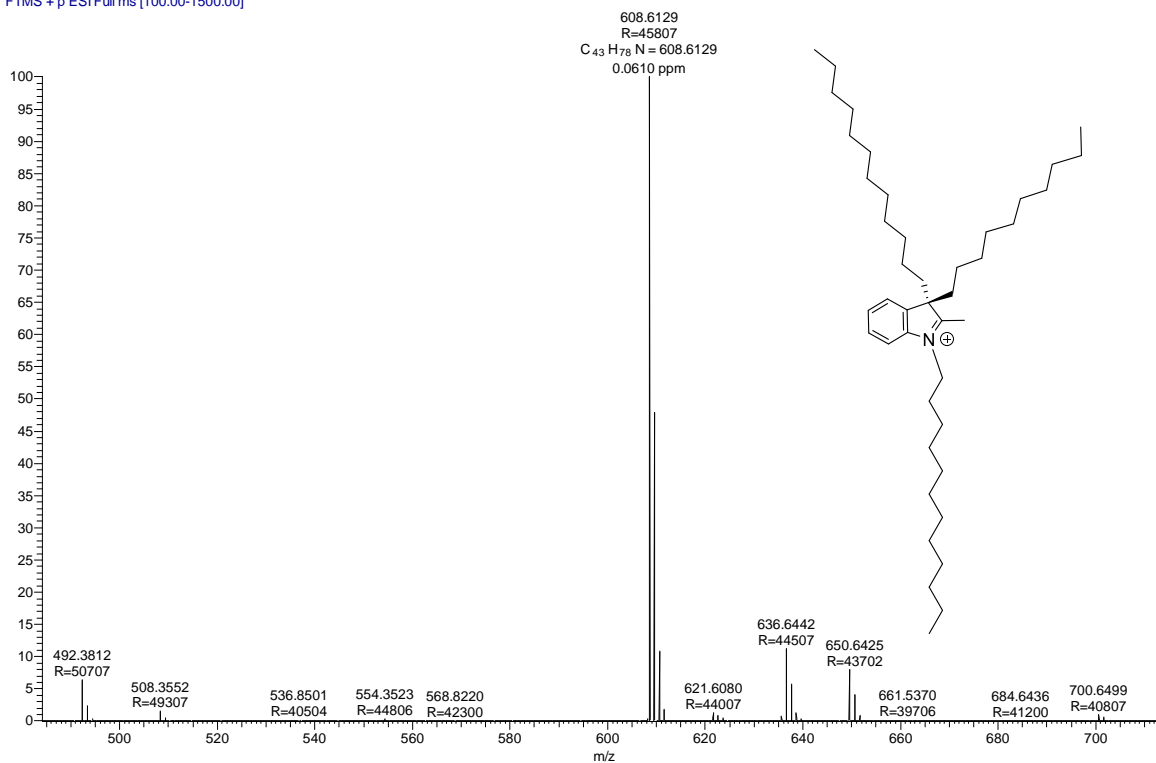
AKS-2-91-C #220 RT: 0.98 AV: 1 NL: 2.27E9
T: FTMS + p ESI Full ms [100.00-1500.00]

454.4400
R=52607
C$_{32}$H$_{56}$N = 454.4407
-1.5950 ppm

391.2823
R=46200

418.8783
R=54300

467.4341
R=51207

580.3350
R=39907

608.6113
R=44607

m/z
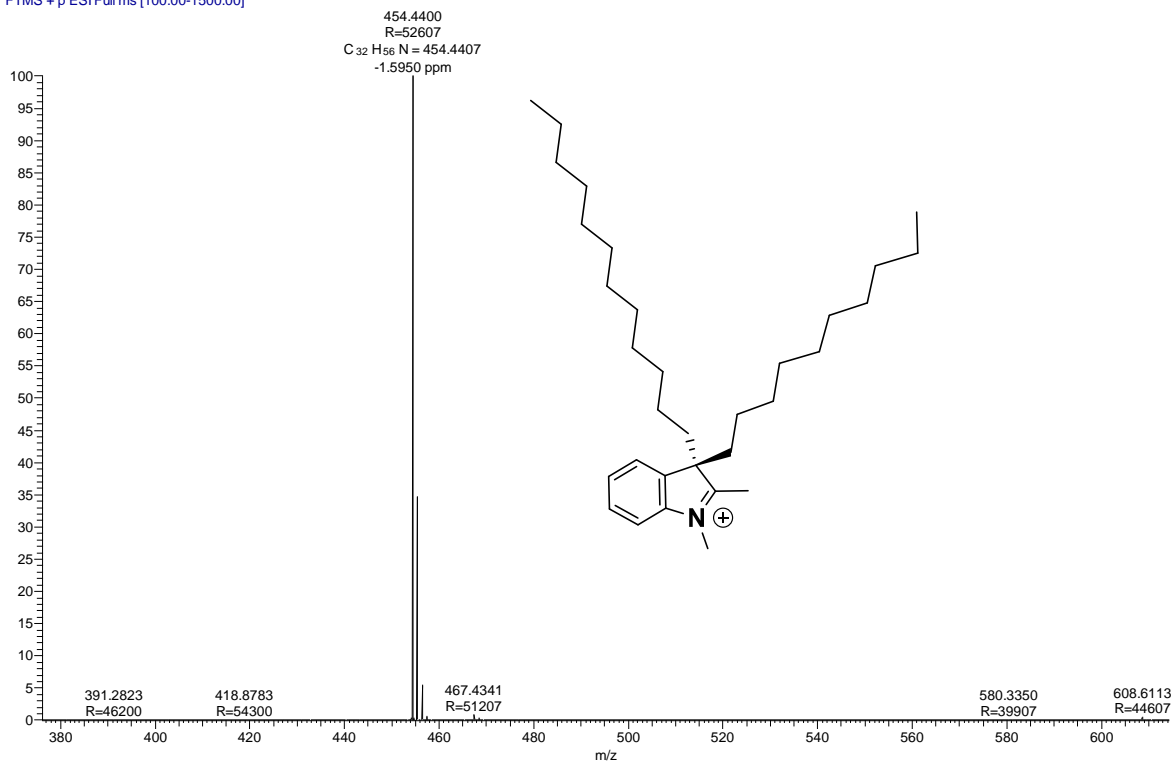
Figure A35. HRMS mass spectrometric analysis for compound **6d** and **6e**.
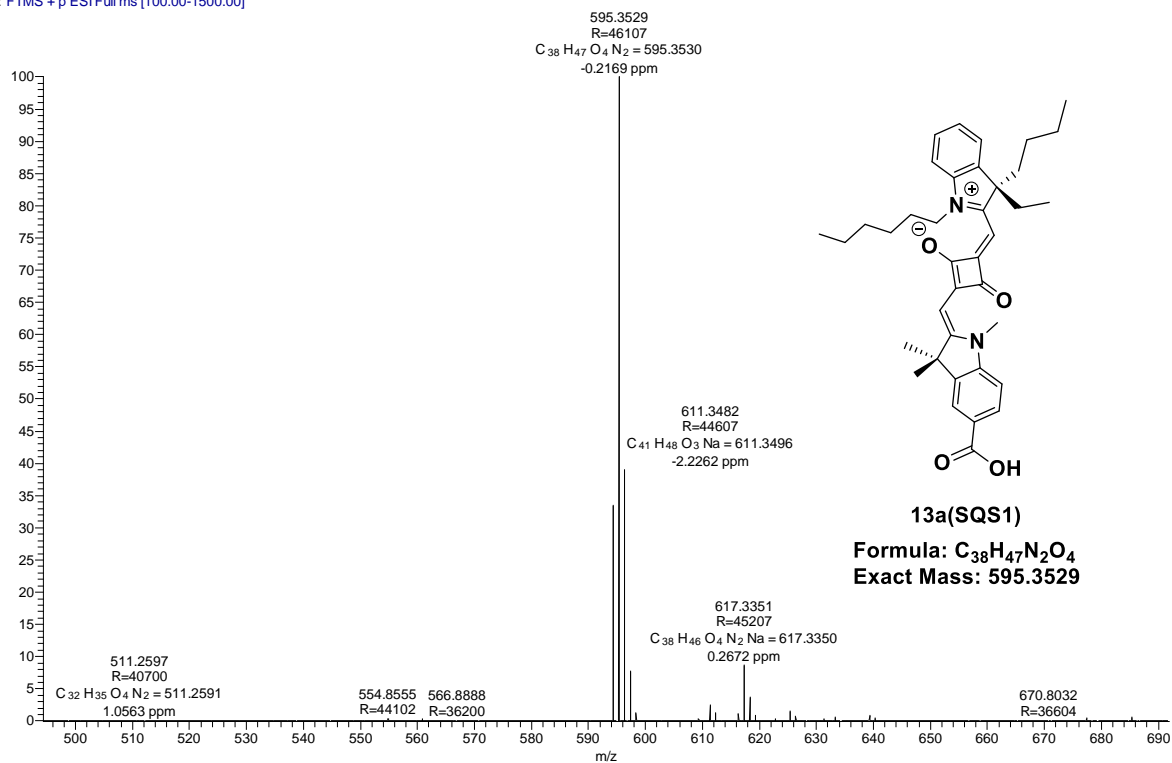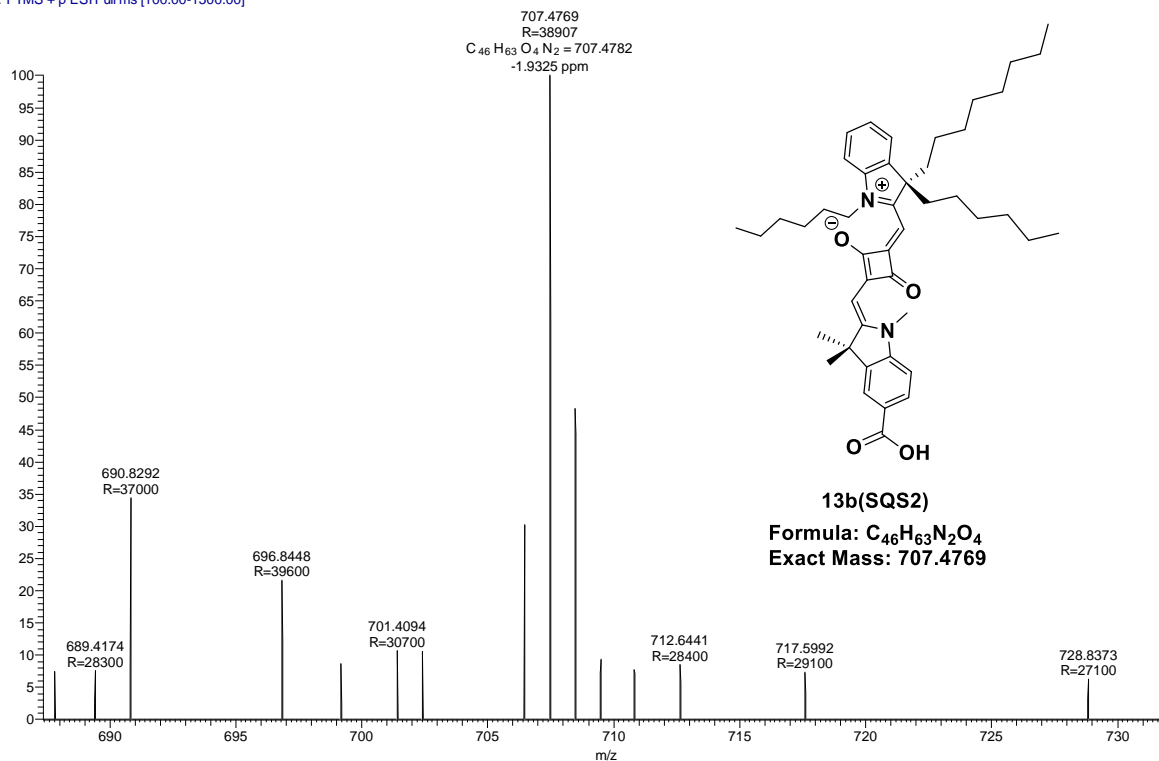
Figure A36. HRMS spectra of compound **13a (SQS1)** and **13b (SQS2).**

AKS-2-37-C #176 RT: 0.78 AV: 1 NL: 4.35E6
T: FTMS + p ESI Full ms [100.00-1500.00]

819.6057
R=38307
C$_{54}$ H$_{79}$ O$_4$ N$_2$ = 819.6034
2.7043 ppm

820.7856
R=24100

804.8096
R=26600

809.3202
R=25800

822.7268
R=24600

828.5187
R=32004

833.4724
R=23500

13c(SQS3)

Formula: C$_{54}$H$_{79}$N$_2$O$_4$
Exact Mass: 819.6057
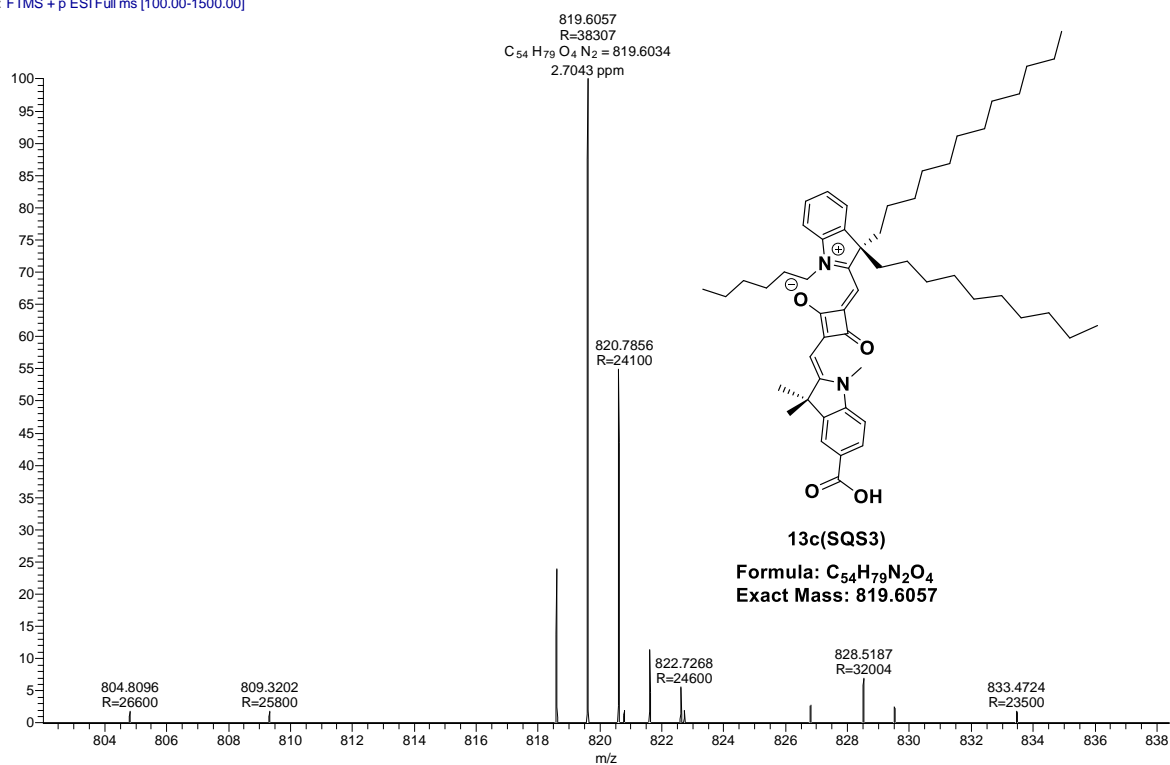
ASK-II-114-C #223 RT: 0.99 AV: 1 NL: 5.01E7
T: FTMS + p ESI Full ms [100.00-1500.00]

749.5228
R=41307
C$_{49}$ H$_{69}$ O$_4$ N$_2$ = 749.5252
-3.2273 ppm

752.5327
R=37702

771.5062
R=40007
C$_{51}$ H$_{67}$ O$_4$ N$_2$ = 771.5095
-4.3687 ppm

710.5621
R=37505
C$_{49}$ H$_{74}$ O$_3$ = 710.5632
-1.5675 ppm

698.7820
R=29300

730.7496
R=26000

735.5049
R=27800

765.5182
R=35207

787.4754
R=30500

793.5147
R=36406

13e(SQS5)
Formula: C$_{49}$H$_{69}$N$_2$O$_4$
Exact Mass: 749.5228
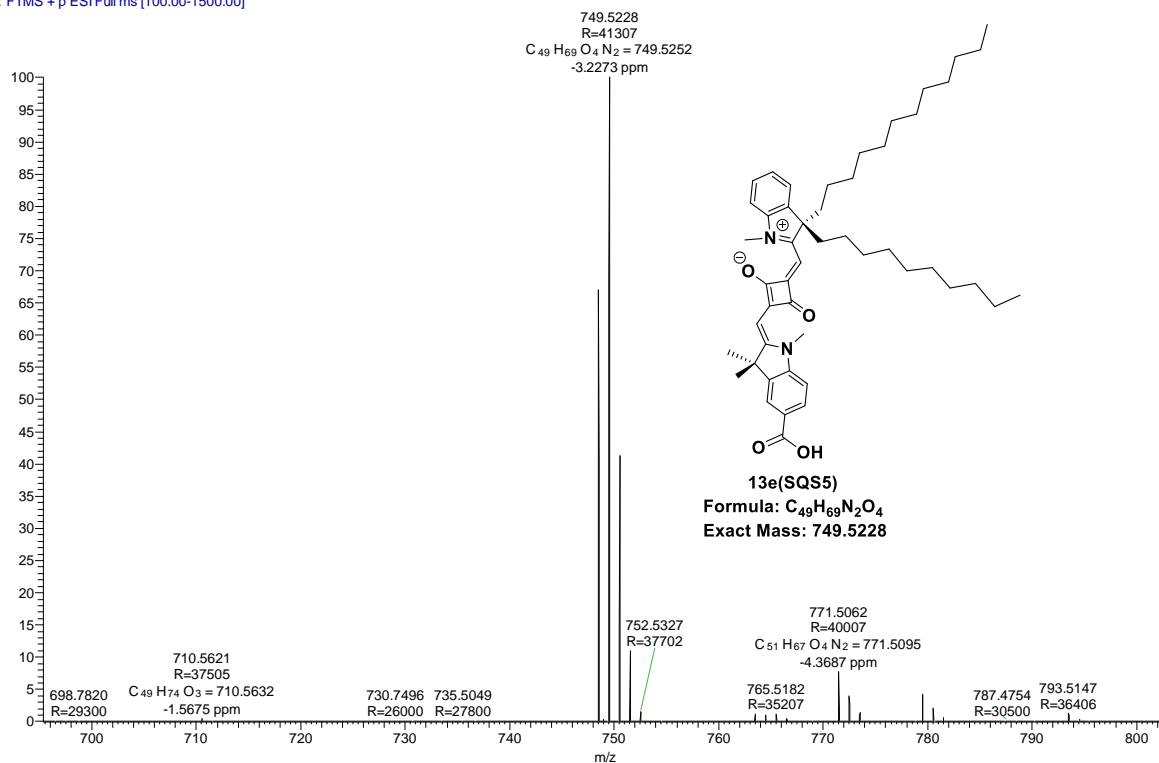
Figure A37. HRMS spectra of compound **13c (SQS3)** and **13e (SQS5)**.

IR spectroscopic studies of SQS dyes have been done to examine the carbonyl stretching frequency of carboxylic acid group, and squaraine unit. The carbonyl stretching frequency of carboxylic acid found at 1699 cm^{-1} for all the dyes, whereas two carbonyl stretching frequency have been found for squaraine unit of dyes which is varies from 1591-1598 cm^{-1} and 1566-1570 cm^{-1} respectively. IR spectrum of SQS4 dye is displayed in **Figure A38a**.

(a)   **(b)**
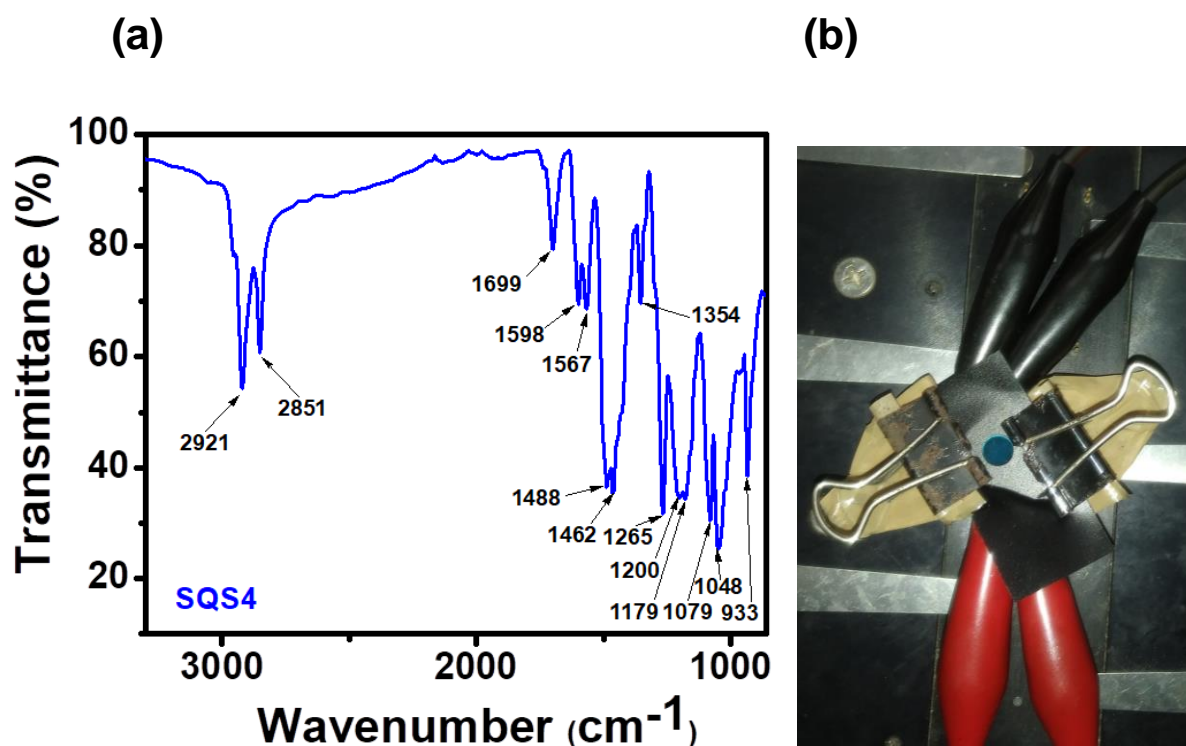
Figure A38. (a) IR spectrum of SQS4 dye, (b) cell active area 0.23 cm^2 with black mask (area 0.23 cm^2) for SQS dyes.

Chapter 3
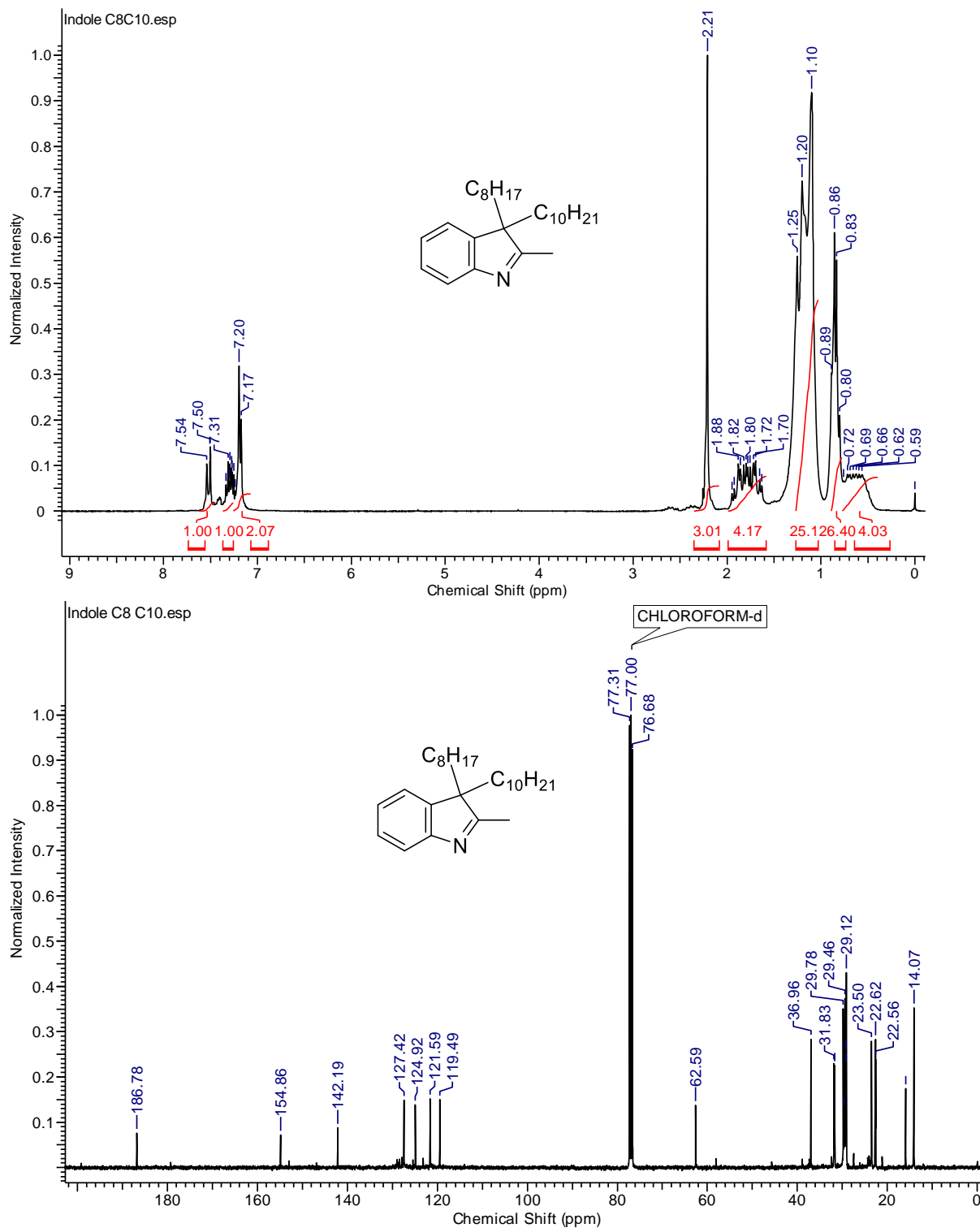
Figure A39. ^{1}H- and ^{13}C- NMR spectra of compound **2** in CDCl$_3$.
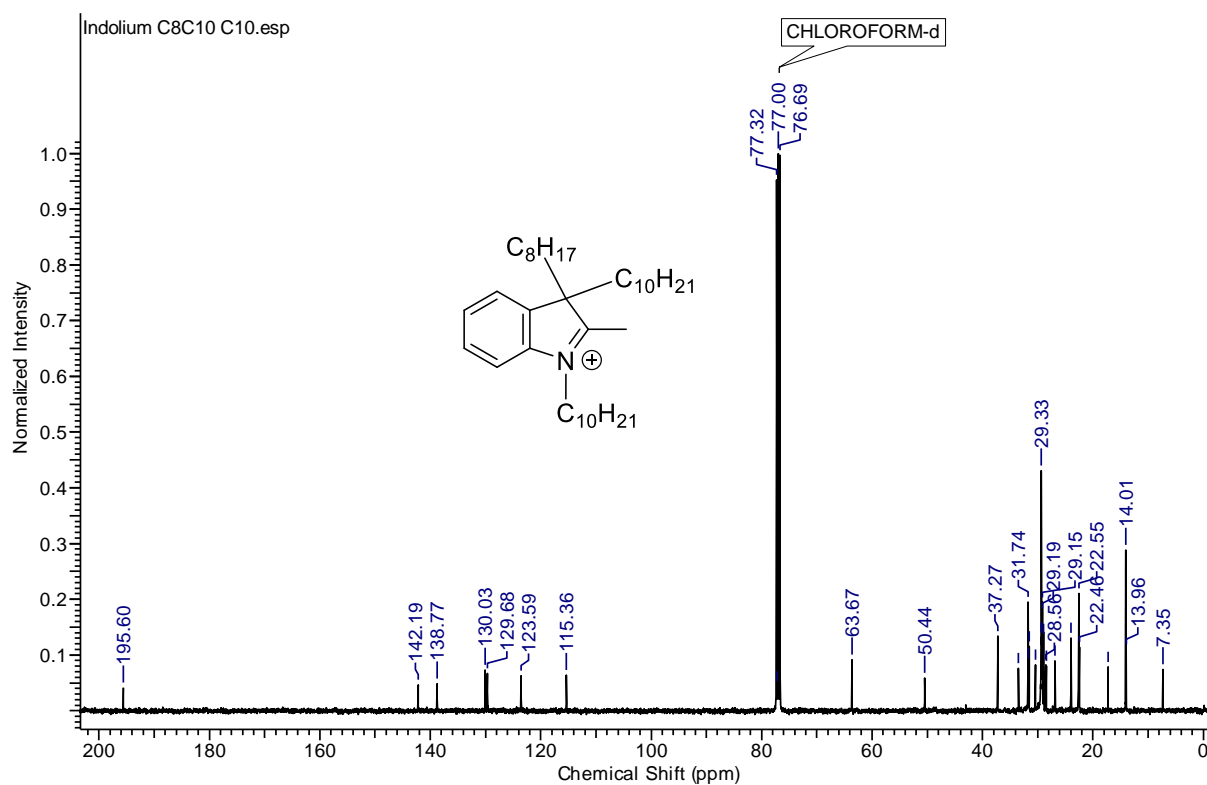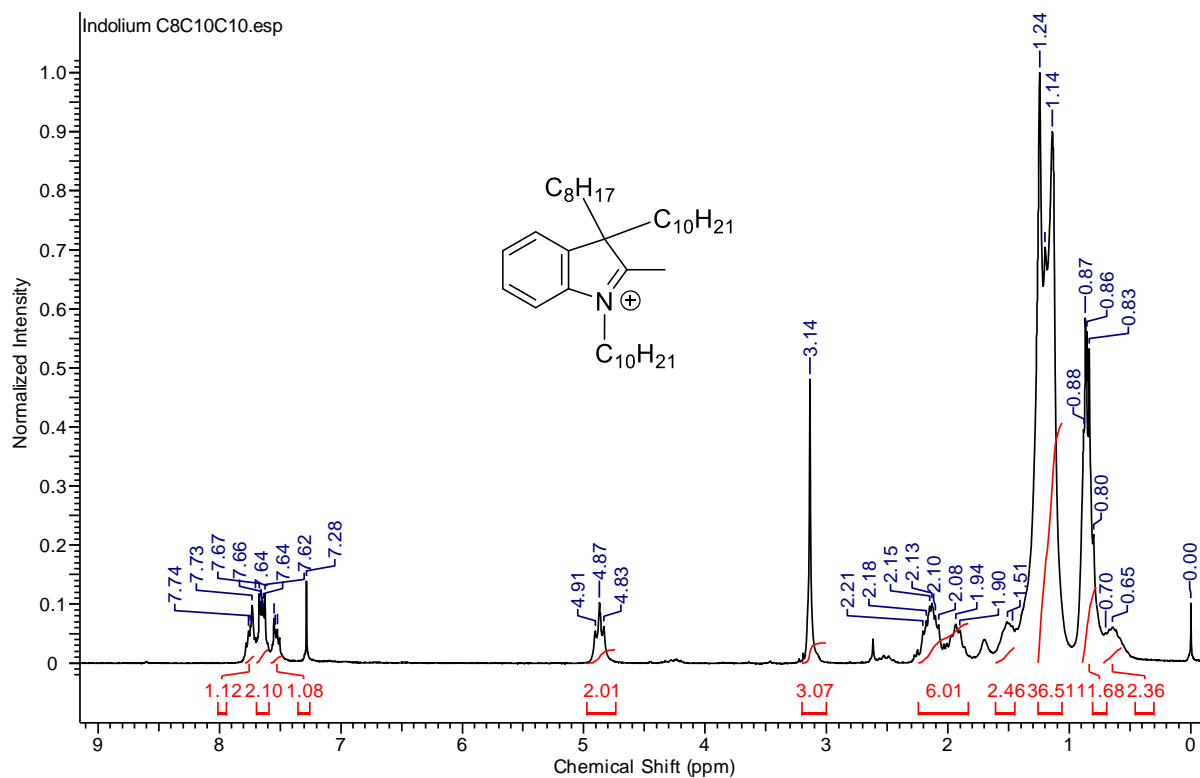
Figure A40. ^{1}H- and ^{13}C- NMR spectra of compound **3** CDCl$_3$.
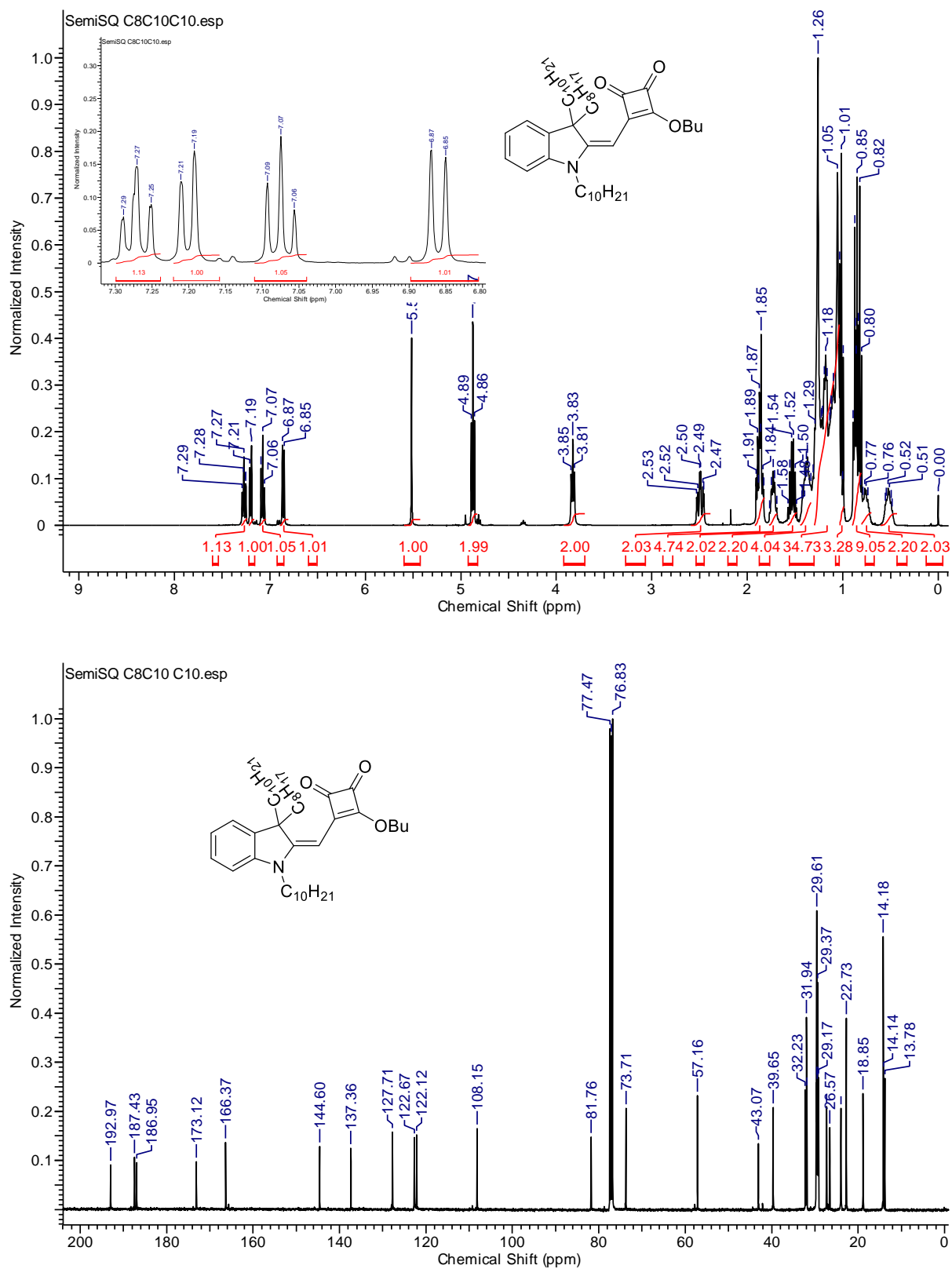
Figure A41. ^{1}H- and ^{13}C- NMR spectra of compound **4** CDCl$_3$.
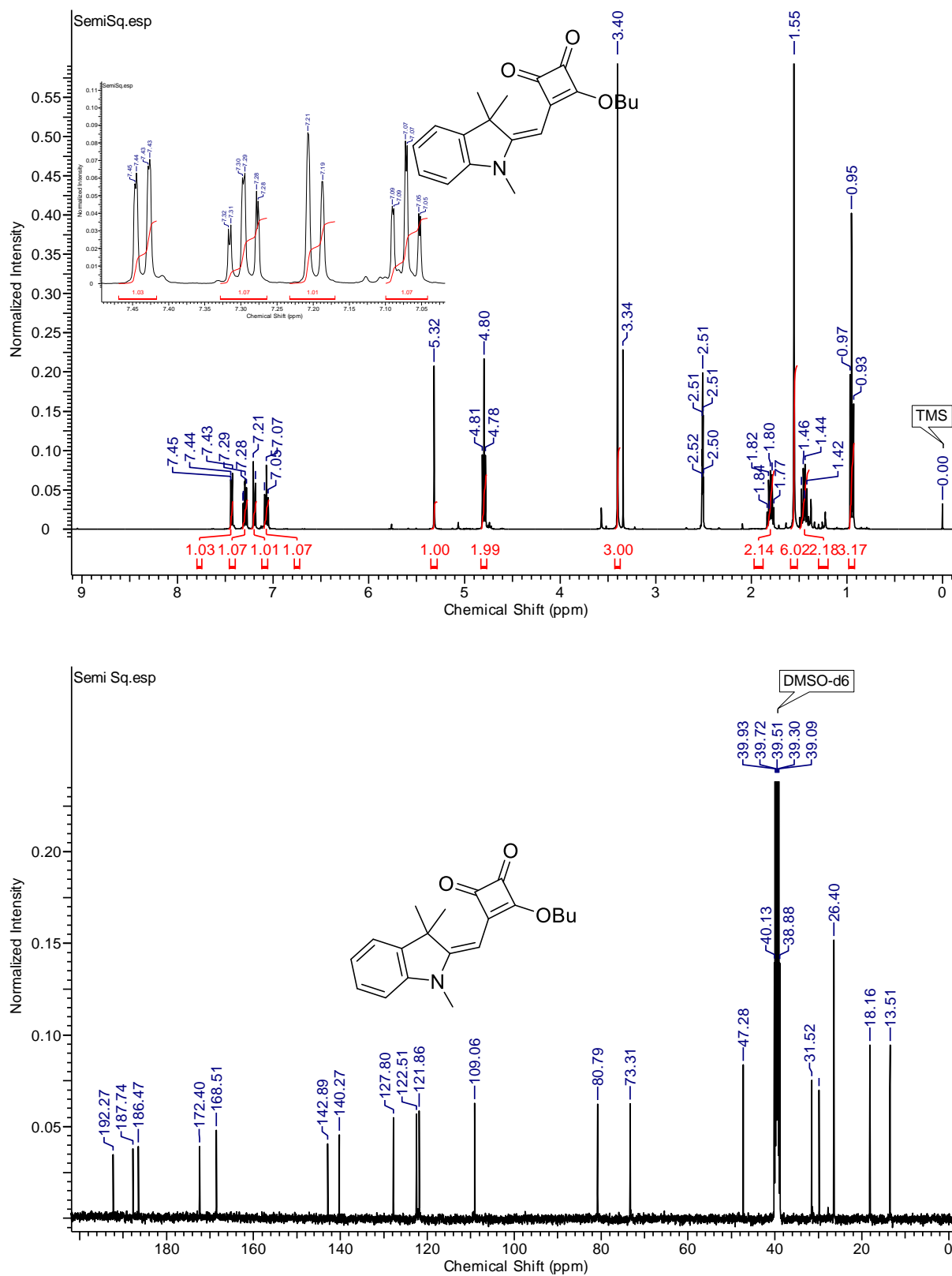
Figure A42. ^{1}H- and ^{13}C- NMR spectra of compound **6** in DMSO-d_6.
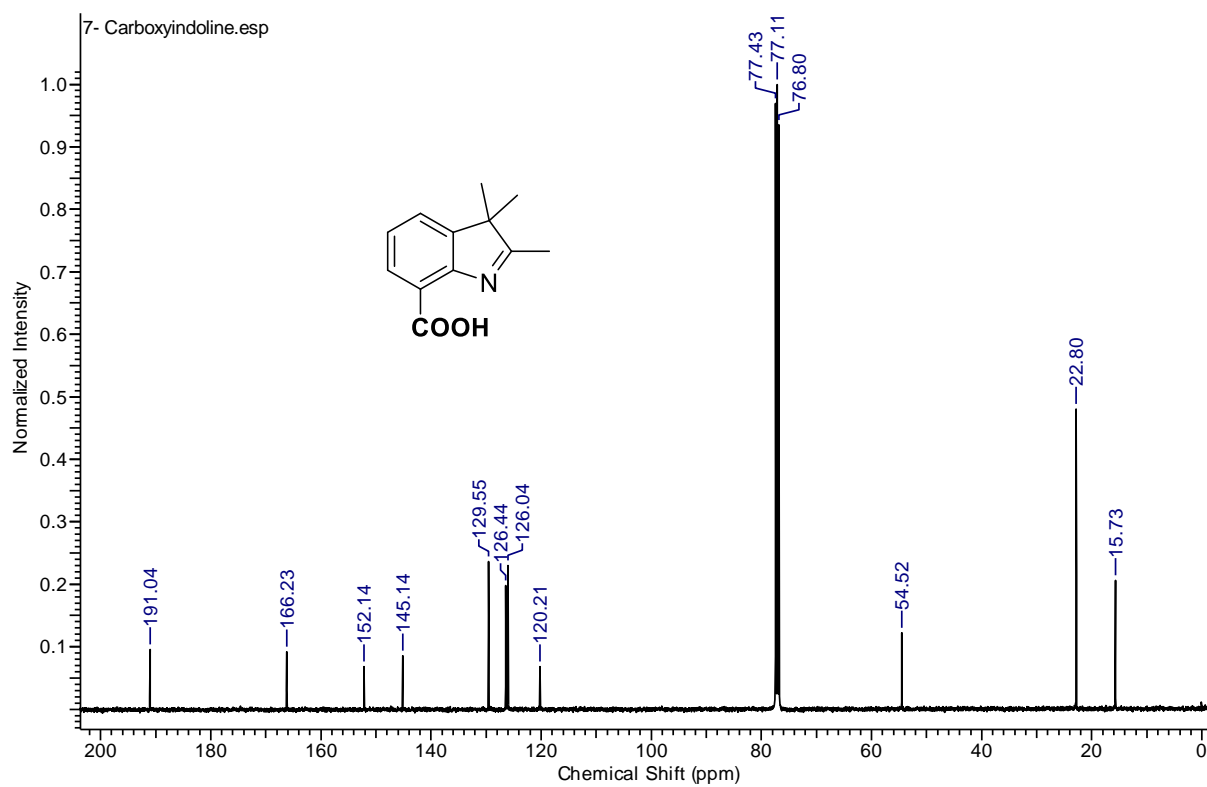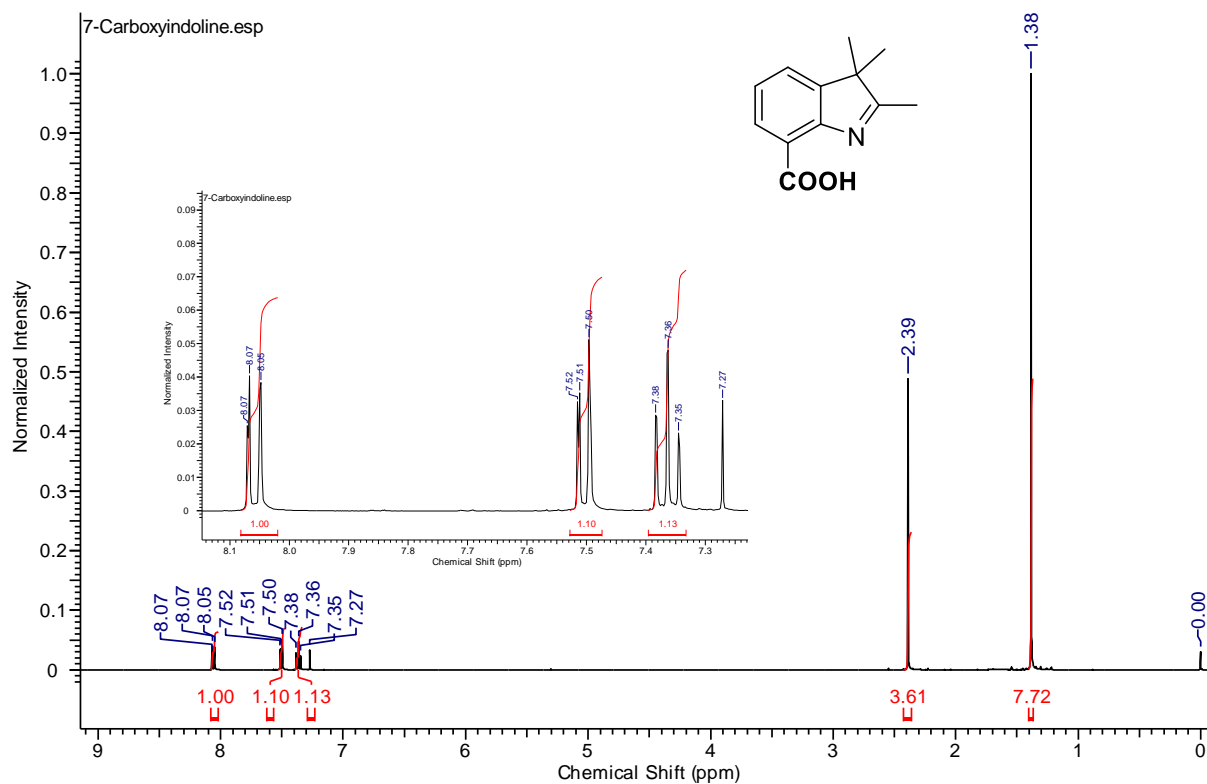
Figure A43. ^{1}H- and ^{13}C- NMR spectra of compound **9** in CDCl$_3$.
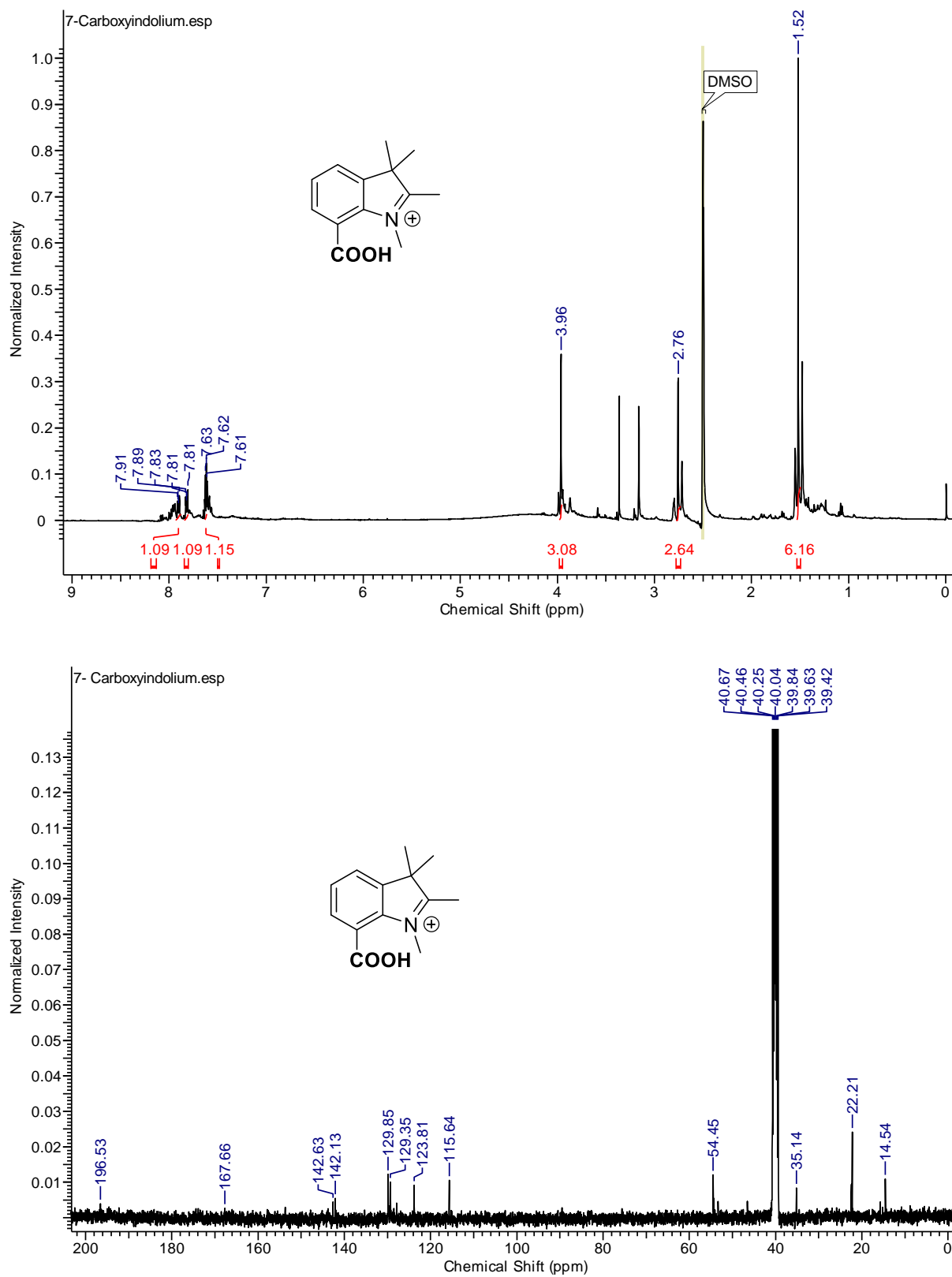
Figure A44. ^{1}H- and ^{13}C- NMR spectra of compound **10** in DMSO-d_6.
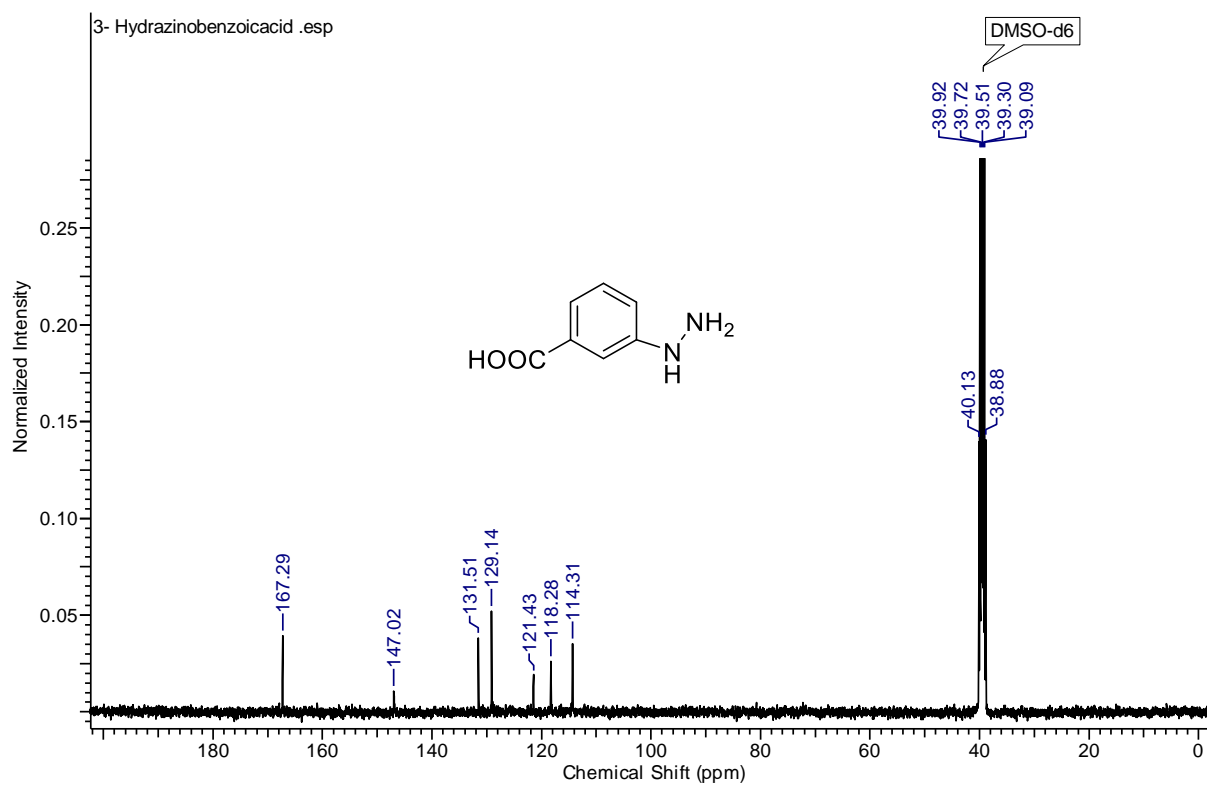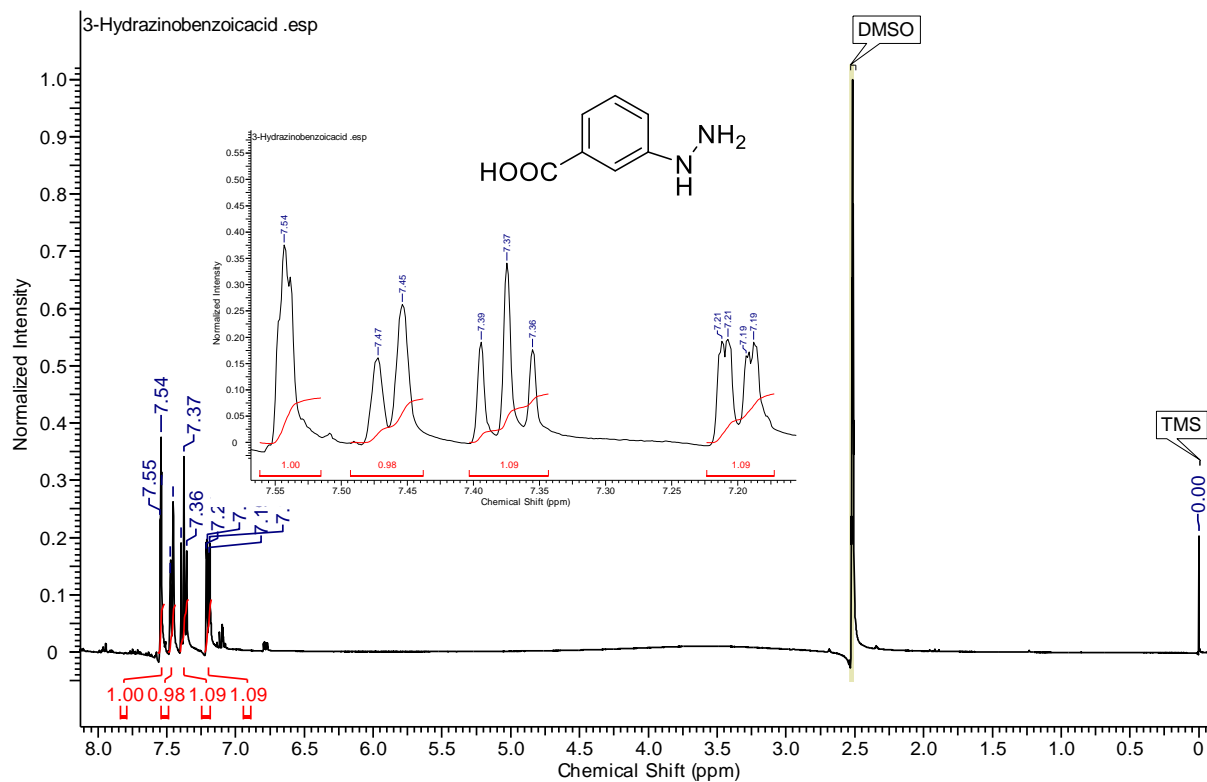
Figure A45. ^{1}H- and ^{13}C- NMR spectra of compound **12** in DMSO-d_6.
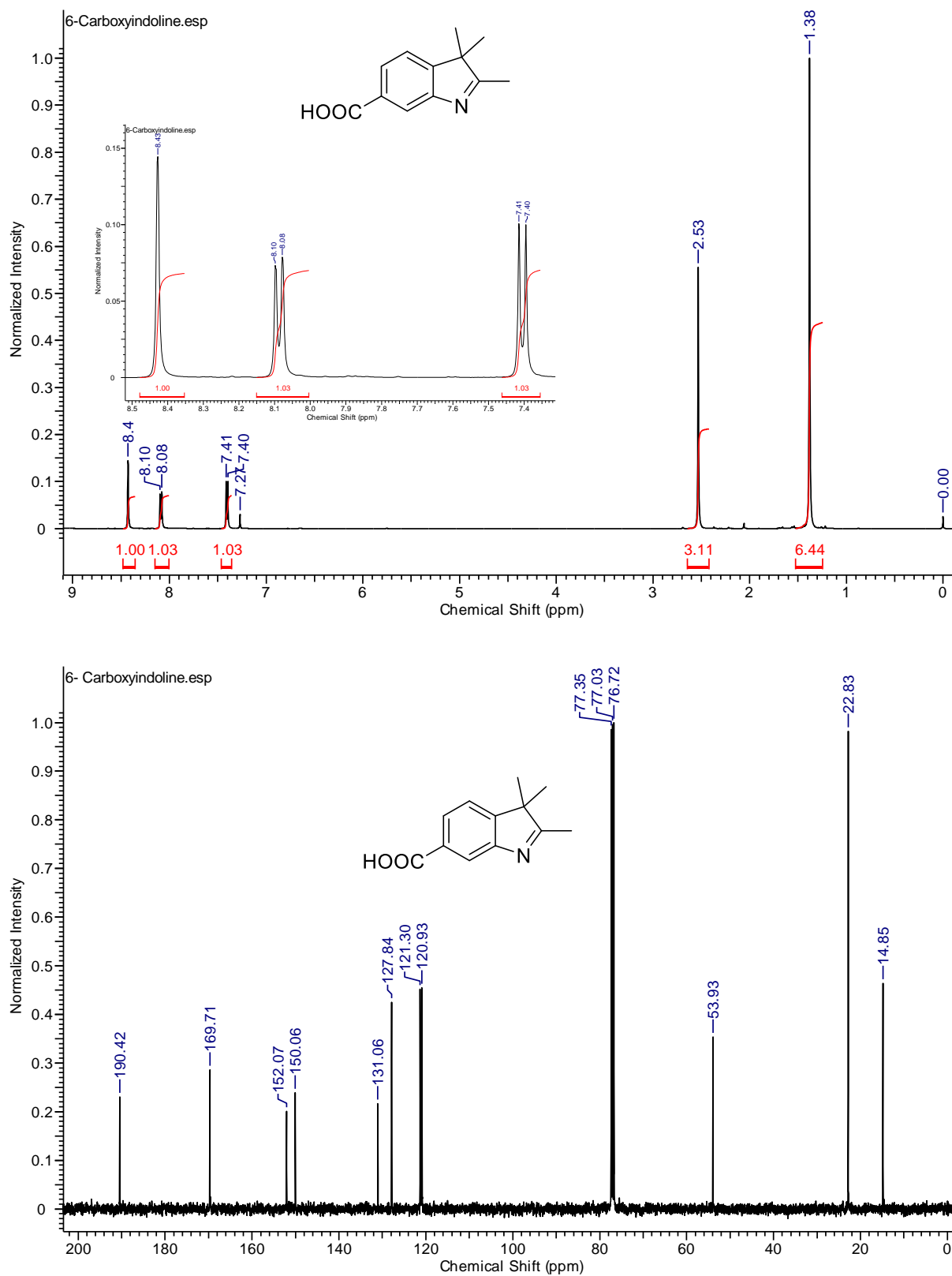
Figure A46. ^{1}H- and ^{13}C- NMR spectra of compound **13a** in CDCl$_3$.
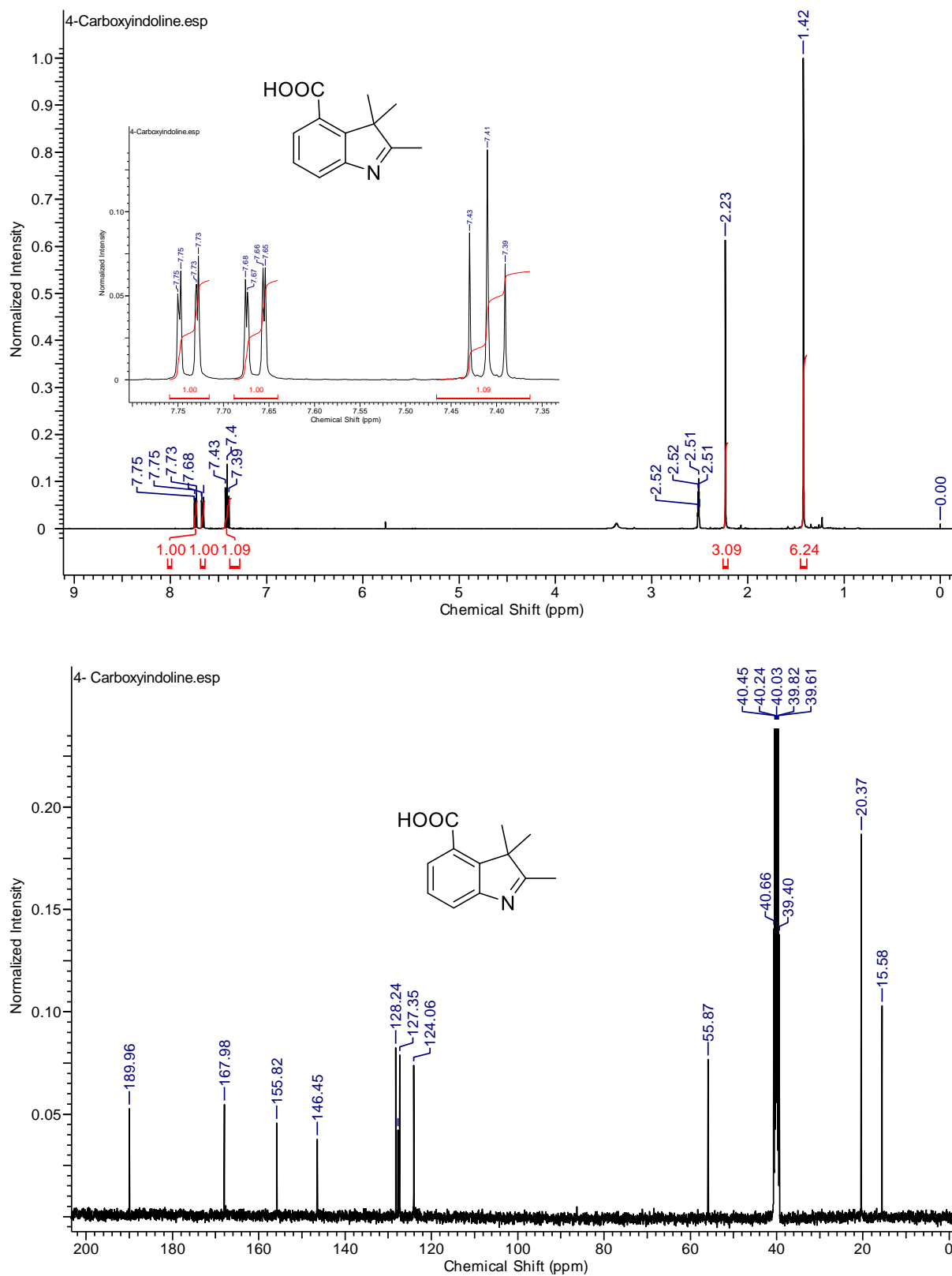
Figure A47. ¹H- and ¹³C- NMR spectra of compound **13b** in DMSO-d_6.
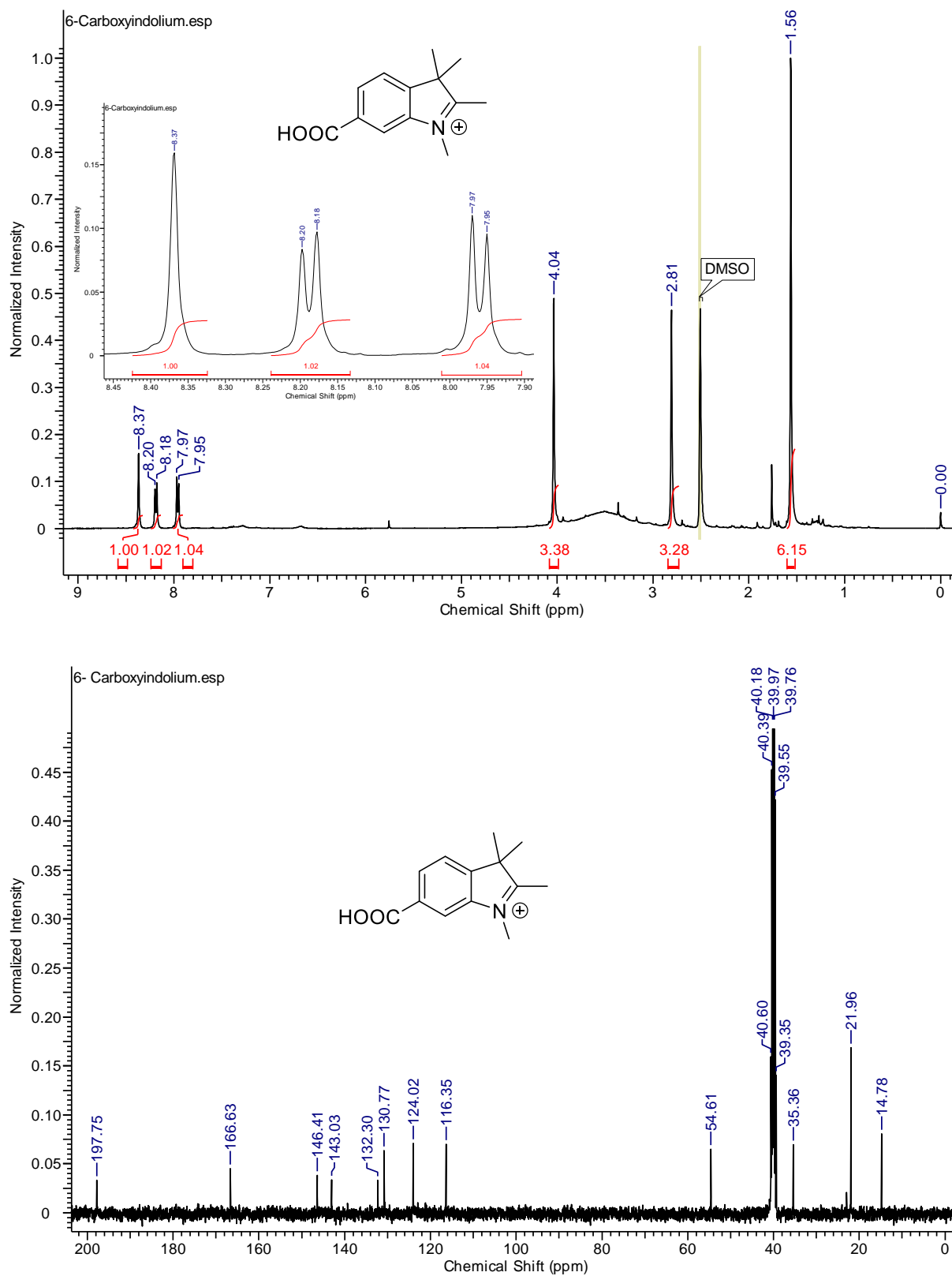
Figure A48. ^{1}H- and ^{13}C- NMR spectra of compound **14a** in DMSO-d_6.
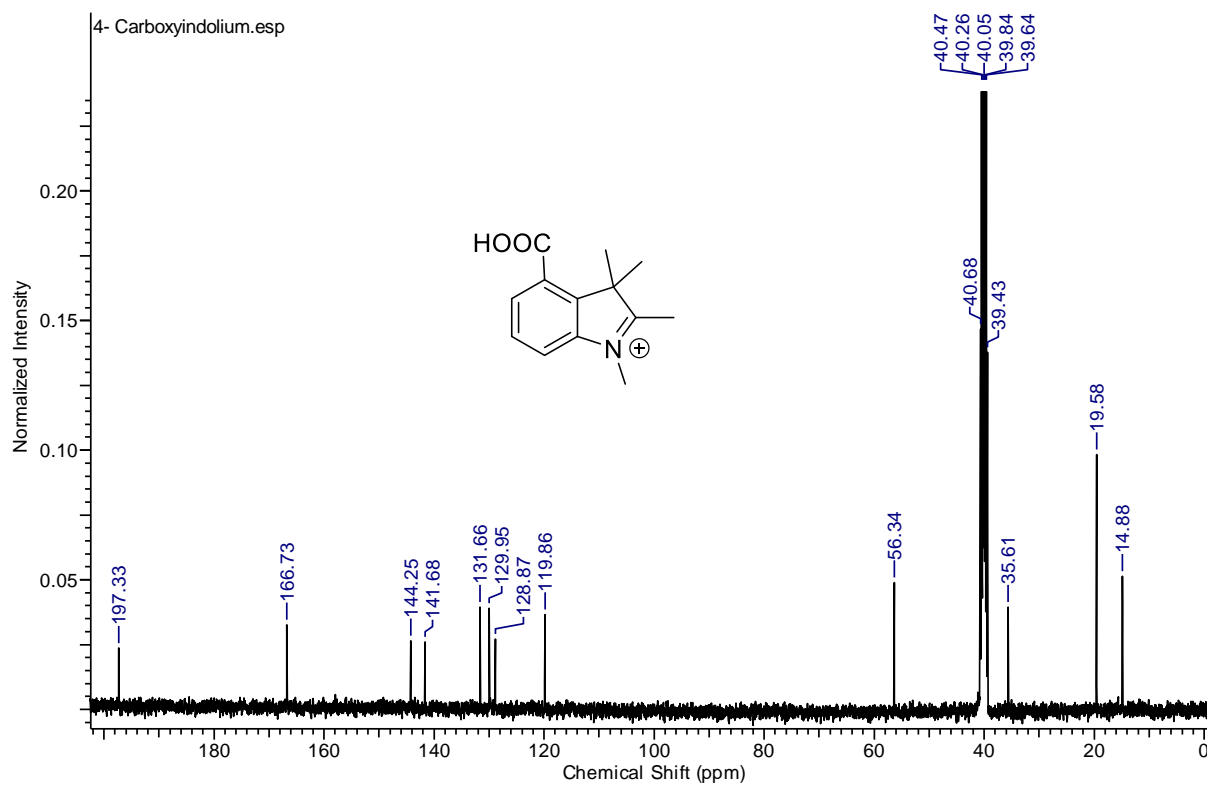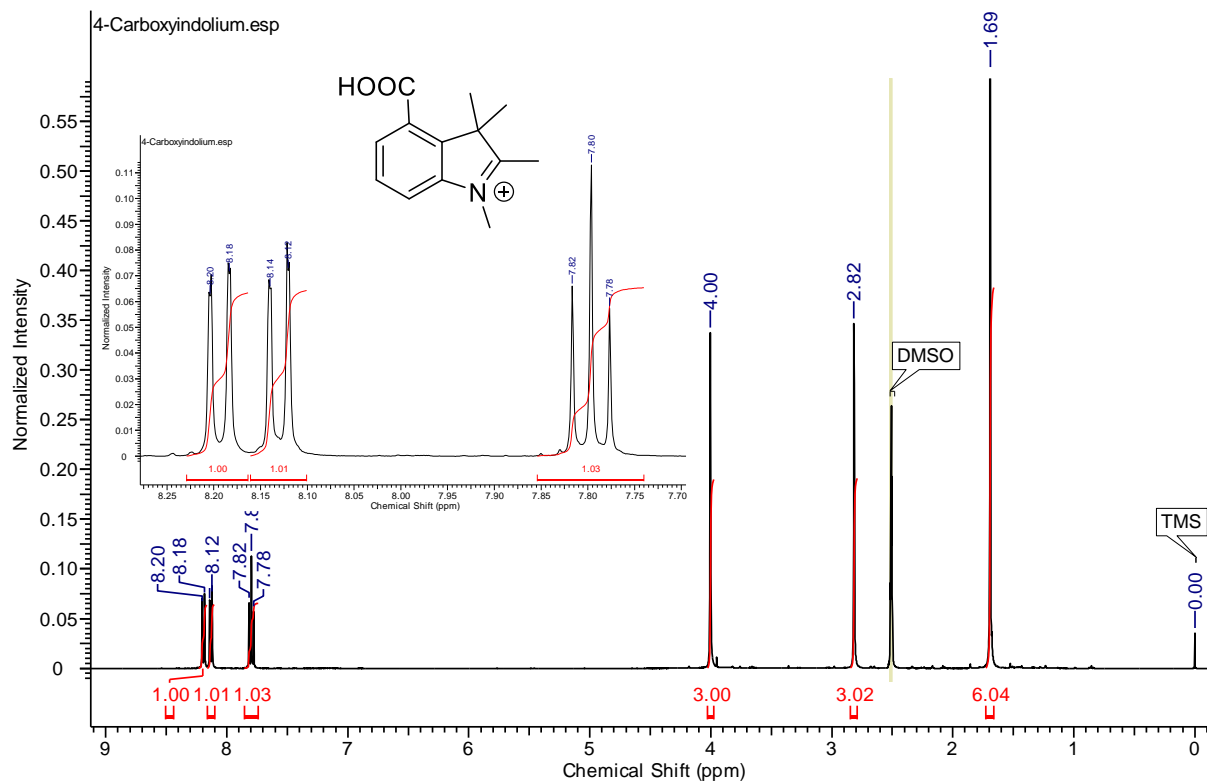
Figure A49. ^{1}H- and ^{13}C- NMR spectra of compound **14b** in DMSO-d_6.
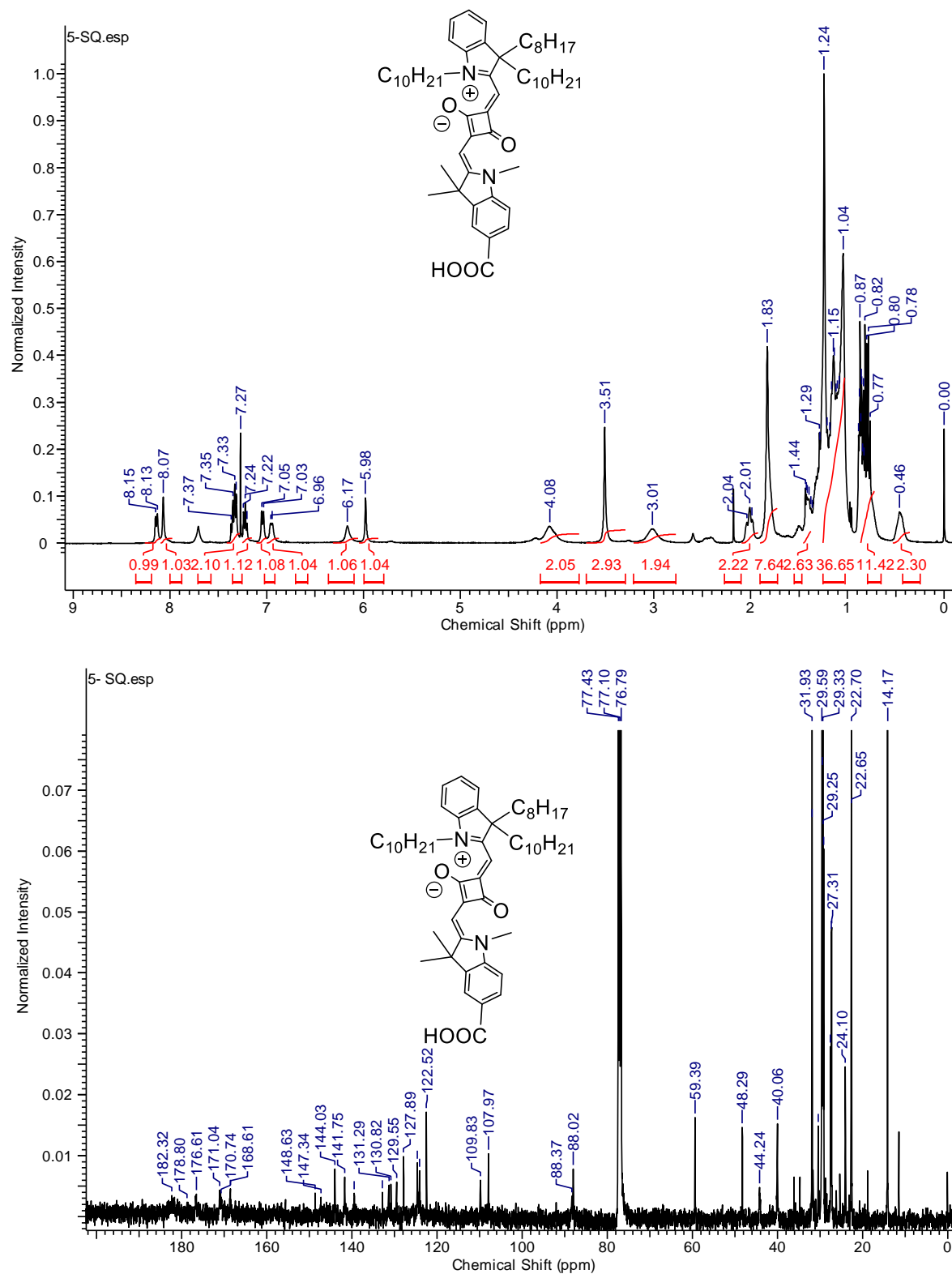
Figure A50. ^{1}H- and ^{13}C- NMR spectra of compound **15 (5-SQ)** in CDCl$_3$.
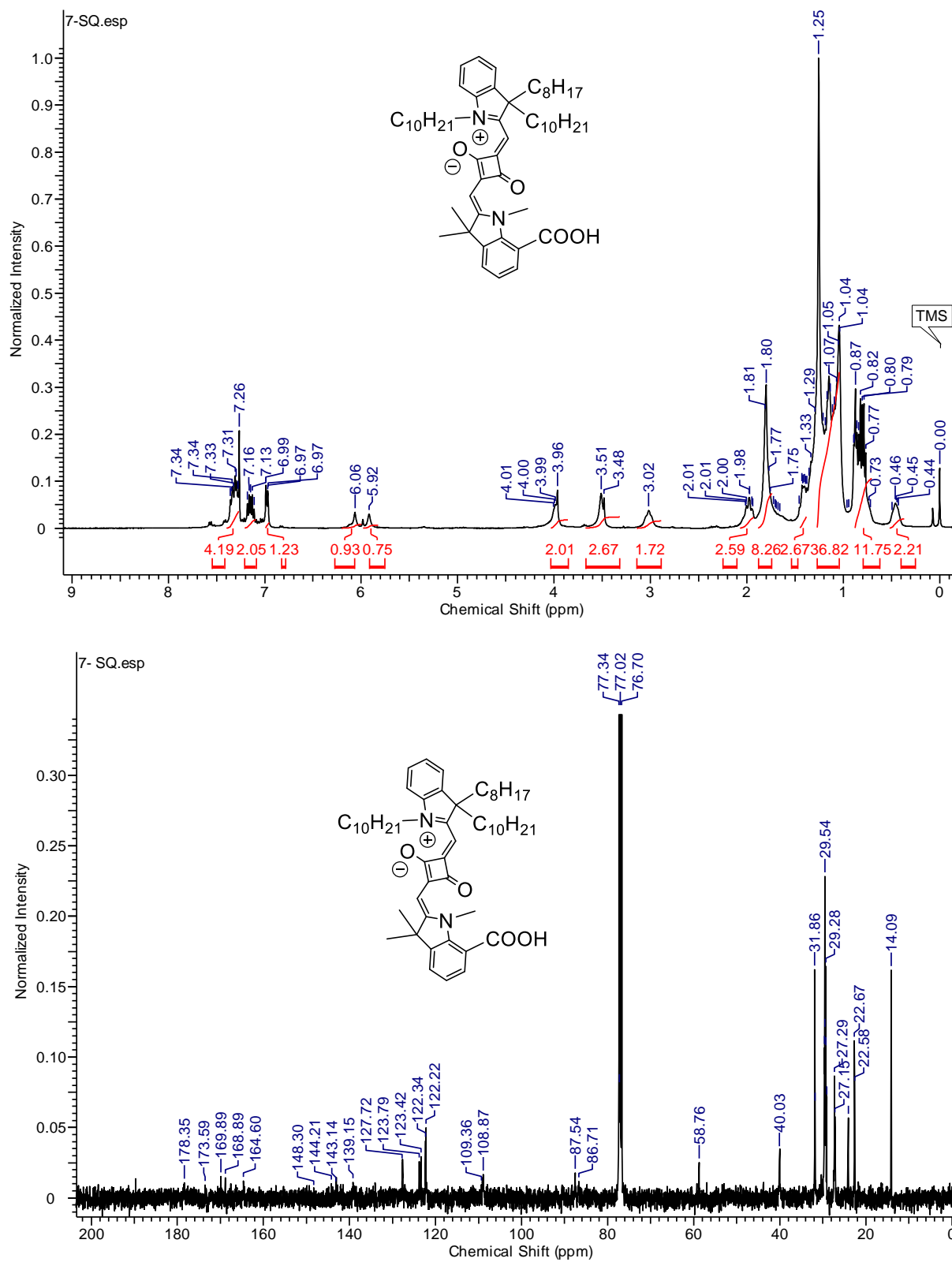
Figure A51. ^{1}H- and ^{13}C- NMR spectra of compound **16** (**7-SQ**) in CDCl$_3$.
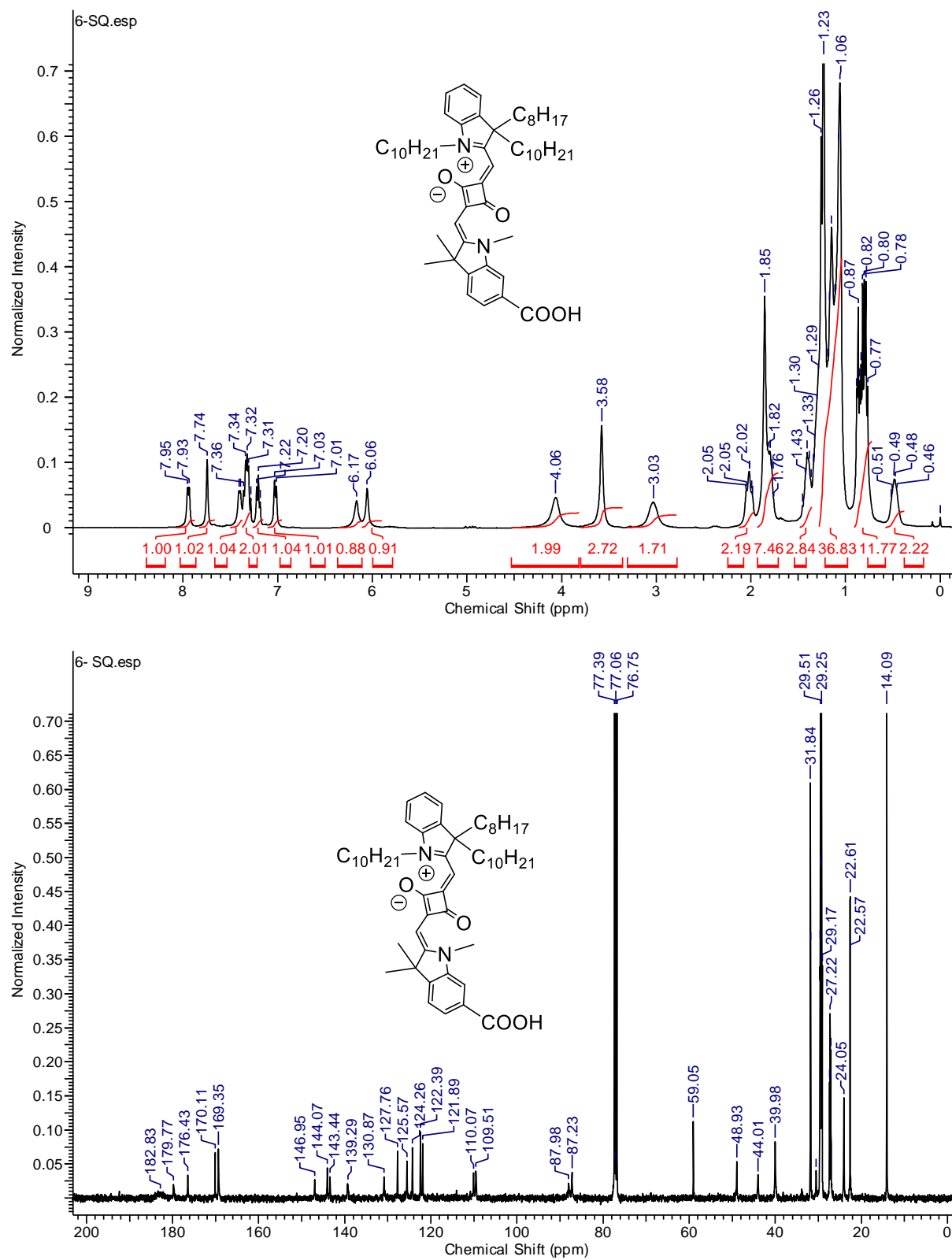
Figure A52. ^{1}H- and ^{13}C- NMR spectra of compound **17** (**6-SQ**) in CDCl$_3$.
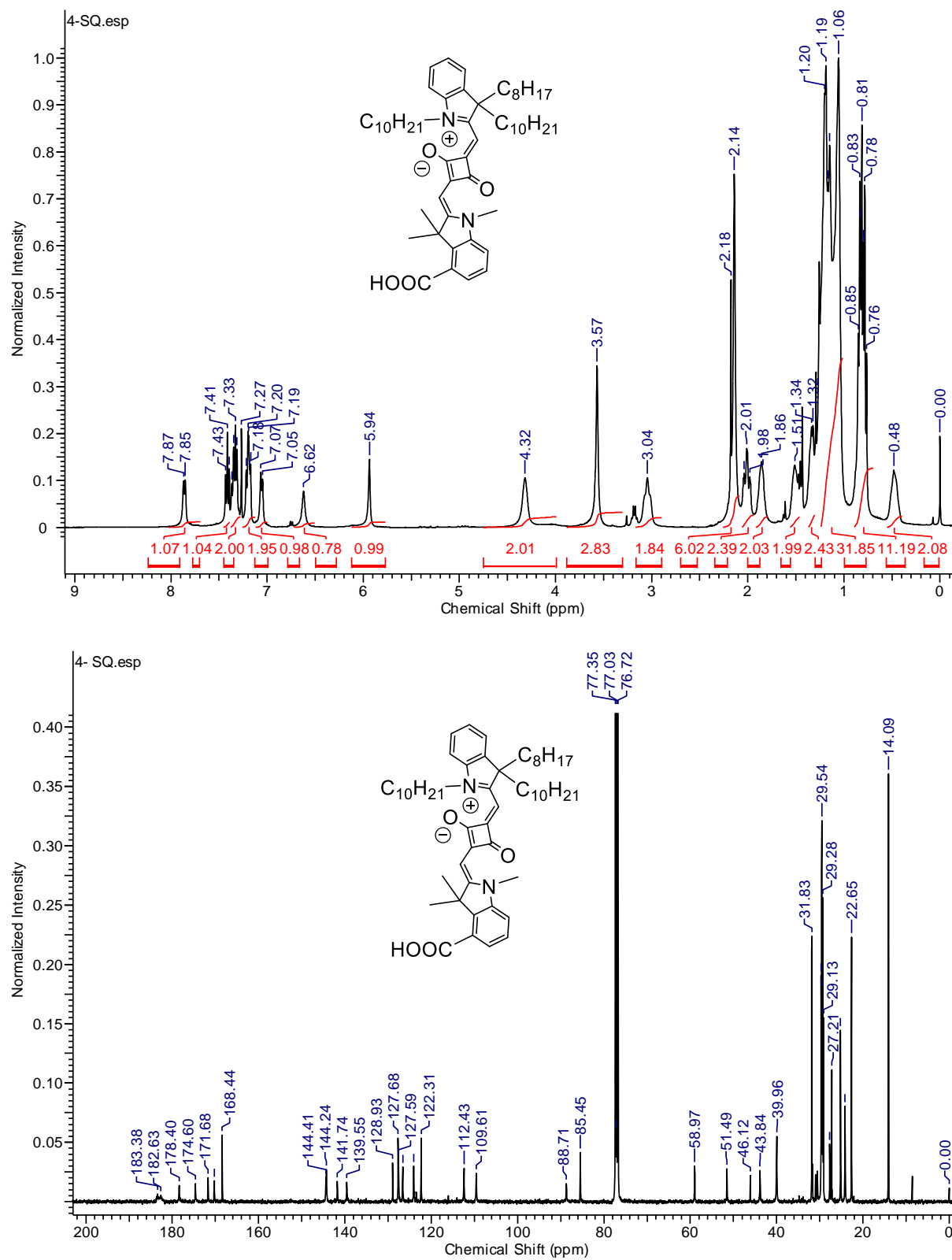
Figure A53. ^{1}H- and ^{13}C- NMR spectra of compound **18** (**4**-SQ) in CDCl$_3$.
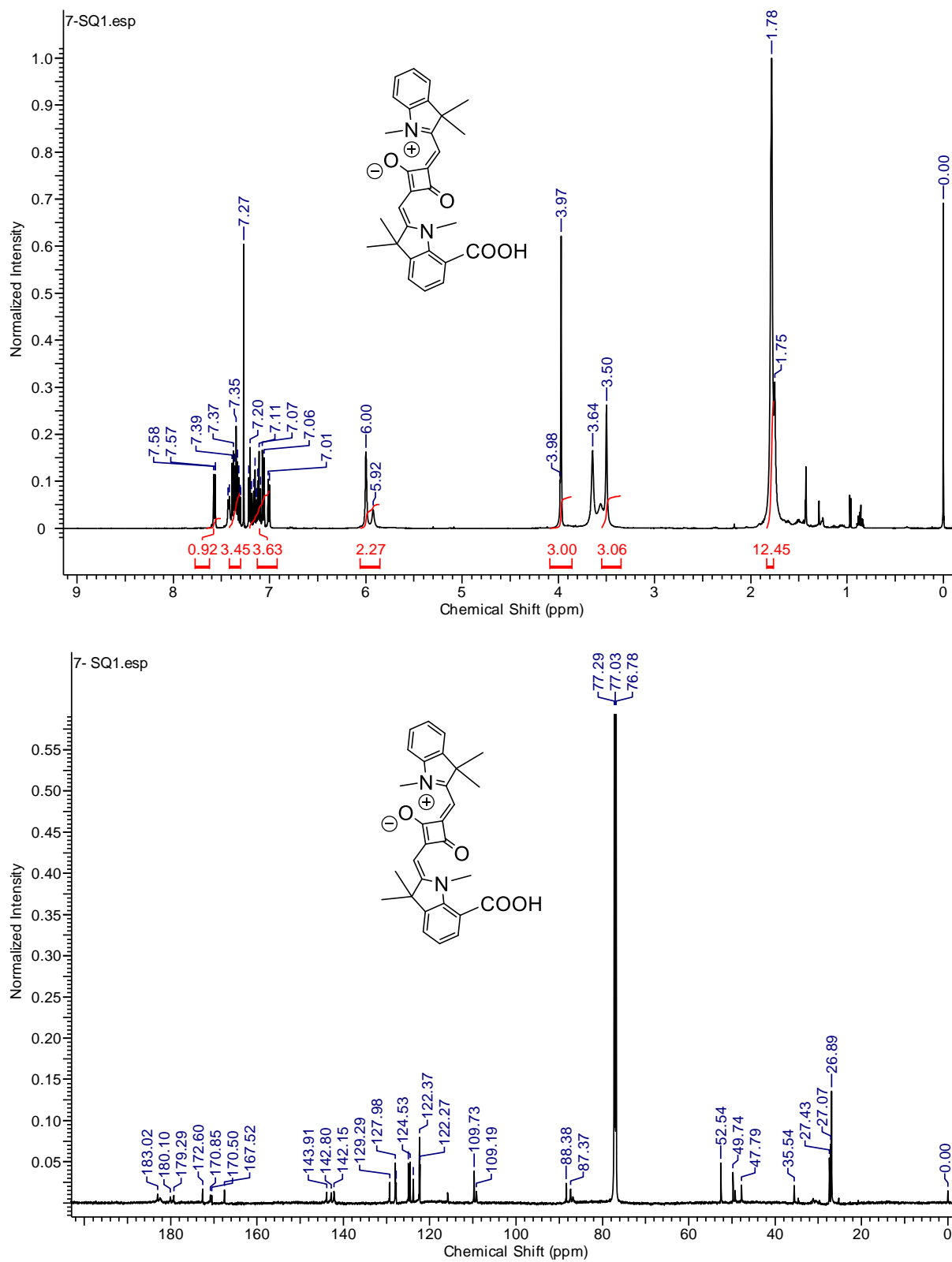
Figure A54. ^{1}H- and ^{13}C- NMR spectra of compound **19 (7-SQ1)** in CDCl$_3$.
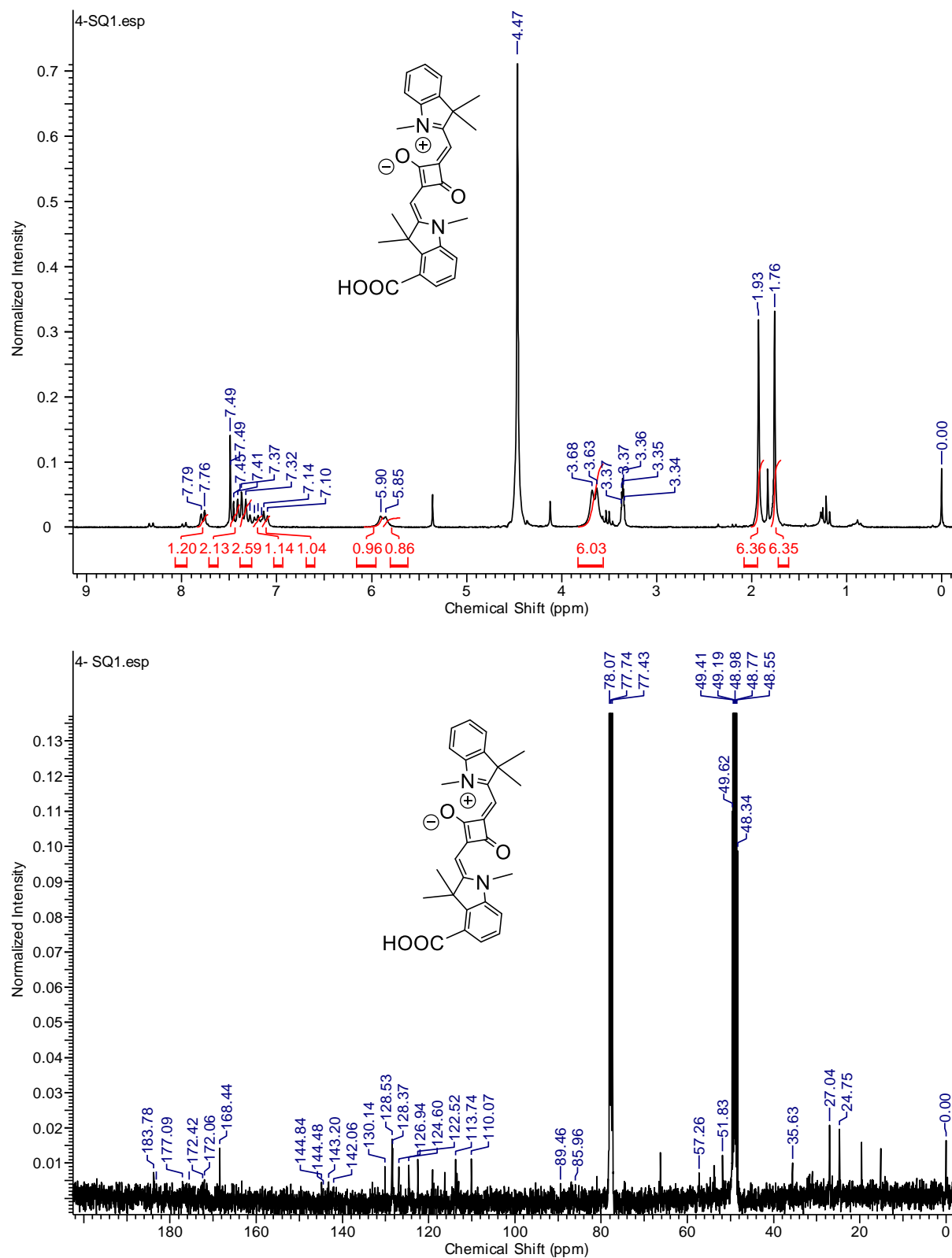
Figure A55. ^{1}H- and ^{13}C- NMR spectra of compound **20 (*4*-SQ1)** in MeOH: CDCl$_3$ (2: 4).

3-Indm #237 RT: 1.27 AV: 1 NL: 8.66E8
T: FTMS + p ESI Full ms [100.0000-1500.0000]

524.5201
R=49507
$C_{37}H_{66}N = 524.5190$
2.1028 ppm

146.0811
R=95207

214.9174
R=74702

279.1588
R=67707

391.2838
R=57307

475.2365
R=51907

570.5245
R=46607

650.4144
R=39802

740.6734
R=33302

831.5732
R=36307

898.7847
R=34607

m/z
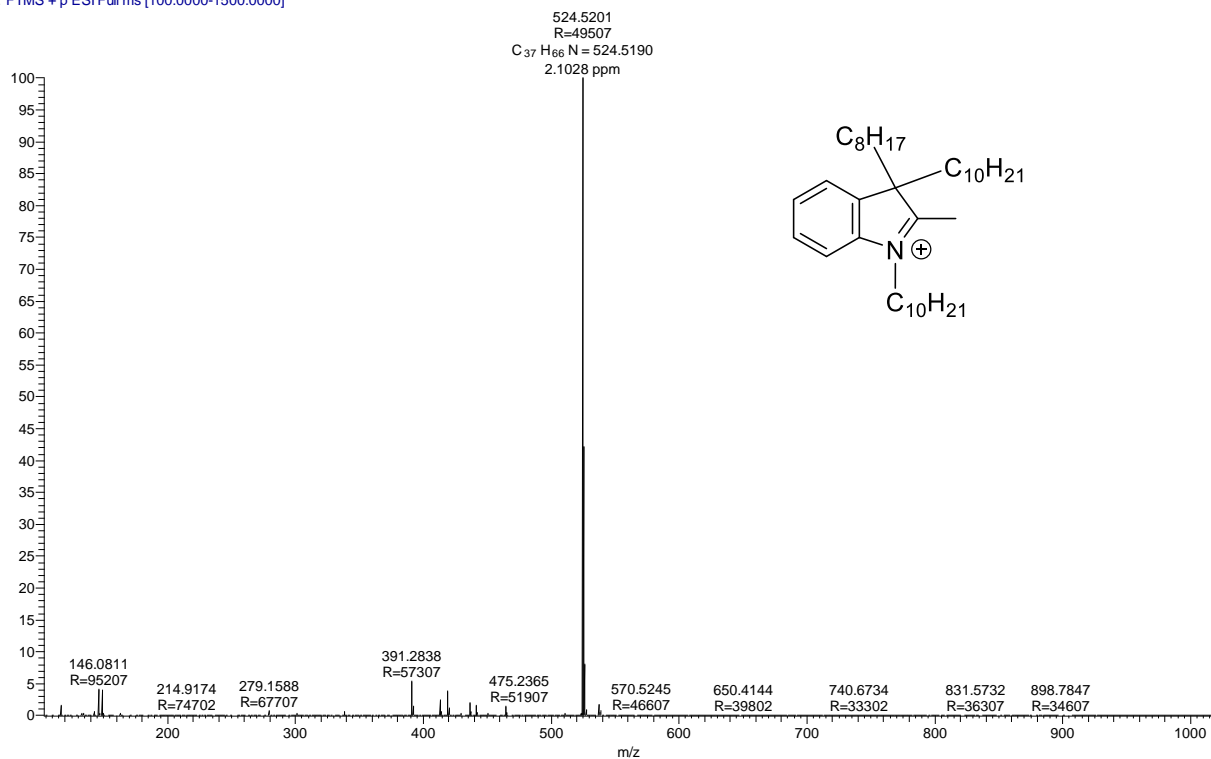
Sm-SQ #324 RT: 1.74 AV: 1 NL: 1.02E9
T: FTMS + p ESI Full ms [100.0000-1500.0000]

326.1754
R=62807
$C_{20}H_{24}O_3N = 326.1751$
0.8703 ppm

149.0232
R=92607
$C_8H_5O_3 = 149.0233$
-0.9559 ppm

214.9174
R=72802

270.1122
R=68707
$C_{16}H_{16}O_3N = 270.1125$
-1.0635 ppm

348.1563
R=60707

391.2837
R=56907

419.3150
R=54507

464.3730
R=50707

503.2675
R=48507

551.5031
R=36605

m/z
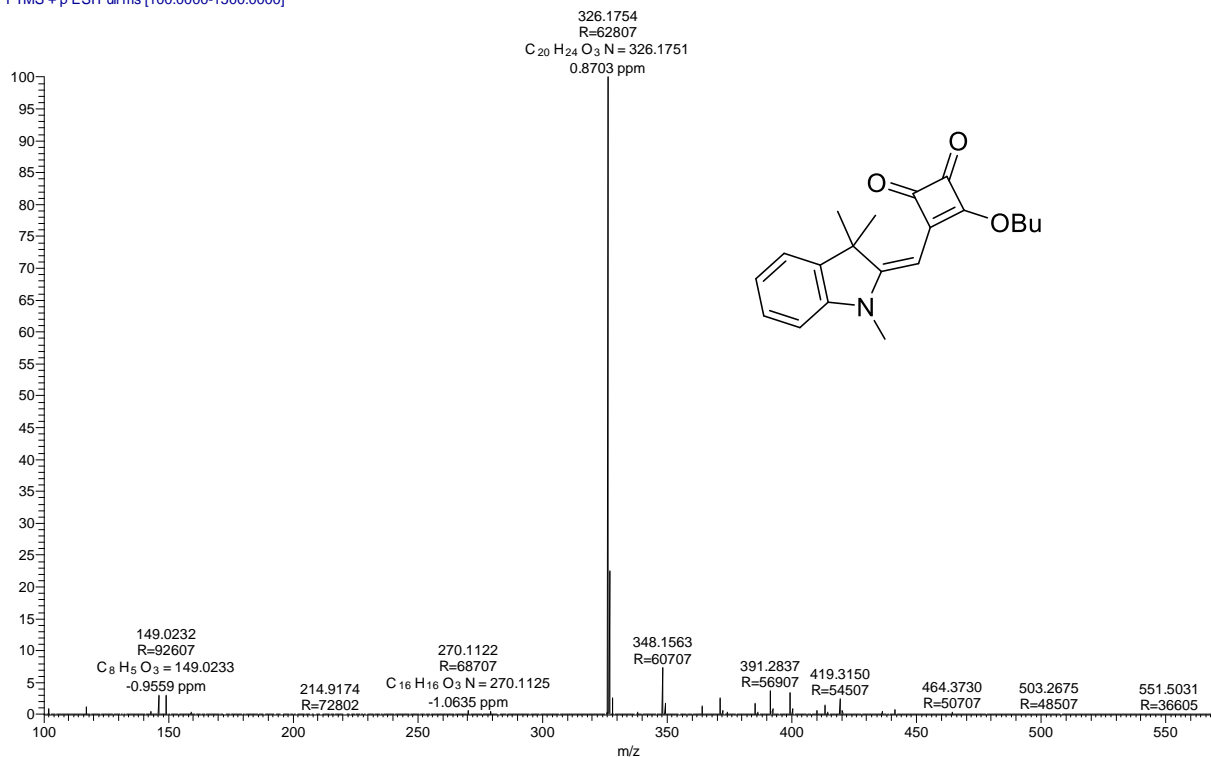
Figure A56. HRMS spectra of compounds **3** and **6**.
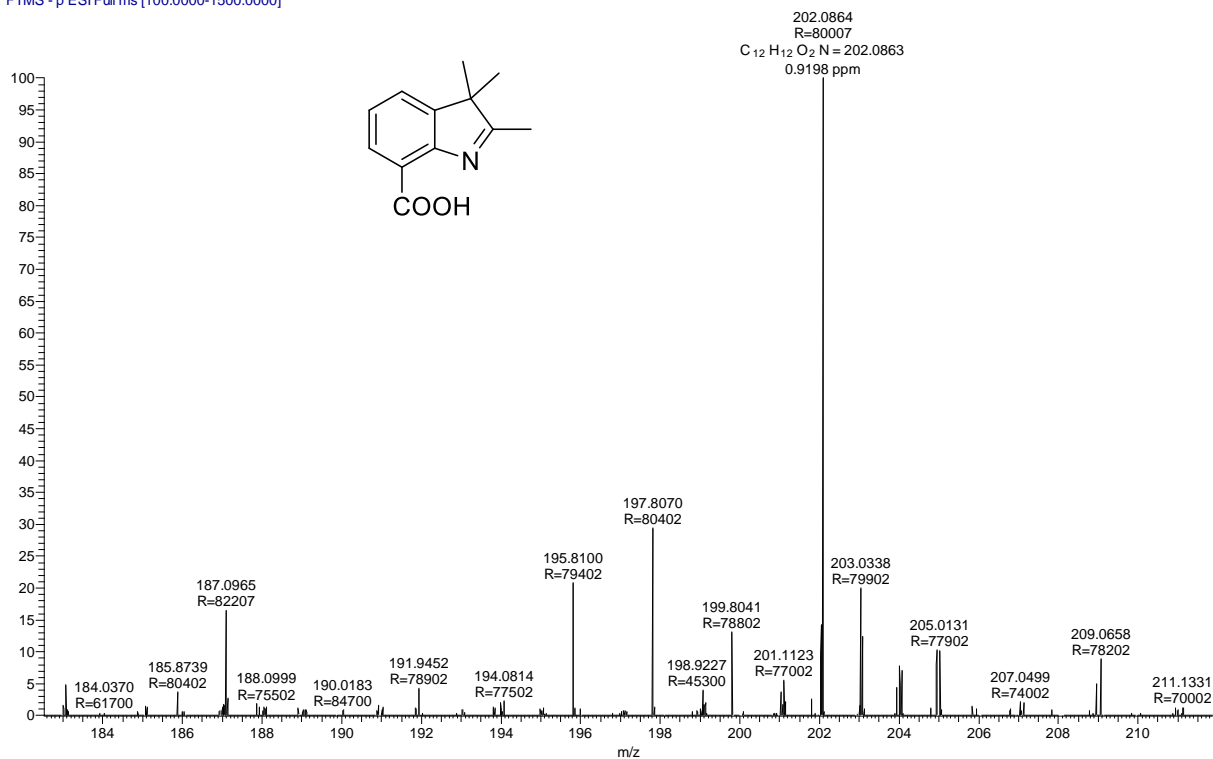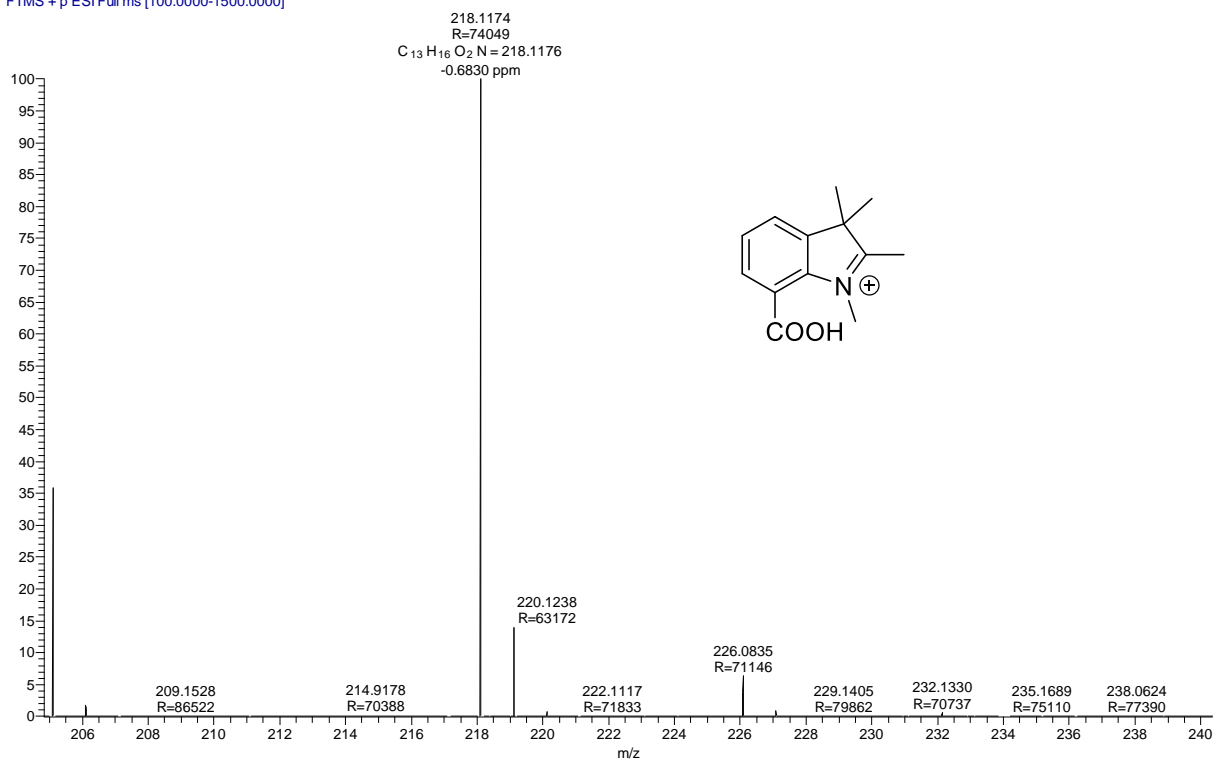
Figure A57. HRMS spectra of compounds **9** and **10**.

m-Hydra #168   RT: 0.90   AV: 1   NL: 5.60E7
T: FTMS + p ESI Full ms [100.0000-1500.0000]
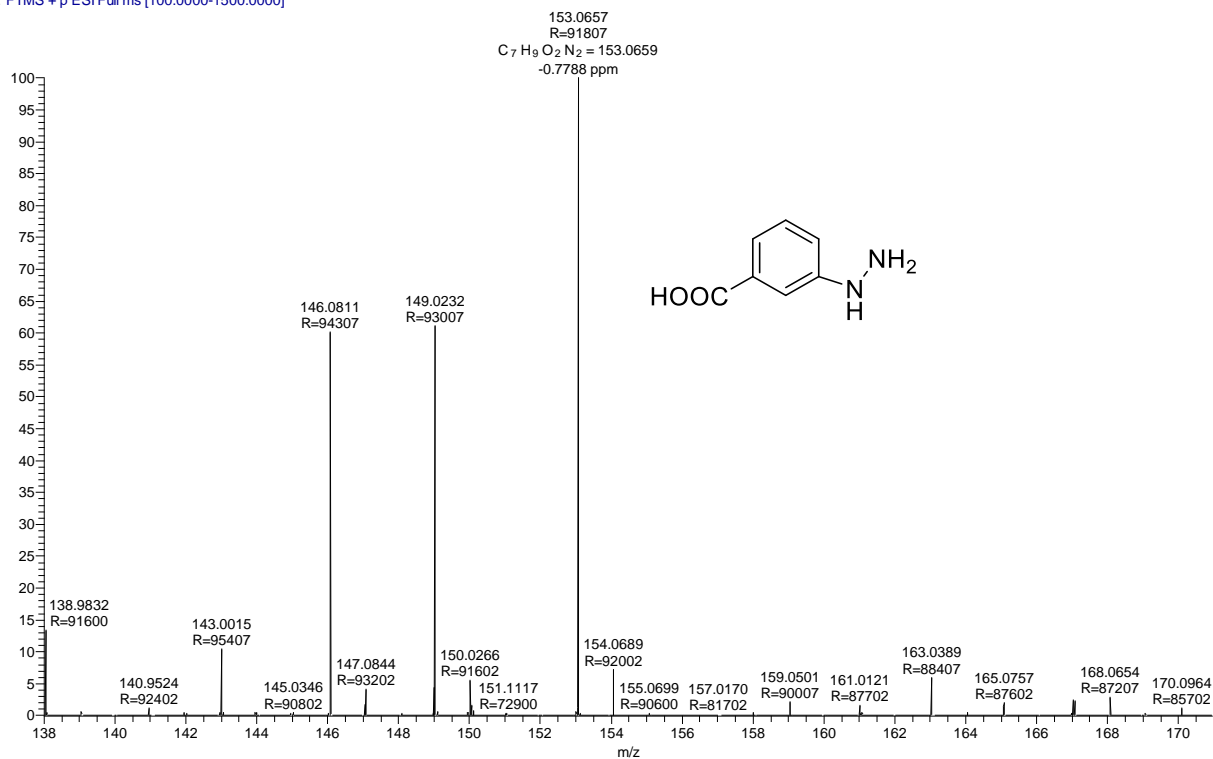
6-Ind #258   RT: 1.49   AV: 1   NL: 4.67E6
T: FTMS - p ESI Full ms [100.0000-1500.0000]
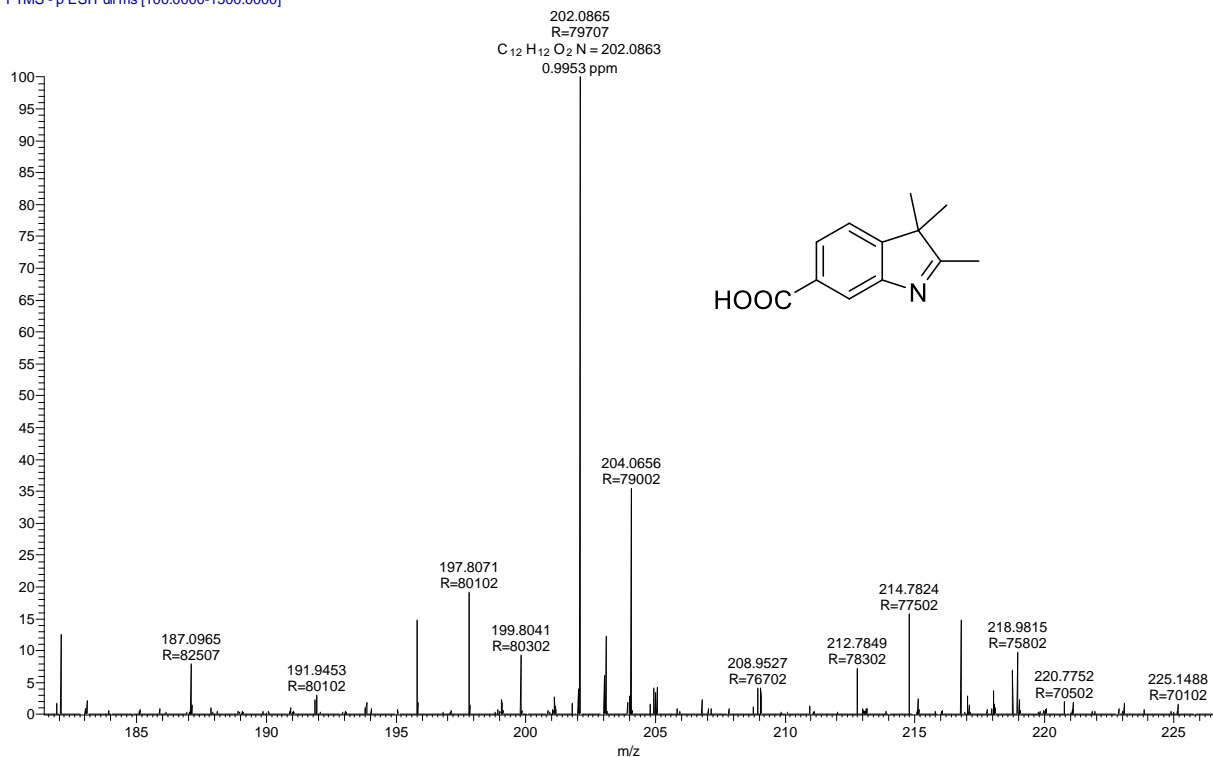
Figure A58. HRMS spectra of compounds **12** and **13a**.

4-Ind #265   RT: 1.52   AV: 1   NL: 3.39E8
T: FTMS - p ESI Full ms [100.0000-1500.0000]

202.0864
R=79307
$C_{12}H_{12}O_2N$ = 202.0863
0.8443 ppm

156.0805
R=91007
$C_{11}H_{10}N$ = 156.0808
-1.5377 ppm

115.9193
R=104207

181.0705
R=85107

214.7821
R=74302

244.0972
R=71907

270.0743
R=69007

287.0644
R=66707

311.1682
R=63607

332.0447
R=62207

m/z
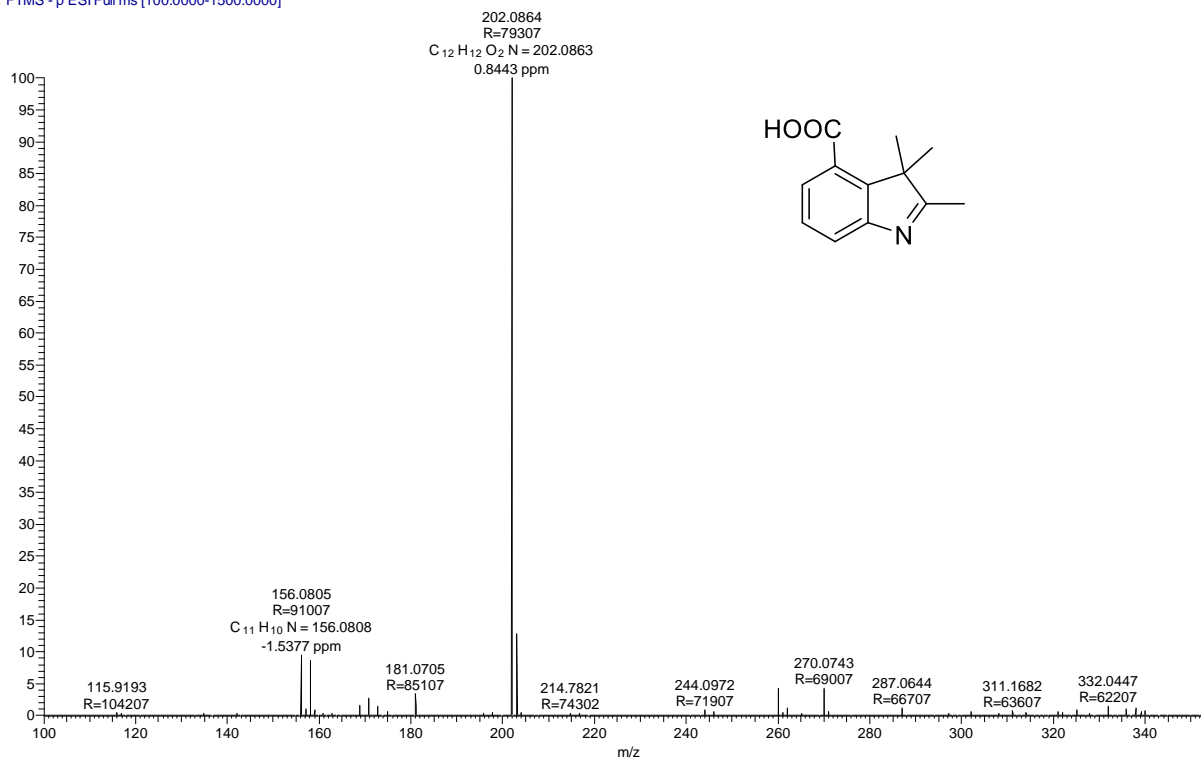
6-Indm #182   RT: 0.97   AV: 1   NL: 7.20E8
T: FTMS + p ESI Full ms [100.0000-1500.0000]

218.1177
R=77007
$C_{13}H_{16}O_2N$ = 218.1176
0.7623 ppm

116.9861
R=104002

149.0232
R=93507

181.0495
R=82407

232.1329
R=74607

250.9999
R=69502

279.1588
R=67307

301.1406
R=64607

338.3414
R=60907

360.3232
R=54607

m/z
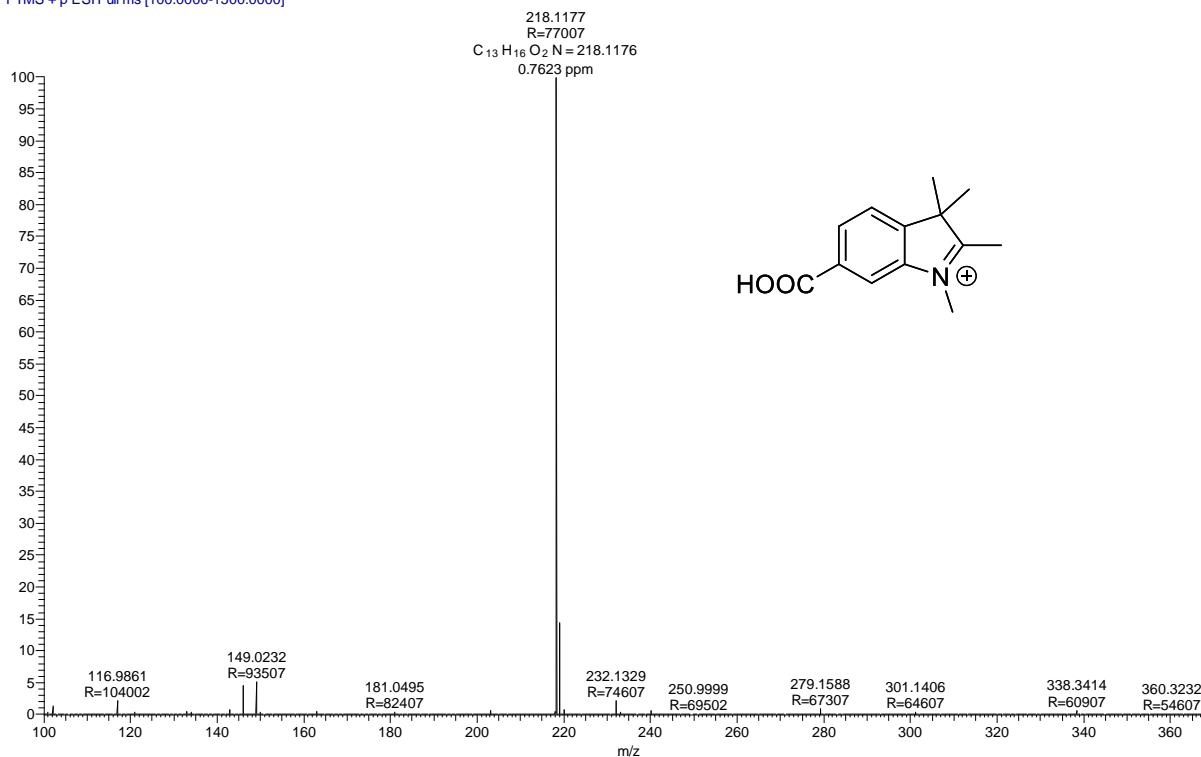
Figure A59. HRMS spectrum of compounds **13b** and **14a**.

Ambarish Kumar Singh
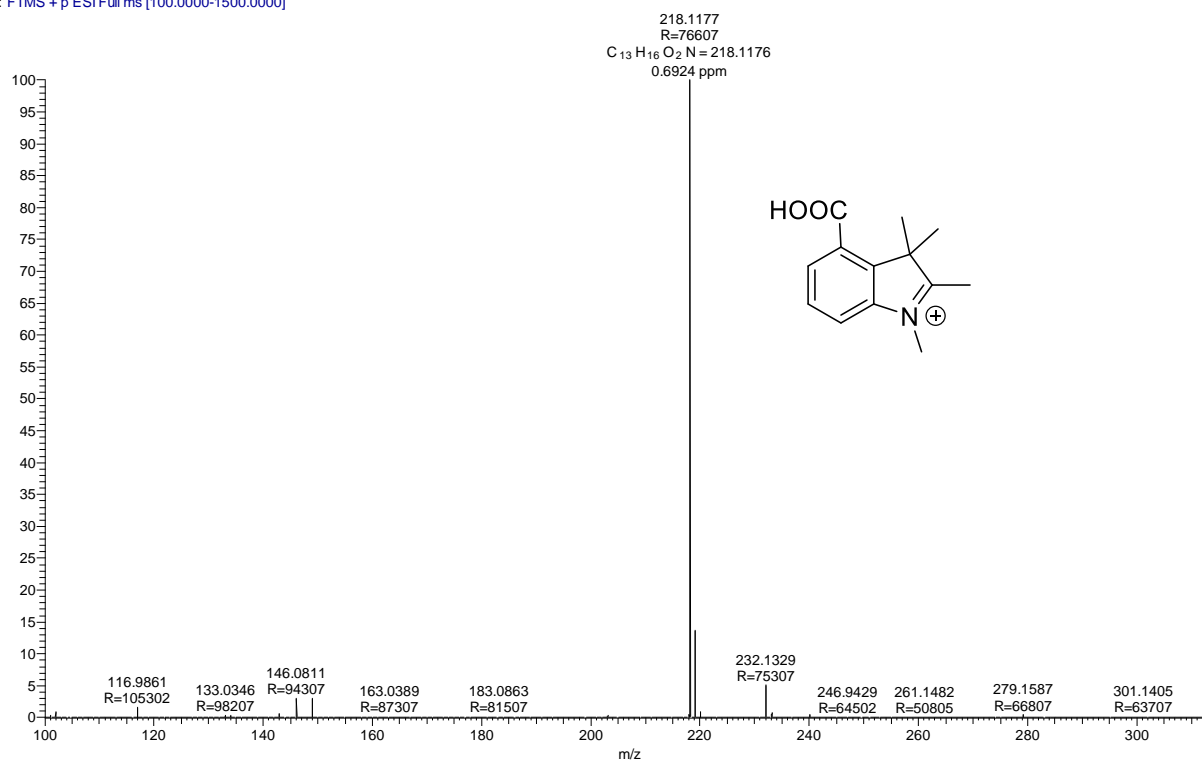
Figure A60. HRMS spectrum of compound **14b**.
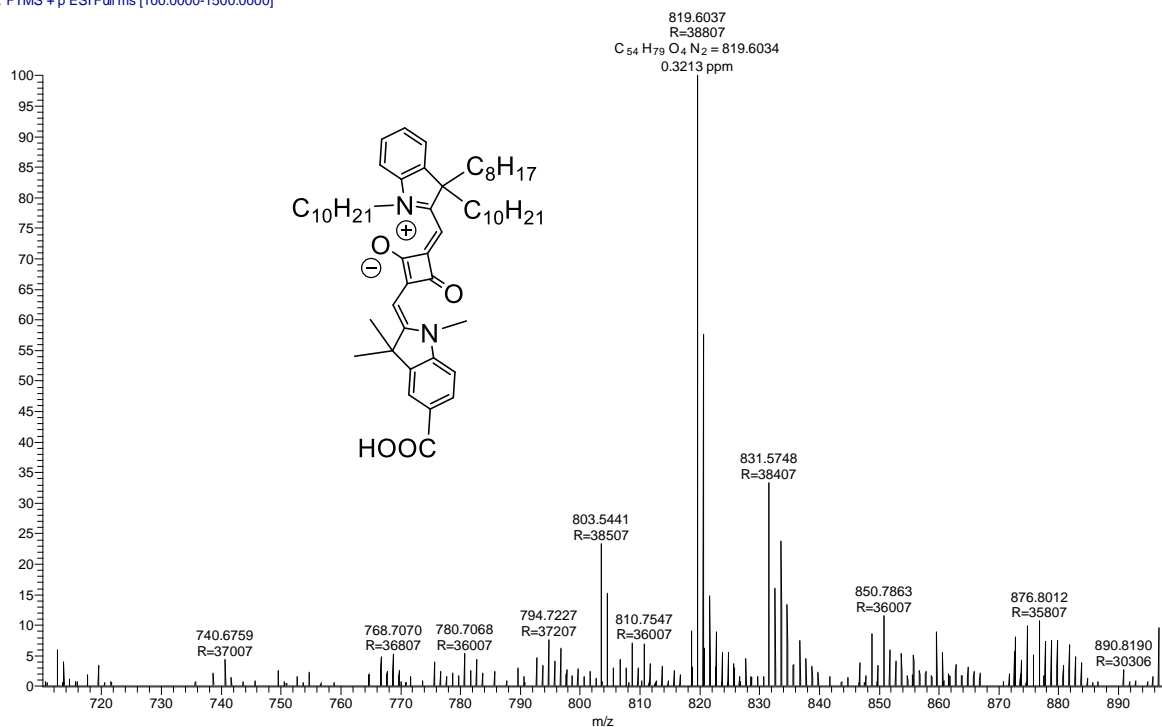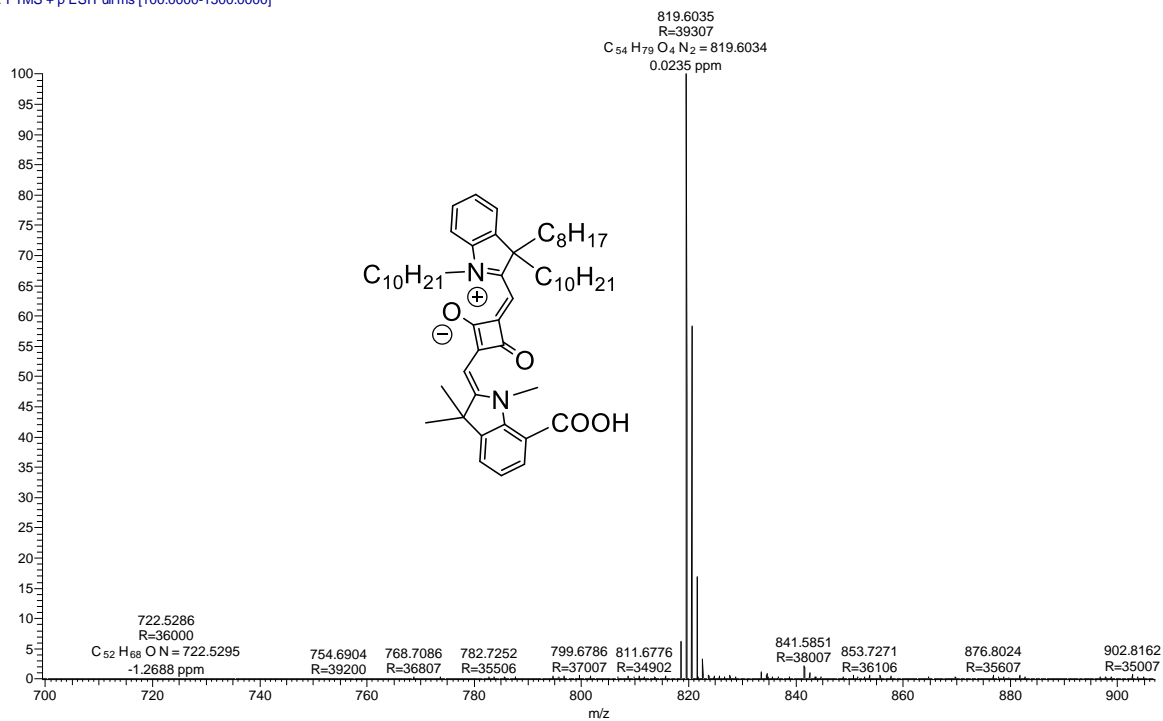
Figure A61. HRMS spectra of compound **15** and **16** (**5-SQ** and **7-SQ**).

6-SQR #305 RT: 1.78 AV: 1 NL: 5.57E6
T: FTMS + p ESI Full ms [100.0000-1500.0000]
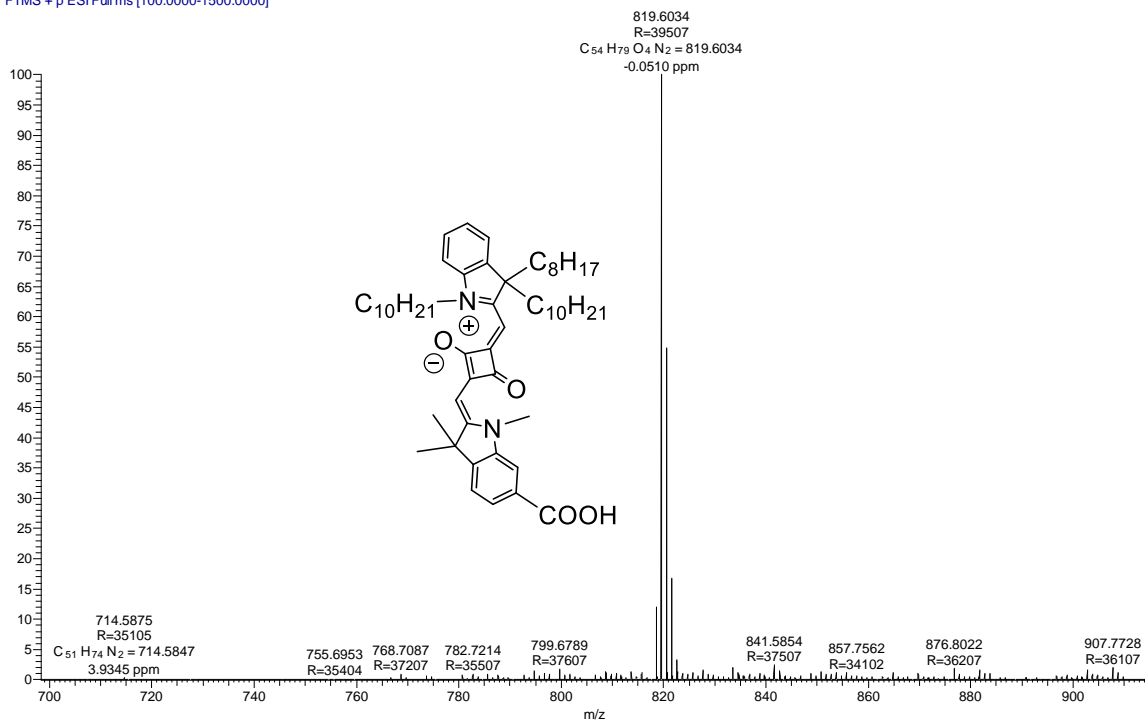
4-SQR #2449 RT: 14.80 AV: 1 NL: 1.04E7
T: FTMS + p ESI Full ms [100.0000-1500.0000]
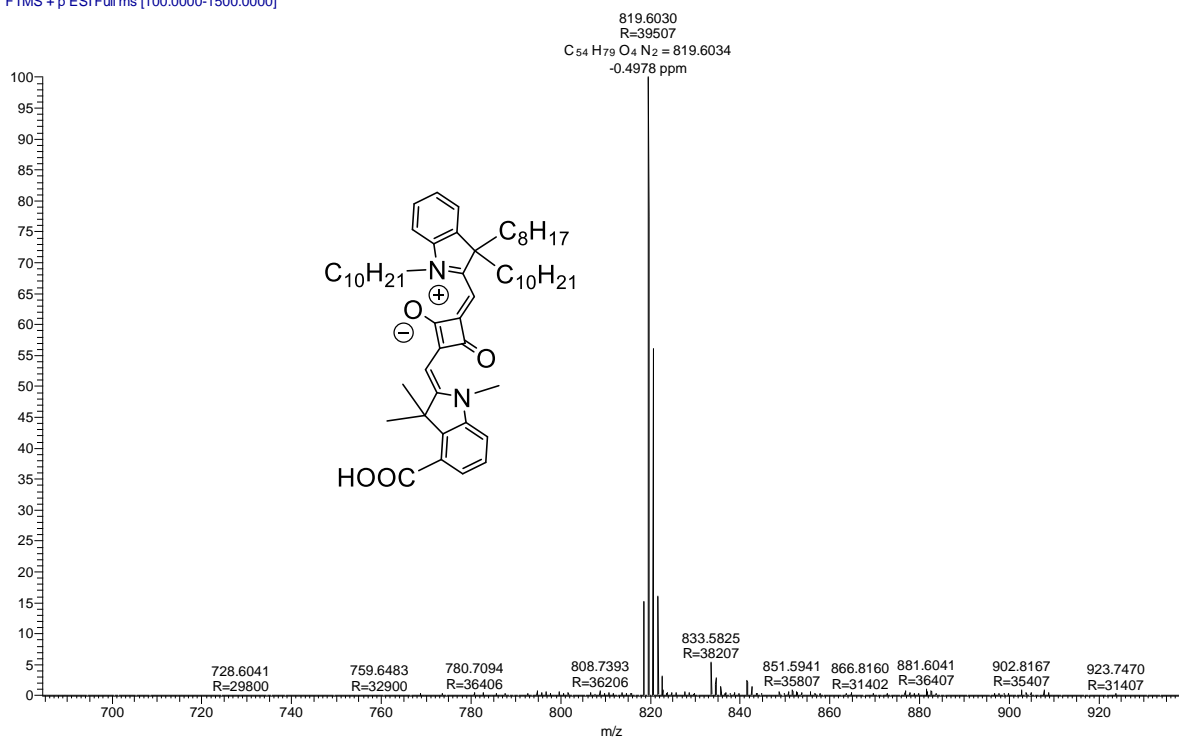
Figure A62. HRMS spectra of compound **17** and **18** (**6**-SQ and **4**-SQ).

7-SQ11 #364 RT: 2.14 AV: 1 NL: 8.89E5
T: FTMS + p ESI Full ms [100.0000-1500.0000]
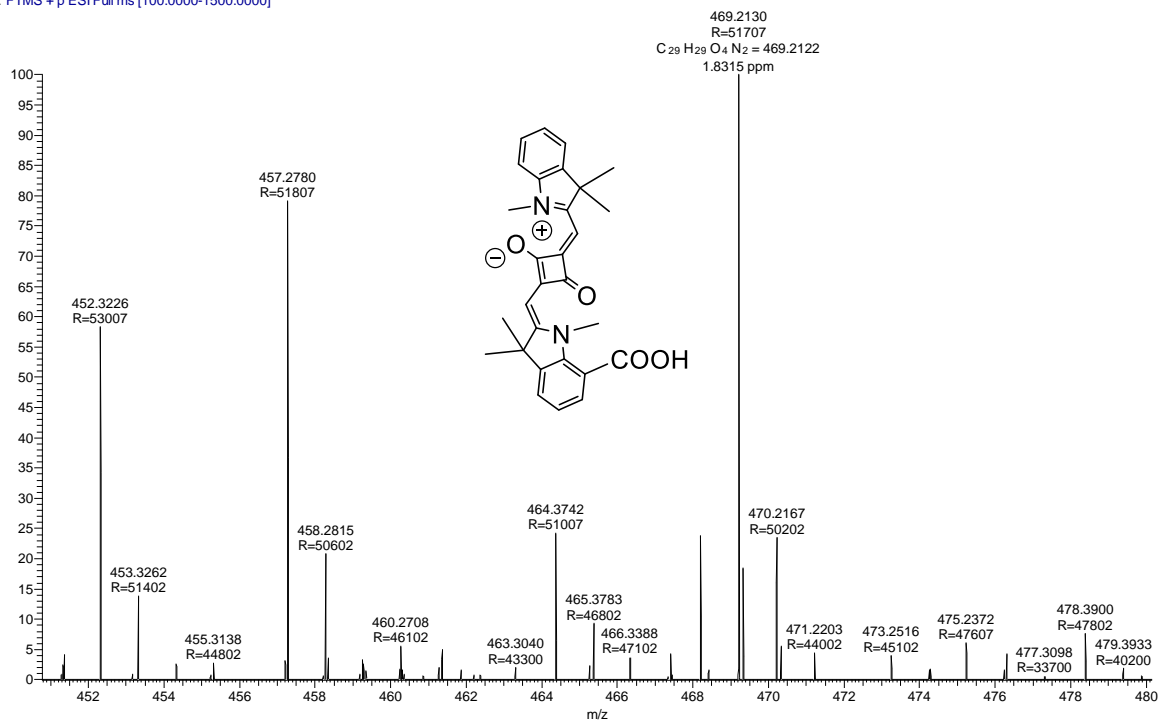
4-SG1 #320 RT: 1.72 AV: 1 NL: 1.09E8
T: FTMS + p ESI Full ms [100.0000-1500.0000]
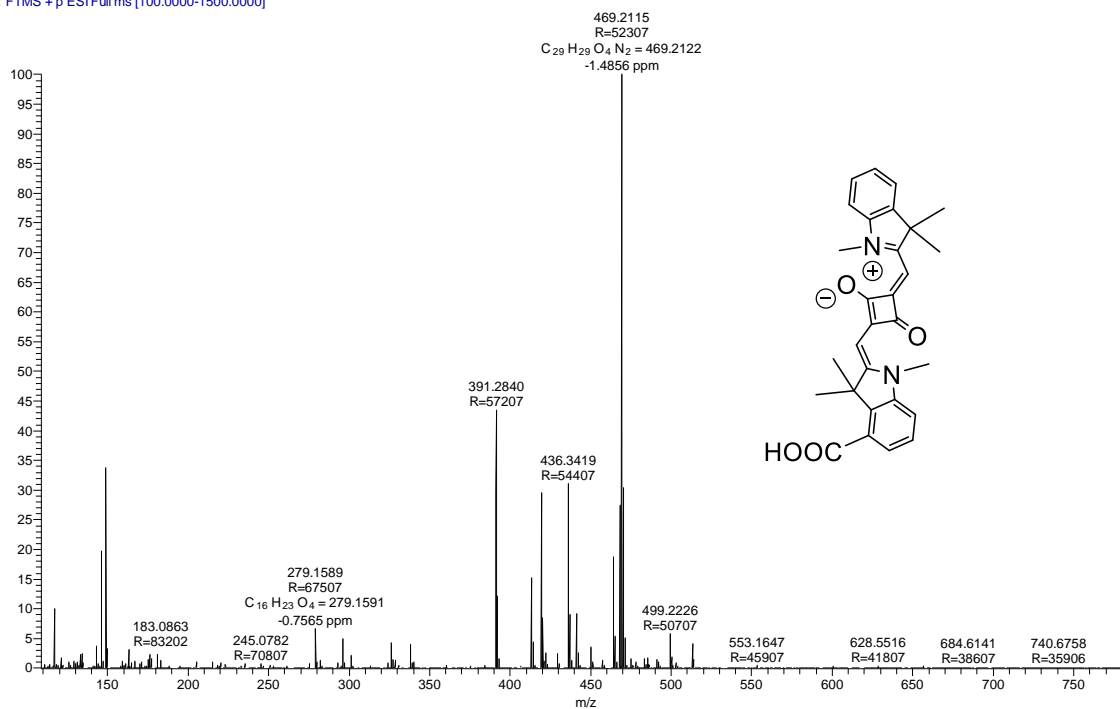
Figure A63. HRMS spectra of compound **19** and **20** (*7*-**SQ1** and *4*-**SQ1**).

Cyclic voltammetry studies SQ dyes.
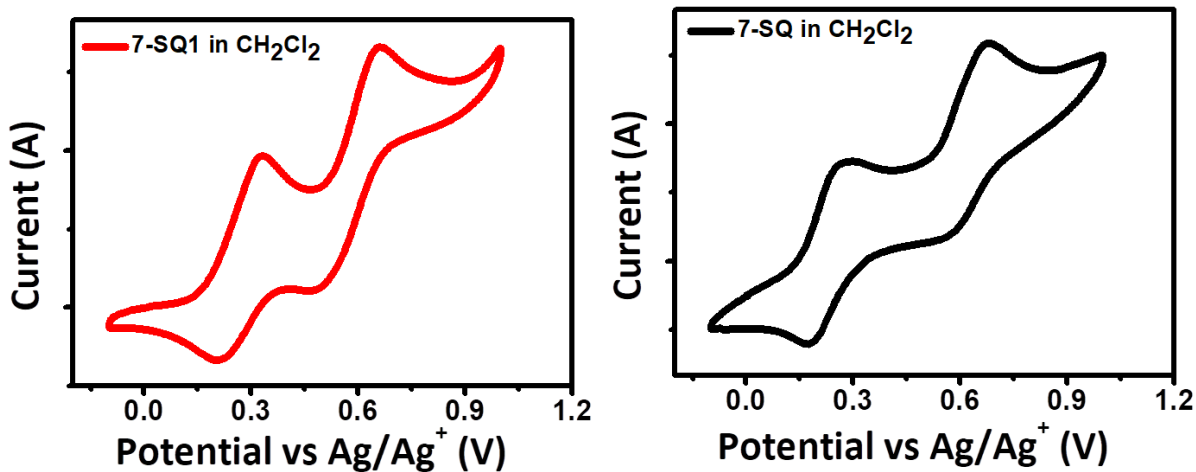
Figure A64. Cyclic voltammograms of **7-SQ1 and 7-SQ** dyes.

IR study of SQ dyes.
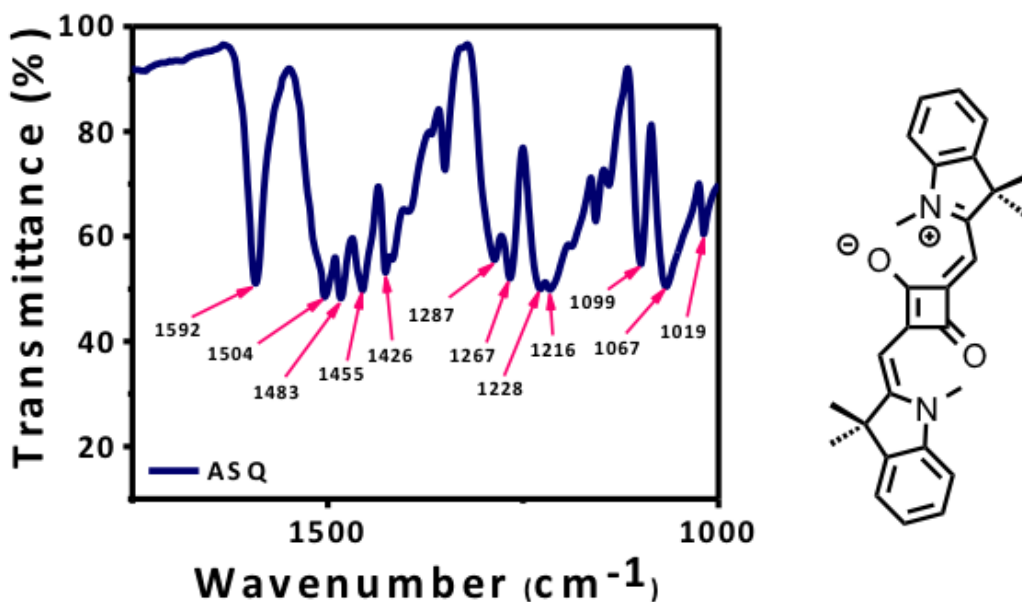
Figure A65. IR spectrum of symmetrical squaraine dye (without carboxylic acid group).
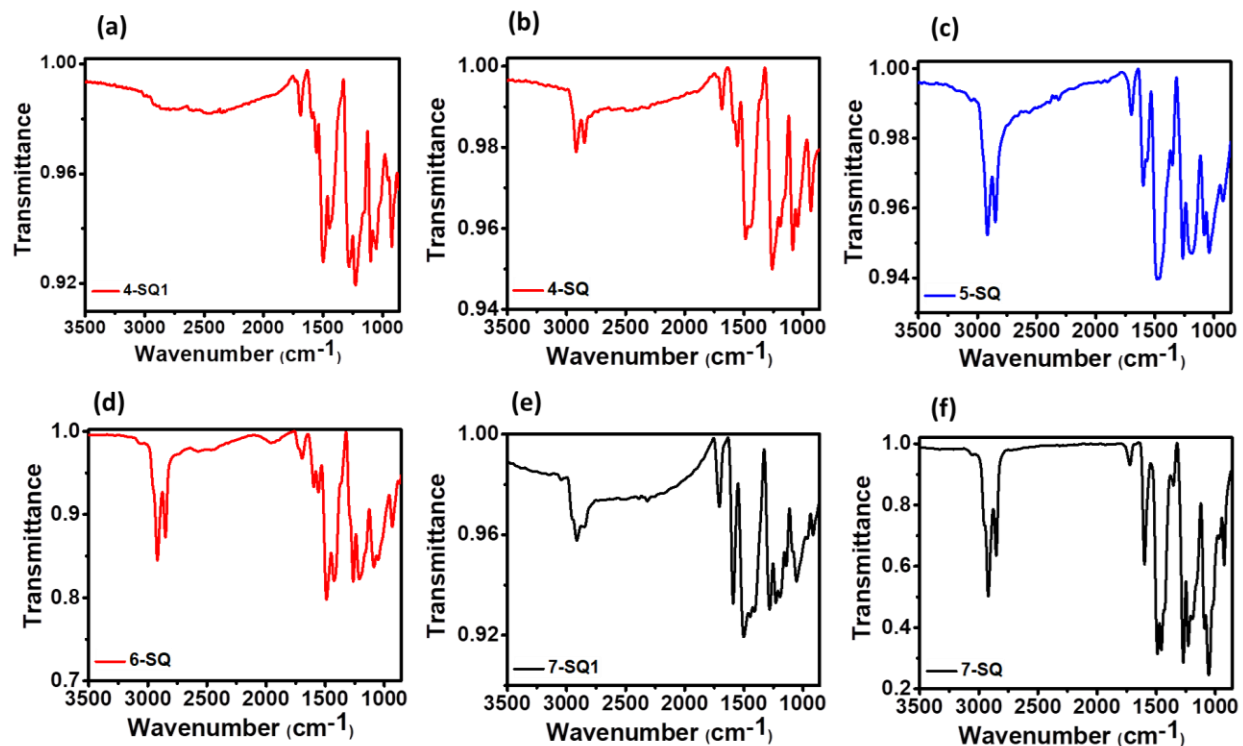
Figure A66. IR spectra of 4-SQ1, 4-SQ, 5-SQ, 6-SQ, 7-SQ1, and 7-SQ dyes.
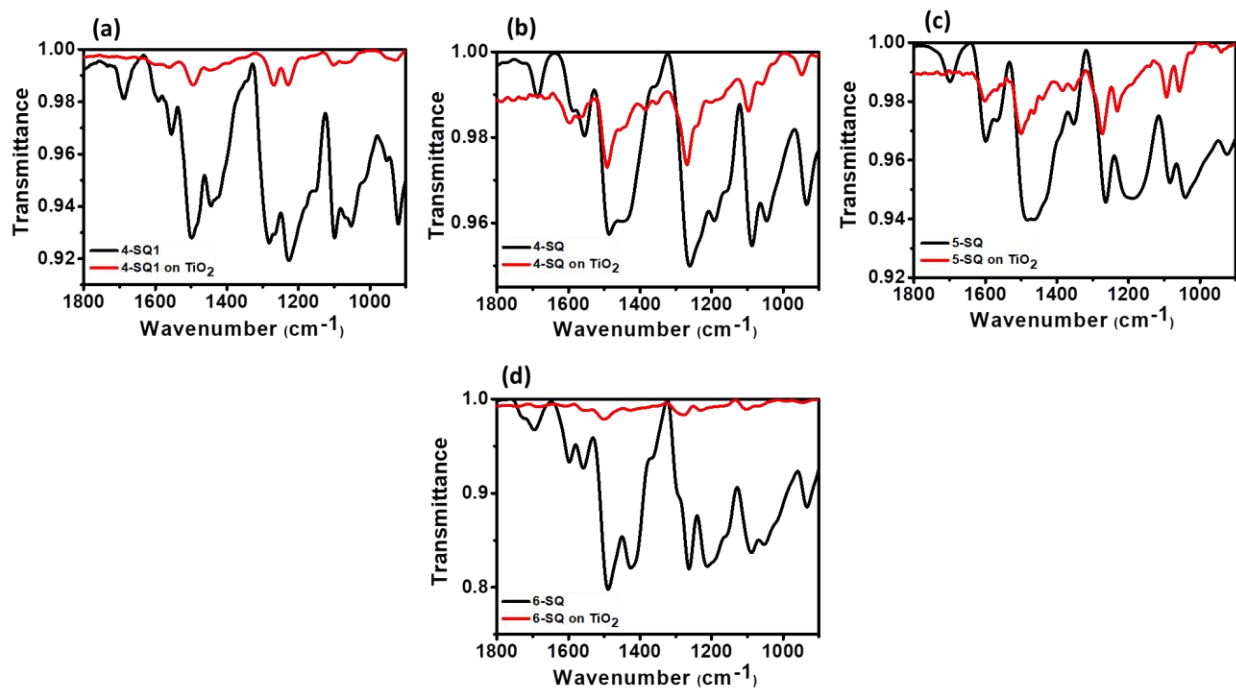
Figure A67. IR spectra of 4-SQ1, 4-SQ, 5-SQ, and 6-SQ dyes as such and on the TiO_2 surface.

Chapter 4
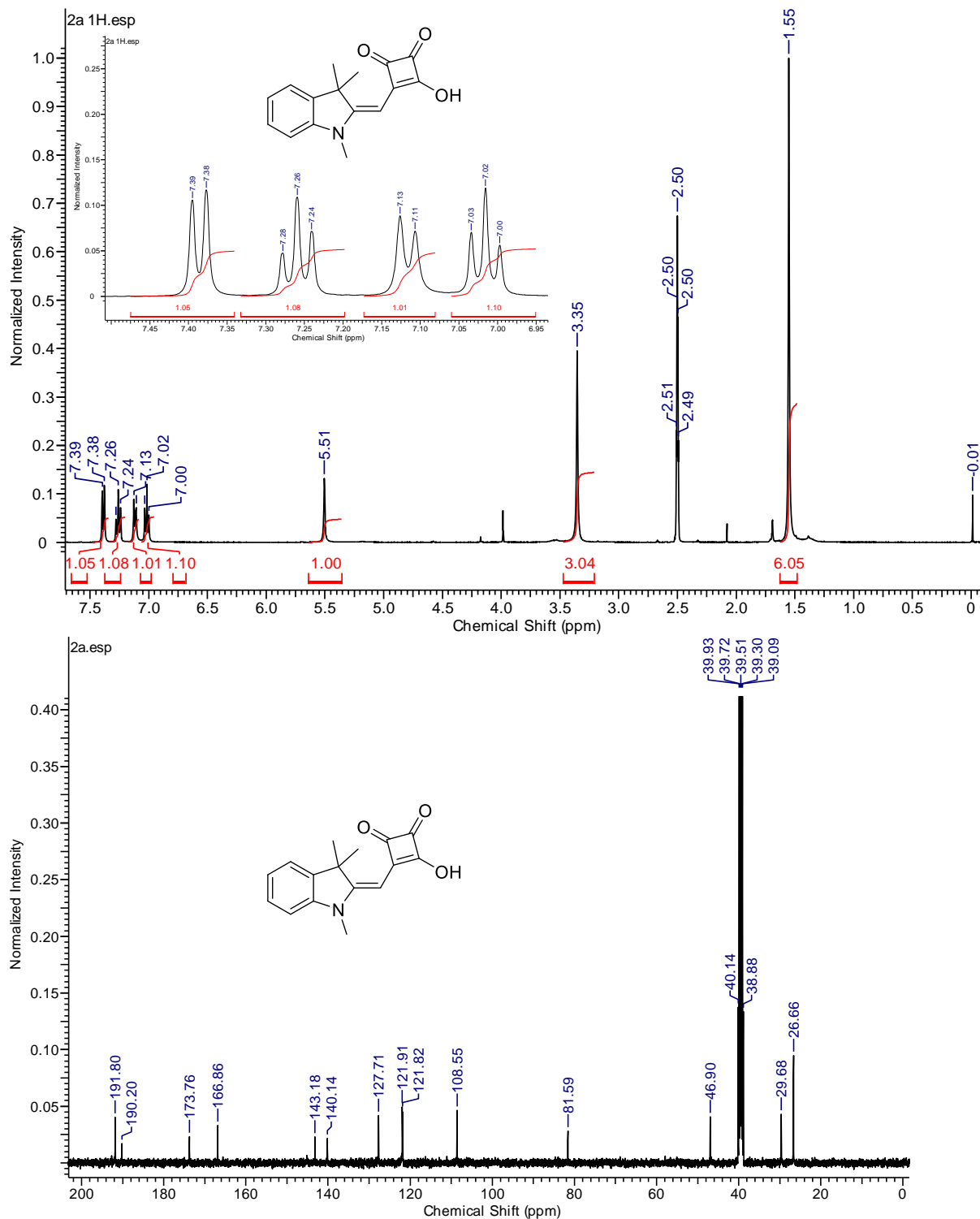
Figure A68. ^{1}H- and ^{13}C- NMR spectra of compound **2a** in DMSO-d_6.

BSSQOH.esp

R₁ = -C₁₀H₂₁, R₂ = -C₁₂H₂₅

B SSQOH.esp

R₁ = -C₁₀H₂₁, R₂ = -C₁₂H₂₅
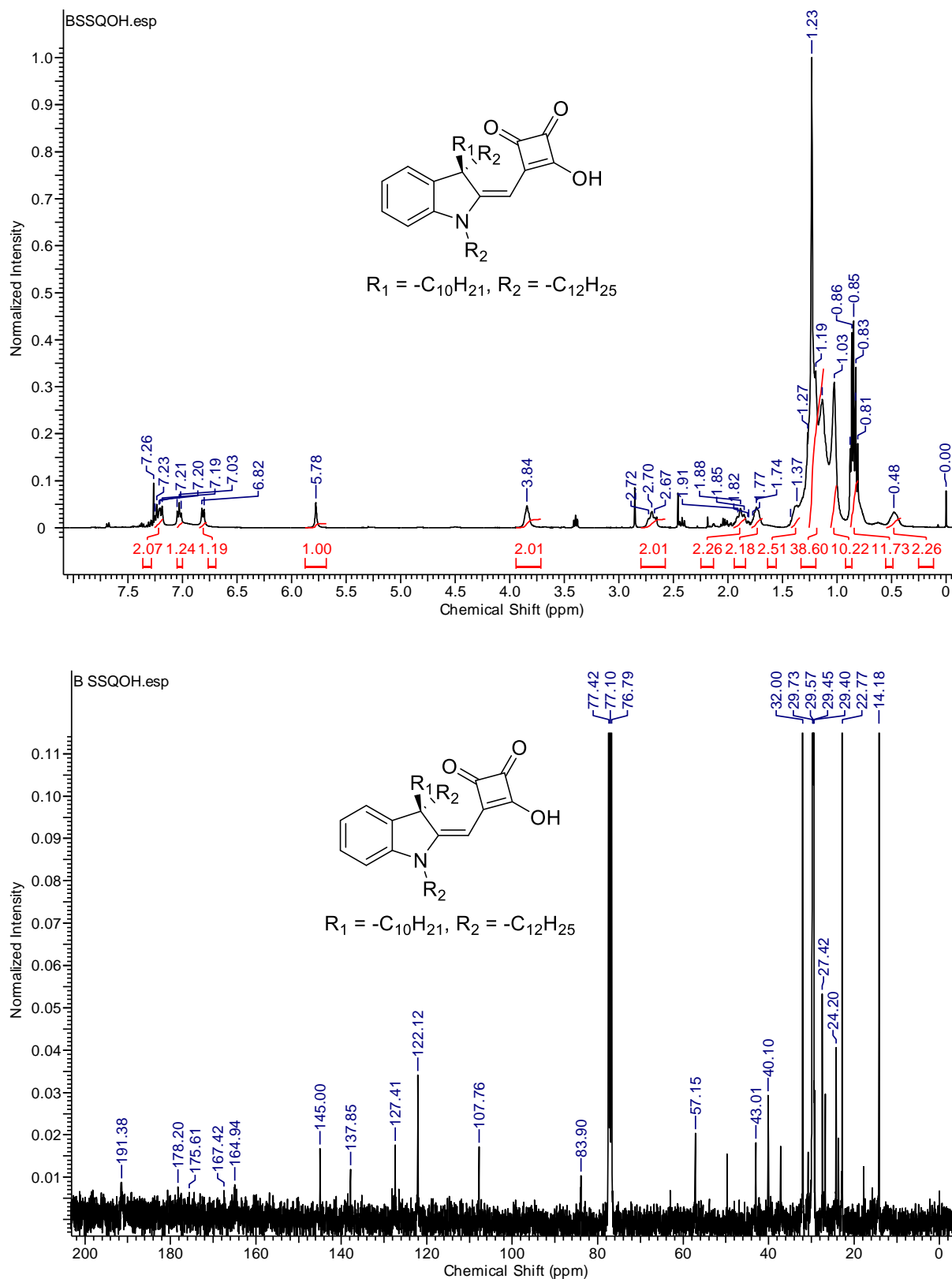
Figure A69. ^{1}H- and ^{13}C- NMR spectra of compound **2b** CDCl₃.
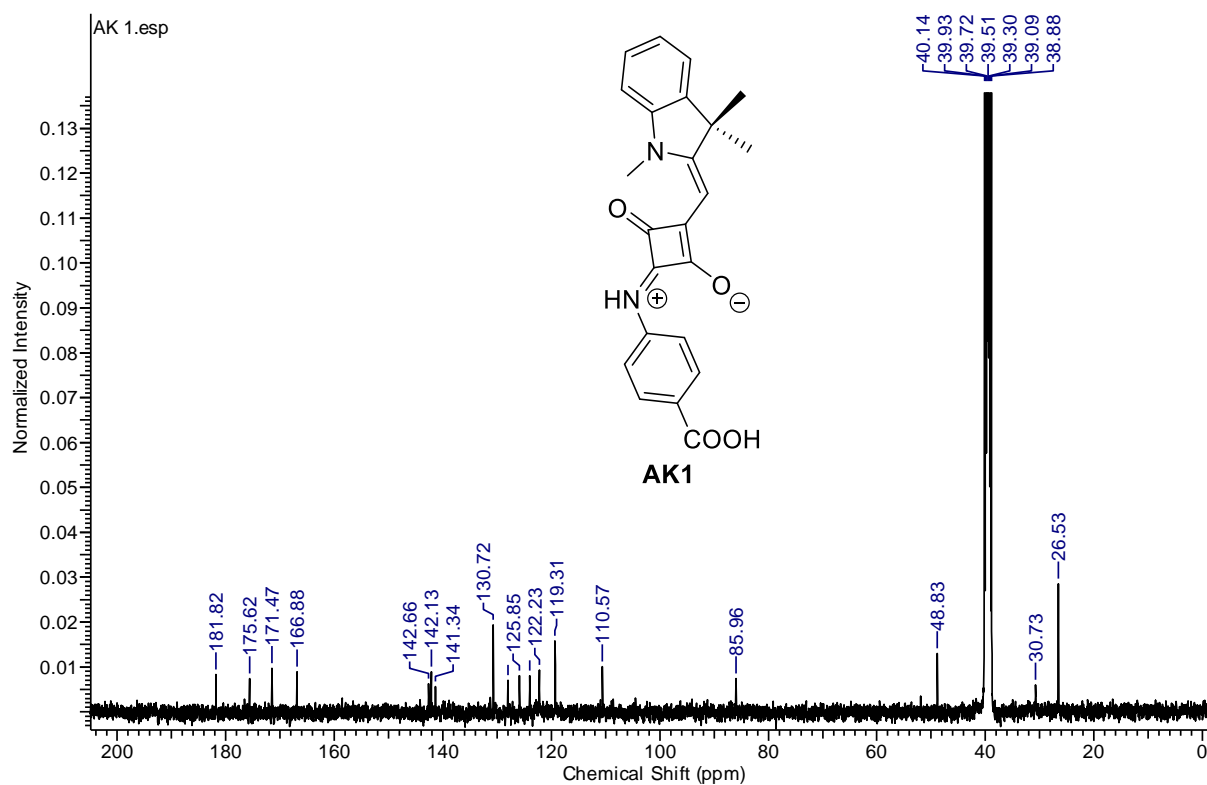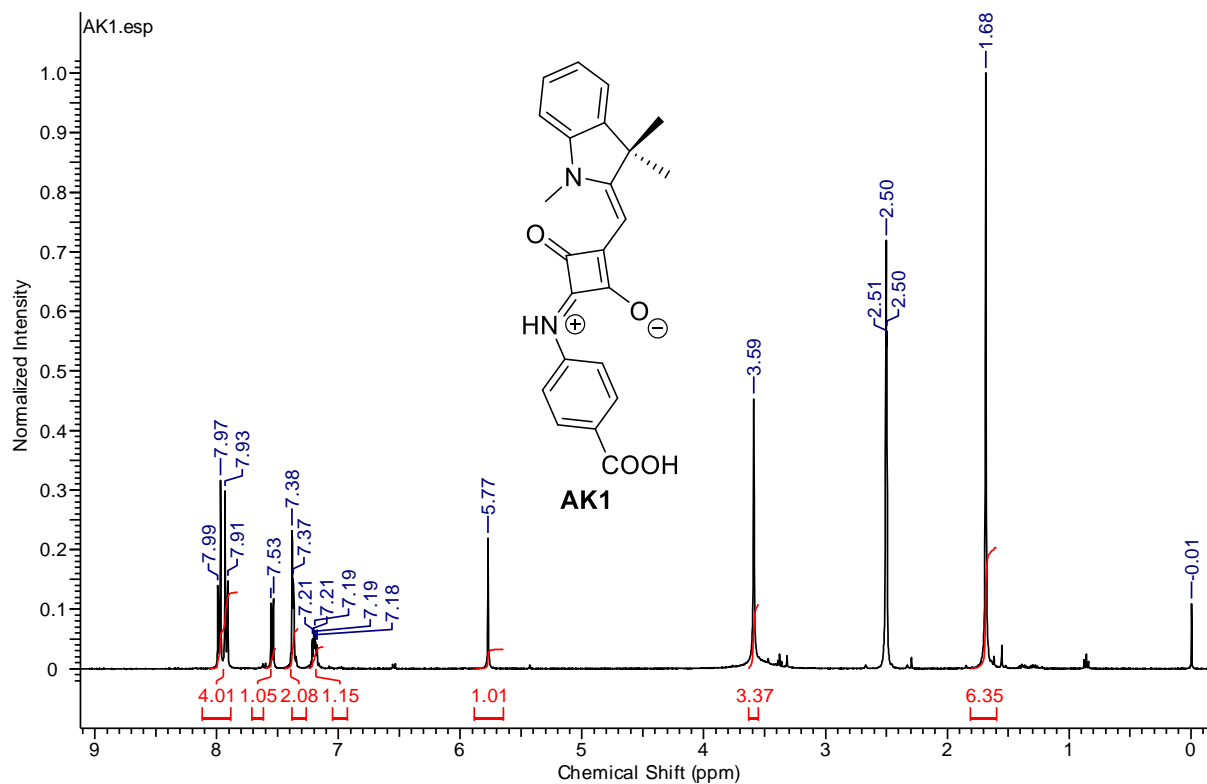
Figure A70. ^{1}H- and ^{13}C- NMR spectra of compound **3** DMSO-d_6.
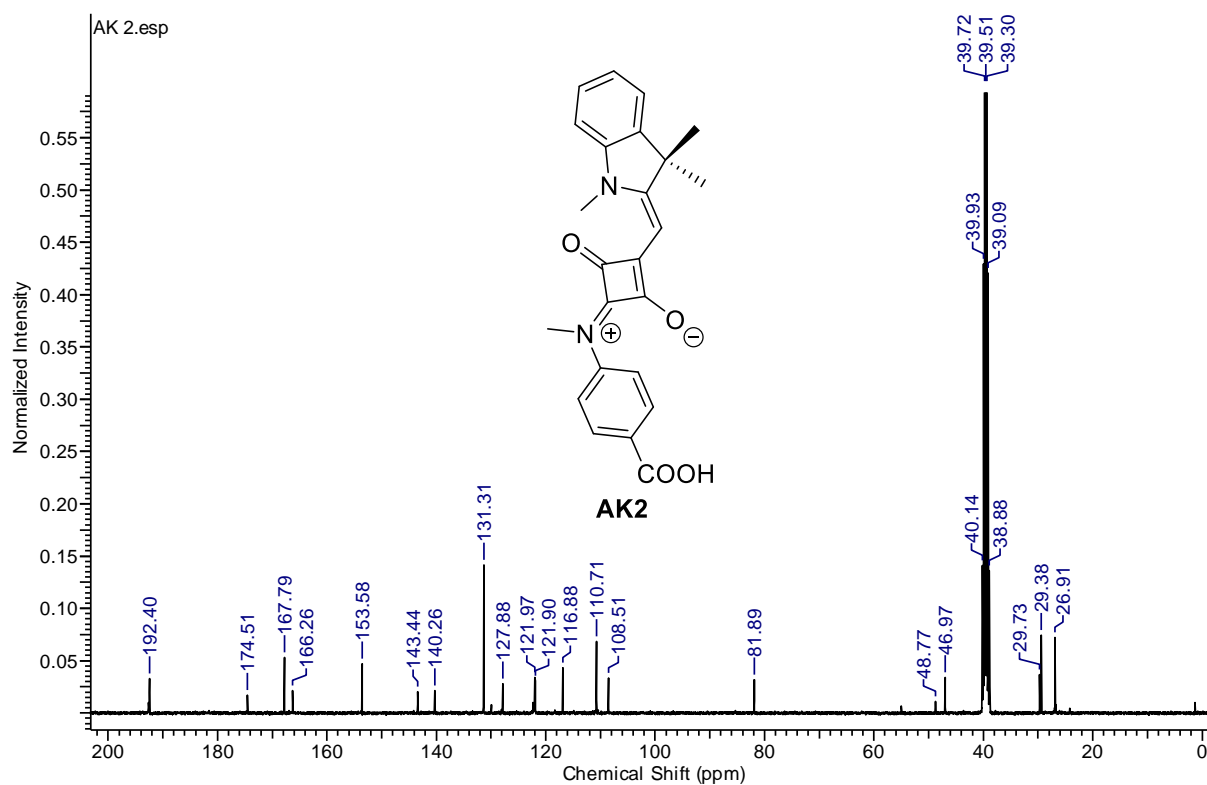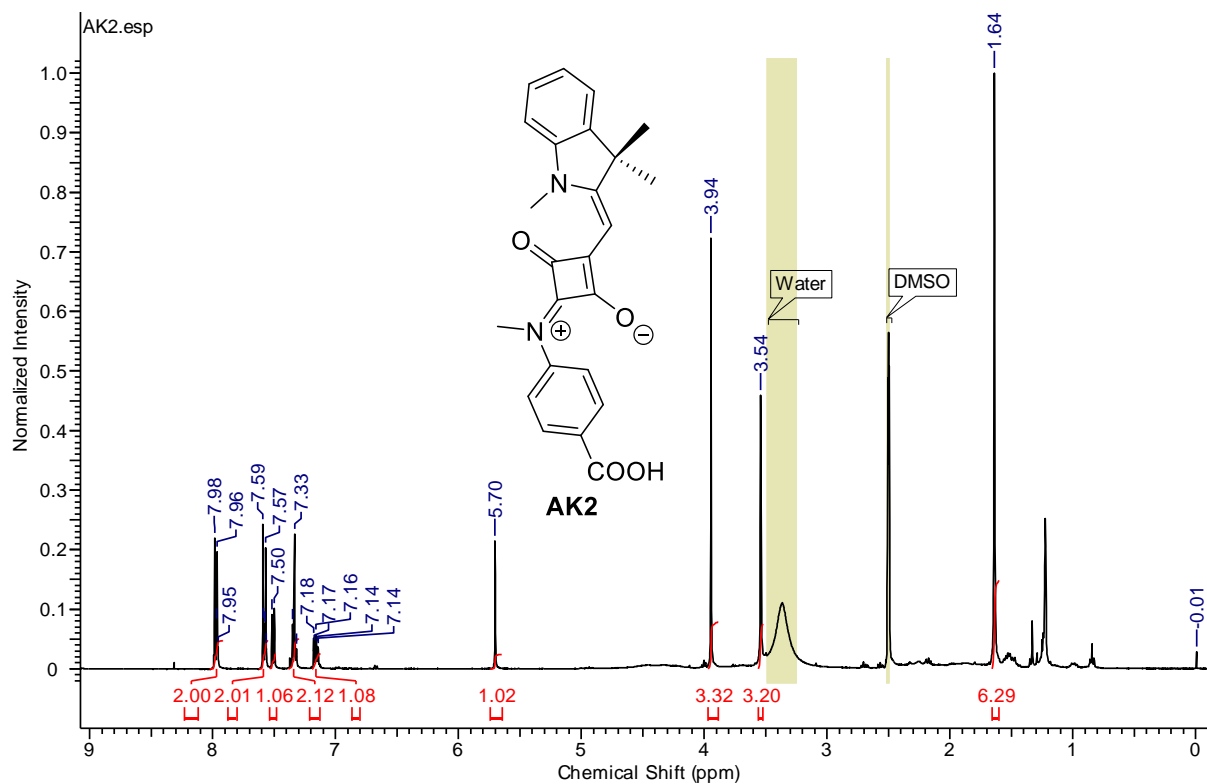
Figure A71. ^{1}H- and ^{13}C- NMR spectra of compound **4 (AK2)** in DMSO-d_6.
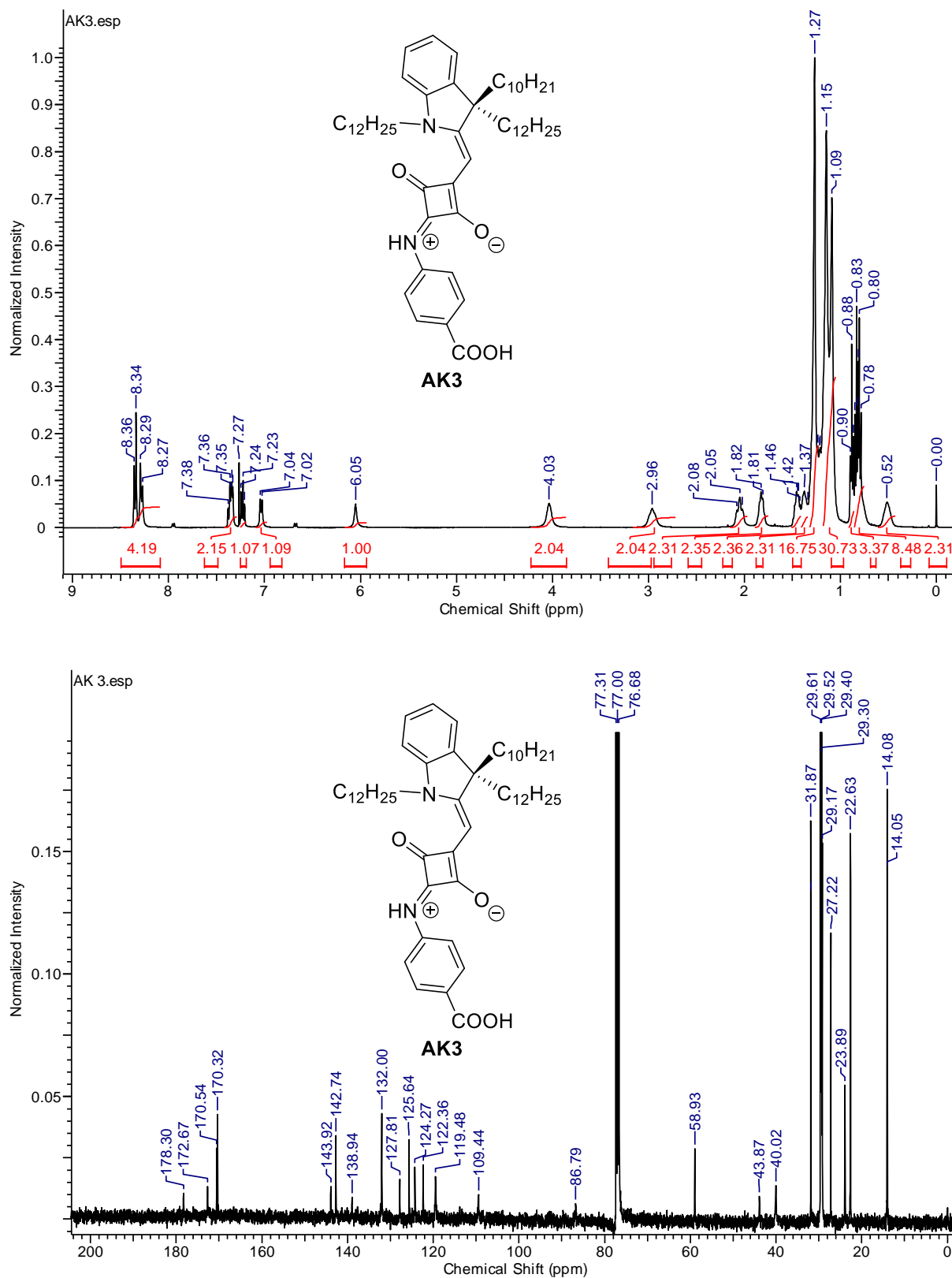
Figure A72. ^{1}H- and ^{13}C- NMR spectra of compound **5 (AK3)** in CDCl$_3$.
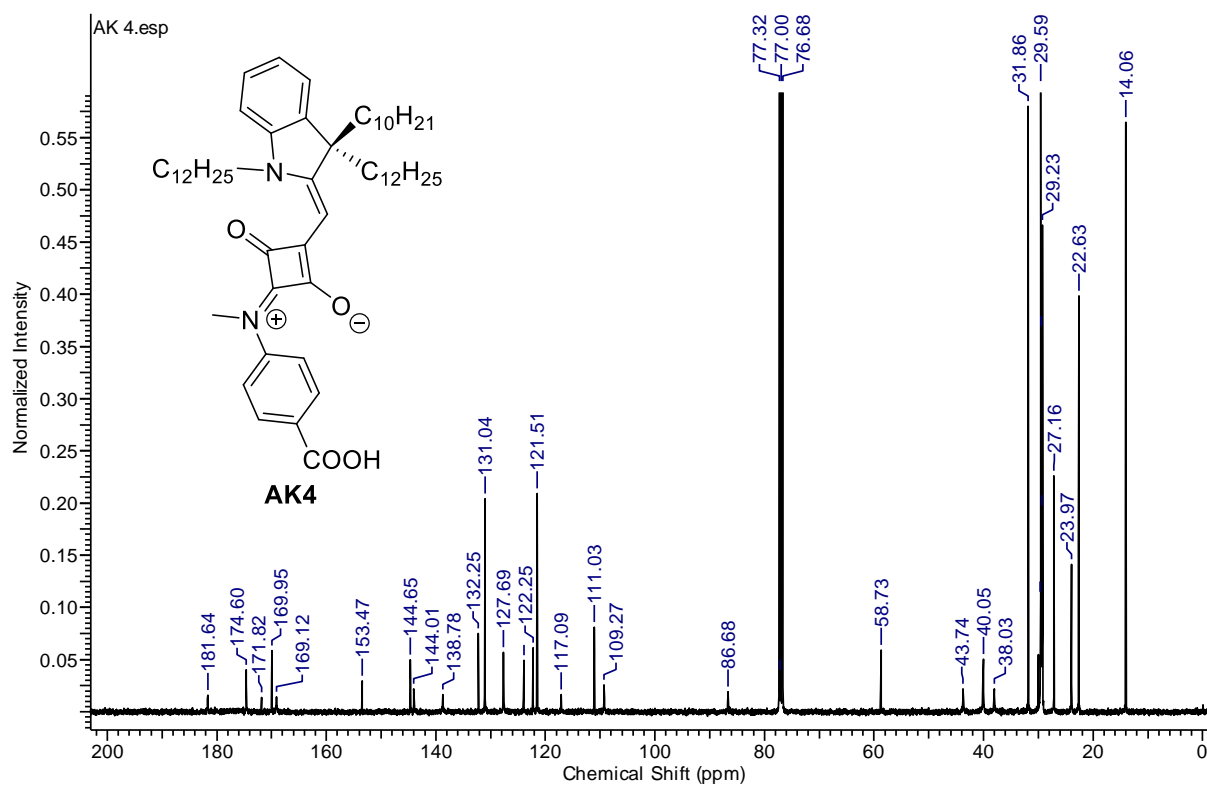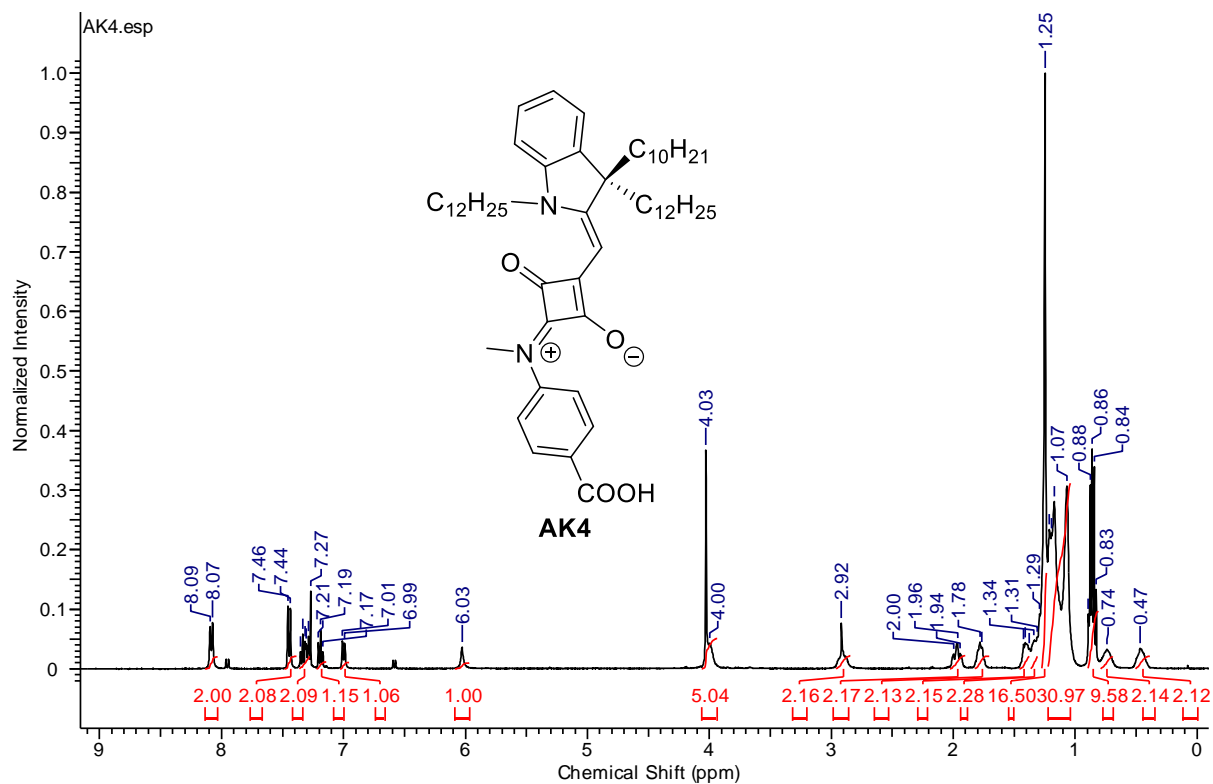
Figure A73. ^{1}H- and ^{13}C- NMR spectra of compound **6 (AK4)** in CDCl$_3$.
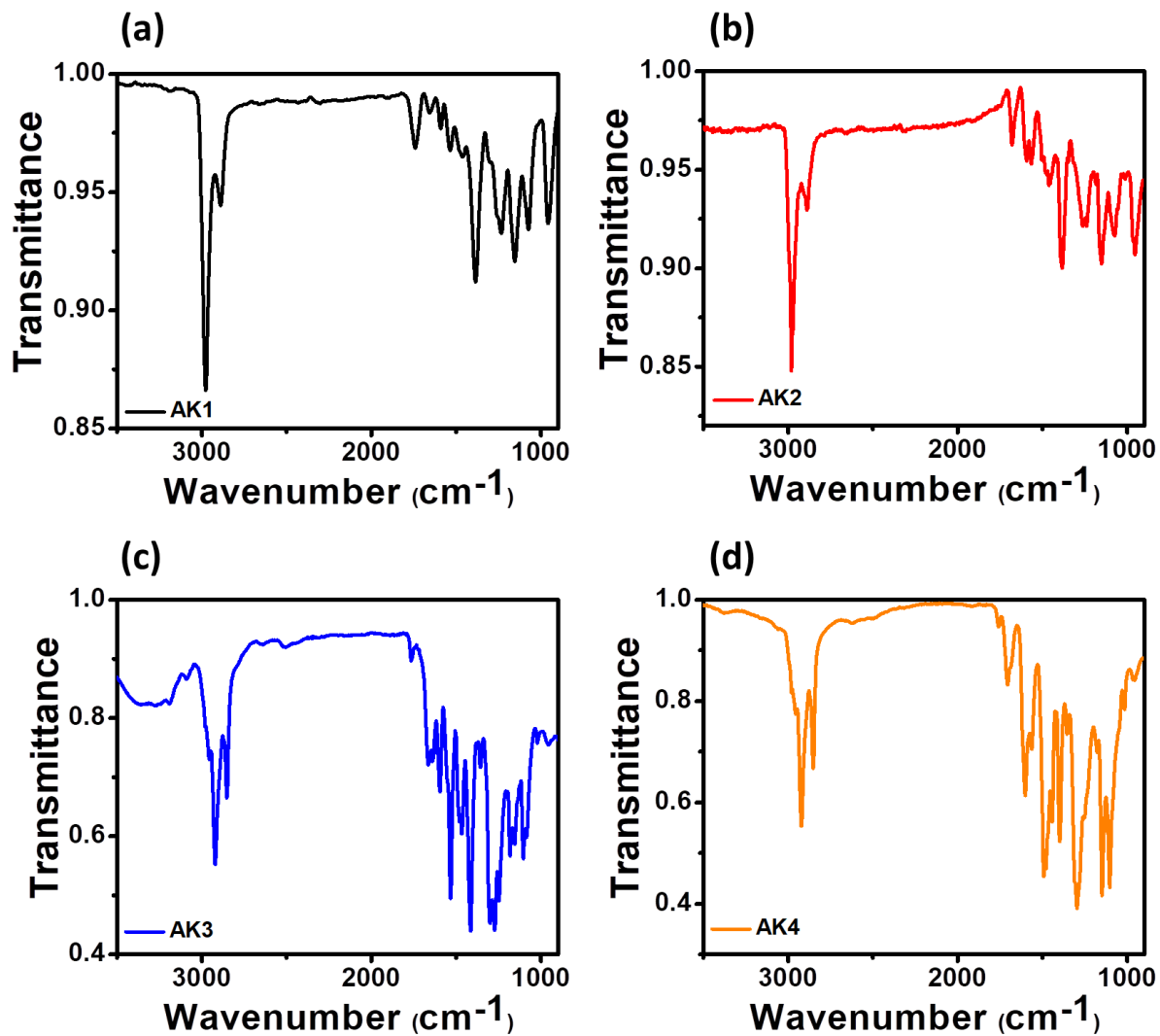
Figure A74. IR-spectra of AK dyes.

Chapter 5
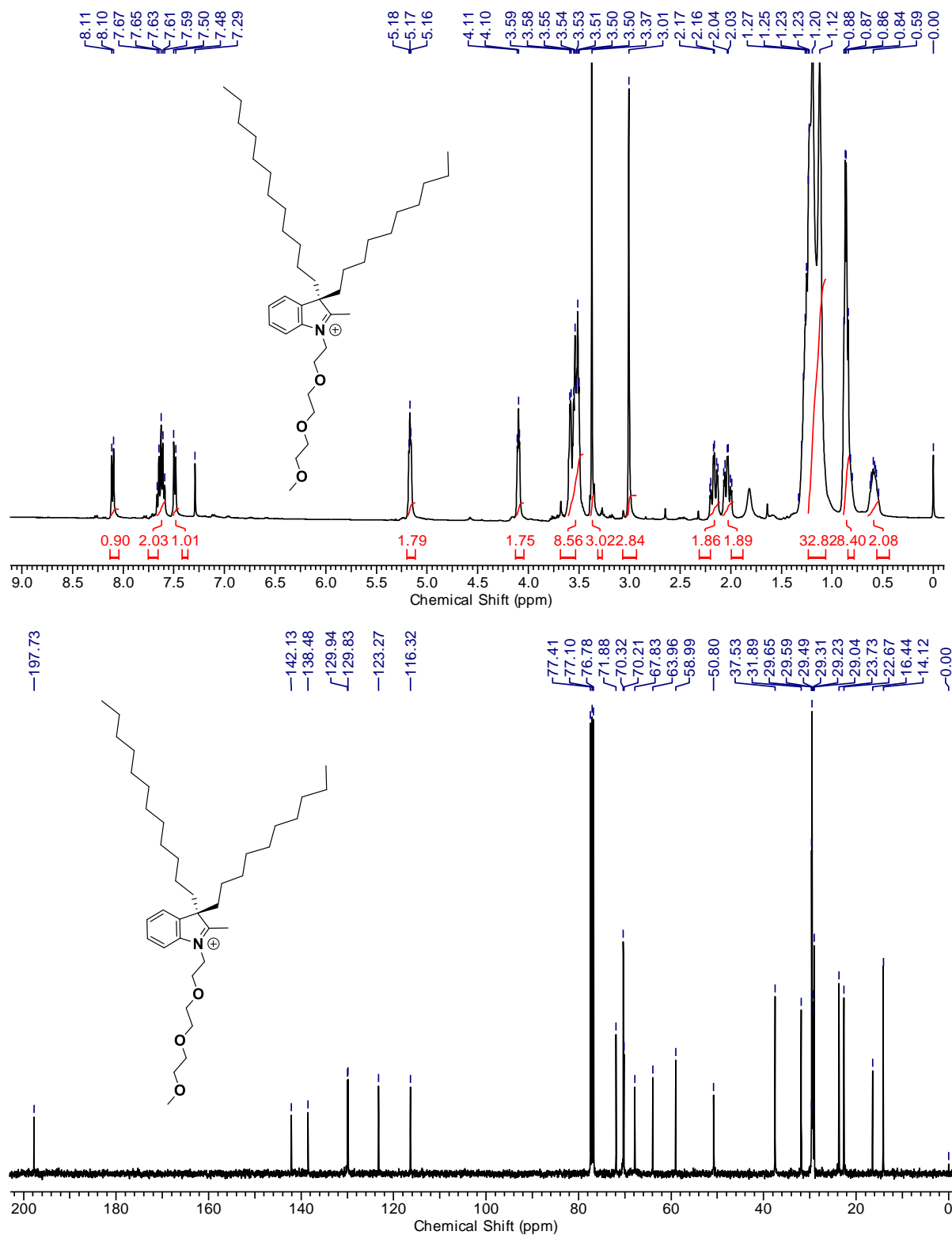
Figure A75. ^{1}H and ^{13}C NMR spectra of compound **2** in CDCl$_3$.
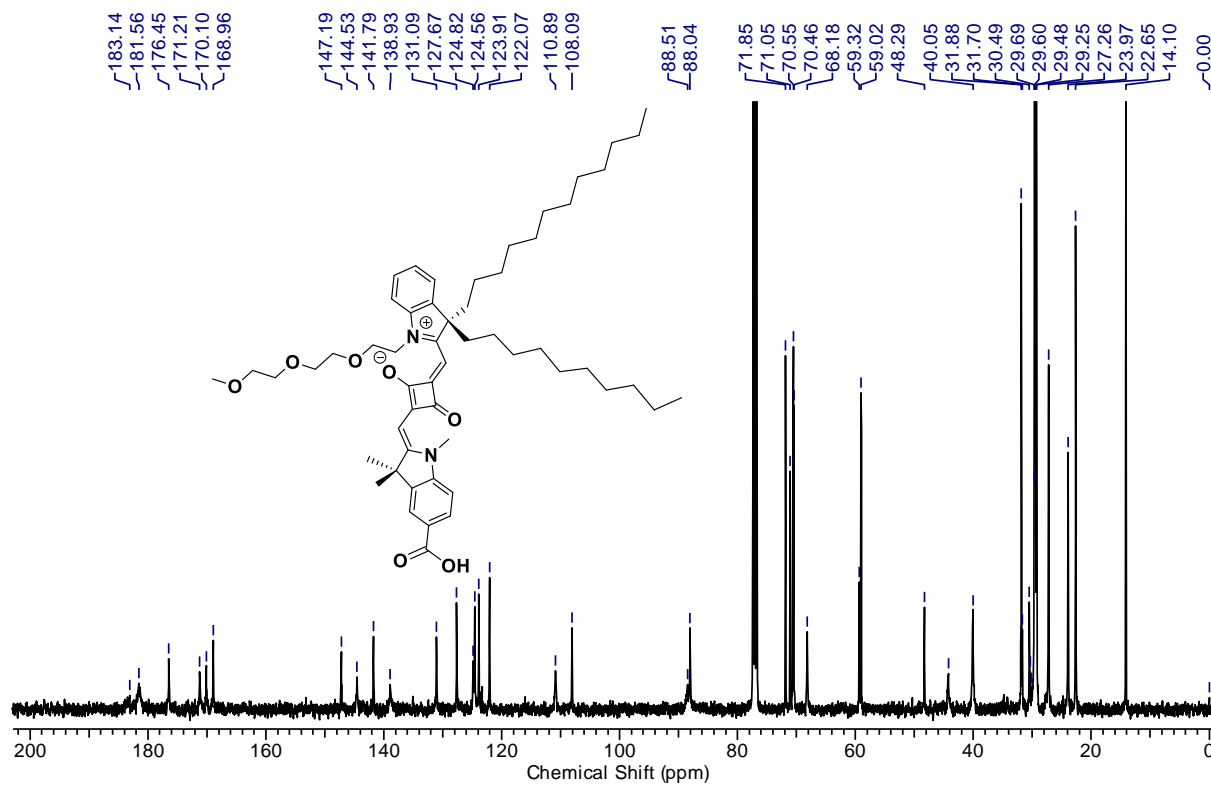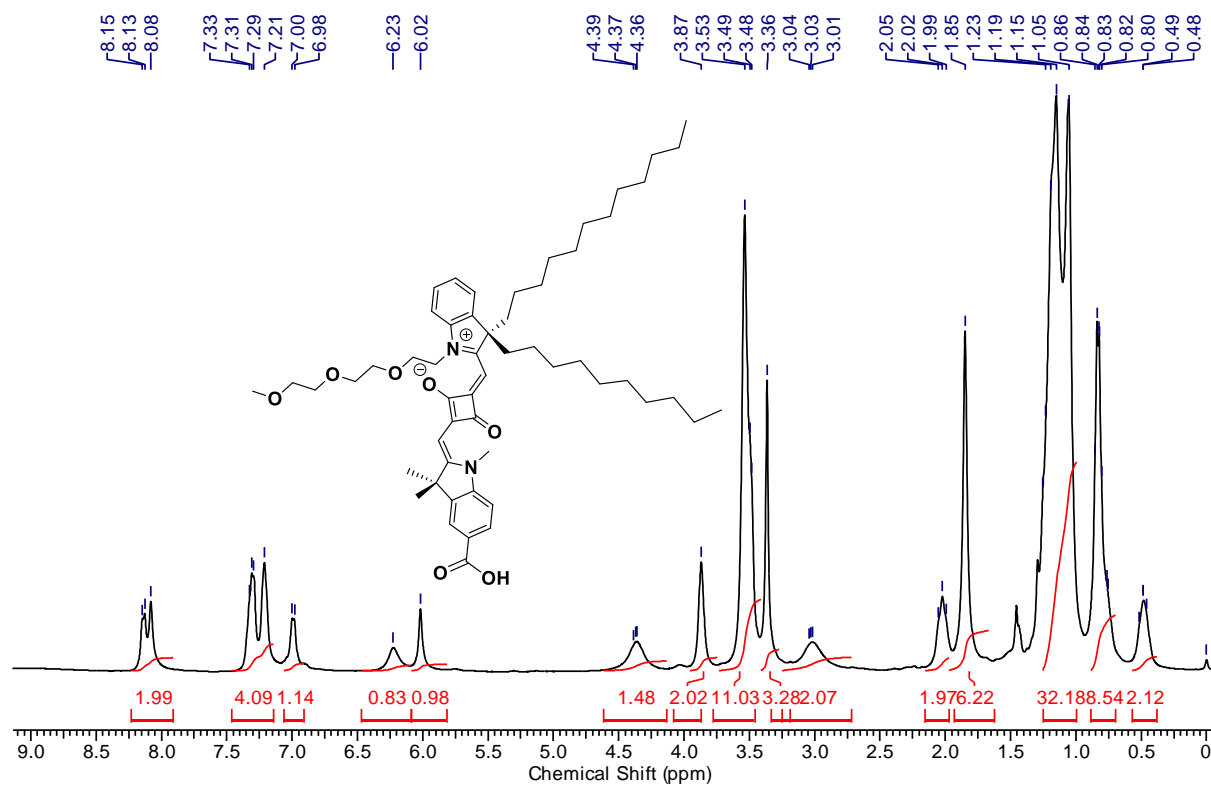
Figure A76. ^{1}H and ^{13}C NMR spectra of compound **4 (ASQ4)** in CDCl$_3$.

AKS-3-29C #29 RT: 0.13 AV: 1 NL: 1.95E8
T: FTMS + p ESI Full ms [100.00-1500.00]
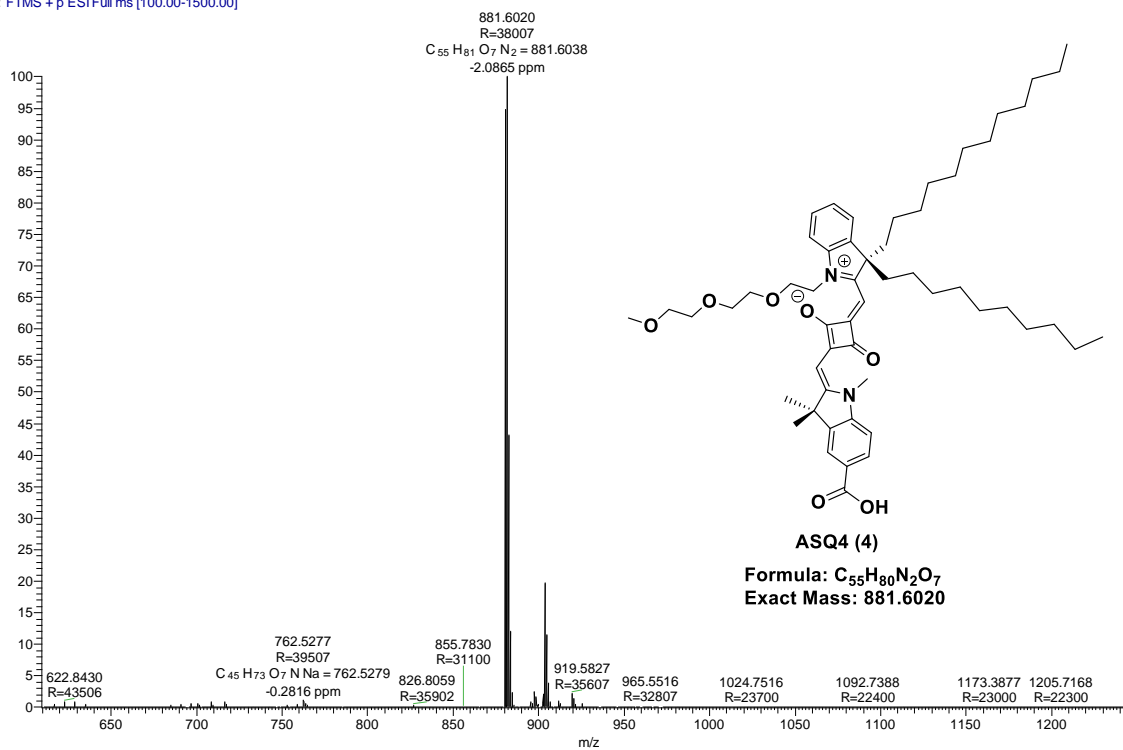
Figure A77. HRMS spectra of compound **4 (ASQ4)**.

ABSTRACT

Controlling the dye aggregation onto the TiO_2 surface plays an important role to achieve high dye-sensitized solar cell (DSSC) efficiency by broadening the IPCE (incident photon to current conversion efficiency) response from visible-light to NIR regions. Squaraine dyes are well known to form well packed aggregated structures onto the TiO_2 surface and aggregation in solution by strong intermolecular attraction between the dye molecules, and also well known for absorbing the visible and NIR-light regions with high molar extinction coefficient. So, here unsymmetrical squaraine dyes have been used to understand the aggregation properties of dyes onto the TiO_2 surface by alkyl group engineering, orienting the dyes, co-sensitization, changing the solvent systems for sensitization, and using the various electrolytes, and its effect on the dye-sensitized solar cell efficiency. By increasing the chain length of in-plane and out-of-plane alkyl groups in squaraine dyes V_{OC} and J_{SC} of DSSC were synergistically increased by the surface passivation of photoanode and controlled aggregation of dyes onto the TiO_2 surface. Further, anchoring group (carboxylic acid) on the *para*-position respect to the amine group of squaraine dyes is best position to achieve high DSSC efficiency than other positions. Further, methyl group on arylamine, in-plane and out-of-plane alkyl groups on the indoline unit of visible-light active unsymmetrical squaraine dyes are very sensitive towards the V_{OC}, J_{SC} and DSSC efficiency. Further, co-sensitization of the visible dyes with NIR active squaraine dyes have achieved the maximum efficiency 9.36% with enhanced J_{SC}. Further, acetonitrile solvent system used for the device fabrication and iodine-based electrolytes are the best combination to achieve the high DSSC efficiencies for the NIR active unsymmetrical squaraine dyes. Furthermore, SQS4 have achieved 5.92% of DSSC efficiency and is maximum obtained efficiency by NIR-light active squaraine dyes with cobalt based electrolyte and PEDOT.

Details of the publications emanating from the thesis work

1) **Ambarish Kumar Singh,** Munavvar Fairoos Mele Kavungathodi, Jayaraj Nithyanandhan. Alkyl-Group-Wrapped Unsymmetrical Squaraine Dyes for Dye Sensitized Solar Cells: Branched Alkyl Chains Modulate the Aggregation of Dyes and Charge Recombination Processes. *ACS Appl. Mater. Interfaces* **2020**, *12,* 2555−2565.

2) **Ambarish Kumar Singh,** Ashakiran Maibam, Bharathkumar H. Javaregowda, Rajesh Bisht, Ashwath Kudlu, Sailaja Krishnamurty, Kothandam Krishnamoorthy, Jayaraj Nithyanandhan. Unsymmetrical Squaraine Dyes for Dye-Sensitized Solar Cells: Position of Anchoring Group Controls the Orientation and Self-Assembly of Sensitizers on TiO_2 Surface and Modulate Its Flat Band Potential. *J. Phys. Chem. C*, **2020**, *124*, 18436−54.

Publications Not-emanating from the thesis work

1) Rajesh Bisht, Munavvar Fairoos M. K., **Ambarish Kumar Singh**, Jayaraj Nithyanandhan. Panchromatic Sensitizer for Dye-Sensitized Solar Cells: Unsymmetrical Squaraine Dyes Incorporating Benzodithiophene π-Spacer with Alkyl Chains to Extend Conjugation, Control the Dye Assembly on TiO_2, and Retard Charge Recombination. *J. Org. Chem.* **2017**, *82*, 1920−1930.

2) Manik Chandra Sil, Vediappan Sudhakar, **Ambarish Kumar Singh,** Munavvar Fairoos Mele Kavungathodi, Jayaraj Nithyanandhan. Homo- and Heterodimeric Dyes for Dye-Sensitized Solar Cells: Panchromatic Light Absorption and Modulated Open Circuit Potential. *ChemPlusChem* **2018**, *83*, 998–1007.

3) Vellimalai Punitharasu, Munavvar Fairoos Mele Kavungathodi, **Ambarish Kumar Singh**, Jayaraj Nithyanandhan. π-Extended cis-Configured Unsymmetrical Squaraine Dyes for Dye Sensitized Solar Cells: Panchromatic Response. *ACS Appl. Energy Mater.* **2019**, *2,* 8464−8472.

Details of the abstract presented (oral/poster) at national/international conferences/seminars

1) Poster presented at International Symposium, "8th East Asia Symposium on Functional Dyes and Advanced Materials (EAS8-2017), conference held on 20-22 September 2017", CSIR-NIIST, Thiruvananthapuram, India.

2) Oral presentation at "NCL-Research Foundation & CSIR-NCL Annual Students Conference 2018, conference held on 29th and 30th November 2018", CSIR-NCL Pune, India.

3) Participated in "SPSI-MACRO-2018, 15th International conference on Polymer Science and Technology, ISSER-Pune and CSIR-NCL Pune India, conference held on 19-22 December 2018".

4) Oral presentation at "Divisional Symposium Physical and Materials Chemistry Division, CSIR-NCL Pune, conference held on 30th November 2017".